National Library
of Canada

Canadian Theses Service

Ottawa, Canada
K1A 0N4

Bibliothèque nationale
du Canada

Services des thèses canadiennes

CANADIAN THESES

THÈSES CANADIENNES

NOTICE

The quality of this microfiche is heavily dependent upon the quality of the original thesis submitted for microfilming. Every effort has been made to ensure the highest quality of reproduction possible.

If pages are missing, contact the university which granted the degree.

Some pages may have indistinct print especially if the original pages were typed with a poor typewriter ribbon or if the university sent us an inferior photocopy.

Previously copyrighted materials (journal articles, published tests, etc.) are not filmed.

Reproduction in full or in part of this film is governed by the Canadian Copyright Act, R.S.C. 1970, c. C-30. Please read the authorization forms which accompany this thesis.

AVIS

La qualité de cette microfiche dépend grandement de la qualité de la thèse soumise au microfilmage. Nous avons tout fait pour assurer une qualité supérieure de reproduction.

S'il manque des pages, veuillez communiquer avec l'université qui a conféré le grade.

La qualité d'impression de certaines pages peut laisser à désirer, surtout si les pages originales ont été dactylographiées à l'aide d'un ruban usé ou si l'université nous a fait parvenir une photocopie de qualité inférieure.

Les documents qui font déjà l'objet d'un droit d'auteur (articles de revue, examens publiés, etc.) ne sont pas microfilmés.

La reproduction, même partielle, de ce microfilm est soumise à la Loi canadienne sur le droit d'auteur, SRC 1970, c. C-30. Veuillez prendre connaissance des formules d'autorisation qui accompagnent cette thèse.

THIS DISSERTATION
HAS BEEN MICROFILMED
EXACTLY AS RECEIVED

LA THÈSE A ÉTÉ
MICROFILMÉE TELLE QUE
NOUS L'AVONS REÇUE

NL 339 (r. 86/01)

Canada

National Library of Canada Bibliothèque nationale du Canada

53

Ottawa, Canada
K1A 0N4

TC –

ISBN 0-315-23251-X

CANADIAN THESES ON MICROFICHE SERVICE – SERVICE DES THÈSES CANADIENNES SUR MICROFICHE

PERMISION TO MICROFILM – AUTORISATION DE MICROFILMER

- Please print or type – Écrire en lettres moulées ou dactylographier

AUTHOR – AUTEUR

Full Name of Author – Nom complet de l'auteur
GREGORY ALAN ROBB

Date of Birth – Date de naissance
August 12 1956

Canadian Citizen – Citoyen canadien
☑ Yes / Oui ☐ No / Non

Country of Birth – Lieu de naissance
Canada

Permanent Address – Résidence fixe
2326 WESTMOUNT ROAD NW
CALGARY, ALBERTA
T2N-3L6

THESIS – THÈSE

Title of Thesis – Titre de la thèse
Sedimentology and Diagenesis of the Viking Formation, Garrington Oil Field, South Central, Alberta

Degree for which thesis was presented / Grade pour lequel cette thèse fut présentée
M Sc

Year this degree conferred / Année d'obtention de ce grade
1985

University – Université
U of Alberta

Name of Supervisor – Nom du directeur de thèse
Dr F.J. Longstaffe & Dr F.J. Hein

AUTHORIZATION – AUTORISATION

Permission is hereby granted to the NATIONAL LIBRARY OF CANADA to **microfilm** this thesis and to **lend** or **sell copies of the film.**

The author reserves other publication rights, and neither the thesis nor extensive extracts from it may be printed or otherwise reproduced without the author's written permission.

L'autorisation est, par la présente, accordée à la BIBLIOTHÈQUE NATIONALE DU CANADA de **microfilmer** cette thèse et de **prêter** ou de **vendre des exemplaires du film.**

L'auteur se réserve les autres droits de publication; ni la thèse ni de longs extraits de celle-ci ne doivent être imprimés ou autrement reproduits sans l'autorisation écrite de l'auteur.

ATTACH FORM TO THESIS – VEUILLEZ JOINDRE CE FORMULAIRE À LA THÈSE

Signature
Greg Robb

Date
Oct 15/85

NL-91 (r. 84/03)

Canada

THE UNIVERSITY OF ALBERTA

Sedimentology and Diagenesis of the Viking Formation, Garrington Oil Field, South-Central Alberta

by

Gregory Alan Robb

A THESIS
SUBMITTED TO THE FACULTY OF GRADUATE STUDIES AND RESEARCH
IN PARTIAL FULFILMENT OF THE REQUIREMENTS FOR THE DEGREE
OF Master of Science

Geology

EDMONTON, ALBERTA
Fall, 1985

THE UNIVERSITY OF ALBERTA

RELEASE FORM

NAME OF AUTHOR Gregory Alan Robb

TITLE OF THESIS Sedimentology and Diagenesis of the Viking Formation, Garrington Oil Field, South-Central Alberta

DEGREE FOR WHICH THESIS WAS PRESENTED Master of Science

YEAR THIS DEGREE GRANTED Fall, 1985

Permission is hereby granted to THE UNIVERSITY OF ALBERTA LIBRARY to reproduce single copies of this thesis and to lend or sell such copies for private, scholarly or scientific research purposes only.

The author reserves other publication rights, and neither the thesis nor extensive extracts from it may be printed or otherwise reproduced without the author's written permission.

(SIGNED) Greg Robb

PERMANENT ADDRESS:

2320 WESTMOUNT ROAD N.W.
CALGARY, ALBERTA
T2N - 3N6

DATED October 14 1985

THE UNIVERSITY OF ALBERTA

FACULTY OF GRADUATE STUDIES AND RESEARCH

The undersigned certify that they have read, and recommend to the Faculty of Graduate Studies and Research, for acceptance, a thesis entitled Sedimentology and Diagenesis of the Viking Formation, Garrington Oil Field, South-Central Alberta submitted by Gregory Alan Robb in partial fulfilment of the requirements for the degree of Master of Science.

F. J. Longstaffe

Supervisor

Frances J. Hein

Supervisor

Frank W. Schwartz

J. O. Scott

Date Oct 14, 1985

DEDICATION

This thesis is dedicated to my mother,

Catherine Robb,

and to my father,

Russell Robb,

whose encouragement and support made this work possible.

ABSTRACT

The Viking Formation at Garrington consists of a laterally extensive coarsening upward sequence of shales, sandstones and conglomerates. Shales at the base of the Viking Formation were deposited in relatively deep water by hemipelagic fallout of fine-grained material from suspension. The sandstones were deposited by storm processes approximately 30 to 50 kilometers from the Albian paleoshoreline. Subsequent reworking by semipermanent geostrophic currents, periodically enhanced by storms, molded these sediments into a northwest to southeast trending topographic high or sand ridge with a maximum thickness of 15 metres. Conglomerate units were deposited unconformably on top of the sandstones. Conglomerate thickness is highly variable; ranging from 0 to 3.6 meters in the study area. Inversely and normally graded conglomerates and massive-disorganized beds are believed to have been emplaced by sediment gravity flows. Other conglomerate beds are low to high angle cross-stratified and are the result of current reworking of the sediment gravity flow deposits into migrating gravel waves and megaripples. The geometry, sedimentary structures, trace fossil assemblage and the general coarsening upward sequence all indicate that the Viking Formation at Garrington was deposited as an offshore bar formed by the complex interaction of marine processes in a regressive seaway.

Diagenesis of the sediments has taken place in a number of discrete events. Earliest diagenesis involved pyrite and siderite cementation as reducing conditions developed at relatively shallow burial depths. This was followed by compaction and quartz cementation. Late pore-filling carbonate cementation followed quartz cementation. From analysis by thin section, X-ray diffraction and scanning electron microscope it appears that the first pore-filling carbonate cement to form was calcite, which was subsequently dolomitized. Dolomite cement was later partially ankeritized at depth. These pore-filling carbonate cements later underwent solution and secondary porosity was created. Clay mineral authigenesis was the last major diagenetic event to occur prior to hydrocarbon migration. Acidic fluids responsible for carbonate solution are also believed to be responsible for the precipitation of kaolinite, illite, illite/smectite, smectite and chlorite.

Diagenesis has had a profound impact on the porosity and permeability of the Viking Formation at Garrington. Porosity has been substantially reduced by compaction and

quartz and carbonate cementation. Permeability is most seriously affected by pore-lining and pore-filling clay mineral cements. Pore-lining and pore-filling minerals are in 100 % contact with drilling, completion and stimulation fluids and may effectively block pore throats and greatly reduce permeability. If enhanced recovery methods, such as fluid injection or hydraulic fracturing are used to stimulate the Viking reservoir rocks the following problems may arise; (1) migration of fine-grained material (mainly kaolinite and quartz), (2) swelling of water sensitive clays (smectite and illite / smectite), and (3) precipitation of iron-rich compounds (derived from chlorite, ankerite and siderite). Reservoir damage would be most severe in the fine-grained sandstones due to the relatively large amount of fine-grained material and iron-rich carbonate cements present in these rocks and the small pore throat sizes. The conglomerates and coarse-grained sandstones have less fine-grained material present in their pore systems, very little carbonate cement and much larger pore throats than the fine-grained sandstones, therefore they should not be as adversely affected by reservoir stimulation.

The Viking Formation throughout much of central Alberta is subpressured. For this reason pressure maintainence is necessary in the Viking reservoir at Garrington. At least three possible cause for the subpressures exist; (1) a chemico-osmotic pressure gradients (2) decompaction due to the removal of overburden, and (3) permeability barriers. Of these three possibilities a chemico-osmotic pressure gradient and permeability barriers are the most likely causes of subpressures in the Garrington area.

ACKNOWLEDGEMENTS

A work of this magnitude is the result of the efforts of many people. This project was generously funded by Candian Superior Oil Ltd. and special thanks must go to the development group there, especially Lauren Pudsey. I wish to thank Dr. Fred Longstaffe and Dr. Fran Hein for their many helpful suggestions and their liberal use of red ink. A very special thank you to Diane Caird for her assistance in the laboratory and her perseverance in spite of very long odds.

Table of Contents

Chapter ... Page

I. INTRODUCTION ... 1

A. PREVIOUS WORK ... 3

B. STRATIGRAPHY ... 6

C. METHODS ... 11

CORE DESCRIPTION ... 12

FACIES DEFINITION ... 12

CORRELATION OF FACIES FROM LITHOLOGIC AND GEOPHYSICAL LOGS ... 12

ISOPACH MAPS, BLOCK DIAGRAMS AND FENCE DIAGRAMS ... 15

SAMPLING METHODS ... 17

PETROGRAPHIC ANALYSIS ... 17

HYDROMETER ANALYSIS ... 17

X-RAY DIFFRACTION ANALYSIS ... 18

SCANNING ELECTRON MICROSCOPY ... 20

GAS-OIL RATIO TRENDS ... 21

LIST OF ABBREVIATIONS ... 22

TERMINOLOGY ... 24

II. SEDIMENTOLOGY AND DEPOSITIONAL ENVIRONMENT ... 25

A. DEPOSITIONAL ENVIRONMENTS AND SEDIMENT DISPERSAL MECHANISMS ... 25

B. CRETACEOUS ANALOGS ... 29

C. LITHOFACIES DESCRIPTION ... 34

D. VIKING DEPOSITIONAL MECHANISMS ... 53

E. FACIES INTERPRETATION AND CORRELATION ... 60

F. DEPOSITIONAL PATTERN AND FACIES DISTRIBUTION ... 76

G. GARRINGTON DEPOSITIONAL ENVIRONMENT ... 86

III. MINERALOGY ... 92

A. BULK MINERALOGY ... 92

TEXTURES ... 103

B. HYDROMETER ANALYSIS ... 109

C. X-RAY DIFFRACTION RESULTS 109
  CONGLOMERATES 113
  COARSE-GRAINED SANDSTONES 113
  FINE-GRAINED SANDSTONES 114
  SUMMARY OF X-RAY DIFFRACTION RESULTS 115
D. SCANNING ELECTRON MICROSCOPY RESULTS 115
E. PARAGENETIC SEQUENCE 138
F. DIAGENESIS 138
  EARLY DIAGENESIS: PYRITE AND SIDERITE FORMATION 139
  COMPACTION 142
  QUARTZ CEMENTATION 143
  FELDSPAR CEMENT 144
  FELDSPAR SOLUTION 145
  LATE CARBONATE CEMENTATION 145
  LATE SECONDARY POROSITY 146
  PRECIPITATION OF CLAY MINERALS 147
  ALBITIZATION OF FELDSPARS 148
  DISCUSSION 149
IV. RESERVOIR CHARACTERISTICS 151
A. RESERVOIR ROCKS 151
B. POROSITY AND PERMEABILITY 152
C. EFFECTS OF PORE-LINING AND PORE-FILLING MINERALS ON RESERVOIR PERFORMANCE 156
  CONGLOMERATES AND COARSE-GRAINED SANDSTONES 156
  FINE-GRAINED SANDSTONES 162
D. GAS-OIL RATIO 163
E. RESERVOIR PRESSURE 165
  CHEMICO-OSMOTIC PRESSURE GRADIENTS 167
  OVERBURDEN REMOVAL 170
  PERMEABILITY BARRIERS 171
F. PETROLEUM RECOVERY 174

V. CONCLUSION 176

VI. REFERENCES CITED 178

APPENDIX A 188

APPENDIX B 253

LIST OF TABLES

Table 2.1 Summary of Facies 39-40

Table 3.1 Samples Investigated 94-96

Table 3.2 Percentages of Grains, Cements and Porosity 97-98

Table 3.3 Bulk Mineralogy: Thin Section Analysis 99-100

Table 3.4 Hydrometer Analysis 110-112

Table 3.5 Mineralogy 5-20 *um* size fraction 116-118

Table 3.6 Mineralogy 2-5 *um* size fraction 119-121

Table 3.7 Mineralogy < 2 *um* size fraction 122-124

Table 4.1 Porosity and Permeability 153-155

LIST OF FIGURES

Figure 1.1 Location map of the Garrington Oil Field 2

Figure 1.2 Location of some Viking Formation Oil and Gas Fields in Alberta and Saskatchewan 5

Figure 1.3 Table of Formations in Alberta and neighboring areas 8

Figure 1.4 Map of the Colorado Sea at the time of Joli Fou deposition 9

Figure 1.5 Map of the Mowry Sea near the time of Viking deposition 10

Figure 1.6 Grain size scales for sediments 13

Figure 1.7 Lithologic symbols and structures 14

Figure 1.8 Typical geophysical log of the Viking Formation in the Garrington Oil Field..... 16

Figure 2.1 Distribution of allochthonous terranes in the Canadian cordillera 31

Figure 2.2 Diagram comparing coarsening upward sequences in the Shannon sandstone, the Cardium Formation and the Viking Formation 33

Figure 2.3 Core photographs of facies 1 and subfacies 2A, 2B and 2C 42

Figure 2.4 Core photographs of subfacies 2D, 2E, 2F and 2G 44

Figure 2.5 Core photographs of facies 3A, 3C, 4A, 4B, and 4C 46

Figure 2.6 Core photographs of facies 5A, 5B, 6A and 6B 48

Figure 2.7 Core photographs of facies 7A, 7B, 7C, 8A and 8B 50

Figure 2.8 Core photographs of facies 9A, 9B, 9C and 10A 52

Figure 2.9 Diagram showing the interrelationships which may occur between the various types of sediment gravity flows 59

Figure 2.10 Diagram showing the general coarsening-upward sequence in the Viking Formation at Garrington 62

Figure 2.11 Fence diagram of the Garrington Oil Field ....(in pocket)

Figure 2.12 Histogram showing the percentages of facies which comprise Facies Association 3 64

Figure 2.13 Bedform stability plots on a size-velocity diagram 65

Figure 2.14 Core photographs of facies-assemblages occurring within the large-scale facies associations 68

Figure 2.15A Histogram showing the percentages of facies which comprise the Viking "B" conglomerate beds of Facies Association 2 71

Figure 2.15B Histogram showing the percentages of facies which comprise the Viking "B" conglomerate beds of Facies Association 2 grouped by similar sedimentary structures or mode of emplacement 71

Figure 2.16 Histogram showing the percentages of facies which comprise the Viking "A" coarse-grained sandstone beds of Facies Association 2 75

Figure 2.17 Block diagram: Bentonite marker to the top of the Viking "B" horizon 77

Figure 2.18 Block diagram: Topographic surface of the Viking "B" unit relative to a Base of Fish Scales datum 78

Figure 2.19 Isopach map: Bentonite marker to the top of the Viking "B" horizon ..(in pocket)

Figure 2.20 Isopach map: Lloydminster shale .... (in pocket)

Figure 2.21 Block diagram: Thickness of the fine-grained sandstone facies association 3 80

Figure 2.22 Isopach map: Fine-grained sandstone facies association 3 .... (in pocket)

Figure 2.23 Block diagram: Thickness of the conglomerate and coarse-grained sandstone facies association 2 82

Figure 2.24 Isopach map: Viking "B" conglomerate and coarse-grained sandstone facies association 2 .... (in pocket)

Figure 2.25 Block diagram: Combined thickness of the fine-grained sandstone and the coarse-grained sandstone and conglomerate (facies associations 3 and2) 83

Figure 2.26 Isopach map: Combined thickness of the fine-grained sandstone and the coarse-grained sandstone and conglomerate (Facies associations 3 and 2)..(in pocket)

Figure 2.27 Block diagram: Regional dip of the Viking "B" unit relative to present sea level 85

Figure 2.28 Structure map of the top of the Viking "B" unit relative to present sea level ....(in pocket)

Figure 2.29 Diagram showing a paleoreconstruction of the Late Early Cretaceous Seaway at the time of Viking deposition 87

Figure 2.30 Diagram relating a major storm to storm-surge tide and storm-surge ebb current 88

Figure 2.31 Diagram showing the hierarchy of shelf sandstone bodies 90

Figure 3.1 Map of the Garrington study area showing sample locations 93

Figure 3.2A Classification of the conglomerates, coarse-grained sandstones and fine-grained sandstones in the Viking Formation at Garrington 102

Figure 3.2B Diagram showing the change in the relative abundance of chert and quartz from conglomerates to fine-grained sandstones 102

Figure 3.3 Photomicrographs of Viking "B" conglomerates showing various textures and cements 106

Figure 3.4 Photomicrographs of coarse-grained sandstones and fine-grained sandstones showing textures and cements 108

Figure 3.5 SEM photographs of Viking "B" conglomerates 127

Figure 3.6 SEM photographs of Viking "B" conglomerates 129

Figure 3.7 SEM photographs of coarse-grained sandstones 131

Figure 3.8 SEM photographs of coarse-grained sandstones 133

Figure 3.9 SEM photographs of fine-grained sandstones 135

Figure 3.10 SEM photographs of fine-grained sandstones 137

Figure 3.11 Interpreted sequence of diagenetic events in the Viking Formation at Garrington 140

Figure 3.12 Diagram showing three earliest zones of diagenesis and the diagenetic products characteristic of each zone 141

Figure 4.1 Plot of porosity versus permeability for 56 samples from the Viking Formation at Garrington 157

Figure 4.2 Plots of porosity versus percentages of fine-grained material present in samples 158

Figure 4.3 Plots of permeability versus percentages of fine-grained material present in the samples 159

Figure 4.4 Map showing the gas-oil ratio (GOR) trends in the Viking Formation at Garrington 164

Figure 4.5 Potentiometric cross-section between Ferrier, Gilby and Joarcam oil fields 166

Figure 4.6 Hydraulic head distribution in the Upper Devonian Woodbend Group of western Canada 168

Figure 4.7 Hydraulic head distribution in the Lower Cretaceous Viking Formation of western Canada 169

Figure 4.8 Isopach map of the calculated thickness of eroded sediments in Alberta 172

Figure 4.9 Cross-sectional model showing potentiometric surface approximation reflecting local permeability change 173

Figure 4.10 Potentiometric map reflecting fluid flow within the Viking sandstone in the Westlock-Joarcam area of Alberta 175

I. INTRODUCTION

The subject of this report is the Lower Cretaceous (Upper Albian) Viking Formation as it occurs in the Garrington Oil Field, Townships 34 and 35, Ranges 2 to 4 west of the Fifth Meridian (Figure 1.1). The data base for this study consists of 69 cores and 150 geophysical logs. Sixty-two samples were examined for mineralogy.

The primary objectives of this study are to:

1. Define the sedimentary facies of the Viking Formation within the study area;
2. Determine the lateral and vertical continuity of the sedimentary facies;
3. Establish a correlation between geophysical and lithologic logs within the study area;
4. Ascertain the bulk mineralogy of the Viking Formation and to classify the main rock types present;
5. Determine the nature and distribution of pore-lining and pore-filling minerals (especially clay minerals) in the three main lithologies;
6. Assess the effect of pore-lining and pore-filling minerals on reservoir performance;
7. Record the diagenetic events that have occurred in these rocks and to determine the extent to which they control porosity and permeability;
8. Determine local trends in gas-oil ratios (GOR) and to suggest explanations for subnormal pressures within the reservoir rocks.

Sedimentological studies were carried out by detailed core logging, definition of facies, correlation of facies from lithological and geophysical logs, and compilation of isopach maps, computer-generated block diagrams, cross-sections and fence diagrams. Details of the sedimentological studies are discussed in Chapter 2. Mineralogical studies were performed on samples taken from cores. Techniques included petrographic analysis, hydrometer analysis, X-ray diffraction (XRD) and scanning electron microscopy (SEM). Chapter 3 presents a discussion of the mineralogy and diagenesis of the Viking Formation. Chapter 4 discusses the porosity and permeability characteristics of the reservoir rocks, mineralogical controls upon reservoir performance and possible reasons for subpressure in the reservoir.

GARRINGTON OIL FIELD

SOUTH-CENTRAL ALBERTA

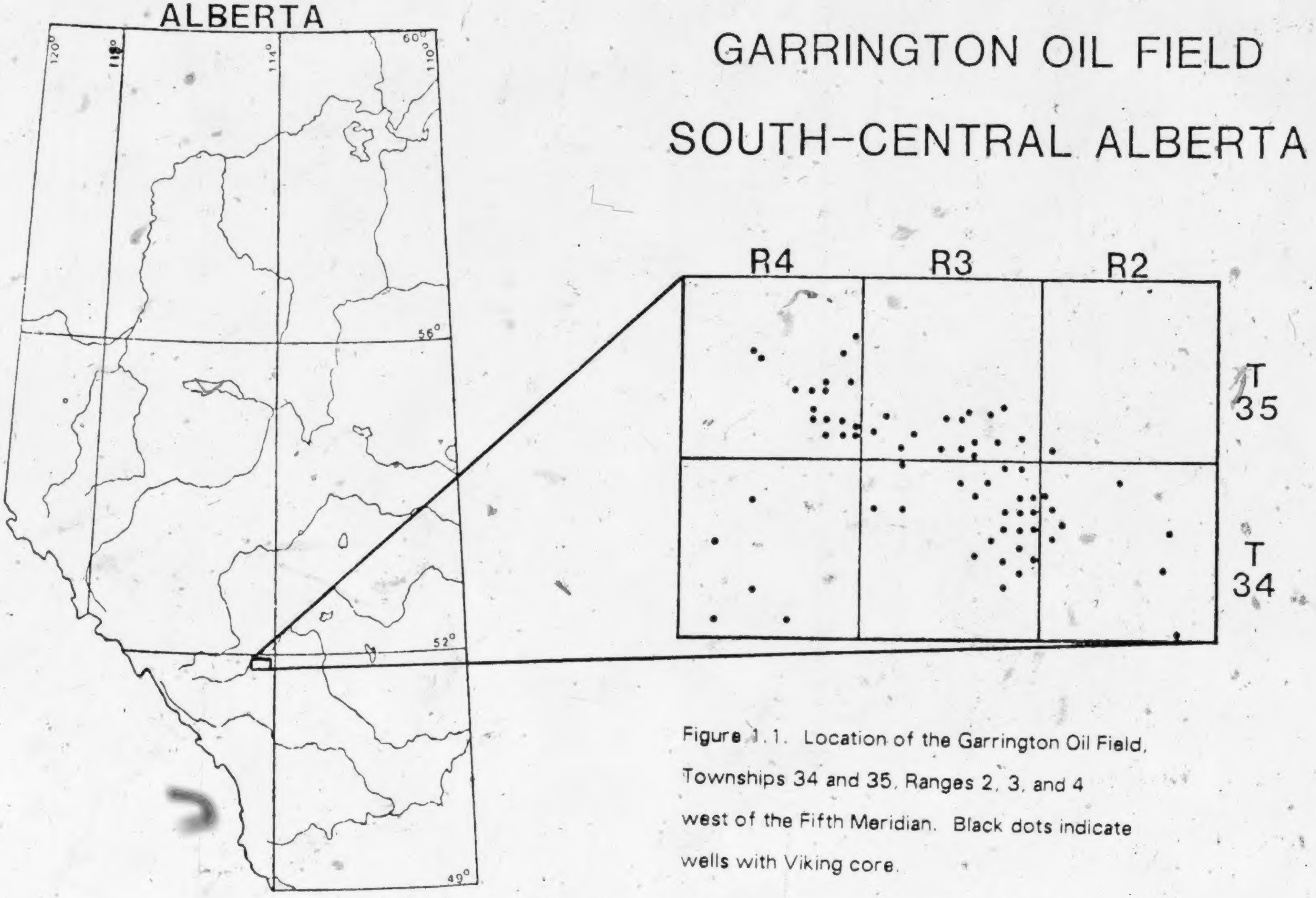
ALBERTA
120°
118°
114°
110°
60°
56°
52°
49°
R4
R3
R2
T 35
T 34

Figure 1.1. Location of the Garrington Oil Field, Townships 34 and 35, Ranges 2, 3, and 4 west of the Fifth Meridian. Black dots indicate wells with Viking core.

A. PREVIOUS WORK

The Viking Formation has been examined extensively in central and southern Alberta and southwest Saskatchewan because of its significance as a hydrocarbon reservoir. The formation has an estimated 247.6 x 10^3 $m^3$of conventional crude oil in place (3.5 % of the total conventional reserves), and 362,869 x 10^6 m^3 of initial raw gas in place (7.5 % of the total gas reserves) (ERCB, 1983, 1984).

The oil and gas prospects of the Viking Formation have been examined by Slipper (1918), Badgley (1952), Reasoner and Hunt (1954), Gammell (1955), Larson (1960), Alho et al.(1977), Boething (1977a) and Thomas (1977). Subsurface lithostratigraphy has been studied by Hume (1933), Nauss (1945), Gammell (1955), Love (1955), Glaister (1958, 1959), Stelck (1958), Tizzard and Lerbekmo (1975), Simpson (1975), Boethling (1977b) and Amajor (1980). Biostratigraphy and paleoecology were studied by Nauss (1947), Bullock (1950), Bahan (1951), Stansberry (1957), Stelck (1958, 1975), Simpson (1975), North and Caldwell (1975) and Caldwell et al.(1978). Bentonite markers within the Viking Formation and the Joli Fou and Lloydminster Formations have been used as time-stratigraphic markers by Roessingh (1959), Jones (1961), Tizzard and Lerbekmo (1975), and Amajor (1978, 1980).

The amount of work done on the Viking Formation and the extensive area which it covers has led to a number of different interpretations of the depositional setting of these sediments. Six types of deposits are commonly invoked: (a) regressive and transgressive shoreline deposits, (b) storm-surge deposits, (c) turbidites, (d) nearshore complexes of beaches, barrier islands and offshore bars, (e) tidal current ridges, and (f) deltas.

Bullock (1950) first proposed the regressive-transgressive shoreline concept and suggested that the Viking Formation represented the sandstone facies of the early Lloydminster transgression. Gammell (1955) used the stratigraphic position of the Viking Formation to conclude that the sandbodies were generally regressive. DeWiel (1956) thought that longshore currents were responsible for transportation of Viking sediments offshore. The Viking equivalent (Bow Island Formation) in southern Alberta has been described by Glaister (1959) as a deposit formed from a series of minor regressions within a generally transgressive sea. Thomas (1977) interpreted the Viking sandstone in the Provost area as a transgressive deposit. The Viking conglomerates in the Caroline area were interpreted by Leckie (in prep, 1984) as transgressive deposits.

Hunt (1954) first proposed the concept of storm-surge deposition for the Viking reservoir sandstones in the Joseph Lake-Armena-Camrose trend (now known as Joarcam, Figure 1.2); he based his conclusion on sedimentary structures and textures and the uniform thickness of the sandstone unit. Koldijk (1976) and Thomas (1977) proposed a storm-surge origin for the Gilby Viking "B" reservoir, regarded as an extension of the Joffre-Bentley trend (Figure 1.2). In 1977, Davies reinterpreted the work of Evans (1970), suggesting that in the Dodsland-Hoosier area of Saskatchewan (Figure 1.2), the Viking Formation was formed as storm deposits.

Turbidity currents were among the first models to be applied to the deposition of the Viking Formation (Beach, 1955, 1956, 1962; Roessingh, 1959). This interpretation was based upon the presence of chert-pebble beds of such widespread extent and unsorted character that they could not be explained by normal marine sedimentation. Bentonites provided evidence of volcanic activity associated with tectonic events in the Cordillera. The tectonic events were thought to be the cause of earthquakes which would trigger turbidity currents capable of moving large boulders and causing slump structures. DeWiel (1956) and Jones (1961) disagreed with the theory of turbidity currents citing the absence of graded bedding and the occurrence of extensive bioturbation as indicators of normal marine sedimentation.

Stelck (1958) proposed that the Viking sandstones comprised shoreline deposits and offshore bars developed along the borders of the Joli Fou sea. Jones (1961) stated that the Viking sandstones in part of southwestern Saskatchewan were beach deposits. Shelton (1973) used the presence of gradational lower and lateral contacts, a high width-thickness ratio (500:1), sedimentary structures and the presence of glauconite as evidence in favor of an offshore bar origin for some of the Viking sand bodies. Sedimentary structures and the shape of spontaneous potential logs led Tizzard and Lerbekmo (1975) to interpret the Viking sandbodies in the Suffield area as barrier bars.

The tidal current ridge concept was invoked by Evans (1970) to explain the deposition of the Viking Formation in the Dodsland-Hoosier area of southwestern Saskatchewan (Figure 1.2). He demonstrated that the sandstone units were stacked in an imbricate manner with the younger units displaced to the south. He concluded that they

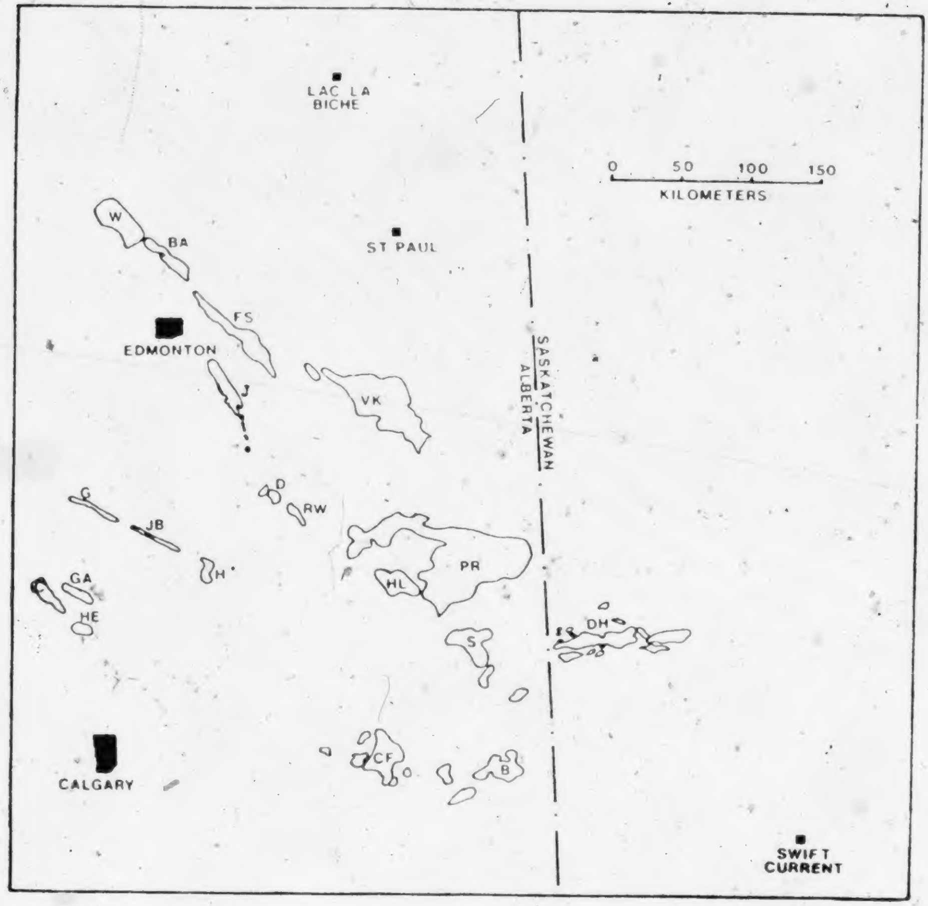
LAC LA BICHE
0 50 100 150
KILOMETERS
ST PAUL
W
BA
FS
EDMONTON
J
VK
SASKATCHEWAN
ALBERTA
D
RW
G
JB
H
GA
HE
PR
HL
S
DH
CF
B
CALGARY
SWIFT CURRENT

Figure 1.2. Location of some Viking Formation Oil and Gas Fields in Alberta and Saskatchewan. W = Westlock, FS = Fort Saskatchewan, VK = Viking-Kinsella, J = Joarcam, D = Donalda, RW = Red Willow, G = Gilby, JB = Joffre-Bentley, H = Huxley, C = Caroline, GA = Garrington, HE = Harmattan East, PR = Provost, HL = Harrison Lake, S = Sedalia, CF = Cessford, B = Blindloss, DH = Dodsland-Hoosier (Modified from Amajor, 1980).

were deposited by eastward-flowing tidal currents far from shore.

Simpson (1975) stated that the Viking nearshore area was characterized by shoreface and barrier island deposits while the shelf sediments were deposited by storm surges, augmented by tidal currents.

The concept of a deltaic depositional environment is a relatively new one for the Viking Formation. Amoco Petroleum (in Amajor, 1980, p.11) has mapped a delta in the Lower Viking near Jasper. Other deltas have not been reported in the Viking literature and these deposits may have been largely removed by erosion or reworked by other marine processes as the Lloydminster transgression occurred.

B. STRATIGRAPHY

During the late Albian the interior of western North America was inundated by transgressive seas advancing from the north and to a lesser degree from the south (Williams and Stelck, 1975). Sediments deposited into these seas comprise the Lower Colorado Group. The Viking Formation in central Alberta is a dominantly marine sandstone encased between two marine shales, the Joli Fou below and the Lloydminster above (Figure 1.3).

The Joli Fou Formation (Wickenden, 1949) is an extensive, dark grey, non-calcareous, fissile, marine shale with bentonitic horizons and minor lenses of fine-and medium-grained sandstone. These sediments represent the first marine deposits of the Colorado Sea. Figure 1.4 shows the configuration of the Colorado Sea at Joli Fou time. Early, onlap sediments are expressed as basal Colorado sandstones throughout the Western Interior. Biostratigraphic equivalents of the Joli Fou Formation are the Skull Creek Formation in Montana, the Thermopolis Formation in Wyoming and the Kiowa Shale in Colorado and Kansas (Figure 1.3). Biostratigraphic evidence within these formations suggests that the Boreal and Gulfian seas merged to form a continous seaway in the interior plains of western North America at Joli Fou time (Stelck, 1958, 1975; Williams and Stelck, 1975).

The contact between the Joli Fou Formation and the Viking Formation is somewhat controversial. It has been described as a slight disconformity (Evans, 1970), a regional disconformity, an angular uncomformity or a hiatus (Beaumont, 1984). In parts of

Wyoming, Montana and Colorado, non-marine conditions are reported to have existed at the top of the Skull Creek-Thermopolis Shale (Stapp, 1967; Scott, 1970; Reinert and Davies, 1976; Berg, 1976) (Figure 1.3). Elsewhere these contacts are comformable (Gopinath, 1978). Biostratigraphic work by Bullock(1950) and North and Caldwell (1975) indicate no significant faunal break between the Joli Fou and the Viking.

The name Viking was first used by Slipper (1918) to denote the gas bearing sands of the Viking-Kinsella Field of east-central Alberta (Figure 1.2). The Viking sandstone was initially classified as a member of the Colorado Group (Hunt, 1954; Reasoner and Hunt, 1954; Gammell, 1955) and later upgraded to formation status (Magditch, 1955; Stelck, 1958). Lithologically the Viking Formation varies from coarse to fine-grained salt-and-pepper sandstone to siltstone and silty shale (Norgaard, 1954). Several sand horizons of variable thickness may be present with intervening beds of dark grey to black shale (Amajor, 1980). The sandstones are primarily quartz with varying amounts of chert and glauconite. Regionally the Viking Formation thins to the east and northeast and "shales out" north and east of a line drawn from Lac La Biche, Alberta to Swift Current, Saskatchewan. Near Calgary it attains a maximum thickness of 200 feet (60 m), decreases to 100 feet (30 m) near Edmonton and to less than 40 feet (12 m) west of St. Paul (Figure 1.2). One interpretation of this pattern is that the interior sea regressed to the east and northeast and that the source area for the Viking sandstones lay to the west and the southwest. Figure 1.5 is an interpretation of the configuration of the Mowry Sea at Viking time.

In southern Alberta the Viking and Joli Fou Formations become indistinguishable and grade into the Bow Island Formation. To the west, in the Alberta foothills, the Joli Fou shale pinches out and the Bow Island (Viking) merges with the Mannville Group to form the Blairmore Group (Glaister, 1959; Rudkin, 1964). To the northeast and to the northwest, in the Alberta plains, sandstones in similar stratigraphic position as the Viking are known as the Pelican Formation and the Paddy Member of the Peace River Formation, respectively. The Viking Formation is the time-stratigraphic equivalent of the Silt Member of the Ashville Formation in southwestern Manitoba, the Muddy Sandstone of Wyoming and the Newcastle Sandstone of Montana and Northern Dakota (Figure 1.3)(Stelck, 1958, 1975; Glaister, 1959; Rudkin, 1964; Berg and Davies, 1968). Macro-and micro-faunal evidence

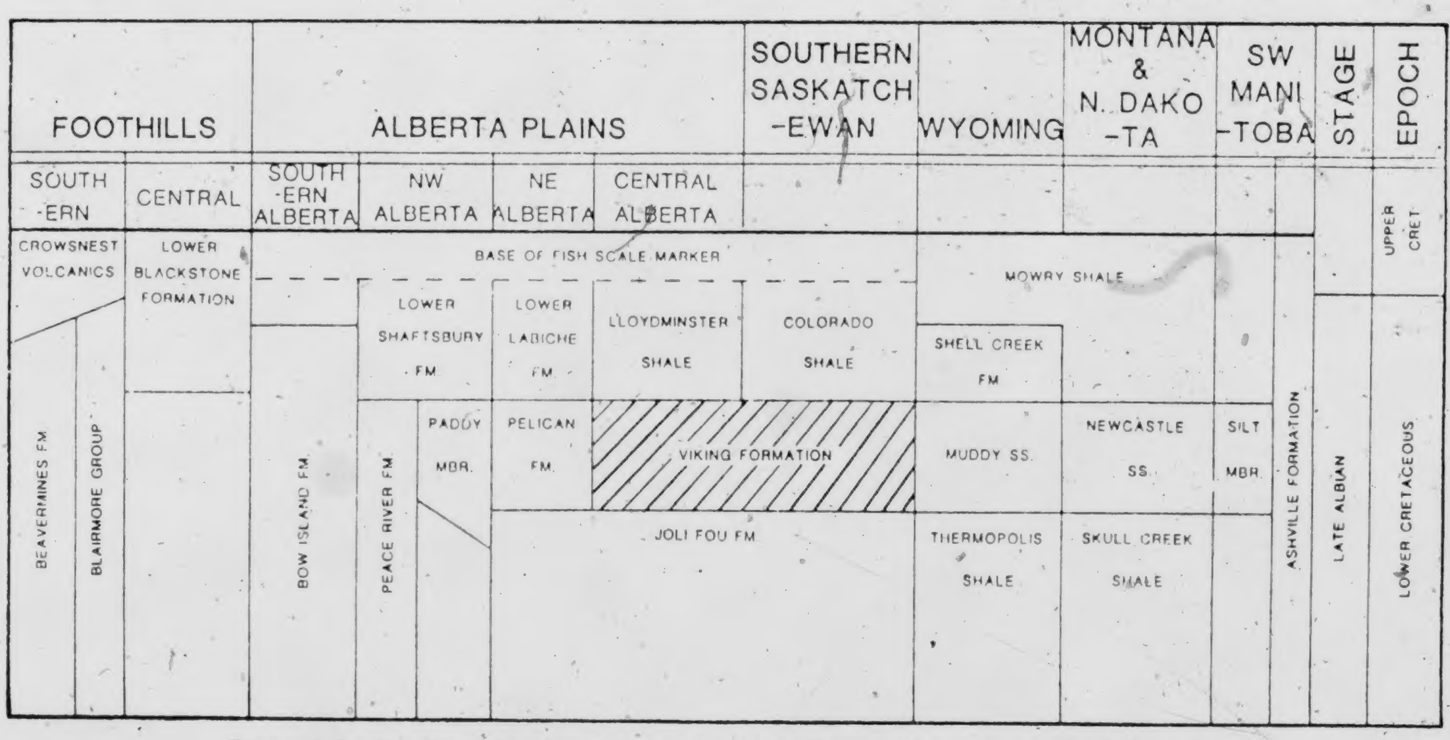
FOOTHILLS
ALBERTA PLAINS
SOUTHERN SASKATCH-EWAN
WYOMING
MONTANA & N. DAKO-TA
SW MANI-TOBA
STAGE
EPOCH
SOUTH-ERN
CENTRAL
SOUTH-ERN ALBERTA
NW ALBERTA
NE ALBERTA
CENTRAL ALBERTA
CROWSNEST VOLCANICS
LOWER BLACKSTONE FORMATION
BASE OF FISH SCALE MARKER
MOWRY SHALE
UPPER CRET
LOWER SHAFTSBURY FM
LOWER LABICHE FM
LLOYDMINSTER SHALE
COLORADO SHALE
SHELL CREEK FM
PADDY MBR.
PELICAN FM.
VIKING FORMATION
MUDDY SS.
NEWCASTLE SS.
SILT MBR.
BEAVERMINES FM
BLAIRMORE GROUP
BOW ISLAND FM
PEACE RIVER FM
JOLI FOU FM
THERMOPOLIS SHALE
SKULL CREEK SHALE
ASHVILLE FORMATION
LATE ALBIAN
LOWER CRETACEOUS

Figure 1.3. Stratigraphic correlation of the Viking Formation in Central Alberta and neighboring areas (Modified from Amajor, 1980).

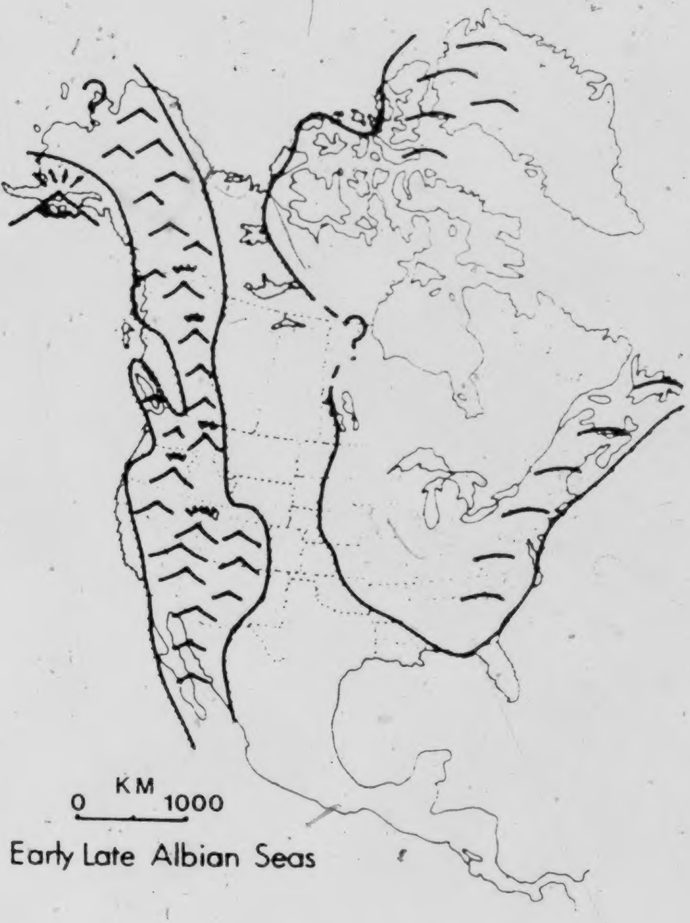
KM
0
1000
Early Late Albian Seas

Figure 1.4. Map showing the Colorado Sea at the time of Joli Fou deposition (Modified from Williams and Stelck, 1975).

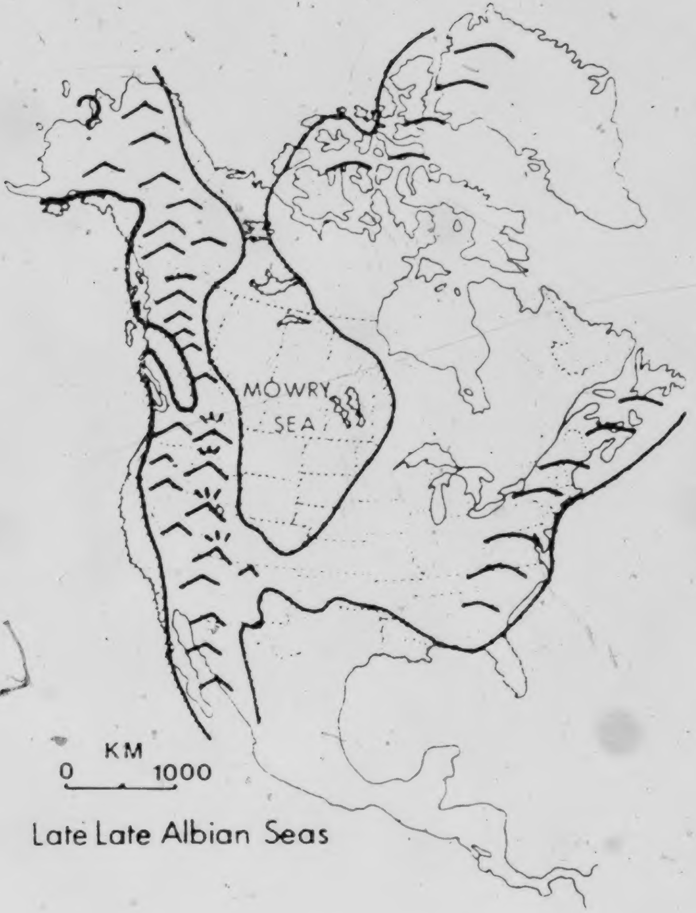
MOWRY
SEA
KM
0
1000
Late Late Albian Seas

Figure 1.5. Map showing the Mowry Sea near the time of Viking deposition (Modified from Williams and Stelck, 1975).

from the Lloydminster and Joli Fou Formations establishes the age of the Viking Formation at the mid-Late Albian stage of the Lower Cretaceous (Stelck, 1958, 1975). Potassium-Argon absolute ages obtained from biotite and sanidine in some Viking bentonites average 100±2 Ma. (Tizzard and Lerbekmo, 1975) and are in agreement with faunal evidence. Weimer (1983), using Potassium-Argon absolute ages from Obradovich and Cobban (1975), dated the Viking Formation at 97±1 Ma.

The top of the Viking Formation is placed at the top of a chert-pebble horizon or pebbly chert sandstone (Stelck, 1958; Glaister, 1959). Because of the presence of numerous chert-pebble beds near the top of the Viking Formation, this pick is difficult. The stratigraphic distribution of the chert-pebble beds appears to have been influenced by the topography of the seafloor and by the migration and stacking of sandbodies (Amajor, 1980; and this study).

The Viking Formation is conformably overlain by a dark marine shale known as the Lloydminster Shale (Tizzard and Lerbekmo, 1975)(Figure 1.3). This formation represents the second flooding of the Boreal Sea during Late Late Albian time. The biostratigraphic equivalents of the Lloydminster Formation include the Shell Creek and the Mowry Shales of Wyoming and Montana (Figure 1.3).

The Fish Scales Zone caps the Lloydminster Shale and terminates Lower Cretaceous sedimentation in a major portion of the Western Canadian Interior Plains. This unit is widely recognized in the subsurface of western Canada and is a useful datum for mapping of the Lower Cretaceous. The Base of Fish Scales is used as a datum in this study.

C. METHODS

Sedimentological studies were carried out by detailed core logging, definition of facies, correlation of facies from lithological and geophysical logs, and by compilations of isopach maps, computer generated block diagrams, cross-sections and fence diagrams. Mineralogical studies included detailed petrographic analysis, hydrometer analysis, X-ray diffraction (XRD), and scanning electron microscopy (SEM).

CORE DESCRIPTION

The cores were described with careful notation of grain size, sedimentary and biogenic structures and the nature of all lithologic contacts. Grain size was determined using a binocular microscope and grain size charts from Canstrat. The phi (0) scale was used as a standard measure of grain size (Figure 1.6). Photographs and sketches were made of representative sedimentary and biogenic structures and lithologic contacts. Sections were drawn using standard lithologic symbols (Figure 1.7). Problems in the logging of core occurred where portions were missing, removed, broken or scored by the core barrel (thus obliterating sedimentary structures).

FACIES DEFINITION

Facies were defined by grain size (Figure 1.6), and sedimentary and biogenic structures (Chapter 2). For the purpose of mapping thicknesses of the lithologies and interpreting facies, four major facies associations were defined for the Viking Formation in the Garrington area (Chapter 2). Facies associations are defined as genetically or environmentally related facies (Reading, 1978, p.5).

CORRELATION OF FACIES FROM LITHOLOGIC AND GEOPHYSICAL LOGS

Correlation between sedimentary facies and geophysical logs on a regional scale was done using lithologic, gamma-ray and shallow resistivity logs. Important picks on the logs include the Base of Fish Scales, the top of the Viking "B" horizon, the Viking "A" sandstones (often referred to as "grits") and a lower bentonite marker (Figure 1.8).

The Base of Fish Scales and the top of the Viking "B" horizon are easy picks on both the gamma-ray and shallow resistivity logs (Figure 1.8). The Viking "A" sandstones are usually quite evident on gamma-ray and resistivity logs; however, no method to accurately determine their thickness has been achieved. The lower bentonite marker is most easily picked from the shallow resistivity log (Cant, 1984) and may show up on the gamma-ray log as well (Figure 1.8). In addition to making specific picks of horizons from geophysical logs, it was found that the thicknesses of the conglomerate and coarse-grained sandstone facies association and the fine-grained sandstone association could be determined from geophysical logs with a high degree of correlation to lithologic descriptions. The thickness

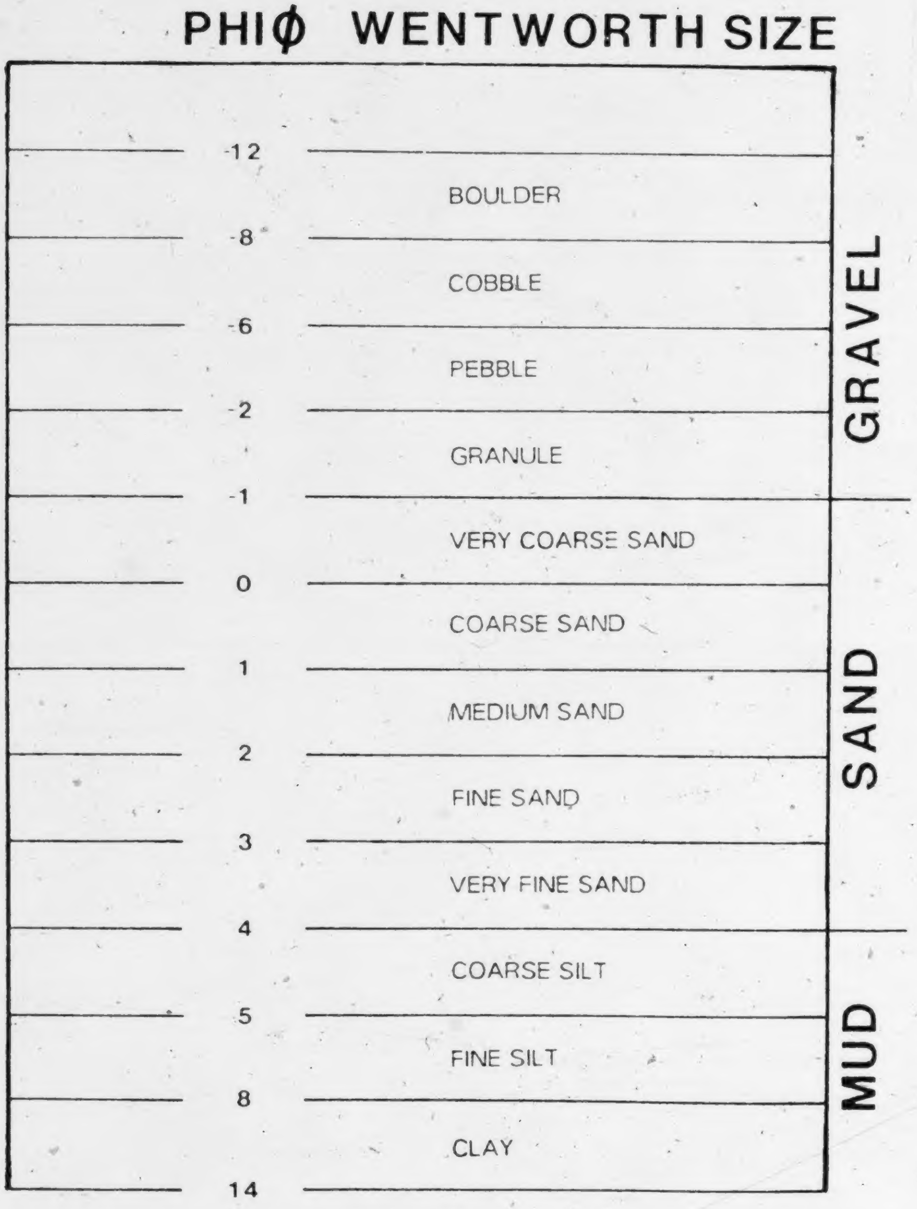
PHIϕ
WENTWORTH SIZE
-12
BOULDER
-8
COBBLE
-6
PEBBLE
-2
GRANULE
-1
VERY COARSE SAND
0
COARSE SAND
1
MEDIUM SAND
2
FINE SAND
3
VERY FINE SAND
4
COARSE SILT
5
FINE SILT
8
CLAY
14
GRAVEL
SAND
MUD

Figure 1.6. Grain size scheme for sediments. Modified from Folk (1968)

Figure 1.7. Lithologic Symbols and Sedimentary Structures

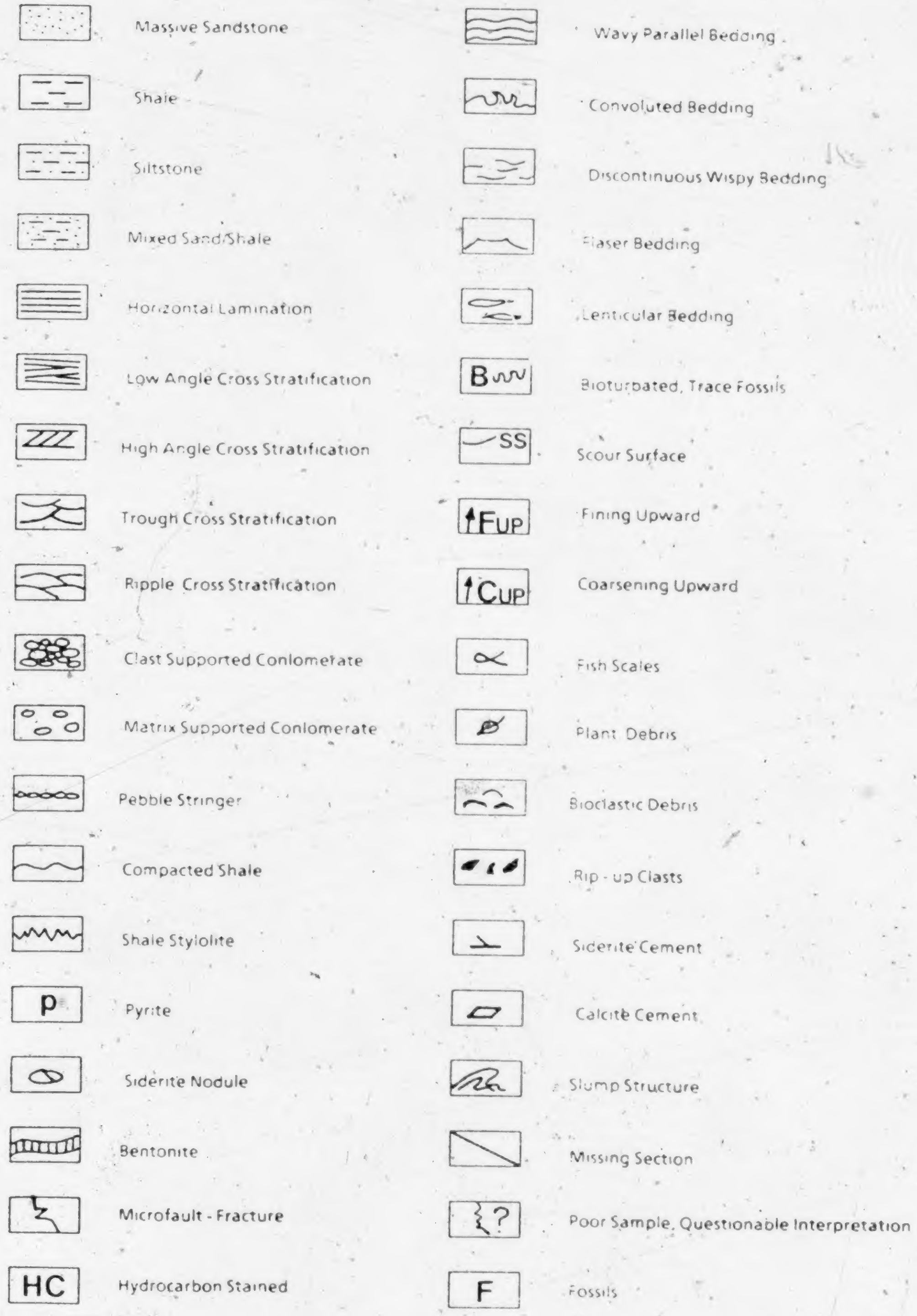
Massive Sandstone
Shale
Siltstone
Mixed Sand/Shale
Horizontal Lamination
Low Angle Cross Stratification
High Angle Cross Stratification
Trough Cross Stratification
Ripple Cross Stratification
Clast Supported Conlometate
Matrix Supported Conlomerate
Pebble Stringer
Compacted Shale
Shale Stylolite
p
Pyrite
Siderite Nodule
Bentonite
Microfault - Fracture
HC
Hydrocarbon Stained
Wavy Parallel Bedding
Convoluted Bedding
Discontinuous Wispy Bedding
Flaser Bedding
Lenticular Bedding
B
Bioturbated, Trace Fossils
SS
Scour Surface
FUP
Fining Upward
CUP
Coarsening Upward
Fish Scales
Plant Debris
Bioclastic Debris
Rip - up Clasts
Siderite Cement
Calcite Cement
Slump Structure
Missing Section
?
Poor Sample, Questionable Interpretation
F
Fossils

of the conglomerate and coarse-grained sandstone facies association was determined by taking the furthest ohm line crossed by the shallow resistivity deflection occurring in the Fish Scales Zone and marking that point onto the Viking "B" shallow resistivity response. Deflections to the right of that point indicate conglomerate (developed by M. Griffin, 1983, pers. comm.). This technique gave consistantly accurate results for the conglomerate and coarse-grained sandstone facies association, for unit thicknesses greater than 0.5 m (Figure 1.8). It was empirically determined in this study that the thickness of the fine-grained sandstone facies association could be ascertained by drawing a "sand line" onto the gamma-ray log at the 90 API units line with deflections to the left of this line giving the net thickness of the fine-grained sandstone facies association (with corrections made by subtracting the previously determined conglomerate and coarse-grained sandstone thickness)(Figure 1.8). The 90 API units line was chosen because it gave consistantly good correlation with the thicknesses of the sandstone seen in core. The interbedded and intermixed fine-grained sandstone and shale facies association comprises the remainder of the Viking Formation below the base of the fine-grained sandstone facies association.

ISOPACH MAPS, BLOCK DIAGRAMS AND FENCE DIAGRAMS

Isopach maps were drawn using thicknesses determined from geophysical and lithological logs. The maps include isopach maps of the Lloydminster Shale, three of the four facies associations defined for the Viking Formation and the Lloydminster shale, and the bentonite marker to the top of the Viking "B" horizon. An isopach map was not drawn for Facies Association 4 (Interbedded and intermixed fine-grained sandstone and shale) because these rocks are not important as reservoir rocks and are very seldom cored. A structure map with sea level used as datum was drawn to reveal the regional dip of the Viking "B" horizon. Depths for this map were taken from scout tickets and geophysical logs. Block diagrams were generated by a computer mapping program (Sampson, 1978), using the same thicknesses as the isopach maps. These plots give a three dimensional view of the distributions of the facies associations. A fence diagram encompasing the study area was drawn by hand using thicknesses picked from geophysical and lithologic logs. This diagram demonstrates the variation in the thicknesses within and among facies

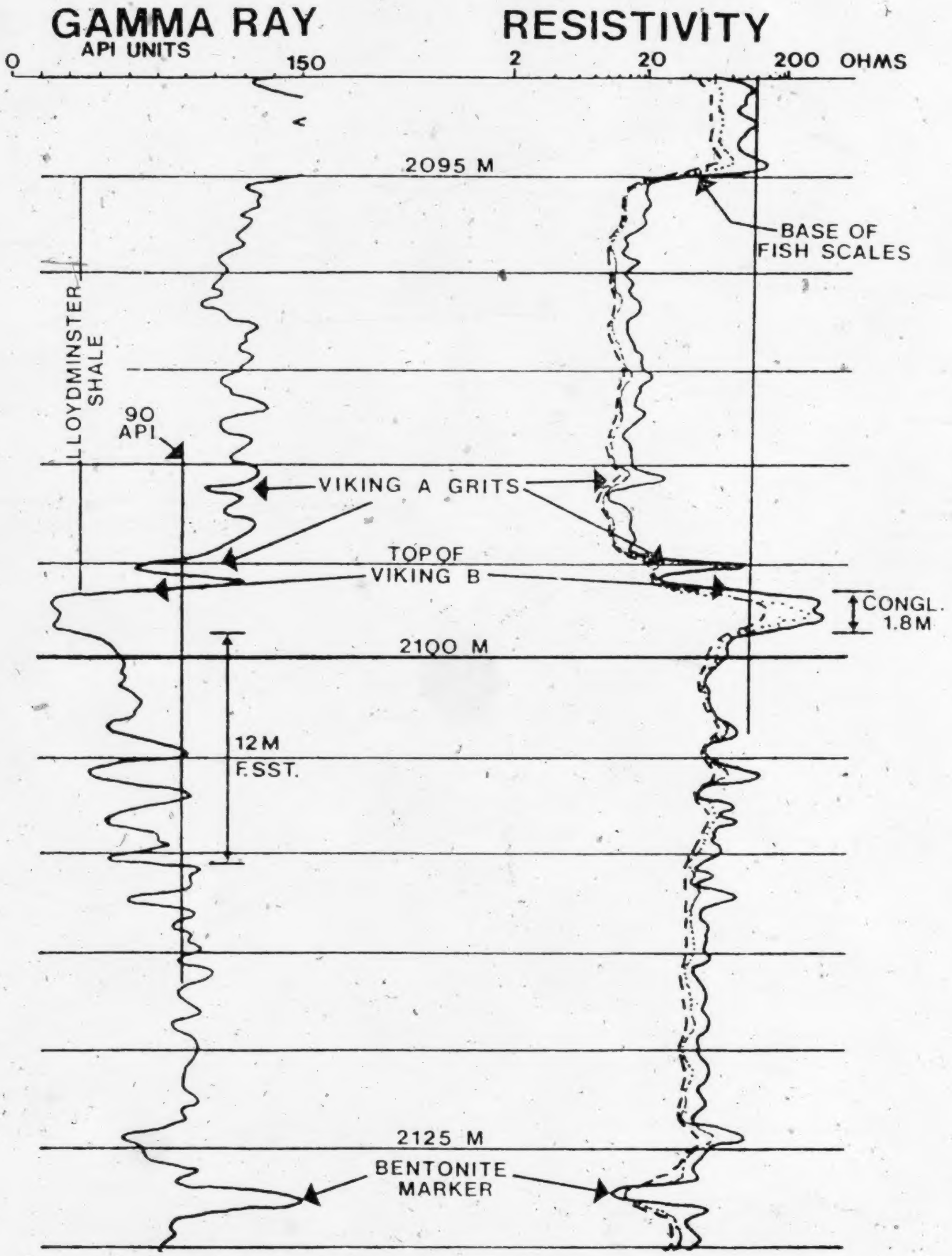

Figure 1.8. Typical geophysical log of the Viking Formation in the Garrington Oil Field showing important stratigraphic horizons and thicknesses as picked from gamma-ray and resistivity logs, from well 1-3-35-3W5.

associations and supplements the information contained in the isopach maps.

SAMPLING METHODS

Sampling for the purpose of mineralogical studies was performed during core logging in compliance with ERCB sampling regulations. The ERCB allows samples of 2.5 cm^3 per 30 cm length of core. Samples were selected from all lithologies, with special emphasis placed on the conglomerates, coarse-grained sandstones and the hydrocarbon stained, fine-grained sandstones. Careful sample selection ensured that adequate coverage occurred in all parts of the study area. Sample locations are shown on lithologs in Appendix A and in Figure 3.1.

PETROGRAPHIC ANALYSIS

The bulk mineralogy of the rocks was determined by petrographic analysis (thin sections). Counts of 500 points per slide were used to calculate the percentages of framework grains, cements and porosity. Percentages of minerals present were noted and the rocks were classified according to Folk's (1968) classification scheme. Sedimentary textures (roundness and sorting), and diagenetic textures (suture contacts, cements and solution features) were also recorded.

HYDROMETER ANALYSIS

The percentage of fine-grained material in each sandstone sample was determined by hydrometer analysis. Each sample was disaggregated, care being taken to preserve the original grain size distribution. Grains larger than 2 mm were removed by dry sieving. A minimum of 20 grams of material from each sample was soaked in 125 ml of a 4 % sodium hexametaphosphate solution for 8 hours to further disperse the particles. Ultrasonic disaggregation was used to ensure thorough dispersion of clay-sized particles. The solution was placed in a graduated cylinder and diluted with distilled water to a total of 1000 ml.

To initiate the analysis, each cylinder was agitated and the dispersed particles then allowed to settle. Hydrometer measurements were taken at 30 seconds, 1, 2, 5, 10, 15, and 30 minutes, and 1, 2, 4, 8, and 24 hours elapsed time for each sample and a control column containing only the distilled water - sodium hexametaphosphate solution. From these data, the following calculations were performed:

1. The hydrometer readings were corrected for variations in temperature and then subtracted from the control hydrometer readings (which takes into account the density of the sodium hexametaphosphate in solution);
2. The corrected hydrometer readings were converted to values of effective depth using calibrated tables;
3. The maximum particle diameter still in suspension at any time was calculated by multiplying its specific gravity (2.65) by the square root of effective depth divided by time. Particle diameter (d) is expressed in units of phi (phi = $-\log_2 d$);
4. The percentage of material still in suspension at any time was calculated by dividing the corrected hydrometer reading by the mass of the sample before sieving (e.g., the mass of any material greater than 2 mm in diameter is included here).

To calculate the percentage of the various size-fractions in each sample a log-probability graph was constructed using particle size (log scale) and percent sediment (probability scale). A smooth curve was drawn through the points. From this graph the percentages of material $<1\ \mu m$, $<2\ \mu m$, $<5\ \mu m$ and $<20\ \mu m$ were determined.

X-RAY DIFFRACTION ANALYSIS

Procedures used in this study follow those reported by Ignasiuk et al., (1983). X-ray diffraction analysis was used primarily to identify clay mineral species present in the samples.

Following hydrometer analysis, the solutions were redispersed and the requisite size-fractions separated at the appropriate time, according to Stoke's Law. To ensure complete separation, the dispersion and settling process was repeated three times for each size-fraction. The mineral matter thus separated was then heated for two days at 50°C to destroy any residual organic matter. Afterwards, the solutions were thoroughly washed with distilled water using a high speed centrifuge. The $< 2\ \mu m$ and $2-5\ \mu m$ materials were then divided into two portions and saturated with Ca^{2+} and K^{+}, respectively. The $5-20\ \mu m$ material was treated with Ca^{2+} only. After saturation, the various size-fractions were washed, freeze-dried and deposited by suction onto a ceramic disc.

X-ray diffractograms for the Ca and K discs were obtained under the following conditions:

1. Co K-alpha radiation, with monochromator;
2. 1 degree divergent slit; time constant = 2;
3. 1 degree two theta/minute at 600 mm/h;
4. 50 KV, 20mA.

The following X-ray charts were obtained for the <2 μm material:

1. Ca-disc at 54% relative humidity, 2-35 degrees two-theta;
2. Ca-glycolated, 2-35 degrees two-theta;
3. K-disc at 0% relative humidity, 2-35 degrees two-theta;
4. K-disc at 54% relative humidity, 2-22 degrees two-theta;
5. K-disc at 300°C, 2-22 degrees two-theta;
6. K-disc at 550°C, 2-22 degrees two-theta.

For the 2-5 μm and the 5-20 μm material, X-ray data was obtained only for the Ca-disc at 54% relative humidity. For all samples the appropriate conditions were maintained prior to, and throughout the X-ray analysis. This combination of procedures permits unambiguous identification of the various clay mineral families present in the samples.

The relative percentage of clay minerals in each size-fraction was determined using Scafe's method (personal communication). For the <2 μm material, the heights of (001) X-ray reflections were measured for smectite, illite and kaolinite using the Ca saturated, ethlyene-glycol treated XRD chart. The (002) or (003) X-ray reflections (d = 13 Å[1]) were used for mixed-layer clays present in the samples. For chlorite, the height of the (001) X-ray reflection was determined from the K-saturated, heat-treated (550°C) XRD pattern. For the 2-5 μm and the 5-20 μm size-fractions, all measurements were made using the Ca-saturated, 54% relative humidity XRD patterns. To account for the variation in crystallinity of each clay mineral family, form factors were assigned in the following manner:

1. Illite (10 Å) = 1.000;
2. Mixed-layer clay (13 Å) = height of 13 Å peak / 2 x height of 10 Å peak;
3. Smectite (17 Å) = height of 17 Å peak / 4 x height of 10 Å peak;

---

[1] 1 Å = 1 X 10^{-10} meters

4. Chlorite (14 Å) = height of 14 Å peak / 3 x height of 10 Å peak;
5. Kaolinite (7 Å) = height of 7 Å peak / 2.5 x height of 10 Å peak.

These form factors were summed and the relative percentages calculated for all the phases. For samples containing both chlorite and kaolinite, the kaolinite (001) and the chlorite (002) basal diffractions overlap. Hence, the amount of kaolinite may be overestimated. To correct for this discrepancy, percentage of chlorite (14 Å) is subtracted from the percentage of kaolinite (7 Å); all results are renormalized to 100% and rounded to the nearest 5%.

Values for relative abundances of quartz, feldspar and clay minerals (Tables 3.5, 3.6, & 3.7, Chapter 3) were determined graphically using standard mixtures of well crystallized kaolinite and quartz for calibration. Carbonate minerals were studied by thin section and identification was verified by bulk X-ray diffraction.

In the tables that follow, abundances are reported as:

1. > 35 % of phase present in sample = major (M),
2. 10-35 % of phase present in sample = moderate (mM),
3. 5-10 % of phase present in sample = minor (m),
4. 2-5 % of phase present in sample = minor to trace (mt),
5. < 2 % of phase present in sample = trace (t).

SCANNING ELECTRON MICROSCOPY

A small chip from the centre of each sample was mounted on a stub using conductive silver paint. The stubs were sputter-coated with 20 nm[2] of gold to ensure proper grounding during the analysis. The instrument used for the microscopy was the Cambridge Stereoscan S100. Its accelerating voltage was fixed at either 10 kV or 25 kV, depending upon the requirements of the analysis. A Kevex System 7000 energy dispersive X-ray Analyzer, coupled to the SEM, was used to obtain qualitative chemical analyses of the pore-lining and pore-filling minerals.

---

[2] 1 nm = 1 X 10^{-9} meters

GAS-OIL RATIO TRENDS

Gas-oil ratio (GOR) trends were studied by plotting GOR versus time and applying statistical analysis to the results. Simple linear regressions, using BMDP (University of California, Los Angeles, Department of Biomathematics Programs) statistical packages, were used to fit lines of correlation to the GOR plots and to calculate correlation coefficients. These plots were then used to determine the trend of the gas-oil ratio within the field.

LIST OF ABBREVIATIONS

Tables, plates and figures presented throughout the report employ the following abbreviations:

ROCK TYPES

Congl. = Conglomerate
C. Sst. = Coarse-Grained Sandstone
F. Sst. = Fine-Grained Sandstone

BULK MINERALOGY FROM THIN SECTION

Ch = Chert
Q = Quartz
F = Feldspar
RF = Rock Fragments
Ca = Carbonate (mainly dolomite and ankerite, minor calcite)
S = Siderite
C = Clay Minerals
NA = Not Available

MINERALOGY FROM X-RAY DIFFRACTION, THIN SECTION, AND SCANNING ELECTRON MICROSCOPY

μm = Micrometre (1 X 10^{-6} metres)
Q = Quartz
F = Feldspar
C = Clay Minerals
IS = Illite-Smectite
SM = Smectite
CL = Chlorite
I = Illite
K = Kaolinite
AF = Authigenic Feldspar
AQ = Authigenic Quartz

S = Siderite

Ca = Carbonate (mainly dolomite and ankerite, minor calcite)

ND = Not determined

TERMINOLOGY

In Chapter 2 the following terms are used to describe sedimentary bedforms:

Sand Waves are low; straight-crested features with well defined avalanche faces. The ratio of height to spacing is much lower than for either dunes or ripples. Spacing may be variable (12-1000 metres). Stoss sides are either flat and featureless or may be covered with low and rapidly migrating ripple-like bedforms (Harms et al., 1975; Amos and King, 1984).

Dunes or Megaripples are downcurrent migrating bedforms with triangular profiles similar to ripples, with gently sloping stoss sides and steep lee slopes which usually are avalanche faces. Height to spacing ratio is on the order of 1:10. Spacing is from 1 to 10 metres. Two-dimensional megaripples are straight, sharp-crested forms with a well developed slip face. Three-dimensional megaripples are highly irregular forms with sinuous to lunate crests and spurs developed in the downcurrent direction. Three-dimensional megaripples have steep profiles and are higher, and have shorter wavelengths, than two-dimensional megaripples (Harms et al., 1975; Amos and King, 1984).

Sand Ridges are mesorelief forms consisting of sand, gravel or silt; they are widespread on continental shelves of the world's oceans. In many locations, they occur in groups forming a rhythmic succession of forms and occupy hundreds of square kilometres of the seafloor. Sand ridges are composite, flow parallel, linear accumulations of sediment, formed by the superposition of sand wave or megaripple fields. They may range in height (thickness) from 1 to 30 metres, and in width from 200 to 8000 metres. They can be tens of kilometres long (Amos and King, 1984).

Shoal-Retreat Massifs are low, broad, shelf-transverse sandbodies which mark the retreat paths of coastal depocenters associated with littoral drift convergences. There are two types of shoal-retreat massifs: (1) estuarine shoal-retreat massifs and (2) cape shoal-retreat massifs. The shoal-retreat massifs are tens of kilometres long and tens of kilometres wide (Swift, 1974).

II. SEDIMENTOLOGY AND DEPOSITIONAL ENVIRONMENT

This chapter presents a detailed examination of the sedimentology and depositional environment of the Viking Formation at Garrington. Lithofacies were defined based on grain-size and biogenic and sedimentary structures. The lithofacies were then grouped into four facies associations. The depositional pattern and facies distribution were mapped based upon these facies associations. A fence diagram (Figure 2.11, in pocket) and numerous block diagrams and isopachs maps show the facies distribution, geometry and depositional pattern throughout the study area. In addition, sediment dispersal mechanisms are discussed and the Viking Formation is briefly compared with other Cretaceous sandbodies.

A. DEPOSITIONAL ENVIRONMENTS AND SEDIMENT DISPERSAL MECHANISMS

In recent years there has been an increasing interest in the study of shallow marine depositional environments, both modern and ancient. Many workers have concentrated their efforts on end-member processes active in the shallow marine, such as storms (Walker, 1979, 1984; Cant, 1980), tides (Off, 1963; Houbolt, 1968; Stride, 1982), oceanic currents (Flemming, 1978, 1980) and sediment gravity flows (Walker, 1979; Hampton, 1972, Middleton and Hampton, 1976; Hein, 1979). Even though there has been much activity there has been no facies model developed that can adequately explain the diversity of sedimentary deposits found in the shallow marine environment. The difficulty in developing a facies model to fully explain the various types of deposits found in the shallow marine environment is partially due to poor understanding of how the various end-member processes interact and partially due to the vast array of different types of deposits found in shallow marine environments. Johnson (1978) gives an excellent overview of the various processes active in the shallow marine environment with comparisons of ancient and recent deposits. Walker (1984) also provides an excellent summary of shelf processes from the viewpoint of the oceanographer, the marine geologist and the land-based geologist. This section will discuss the four main types of currents which operate on modern continental shelves. The section following this will review ancient deposits from the Cretaceous of Western North America and their proposed depositional mechanisms.

Four main types of currents operate on modern continental shelves: oceanic, tidal, meteorological currents and sediment-gravity flows. Oceanic currents result from the differential temperature between high and low latitudes and the subsequent flow of heat from the equator to the polar regions. Oceanic currents have a shallow component driven by global wind circulation patterns and a deep thermohaline component driven by temperature and salinity variations in the stratified ocean waters. Major ocean currents are situated on the oceanward side of the shelf but there is active interchange between oceanic and shelf waters due to large eddies spinning off the main current and onto the outer continental shelf and large scale meandering of currents (Johnson, 1978). Flemming (1978, 1980) studied the Agulhas Boundary Current off the east coast of South Africa and found that this current was responsible for the transportation of large amounts of sand from the inner shelf to the outer shelf. He postulated that the current may go through periods of lateral migration where the current shifts to a position closer to the shelf thereby shifting its shoreward margin onto the inner shelf clastic wedge where it can entrain sediment and carry it to the outer shelf. Flemming (1980) found that the Agulhas Current was capable of moving dune fields in water depths of up to 90 metres. A similar boundary current was noted by Field and Roy (1984) operating on the Australian continental shelf. Johnson (1978) suggests that there is a seasonal variation in ocean currents. The seasonally fluctuating California and Davidson currents migrate onto the shelf during the winter and move offshore during the summer (Johnson, 1978).

Tidal currents are produced by the attraction of the moon and the sun on the surface waters of the earth. Tidal currents in shelf seas result from a tidal wave propagating on to the shelf from the adjacent ocean. Tides may be amplified due to decreasing water depth and width, or resonance, where the oscillation period of the basin corresponds to that of the tide producing force. Local amplification may occur due to flow confinement by topographic features, such as depressions or lows, on the shelf. Net sand transport by tidal currents is caused by tidal current asymmetry. Tidal current-dominated shelves have been studied by many workers, including Off (1963), Houbolt (1968), Caston (1972) and Stride (1982). Off (1963) noted that tidal current ridges often occur as a rhythmic series of ridges oriented parallel with the tidal current and that sand waves occurring on the ridges were oriented perpendicular to the tidal currents. Caston (1972) found that the Norfolk sand banks in the southern North Sea accreted due to the presence of sand streams moving in opposing directions on either side of the sand banks. The asymmetry of the sand bank is a consequence of the flow asymmetry of these sand streams. The size of the sand banks was highly variable; 12 to 52 km long, 0.7 to 2.2 km wide and 24.4 to 42.7 m high. Stride (1982) interpreted tidal environments by herringbone cross-stratification, reactivation surfaces, interference ripples, double-crested ripples, wavy bedding, channels, burrows and normally graded sequences. Tidal currents rework sand so effectively, that a compositionally mature sediment is often produced, commonly with tabular bed geometry, many large sets of cross-stratification and conspicuous horizons of "lag" pebbles.

Meteorological currents are formed where wave- and wind-induced processes are the dominant source of energy on the open shelf. These currents are mainly due to direct wind stress and large fluctuations in barometric pressure. Wind-driven currents are the direct result of wind-shear stress acting on the water surface, with the resulting currents deepening with time as energy is transferred through the water column by turbulent mixing. Surface currents driven by wind stress deviate from the wind direction in response to Coriolis effect, while at depth this deviation is intensified due to Ekman Spiral effect. Storm surges are the result of a large reduction in barometric pressure and / or high wind stress, which produce an abnormally high water level at the coastline followed by a drastic lowering of water level. The seaward-returning ebb current transports nearshore sediment out onto the shelf (Walker, 1979, 1984).

In most of the present shelf areas, especially those associated with pericontinental seas, wind- and wave-induced currents are the most important currents. These areas commonly have a small tidal range and low tidal current velocities. Meteorological factors dominate the hydraulic regime characterised by a strong seasonal aspect. The east coast of the United States is the best documented area of intense storm activity (Swift et al., 1973; Swift, 1974, 1975; Stubblefield and Swift, 1976).

Swift et al. (1973) found in their study of the ridge-and-swale topography of the east coast of the United States that the sand ridges were second order elements superimposed on larger first order elements known as "shoal retreat massifs". The sand ridges occur 2 to 4 km apart, are up to 10 metres thick and extend for tens of kilometres with side slopes of a few degrees or less. The crestlines were observed to climb obliquely across the shelf to the southwest and converge with the shoreline at an angle of 22° (parallel or subparallel to shoreline). Swift et al. (1973) concluded that the ridge topography is primarily of dynamic, nearshore, submarine origin, rather than a relict littoral subaerial feature.

Stubblefield and Swift (1976) suggest that progressive evolution of sand ridge topographies are in response to a changing hydraulic regime associated with transgressive seas. Sustained high velocity currents occur during winter storms when winds from the northeast transport surface water to the coast and result in a coastal set-up of 0.4 to 0.6 m. The resulting hydraulic head induces a southeast return flow near the bottom of the water column (Swift et al., 1973). When this occurs a shelf wide, southward, geostrophic (contour parallel) flow is generated. During major storms, large scale secondary helical flow circulation patterns are developed (Stubblefield and Swift, 1976). Currents descend into the swales, scour the bottom and shift sand up onto the ridge flanks and onto the crestal region in the form of sand waves (Stubblefield and Swift, 1976). The coarsening-upward sequences seen on these ridges are a result of sorting by these helical flows and wave winnowing during periods of waning storm activity.

Sediment-gravity flows occur as the result of mass movement of unstable sediments down a slope due to the force of gravity. Masses involved in slides or slumps may behave in various ways after failure, ranging from slow creeping movements, to rapid debris flows, or fluidized sediment flows and dilute turbidity currents (Karlsrud and Edgers, 1982). Hampton (1972) proved in his experiments that there is a transition from debris flows to turbidity currents. Prior and Coleman (1982) have documented active slides and flows on the underconsolidated marine sediments on the slope of the Mississippi prodelta front. They found that instability could occur on very low slopes, generally less than 1°. On the Mississippi prodelta slope the bottom gradient is 0.7° to 1.5° in water depths of from 10 to 80 m (Prior and Coleman, 1982).

Although the slope angles are small, they do constitute gravitational stresses on the sediment, but are unlikely sufficient to be the sole cause of failure. Pore pressures greater than hydrostatic may be present for a number of reasons including underconsolidation due to rapid sedimentation, generation of biogenic gas within the sediments, artesian gas or water pressures in deeper formations, and pore pressures generated by storm wave loading or earthquakes (Prior and Coleman, 1982; Karlsrud and Edgers, 1982; Koning, 1982). In some shelf environments, especially those seaward or downdrift of large river discharges, sediment transportation and deposition by subaqueous mass movement accounts for a large portion of the shelf deposits (Prior and Coleman, 1982).

Fisher (1971) documented numerous debris flows exhibiting inverse grading. The Wrightwood debris flow of 1941 showed a strongly aligned fabric occurring in association with inverse grading. The Miocene, deep water, Capistrano Formation at San Clemente State Park exhibits inverse grading in poorly sorted coarse-grained marine deposits within turbidite sequences (Fisher, 1971). Davies and Walker (1974), in their work on the deep water, Cap Enrage' Formation in Quebec, developed two models to explain the deposition of these coarse clastic rocks. The inverse-to-normally graded model explained the deposition of conglomerates from highly turbulent flows with clasts supported above the bed by fluid turbulence or dispersive pressure, or both. Graded-stratified portions of the deposit were interpreted in terms of deposition from suspension but with bedload movement becoming increasingly important upwards. Hein (1982) and Hein and Walker (1981), in later studies on the Cap Enrage' Formation, also interpreted the presence of inversely graded beds as the result of dispersive pressures within basal parts of large-scale turbidity currents.

B. CRETACEOUS ANALOGS

During much of the Cretaceous Period the Western Interior of North America was covered by epicontinental seas (Williams and Stelck, 1975). A broad basin in the interior of North America was formed with the Cordilleran fold belt to the west and the Paleozoic platform and Precambrian Shield to the east (Dickinson, 1971; Eisbacher, 1977; Swift and Rice, 1984). Figure 2.1 is a diagram of the tectonic assemblage of western Canada. Terrane I, consisting of the intermontane belt and portions of the omineca crystalline belt and the coast plutonic complex, joined to the western margin of North America during Jurassic time (Monger _et al_., 1982). Shallow marine deposits of the Fernie-Kootenay Transition were derived from mountains formed by this accretion (Monger _et al_., 1982; Hamblin and Walker, 1979). Terrane II, consisting of the insular belt and part of the coast plutonic complex, joined to terrane I and western North America during Cretaceous time (Monger et al., 1982). A large foreland basin which formed to the east of the accretion terranes was the locus for the deposition of sediments derived from the mountains formed during Cretaceous time.

Many sandbodies deposited into this foreland basin are important hydrocarbon reservoirs at the present time. Sandbodies such as the Shannon Sandstone (Spearing, 1976; Seeling, 1978; Shurr, 1984), the Sussex Sandstone (Berg, 1976; Brenner, 1978; Hobson et al., 1982) and the Cardium Formation (Michaelis, 1957; Berven, 1966; Swagor et al., 1976; Wright and Walker, 1981; Griffith, 1981) have been studied extensively in recent years. All of these sandbodies show coarsening-upward sequences very similar to the Viking Formation at Garrington (Figure 2.2).

Spearing (1976) interpreted the Shannon Sandstone at Salt Creek, Wyoming, as a mid-to-outer shelf sand and silt blanket that received sediment episodically by storm-generated currents flowing to the southwest in that area. Seeling (1978) agreed with Spearing, and interpreted the Shannon Sandstone as a prograding sand blanket containing sand ridges. He described the sand ridge at Heldt Draw, Wyoming as a vertical coarsening-upward sequence comprised of (1) a thin bedded shale / sand facies with horizontal and ripple lamination and extensive bioturbation, grading upward into (2) cross-bedded very-fine to fine-grained sandstone, which in turn is capped by (3) medium and coarse-grained sandstone with shale and siderite rip-up clasts. Sand ridges were created by the convergence of strong helical flows (Seeling, 1978) similar to those described by Stubblefield and Swift (1976) for sand ridges off the east coast United States. The sand ridges were asymmetric with a steeper seaward slope (Seeling, 1978).

Berg (1976) interpreted the coarsening-upward sequence in the Sussex Sandstone at House Creek Field, Wyoming, as a prograding sand-sheet that was transported southward by low energy currents. This overall sequence consisted of (1) shales with rippled sand lenses of fine-grained sandstone grading into (2) fine-grained rippled sandstones with thin shale laminae which then pass into (3) fine-grained to medium grained cross-bedded sandstones capped by (4) medium and coarse-grained pebbly sandstones and (5) a bioturbated mudstone with scattered chert pebbles. Berg (1976) suggests that sand invaded a quiet water, muddy, reducing environment, not suited for colonization by

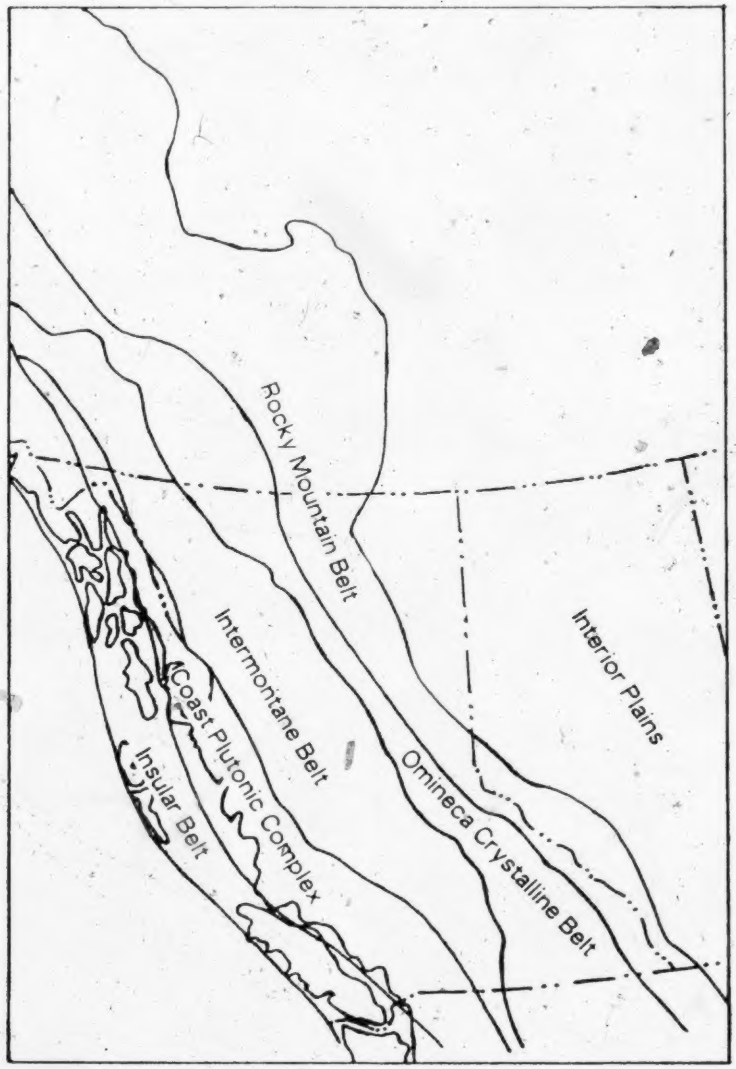
Rocky Mountain Belt
Interior Plains
Intermontane Belt
Coast Plutonic Complex
Insular Belt
Omineca Crystalline Belt

Figure 2.1. Distribution of allochthonous terranes in the Canadian cordillera. Terrane I consists of the intermontane belt and parts of the omineca crystalline belt and the coast plutonic complex. Terrane I accreted to the ancient margin of North America during Jurassic time. Terrane II consists of the insular belt and most of the coast plutonic complex. Terrane II accreted to terrane I (and North America) during Cretaceous time (after Monger et al., 1982).

benthonic fauna. Sand was introduced to the basin by currents of increasing velocity that flowed southward across the shelf, and concentrated the sands at the base of a prograding slope. Hobson et al. (1982) interpreted the Sussex Sandstone at House Creek as a residual sand sheet that was left stranded on the shelf by a transgressive sea. The sand sheet was then further reworked and molded into broad elongate offshore bars by storm-related and other marine currents during marine regressive phases.

The Cardium Formation of Alberta is interpreted to have accumulated in a shoaling, shallow, marine environment (Berven, 1966; Sinha, 1970; Swagor et al., 1976; Wright and Walker, 1981). Wright and Walker (1981) mapped five coarsening-upward sequences at Seebe, Alberta. The sequences begin with bioturbated mudstones and coarsen upwards into sandstones with thin conglomeratic veneers at the top (Figure 2.2). In one sequence, the conglomerate is up to 20 centimetres thick and has been molded into gravel waves with wavelenghts of 1 metres and amplitudes of a few centimetres. Wright and Walker (1981) interpreted the gravel waves as storm emplaced and molded into waves by storm-swell below fair-weather wave base. The sandstone sequences mapped by Wright and Walker (1981) are characterized by hummocky cross-stratification and were interpreted as deposits below fair-weather wave base. No angle-of-repose cross-bedding or other evidence of reworking by fair-weather currents were observed.

The Cardium sandstones in the Alberta foothills and subcrop on the plains frequently form long, narrow, thin deposits parallel to the inferred northwest-southeast striking paleoshoreline. In the Crossfield-Garrington area linear, offshore bars occur from 1.6 to 4.0 km wide, 100 to 130 km long, and up to about 7 m thick (Wright and Walker, 1981). Conglomerates tend to occur on the seaward (northeast) side of the sand bodies (Michaelis, 1957; Swagor et al., 1976; Griffith, 1981). A shelf-break was inferred as a locus for the deposition of conglomerates (Roessingh, 1957; Patterson and Arneson, 1957; Swagor et al., 1976; Griffith, 1981) brought to the shelf edge by storm currents (Swagor et al., 1976; Wright and Walker, 1981) or tidal currents (Michaelis, 1957; Berven, 1966; Michaelis and Dixon, 1969). Figure 2.2 shows a comparison of coarsening-upward sequences from the Shannon Sandstone, the Cardium Formation and the Viking Formation at Garrington. It can be seen that the coarsening-upward sequences in all three formations are very similar. The cycle starts with silty shales and grades to

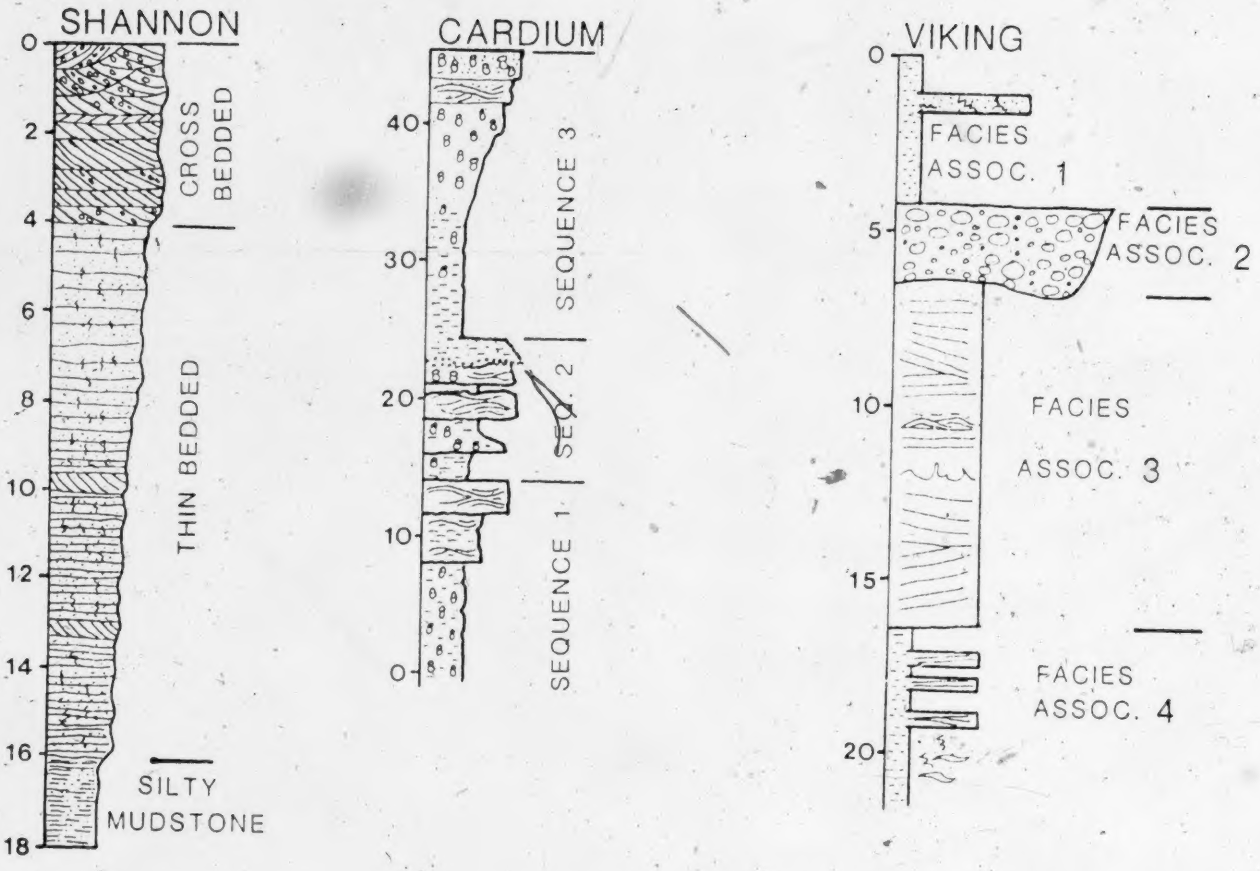
SHANNON
CARDIUM
VIKING
0
2
4
6
8
10
12
14
16
18
CROSS BEDDED
THIN BEDDED
SILTY MUDSTONE
0
10
20
30
40
SEQUENCE 3
SEQ. 2
SEQUENCE 1
0
5
10
15
20
FACIES ASSOC. 1
FACIES ASSOC. 2
FACIES ASSOC. 3
FACIES ASSOC. 4

Figure 2.2. Diagram comparing coarsening upward sequences in the Shannon Sandstone, the Cardium Formation and the Viking Formation. (Modified from Harms et. al., 1975, and Wright and Walker, 1981)

sandstone and shale and finally to sandstone. The top of the cycle may be capped by conglomerate.

C. LITHOFACIES DESCRIPTION

The facies described below are summarized in Table 2.1.

Facies 1. The *Interbedded Shale/Fine-Grained Sandstone Facies* has two end-members. Subfacies 1A: fine-grained sandstones (average grain size: 2 to 3 ϕ) with argillaceous laminations, in which bedding is horizontal to wavy and bioturbation is minor (Figure 2.3A), and Subfacies 1B: shale beds (1 to 2 cm thick) with fine-grained sandstone lenses, showing flaser and lenticular bedding. The shales are black and have varying amounts of coaly or pyritized plant material. Facies 1 units average 10 cm thick (range: a few centimetres to 60 cm).

Facies 2. *Fine-Grained Sandstone* (average grain size: 2 ϕ) constitutes the bulk of the cores from Garrington. This facies is divided into the following seven subfacies;

Subfacies 2A. The *Structureless Fine-Grained Sandstone* is essentially massive with no visible sedimentary structures (Figure 2.3B). Hydrocarbon stained and sideritized zones occur within this subfacies. Subfacies 2A units average 60 cm thick (range: 15 cm to 1.6 m) and comprise 5-10 % of Facies 2.

Subfacies 2B.*Parallel-Stratified Fine-Grained Sandstones* have stratification varying from flat to low-angle wavy, with dip angles of the laminae ranging from 0° to 5° (Figure 2.3C). Siderite nodules and sideritized zones occur in many cores. Hydrocarbon staining may also be present. Subfacies 2B units average 35 cm thick (range: 4 to 96 cm) and comprise 60-65 % of Facies 2.

Subfacies 2C. The *Low-angle (< 10°) Cross-Bedded Fine-Grained Sandstone* is relatively common and occurs in association with Subfacies 2B (Figure 2.3D). Average thickness of Facies 2C is 40 cm (range: 9 to 100 cm). This subfacies represents 20-25 % of Facies 2.

Subfacies 2D and 2E. Both *Trough Cross-stratified* and *Ripple Cross-stratified Fine-Grained Sandstone* commonly occur in the sections and usually overlie, parallel-laminated fine-grained sandstones (Figures 2.4A and 2.4B). Individual ripple formsets or (small scale festoon) trough sets are usually 3 to 5 cm thick (range: 1 to 25 cm) and represent 3-5 % of Facies 2.

Subfacies 2F. *Bioturbated Fine-Grained Sandstone* is fairly common in the sections (Figure 2.4C). Beds are generally on the order of 5 to 10 cm thick with well preserved, medium size (1 cm diameter) burrows. Subfacies 2F represents about 1 % of Facies 2.

Subfacies 2G. *High-angle (>10°) Cross-bedded Fine-Grained Sandstone* occurs primarily where high-angle scour surfaces truncate underlying beds (Figure 2.4D). Usually, the dip decreases quickly to low-angle (<10°) over a thickness interval of 5 or 10 cm. Subfacies 2G represents 1-2 % of Facies 2.

Subfacies 2H. *Convolute Cross-bedded Fine-Grained Sandstone* is relatively rare within the study area. Small scale convolute structures include 2-3 cm thick beds with distorted laminae. Larger scale structures include sections 50 to 60 cm thick with overturned and folded laminations and may be associated with underlying ball-and-pillow-structures or slump deposits. Dish structures are also associated with some convoluted beds.

Conglomerate facies have been defined using the following criteria. A conglomerate has greater than 25 % of its components > 2 mm in diameter. Pebbly sandstones are units with less than 25 % of their components > 2 mm, and the bulk of the framework grains being sand size. Matrix-supported conglomerates have <30% clast contact; clast-supported conglomerates have >30% clast contact. The matrix is sand-size or, rarely, clay-size material.

Facies 3. *Ungraded Matrix-supported Conglomerate* is a common facies within dominantly conglomeratic horizons. This facies is commonly a structureless, poorly sorted, chert-pebble conglomerate with a medium to coarse-grained sandstone matrix (average grain size: 0 to 2 0) (Subfacies 3A, Figure 2.5A, Table 2.1). The matrix may be normally graded in beds near the top of the Viking section where there is a gradational contact between the Viking conglomerate and the Lower Colorado Shales. Less commonly, parallel stratified beds, defined by laminae with flat or low-angle dips (Subfacies 3B, Table 2.1) and rare high-angle cross-bedded units (Subfacies 3C, Figure 2.5B, Table 2.1) also occur. Clast-supported pebble stringers with good porosity and hydrocarbon staining are interbedded with the matrix-supported conglomerates. The average thickness of Facies 3 is 25 cm (range: 2 cm to 130 m).

Facies 4. *Ungraded Clast-supported Conglomerate* is a common facies. It is usually a structureless, poorly sorted, chert-pebble conglomerate (Subfacies 4A, Figure 2.5C, Table 1). Clast-supported conglomerates may be horizontally stratified, show low-angle dipping laminae, some of which are apparently bimodal. (Subfacies 4B, Figure 2.5D, Table 2.1). High angle cross-lamination is less common (Figure 2.5E). Cross-stratification may be planar-tabular or trough cross-stratification although this is difficult to ascertain due to the small diameter of the cores.

Hydrocarbon staining occurs on the cores although this facies is less porous than Facies 3. Sutured contacts between clasts are common. Bed thickness averages 15 cm (range: 2 to 135 cm).

Facies 5. *Graded Matrix-supported Conglomerate* is a common facies. Both normally and inversely graded beds occur (Figures 2.6A,B,C,). Clast size varies from 3 mm to 6 cm clasts. Sorting is generally poor. The average thickness of beds in facies 5 is 30 cm (range: 10 to 70 cm).

Facies 6. *Graded Clast-supported Conglomerate* is not very common in conglomerate sections. An individual normally graded bed was only recorded in one place where it was 24 cm thick (Figure 2.6D). Inversely graded beds (Facies 6B) are also uncommon and average 15 cm in thickness (range 5-25 cm) (Figure 2.6E).

Facies 7. *Mixed Conglomerate / Shale* is common at the top of the section (in contact with the Lloydminster Shale, Subfacies 10A in Table 2.1) and is less common at the base of the section (in contact with bioturbated silty shales, Subfacies 10C in Table 2.1). This mixed lithology is usually structureless with pebbles floating in shale (Figures 2.7A,B). In some places, however, conglomerate may occur as burrow infill or detached pebbly load casts (Figure 2.7C). This mixed conglomerate / shale facies is usually about 10 cm thick and has no apparent porosity.

Facies 8. *Mixed Sandstone / Shale* facies is characterized by a mixing of these lithologies by loading or burrowing processes. Where discernable, internal load or biogenic structures are characteristic. Load structures are commonly well defined ball-and-pillow or flame structures (Figure 2.7F). Bioturbation is indicated by the presence of well preserved burrows or mottled textures (Figures 2.7D and 2.7E). Thick sections of intensively mixed fine-grained sandstone and shale occur in the lower portion of the Viking Formation in certain fields, such as Caroline and Garrington. The amount of bioturbation and amount of shale increase downsection within the Viking Formation. Mixed fine-grained sandstone / shale units up to 1 metre thick locally occur within dominantly fine-grained sandstone (Facies 2) units. Mixed coarse-grained sandstone / shale units are generally restricted to the overlying Lower Colorado shale where the Viking "A" coarse and pebbly coarse sandstone is often present and can be locally correlated between wells. Facies 8 beds in the Viking "A" coarse-grained sandstones and the Viking "B" conglomerates average 20 cm in thickness (range 2-100 cm).

Facies 9. *Coarse and Pebbly Coarse Sandstone* (average grain size: 1 φ to -1 φ) commonly occurs within the Viking "A" or within the main Viking "B" conglomerate section of the core. These coarse and pebbly sandstones have low (< 10°), or high-angle (> 10°), cross-beds (Figures 2.8C and 2.8B). Massive coarse-grained sandstones are rare (Figure

2.8A). Facies 9 beds average 25 cm in thickness (range: 4 to 164 cm). This unit is hydrocarbon-stained and has good porosity.

Facies 10. *Shales* seen in the core are black or dark grey in color. The Lower Colorado shales (Subfacies 10A, Table 2.1) exhibit conchoidal fracture and contain abundant fish scales and minor plant debris. These shales range between 19 and 27 metres thick from the Base of Fish Scales to the top of the underlying Viking Formation. Small lenses of rippled very fine-grained sandstone are commonly interbedded with the shales (Figure 2.8D). Coarse-grained sandstones (Viking "A" of Facies 8 and 9) are locally abundant.

Shales within the Viking Formation (Subfacies 10B, Table 2.1) average about 20 cm in thickness (range: 1 cm to 40 cm). No fish scales are present and these shales often contain coaly and pyritized plant debris.

Bioturbated silty shales (Subfacies 10C, Table 1) occur at the very base of most sections. This unit is completely homogeneous due to extensive bioturbation. Silty shales are commonly dark grey in colour and have a blocky or massive texture due to the presence of silt-sized quartz grains. Extensive sideritization of this unit occurs where it is overlain by coarser detritus.

Table 2.1 Summary of Facies

1. Interbedded Shale / Fine Sandstone (average grain size: 2 to 3 ϕ):

    Generally fine-grained sandstone with argillaceous laminations to shale beds 1 to 2 cm thick with sandstone lenses. Many beds show flaser and lenticular bedding.

    A. Sandstones with argillaceous interlaminae.

    B. Shale beds with fine-grained sandstone lenses.

2. Fine-Grained Sandstone:

    A. Structureless: massive sandstones which exhibit no visible sedimentary structures.

    B. Parallel stratified: stratification varies from flat to slightly wavy.

    C. Low-angle cross-bedded (< 10° dips on cross-laminae).

    D. Trough cross-bedded: variable size festoon crossbeds (range 2 to 10 cm), usually occurring above horizontal stratified sandstones.

    E. Ripple cross-stratified: formsets of variable size (range 2 to 8 cm), usually occurring above horizontally stratified sandstones.

    F. Bioturbated: primary sedimentary structures destroyed by burrowing activity.

    G. High angle cross-bedded (> 10° dips on cross-laminae).

    H. Convolute cross-stratified.

3. Conglomerate (Ungraded matrix-supported; more than 25 % of clasts are > 2 mm):

    A. Structureless.

    B. Horizontal stratified: parallel beds, flat to low-angle dip (< 10° dips on cross-laminae).

    C. High-angle cross-stratified (> 10° dips on cross-laminae).

4. Conglomerate (Ungraded clast-supported; more than 25 % of clasts are > 2 mm):

    A. Structureless to disorganized.

    B. Horizontal to low-angle stratified: parallel beds, flat to low-angle dip (< 10° dips on cross-laminae).

    C. Trough cross-bedded.

5. Conglomerate (Graded matrix-supported; more than 25 % of clasts are > 2 mm):
    A. Structureless: with normal grading.
    B. Structureless: with inverse grading.

6. Conglomerate (Graded clast-supported; more than 25 % of clasts are > 2 mm):
    A. Structureless: with normal grading.
    B. Structureless: with inverse grading.

7. Mixed Conglomerate / Shale:
    A. Structureless.
    B. Burrowed.
    C. Loaded.

8. Mixed Sandstone / Shale:
    A. Structureless.
    B. Burrowed.
    C. Loaded.

9. Coarse and Pebbly Coarse Sandstone (average grain size 1 ϕ to -1 ϕ):
    A. Structureless.
    B. High-angle cross-bedded (> 10° dips on cross-laminae).
    C. Low-angle cross-bedded (< 10° dips on cross-laminae).

10. Shale:
    A. Black, with conchoidal fracture, fish scales, small lenses of rippled very fine sandstone (Lloydminster Shale).
    B. Black, often with coaly and pyritized plant debris (Shales within the Viking Formation).
    C. Dark grey, bioturbated, mixed with silt with blocky or massive texture (Shales at the base of the Viking Formation).

FIGURE 2.3.

(all cores are 10 centimetres in diameter)

2.3A. Photograph of core showing Facies 1; fine-grained sandstone with argillaceous laminations (well 10-13-35-4W5, 2182 m).

2.3B. Photograph of core showing subfacies 2A, structureless (massive) fine-grained sandstone (well 1-3-35-3W5, 2103 m).

2.3C. Photograph of core showing Subfacies 2B, parallel-stratified fine-grained sandstone with low angle dip to the stratification (well 6-25-34-3W5, 2092 m).

2.3D. Core photograph showing Subfacies 2C, low angle (< 10^0) cross-bedded fine-grained sandstone. Note the scour contacts and the

FIGURE 2.3

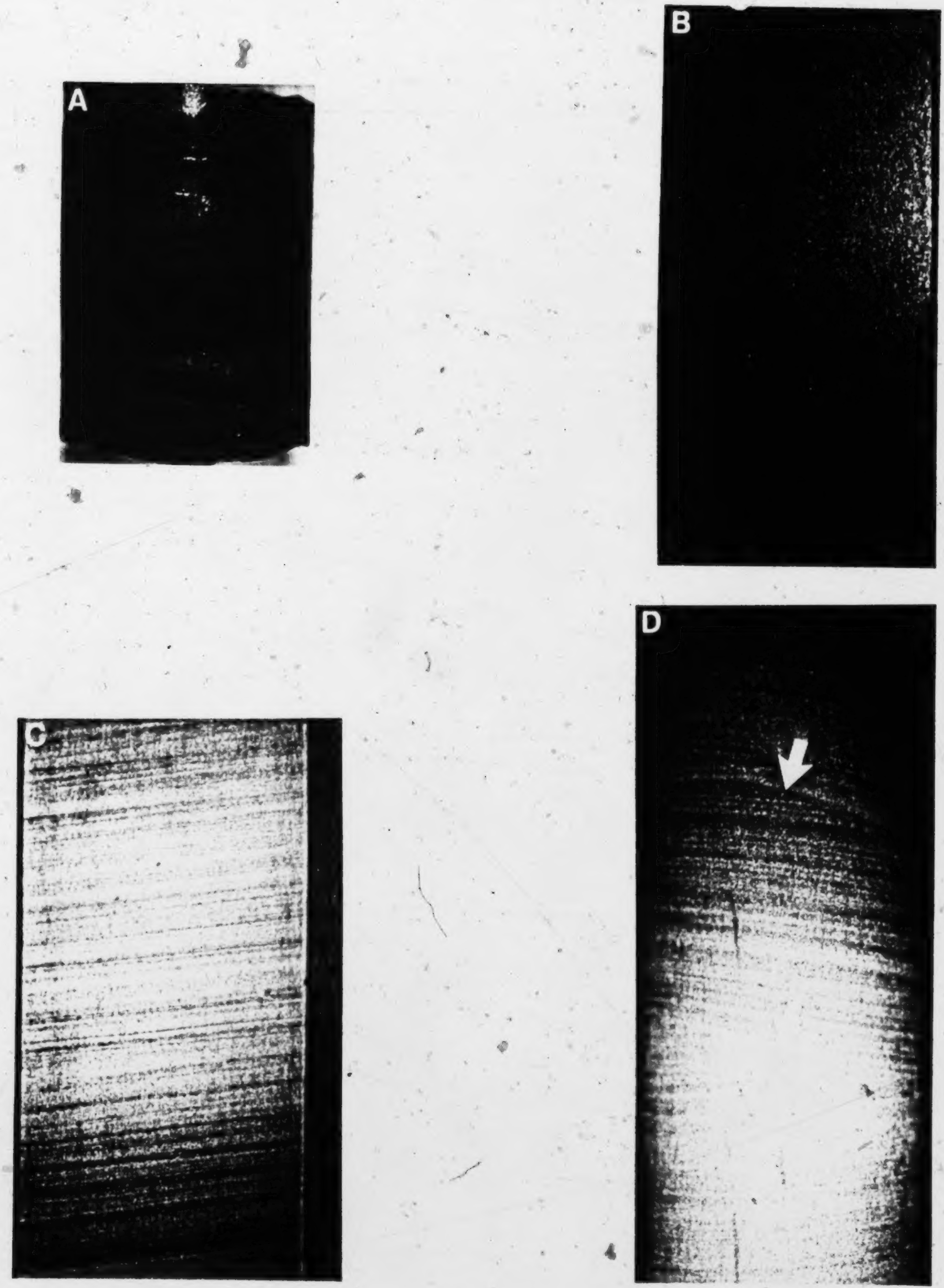

FIGURE 2.4.

(all cores are 10 centimetres in diameter)

2.4A. Photograph of core shows an example of Subfacies 2D, trough cross-stratified fine-grained sandstone (well 10-3-34-4W5, 2300 m).

2.4B. Core photograph showing Subfacies 2E, ripple cross-stratified fine-grained sandstone (well 8-9-35-3W5, 2114 m).

2.4C. Core photograph shows Subfacies 2F, bioturbated fine-grained sandstone. The large burrow (shown by arrows) is probably Rosselia (George Pemberton, pers. comm.)(well 10-3-34-4W5, 2299.5 m).

2.4D. Photograph of core shows Subfacies 2G, high angle (> 10° cross-bedded fine-grained sandstone. The arrow indicates a scour contact (well 14-24-34-3W5, 2087 m).

FIGURE 2.4

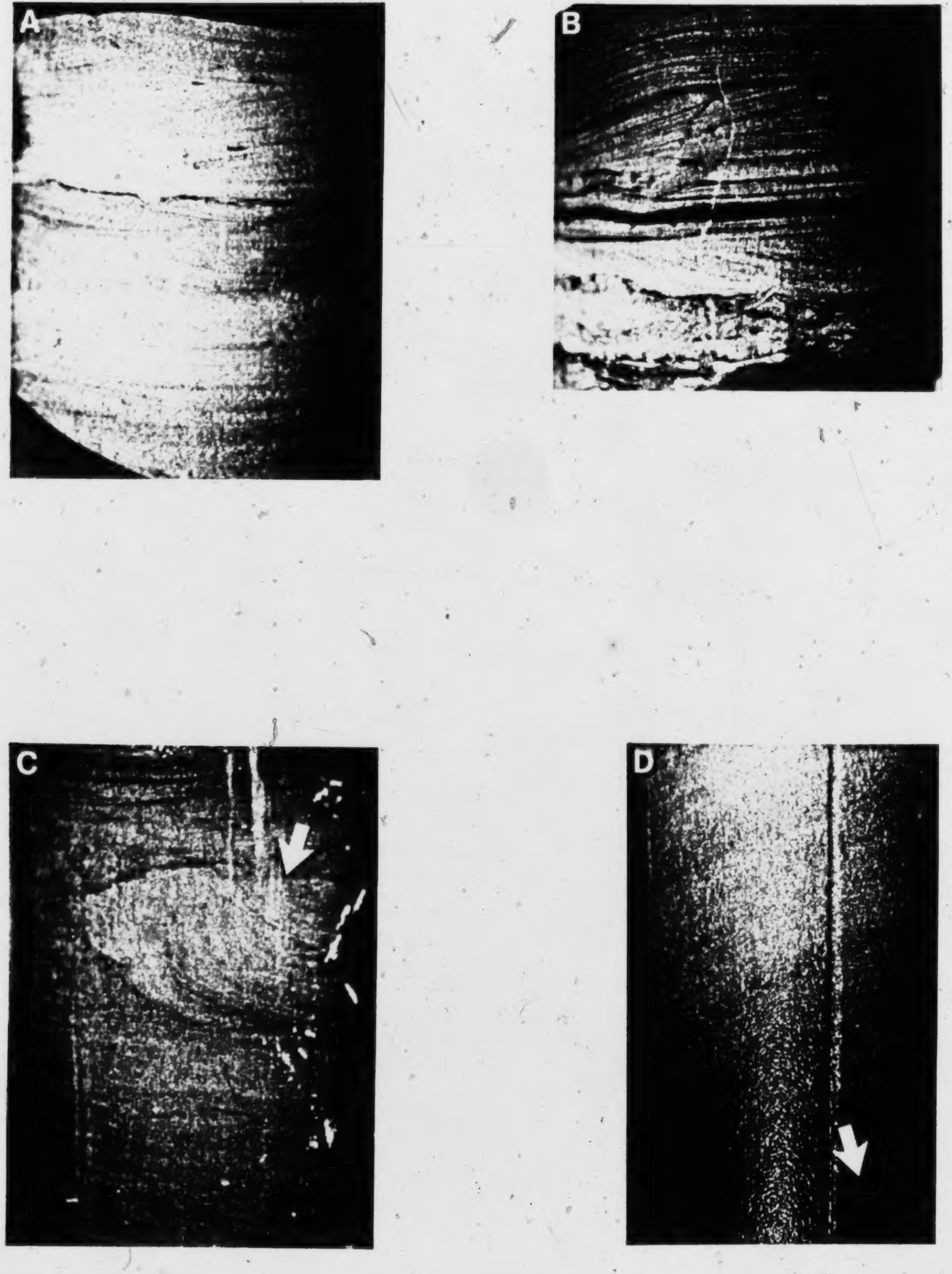

FIGURE 2.5.

(all cores are 10 centimetres in diameter)

2.5A. Core photograph of Facies 3A, structureless, matrix-supported conglomerate (well 14-11-35-4W5, 2216.4 m).

2.5B. Core photograph shows Facies 3C, high angle cross-bedded matrix-supported conglomerate. Crossbeds are marked by arrows (well 6-14-35-4W5, 2212 m).

2.5C. Core photograph of Facies 4A, structureless, clast-supported conglomerate (well 6-23-34-3W5, 2112 m).

2.5D. Core photograph of Facies 4B, clast-supported conglomerate with low angle (< 10°) crossbeds. Arrows indicate low-angle cross-bedding (well 8-14-35-4W5, 2207 m).

2.5E. Photograph of core showing Facies 4C, clast-supported conglomerate with high angle (> 10°) cross-lamination. Arrows indicate cross-lamination (well 1-3-35-3W5, 2094 m).

FIGURE 2.5

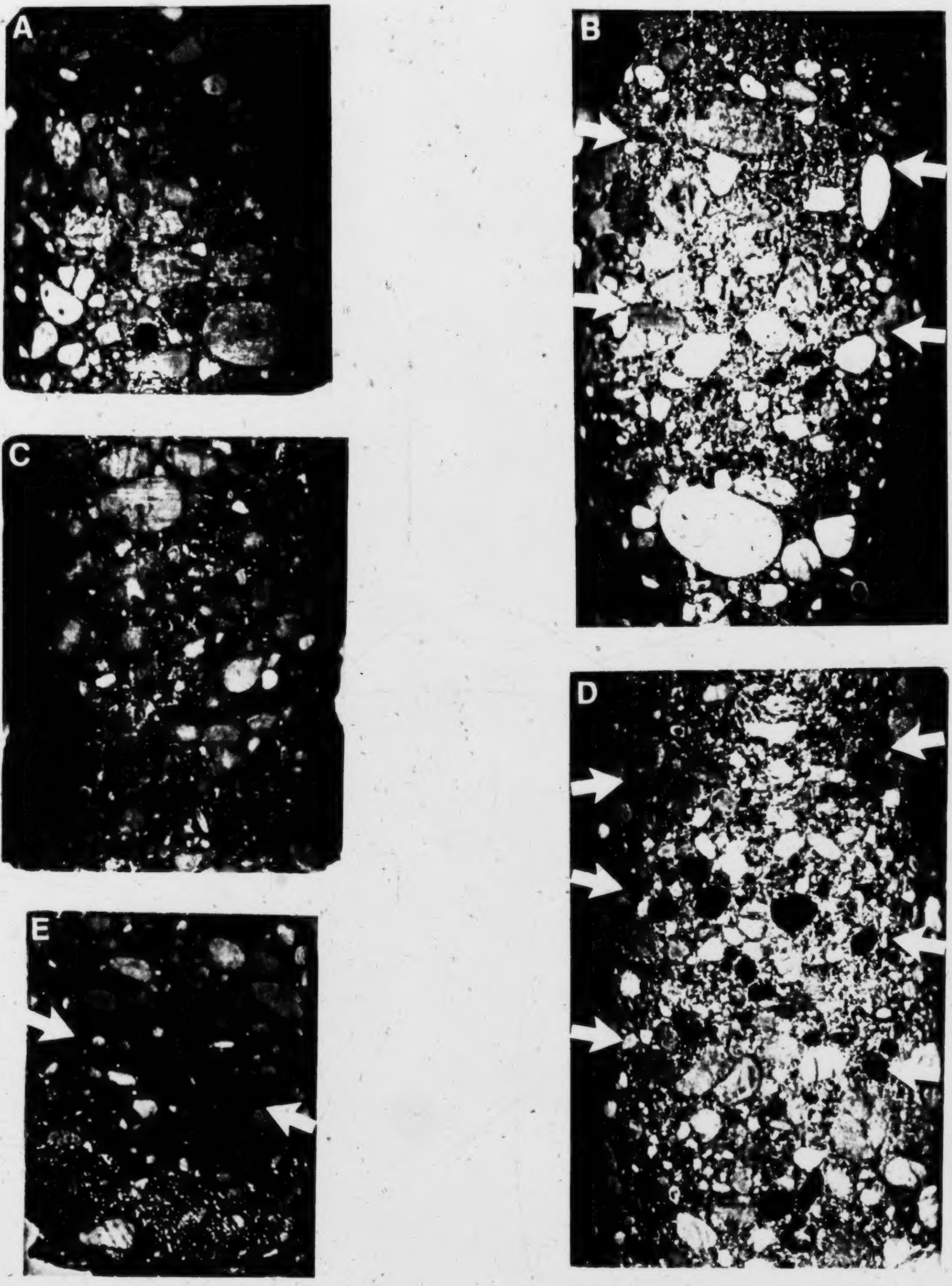

FIGURE 2.6.

(all cores are 10 centimetres in diameter)

2.6A. Photograph of core shows Facies 5A, normally graded, matrix-supported conglomerate. The photograph shows coarse-tail grading indicated by the arrow (well 10-13-35-4W5, 2175.6 m).

2.6B. Core photograph of Facies 5B, inversely graded, matrix-supported conglomerate. Arrow indicates graded portion (well 6-34-34-3W5, 2115 m).

2.6C. Core photograph shows Facies 5B, inversely graded, matrix-supported conglomerate with clasts grading from 0.5 cm up to 3.0 cm as indicated by the arrow (well 14-36-34-3W5, 2064.5 m).

2.6D. Photograph of core showing Facies 6A, normally graded, clast-supported conglomerate with clasts abruptly grading from 6.0 cm to 0.5 cm over 15 cm of core as indicated by the arrow (well 14-25-34-3W5, 2078 m).

2.6E. Photograph of core shows Facies 6B, inversely graded, clast-supported conglomerate with clasts grading from 0.5 to 1.0 cm over 15 cm of core. Arrow indicates graded portion (well 14-11-35-4W5, 2216.8 m).

FIGURE 2.6

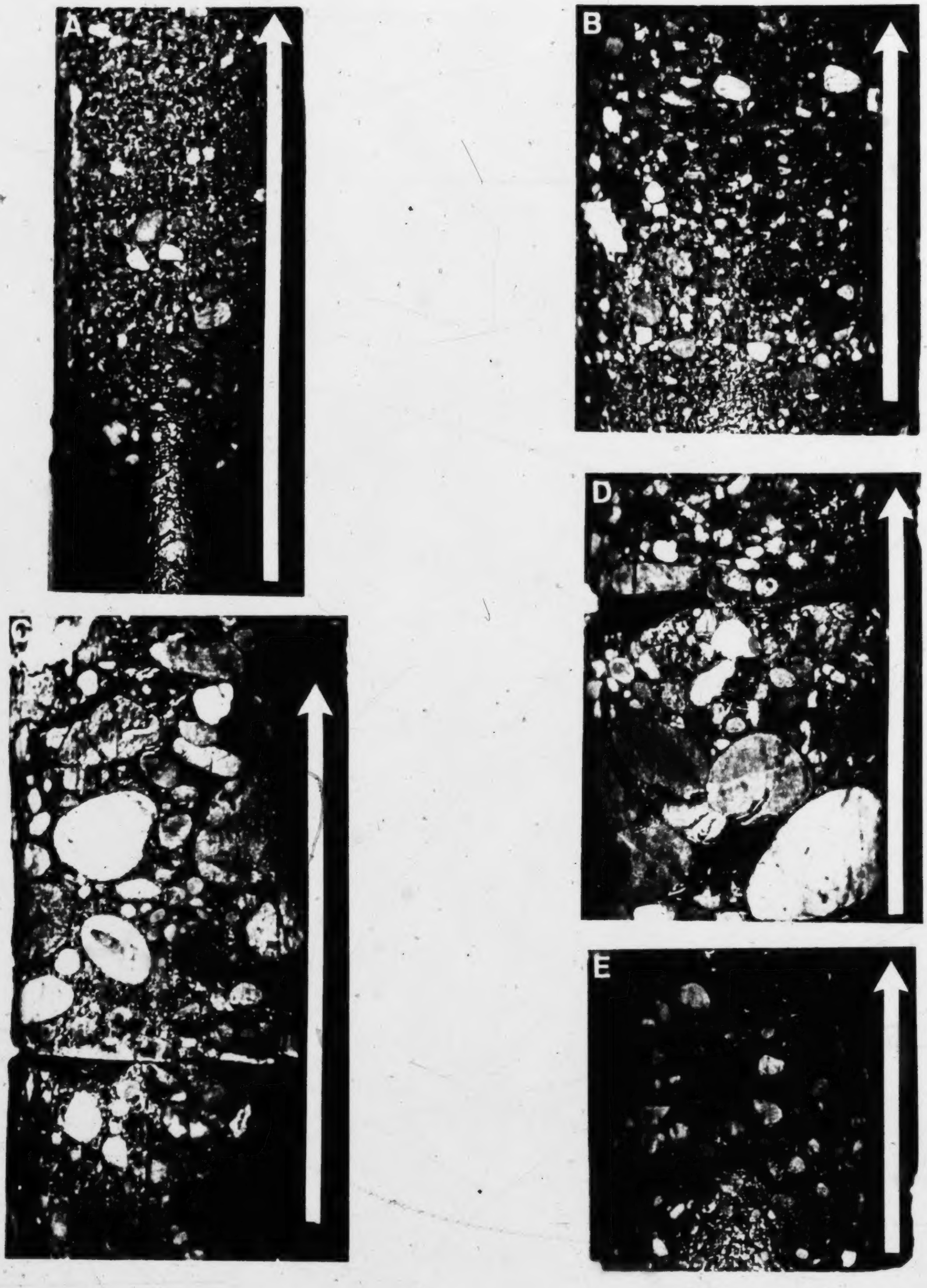

FIGURE 2.7.

(all cores are 10 centimetres in diameter)

2.7A. Core photograph of Facies 7A, structureless, mixed conglomerate and shale near the Viking "B"-Lloydminster Shale contact (well 14-24-34-3W5, 2083 m).

2.7B. Core photograph shows Facies 7A (shown by arrow), structureless, mixed conglomerate and shale near the Viking "B"-Lloydminster Shale contact (well 6-6-35-2W5, 2036 m).

2.7C. Core photograph shows possible pebbly, burrow infill (Facies 7B), or detached, pebbly load cast (Facies 7C), as indicated by arrows (well 14-11-35-4W5, 2216.9 m).

2.7D. Core photograph of Facies 8B, bioturbated, mixed sandstone and shale. This section of core is from the Viking "A" sandstone (well 6-13-34-3W5, 2080.6 m). Well defined burrows are marked by arrows.

2.7E. Core photograph shows Facies 8B, bioturbated, mixed sandstone and shale with a mottled texture. This section of core is from the lower portion of the Viking "B" unit (well 6-19-34-2W5, 2070 m).

2.7F. Core photograph shows Facies 8C, loaded, mixed sandstone and shale. This section of core is from the lower portion of the Viking "B" unit (well 8-14-35-4W5, 2214 m). Flame structures are shown by arrows.

FIGURE 2.7

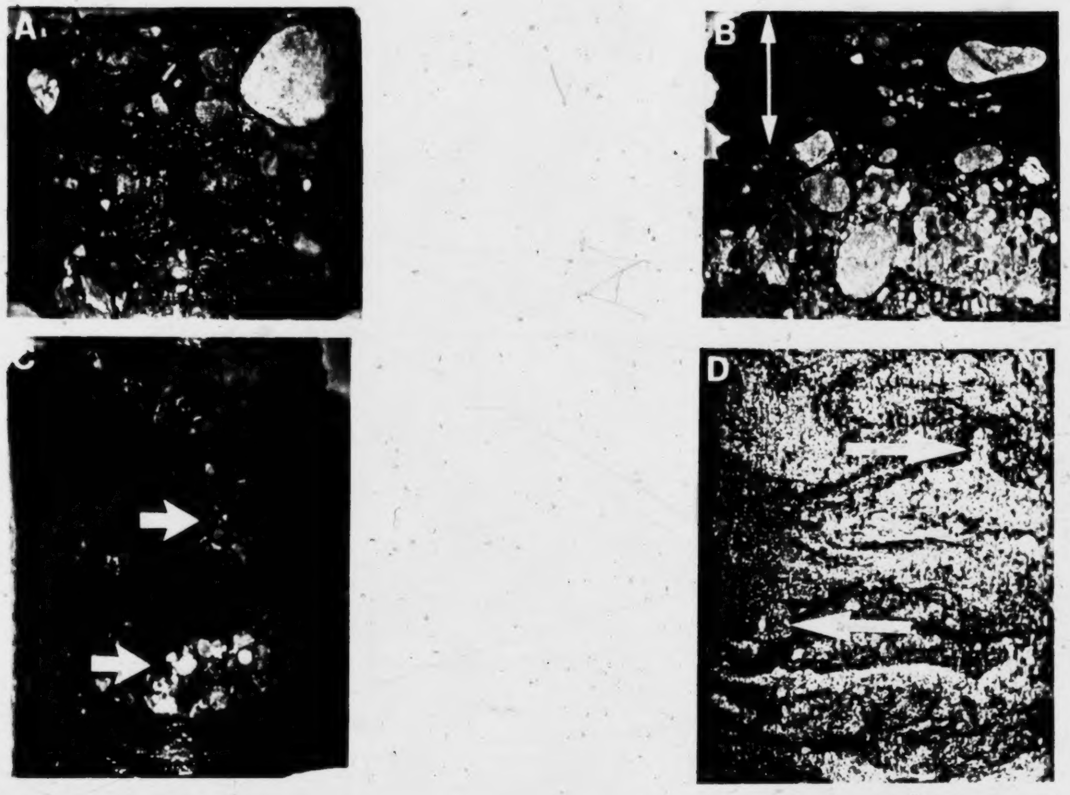

FIGURE 2.8.

(all cores are 10 centimetres in diameter)

2.8A. Core photograph of Facies 9A, structureless, (massive) coarse-grained sandstone (well 16-19-34-2W5, 2054 m).

2.8B. Core photograph of Facies 9B, high-angle (> 10°) cross-bedded coarse and pebbly coarse sandstone. Arrows indicate cross-beds (well 6-34-34-3W5, 2116 m).

2.8C. Photograph of core showing Facies 9C, low-angle (< 10°) cross-bedded coarse and pebbly coarse sandstone. Arrows indicate crossbeds (well 10-7-34-4W5, 2333.8 m).

2.8D. Core photograph showing Facies 10A, black shale (Lloydminster Shale). Note the small, ripple cross-bedded lenses of very fine-grained sandstone (marked by arrow) (well 14-11-35-4W5, 2211 m).

FIGURE 2.8

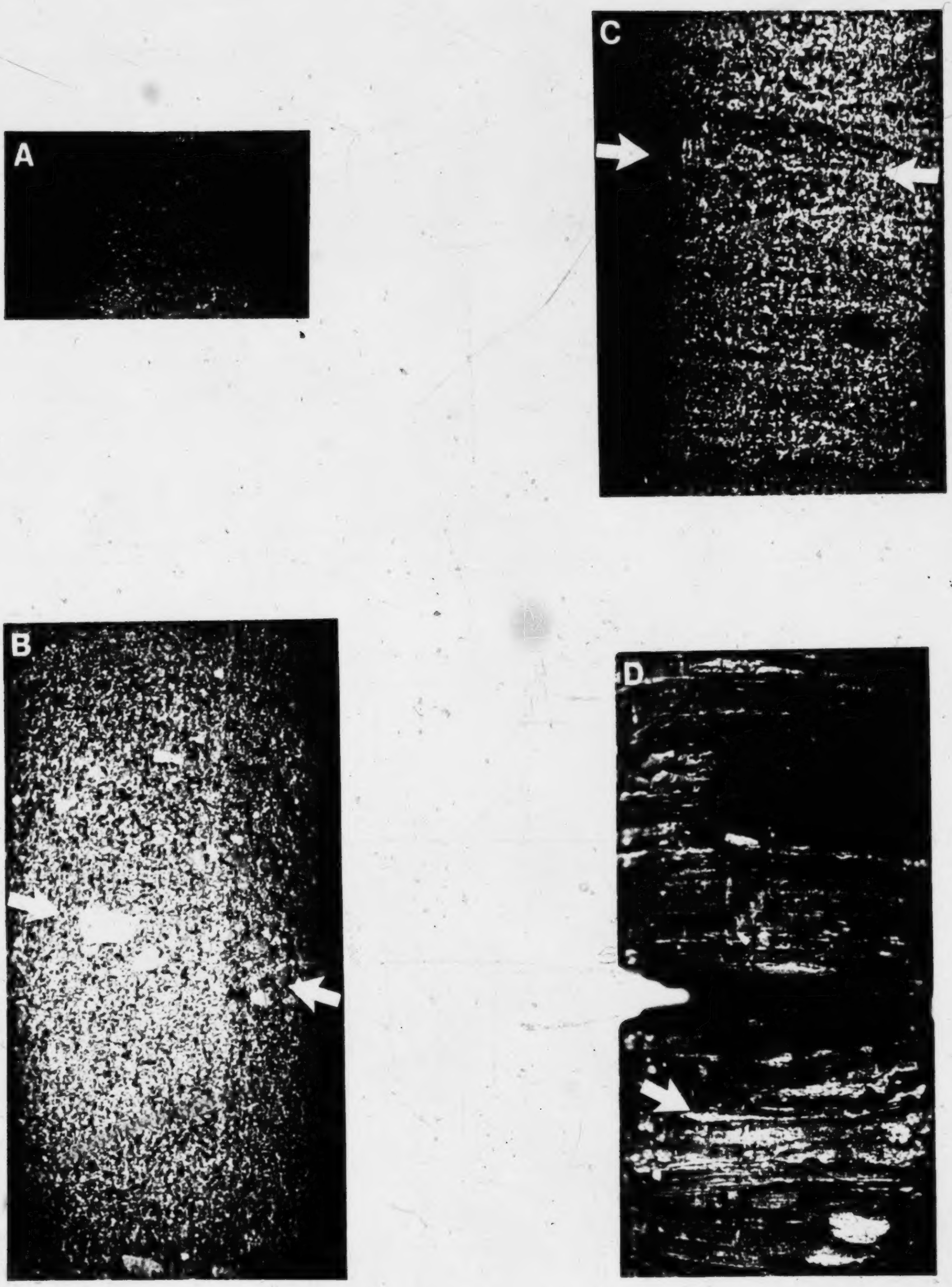

D. VIKING DEPOSITIONAL MECHANISMS

The facies which comprise the Viking Formation at Garrington are characterized by a wide range of sedimentary structures and grain sizes. These features are the result of different depositional processes responsible for the emplacement of individual beds. Fine-grained sediments, such as silts and clays, require only very weak currents to carry them long distances. These sediments are typically deposited as finely laminated beds with only minor current structures. The implication is that these sediments are carried far offshore and deposited in relatively deep water where they are not usually disturbed by current or wave activity. The trace fossils which occur in the fine-grained sediments of the Viking Formation confirm this interpretation.

Fine-grained sandstones seen in the Viking Formation exhibit a variety of sedimentary structures. Grain size characteristics of the fine-grained sandstones and the sedimentary structures suggest that marine currents, storms and wave activity play an important role in the deposition of these sediments. The general coarsening upward sequence suggests that water level must have been decreasing as energy level increased.

Coarse-grained sandstones and conglomerates complete the coarsening upward sequence. Sedimentary structures and grain sizes suggest that these sediments were deposited by very high energy processes. Inversely graded and structureless beds in the conglomerates suggest that these sediments were transported into the shallow marine environment by some type of sediment gravity flow. Other conglomerate beds show evidence of current formed sedimentary structures. Sedimentary structures in the coarse-grained sandstones are believed to be the result of strong current action.

Four major mechanisms are responsible for deposition of the Viking Formation at Garrington;

(1) Hemipelagic fallout of fine-grained material from suspension,
(2) Storm and waning storm currents (oscillatory flows),
(3) Unidirectional marine geostrophic currents, and
(4) Sediment gravity flows.

Deposition from hemipelagic fallout is responsible for the emplacement of fine-grained sediments. In deposition by fallout, without traction, particles are simply sedimented onto the bed and come to rest without further transport. The bed builds up by vertical accretion. This type of sedimentation is characteristic of very low current velocities and very fine-grained sediments, mainly silts and clays (Harms et al., 1982).

Seaward deposition on fine-grained sediment is dependent on the width of the shelf, the energy of marine transport processes and the settling rates of suspended solids. The wider the shelf, the more likely it is that fine-grained sediments will be deposited on it. Fine-grained sediments may be carried great distances by cold, dense, saline, marine currents. In this manner fine-grained terrigenous sediment may move across the shelf by sediment bypass. These currents may flow horizontally at velocities sufficient to maintain silt and clay in suspension, only gradually losing it to underlying stagnant basin waters (Harms et al., 1982). Drake (1976) found that in 20 °C water a 4 micron quartz grain will settle at approximately 1.4×10^{-3} cm/sec and that a clay particle 2 microns in size will settle at approximately 0.3×10^{-3} cm/sec or less. At these rates particles of clay or silt size would settle only about 86 cm in one day in still, vertically homogeneous waters (Drake, 1976). When particles of these sizes are carried into an ocean basin they should remain in suspension for weeks or months over shelves and for years over deep sea areas. Flocculation and biological agglomeration processes may accelerate the settling of clay and silt by two to ten times. These processes have been documented in the Gulf Coast off the Mississippi Delta (Drake, 1976). Blatt et al. (1980) state that laminae in muds of shallow marine environments are produced by seasonal fluctuations in sediment supply or periodic stirring of the bottom by wave action.

Storm processes include wind driven currents, wave processes and storm surges. Deposition from storms and waning storms is characterised by a number of sedimentary structures including hummocky cross-stratification, massive beds and normally graded beds. Hummocky cross-stratification is medium to large scale cross-stratification in fine sand in which sets of fairly gently dipping laminae with erosional upper contacts suggest deposition on a bedding surface in the form of shifting hummocks and depressions. The essential characteristics of hummocky cross-stratification include; (1) lower bounding surfaces which are erosional and slope at low angles, usually less than 10°, (2) laminae above erosional boundaries that are parallel to the erosional surface, (3) laminae that systematically thicken laterally in a set, so that their traces on a vertical sequence are fan-like, and (4) dip directions of erosional set boundaries, and of the underlying laminae, that are scattered (Harms et al., 1982). Hummocky cross-stratification forms by deposition of fine sand during oscillatory flow. The oscillatory flow is caused by wave action at the sea floor with periods of several seconds and moderately high orbital speeds. Hummocky cross-stratification is probably formed from bidirectional oscillatory flow although multidirectional flow may also be important (Harms et al., 1982). The rate of aggradation depends on the erosional sediment source and the water circulation produced by the storm event that molds the bed topography at the depositional site.

Storms are very important for moving sediment offshore. Oscillatory storm surges cause large amounts of fine sand to be suspended in the mid-depth seaward return flow (Goldring and Bridges, 1973; Walker, 1979). If the sediment drops out of suspension very rapidly massive sandstones may form. These deposits may then be molded by wave action into hummocky cross-stratification. Where sand size sediments are deposited far out into the basin, below storm wave base, they occur interbedded with muds and silts (Goldring and Bridges, 1973; Hamblin and Walker, 1980). These sand lenses commonly have very sharp bases indicating sudden emplacement, and bioturbated tops which reflect recolonization by benthonic fauna. Waning storms may deposit graded beds with grain size and sedimentary structures both showing a decrease in energy. Graded sand to mud beds are a common shelf facies and have been reported in the ancient (Cant, 1980) and in the recent (Kontopoulos and Piper, 1982).

Marine geostrophic currents have not been extensively studied and documentation of them is relatively sparse. These currents are permanent or semi-permanent and unidirectional with a strong seasonal aspect. Unidirectional currents form a number of sedimentary structures that are characterised by tractional deposition. Geometry of the depositional surface is typically either planar or rippled on a large or small scale. For sands finer than about 0.6 mm the sequence of bed phases with increasing current velocity is; no movement, ripples, dunes, plane beds and antidunes. For sands coarser than 0.6 mm the sequence of bed phases with increasing current velocity is; no movement, lower plane bed, large ripples, upper plane bed and antidunes.

Small ripples formed at low velocities have sharp crests, planar foresets and angular foreset/toeset contacts. Small ripples formed at higher velocities have rounded crests, sigmoidal foresets and rounded foreset/toeset contacts. The existence of current ripples tells us that current velocities were low but at least sufficient for traction transport. Large ripples formed by relatively weak flows tend to be straight crested and regular in plan view whereas those formed by strong flows tend to be highly three-dimensional and irregular in plan view. Two-dimensional large ripples have stoss sides which are flat or covered with small ripples; crests are sharp, foresets planar and foreset/toeset contacts angular. The lee slope of two-dimensional large ripples is commonly at angle of repose. Three-dimensional large ripples have gentle stoss sides and lee sides that slope at angle of repose or less. These three-dimensional large ripples tend to have rounded crests and smooth transitions from foresets to toesets. Height and spacing of three-dimensional ripples increase with increasing flow velocity and then decrease again toward the transition to a plane bed.

Large scale trough cross-stratification is formed by the migration of large three-dimensional ripples. Cosets of trough cross-strata indicate unidirectional flows with appropriate ranges of depth and velocity to form three-dimensional large ripples in the grain sizes observed in the sets. Large scale tabular cross-stratification is produced by the migration of two-dimensional large ripples. In unidirectional flows, these bedforms indicate lower flow velocities than three-dimensional large ripples. The interpretation of lower flow strength is supported by the steeper and more planar configuration of the cross-laminae as compared to those within trough sets.

Planar lamination is characterised by distinctly laminated sets in muds, sands and fine, pebble gravels that show none of the angular discordance typical of cross-lamination. In steady unidirectional flows, plane beds, or upper flow regime flat beds, are the stable bedform in all sizes of sediment in strong currents. For sediments coarser than about 0.6 mm and low current velocities, lower flow regime plane beds are the stable bedform. Planar stratification should be distinguished from low angle cross-stratification in which laminae in adjacent sets are nearly parallel. Psuedo-planar stratification maybe produced by very low amplitude sand waves with very shallow, near horizontal stoss sides (Smith, 1971; McBride et al., 1975). If current velocities are generally great enough for an upper stage plane bed, but at times decrease and form ripples, planar laminae will be interbedded with cross-laminae formed by ripples climbing at very low angles. Angle of climb of the ripples will approach zero where the cross

7

lamination grades into planar lamination.

Conglomerates may exhibit horizontal or inclined stratification which can vary in angle from a few degrees to angle of repose (Harms et al., 1982). Stratification in conglomerates is shown by changes in clast size or composition, changes in sorting or changes in fabric. Layers may grade into one another where currents are pulsating. Where layers are sharply bounded, separate events or processes are probably responsible for each layer. Angle of repose cross-bedding develops on downstream faces of dunes and probably has an origin similar to sandy cross-bedding. Lower angle inclined stratification may represent lateral accretion on low angle margins of dunes or gravel waves. Where pebble conglomerates occur interbedded with sandstones the amount of current fluctuation does not have to be great. The shear stress necessary to place sand in suspension may be very close to that required to roll pebbles on a bed. Relatively small fluctuations in flow strength can cause rolling of gravel on a bed and suspension of sand or cessation of gravel rolling and simultaneous deposition of sand (Harms et al., 1982).

There are four main types of sediment gravity flows: (1) turbidity currents, (2) fluidized sediment flows, (3) grain flows, and (4) debris flows. Each type of sediment gravity flow has a particular sediment support mechanism. In turbidity currents, sediments are supported by the upward component of fluid turbulence. Fluidized sediment flows are supported by the upward flow of fluid escaping from between the grains as they settle out by gravity. Grain flows are supported by direct grain-to-grain interactions (collisions or close approaches) known as dispersive pressure (Bagnold, 1954). In debris flows larger grains are supported by matrix, a mixture of interstitial fluid and fine-grained sediment which has a finite yield strength. It is difficult to distinguish between deposits formed from the different types of flows because the deposits all have similar sedimentary structures. Middleton and Hampton (1976) show that all four types of sediment gravity flows may be complexly intergradational (Figure 2.9).

Turbidity currents are usually associated with catastrophic events and move as surges (Middleton and Hampton, 1976). They can move down very low slopes; often less than 1°. There must be an initial input of energy to start the flow, but once it has begun to flow it can go for a very long time. All that is necessary to keep the system going is that the energy loss caused by friction should be compensated by the input of gravitational energy as the current moves downslope. The lower part of the bed is commonly massive or normally graded with only faint lamination. Grading is caused by decay of initial turbulence, decreasing competency in the tail of the current and by concentration of coarse grains in the head of the current by flow circulation. Coarse-tail grading and inverse grading are common in high concentration flows. Planar lamination may represent deposits of the upper flow regime. Load structures or scours may form when the bed being deposited is denser than the bed on which it is being deposited.

Grain flows move by upward supportive stress acting on grains within the flowing sediments as a result of grain to grain interaction rather than fluid turbulence. This is known as dispersive pressure, which is proportional to the shear stress transmitted between grains and counteracts the tendency for grains to settle out of the flow (Bagnold, 1954). Grain flows may behave in a viscous fashion, where momentum results from the interaction of grains and interstitial fluid as grains come in close proximaty, or in an inertial fashion, where the influence of the interstitial fluid is negligible and dispersive pressure is generated as grains collide with one another. Grain flows require steep slopes in order to move; approximately 37 ° for viscous flows and 18 ° for inertial flows (Middleton and Hampton, 1976). At high energy conditions turbulence may help support grains in addition to the support provided by dispersive pressure. A continuum may therefore exist between turbidity currents and grain flows.

Deposition of grain flows occurs by mass emplacement due to a sudden freezing of the flow. This occurs when the driving stress becomes less than that required to propel the flow and typically occurs as the result of a reduction in slope. Grain flows are characterised by lateral and vertical inverse grading. Dispersive pressure size sorts grains pushing large ones to the top and small ones downward. A kinetic seive, where small grains fall down between large grains may also operate (Middleton, 1970).

Fluidized sediment flows occur when sediments that have an unstable fabric liquefy or lose strength due to a sudden shock. Sediments that are loosely packed or that have textural properties that are favorable to the breakdown of fabric may be subject to liquefaction. Once the sediment fabric is destroyed the grains must be at least in part supported by pore fluids; the sediment has little strength and behaves like a highly viscous fluid. Fluidized sediment flows are thus able to move rapidly down relatively gentle slopes

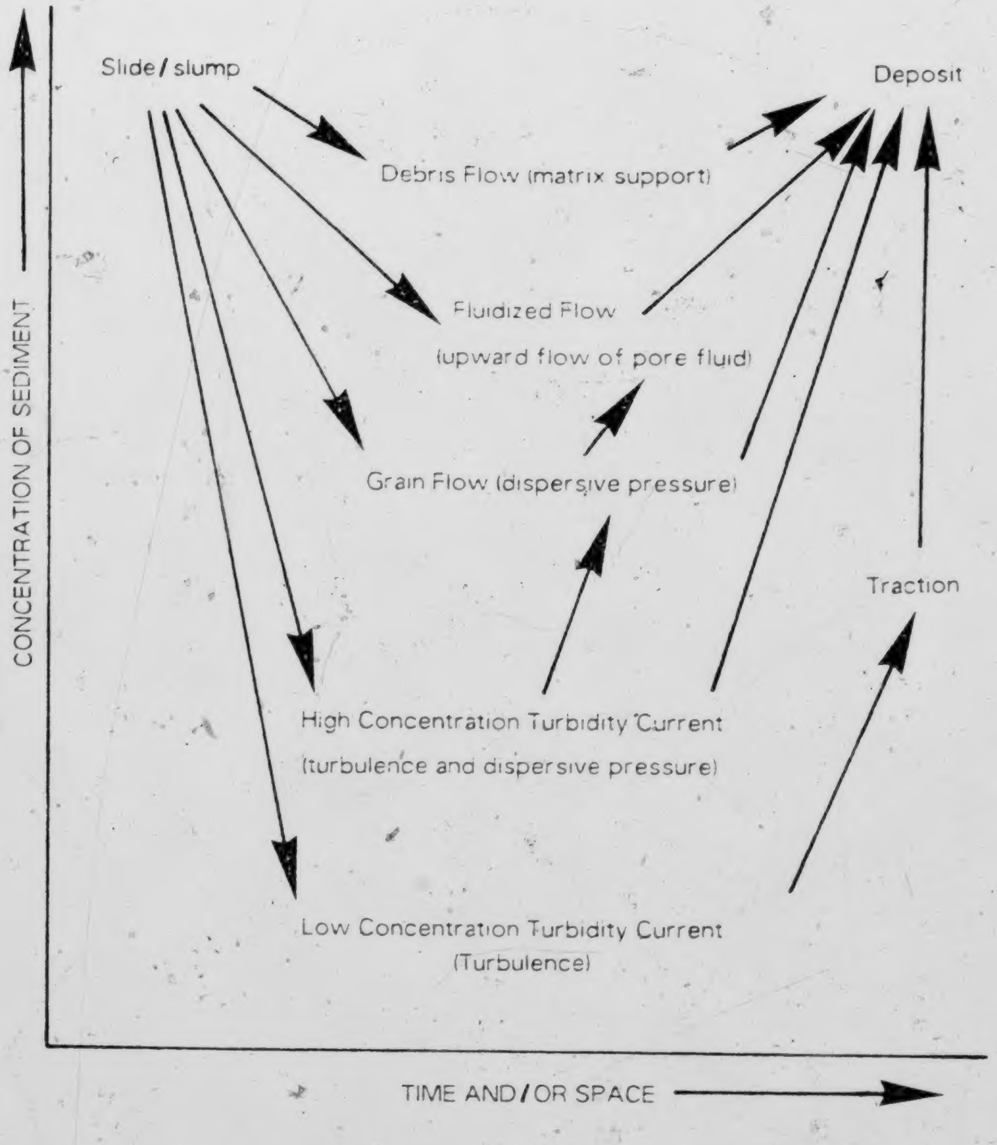
Slide / slump
Deposit
Debris Flow (matrix support)
Fluidized Flow
(upward flow of pore fluid)
Grain Flow (dispersive pressure)
Traction
High Concentration Turbidity Current
(turbulence and dispersive pressure)
Low Concentration Turbidity Current
(Turbulence)
CONCENTRATION OF SEDIMENT
TIME AND / OR SPACE

Figure 2.9. Diagram showing the interrelationships which may occur between the various types of sediment gravity flows (Modified form Middleton and Hampton, 1976).

of 3 to 10 ° (Middleton and Hampton, 1976). These flows are usually so concentrated that normal traction structures do not form. The significance of fluidization is its combined occurrence with other support mechanisms such as turbulence and dispersive pressure.

Debris flows are sluggish downslope movements of mixtures of granular solids, clays and water in response to the pull of gravity. These flows may occur on slopes as low as 1 or 2 ° with relatively low clay (2-20°) and water (9%) contents (Middleton and Hampton, 1976). Flow occurs if the shear stress exceeds the total yield strength of the debris. Grains are supported by buoyancy and matrix strength rather than by turbulence, fluid escape or dispersive pressure. However, dispersive pressure may be significant in debris flows due to the high concentration of grains. Deposition of debris flows occurs by mass emplacement when the driving stress of gravity decreases below the strength of the debris and freezing occurs. Debris flow deposits are typically massive or structureless, or exhibit inverse grading (Middleton and Hampton, 1976; Fisher, 1971). Massive or structureless beds imply that clasts were not free to move relative to one another whereas inverse grading implies that dispersive pressure or kinetic seive mechanisms were operating.

Submarine sediment gravity flows probably result initially from sliding or slumping of delta front sediments. Slumping may be due to rapid deposition of sediment on a slope leading to underconsolidation of sediment, formation of excess pore pressures and consequent low internal angle of friction. Spontaneous liquefaction of sensitive sediments may be produced by relatively minor triggering events. The main requirement for all types of sediment gravity flows is the addition of water. Submarine slides and slumps would be quite likely to incorporate water and evolve into some type of sediment gravity flow. Once a flow begins to move it may evolve, by adding or expelling water, or by flow circulation, into any type of sediment gravity flow. It is therefore probable that two or more types of sediment support mechanisms operate simultaneously in any given flow.

E. FACIES INTERPRETATION AND CORRELATION

In order to interpret facies and correlate general facies patterns throughout the study area, the ten facies have been grouped into four large scale facies associations:

1. Shale (Lloydminster shales); Subfacies 10A and 8;

2. Coarse-grained Sandstone and Conglomerate; Facies 3, 4, 5, 6, 7, 8B and 9;
3. Fine-Grained Sandstone; Facies 1A, Facies 2 and Subfacies 10B (with minor shale interbeds);
4. Interbedded and Intermixed Fine-Grained Sandstone and Shale; Facies 1B, Facies 8 and Subfacies 10C.

Figure 2.10 is a diagram showing the general coarsening-upward sequence of the four facies associations. The Viking Formation at Garrington is interpreted as a prograding clastic wedge which is capped by conglomerate introduced by sediment gravity flows (Figure 2.10). As progradation took place the energy level gradually increased as water level decreased. Deep water deposition was dominated by hemipelagic fallout during fairweather conditions with minor storm pulses inputing sand into the basin periodically. Bioturbation generally kept pace with the rate of sediment accumulation. With continued regression and progradation large amounts of sand were carried into the basin by storm processes. These sand units were then extensively reworked by strong geostrophic currents which molded them into large sand ridges. During fairweather conditions mud deposition, by hemipelagic fallout, took place in interbar areas. Following sand deposition, conglomerate and coarse grained sand were introduced into the basin very abruptly by sediment gravity flows. These coarse deposits were then reworked by strong marine currents (possibly transgressive) into large dunes and gravel waves.

Following conglomerate deposition and reworking, a major marine transgression occurred and the area was once again dominated by hemipelagic fallout deposition during fairweather with minor sand lenses deposited by storm action and rippled by marine bottom currents. At least two minor regressions occurred within the major transgressive episode. These events are characterised by medium- to coarse-grained sandstone deposits with low to high angle crossbeds. These sands were initially deposited by storm activity and were then reworked by unidirectional marine currents into migrating dunes and sand waves.

A fence diagram (Figure 2.11, in pocket) of the facies associations was constructed for the Viking Formation in the Garrington study area. Correlation of the facies associations, using lithologic and geophysical logs, shows their thickness variation throughout the study area.

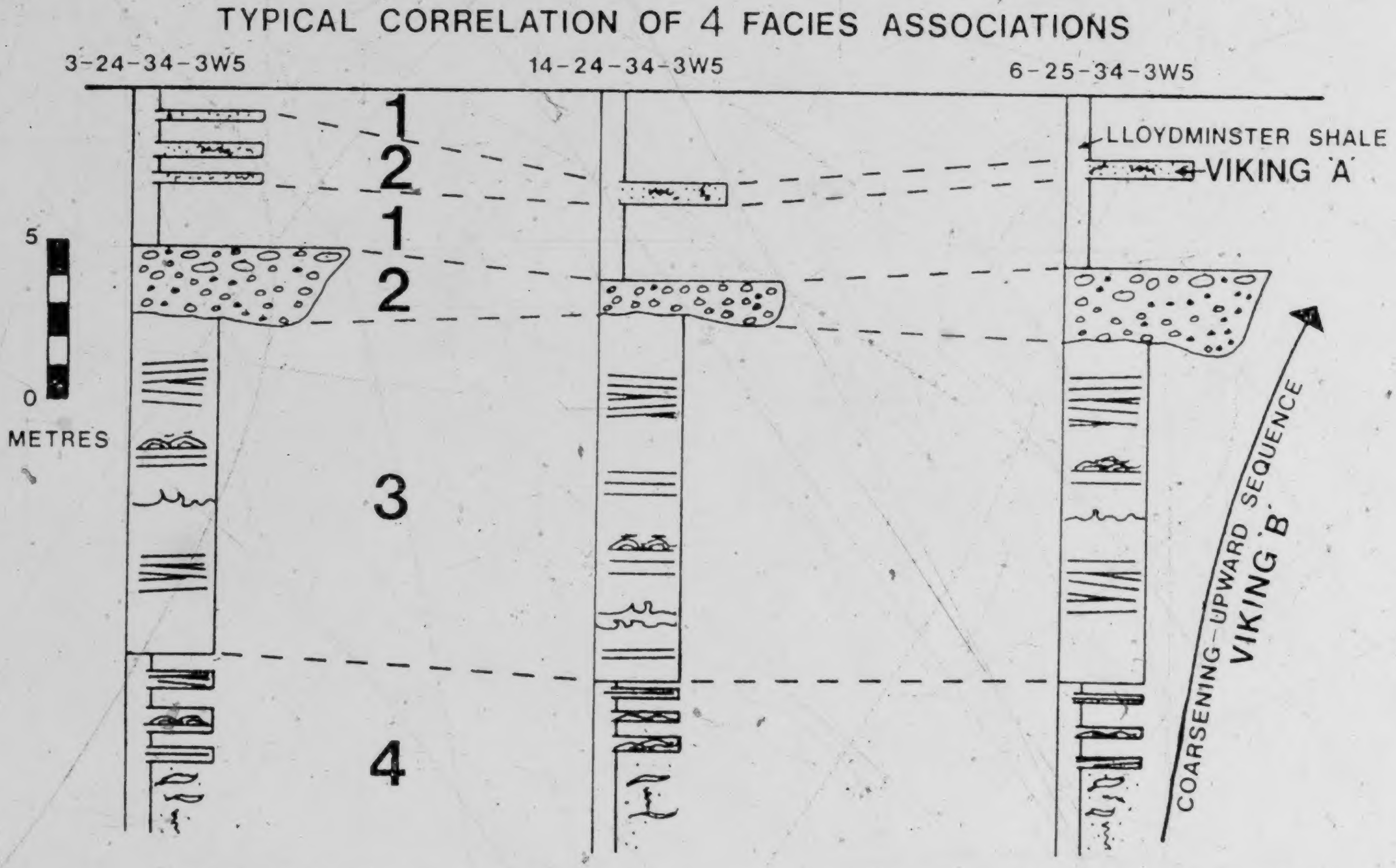
TYPICAL CORRELATION OF 4 FACIES ASSOCIATIONS
3-24-34-3W5
14-24-34-3W5
6-25-34-3W5
LLOYDMINSTER SHALE
VIKING 'A'
5
0
METRES
1
2
1
2
3
4
COARSENING-UPWARD SEQUENCE
VIKING 'B'

Figure 2.10. Diagram showing the general coarsening upward sequence in the Viking Formation at Garrington. Numbers indicate large-scale facies associations.

The four facies associations comprise a 40 metre thick coarsening-upward sequence. At the base of the sequence is Facies Association 4. This facies association is 20-25 metres thick. At the base of this facies association the sediments are extensively bioturbated and mottled (Facies 10C, Bioturbated silty shales). Going upsection, sand input increases and the sediments become dominated by laminated shales interbedded with lenticular sands (Facies 1B). The sandstone lenses always have sharp bases indicating sudden deposition, and most often a sharp upper contact followed by a shale drape.. Where sand lenses are fairly thick (>10 cm) this sequence represents a small facies assemblage consisting of Subfacies 2B (parallel stratified sandstones) overlain by Subfacies 10B (black shale). Where bioturbation of a sand lense is extensive, Subfacies 2F (bioturbated sandstone) is overlain by Subfacies 10B (black shale). Some of the thicker sandstone lenses are ripple or trough crossbedded with minor burrowing (Subfacies 2D and 2E). Recognizable trace fossils within Facies Association 4 include: Planolites, Paleophycus, Rosellia, Teichinus, Terebellina, Ophiomorpha and rare Skolithos indicating a "Cruziana"-equivalent shallow shelf ichnofacies for Facies Association 4 (S.G. Pemberton, pers. com. in Hein et al., submitted 1985). These features imply deposition in an offshore, quiet water, "shelf-type" environment dominated by deposition of fine-grained material by hemipelagic fallout (Facies 10C). Bioturbation was able to keep pace with the rate of sediment deposition at the base of this Facies Association. This environment was periodically interrupted by sudden storm-generated currents which transported sand-size material to the shelf. During fair-weather conditions, these sands were reworked by low velocity, bottom currents and were extensively bioturbated. Storm influence gradually increased upsection and thicker sandstones were deposited. Current produced sedimentary structures also increased upwards as the water level decreased.

The 10 to 15 m thick fine-grained sandstones of Facies Association 3 gradationally overlie Facies Association 4. The fine-grained sandstones are characterized by a wide variety of sedimentary structures as shown in Table 2.1 and Figures 2.3 and 2.4. Figure 2.12 shows the percentage breakdown of the facies which comprise Facies Association 3. Most commonly, the fine-grained sandstones are parallel laminated with horizontal or low angle dips to the laminae (Subfacies 2B). These parallel-laminated sandstones often have scoured contacts between beds. The overwhelming abundance of parallel laminated

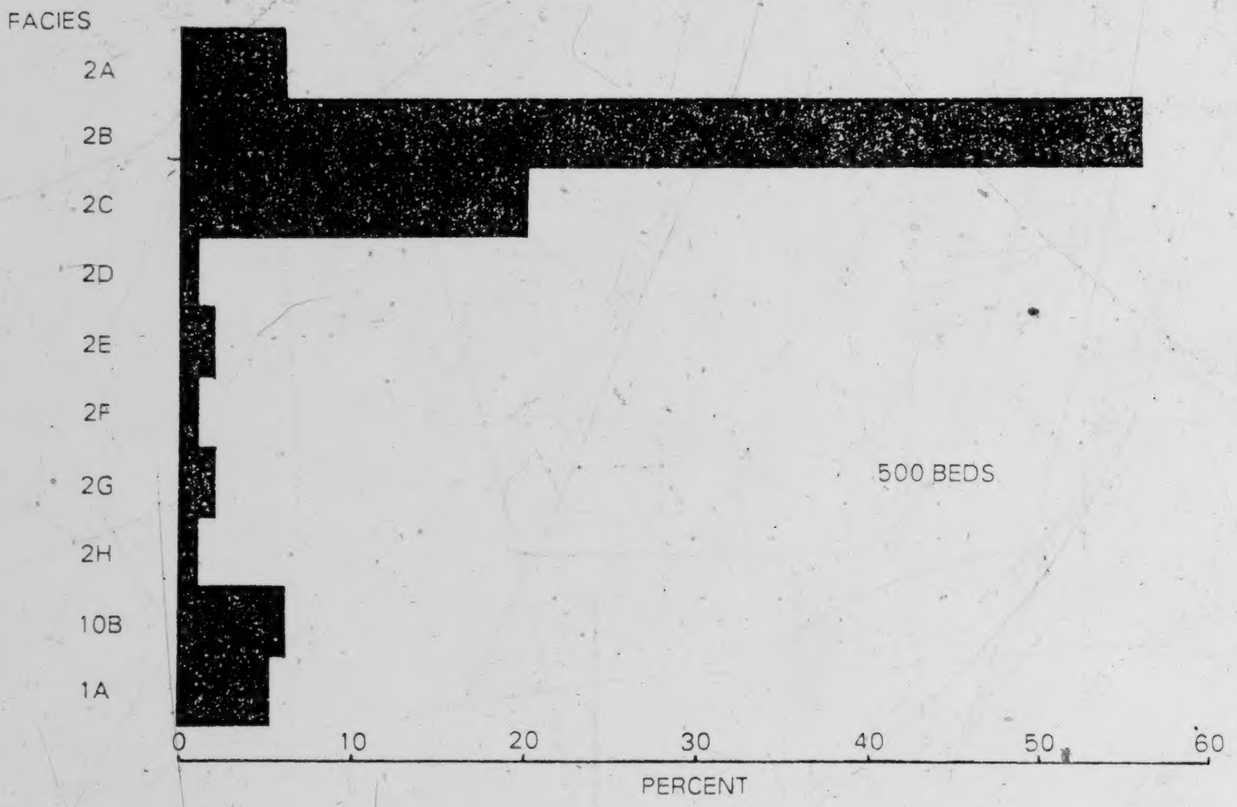

Figure 2.12. Percentage of individual facies which comprise Facies Association 3

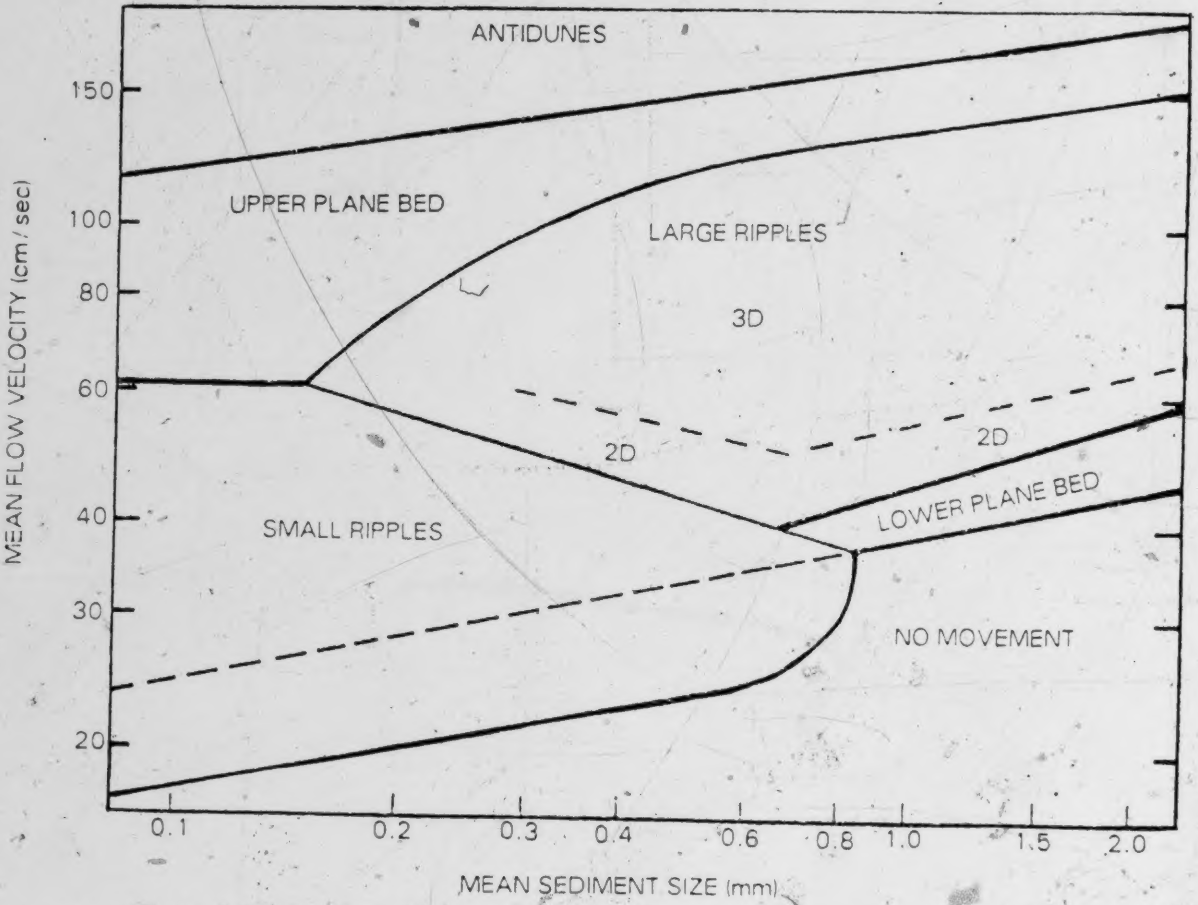

Figure 2.13. Bedform stability plots on size-velocity diagram. Current strength needed to form upper plane beds in 0.2 mm sand is about 80 cm/sec to 120 cm/sec. (Modified from Harms et al., 1982).

sandstones in Facies Association 3 suggests deposition from very high energy, upper flow regime currents. Figure 2.13 shows that the current strength needed to form upper plane beds in 0.2 mm sand is about 80 cm/sec to 120 cm/sec. Because 56 % of Facies Association 3 consists of these upper flow regime parallel laminated sandstones a strong unidirectional current must have been active for much of the period of Facies Association 3 deposition. This current was probably a semi-permanent geostrophic current flowing from north to south that was periodically enhanced by storm activity. In those sandstones with high angle dips (> 10°), the higher cross-bedding angles occur towards the base of the beds and fan over 10 or 15 cm into parallel laminated sandstones with low angle dips (< 5°). This small-scale facies-assemblage of Subfacies 2G (high angle cross-bedded sandstone) overlain by Subfacies 2B or 2C (sandstones with flat or low angle dips) is interpreted as hummocky cross-stratification. Other common sequences consist of parallel laminated sandstones (Subfacies 2B) overlain by ripple or trough crossbeds (Subfacies 2D or2E) capped by a thin shale (Facies 10B, Figure 2.14A). This small-scale facies-assemblage may be interpreted as the B, C and D divisions of the Bouma sequence. The sandstones with Bouma sequences and those with hummocky cross-stratification suggest that these sandstone assemblages within Facies Association 3 were deposited by sediment-gravity flows and strong wave-surge currents, probably recording storm events. These currents were able to scour the underlying sediments and then deposit parallel laminated sands (upper flow regime) and ripple or trough cross-bedded units (lower flow regime) as the current waned. With the onset of low energy, fair-weather conditions, mud drapes were deposited from suspension onto the rippled sandstones, recorded as preserved shale interbeds. When the next high energy event occurred, the scouring action of the current often removed the mud drapes which were then redeposited as intraclasts, suggested by the abundance of shale and siderite rip-up clasts towards the bases of graded beds (Figure 2.14B).

Other facies present in Facies Association 3 are; subfacies 2A (massive sandstones), subfacies 2F (bioturbated sandstones), subfacies 2H (convoluted sandstones), subfacies 10B (black shale) and subfacies 1A (sandstones with argillaceous interlaminae). Subfacies 2A (massive sandstone) beds were deposited very rapidly from suspension with no sedimentary structures forming. These beds are probably associated with storm surge

FIGURE 2.14.

(all cores are 10 centimetres in diameter)

2.14A. Photograph of core shows parallel-laminated fine-grained sandstone (Subfacies 2B) overlain by trough cross-bedded fine-grained sandstone (Subfacies 2E) capped by a thin shale drape (Facies 10B) (shown by arrow) (well 9-3-35-3W5, 2097.5 m).

2.14B. Core photograph of parallel-laminated fine-grained sandstone with abundant shale and siderite rip-up clasts (shown by arrows) (well 14-25-34-3W5, 2078.5 m).

2.14C. Core photograph showing sharp load contact between fine-grained sandstone (Facies Association 3) and conglomerate (Facies Association 2)(well 10-3-34-4W5, 2298 m).

2.14D. Core photograph showing abrupt load contact between fine-grained sandstone (Facies Association 3) and conglomerate (Facies Association 2)(well 6-13-34-3W5, 2083.7 m).

FIGURE 2.14

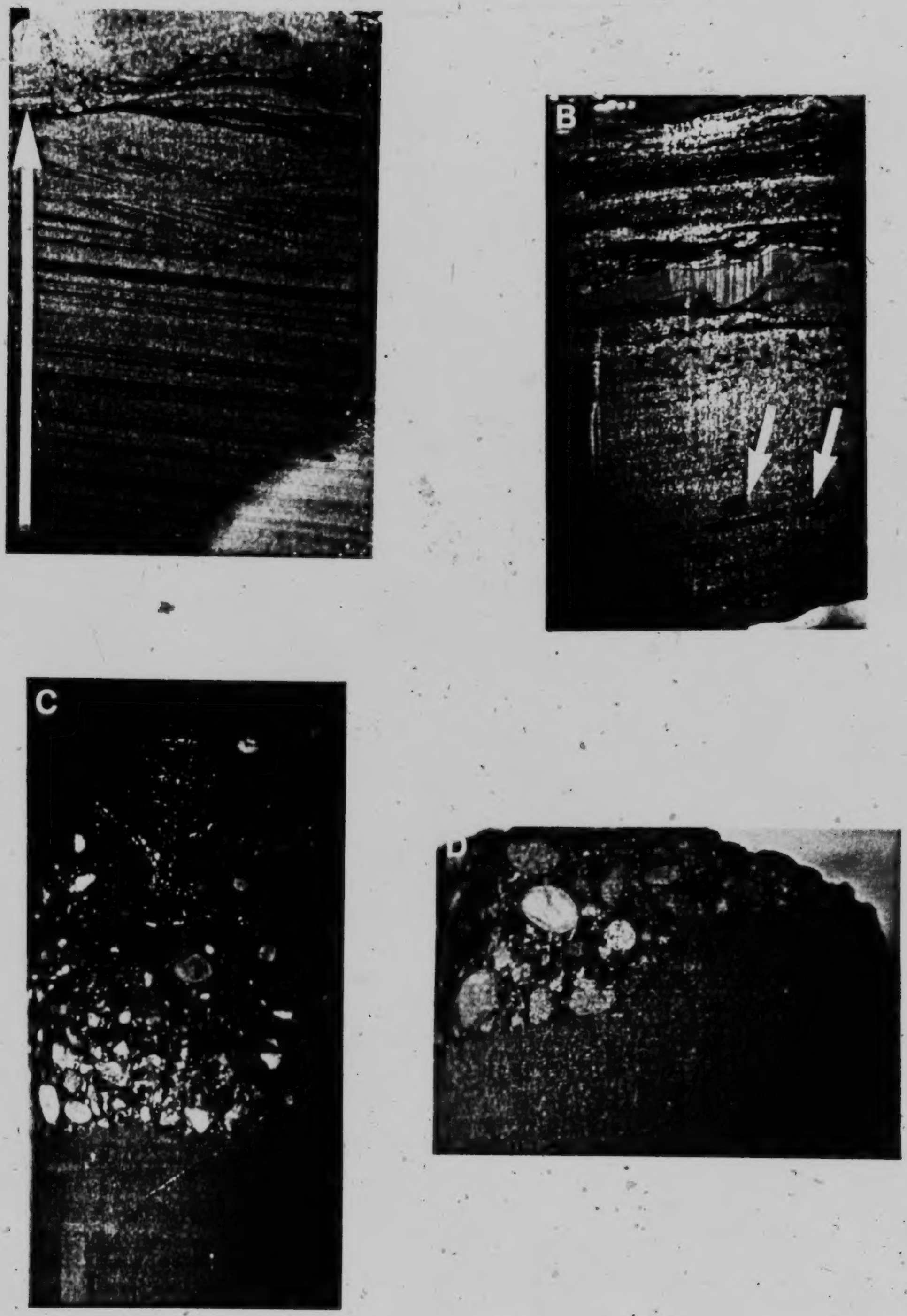

ebb currents which carried sand seaward in suspension and abruptly deposited it as the current waned. Some subfacies 2A beds are probably stratified but stratification is not observed because there is no change in grain size within the bed. In other cases drilling mud and scoring by the core barrel have obstructed the view of stratification.

Bioturbation of the sediments (subfacies 2F) represents recolonization of the substrate by benthonic fauna following a major storm event. Subfacies 2H (convolute crossbedded fine-grained sandstone) beds represent syn-sedimentary or early post depositional liquefaction of sandstone beds. This type of bedding is relatively rare and is formed as a result of abrupt loading of sediments by storm or sediment gravity flow deposits. Subfacies 1A is typical of the base of Facies Association 3 where the gradual transition from Facies Association 4 takes place. These beds were deposited by alternating periods of high and low energy conditions. Periods of high energy were associated with intense storm activity or strong geostrophic currents and the deposition of sand; periods of low energy occurred under fairweather conditions with the deposition of mud from suspension. Other shale breaks which occur within Facies Association 3 (Subfacies 10B) were also deposited during fairweather periods when marine currents and storms were inactive. Where these beds are relatively thick they were deposited in interbar areas where they were not later reworked by currents or storms. The fine-grained sandstone Facies Association 3 is a laterally extensive wedge of sediment, which varies considerably in thickness (Figure 2.11, in pocket). The thickest accumulations of this facies association occur on a topographic high, interpreted as a sand ridge, running from the northwest corner of the diagram to the southeast corner. In the central portion of the map area, the thickness of the fine-grained sandstones reaches 13.5 metres in 16-5-35-3W5 (well 46) and 14.0 metres in 14-9-35-3W5 (well 52). To the southwest and west, and offlapping the topographic high, the fine-grained sandstones thin to 5.5 metres at 11-28-34-4W5 (well 34) and 6.5 metres at 6-8-35-4W5 (well 65). A similar thinning of this facies occurs to the northeast of the fence diagram. Facies Association 3 is dominated by current and storm produced lithofacies (Figure 2.12). Storms initially entrained sediment and carried it from the shoreface out onto the shelf. As the sediments were deposited a marine geostrophic current, enhanced by the storms, continued to transport the sediments by traction. In this way the offshore bar was constructed by reworking of storm transported sediments by a strong marine current.

Facies Association 2 coarse-grained sandstone and conglomerate occurs as three separate units in the study area. Two of these units lie within the Lloydminster Shales and are referred to as the Viking "A" sandstones. The third unit rests on Facies Association 3 with an erosional or loaded contact and is referred to as the Viking "B" conglomerate (Figure 2.14C and 2.14D). The Viking "B" conglomerate is the primary hydrocarbon reservoir rock in the Garrington Oil Field. Figure 2.15A shows the percentages of the various facies which comprise the Viking "B" conglomerate. Figure 2.15B groups together those facies that are formed by similar processes.

The Viking "B" conglomerate is most commonly structureless matrix- or clast-supported, but may also have low-to high-angle crossbeds. Normally and inversely graded conglomerates are common in thick conglomerate sequences. Conglomerates with shale matrix are common at the top of the sequence where the transition to the Lloydminster shales takes place. Coarse-grained sandstones are also common in the Viking "B" conglomerate section. These beds occur randomly interbedded with the conglomerate beds and are usually low-angle crossbedded. Where they occur at the top of the Viking "B" conglomerate section they are bioturbated.

Structureless conglomerates (Facies 3A and Facies 4A) comprise 33.3 % of all Viking "B" conglomerate beds. These beds are interpreted as recording rapid deposition from a density current or sediment gravity flow, possibly associated with storm-surge ebb currents. In these deposits clasts were apparently unable to move relative to one another and thus no sedimentary structures, such as grading or stratification, formed.

Graded conglomerates form approximately 10 % of the Viking "B" conglomerate beds. Inversely graded, matrix-supported conglomerates are the most common type of graded conglomerates (Figure 2.15A). Inversely graded conglomerates maybe overlain by normally graded conglomerates. Where this occurs, a small scale facies assemblage consists of matrix-supported inversely graded conglomerate (Facies 5A) overlain by matrix-supported normally graded conglomerate (Facies 5B). Graded matrix-supported conglomerate was deposited from sediment gravity flows. Inverse grading formed when dispersive pressures were generated within the flow. As clasts collided with each other within the flow smaller ones worked their way down between the larger ones giving rise

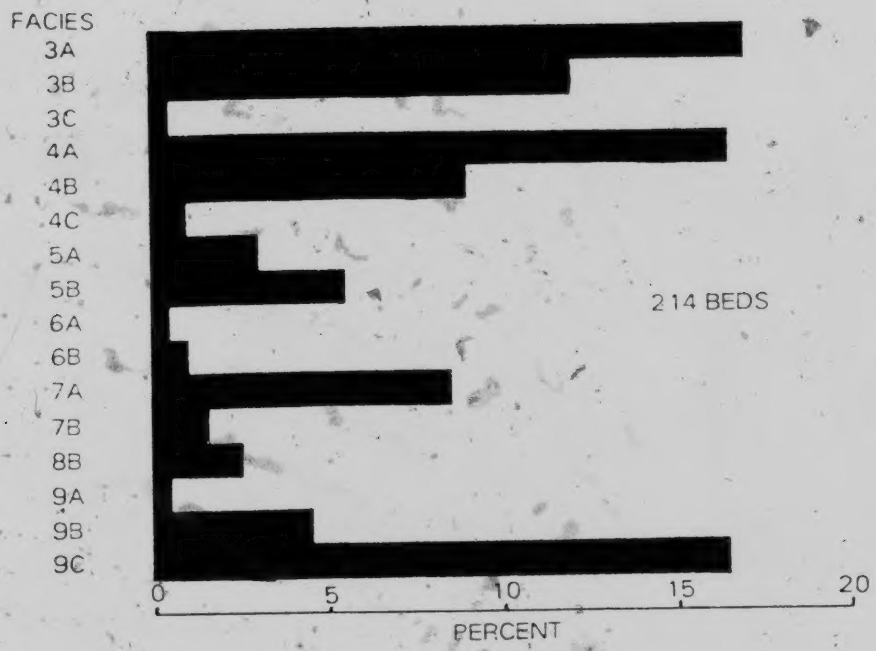

Figure 2.15A. Percentage of facies which comprise the Viking "B" conglomerate beds of Facies Association 2.

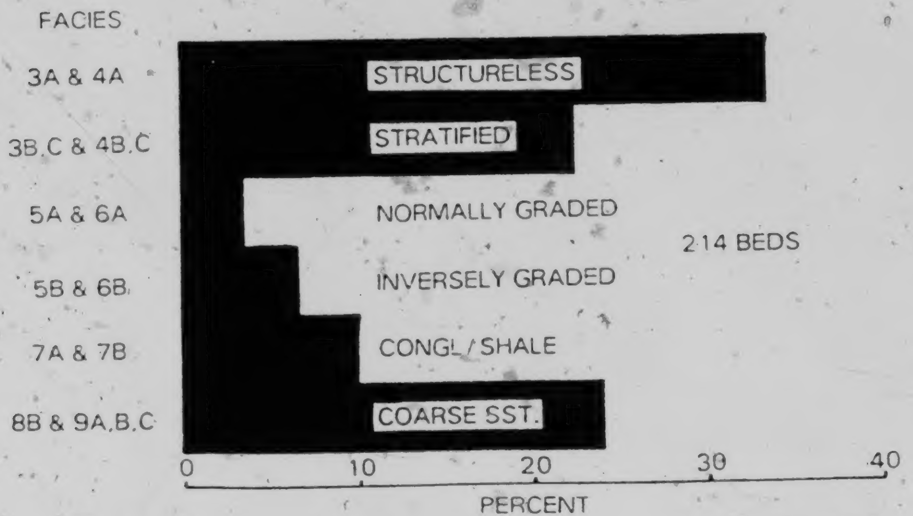

Figure 2.15B. Percentages of facies which comprise the Viking "B" conglomerate beds of Facies Association 2 grouped by similar sedimentary structures or mode of emplacement.

to inverse grading (kinetic sieve of Middleton, 1970). Normally graded matrix-supported conglomerates exhibit mainly coarse tail grading. Normal grading indicates deposition of finer and finer material from one current during bed aggradation, and also implies a sorting of clast sizes within the current and a diminishing flow strength during deposition. The inversely graded-normally graded couplet implies a flow in which sediments at the base are highly concentrated and moving by dispersive pressure while the sediments above are dominated by turbulent motion. Inversely graded and normally graded clast-supported conglomerates are relatively rare in the study area. Where they occur they were probably also emplaced by sediment gravity flows similar to those that emplaced the matrix-supported graded units with fines transported in suspension above the bed.

Quite commonly clast-supported conglomerate interbeds are present in predominantly matrix-supported units. This small scale facies assemblage consists of Facies 4B or 4C (clast-supported low- to high-angle stratified conglomerate) interbedded with Facies 3B or 3C (matrix-supported low- to high-angle stratified conglomerate). This type of assemblage represents the reworking of sediment gravity flow deposits into migrating dunes and gravel waves by pulsating geostrophic or longshore currents. Low- and high-angle cross-bedded conglomerates account for 22.5 % of the Viking "B" conglomerates. Commonly interbedded with these facies are Facies 9B and 9C (high- and low-angle cross-stratified coarse-grained sandstones). The coarse-grained sandstone facies make up 24 % of the Viking "B" conglomerate beds. These beds also represent the migration of dunes and gravel waves. When the currents were relatively strong coarse sand was transported above the bed in suspension and pebbles were rolled on the bed. When current velocity waned the pebbles ceased rolling and the sand fell out of suspension and was transported by traction. In this way cross-stratified matrix- and clast-supported conglomerates and coarse-grained sandstones were interbedded.

Mixed conglomerate / shale beds are common at the top of the Viking "B" conglomerate section. This facies accounts for approximately 10 % of the Viking "B" conglomerate and forms by transgressive currents mixing the top of the Viking "B" into the first deposits of the Lloydminster shale. Minor bioturbation also occurs at this interface and is responsible for some additional mixing of the conglomerate and shale.

From the above discussion it can be seen that the Viking "B" conglomerates are dominated by two types of depositional processes. Sediment gravity flows are responsible for the emplacement of 43.5 % of the Viking "B" conglomerates (Structureless and Graded Facies, Figure 3.15B). Reworking of the sediment gravity flow deposits by marine currents is responsible for 56.5 % of the Viking "B" conglomerates (Stratified, Conglomerate / Shale and Coarse-grained Sandstones, Figure 3.15B). The reworking of the Viking "B" conglomerate into gravel waves and dunes is evident from the isopach map of the conglomerate and coarse-grained sandstone (Figure 2.24). This isopach map clearly shows that the conglomerate has been molded into ridge and swale topography. The thickness of the Viking "B" conglomerate is highly variable and ranges from 0 to 3.6 metres in the study area. The thickest packages of this conglomerate occur on a northwest-southeast trend corresponding to a topographic high or "sand ridge", mentioned above in the description of Facies Association 3. In 10-12-35-3W5 (well 58, Figure 2.11), the conglomerate is 3.6 metres thick, whereas in 14-6-35-3W5 (well 47, Figure 2.11), it is only 0.3 metres thick.

The Viking "A" pebbly and coarse-grained sandstones ("grits") are relatively thick in the southwestern portion of the study area (Well 11-28-34-4W5), corresponding to the southeast end of the Caroline gas field. The Viking "A" pebbly and coarse-grained sandstones are gas-bearing and where they are perforated during completion of Viking "B" oil wells in the western portion of the Garrington Oil Field may cause very high gas-oil ratios, as observed in Well 6-11-35-4W5. In the thicker intervals the sediments are high- to low-angle cross-stratified. Where the units are thin, they are commonly extensively bioturbated, and most of the primary sedimentary structures are often destroyed. Figure 2.16 shows that the Viking "A" sandstone units are comprised of facies 9B and 9C units and facies 8B units. The Viking "A" sandstones occur abruptly within the Lloydminster shales and are interpreted as prograding sand deposits emplaced during minor regressive events during a generally transgressive period. The coarse-grained sandstones were deposited by strong currents probably associated with storms, and subject to reworking by semi-permanent currents and waves. High angle cross-stratified sandstones are interpreted as planar tabular crossbeds and represent the migration of dunes or megaripples moved by unidirectional marine currents. Low angle cross-stratified sandstones with gently curving, convex upward laminae maybe interpreted as hummocky cross-stratification or as trough crossbeds of migrating three dimensional large ripples. Where the Viking "A" sandstones thin to the east they are extensively bioturbated (Facies 8B). This facies represents the recolonization of the substrate by bottom dwelling organisms after the deposition of sand ceased.

The lowermost Viking "A" pebbly and coarse-grained sandstone bed is present primarily in the southern half of the study area and in Township 35, Range 4 west of the Fifth Meridian. This bed pinches out in Township 35, Ranges 2 and 3 west of the Fifth Meridian as shown in the fence diagram (Figure 2.11, in pocket). This bed lies within 50 cm of the underlying Viking "B" conglomerate and should be carefully avoided when completing Viking "B" oil wells.

The uppermost Viking "A" pebbly and coarse-grained sandstone bed is most prevalent in the northern half of the study area and in Township 34, Range 4 west of the Fifth Meridian, where it is up to 2.5 metres thick. This bed is about 4 metres above the Viking "B" in the western portion of the study area and thins to the east where it lies about 6 metres above the Viking "B". Both Viking "A" units are interpreted as representing minor regressive events in a generally transgressive sequence. The coarse-grained sandstones were emplaced by strong currents associated with storms and subject to reworking by semi-permanent currents and waves.

Facies Association 1 consists of the Lloydminster shales. In the study area this facies association varies from 19 to 27 metres in thickess and is primarily comprised of black, fissile, marine shales (subfacies 10B). Rippled, lenticular interbeds of fine-to-very-fine-grained sandstones and rare bentonites also occur within this facies association. The shales were deposited from suspension into quiet water. The sandstone lenses represent occasional pulses of sediment dumped into the basin by strong unidirectional currents. Rippling of the fine-grained sandstones is probably due to weak bottom current action. The bentonites are wind blown volcanic ash deposits derived from volcanic activity to the west, possibly associated with the Crowsnest Volcanics, and were deposited from suspension into quiet water. Facies Association 1 represents a major marine transgression by the Boreal Sea into the Garrington area.

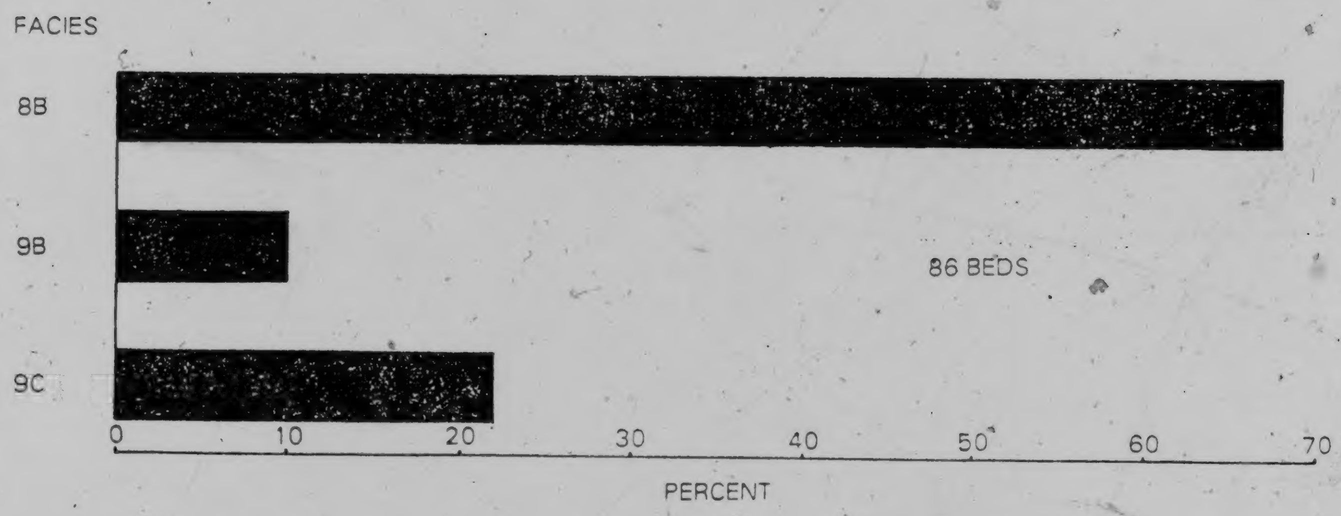

Figure 2.16. Percentages of facies which comprise the Viking "A" coarse-grained sandstone beds of Facies Association 2.

F. DEPOSITIONAL PATTERN AND FACIES DISTRIBUTION

In order to study the depositional pattern and facies distribution a number of isopach maps and computer generated block diagrams were constructed.

Figure 2.17 is a block diagram of the study area with the base representing the lower bentonite marker horizon (picked from logs) and the surface the top of the Viking "B" horizon. The block diagram reveals a complex topography with a general elongate high running from the northwest corner of the block to the southeast corner. To either side of this feature there are topographic low areas which follow the same trend as the topographic high (Northwest-Southeast). Figure 2.18 shows the topographic surface of the top of the Viking "B" unit relative to a datum 30 metres below the Base of Fish Scales marker, as picked from geophysical logs. In general, the same features are seen in this figure as in Figure 2.17. A topographically high feature trends from the northwest corner of the study area through the center and down to the southeast corner and is paralleled by topographically lower areas on either side. Although the two figures are not identical, the similarities are notable. The topographically high area most likely represents a "sand ridge" and the adjacent topographic lows inter-ridge "swales", similar to those documented by Swift et al. (1973) and Stubblefield and Swift (1976) off the east coast of the United States.

Isopach maps corresponding to the above figures are represented by Figures 2.19 and 2.20 (in pockets). Figure 2.19 is an isopach of the Viking Formation from the lower bentonite marker to the top of the Viking "B" horizon. This figure shows the thickest accumulation of Viking sediments occurring as small pods on a generally west-northwest to south-southeast trending topographic high. Parallelling the topographic high to either side are topographically lower areas. The low on the northeast side of the ridge is 10 to 12 meters lower than the highest parts of the ridge. The low on the southwest side is 8 to 10 meters lower than the highest portions of the ridge. The dip of the ridge to the northeast is approximately 0.2° and the dip to the southwest is approximately 0.1°. The main ridge appears to be transversed by a topographically lower swale in the northwest and partially transversed by another low to the southeast. Also of interest in this isopach is a thickening of the sediments in the northern part of the map on the boundary of Range 2 and Range 3. This may represent the southern tip of another ridge occurring parallel to the

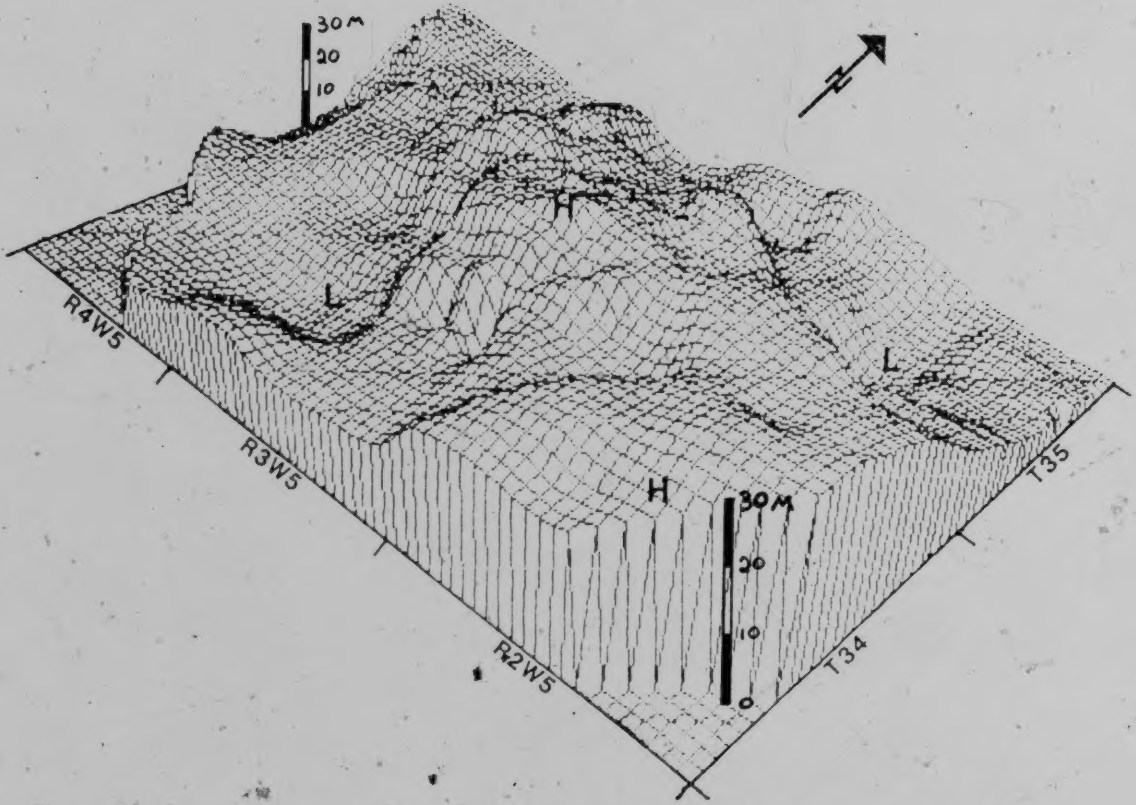
30M
20
10
H
L
H
L
30M
20
10
0
R4W5
R3W5
R2W5
T34
T35

Figure 2.17. Block diagram: Bentonite marker to the top of the Viking "B" horizon. Base of the block is the bentonite marker. The topographic surface is the top of the Viking "B" unit. H = topographic highs, L = topographic lows mentioned in the text.

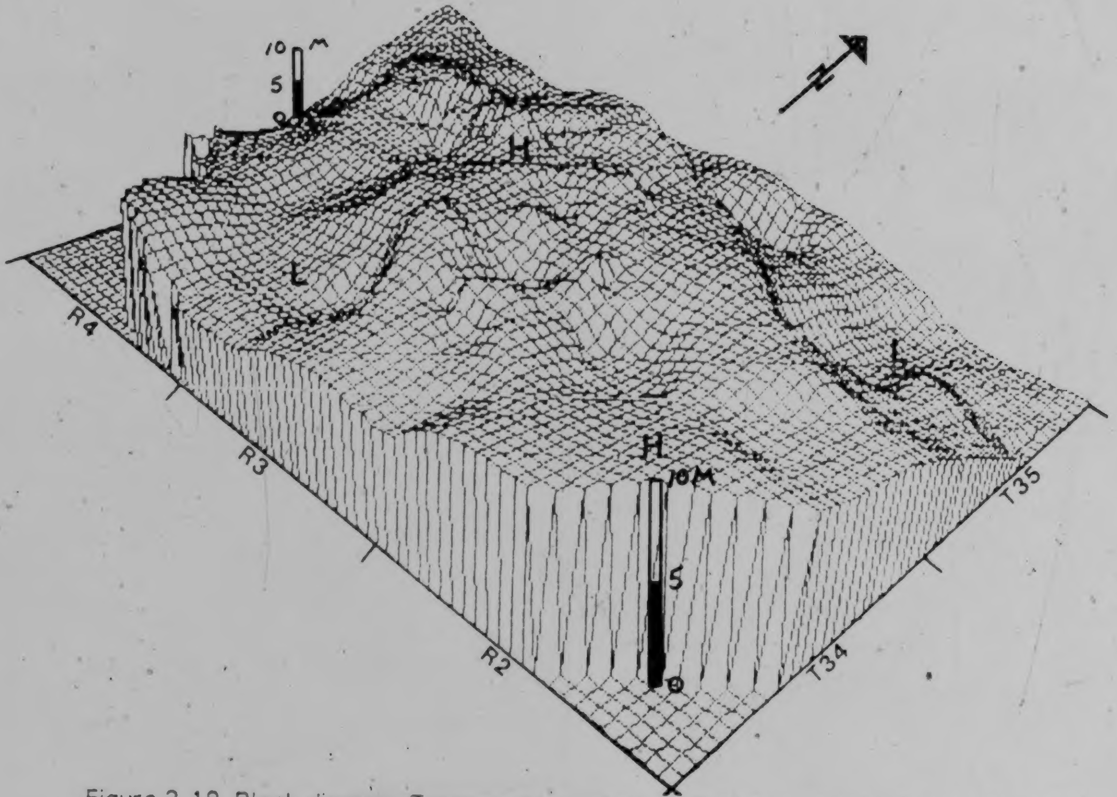

N
10 m
5
0
H
L
L
R4
R3
R2
T34
T35
H
10M
5
0

Figure 2.18. Block diagram: Topographic surface of the Viking "B" unit relative to a Base of Fish Scales datum. Base of the block is 30 m below the Base of Fish Scales marker. The topographic surface is the top of the Viking "B" unit. H = topographic highs. L = topographic lows mentioned in the text.

Garrington Oil Field.

Figure 2.20 (in pocket) is an isopach of the Lloydminster Shale. In general, the thinnest accumulations of this unit occur directly over the thickest portions of Viking sediments (see Figure 2.19). The top of the sand ridge is generally covered by 19 to 21 metres of shale. A thick accumulation of shale occurs to the northeast reaching up to 27 meters, and corresponds to an area of relatively thin Viking sediments as seen in Figure 2.19. To the southwest, the Lloydminster Shale thickens again corresponding to an area of relatively thin Viking deposition.

An embayment in the southeast portion of the ridge with 22 metres of shale corresponds to a similar feature in Figure 2.19. The northwest swale occurring in Figure 2.19 is not as obvious in the trends shown in Figure 2.20. Figure 2.21 is a block diagram representing the thickness of the fine-grained sandstone Facies Association 3. This figure again shows a form similar to Figures 2.17 and 2.18. The west-northwest to east-southeast trending high is flanked on either side by topographically lower areas or areas of thinner sandstone deposition. The northwest and southeast swales are clearly visible. The sandstone thickness on the ridge itself appears to split into two ridges (A and B) about halfway down the main ridge with a low area occurring between them.

An isopach map of the fine-grained sandstone facies-association (Figure 2.22, in pocket) confirms these features. A thick sandstone deposit trends west-northwest to east-southeast through the center of the map area. The thickest sandstone accumulations (12-14m) occur in areas corresponding to the thinnest accumulations of Lloydminster Shale (Figure 2.20) and to the thickest areas of Figure 2.19 (Bentonite marker to top of Viking "B"). The only major exception is the topographically low area in Figure 2.22 where the ridge appears to split into two smaller parts. To the southwest of the main ridge, a large swale runs parallel to the ridge and corresponds to an area of relatively thick Lloydminster sediments. To the northeast another swale runs parallel to the ridge and also corresponds to an area of thicker Lloydminster accumulations. A small tongue of sandstone enters the map area from the north approximately on the boundary of Range 2 and Range 3 and corresponds to a high area seen in Figures 2.17, 2.18 and 2.19 (in pocket).

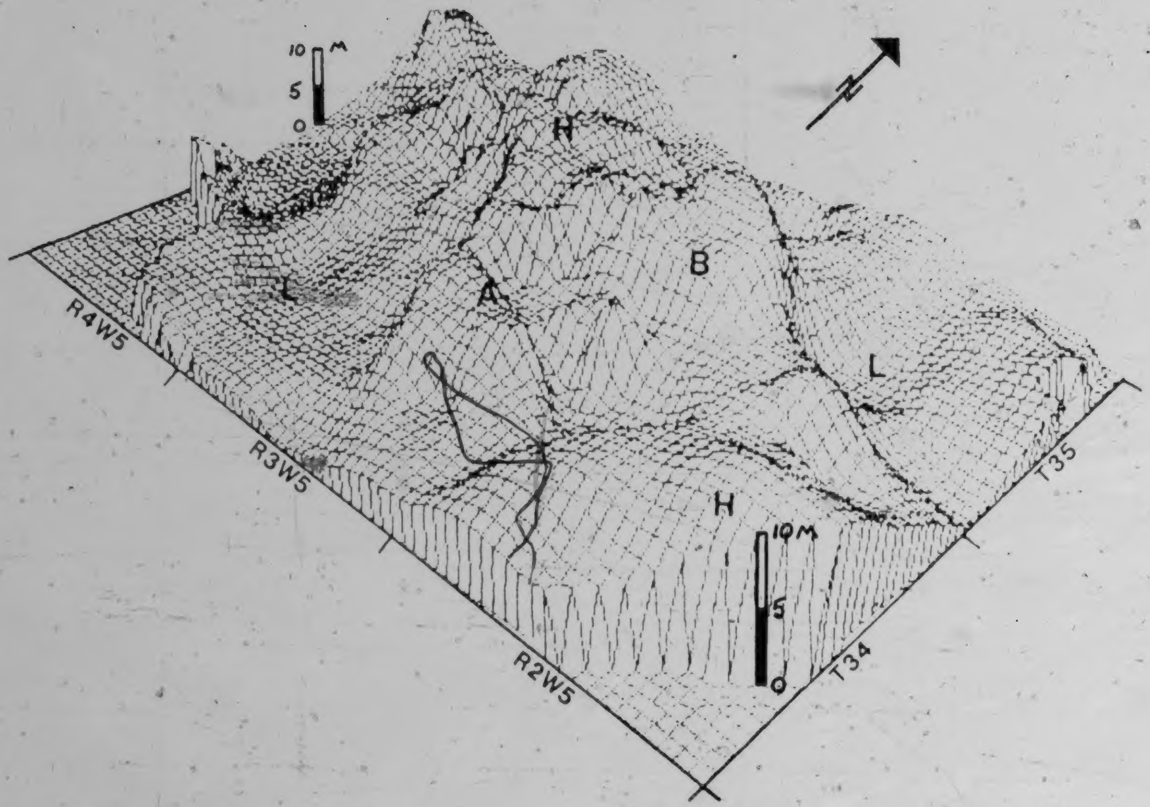
10 M
5
0
N
H
B
A
L
L
H
10 M
5
0
R4W5
R3W5
R2W5
T34
T35

Figure 2.21. Block diagram. Thickness of the fine-grained sandstone Facies Association 3. A and B show where the main ridge separates into two smaller ridges. H = topographic highs. L = topographic lows mentioned in the text.

Figure 2.23 is a block diagram showing the thickness of the conglomerate and coarse grained sandstone Facies Association 2. This figure shows a similarity to previous diagrams, most notably Figure 2.21 (fine-grained sandstone; Facies Association 3); however, the topography appears much more complex. The conglomerate thickens and thins rapidly, with the thickest accumulations occurring sporadically along the main ridge. The area to the southwest of the ridge has little conglomerate and corresponds to the topographic low of earlier figures. The area to the northeast of the ridge also has little conglomerate, with the exception of a small pod of conglomerate intruding into the map area from the north. The northwest and southeast transects are more subdued than in previous figures and the small embayment that bisected the ridge in Figure 2.21 has been partially filled by conglomerate and coarse sand.

The isopach map of the Viking "B" conglomerate and coarse-grained sandstone Facies Association 2 (Figure 2.24, in pocket) confirms the features seen in Figure 2.23. The isopach map reveals a very complex pattern of conglomerates. On the main ridge the conglomerate thickness ranges from less than 50 cm to greater than 3.5 metres. A pattern of small ridges, with relatively thick comglomerate accumulations, and swales, with thinner deposits of conglomerate, appear to have been superimposed on the main ridge. This system of smaller ridges and swales is aligned parallel with the main ridge trend. The thickest conglomerates generally occur in areas where thin accumulations of Lloydminster are present. These areas also correspond to areas of thick sandstone deposition (Figure 2.22, in pocket) and the thickest Viking sediment accumulations as seen in Figure 2.20 (in pocket). To the southwest a long trough runs parallel to the main ridge and represents an area which did not receive conglomerate. Further southwest of this trough another buildup of conglomerate occurs (southeast end of the Caroline gas field). To the northeast another trough feature is observed, trending parallel to the main ridge. A small tongue of conglomerate penetrates the map area from the north at the boundary of Range 2 and Range 3 (Figure 2.24, in pocket).

A block diagram of the combined fine-grained sandstone and conglomerate thicknesses (Facies Associations 3 and 2, Figure 2.25) shows more subdued features than the conglomerate block diagram and more accentuated features than the fine-grained sandstone block diagram. The main ridge and adjacent swales are still clearly visible. An

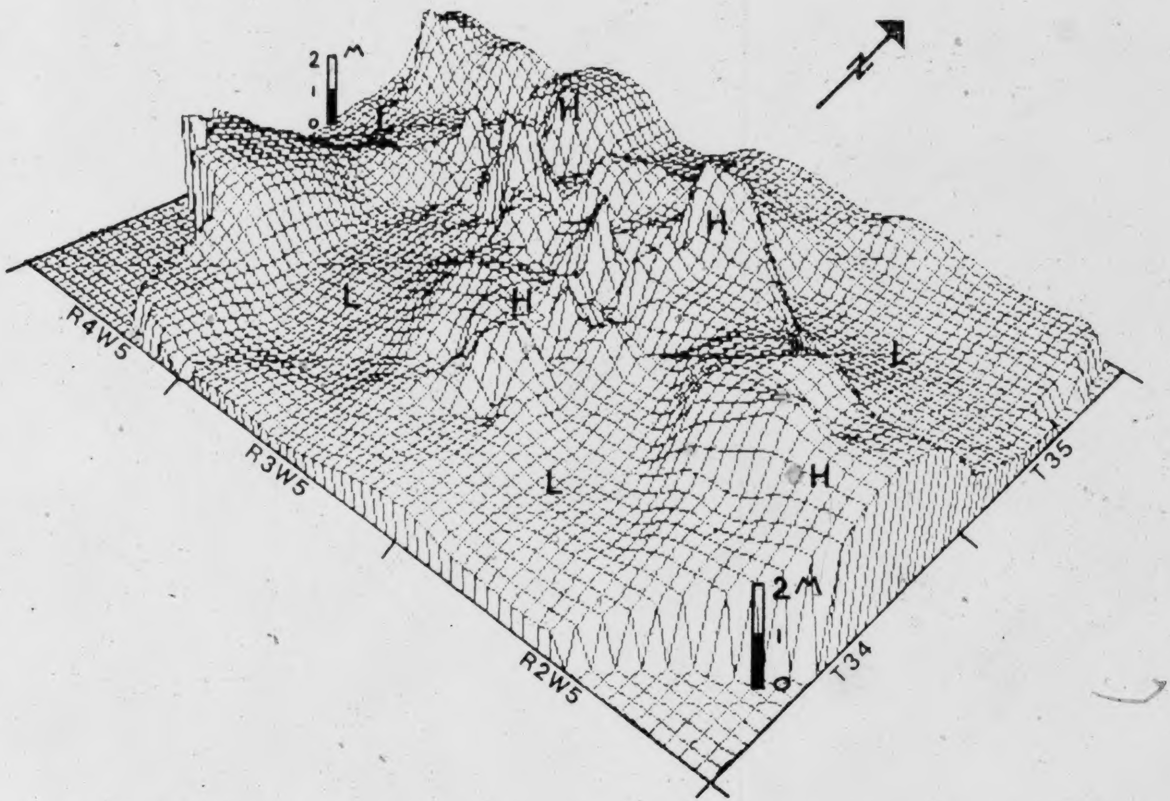
2
1
0
M
L
H
H
H
L
L
H
L
2
1
0
M
N
R4W5
R3W5
R2W5
T34
T35

Figure 2.23. Block diagram: Thickness of the conglomerate and coarse-grained sandstone Facies Association 2. Note the complex topography. H = major topographic highs, L = major topographic lows mentioned in the text.

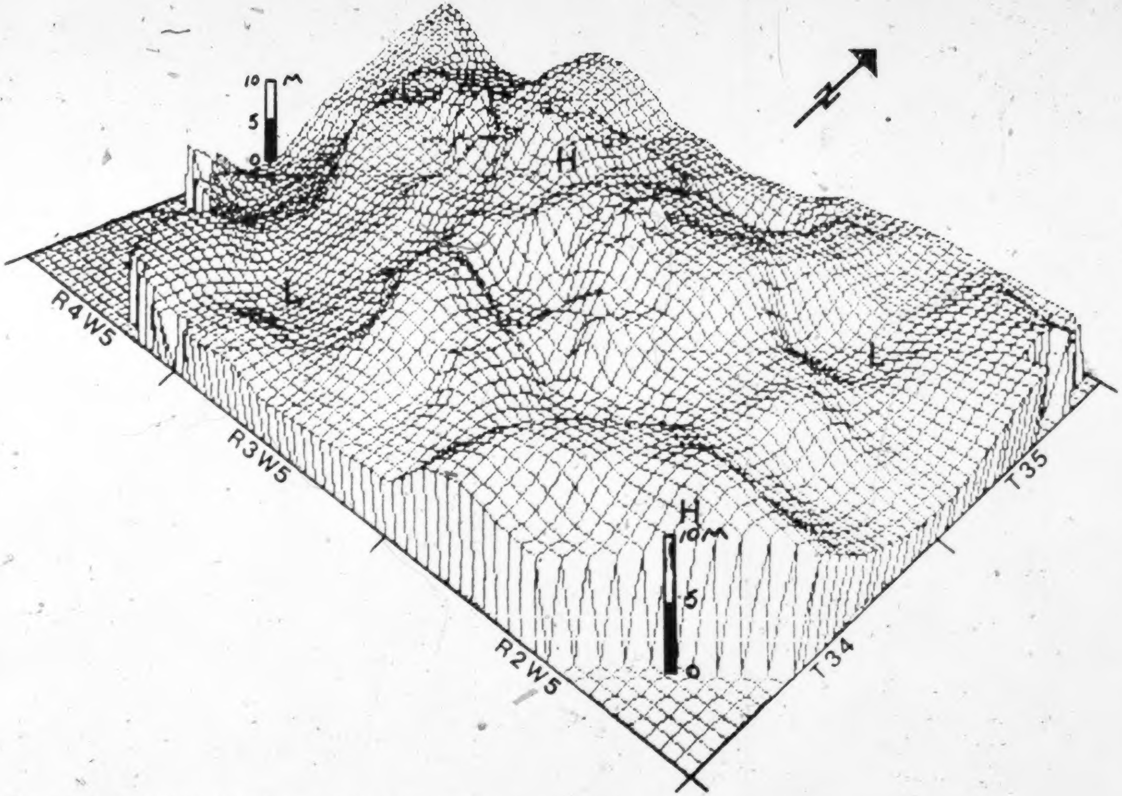
10 M
5
0
H
L
L
H
10 M
5
0
N
R4W5
R3W5
R2W5
T34
T35

Figure 2.25. Block diagram: Combined thicknesses of the fine-grained sandstone and coarse-grained sandstone and conglomerate (Facies Associations 3 and 2). H = topographic highs, L = topographic lows mentioned in the text.

isopach map of the combined fine grained sandstone and conglomerate thicknesses (Figure 2.26, in pocket) confirms these features. The thickest accumulations of fine-grained sandstone and conglomerate occur on the main ridge and exhibit a relatively complex pattern. These thicker areas range from 12 to 15 meters and correspond to the thinnest accumulations of Lloydminster Shale (Figures 2.18 & 2.20, in pocket). A tongue of sediment in the southwest corner of the map area represents the southern tip of another sand ridge comprising part of the Caroline gas field. To the northeast a similar feature once again enters the map area on the boundary of Range 2 and Range 3. This second tongue may represent another sand ridge paralleling the Caroline and Garrington ridges.

Other workers in the Cretaceous of the Western Interior have postulated that structural controls may have been important in determining the positions of shelf sand ridges (Griffith, 1981; Swagor et al., 1976). Griffith (1981) proposed that deposition of sand and conglomerate was localized seaward of a shelf break. No such structure is apparent in the Garrington area. Figure 2.27 is a block diagram of the study area showing the regional dip of the Viking Formation relative to present sealevel. The surface of the diagram (representing the top of the Viking"B" horizon) shows a gently undulating topography with a regional dip to the west-southwest. No large-scale structural features are evident. Small-scale highs and depressions can be seen to follow the trend seen in previous figures and represent the variation in sandstone and conglomerate accumulation in the Garrington oil field. The isopach map of sea level to the top of the Viking "B" horizon (Figure 2.28, in pocket) shows features similar to Figure 2.27. The regional dip is to the west or slightly west-southwest at about 10 m per kilometer (0.57°). In Township 35, Range 4 west of the Fifth Meridian, a minor structural feature occurs, apparently corresponding to an area of relatively thick sandstone and conglomerate accumulation. In the northeast corner of Township 34, Range 3 west of the Fifth Meridian, a small circular structural depression occurs. This area corresponds to a zone of highly complex depositional patterns for the sandstones and conglomerates (Figures 2.21, 2.22, 2.23, 2.24, 2.25, and 2.26, in pocket). In general, however, the structure map shows that large scale structural elements are not important in influencing the facies patterns in the Garrington oil field. Hydrocarbon accumulations occur in stratigraphic traps and in updip

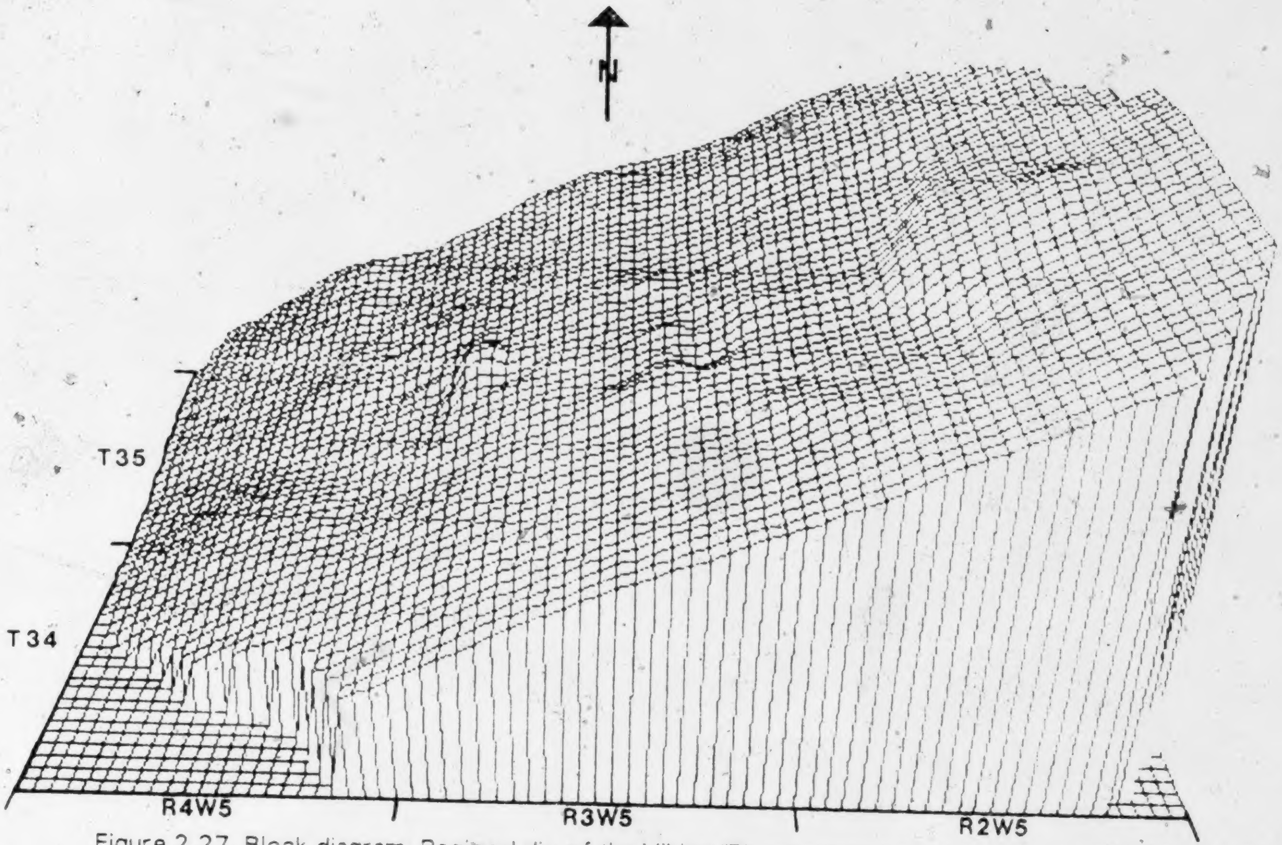
N
T35
T34
R4W5
R3W5
R2W5

Figure 2.27. Block diagram: Regional dip of the Viking "B" unit relative to present sea level.

Vertical exaggeration is approximately 30 times.

pinchouts of sandstone and conglomerate. The Lloydminster Shale acts as a vertical and lateral barrier to petroleum migration.

G. GARRINGTON DEPOSITIONAL ENVIRONMENT

The coarsening-upward sequence in the Viking Formation at Garrington is interpreted as representing a regression associated with progradation of a shoreline-attached clastic wedge. Figure 2.29 is an interpretation of the Cretaceous Seaway at the time of Viking deposition. Sediments were carried to the foreland basin by major river systems and deposited initially along the shoreline. Some sand was transported directly to the shelf by sediment bypass, but the bulk of the sediment was moved basinward by periodic storm-surge ebb currents. Rooted zones to the west and southwest place the Garrington Oil Field 30 to 50 km from the Viking paleoshoreline. Water depth at this position was probably as shallow as 20 to 50 m. Walker (1984) states that fairweather wavebase should be from 5 to 15 meters. The bulk of the Viking Formation at Garrington appears to have been deposited between storm and fairweather wavebase as evidenced by the presence of hummocky cross-stratification in Facies Association 3. Slatt (1984) reported sandridges 40 kilometers long, 25 kilometers offshore in only 20 meters of water along the Gulf Coast. Walker (1984) reported water depths of 21 meters 50 kilometers offshore in the same area. Walker (1984) also reports that the average shelf gradient is only 0.002 degrees so it seems very reasonable that water depth at Garrington during deposition of the Viking Formation was only 20 to 50 meters. The source of the sediment was from the southwest, as indicated by the thickening of the clastic wedge to the southwest and the thinning and "shaling" out to the northeast. Where the sand was deposited in deep water, below storm-wave base, beds were commonly extensively bioturbated with sedimentary structures completely destroyed (Facies Association 4, Figure 2.30). Where bioturbation has not been extensive, the sandstones rest on shales with sharp loaded contacts. In some places, well-defined ball-and-pillow structures and flame structures are seen.

In shallower water (between storm- and fair-weather wave base) a thick sand wedge was deposited (Facies Association 3). This wedge of sediment was deposited in a high energy environment and is dominated by low-angle stratification. With continued

CRETACEOUS SEAWAY : VIKING TIME

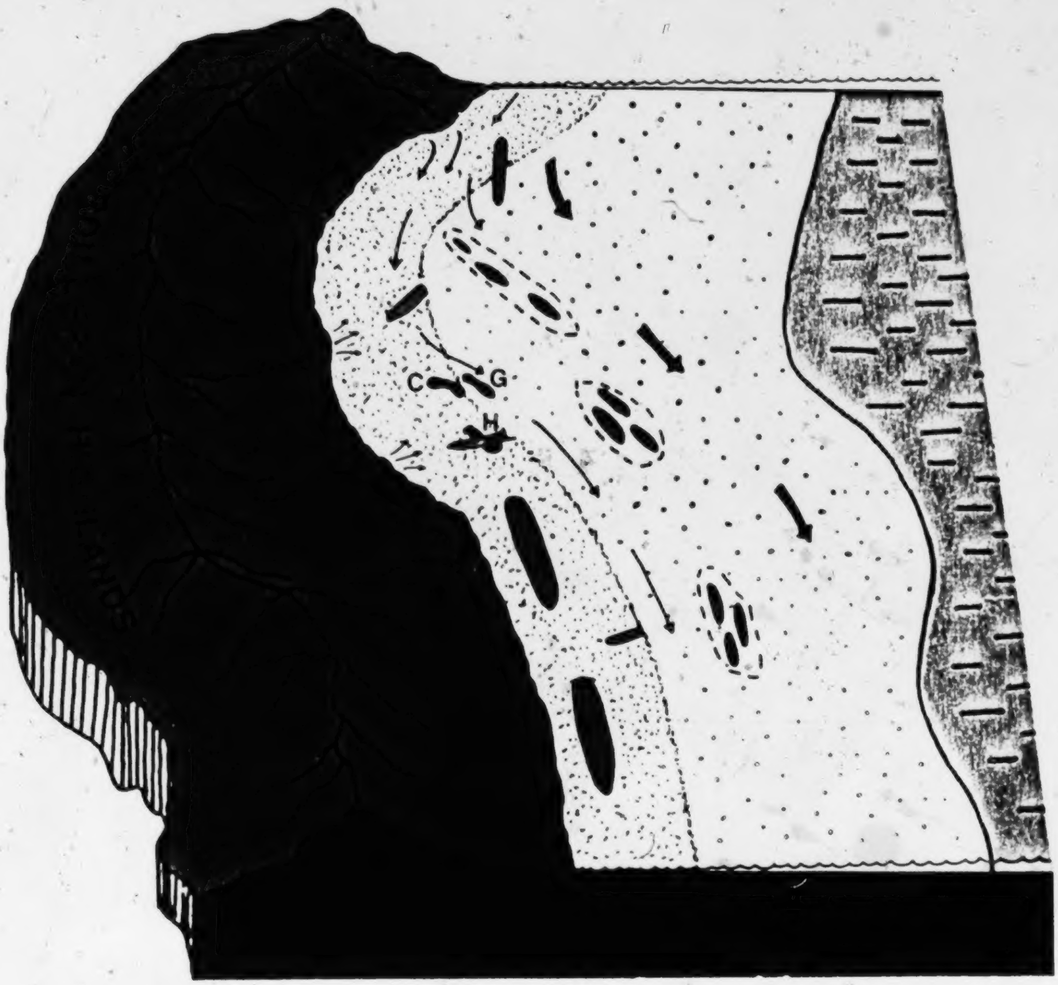

Figure 2.29 Diagram showing a paleoreconstruction of the Late Early Cretaceous Seaway at the time of Viking deposition. Green indicates subaerial exposure, Yellow indicates continental shelf sediments, Brown indicates shale basin. Red patches represent sand ridges; G = Garrington, H = Harmattan East and C = Caroline. Blue areas represent channels which may have been feeder systems from the nearshore to the shelf. Arrows indicate flow direction.

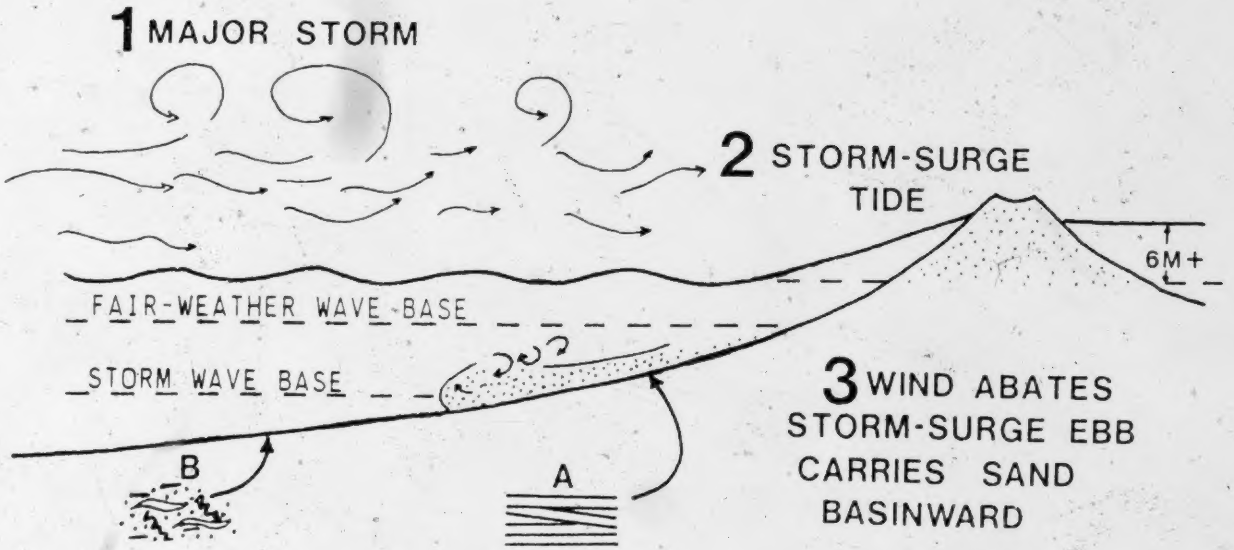
1 MAJOR STORM
2 STORM-SURGE TIDE
6M+
FAIR-WEATHER WAVE BASE
STORM WAVE BASE
3 WIND ABATES STORM-SURGE EBB CARRIES SAND BASINWARD
B
A

Figure 2.30. Diagram relating a major storm (1) to storm surge tide (2) and storm-surge ebb current (3). At Garrington parallel-laminated, low angle cross-stratified sands were deposited between storm and fair-weather wave base (A). Below storm wave base sand was deposited on a muddy bottom. Extensive bioturbation mixed the sand and mud (B). Modified from Walker (1979) with representative facies drawn from this study.

shoaling, the strandline migrated to the northeast and the sand wedge was extensively reworked by storm waves and geostrophic and longshore drift currents. The geostrophic currents and longshore drift transported sand from north to south parallel to the coast. Periodic storms combined with these currents to generate large-scale secondary circulation currents or helical flows which gradually molded the sand wedge into a broad sand-sheet with superimposed dune and megaripple fields (Figure 2.31). Strong geostrophic flows similar to the Agulhas Boundary Current (Flemming, 1980) continued to mold and maintain the ridges during fair-weather periods.

The top of the coarsening-upward sequence in the Viking Formation at Garrington consists of coarse-grained sandstone and conglomerate (Facies Association 2). These rocks rest on the clastic wedge with an erosional or loaded contact. These sediments were deposited by storm-generated or storm-enhanced currents or sediment-gravity flows. An increased gradient to the basin may have been created by uplift in the source area to the west and by subsidence of the foreland basin due to loading of thrust sheets and extensive accumulation of sediment (Beaumont , 1984; Swift and Rice, 1984; Reinson et al., 1983). Rapid transport of the conglomerate and coarse-grained sandstones was probably initated by earthquake shock or storm-wave loading.

Once the sediments were transported to the shelf they were deposited, as the current waned, over paleotopographic highs. During fair-weather conditions the conglomerates and coarse-grained sandstones were extensively reworked by waves and ocean currents to form ridge and swale topography on the top of the sand ridge. After the emplacement of the conglomerates and coarse-grained sandstones, a major transgression occurred and the top of the Viking "B" was covered by marine shales of the Lloydminster Formation. Ocean currents mixed the top of the conglomerate into the shales.

At least two minor regressions occurred within the Lloydminster transgression and these are represented by the Viking "A" sandstones which lie above the Viking "B" unit and are interbedded and often intermixed with the Lloydminster Shale. The Viking "B" conglomerate and coarse-grained sandstone and the Viking "A" coarse-grained sandstones were deposited from a source area to the west. This suggests that prior to deposition of these rocks active tectonism altered the input of sediment to the shelf. A major episode

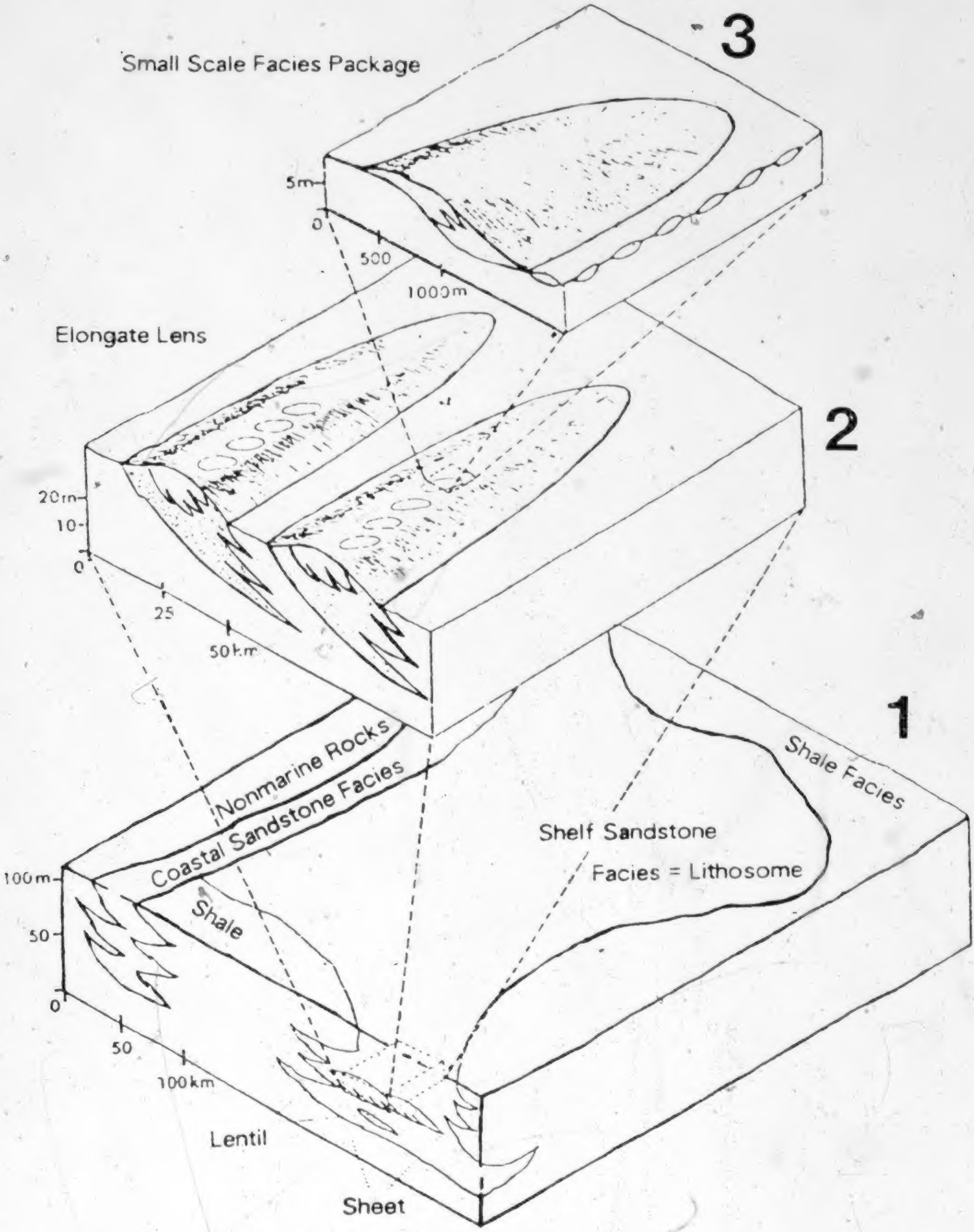
3
Small Scale Facies Package
5m
0
500
1000m
Elongate Lens
2
20m
10
0
25
50km
1
Nonmarine Rocks
Coastal Sandstone Facies
Shale
Shale Facies
Shelf Sandstone
Facies = Lithosome
100m
50
0
50
100km
Lentil
Sheet

Figure 2.31. Diagram showing hierarchy of shelf sandstone bodies. The clastic wedge is molded into broad sand sheets which in turn have smaller bedforms superimposed upon them (Modified from Shurr, 1984, from the Shannon Sandstone of southeastern Montana).

of thrusting could have resulted in the diversion of a large fluvial system, movement of the shoreline and/or delta lobe switching all of which would alter the pattern of sedimentation in the foreland basin.

III. MINERALOGY

This chapter describes the mineralogy of the Viking Formation at Garrington. Sixty-two samples selected from 19 wells were studied, including 14 conglomerates, 15 coarse-grained sandstones, 32 fine-grained sandstones and 1 shale. Figure 3.1 is a map of the study area showing the sample locations.

Methods used in the mineralogical study include hydrometer analysis, X-ray diffraction (XRD), scanning electron microscopy (SEM) and petrographic study. The percentages of clay-sized material were determined by hydrometer analysis. The major phases and the relative percentages of clay minerals were determined by X-ray diffraction. SEM studies provided information on the morphology and distribution of pore-lining and pore-filling clay minerals. Empirical estimates of the size of pores and pore throats were made from SEM studies. Table 3.1 lists the samples investigated. Abbreviations used in the tables and figures that follow are listed on pages 22 and 23.

A. BULK MINERALOGY

Thirty-six thin sections including 14 fine-grained sandstones, 12 coarse-grained sandstones and 10 conglomerates have been studied. Abundances of detrital grains and cements are based on point counts of 500 points per thin section. Porosity values are from core analysis or from point counts where core analysis was not available. The results are summarized in Tables 3.2 and 3.3 (Abbreviations on pages 22-23):

1. The conglomerates average 81 % detrital grains (range 75-85 %), 12 % cements (range 5-17 %) and 7 % porosity (range 3-11 %).
2. The coarse-grained sandstones average 77 % detrital grains (range 70-80 %), 15 % cements (range 8-26 %) and 8 % porosity (range 3-12 %).
3. The fine-grained sandstones average 72 % detrital grains (range 65-80 %), 20 % cements (range 10-28 %) and 8 % porosity (range 3-11 %).

The rocks were classified, based on the mineralogy of the detrital grains, according to Folk's scheme (1968)(Figure 3.2A). All of the conglomerates samples are quartzarenites. The coarse-grained sandstones are equally divided between quartzarenites and sublitharenites, and the fine-grained sandstones are all sublitharenites (Figure 3.2A).

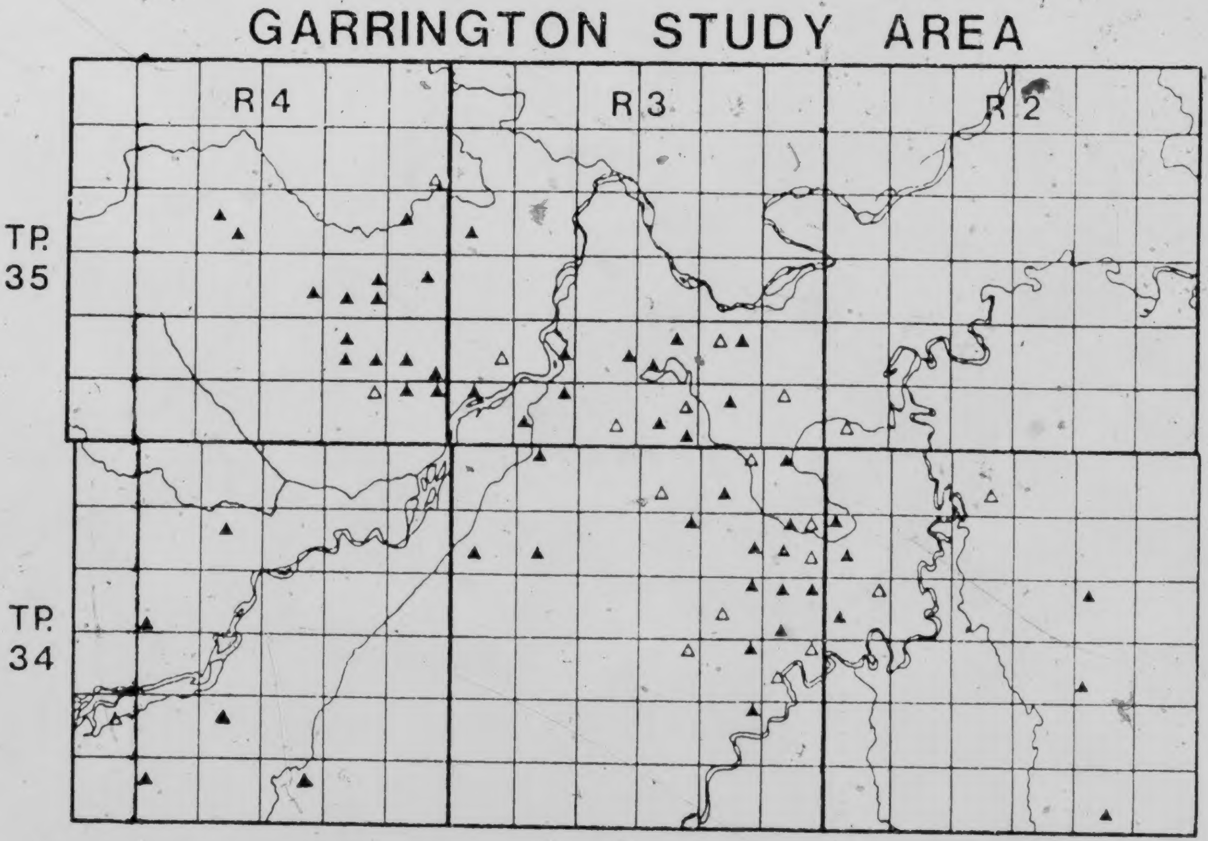
GARRINGTON STUDY AREA
R 4
R 3
R 2
TP. 35
TP. 34

Figure 3.1 Map of the Garrington study area. Triangles indicate wells with Viking core. Open triangles indicate sample locations.

TABLE 3.1 SAMPLES INVESTIGATED

SAMPLE NUMBER	ROCK TYPE	DEPTH (m)	HYDROMETER ANALYSIS	THIN SECTION	XRD SIZE-FRACTION <2 μm	XRD SIZE-FRACTION 2-5 μm	XRD SIZE-FRACTION 5-20 μm	SEM
16-19-34-2W5								
003	Congl.	2053.6	X		X	X	X	X
004	C.Sst.	2053.9	X	X	X	X	X	X
005	F.Sst.	2054.2	X	X	X	X	X	X
1-25-35-4W5								
010	Congl.	2147.5	X	X	X	X	X	X
011	C.Sst.	2147.9	X	X	X	X	X	X
012	F.Sst.	2148.3	X	X	X	X	X	X
16-25-34-3W5								
016	Congl.	2069.1	X	X	X	X	X	X
017	F.Sst.	2071.5	X	X	X	X	X	X
11-11-35-3W5								
019	Congl.	2074.1	X	X	X	X	X	X
020	F.Sst.	2074.6	X	X	X	X	X	
022	F.Sst.	2079.9	X		X	X	X	X
024	C.Sst.	2090.9	X	X	X	X	X	X
6-6-35-2W5								
027	Congl.	2037.5	X	X	X	X	X	X
028	F.Sst.	2037.8	X	X	X	X	X	X
029	F.Sst.	2041.4	X		X	X	X	X
030	F.Sst.	2043.6	X	X	X	X	X	X
031	F.Sst.	2045.3	X		X	X	X	X
032	F.Sst.	2047.5	X		X	X	X	
6-34-34-3W5								
033	C.Sst.	2112.5	X	X	X	X	X	
034	Congl.	2115.0	X	X	X	X	X	X
035	C.Sst.	2115.3	X	X	X	X	X	
036	C.Sst.	2115.7	X		X	X	X	
037	F.Sst.	2116.5	X	X	X	X	X	
038	F.Sst.	2121.1	X		X	X	X	
6-23-34-3W5								
039	Congl.	2111.4	X	X	X	X	X	X
041	Congl.	2112.8	X	X	X	X	X	
042	F.Sst.	2113.3	X	X	X	X	X	
046	F.Sst.	2121.1	X		X	X	X	

TABLE 3.1 SAMPLES INVESTIGATED (CONTINUED)

SAMPLE NUMBER	ROCK TYPE	DEPTH (m)	HYDROMETER ANALYSIS	THIN SECTION	XRD SIZE-FRACTION			SEM
					<2	2-5 µm	5-20	
9-3-35-3W5								
047	Shale	2085.0	X		X	X	X	
048	Congl.	2086.3	X		X	X	X	
049	Congl.	2087.1	X		X	X	X	
050	F.Sst.	2087.6	X		X	X	X	
052	F.Sst.	2094.0	X	X	X	X	X	
16-13-34-3W5								
055	Congl.	2070.5	X		X	X	X	
056	Congl.	2071.0	X	X	X	X	X	
057	F.Sst.	2071.3	X	X	X	X	X	
059	F.Sst.	2076.2	X		X	X	X	
060	C.Sst.	2065.4	X	X	X	X	X	
16-35-34-3W5								
061	C.Sst.	2069.2	X	X	X	X	X	
7-4-35-3W5								
077	C.Sst.	2108.5	X		X	X	X	X
14-1-35-3W5								
085	F.Sst.	2044.5	X		X	X	X	X
086	F.Sst.	2046.7	X		X	X	X	X
088	F.Sst.	2050.4	X		X	X	X	X
089	F.Sst.	2052.5	X		X	X	X	X
16-15-34-3W5								
101	F.Sst.	2131.0	X		X	X	X	X
102	F.Sst.	2132.5	X		X	X	X	X
103	F.Sst.	2134.0	X	X	X	X	X	X
104	F.Sst.	2135.5	X		X	X	X	X
105	F.Sst.	2137.8	X		X	X	X	X
6-13-34-3W5								
107	C.Sst.	2080.7	X	X	X	X	X	
8-25-34-3W5								
111	C.Sst.	2065.7	X		X	X	X	

TABLE 3.1 SAMPLES INVESTIGATED (CONTINUED)

SAMPLE NUMBER	ROCK TYPE	DEPTH (m)	HYDROMETER ANALYSIS	THIN SECTION	XRD SIZE-FRACTION			SEM
					<2	2-5 µm	5-20	
8-7-35-3W5								
117	Congl.	2130.6	X	X	X	X	X	X
118	C.Sst.	2131.1	X	X	X	X	X	X
121	F.Sst.	2135.2	X	X	X	X	X	X
7-33-34-2W5								
124	Congl.	1972.7	X	X	X	X	X	
125	C.Sst.	1973.3	X	X	X	X	X	
126	F.Sst.	1976.0	X	X	X	X	X	
128	F.Sst.	1979.7	X		X	X	X	
10-7-34-4W5								
136	C.Sst.	2335.4	X	X	X	X	X	X
16-2-35-4W5								
146	C.Sst.	2220.5	X	X	X	X	X	X
147	F.Sst.	2224.2	X	X	X	X	X	X
148	F.Sst.	2228.0	X		X	X	X	

TABLE 3.2 PERCENTAGES OF GRAINS, CEMENTS AND POROSITY

SAMPLE NUMBER	ROCK TYPE	DEPTH (m)	FRAMEWORK GRAINS (%)	CEMENTS (%)	POROSITY (%)
16-19-34-2W5					
004	C.Sst.	2053.9	80	10	10
005	F.Sst.	2054.2	70	24	6
1-25-35-4W5					
010	Congl.	2147.5	85	10	5
011	C.Sst.	2147.9	80	13	7
012	F.Sst.	2148.3	70	20	10
16-25-34-3W5					
016	Congl.	2069.1	80	14	6
017	F.Sst.	2071.5	70	21	9
11-11-35-3W5					
019	Congl.	2074.1	80	17	3
020	F.Sst.	2074.6	70	23	7
024	C.Sst.	2090.9	80	16	4
6-6-35-2W5					
027	Congl.	2037.5	82	10	8
028	F.Sst.	2037.8	68	25	7
030	F.Sst.	2043.6	75	14	11
6-34-34-3W5					
033	C.Sst.	2112.5	75	22	3
034	Congl.	2115.0	80	11	9
035	C.Sst.	2115.3	80	8	12
037	F.Sst.	2116.5	65	28	7
6-23-34-3W5					
039	Congl.	2111.4	85	7	8
041	Congl.	2112.8	84	5	11
042	F.Sst.	2113.3	80	10	10
9-3-35-3W5					
052	F.Sst.	2094.0	75	16	9
16-13-34-3W5					
056	Congl.	2071.0	80	12	8
057	F.Sst.	2071.3	70	22	8
060	C.Sst.	2065.4	80	10	10

TABLE 3.2 PERCENTAGES OF GRAINS, CEMENTS AND POROSITY (CONTINUED)

SAMPLE NUMBER	ROCK TYPE	DEPTH (m)	FRAMEWORK GRAINS (%)	CEMENTS (%)	POROSITY (%)
16-35-34-3W5					
061	C.Sst.	2069.2	80	15	5
16-15-34-3W5					
103	F.Sst.	2134.0	70	20	10
6-13-34-3W5					
107	C.Sst.	2080.7	75	17	8
8-7-35-3W5					
117	Congl.	2130.6	75	16	9
118	C.Sst.	2131.1	75	16	9
121	F.Sst.	2135.2	75	17	8
7-33-34-2W5					
124	Congl.	1972.7	83	10	7
125	C.Sst.	1973.3	75	15	10
126	F.Sst.	1976.0	70	22	3
10-7-34-4W5					
136	C.Sst.	2335.4	75	15	10
16-2-35-4W5					
146	C.Sst.	2220.5	70	26	4
147	F.Sst.	2224.2	70	20	10

TABLE 3.3 BULK MINERALOGY : THIN SECTION ANALYSIS

SAMPLE NUMBER	FRAMEWORK GRAINS (%)				CEMENTS (%)				ROCK CLASS (FOLK;1968)
	Ch	Q	F	RF	Q	Ca	S	C	
16-19-34-2W5									
004	48	28	1	3	6	0	3	1	Sublitharenite
005	10	50	2	8	0	2	15	7	Sublitharenite
1-25-35-4W5									
010	69	12	2	2	5	t	t	5	Quartzarenite
011	24	49	3	4	5	0	1	7	Sublitharenite
012	11	50	1	8	2	6	t	12	Sublitharenite
16-25-34-3W5									
016	65	13	0	2	4	0	0	10	Quartzarenite
017	8	52	1	9	1	7	1	12	Sublitharenite
11-11-35-3W5									
019	69	10	0	1	9	0	0	8	Quartzarenite
020	8	52	1	9	1	8	3	11	Sublitharenite
024	62	17	0	1	11	2	0	3	Quartzarenite
6-6-35-2W5									
027	75	6	0	1	5	0	1	4	Quartzarenite
028	1	58	3	6	0	10	6	9	Sublitharenite
030	6	58	2	9	3	1	4	6	Sublitharenite
6-34-34-3W5									
033	37	36	1	1	8	1	1	12	Quartzarenite
034	56	20	2	2	7	1	0	3	Quartzarenite
035	37	38	2	3	2	0	1	5	Sublitharenite
037	3	49	2	11	1	17	2	8	Sublitharenite
6-23-34-3W5									
039	77	8	0	0	4	0	1	2	Quartzarenite
041	25	55	2	2	2	0	0	3	Quartzarenite
042	14	54	3	9	5	3	1	1	Sublitharenite
9-3-35-3W5									
052	12	52	3	8	7	7	1	1	Sublitharenite
16-13-34-3W5									
056	51	26	2	1	3	2	0	7	Quartzarenite
057	4	60	3	3	1	8	9	4	Sublitharenite
060	41	35	2	2	5	3	0	2	Quartzarenite

TABLE 3.3 BULK MINERALOGY : THIN SECTION ANALYSIS

SAMPLE NUMBER	FRAMEWORK GRAINS (%)				CEMENTS (%)				ROCK CLASS (FOLK;1968)
	Ch	Q	F	RF	Q	Ca	S	C	
16-35-34-3W5									
061	21	56	3	0	8	2	4	1	Quartzarenite
16-15-34-3W5									
103	4	56	2	8	6	3	6	5	Sublitharenite
6-13-34-3W5									
107	27	43	1	4	5	8	3	1	Sublitharenite
8-7-35-3W5									
117	52	20	1	2	6	0	1	9	Quartzarenite
118	31	42	1	1	6	0	1	9	Quartzarenite
121	17	55	1	2	1	3	3	10	Sublitharenite
7-33-34-2W5									
124	55	27	1	0	4	0	1	5	Quartzarenite
125	20	46	4	5	4	tr	5	6	Sublitharenite
126	11	49	3	7	1	7	5	9	Sublitharenite
10-7-34-4W5									
136	44	21	2	8	6	1	0	8	Sublitharenite
16-2-35-4W5									
146	32	36	1	1	7	11	tr	8	Quartzarenite
147	8	54	1	7	7	5	0	8	Sublitharenite

The bulk mineralogy of the conglomerates averages 80 % chert (Ch) and quartz (Q)(range 72-85 %), 1 % rock fragments (RF)(range 0-2 %) and 1 % feldspars (F)(range 0-2 %). Cements in the conglomerates are dominated by quartz (Q) and clay(C), quartz averaging 5 % (range 2-9 %) and clays (mainly kaolinite) averaging 6 % (range 2-10 %). Carbonates make up a small proportion of the cements in the conglomerates. Siderite cement (S) averages < 0.5 % (range 0-1 %); dolomite and ankerite (Ca) cements average < 0.5 % (range 0-2 %).

In the coarse-grained sandstones, the bulk mineralogy averages 73 % chert and quartz (range 65-79 %), 3 % rock fragments (range 0-8 %), and 2 % feldspar (range 0-4 %). Cements in the coarse-grained sandstones are dominated by quartz and clay with local occurrences of carbonate cement. Quartz cement averages 6 % (range 2-11 %) and clay cements average 5 % (range 1-12 %). Dolomite and ankerite cements average 2 % (range 0-11 %) and siderite cement averages 2 % (range 0-5 %).

In the fine-grained sandstones, detrital grains average 62 % chert and quartz (range 52-72 %), 7 % rock fragments (range 2-11 %) and 2 % feldspars (range 1-3 %). Cements in the fine-grained sandstones are divided between quartz, carbonate and clays with carbonates making up approximately half of cements. Dolomite and ankerite cements average 6 % (range 1-17 %) and siderite cement averages 4 % (range 0-15 %). Clay cements average 7 % (range 1-12 %) and quartz cement averages 3 % (range 0-7 %).

From the coarsest conglomerates to the finest sandstones, the mineralogy of the detrital grains changes significantly. Quartz and chert abundances gradually decrease from 80 % to about 60 %, while rock fragments increase from 1 % to 7 %; feldspars increase marginally from 1 % to 2 %. Carbonate cementation is more prevalent in the fine-grained sandstones than in the coarse-grained sandstones and conglomerates. The amount of quartz cementation decreases from the coarse conglomerates to the fine-grained sandstones.

The relative abundance of detrital chert versus quartz changes from conglomerates to fine-grained sandstones (Figure 3.2B). In the conglomerates the abundance of chert averages 60 % (range 25-75 %), while quartz averages 20 % (range 6-55 %). In the coarse-grained sandstones, chert averages about 35 % (range 8-62 %); quartz averages about 40 % (range 17-56 %). In the fine-grained sandstones, chert

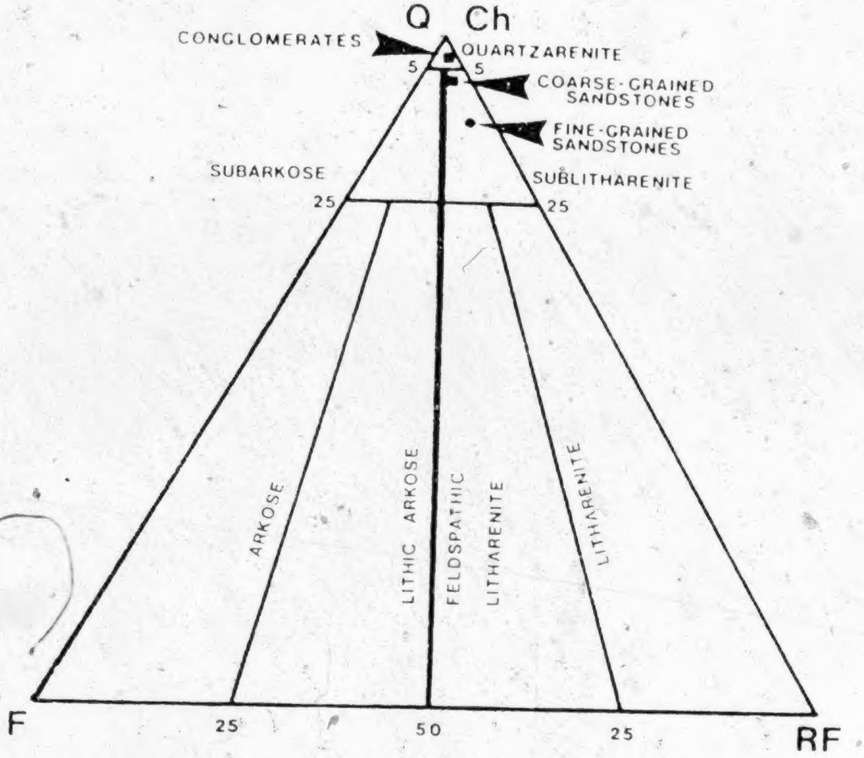
Q Ch
CONGLOMERATES
QUARTZARENITE
5
5
COARSE-GRAINED SANDSTONES
FINE-GRAINED SANDSTONES
SUBARKOSE
SUBLITHARENITE
25
25
ARKOSE
LITHIC ARKOSE
FELDSPATHIC LITHARENITE
LITHARENITE
F
25
50
25
RF

Figure 3.2A Classification of the conglomerates, coarse-grained sandstones and the fine-grained sandstones in the Viking Formation at Garrington (After Folk, 1968). Classifications were based on point counts on 10 conglomerates, 12 coarse-grained sandstones and 14 fine-grained sandstones.

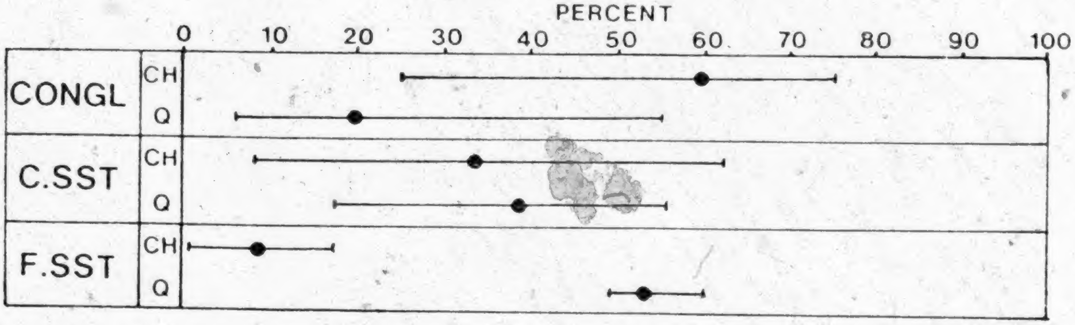

Figure 3.2B Diagram showing the change in the relative abundance of chert and quartz from conglomerates to fine-grained sandstones. Data is from point counts on 10 conglomerates, 12 coarse-grained sandstones and 14 fine-grained sandstones.

averages 10 % (range 1-17 %); quartz averages 55 % (range 49-60 %)(Figure 3.2B). The ranges for quartz and chert abundances in the conglomerates and coarse-grained sandstones are very large; in the fine-grained sandstones the ranges are much narrower. The dominance of chert in the conglomerates and coarse-grained sandstones indicates relatively short transportation and textural immaturity; the abundance of quartz in the fine-grained sandstones reflects the textural maturity of those sediments (Moorhouse, 1959).

TEXTURES

In the conglomerates and coarse-grained sandstones chert and quartz grains are equidimensional and subrounded to rounded. Chert pebbles may contain chalcedony or inclusions of carbonate. Carbonate inclusions reflect incomplete replacement of the original host rock (Blatt et al., 1980). Other chert grains show relict limestone textures such as ghost ooids and shell fragments (Figure 3.3A).

Quartz grains are almost always inclusion-free and generally show uniform extinction. However, some quartz grains show undulatory extinction or strain texture while others are polycrystalline (indicating a sedimentary source rock and second cycle sedimentation). Feldspar grains in the conglomerates and coarse-grained sandstones are rounded to subrounded, have polysynthetic twinning, and are inclusion-free.

Diagenetic features in the conglomerates and coarse-grained sandstones include compaction, cementation, solution and replacement. Compaction is evident from the presence of crenulated contacts between grains and suture contacts between some chert grains and rock fragments (Figure 3.3B). Cementation in the conglomerates and coarse-grained sandstones occurs primarily as quartz overgrowths and diagenetic clay minerals. Quartz cement occurs as overgrowths on chert and quartz grains. Overgrowths on chert grains occur as small individual quartz crystals rimming the grains, giving them a sawtooth texture (Figure 3.3D). Overgrowths on quartz grains occur as complete rims in optical continuity with the detrital grains and have smooth or euhedral terminations (Figures 3.3E and 3.4A). A few feldspar grains have overgrowth cements (Figure 3.4B). Clay cement occurs sporadically throughout the conglomerates and coarse-grained sandstones; locally it completely fills pore space (Figure 3.3C). Dolomite, ankerite and siderite cements are generally not present in the conglomerates but occur in the coarse-grained sandstones in minor or moderate abundance. Dolomite and ankerite occur mainly as pore-filling cements (Figure 3.4C). Siderite cement appears as small rhombs attached to the edges of detrital grains (Figure 3.4D).

Primary intergranular porosity is most abundant in the conglomerates and coarse-grained sandstones. Minor amounts of secondary porosity are associated with solution of chert and feldspar (Figure 3.3F). Solution of relict carbonate rhombs in chert pebbles can also create new pores.

In the fine-grained sandstones, quartz grains are dominant and have a subangular to angular form. Chert grains in the fine-grained sandstones are subangular to subrounded and may show relict carbonate textures. Feldspar grains are subangular to subrounded and equidimensional. Rock fragments are more abundant in the fine-grained sandstones and are usually subangular to angular and elongate, especially micas. The fine-grained sandstones often exhibit obvious parallel laminations which may cause directional permeability.

Diagenetic features in the fine-grained sandstones include compaction, cementation, solution and replacement textures. Compaction is evident where ductile rock fragments are squeezed between (or bent around) quartz grains and where quartz grains show concavo-convex contacts indicative of pressure solution.

Cements include quartz, siderite, dolomite, ankerite and clay. Quartz cement occurs as optically continuous overgrowths which terminate with smooth or euhedral surfaces and often form triple junctions where they meet. Siderite cement is common in the fine-grained sandstones as small rhombs on grain surfaces; in some cases the siderite completely encloses quartz grains. Where siderite cementation is extensive quartz overgrowths are inhibited (Figure 3.4E). Dolomite and ankerite cements fill pores and often rest on an earlier quartz or siderite cement (Figure 3.4F). Clay minerals occur as pore-linings and pore-fillings and are often amorphous. Pyrite also occurs as a cement forming euhedral crystals on grain surfaces or as inclusions in grains.

Porosity in the fine-grained sandstones is dominated by primary intergranular porosity. Very minor amounts of secondary porosity exist where chert and feldspars have undergone solution. Siderite replaces chert in some samples.

FIGURE 3.3.

3.3A. Photomicrograph of a chert pebble showing limestone texture. Note the ghost ooids (well 8-7-35-3W5, 2130.6 m, sample # 117, plane polars, 6.3 X magnification).

3.3B. Photomicrograph of a conglomerate showing a suture contact between a chert pebble and a rock fragment (arrow)(well 8-7-35-3W5, 2130.6 m, sample # 117, plane polars, 6.3 X magnification).

3.3C. Photomicrograph of a chert-pebble conglomerate showing abundant pore-filling kaolinite (K) (well 11-11-35-3W5, 2074.1 m, sample # 019, plane polars, 6.3 X magnification).

3.3D. Photomicrograph of a chert-pebble conglomerate showing incomplete quartz overgrowths (AQ) on chert pebbles (well 11-11-35-3W5, 2074.1 m, sample # 019, plane polars, 6.3 X magnification).

3.3E. Photomicrograph of a conglomerate showing complete quartz overgrowths on detrital quartz grains (AQ). Note the euhedral nature of the quartz overgrowths and the formation of triple junctions where three overgrowths meet (well 6-23-34-3W5, 2112.8 m, sample # 041, plane polars, 6.3 X magnification).

3.3F. Photomicrograph of a conglomerate shows the development of secondary porosity as a result of solution of chert (well 11-11-35-3W5, 2074.1 m, sample # 019, plane polars, 6.3 X magnification).

FIGURE 3.3

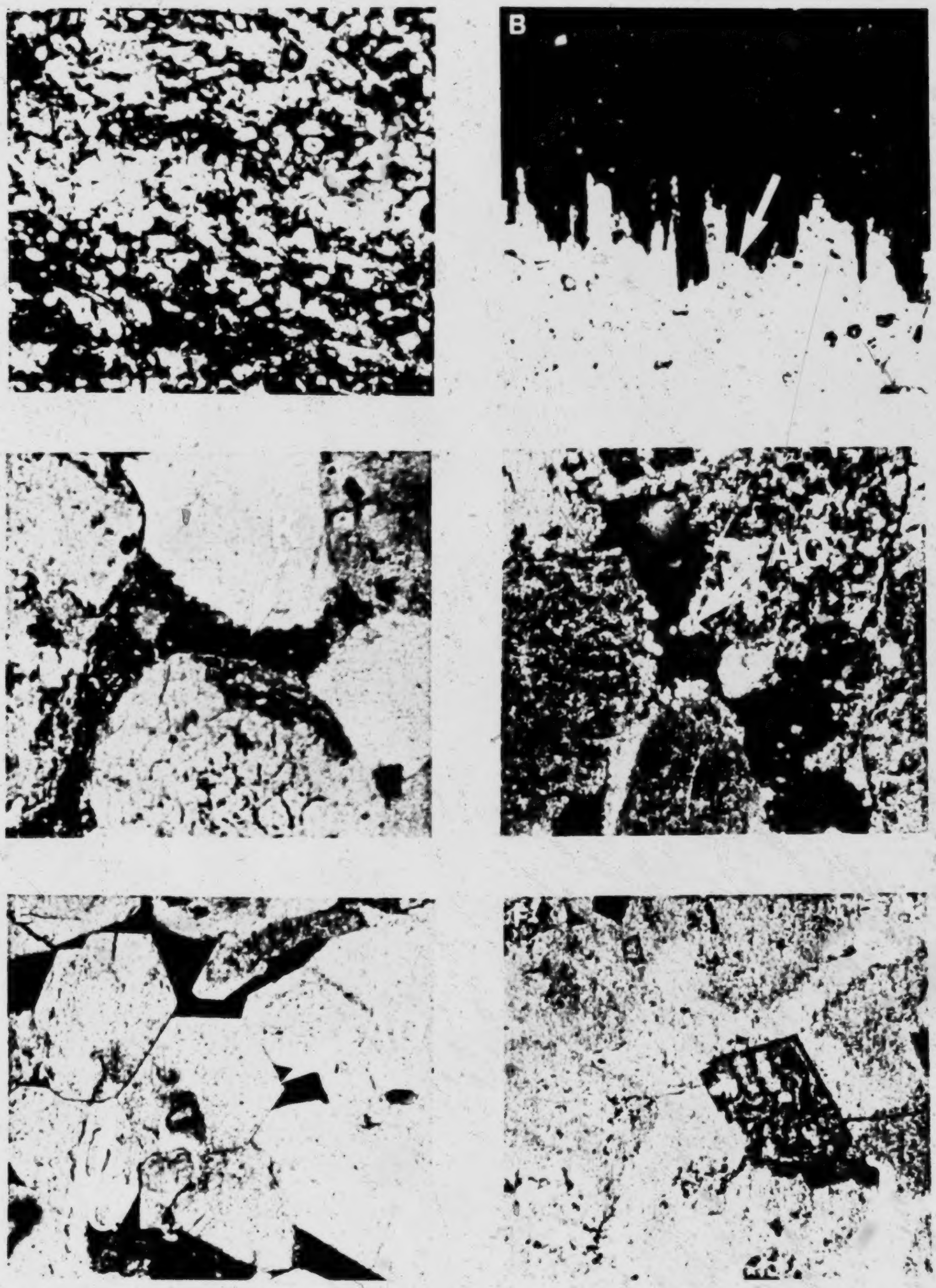

FIGURE 3.4.

3.4A. Photomicrograph of a coarse-grained sandstone showing a complete quartz overgrowth (AQ) on a detrital quartz grain. Note the presence of a dust rim on the detrital grain (well 8-7-35-3W5, 2131.1 m, sample # 118, cross polars, 6.3 X magnification).

3.4B. Photomicrograph of a coarse-grained sandstone showing a rim of authigenic feldspar on a plagioclase grain (AF). Note also the presence of pore-filling carbonate cement to the right of the feldspar (well 6-34-34-3W5, 2112.5 m, sample # 033, cross polars, 6.3 X magnification).

3.4C. Photomicrograph of a coarse-grained sandstone showing abundant pore-filling carbonate cement (Ca)(well 16-2-35-4W5, 2220.5 m, sample # 146, cross polars, 6.3 X magnification).

3.4D. Photomicrograph of a coarse-grained sandstone showing siderite cementation (S). Note that the siderite occurs as small crystals attached to grain surfaces. Where siderite is present quartz overgrowths are absent (well 7-33-34-2W5, 1973.3 m, sample # 125, cross polars, 6.3 X magnification).

3.4E. Photomicrograph of a fine-grained sandstone showing abundant siderite cement occurring as small crystals attached to grain surfaces (well 11-11-35-3W5, 2079.9 m, sample # 022, cross polars, 6.3 X magnification).

3.4F. Photomicrograph of a fine-grained sandstone showing cementation by pore-filling carbonate (Ca)(well 16-25-34-3W5, 2071.5 m, sample # 017, crosspolars, 6.3 X magnification).

FIGURE 3.4

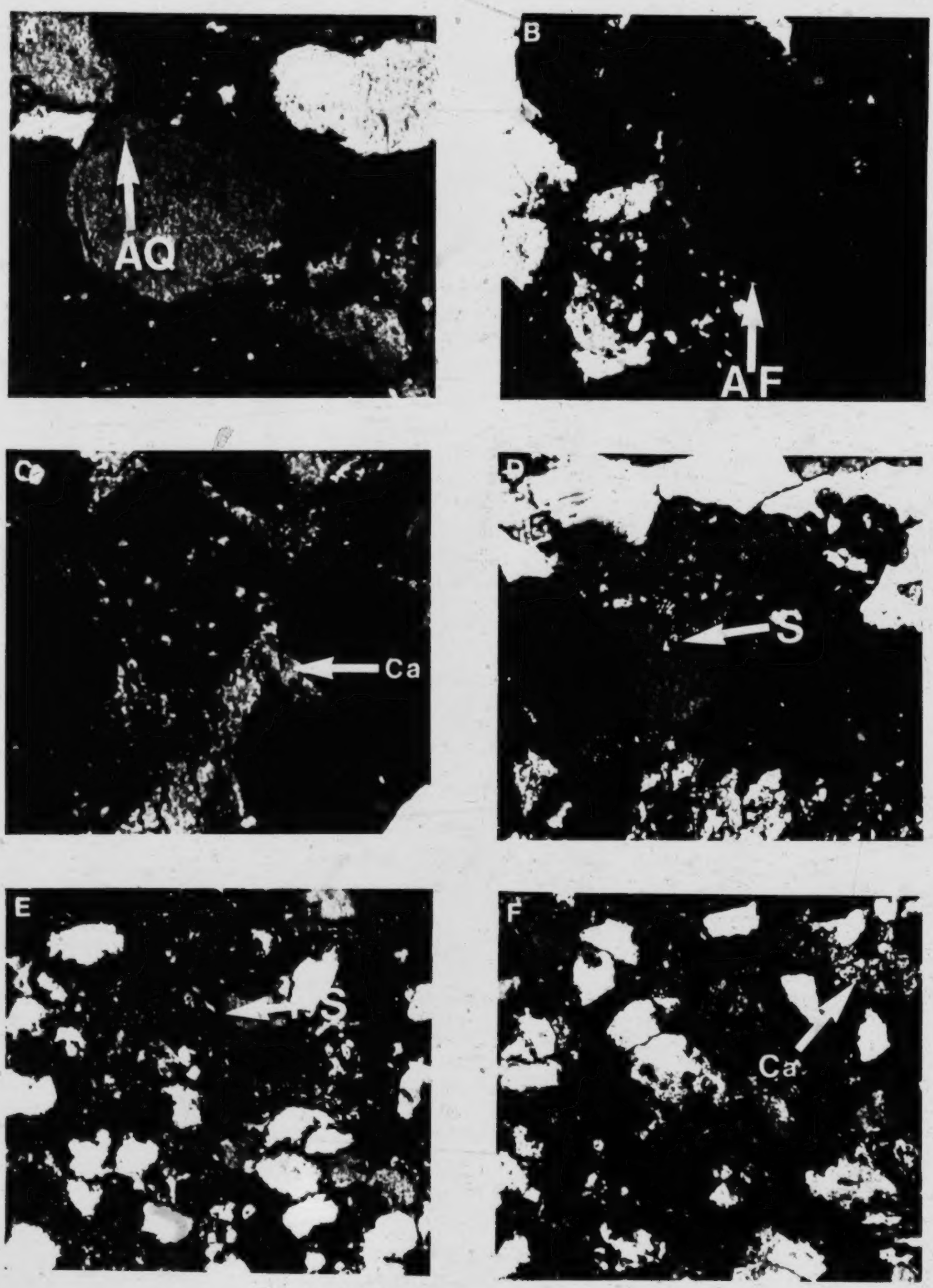
A
AQ
B
A F
C
Ca
D
S
E
S
F
Ca

B. HYDROMETER ANALYSIS

Three size fractions of the samples were studied using X-ray diffraction; $< 2\,\mu m$, 2-5 μm and 5-20 μm. Sixty-two samples were examined including 14 conglomerates, 15 coarse-grained sandstones, 32 fine-grained sandstones and 1 shale. The abundance of material in the three size fractions was determined by hydrometer analysis. All values are weight percentages for the total sample. The hydrometer results are presented in Table 3.4.

Average values for the conglomerates are:

1. 1.5% $< 2\,\mu m$;
2. 2.0% 2-5 μm;
3. 3.3% 5-20 μm.

Average values for the coarse-grained sandstones are:

1. 1.6% $< 2\,\mu m$;
2. 2.6% 2-5 μm;
3. 4.3% 5-20 μm.

Average values for the fine-grained sandstones are:

1. 5.0% $< 2\,\mu m$;
2. 8.0% 2-5 μm;
3. 13.5% 5-20 μm.

C. X-RAY DIFFRACTION RESULTS

X-ray diffraction was used to identify the clay mineral species present in the samples. Other important minerals detected by XRD in the $< 20\,\mu m$ size-fractions were quartz and feldspar. Carbonates were not studied by XRD in the fine size fractions. Instead they were examined using thin sections and their identities confirmed by XRD of bulk rock samples. In the discussion that follows, abundances of clay minerals are listed as relative percentages of the total amount (100 %) of clay minerals present in each size fraction. Abbreviations used in the tables that follow are listed on pages 22 and 23.

Mineral abundances were assigned as follows:

1. >35% of phase present in sample = major (M),
2. 10-35% of phase present in the sample = moderate (mM),

TABLE 3.4 HYDROMETER ANALYSIS

SAMPLE NUMBER	ROCK TYPE	DEPTH (m)	% MATERIAL IN SAMPLE <1 μm	<2 μm	<5 μm	<20 μm
16-19-34-2W5						
003	Congl.	2053.6	0.2	1.5	-	
004	C.Sst.	2053.9	0.5	1.0	3.0	6.0
005	F.Sst.	2054.2	3.0	5.0	9.0	14.0
1-25-35-4W5						
010	Congl.	2147.5	0.5	1.0	2.0	2.5
011	C.Sst.	2147.9	0.5	1.5	2.5	3.5
012	F.Sst.	2148.3	3.0	4.5	7.0	12.0
16-25-34-3W5						
016	Congl.	2069.1	1.5	2.0		
017	F.Sst.	2071.5	3.5	6.0	9.5	17.0
11-11-35-3W5						
019	Congl.	2074.1	<0.5	0.5	1.0	2.0
020	F.Sst.	2074.6	4.0	5.5	10.0	20.0
022	F.Sst.	2079.9	3.5	4.0	7.0	13.0
024	C.Sst.	2090.9	<1.0	<1.0	<1.0	2.0
6-6-35-2W5						
027	Congl.	2037.5	<1.0	<1.0	<1.0	1.0
028	F.Sst.	2037.8	3.0	5.5	11.0	24.0
029	F.Sst.	2041.4	3.0	4.5	8.5	12.5
030	F.Sst.	2043.6	1.0	3.0	4.2	9.2
031	F.Sst.	2045.3	2.0	5.5	7.0	12.0
032	F.Sst.	2047.5	2.0	3.0	5.0	13.0
6-34-34-3W5						
033	C.Sst.	2112.5	1.5	2.5	3.5	
034	Congl.	2115.0	0.5	1.5	2.0	
035	C.Sst.	2115.3	0.5	1.5	2.5	
036	C.Sst.	2115.7	0.5	1.5	3.0	
037	F.Sst.	2116.5	4.5	5.5	8.0	
038	F.Sst.	2121.1	1.0	2.0	3.0	
6-23-34-3W5						
039	Congl.	2111.4	0.5	1.0	1.5	
041	Congl.	2112.8	<1.0	1.0	2.0	
042	F.Sst.	2113.3	2.0	2.5	6.0	
046	F.Sst.	2121.1	3.5	4.5	6.5	

TABLE 3.4 HYDROMETER ANALYSIS (CONTINUED)

SAMPLE NUMBER	ROCK TYPE	DEPTH (m)	% MATERIAL IN SAMPLE			
			<1 μm	<2 μm	<5 μm	<20 μm
9-3-35-3W5						
047	Shale	2085.0	8.0	10.0	15.0	28.0
048	Congl.	2086.3	<1.0	1.0	1.0	1.5
049	Congl.	2087.1	2.0	3.0	3.5	7.0
050	F.Sst.	2087.6	3.5	4.0	5.0	11.0
052	F.Sst.	2094.0	4.5	5.0	6.0	10.0
16-13-34-3W5						
055	Congl.	2070.5	1.5	2.0	4.0	6.0
056	Congl.	2071.0	1.5	2.0	2.5	4.0
057	F.Sst.	2071.3	3.0	3.5	6.0	11.0
059	F.Sst.	2076.2	2.5	3.5	4.5	8.0
060	C.Sst.	2065.4	< 1.0	1.0	2.0	3.5
16-35-34-3W5						
061	C.Sst.	2069.2	1.0	1.5	2.0	4.0
7-4-35-3W5						
077	C.Sst.	2108.5	0.5	1.0	1.5	2.0
14-1-35-3W5						
085	F.Sst.	2044.5	2.5	8.0	12.0	13.5
086	F.Sst.	2046.7	2.5	8.0	12.0	16.0
088	F.Sst.	2050.4	2.0	8.0	11.0	16.0
089	F.Sst.	2052.5	2.0	8.0	10.5	16.0
16-15-34-3W5						
101	F.Sst.	2131.0	2.0	6.5	10.0	14.0
102	F.Sst.	2132.5	2.0	7.0	10.0	12.5
103	F.Sst.	2134.0	2.5	5.5	8.5	13.5
104	F.Sst.	2135.5	1.0	5.0	10.0	15.0
105	F.Sst.	2137.8	2.0	4.0	9.5	13.0
6-13-34-3W5						
107	C.Sst.	2080.7	1.0	1.5	2.0	4.0
8-25-34-3W5						
111	C.Sst.	2065.7	1.5	2.0	2.5	3.5

TABLE 3.4 HYDROMETER ANALYSIS (CONTINUED)

SAMPLE NUMBER	ROCK TYPE	DEPTH (m)	% MATERIAL IN SAMPLE <1 μm	<2 μm	<5 μm	<20 μm
8-7-35-3W5						
117	Congl.	2130.6	1.0	1.5	2.0	3.0
118	C.Sst.	2131.1	2.0	3.0	4.5	6.0
121	F.Sst.	2135.2	3.0	4.5	7.0	13.0
7-33-34-2W5						
124	Congl.	1972.7	1.0	1.5	2.0	2.5
125	C.Sst.	1973.3	1.5	2.0	4.5	7.5
126	F.Sst.	1976.0	3.0	6.0	9.5	15.0
128	F.Sst.	1979.7	3.0	4.5	8.0	12.5
10-7-34-4W5						
136	C.Sst.	2335.4	0.5	1.0	1.5	5.0
16-2-35-4W5						
146	C.Sst.	2220.5	1.0	2.0	3.0	4.0
147	F.Sst.	2224.2	2.5	3.0	5.5	11.0
148	F.Sst.	2228.0	3.0	4.0	5.0	8.5

3. 5-10% of phase present in the sample = minor (m),
4. 2-5% of phase present in the sample = minor-trace (mt),
5. <2% of phase present in the sample = trace (t).

CONGLOMERATES

5-20 μm Size Fraction (Table 3.5)

Quartz is the major phase in the 5-20 μm size-fraction; clay minerals are moderately abundant and feldspars occur in minor or trace amounts. Of the clay minerals kaolinite is the most abundant (60-95%) followed by illite (trace-25%). Illite / smectite, smectite and chlorite occur in only minor or trace quantities.

2-5 μm Size Fraction (Table 3.6)

In all the conglomerate samples quartz is the major phase in the 2-5 μm size fraction. Clay minerals occur in moderate or major amounts; feldspars are present in minor or trace quantities. Kaolinite is the most abundant clay mineral (35-95%), followed by illite (minor / trace-35%), illite / smectite (trace-20%), chlorite (trace-10%), and smectite (not detected to trace).

<2 μm Size Fraction (Table 3.7)

Quartz is present in moderate to major amounts in the <2 μm size fraction. Clay minerals are always present in major amounts; feldspars occur in minor or trace quantities. The clay minerals present are dominated by kaolinite (20-85%), with lower amounts of illite (5-55), illite / smectite (trace-15%) and chlorite (trace-10%). Smectite generally occurs in trace quantities; three samples have anomalously high smectite contents (up to 30% of clay minerals).

COARSE-GRAINED SANDSTONES

5-20 μm Size Fraction (Table 3.5)

Quartz is the most abundant phase in the 5-20 μm size fraction always occurring in major amounts. Clay minerals occur in moderate or major amounts; feldspars occur in minor to trace quantities. Kaolinite is the most abundant clay mineral (65-95%), followed by illite (trace-25%). Illite / smectite , chlorite and smectite occur in minor or trace amounts.

2-5 μm Size Fraction (Table 3.6)

In the 2-5 μm size fraction, quartz occurs in moderate or major amounts; clay minerals in minor or major amounts and feldspars in minor or trace amounts. Kaolinite is the most abundant clay mineral (60-95%), followed by illite (minor-trace-20%). Illite / smectite, chlorite and smectite occur in minor or trace amounts.

<2 μm Size Fraction (Table 3.7)

In the <2 μm size fraction, quartz is present in minor or major amounts; clay minerals occur in moderate or major amounts and feldspars in minor or trace amounts. Clay minerals are dominated by kaolinite (30-90%). Illite is the next most abundant clay mineral (5-45%). Illite / smectite occurs in amounts from trace to 15% and chlorite in amounts from trace to 20%. Smectite usually occurs in only trace quantities but three samples have anomalously high smectite quantities (up to 30% of clay minerals).

FINE-GRAINED SANDSTONES

5-20 μm Size Fraction (Table 3.5)

Quartz is the major phase present in the 5-20 μm size fraction. Clay minerals occur in moderate abundance and feldspars are present in minor or trace amounts. Clay minerals are dominated by kaolinite (40-90%), and illite (minor-40%). Illite / smectite occurs in amounts form trace to 15%. Chlorite is present in minor or trace quantities. Smectite is either not detected or only occurs in minor or trace quantities.

2-5 μm Size Fraction (Table 3.6)

In the 2-5 μm size fraction quartz is the major phase present. Clay minerals occur in moderate or major abundance; feldspars in minor or trace amounts. Kaolinite is the most abundant clay mineral (40-85%), followed by illite (minor- 40%), illite / smectite (trace- 15%) and chlorite (trace- 10%). Smectite is either not detected or occurs in trace quantities.

<2 μm Size Fraction (Table 3.7)

Clay minerals are the major phase present in the <2 μm size-fraction. Quartz occurs in minor or major quantities (generally moderate) and feldspars only in trace amounts. Kaolinite and illite are the most abundant clay minerals (25-75% and 20-60%, respectively) followed by illite / smectite (minor / trace- 15%) and chlorite (minor / trace- 10%). Smectite is either not detected or occurs in trace quantities.

Examination of thin sections and XRD of bulk rock samples indicated that carbonate minerals (dolomite and ankerite) were present mainly in the fine-grained sandstones.

SUMMARY OF X-RAY DIFFRACTION RESULTS

In the three main lithologies quartz is a major phase in the 5-20 and 2- 5 μm size fractions and a moderate phase in the $< 2 \mu m$ size fraction. Quartz abundance increases in the larger size fractions. Clay minerals occur in moderate abundance in the 5-20 μm size fraction, increasing to a moderate or major abundance in the $< 2 \mu m$ size fraction. Feldspars occur in minor or trace amounts in all size fractions. Of the clay minerals, kaolinite is the most abundant occurring in major amounts in all lithologies and in all size fractions. The amount of illite decreases as the size fraction gets larger, while kaolinite values show a corresponding increase. Illite occurs in moderate or major abundance in the < 2 and 2-5 μm size fractions and falls to moderate abundance in the 5-20 μm size fraction. Illite / smectite and chlorite abundances also decrease in the larger size fractions. These minerals occur in minor amounts. Smectite usually occurs in trace amounts, however, six (6) samples have large amounts of smectite in the $< 2 \mu m$ size fraction. These anomalous smectite values either represent the infiltration of drilling mud into the cores or a bentonite horizon.

D. SCANNING ELECTRON MICROSCOPY RESULTS

The results of scanning electron microscopy for the conglomerates, coarse-grained sandstones and fine-grained sandstones of the Viking Formation are summarized in Figures 3.5 to 3.10. The main objectives of the SEM study were to determine the nature and distribution of the pore-lining and pore-filling minerals and to determine the sizes and shapes of pores and pore throats. Thirty-two samples were examined including seven (7) conglomerates, eight (8) coarse-grained sandstones and fifteen (15) fine-grained sandstones.

In all lithologies the presence of pore-lining and pore-filling minerals has significantly reduced porosity. The conglomerates and coarse-grained sandstones are primarily affected by quartz and kaolinite and to a lesser extent by illite, pyrite, siderite and

TABLE 3.5 MINERALOGY 5-20 *μm* SIZE-FRACTION

SAMPLE NUMBER	ROCK TYPE	DEPTH (m)	Q	F	C	RELATIVE % CLAYS				
						IS	SM	CL	I	K
16-19-34-2W5										
003	Congl.	2053.6	M	t	M	nd	nd	t	t	95
004	C.Sst.	2053.9	M	t	M	t	t	t	t	95
005	F.Sst.	2054.2	M	t	M	t	t	mt	30	65
1-25-35-4W5										
010	Congl.	2147.5	M	t	M	t	t	t	5	90
011	C.Sst.	2147.9	M	mt	M	nd	nd	t	mt	95
012	F.Sst.	2148.3	M	mt	mM	mt	t	mt	25	70
16-25-34-3W5										
016	Congl.	2069.1	M	mt	M	t	t	t	t	95
017	F.Sst.	2071.5	M	mt	mM	t	nd	mt	15	80
11-11-35-3W5										
019	Congl.	2074.1	M	mt	mM	mt	nd	mt	10	85
020	F.Sst.	2074.6	M	m	mM	t	t	mt	35	60
022	F.Sst.	2079.9	M	m	mM	m	mt	m	30	55
024	C.Sst.	2090.9	M	m	m	nd	nd	nd	25	75
6-6-35-2W5										
027	Congl.	2037.5	M	mt	M	t	nd	t	mt	95
028	F.Sst.	2037.8	M	mt	mM	mt	nd	mt	35	60
029	F.Sst.	2041.4	M	mt	M	nd	nd	mt	15	80
030	F.Sst.	2043.6	M	m	mM	mt	nd	mt	m	90
031	F.Sst.	2045.3	M	mt	mM	10	nd	m	35	45
032	F.Sst.	2047.5	M	mt	m	15	t	mt	40	40
6-34-34-3W5										
033	C.Sst.	2112.5	M	mt	mM	mt	t	t	m	90
034	Congl.	2115.0	M	mt	M	t	t	t	mt	95
035	C.Sst.	2115.3	M	m	M	t	t	t	t	95
036	C.Sst.	2115.7	M	m	M	t	nd	t	t	95
037	F.Sst.	2116.5	M	mt	mM	mt	nd	mt	25	70
038	F.Sst.	2121.1	M	m	mM	mt	t	mt	20	70
6-23-34-3W5										
039	Congl.	2111.4	M	t	M	t	nd	t	t	95
041	Congl.	2112.8	M	t	M	nd	nd	t	t	95
042	F.Sst.	2113.3	M	m	M	mt	nd	mt	30	60
046	F.Sst.	2121.1	M	mt	mM	mt	nd	mt	25	65

TABLE 3.5 MINERALOGY 5-20 μm SIZE-FRACTION (CONTINUED)

SAMPLE NUMBER	ROCK TYPE	DEPTH (m)	Q	F	C	RELATIVE % CLAYS				
						IS	SM	CL	I	K
9-3-35-3W5										
047	Shale	2085.0	M	mt	mM	25	5	15	45	10
048	Congl.	2086.3	M	t	mM	nd	nd	t	mt	95
049	Congl.	2087.1	M	mt	mM	t	nd	mt	20	75
050	F.Sst.	2087.6	M	mt	mM	t	nd	mt	15	80
052	F.Sst.	2094.0	M	mt	mM	mt	nd	mt	20	75
16-13-34-3W5										
055	Congl.	2070.5	M	t	mM	10	nd	mt	25	60
056	Congl.	2071.0	M	mt	mM	t	nd	t	5	90
057	F.Sst.	2071.3	M	mt	mM	mt	nd	5	30	60
059	F.Sst.	2076.2	M	mt	mM	mt	nd	m	30	60
060	C.Sst.	2065.4	M	t	mM	t	nd	t	m	90
16-35-34-3W5										
061	C.Sst.	2069.2	M	t	mM	t	nd	t	mt	95
7-4-35-3W5										
077	C.Sst.	2108.5	M	t	M	t	t	t	mt	95
14-1-35-3W5										
085	F.Sst.	2044.5	M	mt	mM	mt	nd	mt	40	55
086	F.Sst.	2046.7	M	mt	mM	mt	nd	mt	35	60
088	F.Sst.	2050.4	M	t	M	mt	nd	mt	20	75
089	F.Sst.	2052.5	M	t	M	mt	nd	mt	25	70
16-15-34-3W5										
101	F.Sst.	2131.0	M	mt	mM	nd	nd	mt	15	80
102	F.Sst.	2132.5	M	mt	mM	t	nd	mt	15	80
103	F.Sst.	2134.0	M	mt	mM	mt	nd	mt	20	75
104	F.Sst.	2135.5	M	mt	mM	t	nd	t	10	85
105	F.Sst.	2137.8	M	mt	mM	5	nd	5	25	65
6-13-34-3W5										
107	C.Sst.	2080.7	M	mt	mM	t	t	nd	mt	95
8-25-34-3W5										
111	C.Sst.	2065.7	M	mt	M	t	nd	t	mt	95

TABLE 3.5 MINERALOGY 5-20 *µm* SIZE-FRACTION (CONTINUED)

SAMPLE NUMBER	ROCK TYPE	DEPTH (m)	Q	F	C	RELATIVE % CLAYS IS	SM	CL	I	K
8-7-35-3W5										
117	Congl.	2130.6	M	mt	M	t	nd	t	mt	95
118	C.Sst.	2131.1	M	mt	M	t	nd	t	mt	95
121	F.Sst.	2135.2	M	mt	M	mt	nd	mt	20	75
7-33-34-2W5										
124	Congl.	1972.7	M	mt	M	t	nd	t	mt	95
125	C.Sst.	1973.3	M	mt	M	t	nd	t	m	90
126	F.Sst.	1976.0	M	mt	mM	mt	nd	mt	30	60
128	F.Sst.	1979.7	M	mt	mM	m	nd	mt	45	45
10-7-34-4W5										
136	C.Sst.	2335.4	M	mt	M	t	nd	t	m	90
16-2-35-4W5										
146	C.Sst.	2220.5	M	t	mM	m	nd	mt	20	65
147	F.Sst.	2224.2	M	mt	mM	t	t	mt	15	80
148	F.Sst.	2228.0	M	mt	mM	mt	nd	m	30	60

TABLE 3.6 MINERALOGY 2-5 μm SIZE-FRACTION

SAMPLE NUMBER	ROCK TYPE	DEPTH (m)	Q	F	C	RELATIVE % CLAYS IS	SM	CL	I	K
16-19-34-2W5										
003	Congl.	2053.6	M	mt	M	t	t	t	mt	95
004	C.Sst.	2053.9	M	t	M	t	nd	t	mt	95
005	F.Sst.	2054.2	M	mt	M	mt	t	mt	30	60
1-25-35-4W5										
010	Congl.	2147.5	M	t	M	10	nd	mt	20	60
011	C.Sst.	2147.9	mM	mt	M	t	t	t	mt	95
012	F.Sst.	2148.3	M	mt	M	5	t	mt	30	60
16-25-34-3W5										
016	Congl.	2069.1	M	mt	M	t	nd	t	mt	95
017	F.Sst.	2071.5	M	mt	M	t	nd	mt	20	75
11-11-35-3W5										
019	Congl.	2074.1	M	mt	M	10	nd	10	35	45
020	F.Sst.	2074.6	M	mt	mM	mt	t	mt	30	60
022	F.Sst.	2079.9	M	mt	mM	5	mt	m	25	60
024	C.Sst.	2090.9	M	m	mM	mt	nd	mt	10	80
6-6-35-2W5										
027	Congl.	2037.5	M	mt	mM	mt	t	mt	10	85
028	F.Sst.	2037.8	M	mt	mM	mt	nd	mt	25	65
029	F.Sst.	2041.4	M	mt	M	mt	nd	mt	25	70
030	F.Sst.	2043.6	M	mt	M	mt	nd	t	m	85
031	F.Sst.	2045.3	M	mt	mM	m	nd	5	30	60
032	F.Sst.	2047.5	M	mt	mM	15	nd	mt	40	40
6-34-34-3W5										
033	C.Sst.	2112.5	M	mt	mM	m	t	mt	15	75
034	Congl.	2115.0	M	mt	M	t	nd	t	mt	95
035	C.Sst.	2115.3	mM	mt	M	t	t	t	mt	95
036	C.Sst.	2115.7	mM	mt	M	t	nd	t	mt	95
037	F.Sst.	2116.5	M	mt	mM	mt	nd	mt	25	65
038	F.Sst.	2121.1	M	mt	M	10	t	15	35	45
6-23-34-3W5										
039	Congl.	2111.4	M	mt	mM	t	t	mt	5	90
041	Congl.	2112.8	M	mt	M	t	t	t	5	90
042	F.Sst.	2113.3	M	mt	M	mt	t	mt	25	70
046	F.Sst.	2121.1	M	mt	mM	m	nd	5	35	55

TABLE 3.6 MINERALOGY 2-5 μm SIZE-FRACTION (CONTINUED)

SAMPLE NUMBER	ROCK TYPE	DEPTH (m)	Q	F	C	RELATIVE % CLAYS				
						IS	SM	CL	I	K
9-3-35-3W5										
047	Shale	2085.0	M	mt	mM	20	5	10	45	10
048	Congl.	2086.3	M	t	mM	mt	nd	t	5	90
049	Congl.	2087.1	M	mt	mM	mt	nd	mt	20	70
050	F.Sst.	2087.6	M	mt	mM	t	nd	t	15	80
052	F.Sst.	2094.0	M	mt	M	5	nd	mt	25	65
16-13-34-3W5										
055	Congl.	2070.5	M	t	mM	20	nd	m	35	35
056	Congl.	2071.0	M	mt	mM	mt	nd	t	m	90
057	F.Sst.	2071.3	M	t	mM	mt	nd	mt	35	60
059	F.Sst.	2076.2	M	t	mM	10	nd	5	25	60
060	C.Sst.	2065.4	M	mt	m	nd	nd	5	20	75
16-35-34-3W5										
061	C.Sst.	2069.2	M	t	mM	mt	nd	mt	15	80
7-4-35-3W5										
077	C.Sst.	2108.5	mM	t	M	t	t	t	mt	95
14-1-35-3W5										
085	F.Sst.	2044.5	M	t	M	m	nd	mt	35	55
086	F.Sst.	2046.7	M	mt	mM	m	nd	mt	30	60
088	F.Sst.	2050.4	M	t	mM	m	nd	mt	30	60
089	F.Sst.	2052.5	M	t	M	m	nd	mt	15	75
16-15-34-3W5										
101	F.Sst.	2131.0	M	t	M	mt	nd	mt	25	70
102	F.Sst.	2132.5	M	mt	M	mt	nd	mt	20	75
103	F.Sst.	2134.0	M	mt	mM	10	nd	5	30	55
104	F.Sst.	2135.5	M	mt	M	m	nd	mt	25	65
105	F.Sst.	2137.8	M	mt	M	mt	nd	t	20	75
6-13-34-3W5										
107	C.Sst.	2080.7	M	mt	mM	mt	nd	nd	15	80
8-25-34-3W5										
111	C.Sst.	2065.7	M	mt	mM	mt	t	mt	10	80

TABLE 3.6 MINERALOGY 2-5 μm SIZE-FRACTION (CONTINUED)

SAMPLE NUMBER	ROCK TYPE	DEPTH (m)	Q	F	C	RELATIVE % CLAYS IS	SM	CL	I	K
8-7-35-3W5										
117	Congl.	2130.6	M	mt	M	t	nd	t	mt	95
118	C.Sst.	2131.1	M	mt	M	t	t	t	5	90
121	F.Sst.	2135.2	M	mt	M	mt	t	mt	20	70
7-33-34-2W5										
124	Congl.	1972.7	M	mt	M	t	nd	t	5	90
125	C.Sst.	1973.3	M	mt	M	t	nd	t	mt	95
126	F.Sst.	1976.0	M	t	mM	mt	nd	mt	30	60
128	F.Sst.	1979.7	M	mt	mM	mt	nd	mt	40	50
10-7-34-4W5										
136	C.Sst.	2335.4	M	mt	M	t	nd	t	5	90
16-2-35-4W5										
146	C.Sst.	2220.5	M	mt	mM	10	mt	mt	25	60
147	F.Sst.	2224.2	M	mt	M	mt	nd	t	15	80
148	F.Sst.	2228.0	M	mt	mM	m	t	mt	30	55

TABLE 3.7 MINERALOGY < 2 μm SIZE-FRACTION

SAMPLE NUMBER	ROCK TYPE	DEPTH (m)	Q	F	C	RELATIVE % CLAYS				
						IS	SM	CL	I	K
16-19-34-2W5										
003	Congl.	2053.6	mM	t	M	t	mt	t	5	85
004	C.Sst.	2053.9	mM	t	M	t	t	mt	m	90
005	F.Sst.	2054.2	m	t	M	m	t	m	50	35
1-25-35-4W5										
010	Congl.	2147.5	mM	t	M	m	t	mt	25	60
011	C.Sst.	2147.9	mM	t	M	t	t	t	5	90
012	F.Sst.	2148.3	m	t	M	m	t	mt	50	40
16-25-34-3W5										
016	Congl.	2069.1	mM	t	M	mt	mt	mt	15	75
017	F.Sst.	2071.5	m	t	M	15	t	5	35	45
11-11-35-3W5										
019	Congl.	2074.1	M	mt	M	15	t	10	55	20
020	F.Sst.	2074.6	mM	t	M	m	nd	m	50	35
022	F.Sst.	2079.9	m	t	M	10	t	m	40	45
024	C.Sst.	2090.9	M	t	M	m	m	20	25	45
6-6-35-2W5										
027	Congl.	2037.5	M	t	M	t	30	5	25	40
028	F.Sst.	2037.8	mM	t	M	m	t	mt	50	40
029	F.Sst.	2041.4	M	t	M	5	t	10	40	40
030	F.Sst.	2043.6	mM	t	M	mt	t	mt	20	75
031	F.Sst.	2045.3	mM	t	M	15	t	m	50	25
032	F.Sst.	2047.5	M	t	M	10	t	5	55	25
6-34-34-3W5										
033	C.Sst.	2112.5	M	t	M	15	mt	m	40	35
034	Congl.	2115.0	mM	mt	M	5	5	5	15	70
035	C.Sst.	2115.3	m	t	M	t	t	5	5	85
036	C.Sst.	2115.7	mM	t	M	t	5	mt	10	80
037	F.Sst.	2116.5	m	t	M	m	t	5	40	45
038	F.Sst.	2121.1	mM	nd	M	15	t	m	50	25
6-23-34-3W5										
039	Congl.	2111.4	M	t	M	mt	25	m	25	40
041	Congl.	2112.8	mM	t	M	mt	10	m	15	65
042	F.Sst.	2113.3	mM	t	M	5	t	m	45	45
046	F.Sst.	2121.1	mM	t	M	10	nd	m	50	35

TABLE 3.7 MINERALOGY < 2 μm SIZE-FRACTION (CONTINUED)

SAMPLE NUMBER	ROCK TYPE	DEPTH (m)	Q	F	C	RELATIVE % CLAYS IS	SM	CL	I	K
9-3-35-3W5										
047	Shale	2085.0	mM	nd	M	15	10	5	60	10
048	Congl.	2086.3	M	t	M	10	5	m	35	45
049	Congl.	2087.1	mM	t	M	5	t	mt	45	45
050	F.Sst.	2087.6	mM	t	M	5	t	mt	40	45
052	F.Sst.	2094.0	mM	t	M	10	t	5	50	35
16-13-34-3W5										
055	Congl.	2070.5	mM	t	M	15	t	mt	50	25
056	Congl.	2071.0	mM	t	M	5	t	5	25	65
057	F.Sst.	2071.3	mM	t	M	m	nd	5	45	40
059	F.Sst.	2076.2	mM	t	M	15	t	5	50	25
060	C.Sst.	2065.4	M	t	M	t	25	5	40	30
16-35-34-3W5										
061	C.Sst.	2069.2	M	t	mM	t	5	m	35	50
7-4-35-3W5										
077	C.Sst.	2108.5	M	mt	M	t	t	mt	m	90
14-1-35-3W5										
085	F.Sst.	2044.5	m	t	M	10	t	m	50	35
086	F.Sst.	2046.7	m	t	M	15	mt	5	50	25
088	F.Sst.	2050.4	m	t	M	10	t	5	55	25
089	F.Sst.	2052.5	m	t	M	15	t	m	40	35
16-15-34-3W5										
101	F.Sst.	2131.0	m	t	M	m	t	5	45	40
102	F.Sst.	2132.5	m	t	M	10	t	5	50	35
103	F.Sst.	2134.0	mM	t	M	10	t	5	55	30
104	F.Sst.	2135.5	mM	t	M	15	t	m	50	30
105	F.Sst.	2137.8	mM	t	M	10	t	5	60	20
6-13-34-3W5										
107	C.Sst.	2080.7	M	t	M	mt	30	5	30	30
8-25-34-3W5										
111	C.Sst.	2065.7	mM	t	M	mt	15	mt	30	45

TABLE 3.7 MINERALOGY < 2 μm SIZE-FRACTION (CONTINUED)

SAMPLE NUMBER	ROCK TYPE	DEPTH (m)	Q	F	C	RELATIVE % CLAYS				
						IS	SM	CL	I	K
8-7-35-3W5										
117	Congl.	2130.6	mM	mt	M	mt	mt	mt	20	70
118	C.Sst.	2131.1	mM	t	M	m	t	m	30	55
121	F.Sst.	2135.2	m	nd	M	10	t	mt	50	35
7-33-34-2W5										
124	Congl.	1972.7	mM	mt	M	10	15	5	35	35
125	C.Sst.	1973.3	mM	t	M	5	t	m	15	70
126	F.Sst.	1976.0	mM	t	M	m	nd	5	45	45
128	F.Sst.	1979.7	mM	t	M	10	t	m	55	25
10-7-34-4W5										
136	C.Sst.	2335.4	mM	t	M	m	nd	mt	35	55
16-2-35-4W5										
146	C.Sst.	2220.5	M	t	M	10	mt	m	45	35
147	F.Sst.	2224.2	mM	t	M	m	t	mt	35	50
148	F.Sst.	2228.0	mM	t	M	m	t	m	55	30

smectite. Carbonate cement (dolomite and ankerite) occurs only rarely in the conglomerates and coarse-grained sandstones. Quartz is a major cement and occurs as pore-lining crystals (Figures 3.5A,B,E, 3.8C) and complete overgrowths (Figures 3.5D and 3.6A). Pore-filling kaolinite occurs in major abundance in the conglomerates and coarse-grained sandstones (Figures 3.5C, 3.6C,D, 3.7D,E and 3.8A). Individual kaolinite crystals can grow to 15 or 20 μm in size (Figures 3.5D, 3.6E, 3.7C and 3.8B).

In the conglomerates, the average kaolinite diameter is 12 to 25 μm; authigenic quartz crystals average 10 to 20 μm. Estimates of pore throat diameters (from SEM photographs) range from 20 to 40 μm and pores are from 75 to 250 μm (Figures 3.5A,E and 3.6C). This gives a ratio of kaolinite diameter to pore throat diameter of approximately 0.5.[3] The coarse-grained sandstones have average kaolinite diameters of 10 to 12 μm; authigenic quartz crystals average 10 to 20 μm (Figures 3.7B and 3.8B,C). Estimates of pore throat diameters (from SEM photographs) range from 10 to 20 μm and pores are from 50 to 150 μm in size (Figures 3.7A,D). The ratio of kaolinite crystal diameter to pore throat diameter is approximately 0.7.

Illite and illite / smectite occur as pore-lining cements in the conglomerates and coarse-grained sandstones (Figures 3.6A, 3.6F, 3.8E). Smectite cement is relatively rare and occurs as a pore-lining phase (Figures 3.6B, 3.8D). Pyrite is also a rare cement; it occurs as framboids attached to grain surfaces or filling pores (Figure 3.5F). Siderite was not recognized in any of the conglomerates but can be seen as small rhombs attached to grain surfaces in the coarse-grained sandstones (Figures 3.7F, 3.8F).

The fine-grained sandstones are also primarily affected by quartz and kaolinite cements, but carbonate cements are also very important and are locally dominant. Illite and illite / smectite are also common. Quartz cement occurs mainly as complete overgrowths (Figures 3.9B,D and 3.10E) or, less commonly, as pore-lining crystals (Figures 3.9B and 3.10C). Kaolinite occurs as a pore-filling (Figures 3.10B,C). In the fine-grained sandstones kaolinite diameters average 7 to 10 μm (Figures 3.10B,C) and quartz crystals average 10 to 15 μm in size (Figure 3.9B). Pore throat estimates in the fine-grained sandstones range from 5 to 10 μm (Figures 3.9A,C) and pores are from < 20 to > 100 μm (Figures 3.9A,C).

---

[3] *It is important to note that pore-throats measured in this manner provide only a crude estimate*; other techniques, such as acetate peels and mercury injection (which are beyond our existing analytical capabilities), should be used to verify these estimates.

FIGURE 3.5

3.5A. SEM photograph of a conglomerate showing quartz (AQ) and kaolinite (K) cementation (well 11-11-35-3W5, 2074.1 m, sample # 019).

3.5B. SEM photograph of a conglomerate showing pore-lining, authigenic, quartz crystals (AQ)(well 11-11-35-3W5, 2074.1 m, sample # 019).

3.5C. SEM photograph of a conglomerate showing pore-filling, authigenic, kaolinite cement (K)(well 11-11-35-3W5, 2074.1 m, sample # 019).

3.5D. SEM photograph showing a conglomerate with large, euhedral quartz overgrowths (AQ) and pore-filling kaolinite (K). Note the large size of the kaolinite crystals (well 11-11-35-3W5, 2074.1 m, sample # 019).

3.5E. SEM photograph showing a conglomerate with large size pores and minor, pore-lining, authigenic quartz (AQ)(well 16-25-34-3W5, 2069.1 m, sample # 016).

3.5F. SEM photograph of a conglomerate showing pyrite cementation. The pyrite (PY) occurs as framboids attached to grain surfaces and partially filling pores (well 16-25-34-3W5, 2069.1 m, sample # 016).

FIGURE 3.5

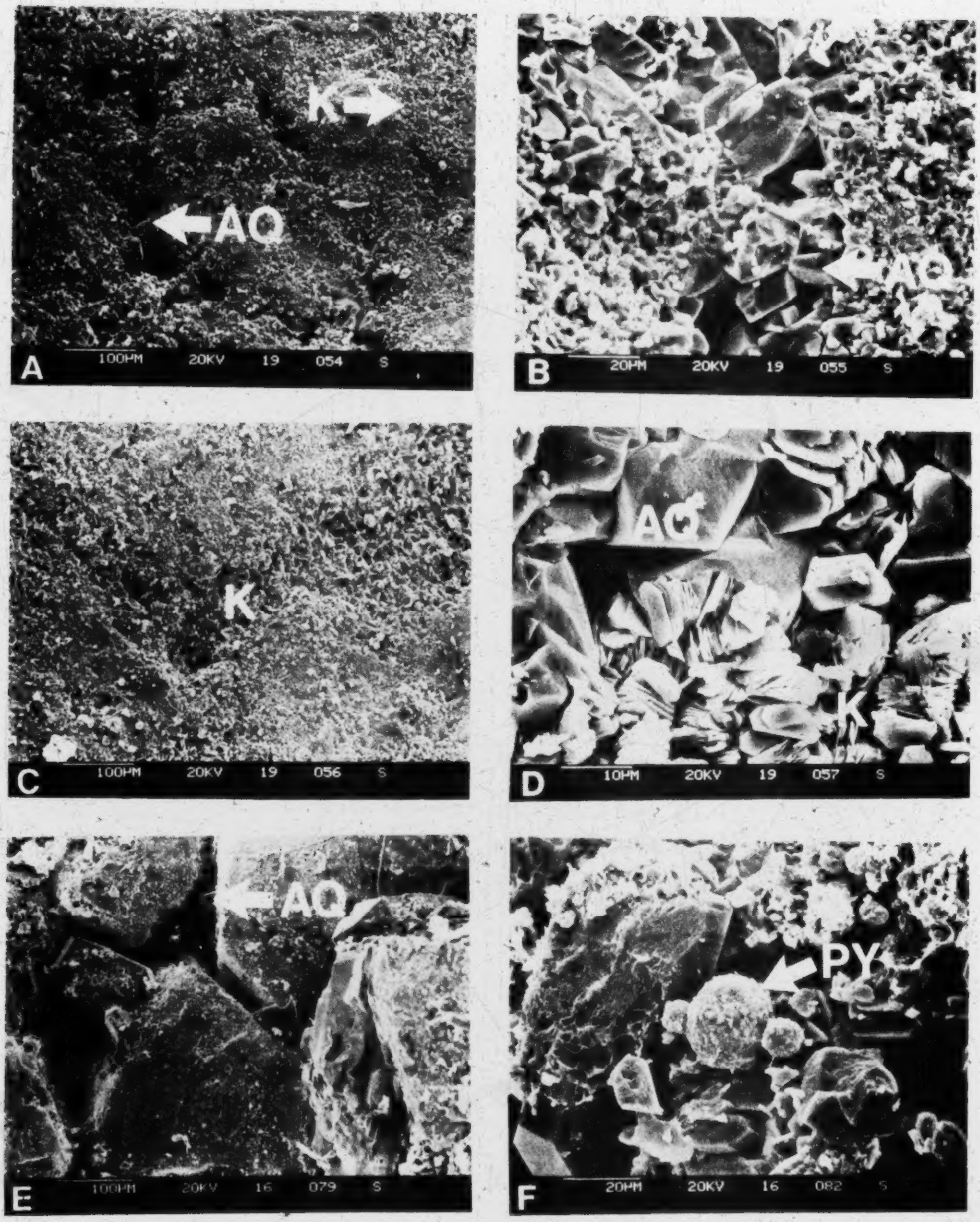
K
AQ
A
100PM 20KV 19 054 S
AQ
B
20PM 20KV 19 055 S
K
C
100PM 20KV 19 056 S
AQ
K
D
10PM 20KV 19 057 S
AQ
E
100PM 20KV 16 079 S
PY
F
20PM 20KV 16 082 S

FIGURE 3.6

3.6A. SEM photograph showing a conglomerate with large, euhedral, quartz overgrowths (AQ) and abundant pore-lining illite and illite / smectite (I-IS)(well 8-7-35-3W5, 2130.6 m, sample # 117).

3.6B. SEM photograph of a conglomerate showing pore-lining smectite cement (SM)(well 6-34-34-3W5, 2115.0 m, sample # 034).

3.6C. SEM photograph of a conglomerate showing good, interconnected porosity with scattered patches of pore-filling kaolinite (K)(well 6-6-35-2W5, 2037.5 m, sample # 027).

3.6D. SEM photograph showing a close-up of pore-filling kaolinite from Figure 3.6C (well 6-6-35-2W5, 2037.5 m, sample # 027).

3.6E. SEM photograph showing a close-up of kaolinite crystals in Figures 3.6C and 3.6D. Note the large size of the individual kaolinite crystals (K)(well 6-6-35-2W5, 2037.5 m, sample # 027).

3.6F. SEM photograph of a conglomerate showing abundant pore-lining illite (I). Note the delicate morphology of the crystals (well 8-7-35-3W5, 2130.6 m, sample # 117).

FIGURE 3.6

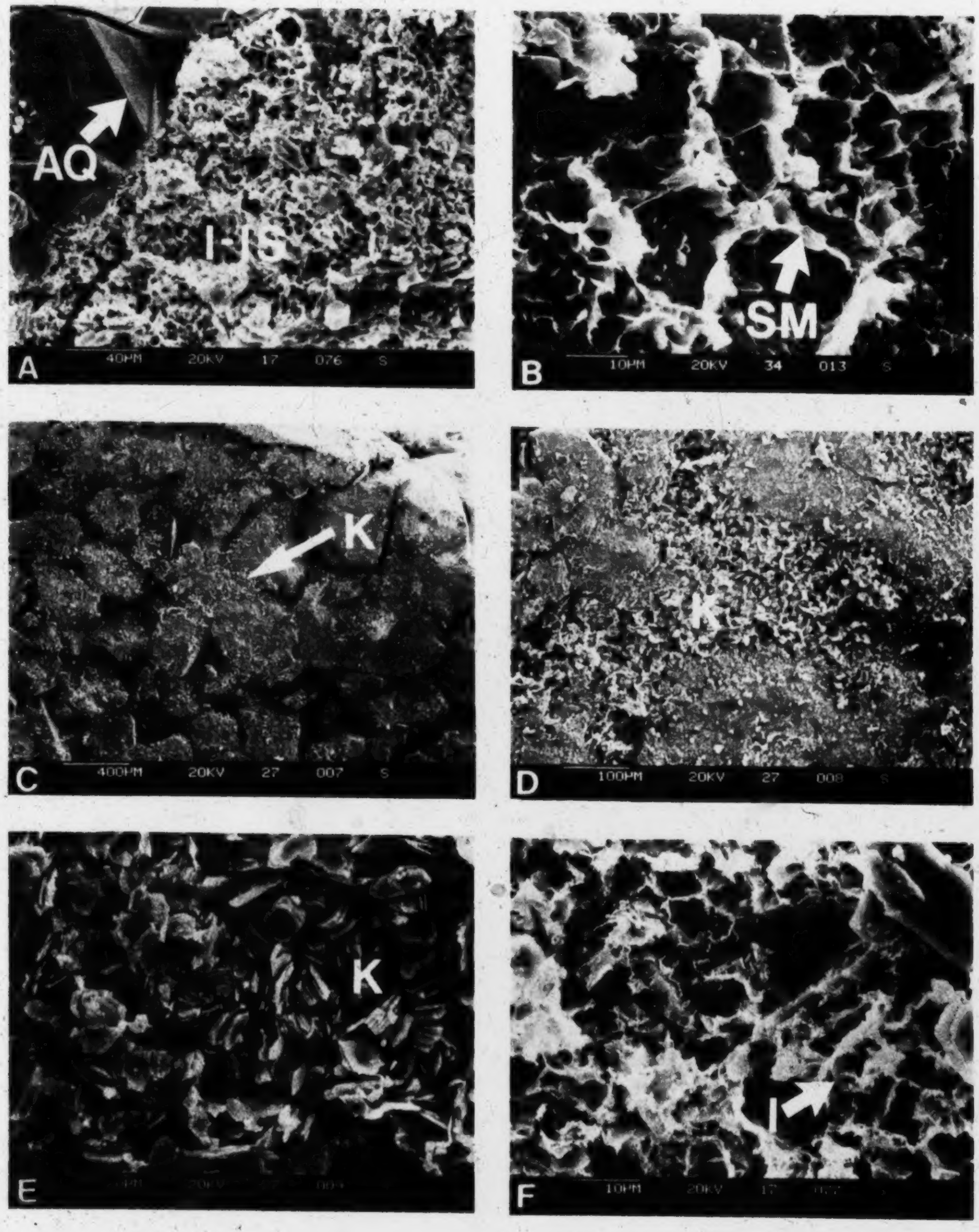
AQ
I/S
A
40PM 20KV 17 076 S
SM
B
10PM 20KV 34 013 S
K
C
400PM 20KV 27 007 S
K
D
100PM 20KV 27 008 S
K
E
20KV 009
I
F
10PM 20KV 17

FIGURE 3.7

3.7A. SEM photograph of a coarse-grained sandstone showing interconnected, primary, intergranular porosity. Note the large size of the pores (well 7-4-35-3W5, 2108.5 m, sample # 077).

3.7B. SEM photograph showing a coarse-grained sandstone with large, euhedral, pore-lining, quartz crystals (AQ). Note the large size of the individual quartz crystals (well 7-4-35-3W5, 2108.5 m, sample # 077).

3.7C. SEM photograph of a coarse-grained sandstone showing pore-lining kaolinite (K). Note the large size of the individual kaolinite crystals and the booklet-like aggregates (well 7-4-35-3W5, 2108.5 m, sample # 077).

3.7D. SEM photograph of a coarse-grained sandstone showing some of the pores filled with kaolinite while others are unoccluded (well 16-19-34-2W5, 2053.9 m, sample # 004).

3.7E. SEM photograph a large pore in a coarse-grained sandstone completely filled with authigenic kaolinite (K)(well 16-19-34-2W5, 2053.9 m, sample # 004).

3.7F. SEM photograph of a coarse-grained sandstone showing siderite rhombs (S) attached to grain surfaces (well 16-19-34-2W5, 2053.9 m, sample # 004).

FIGURE 3.7

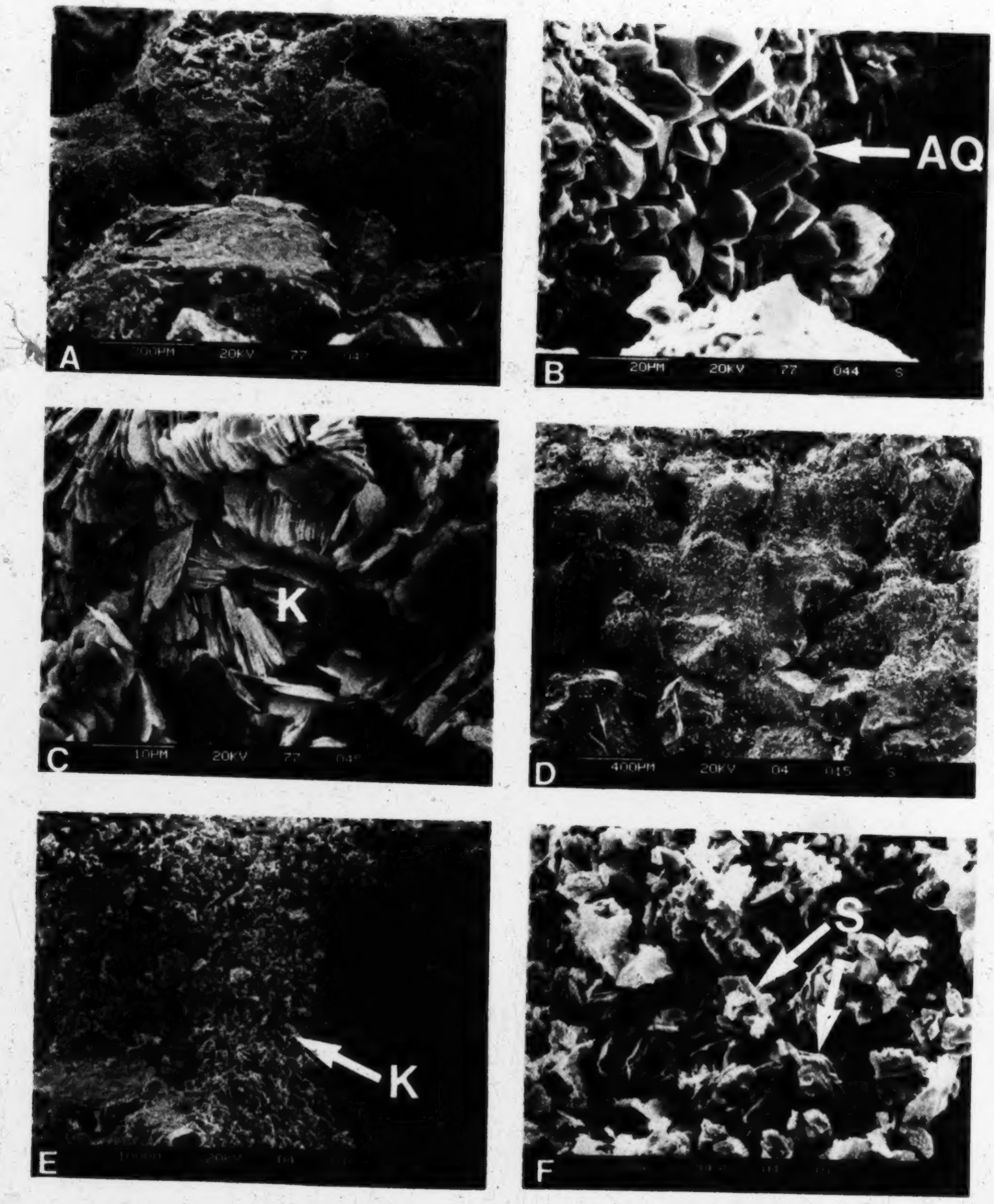
A
200PM 20KV 77 047
B
20PM 20KV 77 044 S
AQ
C
10PM 20KV 77
K
D
400PM 20KV 04 015 S
E
K
F
S

FIGURE 3.8

3.8A. SEM photograph of a coarse-grained sandstone showing abundant pore-filling kaolinite (K)(well 1-25-35-4W5, 2147.9 m, sample # 011).

3.8B. SEM photograph showing a close-up of Figure 3.8A. Note the booklets of kaolinite (K) and the size of the individual crystals (well 1-25-35-4W5, 2147.9 m, sample # 011).

3.8C. Sem photograph of a coarse-grained sandstone showing euhedral, authigenic, quartz crystals (AQ) lining a pore. Many of the quartz crystals are greater than 20 *um* long (well 1-25-35-4W5, 2147.9 m, sample # 011).

3.8D. SEM photograph showing grain coating smectite (SM) in a coarse-grained sandstone (well 1-25-35-4W5, 2147.9 m, sample # 011).

3.8E. SEM photograph of a coarse-grained sandstone showing pore-lining illite (I). Notice the delicate morphology of the illite crystals (well 8-7-35-3W5, 2131.1 m, sample # 118).

3.8F. SEM photograph showing large rhombs of siderite (S) attached to a grain surface in a coarse-grained sandstone (well 16-19-34-2W5, 2053.9 m, sample # 004).

FIGURE 3.8

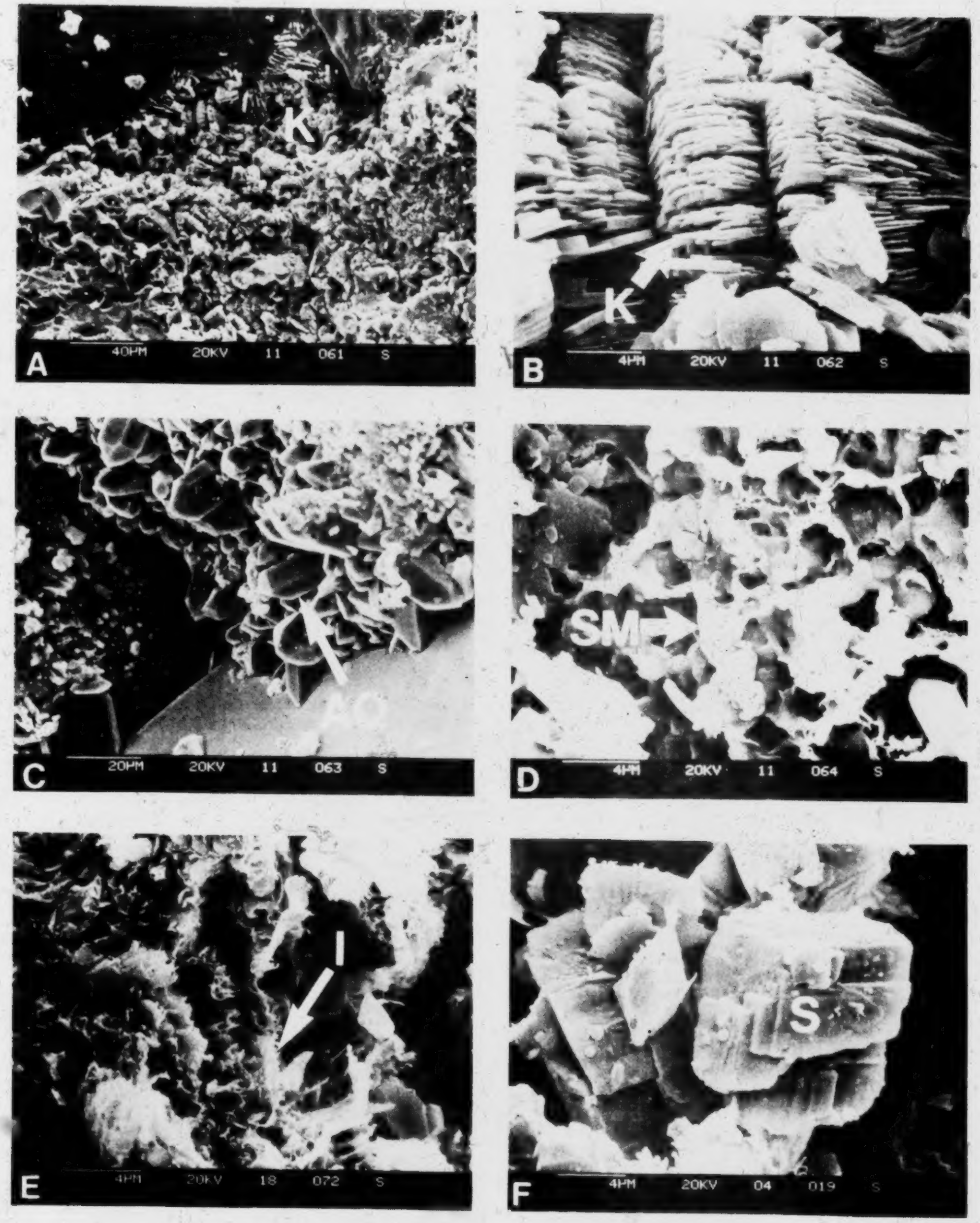
K
A
40PM 20KV 11 061 S
K
B
4PM 20KV 11 062 S
AQ
C
20PM 20KV 11 063 S
SM
D
4PM 20KV 11 064 S
I
E
4PM 20KV 18 072 S
S
F
4PM 20KV 04 019 S

FIGURE 3.9

3.9A. SEM photograph of a fine-grained sandstone showing the size of the pores and pore throats (arrow)(well 8-7-35-3W5, 2135.2 m, sample # 121).

3.9B. SEM photograph of a fine-grained sandstone showing large, euhedral, complete, quartz overgrowths (AQ) and large pore-lining crystals (well 8-7-35-3W5, 2135.2 m, sample # 121).

3.9C. SEM photograph showing a general view of a fine-grained sandstone with poor porosity (well 8-7-35-3W5, 2135.2 m, sample # 121).

3.9D. SEM photograph showing a close-up of Figure 3.9C. The poor porosity is due to extensive, quartz cementation (well 8-7-35-3W5, 2135.2 m, sample # 121).

3.9E. SEM photograph of a fine-grained sandstone with extensive siderite cementation. The siderite (S) occurs as small rhombs attached to grain surfaces (well 11-11-35-3W5, 2079.9 m, sample # 022).

3.9F. SEM photograph showing a fine-grained sandstone with pore-throat-bridging illite (I) cement and carbonate (dolomite-ankerite) cement (CA) (well 11-11-35-3W5, 2079.9 m, sample # 022).

FIGURE 3.9

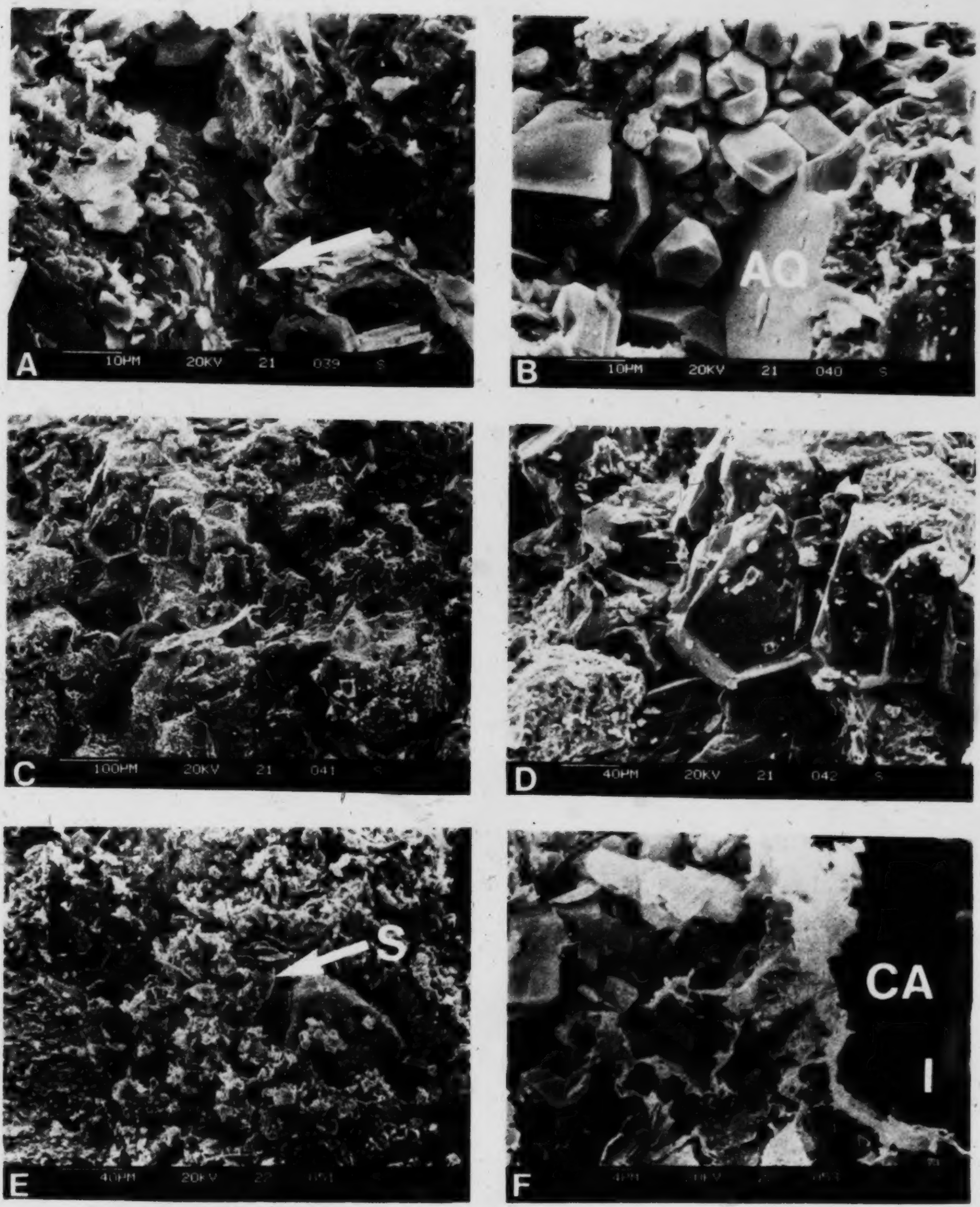
A
10µM 20KV 21 039 S
B
AQ
10µM 20KV 21 040 S
C
100µM 20KV 21 041 S
D
40µM 20KV 21 042 S
E
S
40µM 20KV 22 051 S
F
CA
I
4µM

FIGURE 3.10

3.10A. SEM photograph of a fine-grained sandstone showing pore-filling carbonate (dolomite-ankerite) cement (CA)(well 16-25-34-3W5, 2071.5 m, sample # 017).

3.10B. SEM photograph showing a fine-grained sandstone with abundant pore-filling kaolinite (K). Notice the booklets of kaolinite and the large size of the individual crystals (well 16-25-34-3W5, 2071.5 m, sample # 017).

3.10C. SEM photograph of a fine-grained sandstone showing pore-lining, authigenic, quartz crystals (AQ), many greater than 20 *um* in size (well 16-25-34-3W5, 2071.5 m, sample # 017).

3.10D. SEM photograph showing grain-coating siderite cement(s) in a fine-grained sandstone (well 11-11-35-3W5, 2079.9 m, sample # 022).

3.10E. SEM photograph of a fine-grained sandstone showing a complete, quartz overgrowth (AQ) growing into a pore (well 1-25-35-4W5, 2148.3 m, sample # 012).

3.10F. SEM photograph showing a fine-grained sandstone with abundant, pore-lining illite and illite / smectite (I-IS). Note the delicate crystal morphology (well 1-25-35-4W5, 2148.3 m, sample # 012).

FIGURE 3.10

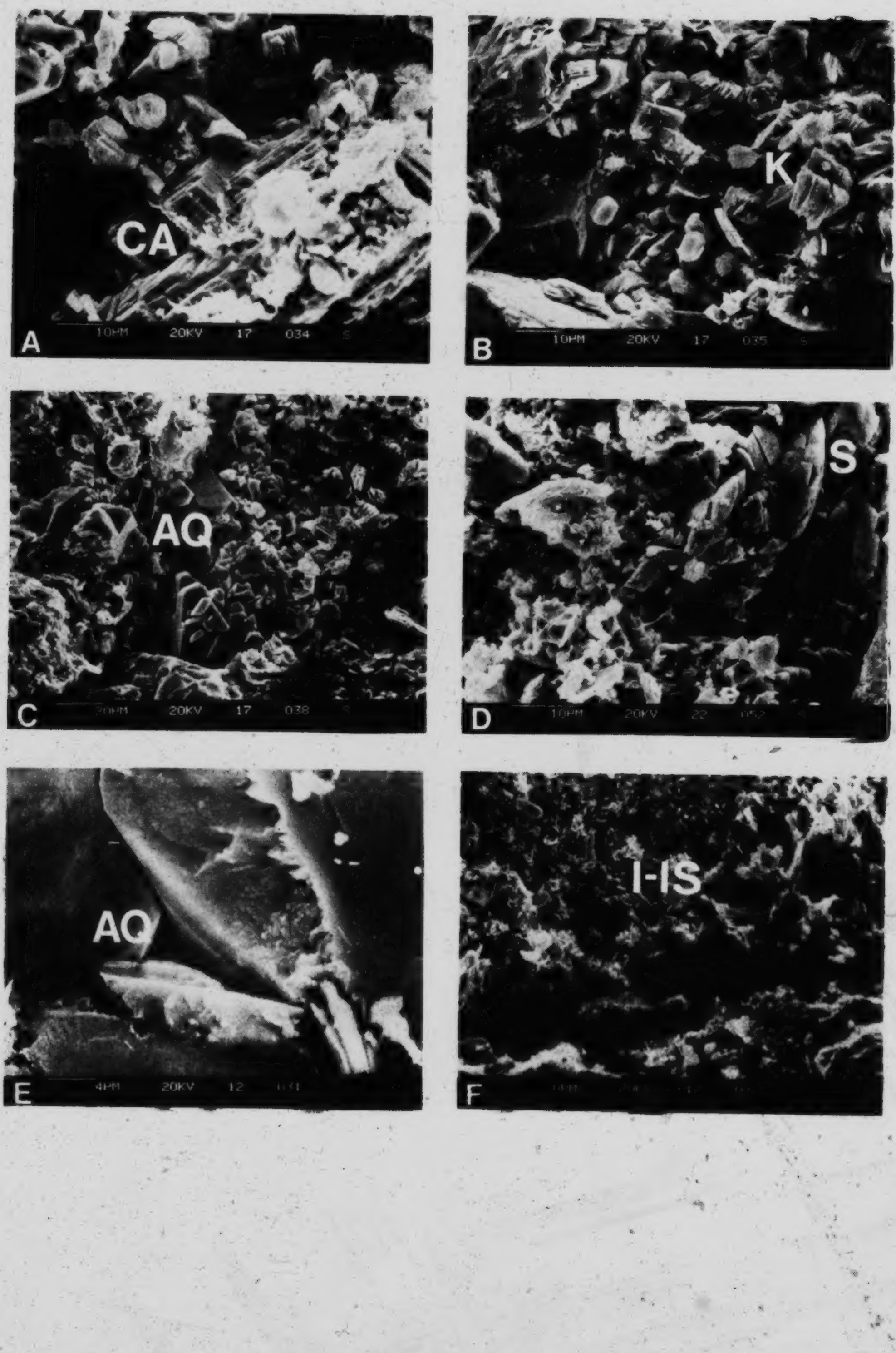
CA
A
10HM 20KV 17 034 S
K
B
10HM 20KV 17 035 S
AQ
C
20HM 20KV 17 038 S
S
D
10HM 20KV 22 052
AQ
E
4HM 20KV 12
I-IS
F

The ratio of kaolinite diameter to pore throat width is close to 1.0 in the fine-grained sandstones. This value is considerably higher than those found in the conglomerates and coarse-grained sandstones. Illite and illite/smectite occur as pore throat bridging (Figure 3.9F) or pore-lining phases (Figure 3.10F). Siderite occurs as small rhombs attached to grain surfaces (Figures 3.9E and 3.10D); dolomite and ankerite occur as pore-filling cements (Figures 3.9F and 3.10A).

E. PARAGENETIC SEQUENCE

From the study of thin sections and scanning electron micrographs the paragenetic sequence in the Viking Formation may be deduced. Pyrite and siderite cements were formed prior to quartz cementation (Figures 3.4E and 3.5F) and appear to have formed very early and at shallow burial depths. Dolomite and ankerite cements occur after quartz cementation, prior to clay mineral authigenesis and at relatively deep burial depths. (Figures 3.4F and 3.10A). Solution of carbonate cements took place before clay minerals precipitated. The last event to occur was the migration of hydrocarbons which are seen staining pore-filling clay minerals in many samples (Figure 3.3C).

F. DIAGENESIS

Alteration of porosity and permeability in the Viking Formation at Garrington has occurred due to several distinct diagenetic events. Early diagenesis involved pyrite and siderite cementation, mechanical compaction and creation of pseudomatrix. These events were followed by chemical compaction and crystallization of quartz and feldspar overgrowths. Feldspar solution followed these events. With continued burial pore-filling carbonate cements formed. The first pore-filling carbonate to form was probably calcite which was subsequently dolomitized. Dolomite cement was later ankeritized at depth. Secondary porosity was formed when dolomite and ankerite cements were dissolved by acidic fluids generated by the maturation of organic matter in adjacent shales. Once the acidic fluids became neutralized they precipitated clay minerals into primary and secondary pore spaces. At the greatest depths of burial albitization of feldspars may have taken place. Albitization could have provided Ca^{2+} for late calcite cements and Al^{3+} for clay mineral genesis. The last diagenetic event to occur was the migration of hydrocarbons.

Figure 3.11 is a summary diagram of the diagenetic events.

EARLY DIAGENESIS: PYRITE AND SIDERITE FORMATION

Chemical pathways followed by early diagenetic reactions are affected by rates of sedimentation and accumulation of organic matter (Gautier, 1983; Curtis, 1978; Irwin and Curtis, 1977). In marine sediments with excess organic matter early diagenesis takes place in three depth related metabolic zones: (1) a zone of aerobic oxidation, (2) a zone of sulfate reduction and (3) a zone of methanogenesis or fermentation (Gautier, 1983; Curtis, 1978; Irwin and Curtis, 1977)(Figure 3.12). The transition from one metabolic zone to another results from biological responses to changes in the chemistry of the water column or to biogeochemical changes in the interstitial waters. Aerobic oxidation proceeds in zone 1 until oxygen is depleted. In this zone diffuse input of oxygen maintains high oxidation states and supports oxidative breakdown of organic matter according to the reaction:

$CH_2O + O_2 = CO_2 + H_2O$ (Irwin and Curtis, 1977).

Soluble products will tend to dissipate into the water column. For this reason carbonate supersaturation does not occur and carbonates do not normally precipitate. In the Viking Formation zone 1 is characterized by burrow mottling and extensive bioturbation (Figure 3.12).

Reducing conditions are established as the rate of molecular oxygen uptake exceeds diffusive supply. Oxygen depletion corresponds with the anoxic / oxic boundary at the top of the sulfate reduction zone. Sulfidic conditions are brought about by bacterial reduction of sulfate which accompanies the anaerobic oxidation of organic matter (Gautier, 1983; Curtis, 1978; Irwin and Curtis, 1977). The reaction is:

$2CH_2O + SO_4^{2-} = 2CO_2 + S^{2-} + H_2O$ (Irwin and Curtis, 1977).

The reduced sulfur species combine with Fe^{2+} to precipitate pyrite in zone 2 (Gautier, 1983; Curtis, 1978; Berner, 1970)(Figures 3.5F, 3.11 and 3.12). Sulfate reducing bacteria thrive as long as diffusive supply of sulfate from depositional waters lasts. In the fine-grained sandstones of the Viking Formation early pyrite cement is seen as small euhedral crystals occurring as grain coats or as inclusions in detrital grains (Figure 3.5F). Pyrite cements are not extensive within the fine-grained sandstones and are quantitatively

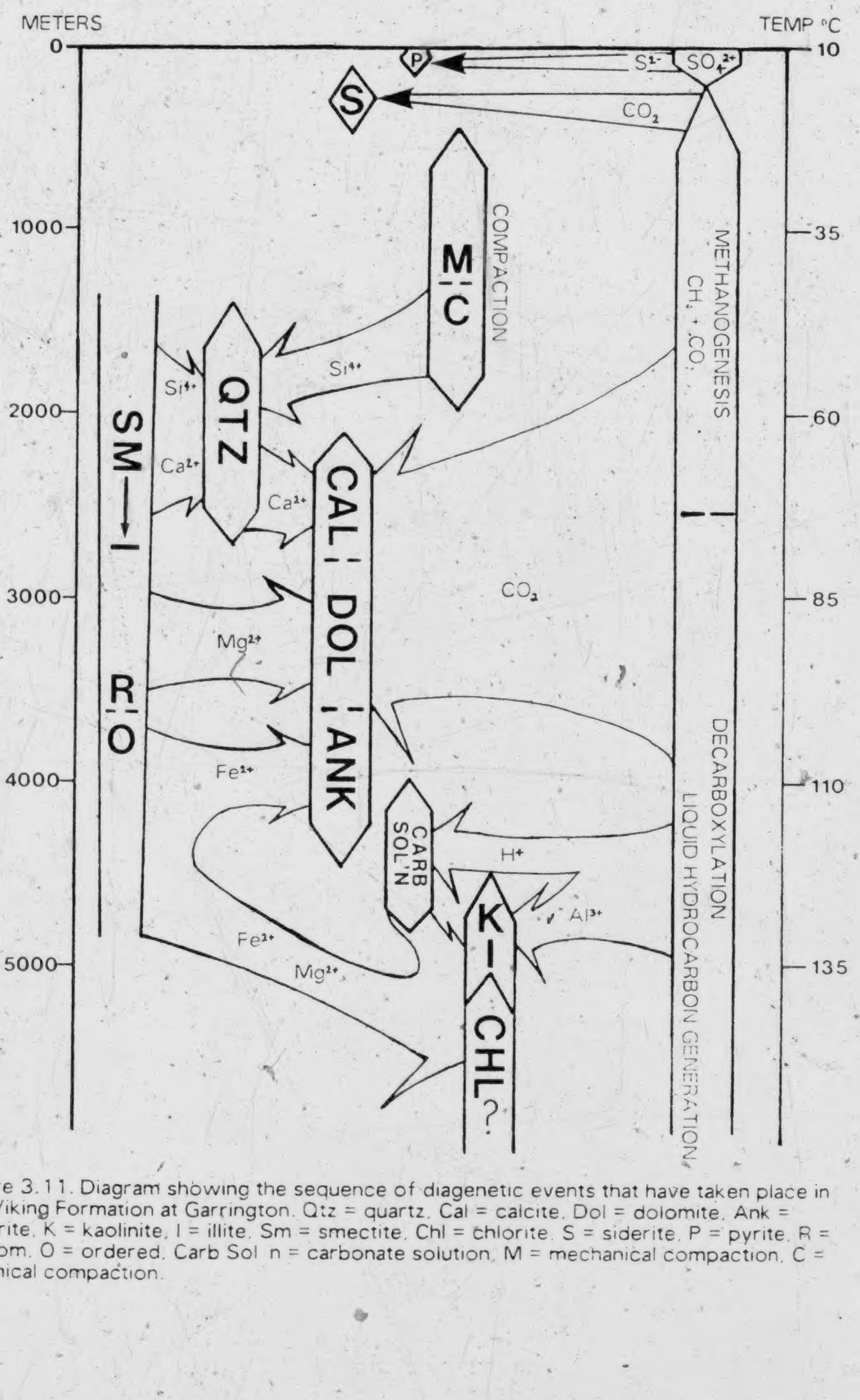
METERS
TEMP °C
0
1000
2000
3000
4000
5000
10
35
60
85
110
135
P
S
S^{2-}
SO_4^{2+}
CO_2
M
C
COMPACTION
METHANOGENESIS
$CH_4 + CO_2$
Si^{4+}
Si^{4+}
QTZ
SM—I
Ca^{2+}
Ca^{2+}
CAL
DOL
ANK
CO_2
Mg^{2+}
R
O
Fe^{2+}
CARB SOL'N
H^+
Al^{3+}
K
I
CHL?
Fe^{2+}
Mg^{2+}
DECARBOXYLATION
LIQUID HYDROCARBON GENERATION

Figure 3.11. Diagram showing the sequence of diagenetic events that have taken place in the Viking Formation at Garrington. Qtz = quartz, Cal = calcite, Dol = dolomite, Ank = ankerite, K = kaolinite, I = illite, Sm = smectite, Chl = chlorite, S = siderite, P = pyrite, R = random, O = ordered, Carb Sol n = carbonate solution, M = mechanical compaction, C = chemical compaction.

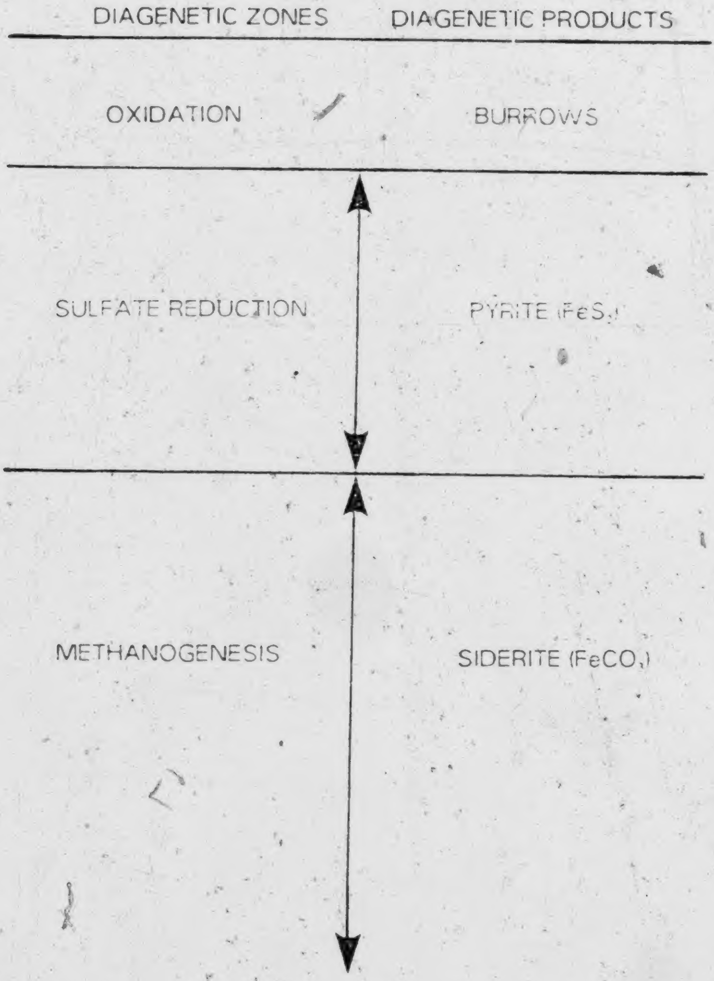
DIAGENETIC ZONES
DIAGENETIC PRODUCTS
OXIDATION
BURROWS
SULFATE REDUCTION
PYRITE (FeS$_2$)
METHANOGENESIS
SIDERITE (FeCO$_3$)

Figure 3.12. Diagram showing the three earliest zones of diagenesis and the diagenetic products characteristic of each zone (modified from Gautier, 1983).

unimportant. This cement is rarer still in the conglomerates and coarse-grained sandstones suggesting that sulfate reducing conditions rarely occurred in these rock types.

The third zone of early diagenesis is a zone of methanogenesis or fermentation. Methanic diagenesis commonly occurs over a depth interval from a few metres to depths at which early stages of thermal decarboxylation of organic matter take over as the principle diagenetic processes. Thus the zone of carbonate reduction and methane generation is generally coincident with those depths at which most sediment dewatering occurs. The basic reaction of methanogenesis is,

$2CH_2O = CH_4 + CO_2$ (Irwin and Curtis, 1977).

Siderite cement is characteristic of this zone (Figure 3.12).

Siderite cement is very common in the fine-grained sandstones but is only quantitatively important in a few of the samples (Figures 3.4D,E and 3.10D). In the conglomerates and coarse-grained sandstones siderite was very minor. Siderite cement most often occurs as small euhedral rhombs attached to grain surfaces. In extreme cases siderite cement totally encases individual detrital grains completely cementing the sandstone and inhibiting later diagenesis. Siderite also replaces chert grains. Where this occurs, the siderite appears to initially replace carbonate inclusions within the chert grains and then to replace the rest of the grain. This type of sideritization was seen in all lithologies within the Viking Formation and occurs in all stages of completion. Siderite also occurs as nodules and rip-up clasts within the sediments.

COMPACTION

As sediments are buried, compaction and dewatering takes place. Dewatering initially occurs by upward transmission of water out of the sediment but as mechanical compaction takes place vertical permeability is greatly reduced and expelled water begins to move updip through the more permeable conduits of sandstones (Gautier, 1983). Pore fluids carrying the products of methanic diagenesis evolve through the addition of shale waters and chemical reactions with sandstones. These fluids have a significant influence on sandstone diagenesis.

Mechanical compaction in the Viking Formation has reduced porosity and permeability by progressive tighter packing of the framework grains. Ductile grains, such as micas and shaly rock fragments, occur bent about more competent chert or quartz grains or squeezed between grains resulting in the creation of shaley-pseudomatrix (Thomas and Oliver, 1979). Because of the large grain size and poor sorting of the conglomerates, these rocks are subject to the most mechanical compaction. Mechanical compaction is inhibited in the fine-grained sandstones due to the fine grain size and the large number of grain contacts (Thomas and Oliver, 1979). Where fine-grained sandstones were previously extensively cemented by siderite mechanical compaction is further inhibited.

Chemical compaction follows mechanical compaction. Chemical compaction is evident where suture contacts exist between chert or quartz grains and softer rock fragments and where crenulated or concave-convex contacts exist between chert and quartz grains. In contrast to mechanical compaction chemical compaction is enhanced by fine grain size and is evident in the fine-grained sandstones where highly developed grain to grain contacts and secondary quartz overgrowths exist (Thomas and Oliver, 1979). In the conglomerates and coarse-grained sandstones chemical compaction is manifested by the presence of sutured contacts between detrital grains (Figure 3.3B).

QUARTZ CEMENTATION

The formation of quartz cement is a relatively early diagenetic event associated with increased chemical compaction with depth of burial (Figure 3.11). Other sources of silica for quartz overgrowths are clay mineral diagenesis and alteration of feldspars. Boles and Franks (1979) report that Si^{4+} released by illitization of smectite is transferred from shales to sandstones and produces quartz overgrowths at temperatures as low as 60° C. They propose the reaction:

$3.93\,K^{+} + 1.57\,KNaCa_2Mg_4Fe_4Al_{14}\,Si_{38}O_{100} \times 10H_2O =$

$K_{5.5}Mg_2Fe_{1.5}Al_{22}\,Si_{35}O_{100} + 1.57Na^{+} + 3.14Ca^{2+}$

$+ 4.28Mg^{2+} + 4.78Fe^{2+} + 24.66\,Si^{4+} + 57O^{2-} + 11.40OH^{-} + 15.7H_2O$

where each mole of illite formed releases approximately 24 moles of Si^{4+} which can form quartz overgrowths in adjacent sandstones (see Figure 3.11).

Hower et al. (1976) suggest that the main factor controlling the extent of the smectite to illite transition is temperature. Eberl and Hower (1976) state that the smectite to illite transition takes place in a temperature range from 50° C to 100° C, with expandable layers decreasing from 80 % to approximately 20 %. Much of the K^+ needed in the smectite to illite conversion is believed to be provided by feldspars and micas in the shales. Feldspars and micas in the shales may also provide Si^{4+} for quartz cement.

In the Viking rocks examined quartz cements occur in two different styles. On chert grains quartz overgrowths occur as small individual crystals attached to the polycrystalline chert (Figures 3.3D and 3.7B). These overgrowths are generally incomplete or not as well developed as those which occur on monocrystalline quartz grains. This is due to the random orientation of the c-axes of the polycrystalline chert grains. The result is a rim of quartz crystals in optical discontinuity showing a jagged or sawtooth structure. Overgrowths on monocrystalline quartz grains occur in optical continuity with the quartz grains and have euhedral terminations (Figures 3.3E and 3.4A).

The conglomerates, because of the large quantities of chert present and conditions unfavorable for chemical compaction, are dominated by incomplete quartz overgrowths. Coarse-grained sandstones have a higher quartz content than the conglomerates and more complete quartz overgrowths; fine-grained sandstones are dominated by quartz and generally have complete quartz overgrowths. In fine-grained sandstones with extensive quartz cement pore networks occur as small angular shaped voids where quartz overgrowths have not grown together (Figure 3.10E). Triple junctions are present where a number of quartz overgrowths meet (Figure 3.3E). A few fine-grained sandstones have very minor amounts of quartz cement due to early siderite cement poisoning grain surfaces and inhibiting quartz overgrowths (Figure 3.4E).

FELDSPAR CEMENT

Feldspar cement is very rare in the samples studied. Chemical conditions favoring feldspar overgrowths require a supply of Na^+, K^+, Si^{4+} and Al^{3+}. The source of feldspar cement was probably from solution of feldspars of intermediate composition which are not as stable as end members (Westcott, 1983). This cement occurs as rims on detrital feldspar grains and is probably associated with pressure solution and leaching of feldspars (Figure 3.4B).

FELDSPAR SOLUTION

Solution of feldspar is related to its instability with increasing pressure and temperature (Hower et al., 1976; Boles and Franks, 1979). Most feldspar solution appears to be due to leaching. Products of feldspar solution are quartz and feldspar overgrowths. Some feldspar solution may also be related to the formation of kaolinite during later diagenesis.

LATE CARBONATE CEMENTATION

Late carbonate cementation follows quartz cementation and appears to be very complex. The most common late carbonate cements observed are dolomite and ankerite; calcite was observed in only one sample. These carbonate cements occur as a pore-fillings or as replacements of detrital quartz grains (Figure 3.4C). Quartz and chert grains are often etched and pitted and may be partially to totally replaced. Late carbonate cement is also seen filling in voids in partially dissolved feldspars.

The first late carbonate cement to form was probably calcite. This cement formed in the lower methanogenesis zone or very early in the zone of decarboxylation (Figure 3.11). Bicarbonate produced by anaerobic oxidation of organic matter or by early stages of thermal decarboxylation combined with Ca^{2+} released as the interlayer cation from the ongoing smectite to illite transition to form the earliest carbonate cements (Figure 3.11). Curtis (1978) states that the extent of magnesium concentration in carbonate cement depends on the rate of precipitation as well as the magnesium content of the solution. The fact that calcite was only observed in one sample may indicate that dolomite cement was formed concurrently with the calcite. Alternatively, early calcite may have been dolomitized by Mg-bearing solutions released from shales as the smectite to illite transition proceeded. In the one sample which contains calcite, it is observed filling the centre of the pore space. Moving toward the detrital grains there is a rim of dolomite followed by a rim of ankerite which abuts framework grains. This arrangement suggests an early phase of calcite cement which filled pore space, followed by dolomitization along the grain boundaries. Dolomite cements were subsequently ankeritized at depth.

Iron enrichment of carbonate cements with depth has been reported by many workers (Boles and Franks, 1979; Boles, 1978; Pitman et al., 1982; Nash and Pittman, 1975; Land and Dutton, 1978). Late stage iron and magnesium enrichment of carbonates is related to clay mineral diagenesis in adjacent shales (Boles and Franks, 1979; Boles, 1978). With increasing depth and temperature the percentage of expandable layers in the mixed layer illite / smectite clays in the shales decreases and the interlayering changes from random to ordered. The transition from randomly interlayered illite / smectite to ordered interlayered illite / smectite takes place at a temperature of approximately 100° C (Boles and Franks, 1979; Boles, 1978; Eberl and Hower, 1976). Perry and Hower (1970) indicate that ordering takes place when the mixed layer illite / smectite has approximately 35 % expandable layers. X-ray diffraction analysis of 62 samples from the Viking Formation in the study area indicated that the mixed layer illite / smectite clays have approximately 35 % expandable layers. This evidence is further supported by the presence of small superlattice reflections beginning to appear on the x-ray diffractograms of many of the samples studied indicating ordering of the mixed layer clays. Results from the work of Boles and Franks (1979) indicate an apparent enrichment of iron and magnesium in unreacted smectite layers with increasing depth until ordering occurs. They suggest that the increase in iron and magnesium is due to the reaction of more aluminous smectite layers to illite, leaving behind iron and magnesium rich smectite layers. With the commencement of ordering iron and magnesium rich smectite layers are also converted to illite with large quantities of iron and magnesium released and incorporated into late diagenetic ankerite (see Figure 3.11). Pitman et al. (1982) found that pre-existing dolomite serves as nucleation sites for syntaxial overgrowths of ankerite. Ankerite cement in the Viking samples was always observed surrounding a dolomite core as a syntaxial overgrowth or as a replacement of the dolomite. Boles and Franks (1979) found that ankeritization takes place at temperatures of 117° C to 120° C in Gulf Coast sandstones. Ankerite cement is present in many Viking sandstones studied but none of the carbonate cement has been completely ankeritized which suggests that temperatures were only in the 120° C range for a short period of time or that Fe^{2+} availability was limited.

LATE SECONDARY POROSITY

Late secondary porosity was formed in the Viking Formation by the solution of carbonate cements (see Figure 3.11). Thermal decarboxylation of organic matter in shales results in evolution of significant amounts of organic acids and carbon dioxide (Curtis, 1983; Surdam et al., 1982; Land and Dutton, 1978). Dissolved CO_2 may dissociate to form carbonic acid further reducing the pH (Curtis, 1983; Porter Weimer, 1982). Sediment compaction and CO_2 gas force the pore fluids from shales into sandstones where they dissolve carbonate cements. In this manner secondary porosity was created at depth in the Viking Formation sandstones and conglomerates by the solution of dolomite and ankerite cements. These carbonates may be partially to totally dissolved.

PRECIPITATION OF CLAY MINERALS

The last major diagenetic event to occur prior to hydrocarbon migration was the precipitation of clay mineral cements. The main clay minerals present in the Viking Formation at Garrington are kaolinite and illite (Figures 3.3C, 3.6D,F, 3.7C, and 3.8B), mixed layer illite / smectite, chlorite and smectite occur in lesser amounts (Figures 3.6A, and 3.8D).

Acidic fluids associated with carbonate solution significantly increase the mobility of aluminum and transport it as an organic complex (Surdam et al., 1982; Curtis, 1983). These acidic fluids also contain significant quantities of Fe, Mg and Si released by the smectite to illite transformation in shales (Boles and Franks, 1979). As the acidic pore fluids become neutralized by hydrogen consuming reactions clay minerals precipitate (Curtis, 1983)(see Figure 3.11).

Kaolinite is the most abundant clay mineral in the Viking Formation at Garrington. It occurs most commonly as extensive pore-fillings in conglomerates and coarse-grained sandstones (Figures 3.6C and 3.8A). Kaolinite is also an important pore-filling phase in the fine-grained sandstones (Figure 3.10B). Carrigy and Mellon (1964), in their study of Cretaceous and Tertiary sandstones of Alberta, reported that kaolinite was the most common authigenic clay mineral in quartzose sandstones low in feldspar and volcanic detritus and that it was commonly associated with authigenic quartz and carbonate. They proposed that the kaolinite in such rocks was formed by precipitation from Al-rich solutions expelled from adjacent shaley strata. Shelton (1964) agreed that formation water was responsible for the formation of kaolinite.

The rocks of the Viking Formation at Garrington are quartz rich with only minor amounts of feldspar and little or no volcanic material. Most of the kaolinite present in these rocks appears to have precipitated from aluminum-rich solutions, however, some kaolinite also appears to be associated with the solution of feldspars.

Illite is the next most abundant clay mineral in the samples studied. It occurs as lath shaped crystals growing from pore walls into pore openings (Figure 3.8E). Illite is present in all lithologies but is most abundant in the fine-grained sandstones. This concentration in the fine-grained sandstones may indicate that much of the illite in this rock type is detrital. Authigenic illite was probably formed from the same fluids which precipitated kaolinite. Alternatively, kaolinite may have been altered to illite at depth, by the introduction of excess potassium from shales (Wilson, 1982).

Illite / smectite and chlorite are relatively minor components in the Viking Formation at Garrington. Illite / smectite clays may be a detrital phase; more probably they were formed by the same fluids which generated kaolinite and illite. Chlorite may also be present mainly as a detrital component, however, it may also have formed by the reaction of kaolinite with iron and magnesium released by the illitization reactions in shales or from solution of ferro-magnesian carbonates (Boles and Franks, 1979). Boles and Franks (1979) state that the transformation of kaolinite to chlorite takes place at temperatures of 150° C to 200° C. Peak hydrocarbon generation occurs at temperatures of 100° C to 120° C (Milliken et al., 1981). The minor occurrence of chlorite cement in the Viking Formation indicates that hydrocarbon migration may have truncated chlorite generation. Alternatively, temperatures necessary for rapid chlorite generation may have never been reached in the Viking Formation in the Garrington area. Chlorite can also form at low temperatures and may occur very early in the diagenetic sequence particularly where large amounts of unstable feldspars are present (Michael Dean, personnal communication, 1985).

ALBITIZATION OF FELDSPARS

Albitization of feldspars may have taken place in the Viking Formation but because of the relatively minor amounts of feldspar present in these rocks this event is quantitatively unimportant. The products of albitization are albite, kaolinite and calcite (Boles, 1982). Boles (1982) reported that the zone of albitization occurred at temperatures of 110° C to 120° C. Albitization may have contributed to clay mineral genesis and possibly to a late stage calcite cement in the Viking Formation (Figure 3.11).

DISCUSSION

The extent of mineral diagenesis differs between the coarse facies (conglomerates and coarse-grained sandstones) and the fine-grained sandstones in the Viking Formation at Garrington. The fine-grained sandstones have been affected to a greater degree by pyrite, siderite and quartz cementation than have the conglomerates and coarse-grained sandstones. All three lithologies were affected by carbonate and clay mineral cements. Solution of carbonate minerals to create secondary porosity also occurred in all three lithologies but may be most significant in the conglomerates and coarse-grained sandstones where only minor amounts of carbonate cements are seen at the present time.

The coarse facies and the fine-grained sandstones are affected to different degrees by diagenetic events because of the fluid flow characteristics of the rock types and kinetic factors (Thomas, 1978). The coarse facies have much larger pores and pore throats than the fine-grained sandstones and much lower surface area to volume ratios. Therefore fluids are transmitted through the coarse facies more rapidly than in the fine-grained sandstones and cements have less opportunity to nucleate onto grain surfaces. This causes the fine-grained sandstones to be more extensively cemented by early diagenetic events than the coarser grained rock types.

The current temperature of the Viking Formation at Garrington is approximately 63° C (pers. comm. Engineering Department, Canadian Superior Oil Ltd.). The diagenetic signiture of the samples examined indicates that in the past temperatures must have been much higher. From the interpreted sequence of events it is obvious that temperatures must have peaked at approximately 110° C to 120° C. Hitchon (1984) indicates that the geothermal gradient in the Garrington area is approximately 25° C/kilometer and probably has not changed significantly in the geologic past. The Viking Formation is currently buried at depths of 1950 meters to 2350 meters in the Garrington study area. In order to attain temperatures of 110° C to 120° C these rocks must have been buried much deeper in the past. Hitchon's (1984) work shows that as much as 2250 meters of overburden have been removed in the Garrington area. This amount of sediment would increase the temperature of the Viking Formation at Garrington by approximately 55° C and place it in the temperature range indicated by the diagenetic sequence (Figure 3.11).

IV. RESERVOIR CHARACTERISTICS

This chapter presents a discussion on the reservoir rocks with emphasis on their porosity and permeability, and the effects of the pore-lining and pore-filling minerals on the reservoir performance. In addition, the gas-oil ratio trend in the reservoir has been studied and several explanations for reservoir subpressures have been examined. The final portion of the chapter deals with petroleum recovery.

A. RESERVOIR ROCKS

The Viking Formation in the Garrington Oil Field has two main reservoir facies the Viking "B" conglomerate (Facies Association 2) and the Viking "B" fine-grained sandstones which lie below the conglomerate (Facies Association 3).

The conglomerate facies appears to be laterally continuous over the main sand ridge complex and pinches out along the edges of this ridge (Figure 2.24, in pocket). These rocks have low to moderate porosities (average 7.6 %, Table 4.1) and moderate permeabilities (range 0-4210 md, average approximately 70 md).[4] Where the conglomerate thins the matrix may become shaley and the rocks lose permeability. This occurs in some of the swales associated with the ridge-and-swale topography within the Viking "B" horizon and also at the top of the conglomerate where the Viking Formation and the Lloydminster shale meet.

The fine-grained sandstones are laterally continuous and extend beyond the study area. They have low to moderate porosities (average 8.4 %) and very low permeabilities (average < 1.0 md) Where fracturing has occurred the fine-grained sandstones may locally have relatively high permeabilities (for example 62 md in well 9-14-35-4W5).

Examination of core analysis reveals that there is little or no communication between the fine-grained sandstones and the conglomerates. While both facies may be hydrocarbon stained, the permeabilities in the fine-grained sandstones are generally too low for them to contribute to significant oil production. However, the fine-grained sandstones may be gas permeable and transmit gas upwards into the conglomerates (Engineering Department of Canadian Superior Oil Ltd., pers. comm.). As the geometry of the pores in the fine-grained sandstones change towards microporosity, pores become more tabular in nature. Under these conditions gas slippage (Klinkenberg effect) causes more rapid flow of gas than water or oil (Thomas, 1981). The water and oil are trapped because capillary forces exceed the buoyant forces for water and oil; in contrast gas may be released from pore geometries in the microdarcy range (Thomas, 1981; Jones and Owens, 1980). The reason for poor communication between the fine-grained sandstones and the conglomerates is that more cementation has occurred in the fine-grained sandstones than in the conglomerates, resulting in a large loss of permeability (see Chapter 3).

---

[4] All porosity and permeability data were obtained from core analysis performed by Core Laboratories Canada Ltd. and Geotech Ltd.

The Viking "A" sandstones lie above the Viking "B" reservoir and are separated from it by the Lloydminster shales (Figures 2.10 and 2.11). The Viking "A" sandstones are not included in the reservoir facies of the Garrington Oil Field. These sandstones, however, are gas-bearing and may contribute to Garrington production where they are perforated along with the Viking "B" or where they have been affected by fracture treatments performed on the underlying Viking "B" conglomerates and fine-grained sandstones. Where either of these situations occur high gas-oil ratios (GOR) may result.

B. POROSITY AND PERMEABILITY

Table 4.1 lists porosity and permeability data for samples from the Viking Formation of the Garrington Oil Field. Figure 4.1 is a plot of porosity versus permeability for 56 samples (31 fine-grained sandstones, 12 coarse-grained sandstones and 13 conglomerates). This plot shows that the coarse-grained sandstones and conglomerates have significantly higher permeabilities than the fine-grained sandstones, with the exception of three samples (033, 049 and 060). Samples 033 and 060 are both Viking "A" coarse-grained sandstones and have appreciable amounts of shale mixed in with the coarse sand by bioturbation. Sample 049 has a high percentage of clay-size material present within its pore system. The conglomerates and coarse-grained sandstones generally have permeabilities greater than 10 md, and in many cases, greater than 100 md. In contrast the fine-grained sandstones have permeabilities less than 2 md, and usually less than 1 md. Porosity values do not differ between the coarse facies (conglomerates and coarse-grained sandstones) and the fine-grained sandstones. Plots of porosity versus percentage of fine-grained material show a polarity, with the coarse facies having less

TABLE 4.1 POROSITY AND PERMEABILITY

SAMPLE NUMBER	ROCK TYPE	DEPTH (m)	POROSITY %	PERMEABILITY millidarcies
16-19-34-2W5				
003	Congl.	2053.6	5.2	10.5
004	C.Sst.	2053.9	9.6	37.8
005	F.Sst.	2054.2	6.5	0.02
1-25-35-4W5				
010	Congl.	2147.5	5.0	159.0
011	C.Sst.	2147.9	7.5	28.0
012	F.Sst.	2148.3	9.5	0.67
16-25-34-3W5				
016	Congl.	2069.1	6.4	63.1
017	F.Sst.	2071.5	9.1	0.28
11-11-35-3W5				
019	Congl.	2074.1	3.3	133.0
020	F.Sst.	2074.6	6.9	0.99
022	F.Sst.	2079.9	11.0	0.95
024	C.Sst.	2090.9	4.2	713.0
6-6-35-2W5				
026	Congl.	2036.2	ND	ND
027	Congl.	2037.5	7.9	105.0
028	F.Sst.	2037.8	6.7	1.47
029	F.Sst.	2041.4	11.7	1.93
030	F.Sst.	2043.6	11.2	1.60
031	F.Sst.	2045.3	11.3	0.65
032	F.Sst.	2047.5	3.9	0.32
6-34-34-3W5				
033	C.Sst.	2112.5	2.7	0.01
034	Congl.	2115.0	8.7	58.4
035	C.Sst.	2115.3	12.5	42.0
036	C.Sst.	2115.7	12.5	46.1
037	F.Sst.	2116.5	7.3	0.21
038	F.Sst.	2121.1	11.3	0.77
6-23-34-3W5				
039	Congl.	2111.4	7.7	155.0
041	Congl.	2112.8	11.1	121.0
042	F.Sst.	2113.3	10.4	0.68
046	F.Sst.	2121.1	4.7	0.06

7

TABLE 4.1 POROSITY AND PERMEABILITY (CONTINUED)

SAMPLE NUMBER	ROCK TYPE	DEPTH (m)	POROSITY %	PERMEABILITY millidarcies
9-3-35-3W5				
047	Shale	2085.0	ND	ND
048	Congl.	2086.3	5.7	4210.0
049	Congl.	2087.1	4.2	1.48
050	F.Sst.	2087.6	7.8	0.67
052	F.Sst.	2094.0	8.8	0.61
16-13-34-3W5				
055	Congl.	2070.5	6.7	24.3
056	Congl.	2071.0	7.9	118.0
057	F.Sst.	2071.3	8.0	0.10
059	F.Sst.	2076.2	10.2	0.10
060	C.Sst.	2065.4	6.0	0.06
16-35-34-3W5				
061	C.Sst.	2069.2	NA	NA
7-4-35-3W5				
077	C.Sst.	2108.5	12.5	83.1
14-1-35-3W5				
084	Congl.	2044.0	7.6	249.0
085	F.Sst.	2044.5	3.8	0.05
086	F.Sst.	2046.7	5.0	0.04
087	Congl.	2048.6	10.6	0.96
088	F.Sst.	2050.4	8.5	0.26
089	F.Sst.	2052.5	11.9	1.13
16-15-34-3W5				
101	F.Sst.	2131.0	8.8	0.25
102	F.Sst.	2132.5	9.8	0.51
103	F.Sst.	2134.0	10.3	0.91
104	F.Sst.	2135.5	0.8	0.09
105	F.Sst.	2137.8	10.5	0.52
6-13-34-3W5				
107	C.Sst.	2080.7	18.2	385.8
8-25-34-3W5				
111	C.Sst.	2065.7	13.7	71.93

TABLE 4.1 POROSITY AND PERMEABILITY (CONTINUED)

SAMPLE NUMBER	ROCK TYPE	DEPTH (m)	POROSITY %	PERMEABILITY millidarcies
8-7-35-3W5				
117	Congl.	2130.6	14.2	82.0
118	C.Sst.	2131.1	15.7	26.0
121	F.Sst.	2135.2	8.3	0.20
7-33-34-2W5				
124	Congl.	1972.7	NA	NA
125	C.Sst.	1973.3	NA	NA
126	F.Sst.	1976.0	NA	NA
128	F.Sst.	1979.7	6.8	0.20
10-7-34-4W5				
136	C.Sst.	2335.4	NA	NA
16-2-35-4W5				
146	C.Sst.	2220.5	3.4	31.0
147	F.Sst.	2224.2	9.9	0.79
148	F.Sst.	2228.0	8.1	0.24

fine-grained material within their pore systems than the fine-grained sandstones (Figure 4.2). The percentage of fine-grained material present does not seem to affect porosity. Plots of permeability versus percentage of fine-grained material again show a polarity with the fine-grained sandstones having the highest percentages of fine-grained material and the lowest permeabilities, while the coarse-grained sandstones and conglomerates have low percentages of fine-grained material and much higher permeabilities (Figure 4.3).

With no difference in porosity, permeability of a fine-grained sandstone should be an order of magnitude less than a coarse-grained sandstone, mostly because of the differences in surface area (Blatt et al., 1980). Figure 4.1 shows that the differences in permeability between the coarse facies and the fine-grained sandstones in the Viking Formation is in many cases two or more orders of magnitude. This indicates that the presence of diagenetic minerals has a direct affect upon permeability. Porosity has been lowered in all facies by compaction and cementation. In the coarse-grained sandstones and conglomerates, quartz and clay cements are of primary importance. In the fine-grained sandstones, carbonate cements (dolomite, ankerite and siderite) are important in addition to quartz and clay.

C. EFFECTS OF PORE-LINING AND PORE-FILLING MINERALS ON RESERVOIR PERFORMANCE

It is now understood that framework grains cause little or no formation damage and that pore-lining and pore-filling minerals (mostly clay minerals) are responsible for most types of formation damage incurred in drilling, completion and stimulation. Pore-lining and pore-filling clays are of significance for two reasons: (1) these materials can effectively block pore throats and greatly reduce permeability, and (2) pore-linings are in 100 % contact with drilling, completion and stimulation fluids (Almon and Davies, 1981).

CONGLOMERATES AND COARSE-GRAINED SANDSTONES

Small, but significant, amounts of fine-grained material are present in the conglomerates (3.5 % $< 5\,\mu m$) and coarse-grained sandstones (4.1 % $< 5\,\mu m$) (see p. 109 and Table 3.4). These fractions are comprised mostly of diagenetic minerals. The main authigenic minerals that could cause formation damage are quartz, kaolinite, illite,

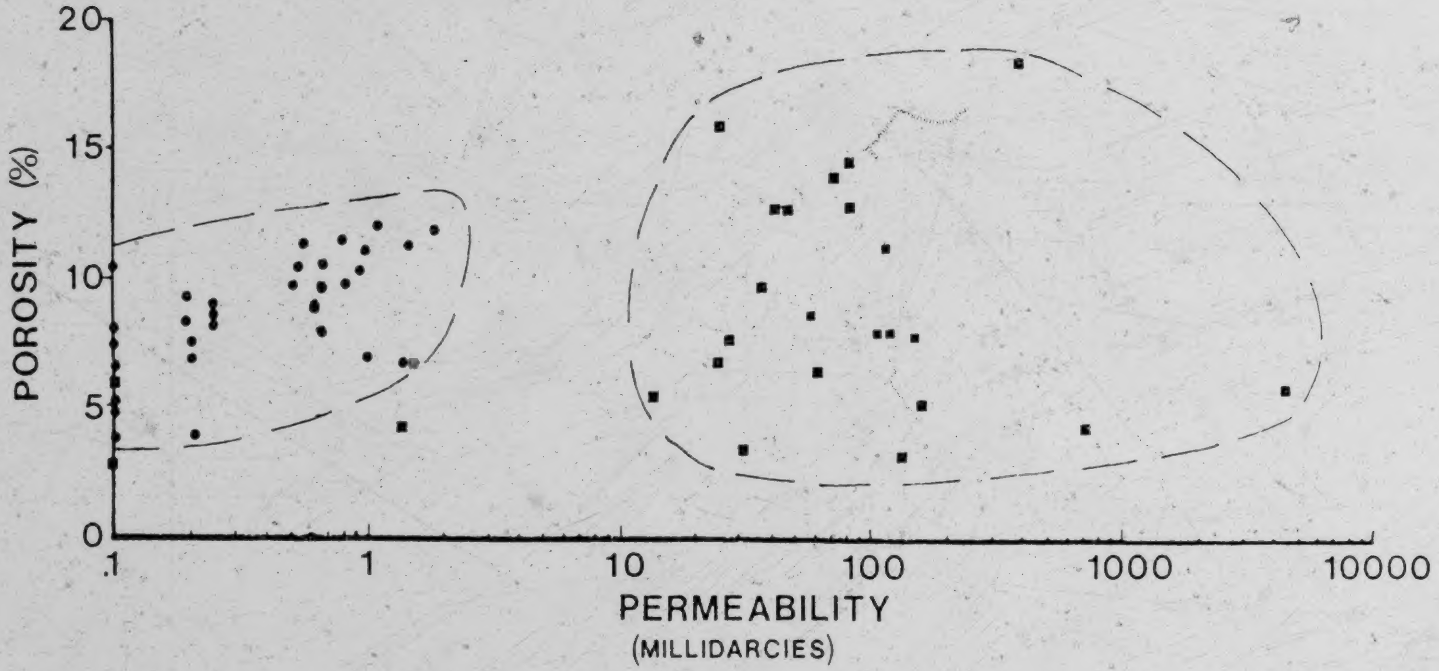

Figure 4.1. Porosity versus permeability: Squares indicate conglomerates and coarse-grained sandstones. Circles indicate fine-grained sandstones.

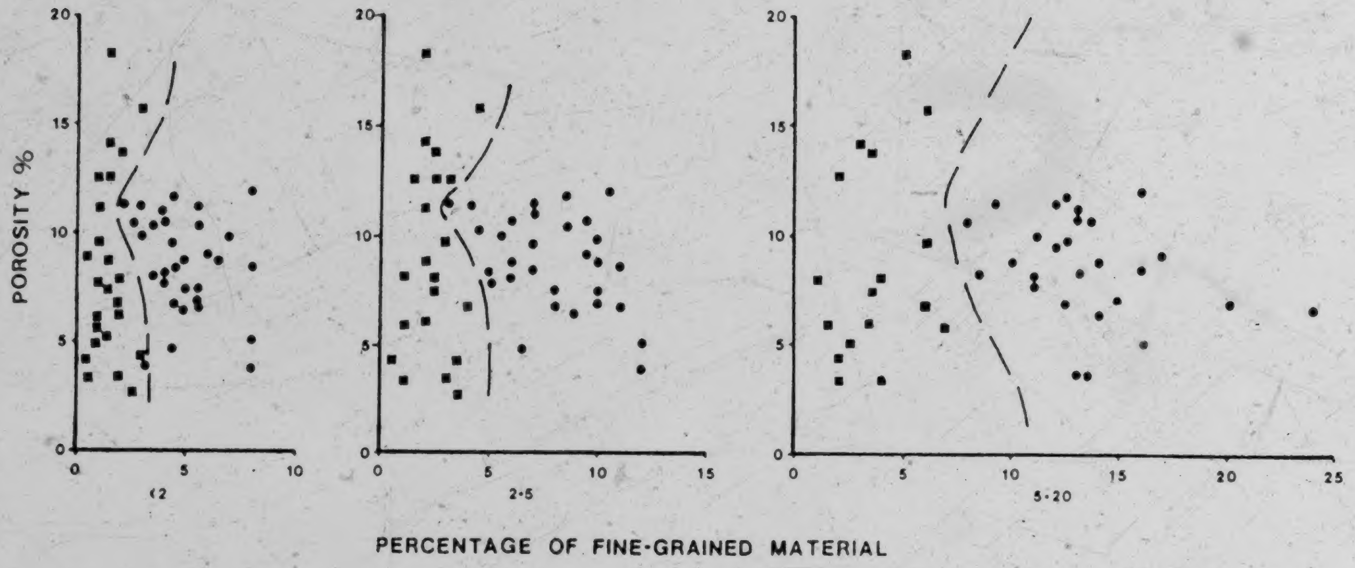

Figure 4.2. Porosity versus percentage of fine-grained material present in the sample. Squares indicate conglomerates and coarse-grained sandstones. Circles indicate fine-grained sandstones.

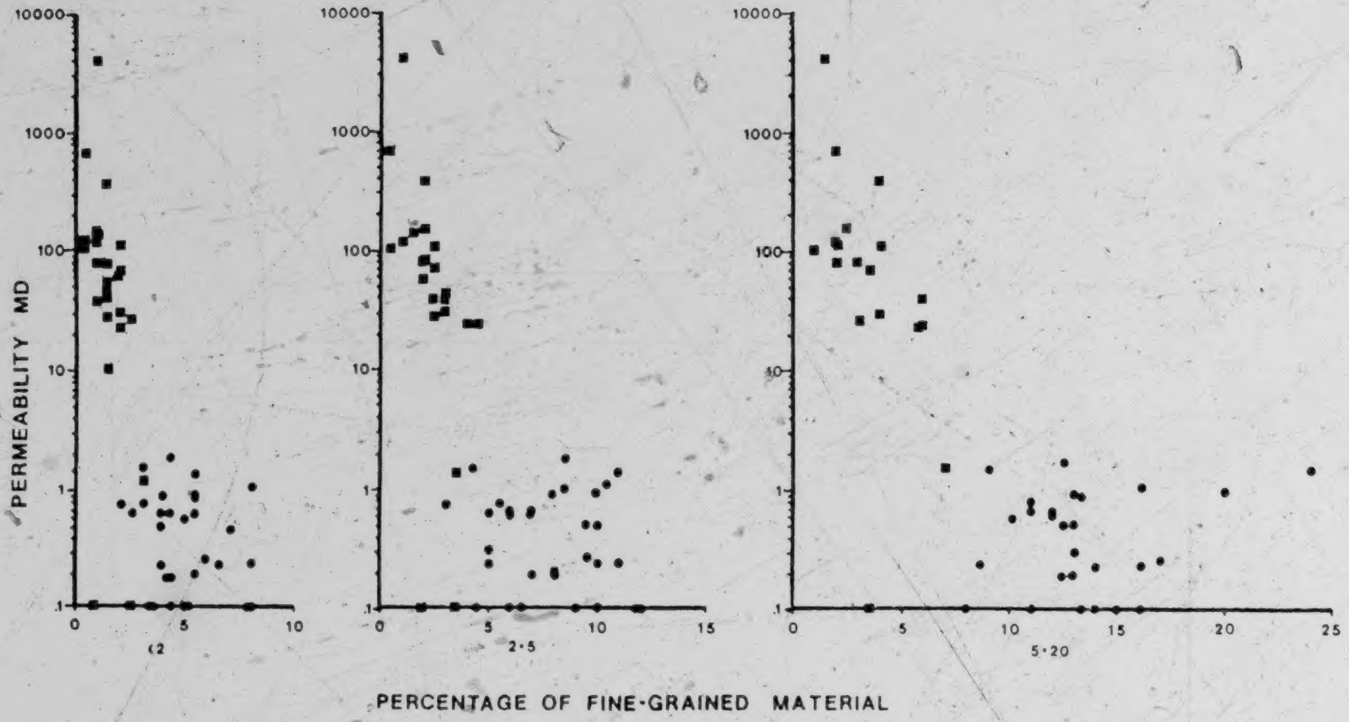

Figure 4.3. Permeability versus percentage of fine-grained material present in the sample: Squares indicate conglomerates and coarse-grained sandstones. Circles indicate fine-grained sandstones.

illite / smectite, smectite, chlorite and siderite. Clay minerals, especially kaolinite, have a patchy mode of occurrence in the conglomerates and coarse-grained sandstones and can be abundant locally, causing a reduction in porosity due to their pore-filling nature. Illite and illite / smectite have high surface area to volume ratios which create high irreducible water saturations, high amounts of microporosity and, where bridging of pore throats occurs, increased pore tortuosity. Authigenic quartz, occurring as prismatic crystals on detrital grains, can contribute to a significant decrease in porosity. If enhanced oil recovery methods, such as fluid injection and hydraulic fracturing are used to stimulate the Viking reservoir rocks, the following problems may arise:

1. Migration of fine-grained material;
2. Swelling of water sensitive clays;
3. Precipitation of iron-rich compounds.

MIGRATION OF FINE-GRAINED MATERIAL

Migration of fine-grained material will be the most serious problem encountered in the conglomerates and coarse-grained sandstones due to the extensive development of kaolinite. Kaolinite is loosely attached to grain surfaces or rests on other grains within the pores. High fluid velocities associated with reservoir stimulation may dislodge the kaolinite booklets. This is particularly true in areas of high fluid flow rate such as near the well bore. Dislodged kaolinite may migrate towards pore throats where, because of its large crystal size (up to 15 *μm*) and the high ratio of crystal diameter to pore throat diameter (0.5 to 0.7), it may become trapped and act like a check valve causing a loss of permeability (Almon and Davies; 1981).

Quartz may also present a migration of fines problem. XRD and SEM results reveal that quartz is very abundant in the conglomerates and coarse-grained sandstones, particularly in the 2-5 *μm* and 5-20 *μm* size fractions. Quartz occurs as small prismatic crystals on chert pebbles and as complete overgrowths on detrital quartz grains. If fluid injection velocities are too high these small crystals may be broken from their substrates, migrate into pore throats, become trapped and reduce permeability.

Because the pore throats in the conglomerates are relatively large (20-40 *μm* estimated from SEM) and the percentage of fine-grained material relatively low, problems of migration of fines will be less severe than in the coarse-grained sandstones where pore throats are smaller (10-20 μm estimated from SEM) and fine-grained material is slightly more abundant.

To prevent a serious migration-of-fines problem, low fluid velocities should be used during injection. Addition of clay stabilizers such as polyhydroxy aluminum compounds and cationic polymers may also help to secure kaolinite to the framework grains. This treatment should be done early in the well history because kaolinite is relatively inert to acid. Once fines have "plugged-up" the pore throats the situation is difficult to reverse.

SWELLING OF WATER SENSITIVE CLAYS

Problems with water sensitive clays will be of less concern than migration of fines in the conglomerates and coarse-grained sandstones. The relative percentage of swelling clays in the conglomerates and coarse-grained sandstones is usually a trace amount, although it can range up to 30 %. Swelling clays are found in abundance in only six samples and then only in the < 2 μm size-fraction. The largest amounts of swelling clays constitute less than 1 % of the bulk mineralogy of the reservoir, assuming that 3 % of the conglomerates and coarse-grained sandstones are clay minerals. Swelling clays do warrant some concern, particularly in the eastern portion of the oil field where all six anomalous smectite values occur. Both smectite and illite / smectite are found in the conglomerates and coarse-grained sandstones. The addition of fresh water to the reservoir would cause the smectite and the smectite component of the illite / smectite to swell. The swelling clays could seal pore throats and result in a reduction of permeability. As the clay swells, the bonds between layers are weakened. The layers may then separate and disperse, possibly adding to a migration-of-fines problem.

Clay swelling problems can be overcome by the use of oil-base, potassium or ammonium chloride drilling, completion and stimulation fluids. Permanent protection against clay swelling can be achieved by the use of cationic polymers. However, because of the high costs and limited benefits, this treatment is probably not warranted in this particular situation.

PRECIPITATION OF IRON-RICH COMPOUNDS

The precipitation of iron-rich compounds will be of minor concern in the conglomerates and coarse-grained sandstones except where local concentrations of iron-bearing clays and carbonates occur. Chlorite and siderite are both present in the conglomerates and coarse-grained sandstones. Dolomite and ankerite occur as a pore-filling cements in a few of the Viking "A" coarse-grained sandstones. The chlorite commonly occurs in only trace or minor quantities in all size fractions. Siderite occurs mainly in the form of large concretions and rip up clasts and is also present as a minor cement or a replacement of chert pebbles. Chlorite, siderite and ankerite can be dissolved in acidic or well oxygenated fluids, liberating iron into solution. The iron can precipitate as an iron-rich gel such as ferric hydroxide ($Fe(OH)_3$) when the stimulation fluids become neutralized. Ferric hydroxide has a large crystal size and can block pore throats, resulting in a loss in permeability. To minimize this problem, oxygen scavengers and iron-chelating agents can be added to the fluids prior to injection. The injection fluids should also be recovered as soon as possible. Use of oxygen scavengers and iron-chelating agents is not warranted in this case.

FINE-GRAINED SANDSTONES

A much higher percentage of fine-grained material (13.0 % $< 5\ \mu m$) is present in the fine-grained sandstones. This material is comprised mostly of pore-lining and pore-filling kaolinite, illite and quartz; however, significant amounts of detrital clay minerals are also present. Migration of fine-grained material will be the most serious problem encountered in the fine-grained sandstones. Of the three lithologies studied, the fine-grained sandstones contain the highest percentage of fine-grained material and have the smallest pore throat sizes (5-10 μm estimated from SEM). Kaolinite diameters range from 7-10 μm. The ratio of kaolinite crystal diameter to pore throat diameter is close to 1.0; only a small amount of material needs to move through the pore system to cause a serious loss of permeability.

Swelling of water sensitive clays will be of less concern in the fine-grained sandstones because smectite occurs in only trace amounts and illite / smectite in only minor amounts. The swelling clays make up less than 1 % of the bulk mineralogy of the fine-grained sandstones.

Precipitation of iron-rich compounds will be of minor concern in the fine-grained sandstones, except where local concentrations of iron carbonate occur. Chlorite and siderite are both present in the fine-grained sandstones. Chlorite is present in only minor concentrations; siderite occurs both as nodules or rip up clasts and as cement. Siderite accumulations appear to be local but may be extensive where the siderite occurs as a cement. Dolomite and ankerite cements are locally extensive in the fine-grained sandstones but are dominated by the dolomite end member and as such should not contribute significantly to iron compound precipitation. Procedures to control iron precipitation should be determined on a well by well basis.

D. GAS-OIL RATIO

To study the gas-oil ratio (GOR) and to determine the relationship of reservoir pressure to GOR, the GOR values were plotted against time for 34 wells. At the same time a linear regression line was fitted to each of the plots and a correlation coefficient was calculated (see Appendix B). The GOR-Time plots show large variability, correlation coefficients ranging from 0.0241 to 0.9369 . The large variance in the correlation coefficients results from the non-linear nature of many of the GOR plots. Of the 34 wells studied, 11 plots show rapidly rising GOR's, 16 plots show slowly or moderately rising GOR's, 3 plots show extreme fluctuations in GOR, 2 plots exhibit slowly falling GOR's and 2 are flat (see Appendix B).

Of the rapidly rising GOR plots, 8 of the 11 are located in the eastern portion of the oil field, very close to the gas-oil contact, which explains their high GOR's (Figure 4.4). The other 3 wells with rapidly rising GOR's are located in the northwest portion of the oil field in sections 11 and 14 of Township 35, Range 4 west of the Fifth Meridian (Figure 4.4). Three wells, with widely fluctuating GOR's, are also located in this area of the oil field. It has been postulated that the Viking "B" in this area represents a distinct oil field from that further to the east and has a separate gas cap. Mapping of the area (Chapter 2; Figures 2.11 and 2.17 to 2.26) does not support this interpretation. Instead the high GOR's in this area are probably due to communication between the gas-bearing Viking "A" sandstones and the Viking "B" conglomerates which lie below. In this area these two

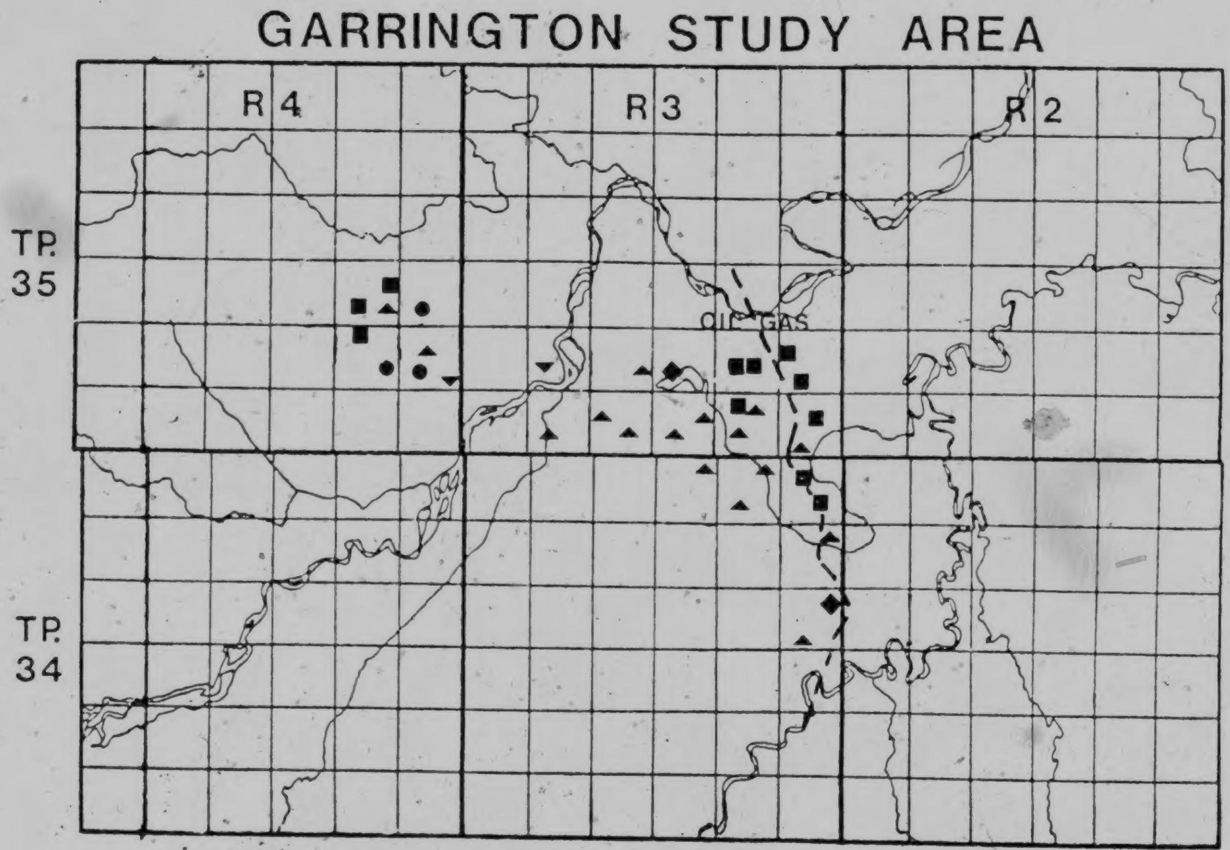
GARRINGTON STUDY AREA
R 4
R 3
R 2
TP. 35
TP. 34
OIL
GAS

Figure 4.4. Map showing the gas-oil ratio trends (GOR) in the Viking Formation in the Garrington Study Area. Squares indicate wells with rapidly rising GOR, circles indicate fluctuating GOR, upward-pointing triangles indicate slowly rising GOR, downward pointing triangles indicate slowly falling GOR and diamonds indicate flat GOR.

reservoirs are often only separated by a metre or less of shale. In one well, 6-11-35-4W5, the Viking "A" and the Viking "B" were both perforated and a GOR of over 4,000 resulted (ERCB, 1984). In other cases, fracture treatments may have provided the link between the two reservoirs.

Where GOR fluctuates up and down, it is probably due to the method of production, that is, periods of rapid production (and rising GOR) are followed by shut-in periods where pressure buildup occurs and gas is redissolved in the oil. When gas evolves in the wellbore area, the oil productivity decreases because of the decrease in the relative permeability of oil. Kazemi (1975) found that long shut-in periods will improve oil productivity for only a short period of time, and that long term oil productivity will be essentially unchanged. This implies that pressure pulsing of oil-gas reservoirs is unlikely to improve oil recovery.

The central area of the Garrington Oil Field is dominated by wells with slowly or moderately rising GOR's. In this area the Viking "A" sandstones are relatively thin and do not appear to affect the Viking "B" reservoir. The GOR's are, however, rising in this portion of the oil field because the reservoir is very near or perhaps below bubble point (Engineering Department of Canadian Superior Oil Ltd., pers. comm.).

E. RESERVOIR PRESSURE

The average reservoir pressure in the Viking Formation of the Garrington Oil Field is about 9,100 kPa (Engineering Department of Canadian Superior Oil Ltd., pers. comm.). A normal hydrostatic gradient of 9.8 kPa/m would give pressures of 19,500 to 22,500 kPa in the Viking Formation at Garrington; therefore, the Viking Formation at this location is underpressured. A search of available literature suggests that much of the Viking Formation in Central Alberta is subpressured. Figure 4.5 shows that pressures in the Viking Formation maybe highly variable. The Gilby reservoir had an initial pressure of 1,445 psi corresponding to a potentiometric surface 411 feet above sea level. Twenty-five miles downdip the Viking Formation, Ferrier and Leafland pools had initial pressures of 4,170 psi and a potentiometric surface 4,400 feet above sea level. This shows a hydraulic head gradient of almost 4,000 feet over the few kilometres between Ferrier and Gilby (Dickey and Cox, 1977).

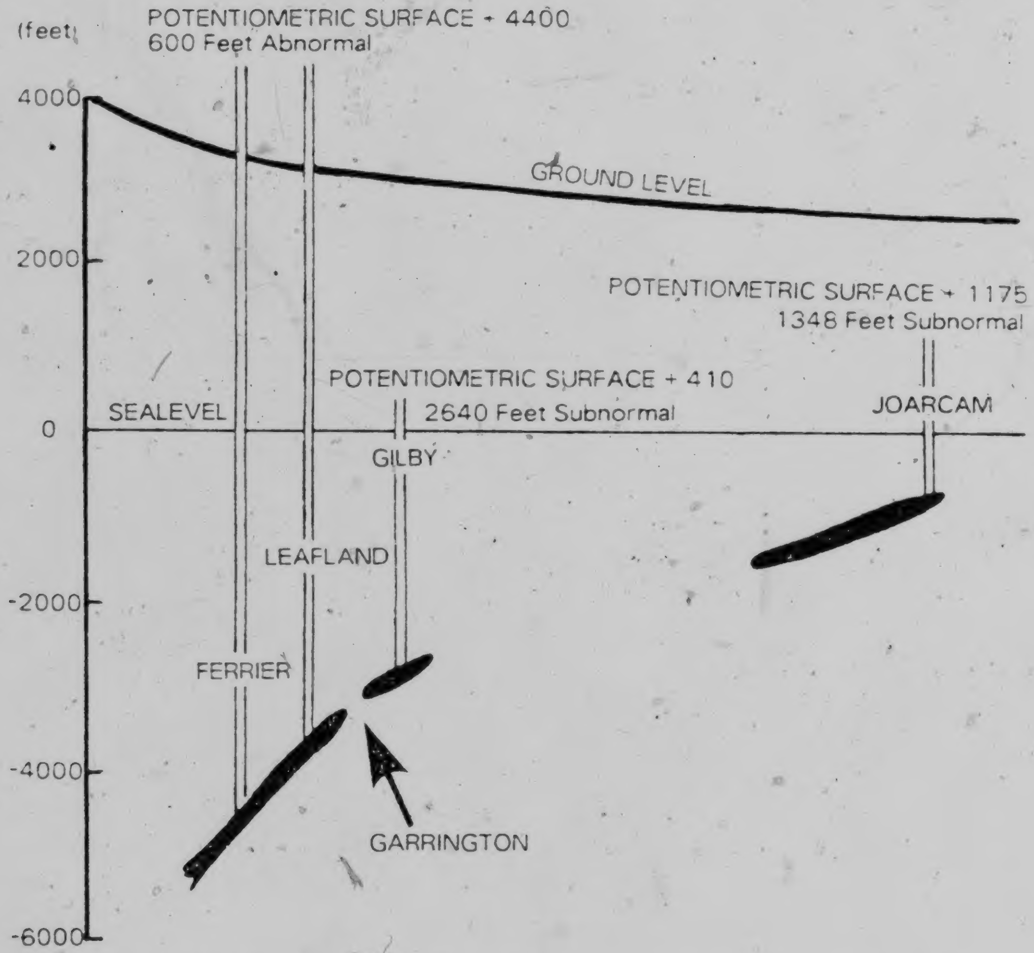
(feet)
POTENTIOMETRIC SURFACE + 4400
600 Feet Abnormal
4000
2000
0
-2000
-4000
-6000
GROUND LEVEL
POTENTIOMETRIC SURFACE + 1175
1348 Feet Subnormal
POTENTIOMETRIC SURFACE + 410
2640 Feet Subnormal
SEALEVEL
GILBY
JOARCAM
LEAFLAND
FERRIER
GARRINGTON

Figure 4.5. Schematic west-east cross-section between Ferrier, Gilby and Joarcam oil fields. Bars show height at which column of fresh water would stand if sustained by original reservoir pressure. Ferrier is abnormally high and Gilby is abnormally low, although they produce from the same zone. Arrow marks the approximate position of the Garrington Oil Field. (Modified from Dickey and Cox, 1977).

At least three possible causes for the subpressures exist;

1. chemico-osmotic pressure gradients,
2. overburden removal, and
3. permeability barriers.

CHEMICO-OSMOTIC PRESSURE GRADIENTS

Several authors have discussed the possibility of chemico-osmotic forces acting to create subpressures in the Viking Formation in Central Alberta (Berry, 1960; Hitchon, 1969, 1984; Dickey and Cox, 1977; Dahlberg, 1982). Berry (1960) stated that anomalous potentials and salinities could be explained by the movement of water cross-formationally through shales which act as semi-permeable membranes. Osmotic potential would result from differences in salt concentration across a shale barrier. Pressure would tend to increase in the reservoir rock on the emergent side of the shale membrane and decrease in the reservoir rock on the influx side. Dickey and Cox (1977) agreed that osmotic pressures across semi-permeable membranes could be high if there was a large difference in salinity across the membrane.

Hitchon (1969) studied fluid potential distribution in the Western Canada Sedimentary Basin by considering the three-dimensional flow net by stratigraphic units. By mapping the fluid potentials of the stratigraphic units, Hitchon found that a low fluid-potential drain exists within the Upper Devonian and Carboniferous carbonate rocks in Central Alberta (Figure 4.6). He further concluded that the drawdown of fluid potentials by some of the low fluid potential channels is reflected through up to 2,500 feet of strata and across the Paleozoic-Mesozoic unconformity. An apparent three-dimensionally closed hydraulic head low in the Viking Formation in Central Alberta is most likely the result of chemico-osmotic potential (Figure 4.7).

Hitchon (1969) found that the position of the lowest hydraulic head elevation at Gilby overlies the southern end of the Rimbey-Meadowbrook reef trend. The Rimbey-Meadowbrook reef complex has excellent high permeability continuity through the basal platform carbonates to the Grosmont reef complex and the subcrop edge (Hitchon 1969, 1984). Exposure of the Beaverhill Lake Formation at Fort McMurray and the resultant discharge causes a drawdown in the Rimbey-Meadowbrook reef trend and

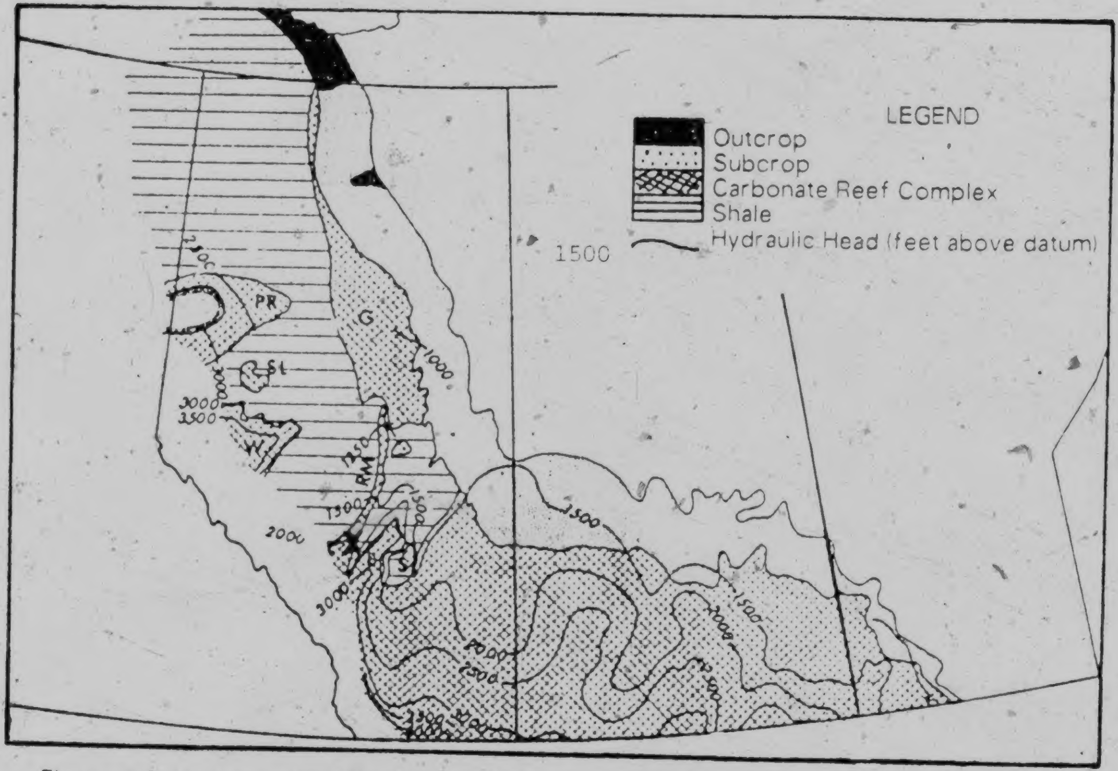
LEGEND
Outcrop
Subcrop
Carbonate Reef Complex
Shale
1500 Hydraulic Head (feet above datum)
PR
SL
W
G
RM
S
B
X
1000
1500
2000
2500
3000
3500
2100

Figure 4.6. Hydraulic head distribution in the Upper Devonian Woodbend Group of western Canada. Lithologic data from Belyea (1964). X marks the position of the Garrington Oil Field. The reef complexes are identified as follows: B=Bashaw; G=Grosmont; PR=Peace River; RM=Rimbey-Meadowbrook; S=Stettler, SL=Sturgeon Lake; W=Windfall (Modified from Hitchon, 1969).

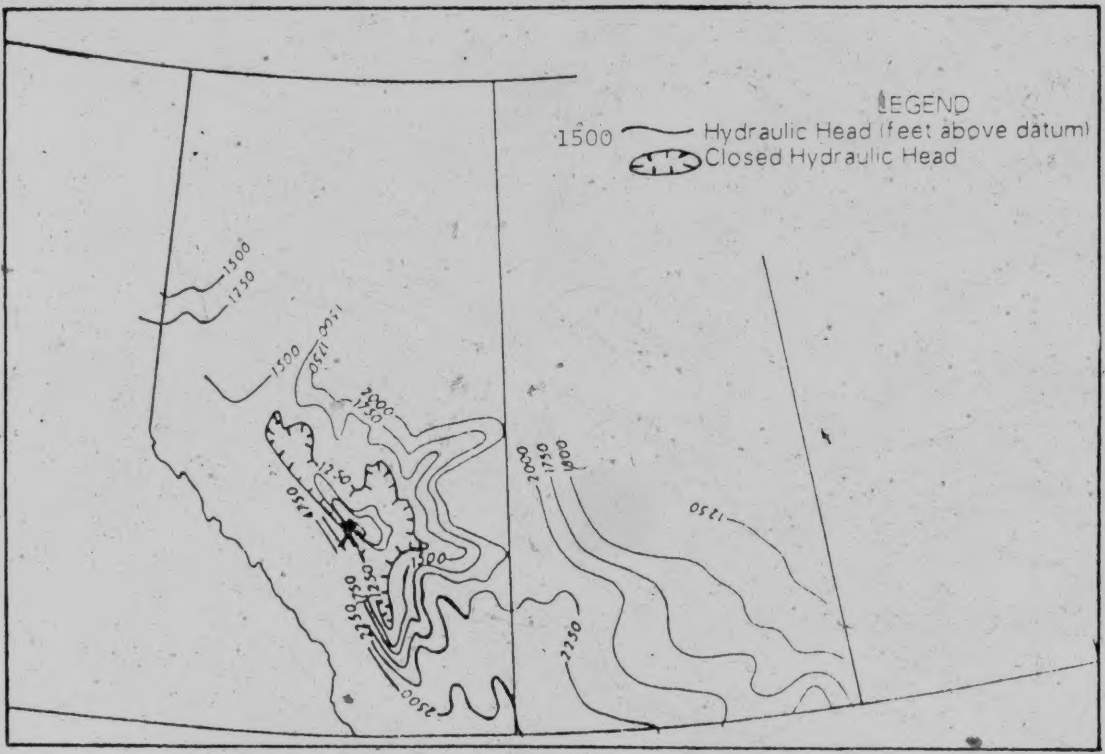
LEGEND
1500 Hydraulic Head (feet above datum)
Closed Hydraulic Head
1500
1250
1500
1750
2000
1750
1250
1250
1500
1750
2250
2500
2000
1750
1500
1250
2250

Figure 4.7. Hydraulic head distribution in the Lower Cretaceous Viking Formation of western Canada. X marks the position of the Garrington Oil Field. (Modified from Hitchon, 1969).

enhances the chemico-osmotic effects down the reef trend. The differences of 1,390 psi and 200,000 ppm salinity between the fluids in the Viking Formation at Gilby and the those in the Rimbey-Meadowbrook reef complex strongly suggest that chemico-osmotic forces are active throughout the basin. The Viking Formation at Garrington appears to be part of this same fluid potential system and this may explain the subpressures there. The position of the Garrington Oil Field (Figure 4.7) clearly places it within the closed hydraulic head low mapped by Hitchon (1969), while other Viking oil and gas pools such as Ferrier and Caroline would be located outside of the closed hydraulic head low.

OVERBURDEN REMOVAL

The cause of subpressures may be related to the removal of overburden, resulting in dilation in pore volume in the rocks and a decrease in reservoir pressure. This is due to the elastic compression of shales and sandstones. Ferran (1973) identified three processes that were responsible for pore pressure change caused by the removal of overburden:

1. The effect of decompressional expansion of the shales surrounding the overpressured sandstones, and the resaturation of the pore space of the shales with fluids absorbed from the sands,
2. The effect of decompressional expansion of the bulk volume of the overpressured reservoirs, and
3. The effect of temperature reduction due to the depth change of the sediments.

Of these three processes, the first was considered thre most important. As overburden is removed, the pore volume dilates, but the interstitial water expands very little and does not fill the new pore volume created. As a consequence the pressure will drop. As the pressure of the pore water in the shales drops, water (but not oil or gas) will seep out of the sandstones into the adjacent shales (Dickey and Cox, 1977). This results in low pressure in the oil and gas reservoir and only a small amount of water remaining in the reservoir.

Hacquebard (1977) estimates the maximum thickness of eroded sediments in the Alberta Basin at about 3,000 metres in the west and 800 metres in the east based on coalification data. Hitchon (1984) calculated the thickness of eroded sediment in the

Alberta Basin by estimating the paleogeothermal gradient. Figure 4.8 is an isopach map of the thickness of eroded sediment as calculated by Hitchon. According to Hitchon's calculations 2,250 to 2,500 metres of overburden have been removed in the Garrington area. If these estimates are correct then the fluid pressure could have been substantially reduced by the removal of overburden, perhaps even to a subnormal pressure.

As overburden is removed, the subsurface becomes cooler. Water contracts as it cools, and this effect would also cause a drop in pressure in the pore water. Hitchon (1984) has determined the geothermal gradient in the Garrington area at 23° C per kilometre. The current temperature of the Viking Formation at Garrington is approximately 63° C but according to Hitchon's estimate it was probably over 100° C in the past. This reservoir has then cooled by over 40° C. This cooling has probably contributed to a reduction in the pressure in the Viking Formation at Garrington.

PERMEABILITY BARRIERS

The existence of low pressure can also be interpreted as a function of permeability. A complete seal is required for a aquifer to continue with a subnormal pressure for a long time (Dickey and Cox, 1977). Dickey and Cox (1977) point out that most low pressure reservoirs are stratigraphic traps. These sandstone bodies are limited in extent and the edge water shows little tendency to advance. In some fields there appears to be little downdip water and the porous and permeable sandbodies are practically full of oil and gas. These reservoirs are often depleted by solution gas drive. The effect of formation water flow interrupted by a semi-permeable barrier, such as a shaley zone within the reservoir, is shown in Figure 4.9. The abrupt change in slope reflects a sudden decrease in the potential energy of the moving water. Increased frictional resistance is caused by the reduced porosity and permeability.

Toth (1980) advanced the theory that in geologically mature basins, gravity-induced cross-formational flow is the principal agent in the transportation and accumulation of hydrocarbons. This theory is based on the observation that where flow systems meet or part, "quasi-stagnant zones" develop, flow directions change abruptly, and a propensity for hydrocarbon accumulations is created (Toth, 1970, 1978, 1979). Dahlberg (1982) shows how a drop in the potentiometric surface in the Viking Formation in the

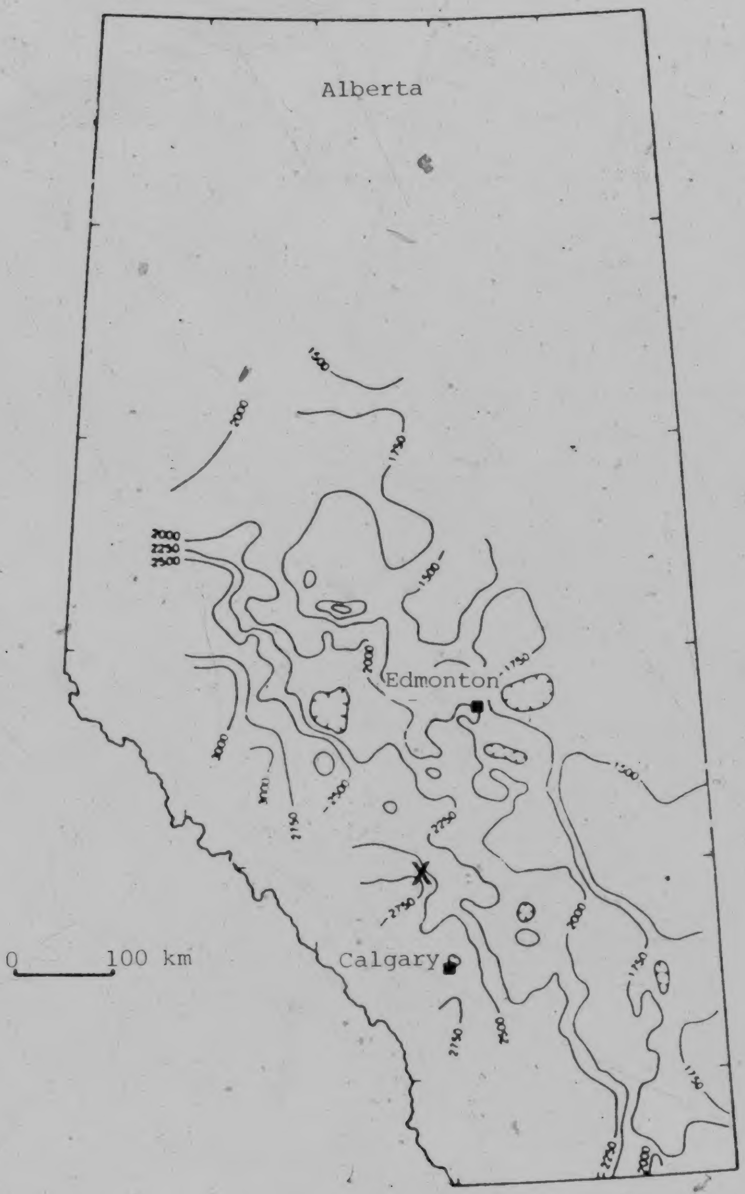
Alberta
1500
2000
1750
2000
2250
2500
1500
2000
1750
Edmonton
3000
3000
2750
2500
2750
1500
2750
X
2000
1750
0
100 km
Calgary
2750
2500
1750
2750
2000

Figure 4.8. Isopach map of calculated thickness of eroded sediments (metres) in Alberta. X marks the position of the Garrington Oil Field (Modified from Hitchon, 1984).

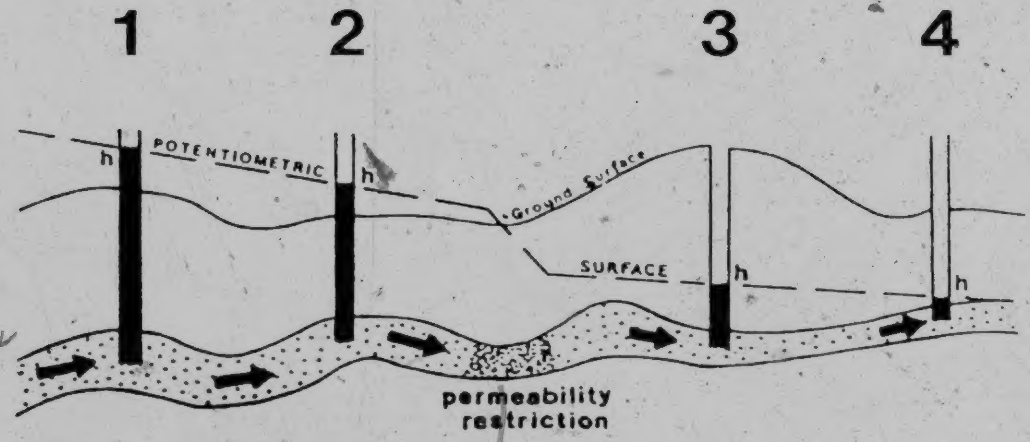
1
2
3
4
h
h
h
h
POTENTIOMETRIC
SURFACE
Ground Surface
permeability restriction

Figure 4.9. Cross-sectional model showing potentiometric surface approximation reflecting local permeability change (Modified from Dahlberg, 1982).

Joarcam-Westlock area coincides with the trapping of oil (Figure 4.10). Considering the low permeability of the fine-grained sandstones in the Viking Formation at Garrington, this mechanism may be responsible for both the low pressure and the emplacement of hydrocarbons at this locality.

All three of the processes mentioned above could be responsible for the subpressures in the Viking Formation at Garrington. However, chemico-csmotic gradients and permeability barriers are probably more likely causes than overburden removal. Other fields which are normally pressured, such as Ferrier and Leafland, exist in areas where substantial amounts of overburden have been removed. More detailed work may provide a more definitive answer to this problem.

F. PETROLEUM RECOVERY

The total original oil in place in the Viking Formation at Garrington has been estimated by Canadian Superior Oil Ltd. at 42 X 10^6 m^3. The total original gas in place has been estimated at 5.5 X 10^9 m^3, of which 3.5 X 10^9 m^3 is free gas and 2.0 X 10^9 m^3 is solution gas. Up to 80 % of the hydrocarbons may be contained in the fine-grained sandstones. The ultimate recovery of original oil in place (OOIP) is estimated at 4.2 % (1.75 X 10^6 m^3) by primary recovery methods. This could be improved to 6.0 % (2.5 X 10^6 m^3) with reinjection of produced gas (Engineering Department of Canadian Superior Oil Ltd., pers. comm.). Because the reservoir is subpressured, pressure maintainence should be initiated in the early stages of development of the oil field.

Studies by Canadian Superior Oil Ltd. indicate that a water flood scheme may be the optimal depletion method. The study by Canadian Superior indicates that an optimized north-south line drive water flood in the Garrington Oil Field could recover 25 % of the total OOIP (10.5 X 10^6 m^3. The majority of the oil produced under waterflood is predicted to originate in the fine-grained sandstones and to be recoverable due to gravity segregation of the injected water. Mineralogical analysis indicates that some difficulties may result; the sandstones have very high abundances of clay minerals (Chapter 3) which could cause severe reservoir damage and inhibit secondary recovery.

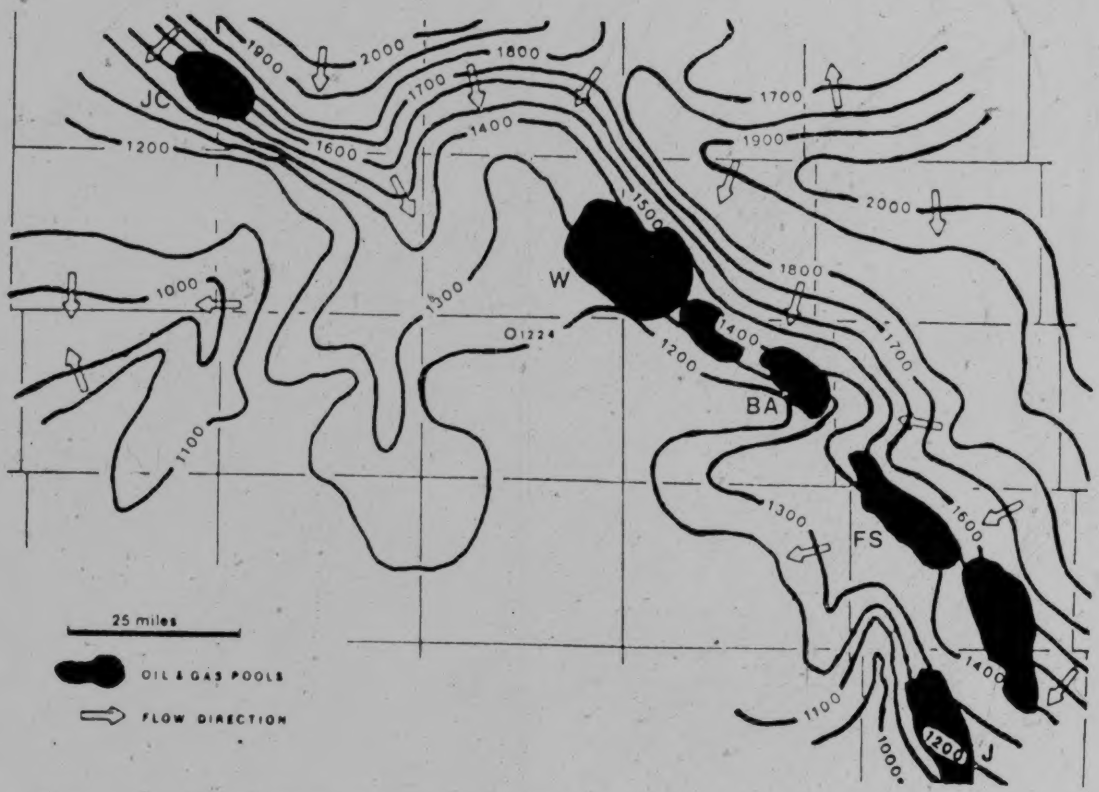
JC
1900
2000
1800
1700
1600
1400
1200
1500
1700
1900
2000
1800
1700
W
1300
1000
O1224
1400
1200
BA
1100
1300
FS
1600
1400
1100
1000
1200
J
25 miles
OIL & GAS POOLS
FLOW DIRECTION

Figure 4.10. Potentiometric map reflecting fluid flow within the Viking sandstone in the Westlock-Joarcam area of Alberta. JC = Judy Creek, W = Westlock, BA = Bon Accord, FS = Fort Saskatchewan, J = Joarcam. (Modified from Dahlberg, 1982, after Dickey and Cox, 1977).

V. CONCLUSION

The Viking Formation has been studied extensively in Alberta and Saskatchewan because of its importance as a hydrocarbon reservoir. At Garrington, the Viking Formation consists of a coarsening-upward sequence of shales, sandstones and conglomerates that were deposited into a shallow epeiric sea. Deposition was due to frequent storm-surge ebb currents and sediment-gravity flows moving detritus from the nearshore to offshore regions. Sediments were reworked into a large scale ridge and swale topography by strong unidirectional currents. Detailed subsurface mapping has revealed that the Garrington Oil Field consists of a sandstone and conglomerate ridge approximately 25 km long, 5 to 10 km wide and 10 to 15 m thick. The ridge is oriented west-northwest to south-southeast, parallel to the paleoshoreline. Longshore drift currents and offshore geostrophic currents are responsible for this orientation. Mapping has delineated the possible presence of another ridge, occurring to the northeast and parallel to the Garrington Oil Field.

Upon burial the rocks of the Viking Formation underwent intense diagenesis. Early diagenesis included cementation by siderite and pyrite which mainly affected the fine-grained sandstones. Late diagenesis involved compaction, quartz and late carbonate cementation (mainly dolomite and ankerite), and growth of authigenic, pore-lining and pore-filling clay minerals. Hydrocarbon migration probably ended diagenesis. Diagenesis caused a reduction in porosity and permeability. Porosity values for the conglomerates, coarse-grained sandstones and fine-grained sandstones are similar, averaging about 8 %. Permeability, however, differs considerably between the coarse-grained rocks and the fine-grained sandstones, averaging 70 md in the conglomerates and coarse-grained sandstones and less than 1 md in the fine-grained sandstones. Permeability is very low in the fine-grained sandstones due to the large amount of fine-grained material present in the pore systems of these rocks.

During enhanced oil recovery operations pore-lining and pore-filling minerals can effect reservoir performance in three ways: (1) by the migration of fine-grained material (kaolinite), (2) by the swelling of water sensitive clays (smectite and illite/smectite) and (3) by the precipitation of iron-rich compounds (derived from chlorite, ankerite and siderite). Migration of fine-grained material will be the most serious problem due to the large abundances of kaolinite present in the reservoir rocks. This problem will be particularly acute in the fine-grained sandstones as they have the largest amounts of fine-grained material present in their pore systems and the smallest pore throats.

The Viking "B" unit of the Viking Formation at Garrington is underpressured and primary production is by gas drive. The subpressure may be due to a chemico-osmotic gradient existing between the Viking Formation and underlying Devonian and Carboniferous carbonate rocks, the removal of up to 2500 m of overburden, or the presence of a permeability barrier restricting the flow of formation water. High gas-oil ratios result from the subpressures and also occur where there is communication between the Viking "B" unit and the overlying Viking "A" sandstones. Ultimate recovery of the original oil in place is estimated at 1.75 X 10^6 m^3 by primary recovery methods. This amount could be significantly increased by the use of secondary recovery methods; however, appropriate clay stabilization measures should be investigated.

VI. REFERENCES CITED

Alho, L.O., F.F. Gray and J.R. Kassube, 1977, The Provost Viking 'C' Oil Pool east-central Alberta, Bulletin of Canadian Petroleum Geology, v. 25, p. 396-409.

Almon, W.R., and D.K. Davies, 1981, Formation damage and the crystal chemistry of clays: In Longstaffe, F.J., Short Course in Clays and the Resource Geologist: Mineralogical Association of Canada, p. 81-103.

Amajor, L.C. 1978, Some Viking bentonites, south-central Alberta: Unpublished M.Sc. Thesis, University of Alberta, 104 pp.

______, 1980, Chronostratigraphy, depositional patterns and environmental analysis of sub-surface Lower Cretaceous (Albian) Viking reservoir sandstones in central Alberta and part of southwestern Saskatchewan: Unpublished Ph.D. Thesis, University of Alberta, Edmonton, 596 pp.

Amos, C.L., and E.L. King, 1984, Sand waves and sand ridges of the Canadian Eastern Seaboard: A comparison to global occurrences, in press.

Badgley, P.C., 1952, Notes on the subsurface stratigraphy and oil and gas geology of the Lower Cretaceous Series in central Alberta: Geological Survey of Canada, paper 52-11, p. 1-12.

Bagnold, R.A., 1954, Experiments on gravity free dispersion of large solid spheres in a Newtonian fluid under shear: Proceedings of the Geological Society of London, v. 225, series A, p. 49-63.

Bahan, W.G., 1951, Microfauna of the Joli Fou Formation in north-central Alberta: Unpublished M.Sc. Thesis, University of Alberta, 43 pp.

Beach, F.K., 1955, Cardium, a turbidity current deposit: Bulletin of the Alberta Society of Petroleum Geologists, v. 3 , p. 123-125.

______, 1956, Reply to DeWiel on turbidity current deposits: Bulletin of the Alberta Society of Petroleum Geologists, v. 4, p. 175-177.

______, 1962, Viking deposition (discussion): Bulletin of the Alberta Society of Petroleum Geologists, v. 10, p. 210-212.

Beaumont, E.A., 1984, Retrogradatioanl shelf sedimentation: Lower Cretaceous Viking Formation, central Alberta: In Tillman, R.W. and C.T. Siemers,(eds.), Siliclastic Shelf Sediments: Society of Economic Paleontologists and Mineralogists, Tulsa, Oklahoma, Special Publication No. 34, p. 163-177.

Belyea, H.R., 1964, Upper Devonian, Chapter 6: In McCrossan, R.G., and R.P. Glaister,(eds.), Geological History of Western Canada; Alberta Society of Petroleum Geologists, Calgary, Alberta., p. 60-85.

Berg, R.R., 1976, Highlight Muddy Field, Lower Cretaceous transgressive deposits in the Powder River Basin, Wyoming: Mountain Geologist, v. 13, p. 33-45.

______, and D.K. Davies, 1968, Origin of Lower Cretaceous Muddy Sandstone at Bell Creek Field, Montana: Bulletin of the American Association of Petroleum Geologists, v. 52, p. 1888-1898.

______, and D.K. Davies, 1975, Depositional environment of Upper Cretaceous Sussex

Sandstone, House Creek Field, Wyoming: Bulletin of the American Association of Petroleum Geologists, v. 59, p. 2099-2100.

Berner, R.A., 1970, Sedimentary pyrite formation: American Journal of Science, v. 268, p. 1-23.

Berry, F.A.F., 1960, Geologic field evidence suggesting membrane properties of shales: Bulletin of the American Association of Petroleum Geologists, v. 44, p. 953-954.

Berven, R.J., 1966, Cardium Sandstone bodies, Crossfield-Garrington area, Alberta: Bulletin of Canadian Petroleum Geology, v. 14, p. 208-240.

Blatt, H., Middleton, G. V., Murray, R. C., 1980, Origin of sedimentary rocks: Prentice-Hall Inc., New Jersey, Second Edition, 782 pp.

Boethling, Jr., F.C., 1977a, Increase in gas prices rekindles Viking-sandstone interest: Oil and Gas Journal, v. 75, p. 196-200.

______, 1977b, Typical Viking sequence: A marine sand enclosed with marine shales: Oil and Gas Journal, v. 75, p. 172-176.

Boles, J.R., 1978, Active ankerite cementation in the subsurface Eocene of southwest Texas: Contributions to Mineralogy and Petrology, v. 68, p. 13-22.

______, 1982, Active albitization of plagioclase, Gulf Coast Tertiary: American Journal of Science, v. 282, p. 165-180.

______ and Franks, S.G., 1979, Clay diagenesis in Wilcox Sandstones of southwest Texas: implications of smectite diagenesis on sandstone cementation: Journal of Sedimentary Petrology, v. 49, p. 55-70.

Brenner, R.L., 1978, Sussex Sandstone of Wyoming - Example of Cretaceous offshore sedimentation, Bulletin of the American Association of Petroleum Geologists, v. 62, p. 181-200.

Bullock, D.B., 1950, A microfaunal study of the Basal Lloydminster Shale: Unpublished. M.Sc. Thesis, University of Alberta, 43 pp.

Caldwell, W.G.E., B.R. North, C.R. Stelck, and J.H. Wall, 1978, A foraminiferal zonal scheme for the Cretaceous System in the Interior Plains of Canada: In Stelck, C.R., and B.D.E. Chatterton,(eds.), Western and Arctic Canadian Biostratigraphy, Percival Sydney Warren Memorial Volume, Geological Association of Canada Special Paper No. 18, p. 475-575.

Cant, D.G., 1980, Storm-dominated shallow marine sediments of the Arisaig Group (Silurian-Devonian) of Nova Scotia: Canadian Journal of Earth Science, v. 17, p. 120-131.

______, 1983, Subsurface Sedimentology: Geoscience Canada, v. 10, p. 115-121.

Carrigy, M.A., and Mellon, G.B., 1964, Authigenic clay mineral cements in Cretaceous and Tertiary sandstones of Alberta: Journal of Sedimentary Petrology, v. 34, p. 461-472.

Caston, V.N.D., 1972, Linear sand banks in the southern North Sea: Sedimentology, v. 18, p. 63-78.

Curtis, C.D., 1978, Possible links between sandstone diagenesis and depth related geochemical reactions occurring in enclosing mudstones: Journal of the Geological Society of London, v.135, p. 107-117.

______, 1983, Link between aluminum mobility and destruction of secondary porosity: Bulletin of the American Association of Petroleum Geologists, v.63, p. 380-384

Dahlberg, E.C., 1982, Applied hydrodynamics in petroleum exploration: Springer-Verlag, New York, 161 pp.

Davies, I.C., and R. G. Walker, 1974, Transport and deposition of resedimented conglomerates: the Cap Enrage Formation, Cambro-Ordovician, Gaspe', Quebec: Journal of Sedimentary Petrology, v. 44, p. 1200-1216.

Dickenson, W.R., 1971. Plate tectonic models of geosynclines: Earth and Planetary Science Letters, v. 10, p. 165-174.

DeWiel, J.E.F., 1956, Viking and Cardium not turbidity current deposits, Bulletin of the Alberta Society of Petroleum Geologists, v. 4, p. 173-174.

Dickey, P.A. and W.C. Cox, 1977, Oil and gas in reservoirs with subnormal pressures: Bulletin of the American Association of Petroleum Geologists, v. 61, p. 2134-2142.

Drake, D.E., 1976, Suspended sediment transport and mud deposition on continental shelves: Chapter 9 In Stanley, D.J., and Swift, D.J.P., (eds.), Marine sediment transport and environmental management: John Wiley and Sons, New York, 602 pp.

Eberl, D., and Hower, J., 1976, Kinetics of illite formation: Bulletin of the Geological Society of America, v. 87, p 1326-1330.

Eisbacher, G.H., 1977, Mesozoic-Tertiary basin models for the Canadian Cordillera and their geological constraints: Canadian Journal of Earth Science, v. 14, p. 2414-2417.

E.R.C.B., 1983, Alberta's Reserves of Gas, Complete Listing (Volumes 1,2,3) at 31 December, 1982: ERCB Report 83-35.

______, 1984, Alberta's Reserves of Crude Oil, Oil Sands, Gas, Natural Gas Liquids, and Sulphur at 31 December, 1983. ERCB Report 84-18.

Evans, W.E., 1970, Imbricate linear sandstone bodies of the Viking Formation in Dodsland-Hoosier area of southwestern Saskatchewan: Bulletin of the American Association of Petroleum Geologists, v. 54, p. 469-486.

Ferran, L.H., 1973, Evaluation of abnormally high and low pressured Morrow Sands in northwestern Oklahoma, using well logs and water sample data: Unpublished M.Sc. Thesis, University of Tulsa, Tulsa, Oklahoma., 110 pp.

Field, M.E., and P.S. Roy, 1984, Large storm and current shaped sandbodies on the southeastern Australian shelf: In Research Symposium, Sedimentology of Shelf Sands and Sandstones, program and abstracts, Calgary, p. 36.

Fisher, R.V., 1971, Features of coarse-grained high-concentration fluids and their deposits: Journal of Sedimentary Petrology, v. 41, p. 916-927.

Flemming, B.W., 1978, Underwater sand dunes along the southeast African Continental Margin - observations and implications: Marine Ecology, v. 26, p. 177-198.

______, 1980, Sand transport and bedform patterns on the continental shelf between Durban and Port Elizabeth (Southeast African Continental Margin): Sedimentary Geology, v. 26, p. 179-205.

Folk, R.L., 1968, Petrology of sedimentary rocks: Austin, Texas: Hemphill's book store.

Gammell, H.G., 1955, The Viking Member in central Alberta, Bulletin of the Alberta Society of Petroleum Geologists, v. 3, p. 63-69.

Gopinath, T.R., 1978, Depositional environments of the Muddy Sandstone (Lower Cretaceous) Wind River Basin, Wyoming: Mountain Geologist, v. 15, p. 27-47.

Glaister, R.P., 1958, Petrology of the Blairmore Sandstones: Bulletin of the Alberta Society of Petroleum Geologists, v. 6, p. 43-49.

______, 1959, Lower Cretaceous of southern Alberta and adjoining areas, Bulletin of the American Association of Petroleum Geologists, v. 43, p. 590-640.

Goldring, R., and Bridges, P., 1973, Sublittoral sheet sandstones: Journal of Sedimentary Petrology, v. 43, p. 736-747.

Griffith, L.A., 1981, Depositional environment and conglomerate diagenesis of the Cardium Formation, Ferrier Field, Alberta: Unpublished M.Sc. Thesis, University of Calgary, 132 pp.

Hacquebard, P. A., 1977, Rank of coal as an index of organic metamorphism for Oil and Gas in Alberta: In Deroo, G., T. G. Powell, B. Tissot, and R. G. McCrossan with contributions by P. A. Hacquebard, The origin and migration of petroleum in the Western Canada Sedimentary Basin, Alberta: Geological Survey of Canada Bulletin 262, p. 11-22.

Hamblin, A.P., and Walker, R.G., 1979, Storm-dominated shallow marine deposits: the Fernie-Kootenay (Jurassic) transition, southern Rocky Mountains: Canadian Journal of Earth Science, v. 16, p. 1673-1690.

Hampton, M.A., 1972, The role of subaqueous debris flow in generating turbidity currents: Journal of Sedimentary Petrology, v. 42, p. 775-793.

Harms, J.C., J.B. Southard, D.R. Spearing and R.G. Walker, 1975, Depositional Environments as interpreted from primary sedimentary structures andstratification sequences: Society of Economic Paleontologists and Mineralogists, Lecture Notes 2, 161 pp.

______, J.B. Southard, and R.G. Walker, 1982, Depositional Environments as interpreted from primary sedimentary structures and stratification sequences: Society of Economic Paleontologists and Mineralogists, Lecture Notes 9, 249 pp.

Hein, F.J., 1981, Depositional mechanisms of deep sea coarse clastic sediments, Cap Enrage' Formation, Quebec: Canadian Journal of Earth Science, v. 19, p. 267-287.

______, 1984, Deep-Sea and Fluvial Braided Channel conglomerates: A comparison of two case studies. in press: Canadian Society of Petroleum Geologists memoir.

______, and R.G. Walker, 1982, The Cambro-Ordovician Cap Enrage' Formation, Quebec, Canada: Conglomerate deposits of a braided submarine channel with terraces: Sedimentology, v. 29, p. 309-329.

______, Dean, M.E., Delure, A.M., Grant, S.K., Robb, G.A., and Longstaffe, F.J. 1984. Regional Sedimentology of the Viking Formation, Caroline, Garrington, and Harmattan East Fields, South-central Alberta, storm and current influenced shelf settings: in preparation.

Hitchon, B., 1969, Fluid Flow in the Western Canada Sedimentary Basin, 2. Effect of Geology: Water Resources Research, v. 5, p. 460-469.

______, 1984, Geothermal gradients, hydrodynamics and hydrocarbon occurrences, Alberta, Canada: Bulletin of the American Association of Petroleum Geologists,

v. 68, p. 713-743.

Hobson, J.P., M.L. Fowler and E.A. Beaumont, 1982, Depositional and Statistical Exploration Models, Upper Cretaceous offshore sandstone complex, Sussex member, House Creek Field, Wyoming: Bulletin of the American Association of Petroleum Geologists, v. 66, p. 689-707.

Houbolt, J.J.H.C., 1968, Recent sediments in the southern bight of the North Sea: Geology Mijnbouw, v. 47, p. 245-273.

Hower, J., E.V. Eslinger, M.E. Hower and E.A. Perry, 1976, Mechanism of burial metamorphism of argillaceous sediment: 1 mineralogical and chemical evidence: Bulletin of the Geological Society of America, v. 87, p. 725-737.

Hume, G.S., 1933, Oil and gas in Western Canada: Geological Survey of Canada, Economic Geology Series No. 5, 359 pp.

Hunt, W.C., 1954, The Joseph Lake-Armena-Camrose producing trend, Alberta: In Clark, L. M., (ed.) Western Canada Sedimentary Basin, p. 452-463.

Ignasiuk, T.M., L. Kotlyar, F.J. Longstaffe, O.P. Strausz and D.S. Montgomery, 1983, Separation and characterization of clay from Athabasca asphaltene: Fuel, v. 62, p. 353-362.

Irwin, H., and Curtis, C., 1977, Isotopic evidence for source of diagenetic carbonates formed during burial of organic rich sediments: Nature, v. 269, p. 209-213.

Jones, F.O., and W.W. Owens, 1980, A laboratory study of low permeability gas sands: Journal of Petroleum Technology, v. 32, p. 1631-1639.

Jones, H.L., 1961, Viking deposition in southwestern Saskatchewan with a note on the source of the sediments, Bulletin of the Alberta Society of Petroleum Geologists, v. 9, p. 231-244.

Karlsrud, K., and L. Edgers, 1982, Some aspects of submarine slope stability: In Saxov, S., and J. K. Nieuwenhuis, (eds.), Marine slides and other mass movements, NATO conference series, Series IV: marine sciences., Plenum Press, New York., p. 63-81.

Kazemi, H., 1975, A reservoir simulator for studying productivity variation and transient behavior of a well in a reservoir undergoing gas evolution: Journal of Petroleum Technology, v. 27, p. 1401-1412.

Koldijk, W.S., 1976, Gilby Viking 'B': A storm deposit, In Lerand, M.M., (ed.), The sedimentology of selected clastic oil and gas reservoirs in Alberta, Canadian Society of Petroleum Geologists, p. 62-77.

Koning, H.L., 1982, On an explanation of marine flow slides in sand: In Saxov, S., and J. K. Nieuwenhuis, (eds.), Marine slides and other mass movements, NATO conference series, Series IV, marine sciences., Plenum Press, New York., p. 83-94.

Kontopoulos, N., and Piper, D.J.W., 1982, Storm graded sand at 200 m water depth, Scotian Shelf, eastern Canada: Geomarine Letters, v. 2, p. 77-81.

Land, L.S., and Dutton, S.P., 1978, Cementation of a Pennsylvanian deltaic sandstone: Isotopic data: Journal of Sedimentary Petrology, v. 48, p. 1167-1176.

Larson, L. H., 1960 (ed.), Gas fields of Alberta: Alberta Society of Petroleum Geologists, 407 pp.

Leckie, D., in prep, Viking Formation, Caroline Area, A transgressive Shelf-Ridge complex:

Bulletin of Canadian Petroleum Geology, 56 pp., submitted.

Love, M., 1955, The Joffre Oil Field, geology and development, Oil in Canada, v. 7, p. 12884-12890.

Magditch, F.S., 1955, The Viking Formation in Saskatchewan: Unpublished M.Sc. Thesis, University of Saskatchewan, Saskatoon.

McBride, E.F., R.G. Shepherd, and R.A. Crawley, 1975, Origin of parallel, near horizontal laminae by migration of bedforms in a small flume: Journal of Sedimentary Petrology, v. 45, p. 132-139.

Michaelis, E.R., 1957, Cardium sedimentation in the Pembina River area: Bulletin of the Alberta Society of Petroleum geologists, v. 5, p. 73-77.

______, and G. Dixon, 1969, Interpretation of the depositional process from sedimentary structures in the Cardium sand: Bulletin of Canadian Petroleum Geology, v. 17, p. 410-433.

Middleton, G.V., 1970, Experimental studies related to problems of flysh sedimentation: In Lajoie, J., (ed.), Flysh sedimentology in North America: Geological Association of Canada, Special Paper No. 7, p. 253-272.

______, and Hampton, M.A., 1976, Subaqueous sediment transport and deposition by sediment gravity flows: Chapter 11 in Stanley, D.J., and Swift, D.J.P., (eds.), Marine sediment transport and environmental management: John Wiley and Sons, New York, 602 pp.

Milliken, K.L., L.S. Land and R.G. Loucks, 1981, History of burial diagenesis determined from isotopic geochemistry, Frio Formation, Brazoria County, Texas: Bulletin of the American Association of Petroleum Geologists, v. 65, p. 1397-1413.

Monger, J.W.H., R.A. Price and D.J. Templeman-Kluit, 1982, Tectonic accretion and the origin of two major metamorphic belts and plutonic welts in the Canadian Cordillera: Geology, v. 10, p. 70-75

Moorhouse, W.W., 1959, The study of rocks in thin section: Harper and Row, New York, 514 pp.

Nash, A.J., and Pittman, E.D., 1975, Ferro-magnesian calcite cement in sandstones: Journal of Sedimentary Petrology, v. 45, p. 258-265.

Nauss, A.W., 1945, Cretaceous Stratigraphy of Vermilion area, Alberta, Canada: Bulletin of the American Association of Petroleum Geologists, v. 29, p. 1615-1618.

______, 1947, Cretaceous microfossils of the Vermillion area, Alberta: Journal of Paleontology, v. 21, p. 329-343.

Norgaard, G. A., 1954, Viking Formation, Colorado Group, Lower Cretaceous: In Lexicon of Geologic names in the western Canadian Sedimentary Basin and Arctic Archipelago: Alberta Society of Petroleum Geologists, Calgary, p. 360-361.

North, B.R., and W.G.E. Caldwell, 1975, Foraminiferal faunas in the Cretaceous system of Saskatchewan: In Caldwell, W.G.E. (ed.), The Cretaceous system in the Western Interior of North America, Geological Association of Canada, Special Paper No. 13, p. 303-332.

Obradovich, J.D., and W.A. Cobban, 1975, A time scale for the Late Cretaceous of the Western Interior of North America: In Caldwell, W.G.E., (ed.), The Cretaceous System in the Western Interior of North America: Geological Association of Canada, Special Paper No. 13, p. 31-54.

Off, T., 1963, Rhythmic linear sandbodies caused by tidal currents: Bulletin of the American Association of Petroleum Geologists, v. 47, p. 324-341.

Patterson, A.M., and A.A. Arneson, 1957, Geology of the Pembina field, Alberta: Bulletin of the American Association of Petroleum Geologists, v. 41, p. 937-949.

Perry, E., and Hower, J., 1970, Burial diagenesis in Gulf Coast pelitic sediments: Clays and Clay Minerals, v. 18, p. 165-177.

Pitman, J.K., T.D. Fouch and M.B. Goldhaber, 1982, Depositional setting and diagenetic evolution of some Tertiary unconventiional reservoir rocks, Uinta Basin, Utah: Bulletin of the American Association of Petroleum Geologists, v. 66, p. 1581-1596.

Porter, K.W., and Weimer, R.J., 1982, Diagenetic sequence related to structural history and petroleum accumulation: Spindle field, Colorado: Bulletin of the American Association of Petroleum Geologists, v. 66, p. 2543-2560.

Prior, D.B., and J.M. Coleman, 1982, Active slides and flows inm underconsolidated marine sediments on the slopes of the Mississippi delta: In Saxov, S., and J. K. Nieuwenhuis, (eds.), Marine slides and other mass movements, NATO conference series, Series IV, marine sciences., Plenum Press, New York, p. 21-49.

Reading, H.G., 1978, Sedimentary environments and facies: Elsevier, New York, 557 pp.

Reasoner, M.A. and Hunt, A.D., 1954, Smiley Oil Field, Saskatchewan: Bulletin of Canadian Mining and Metallurgy, v. 47, p. 612-617.

Reinert, S.L., and D.K. Davies, 1976, Third Creek Field, Colorado: A study of sandstone environments and diagenesis: Mountain Geologist, v. 13, p. 47-60.

Reinson, G.E., A.E. Foscolos and T.G. Powell, 1983, Comparison of Viking Sandstone sequences, Joffre and Caroline fields: In McLean, J.R., and Reinson, G.E., (eds.), Sedimentology of selected Mesozoic clastic sequences, Canadian Society of Petroleum Geologists, Calgary, p. 101-117.

Reynolds, R.C., and Hower, J., 1970, The nature of interlayering in mixed-layer illite-montmorillonites: Clays and Clay Minerals, v. 18, p. 25-36.

Roessingh, H.K., 1957, Cardium Formation in the Alberta Plains between the Athabasca and Bow Rivers: Bulletin of the Alberta Society of Petroleum Geologists, v. 5, p. 78-81.

_______, 1959, Viking deposition in the southern Alberta Plains: Alberta Society of Petroleum Geologists, 9th Annual Field Conference, p. 130-137.

Rudkin, R.A., 1964, Chapter II: Lower Cretaceous, In McCrossan, R.G., and Glaister, R.P.(eds.), Geological History of Western Canada, Canadian Society of Petroleum Geologists, Calgary, Alberta, p. 156-168.

Scott, R.W., 1970, Stratigraphy and sedimentary environments of Lower Cretaceous rocks, southern Western Interior: Bulletin of the American Association of Petroleum Geologists, v. 54, p. 1225-1244.

Seeling, A., 1978, The Shannon sandstone, a further look at the environment of deposition at Heldt Draw Field, Wyoming: Mountain Geologist, v. 15, p. 133-144.

Shelton, J.W., 1964, Authigenic kaolinite in sandstone: Journal of Sedimentary Petrology, v. 34, p. 102-111.

______, 1973, Models of sand and sandstone deposits: a methodology for determining sand genesis and trend: Viking Sandstone, Cretaceous, Joffre Field, Alberta, Bulletin of the Oklahoma Geological Survey, v. 118, p. 91-94.

Shurr, G.W., 1984, Geometry of shelf sandstone bodies in the Shannon Sandstone of southeastern Montana: In Tillman, R. W., and C. T. Siemers (eds.), Siliciclastic Shelf Sediments: Society of Economic Paleontologists and Mineralogists, Tulsa, Oklahoma, Special Publication No. 34, p. 63-83.

Simpson, F., 1975, Marine Lithofacies and Biofacies of the Colorado Group (Middle Albian to Santonian) in Saskatchewan, In Caldwell, W.G.E. (ed.), The Cretaceous system in the Western Interior of North America, Geological Association of Canada, Special Paper No. 13, p. 553-587.

Sinha, R.N., 1970, Cardium Formation, Edson area, Alberta: Geological Survey of Canada Paper 68-30, p. 1-45.

Slatt, R.M., 1984, Continental shelf topography: key to understanding distribution of shelf sand-ridge deposits from Cretaceous western interior seaway: Bulletin of the American Association of Petroleum Geologists, v. 68, p. 1107-1120.

Slipper, S.E. 1918, Viking Gas Field, Structure of Area: Geological Survey Summary Department, 1917, Part C, p. 8c.

Smith, N.D., 1971, Pseudo-planar stratification produced by very low amplitude sand waves: Journal of Sedimentary Petrology, v. 41, p. 69-73.

Spearing, D.R. 1976, Upper Cretaceous Shannon Sandstone: An offshore shallow marine sandbody, Wyoming Geological Association, 28th Annual Guidebook, p. 65-72.

Stansberry, G.F., 1957, The Viking Formation, Central Alberta: Unpublished M.Sc. Thesis, University of Alberta, 124 pp.

Stapp, R.W., 1967, Relationship of Lower Cretaceous depositional environments to oil accumulation, Northeast Powder River Basin, Wyoming: Bulletin of the American Association of Petroleum Geologists, v. 51, p. 2044-2055.

Stelck, C.R. 1958, Stratigraphic position of Viking Sand: Bulletin of the Alberta Society of Petroleum Geologists, v. 6, p. 2-7.

______, 1975, The Upper Albian *Miliammina manitobensis* zone in northeastern British Columbia: In Caldwell, W.G.E., (ed.), The Cretaceous system in the Western Interior of North America: Geological Association of Canada, Special Paper No. 13, p. 253-275.

Stride, A.H., 1982, Offshore Tidal Sands: Processes and Deposits. Chapman and Hall Ltd., New York., 222 pp.

Stubblefield, W.L., and D.J.P. Swift, 1976, Ridge development as revealed by subbottom profiles on the central New Jersey shelf: Marine Geology, v. 20, p. 315-334.

Surdam, R.C., S. Boese and L.J. Crossey, 1982, Role of organic and inorganic reactions in development of secondary porosity in sandstones (abstract): Bulletin of the American Association of Petroleum Geologists, v. 66, p. 635.

Swagor, N.S., T.A. Oliver and B.A. Johnson, 1976, Carrot Creek Field, Central Alberta: In Lerand, M.M., (ed.) The sedimentology of selected clastic oil and gas reservoirs in Alberta: Canadian Society of Petroleum Geologists, Calgary, p. 78-95.

Swift, D.J.P., 1974, Continental shelf sedimentation: In Burke, C. A., and C. L. Drake, (eds.), The Geology of continental margins, Springer-Verlag, p. 117-124

______, 1975, Tidal sand ridges and shoal retreat massifs: Marine Geology, v. 18, p. 105-134

______, D.B. Duane, and T.F. McKinney, 1973, Ridge and swale topography of the Middle Atlantic Bight: Scalar response to Holocene hydraulic regime: Marine Geology, v. 15, p. 227-247.

______, and D.D. Rice, 1984, Sand bodies on muddy shelves: a model for sedimentation in the Western Interior Seaway, North America: In Tillman, R. W., and C. T. Seimers (eds.), Siliciclastic Shelf Sediments: Society of Economic Paleontologists and Mineralogists, Tulsa, Oklahoma, Special Publication No. 34, p. 43-62.

Thomas, J.B., 1978, Diagenetic sequences in low-permeability argillaceous sandstones, Geological Society of London, v. 135, p. 93-99.

______, 1981, Classification and diagenesis of clay minerals in tight gas sandstones: Case studies in which clay minerals properties are crutial to drilling fluid selection, formation evaluation and completion techniques: In Longstaffe, F.J., (ed.) Short Course in clays and the resource geologist: Mineralogical Association of Canada, p. 104-118.

Thomas, M.B., 1977, Depth-Porosity relationships in the Viking and Cardium Formations in Central Alberta: Unpublished M.Sc. Thesis, University of Calgary, 147 pp.

______, and Oliver, T.A. (1979). Depth-Porosity Relationships in the Viking and Cardium Formations of Central Alberta, Bulletin of Canadian Petroleum Geology, v. 27, p. 209-228.

Tizzard, P.G., and J.F. Lerbekmo, 1975, Depositional history of the Viking formation, Suffield area, Alberta, Canada: Bulletin of the Canadian Society of Petroleum Geologists, v. 23, p. 715-752.

Toth, J., 1970, Relations between electric analog patterns of ground water flow and accumulation of hydrocarbons: Canadian Journal of Earth Science, v. 7, p. 988-1007.

______, 1978, Gravity induced cross-formational flow of formation fluids, Red Earth region, Alberta, Canada: Analysis, patterns and evolution: Water Resources Research, v. 14, p. 805-843.

______, 1979, Patterns of dynamic pressure increment of formation-fluid flow in large drainage basins, exemplified by the Red Earth region, Alberta, Canada: Bulletin of Canadian Petroleum Geology, v. 27, p. 63-83.

______, 1980, Cross-formational gravity-flow of ground water: a mechanism for the transport and accumulation of petroleum (the generalized hydraulic theory of petroleum migration): In Roberts, W. H., III, and R. J. Cordell, (eds.) Problems of petroleum migration: AAPG studies in Geology 10, p. 121-167.

Walker, R.G., 1979, Facies Model 7: Shallow Marine Sands: In Walker, R.G., (ed.), Facies Models: Geoscience Canada, Reprint series I, p. 75-89.

______, 1984, Shelf and shallow marine sands: In Walker, R.G., (ed), Facies Models: Geoscience Canada, Reprint series I, second edition, p. 141-169.

Weimer, R.J., 1983, Relation of unconformities, tectonics, and sea level changes, Cretaceous of the Denver Basin and adjacent areas: In Reynolds, M.W., and E.D. Dolly, (eds.), Mesozoic paleogeography of west-central United States: Denver, Rocky Mountain Section, Society of Economic Paleontologists and Mineralogists, p. 359-376.

Westcott, W.A., 1983, Diagenesis of Cotton Valley Sandstone (Upper Jurassic), east Texas: implications for tight gas formation pay recognition: Bulletin of the American Association of Petroleum Geologists, v. 67, p. 1002-1013.

Wickenden, R.T.D., 1949, Some Cretaceous sections along Athabasca River from the mouth of Calling River to below Grand Rapids, Alberta, Geological Survey of Canada, Paper 49-15, p. 3-16.

Williams, G.D., and C.R. Stelck, 1975, Speculations on the Cretaceous Paleogeography of North America: In Caldwell, W.G.E., (ed.), The Cretaceous System in the Western Interior of North America: Geological Association of Canada, Special Paper No. 13, p. 1-7.

Wilson, M.D., 1982, Origins of clays controlling permeability in tight gas sands: Journal of Petroleum Technology, v.34, p. 2871-2876.

______, and Pittman, E.D., 1977, Authigenic clays in sandstones: recognition and influence on reservoir properties and paleoenvironmental analysis: Journal of Sedimentary Petrology, v. 47, p. 3-31.

Wright, M.E., and R.G. Walker, 1981, Cardium Formation (Upper Cretaceous), at Seebe, Alberta: storm-transported sandstones and conglomerates in shallow marine depositional environments below fairweather wave base: Canadian Journal of Earth Science, v. 18, p. 795-809.

APPENDIX A

Appendix A contains lithologs drawn from core descriptions. Samples that were selected for mineralogical studies are plotted on the appropriate lithologs.

2-2-34-2W5

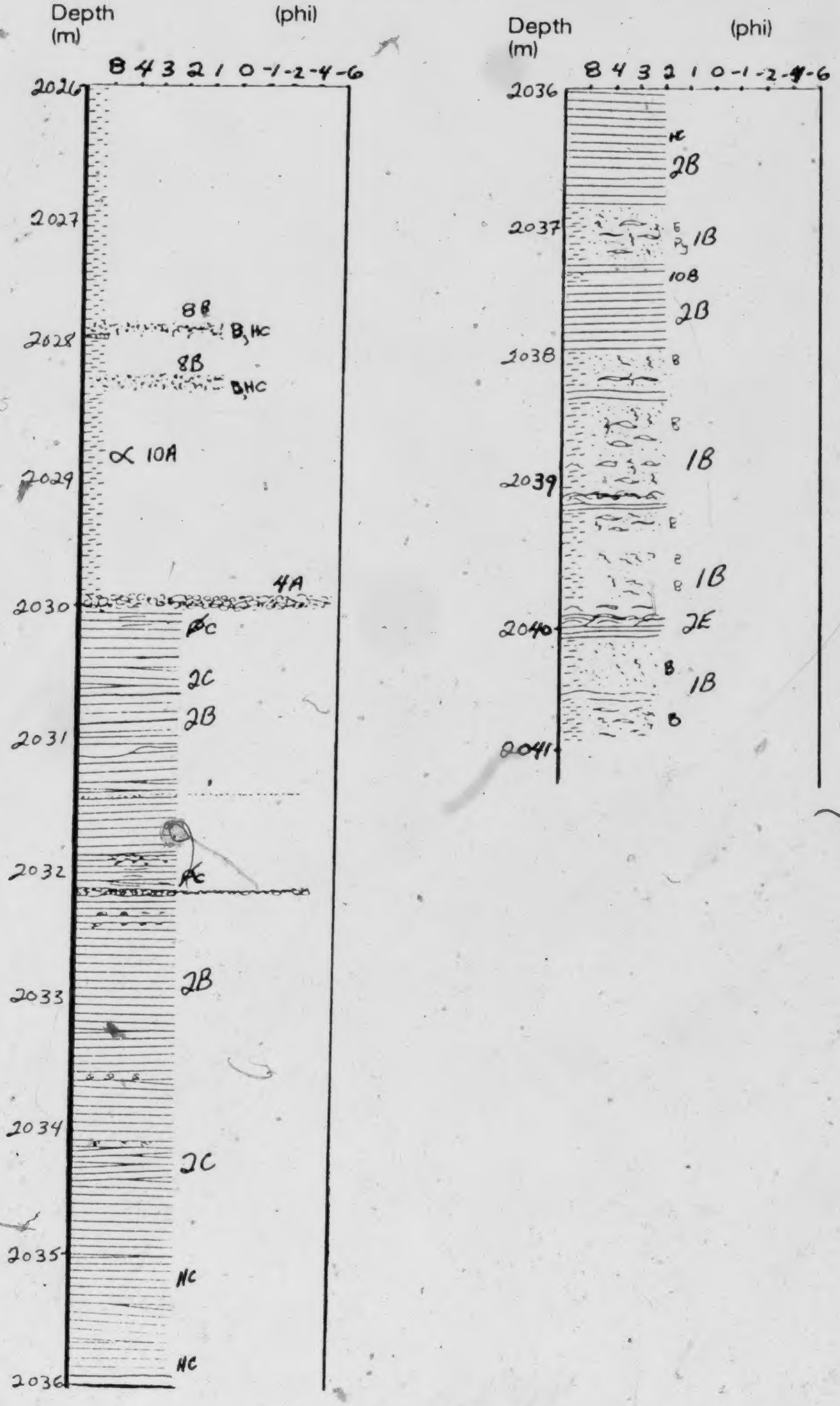
Depth
(m)
(phi)
8 4 3 2 1 0 -1 -2 -4 -6
2026
2027
8B
B, HC
2028
8B
B, HC
α 10A
2029
4A
2030
ØC
2C
2B
2031
2032
ØC
2B
2033
2034
2C
2035
HC
HC
2036
Depth
(m)
(phi)
8 4 3 2 1 0 -1 -2 -4 -6
2036
HC
2B
2037
B
1B
10B
2B
2038
B
B
1B
2039
B
B
B
1B
2040
2E
B
1B
2041
B

5-14-34-2W5

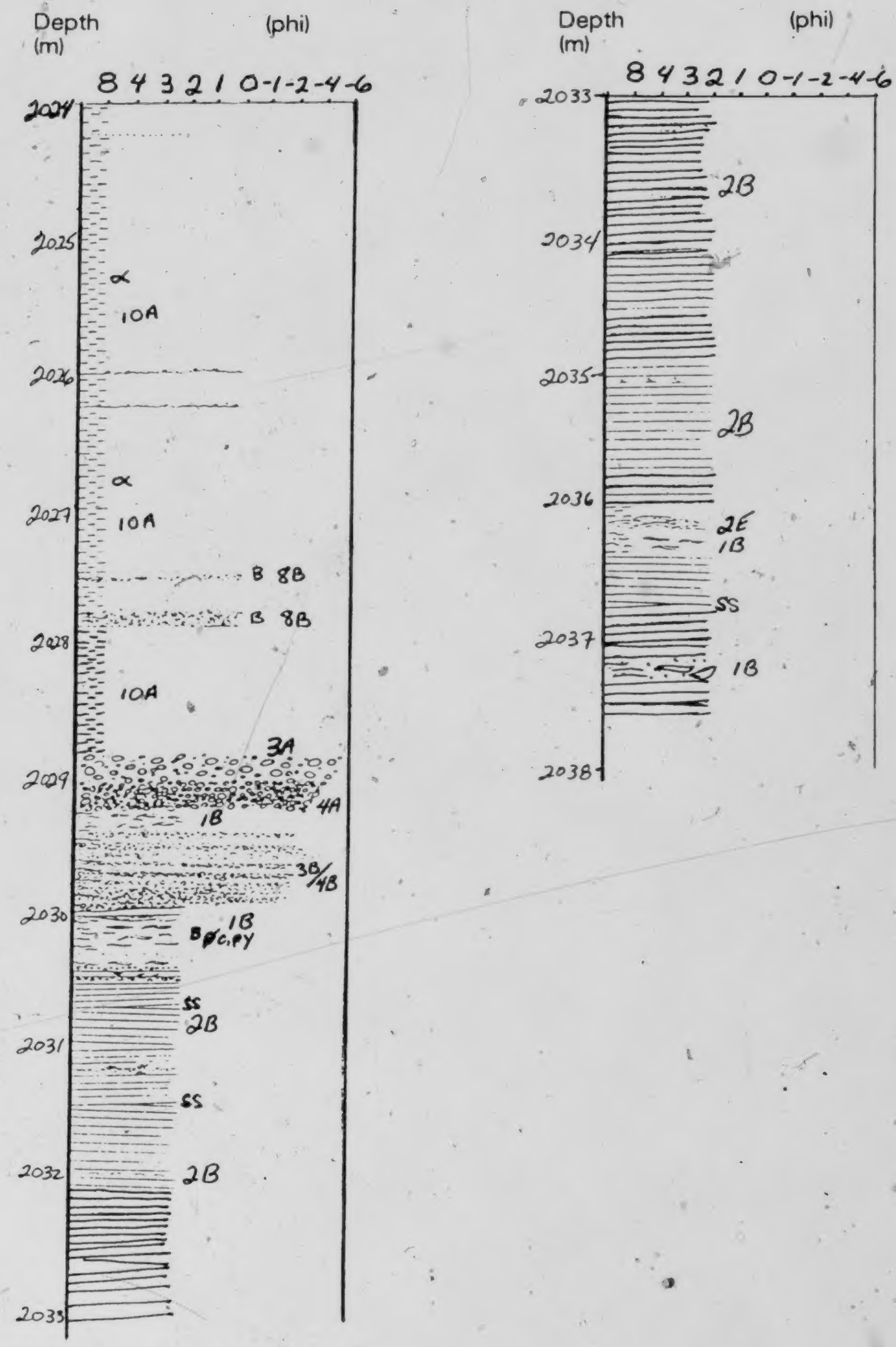
Depth (m)
(phi)
8 4 3 2 1 0 -1 -2 -4 -6
2024
2025
2026
2027
2028
2029
2030
2031
2032
2033
α
10A
α
10A
B 8B
B 8B
10A
3A
4A
1B
3B/4B
1B
B ØC,PY
SS
2B
SS
2B
Depth (m)
(phi)
8 4 3 2 1 0 -1 -2 -4 -6
2033
2034
2035
2036
2037
2038
2B
2B
2E
1B
SS
1B

6-19-34-2W5

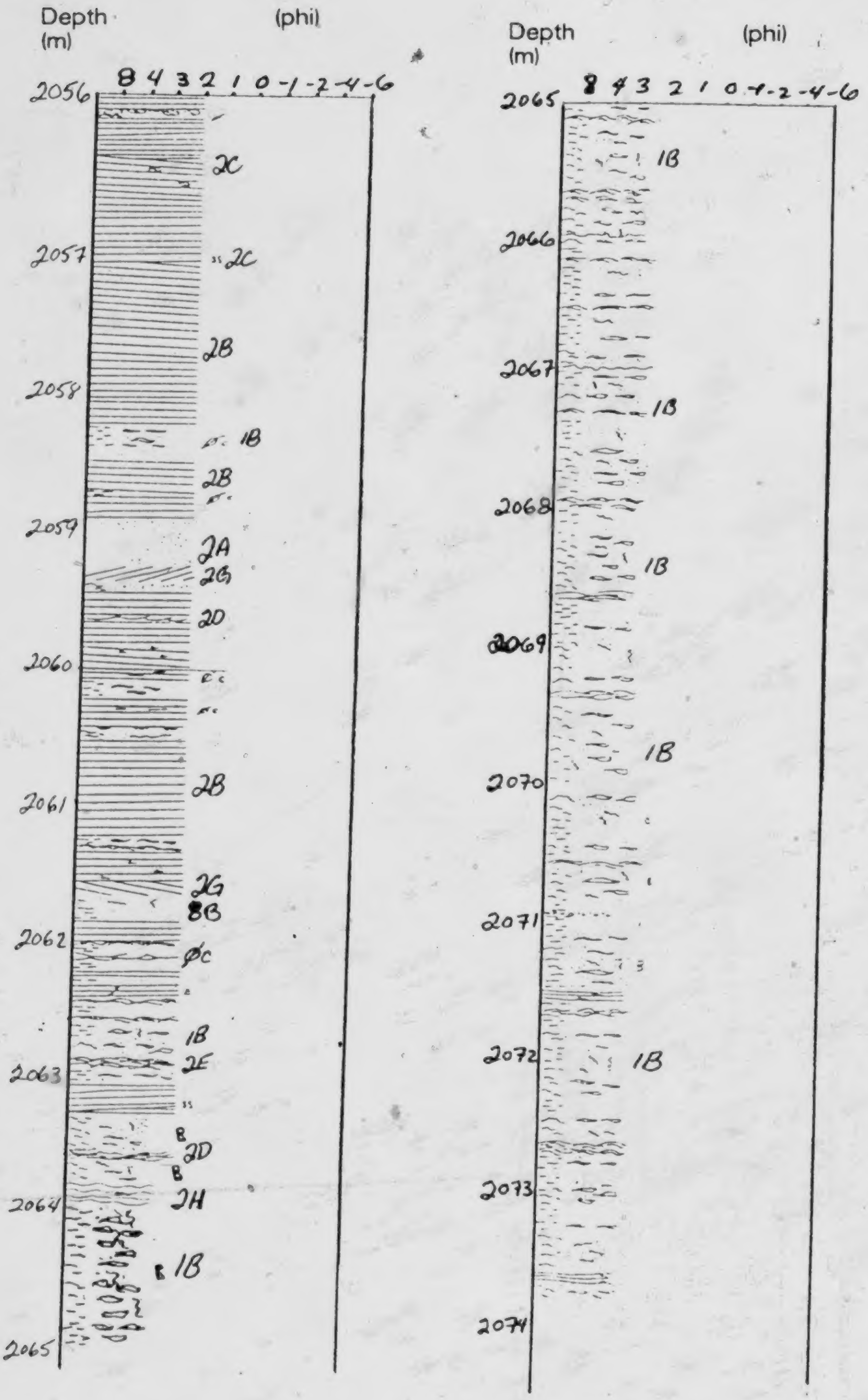
Depth (m)
(phi)
8 4 3 2 1 0 -1 -2 -4 -6
2056
2C
2057
2C
2B
2058
1B
2B
2059
2A
2G
2D
2060
2B
2061
2G
8B
2062
0C
1B
2E
2063
B
2D
B
2H
2064
B
1B
2065
Depth (m)
(phi)
8 4 3 2 1 0 -1 -2 -4 -6
2065
1B
2066
2067
1B
2068
1B
2069
1B
2070
2071
2072
1B
2073
2074

16-19-34-2W5

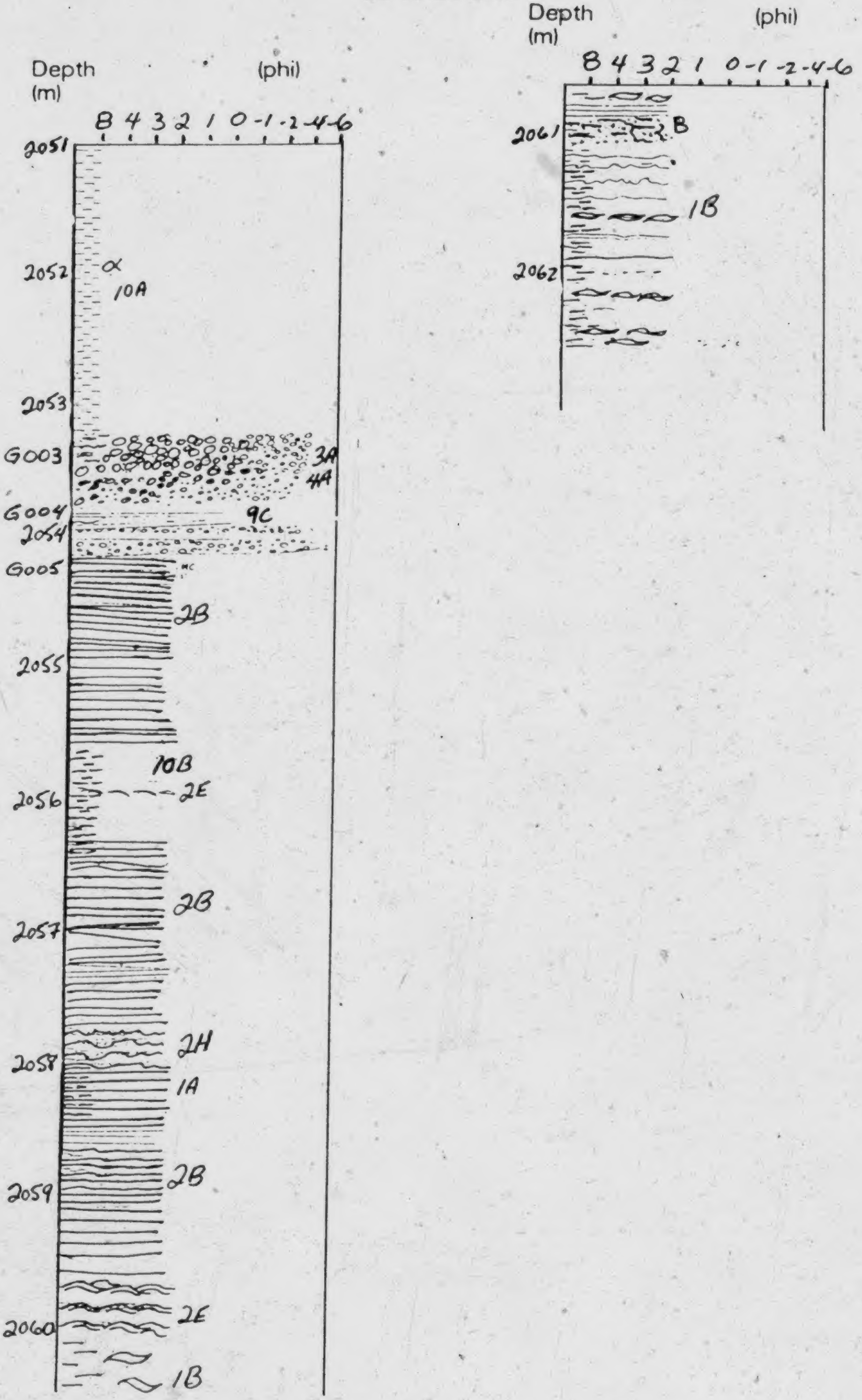
Depth (m)
(phi)
8 4 3 2 1 0 -1 -2 -4 -6
2051
2052
α
10A
2053
G003
3A
4A
G004
9C
2054
G005
2B
2055
10B
2056
2E
2B
2057
2H
2058
1A
2B
2059
2E
2060
1B
Depth (m)
(phi)
8 4 3 2 1 0 -1 -2 -4 -6
2061
B
1B
2062

12-23-34-2W5

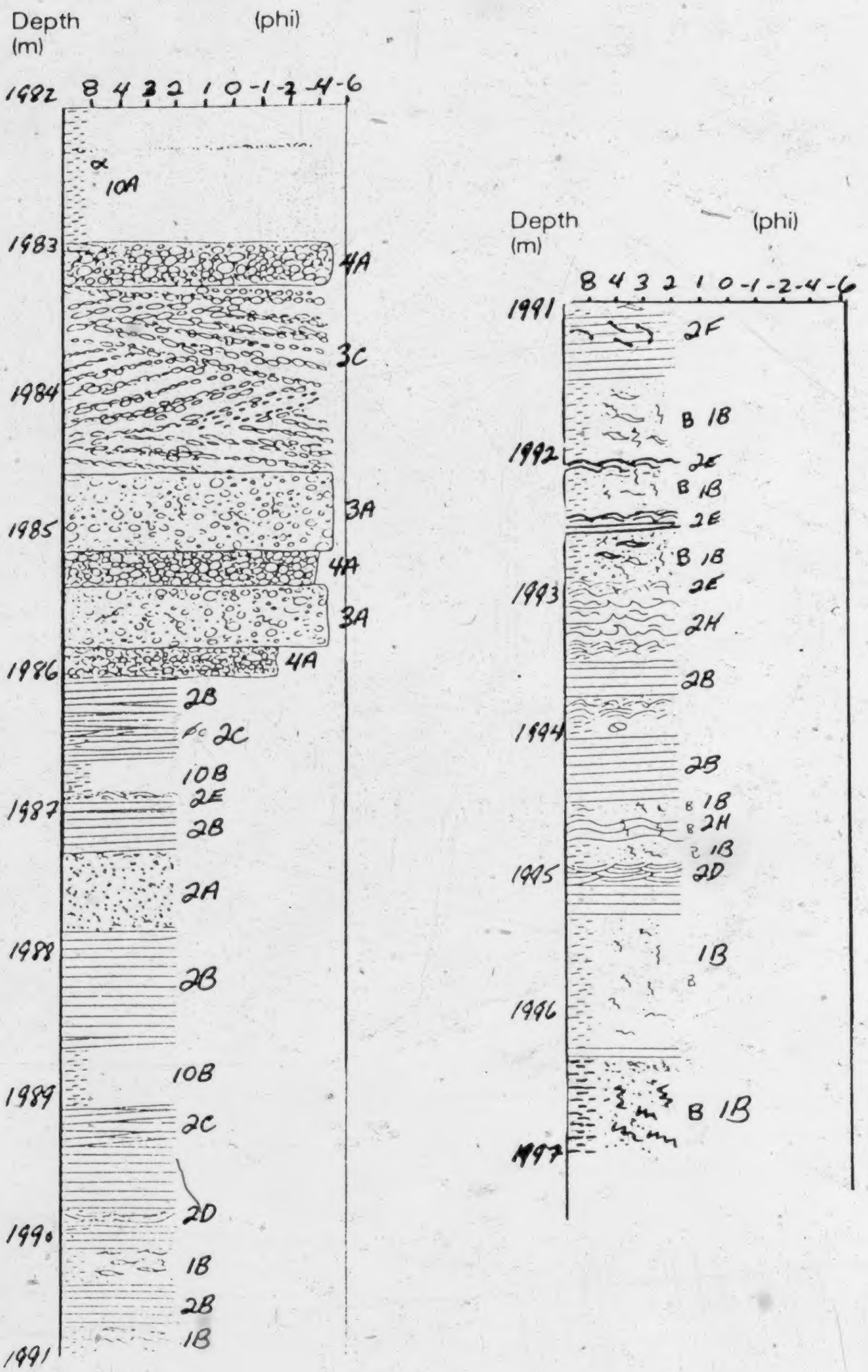
Depth (m)
(phi)
8 4 3 2 1 0 -1 -2 -4 -6
1982
α
10A
1983
4A
3C
1984
3A
1985
4A
3A
1986
4A
2B
2C
10B
2E
1987
2B
2A
1988
2B
10B
1989
2C
2D
1990
1B
2B
1B
1991
Depth (m)
(phi)
8 4 3 2 1 0 -1 -2 -4 -6
1991
2F
B 1B
1992
2E
B 1B
2E
B 1B
1993
2E
2H
2B
1994
2B
B 1B
B 2H
B 1B
1995
2D
1B
B
1996
B 1B
1997

6-30-34-2W5

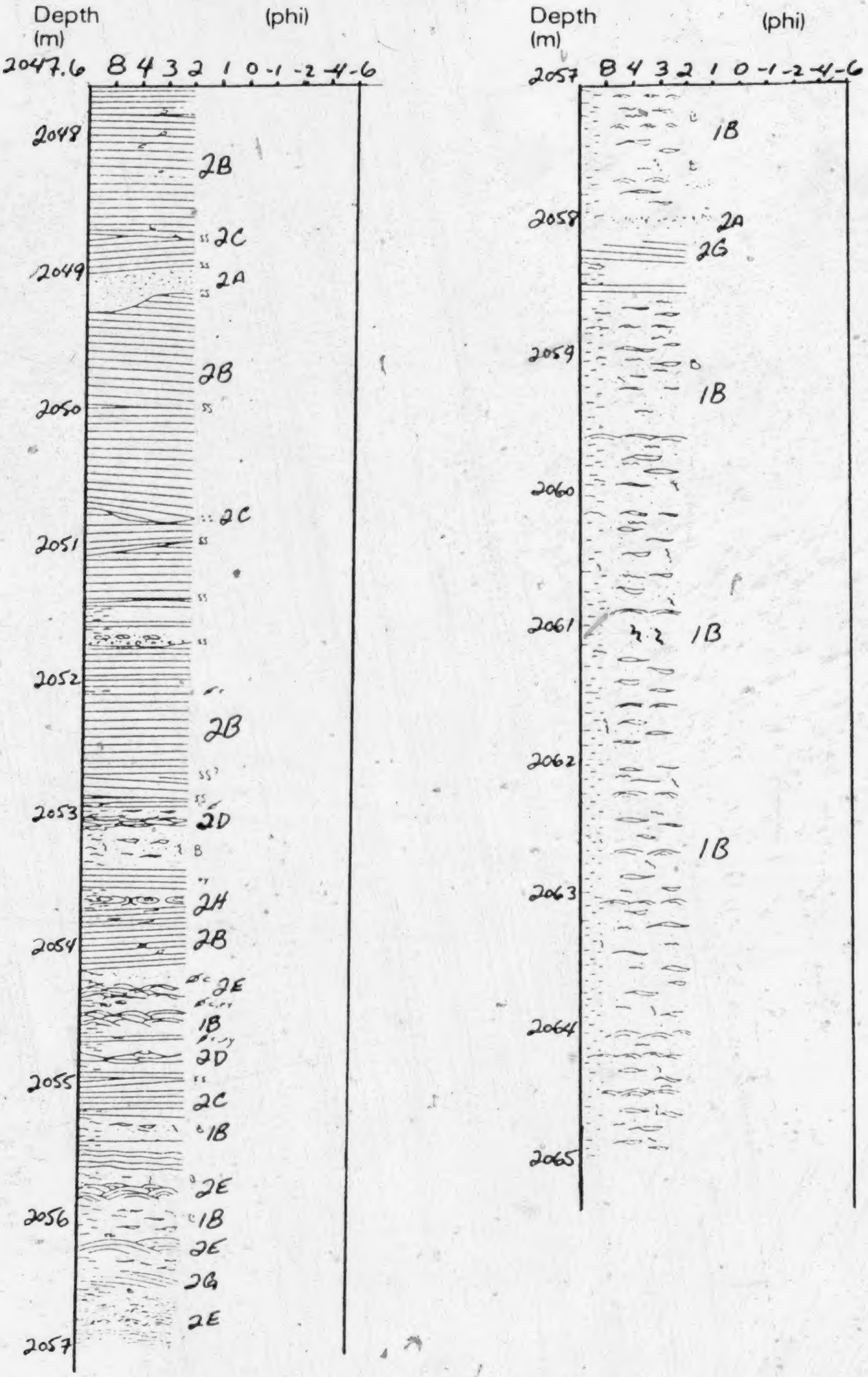
Depth (m)
(phi)
2047.6
8 4 3 2 1 0 -1 -2 -4 -6
2048
2B
2C
2049
2A
2B
2050
2C
2051
2052
2B
2053
2D
B
2H
2054
2B
2E
1B
2D
2055
2C
1B
2E
2056
1B
2E
2G
2E
2057
Depth (m)
(phi)
2057
8 4 3 2 1 0 -1 -2 -4 -6
1B
2058
2A
2G
2059
1B
2060
2061
1B
2062
1B
2063
2064
2065

13-30-34-2W5

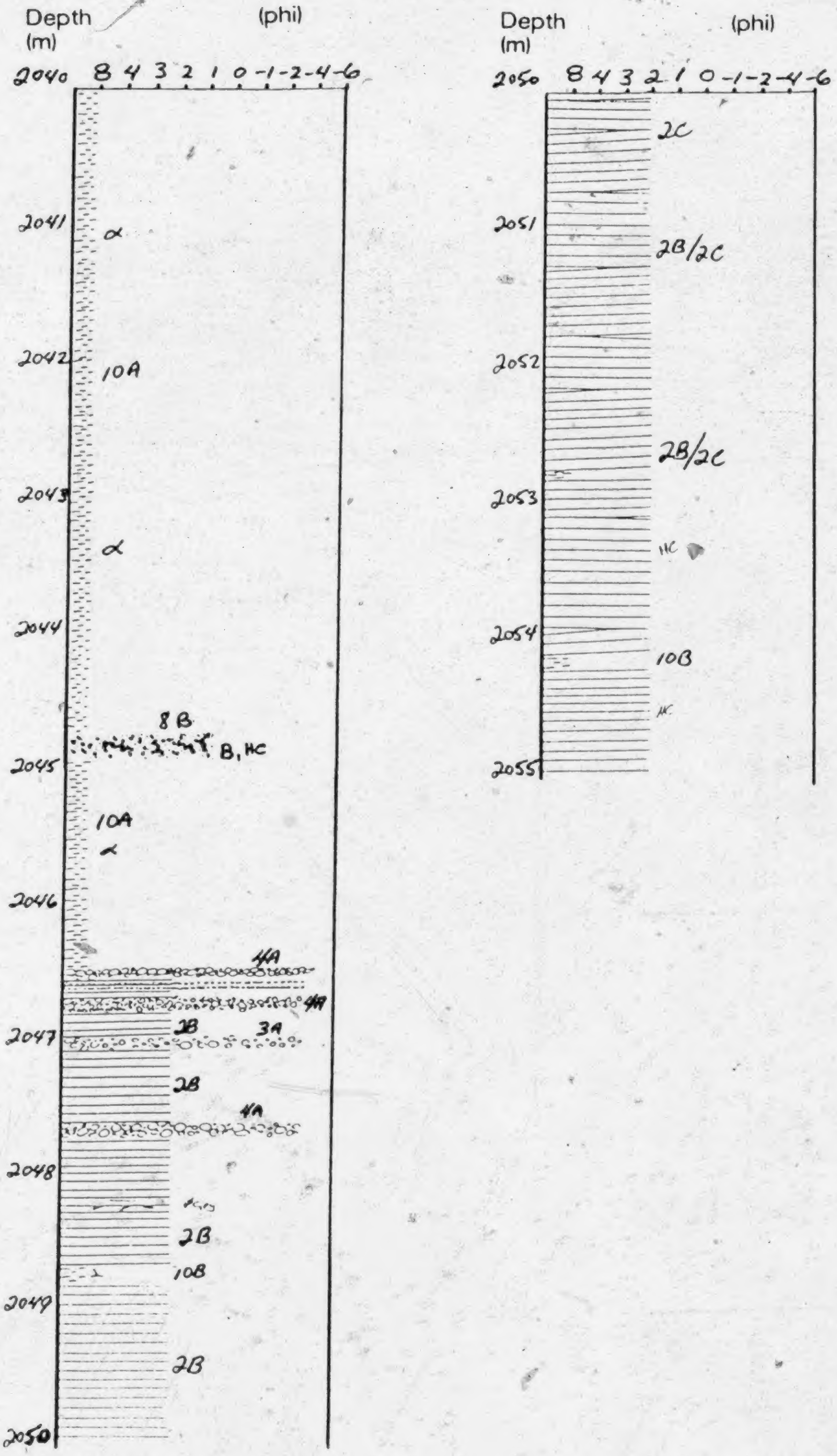
Depth (m)
(phi)
8 4 3 2 1 0 -1 -2 -4 -6
2040
2041
2042
2043
2044
2045
2046
2047
2048
2049
2050
α
10A
α
8B
B, HC
10A
α
4A
4A
2B
3A
2B
4A
2B
10B
2B
Depth (m)
(phi)
8 4 3 2 1 0 -1 -2 -4 -6
2050
2051
2052
2053
2054
2055
2C
2B/2C
2B/2C
HC
10B
HC

7-33-34-2W5

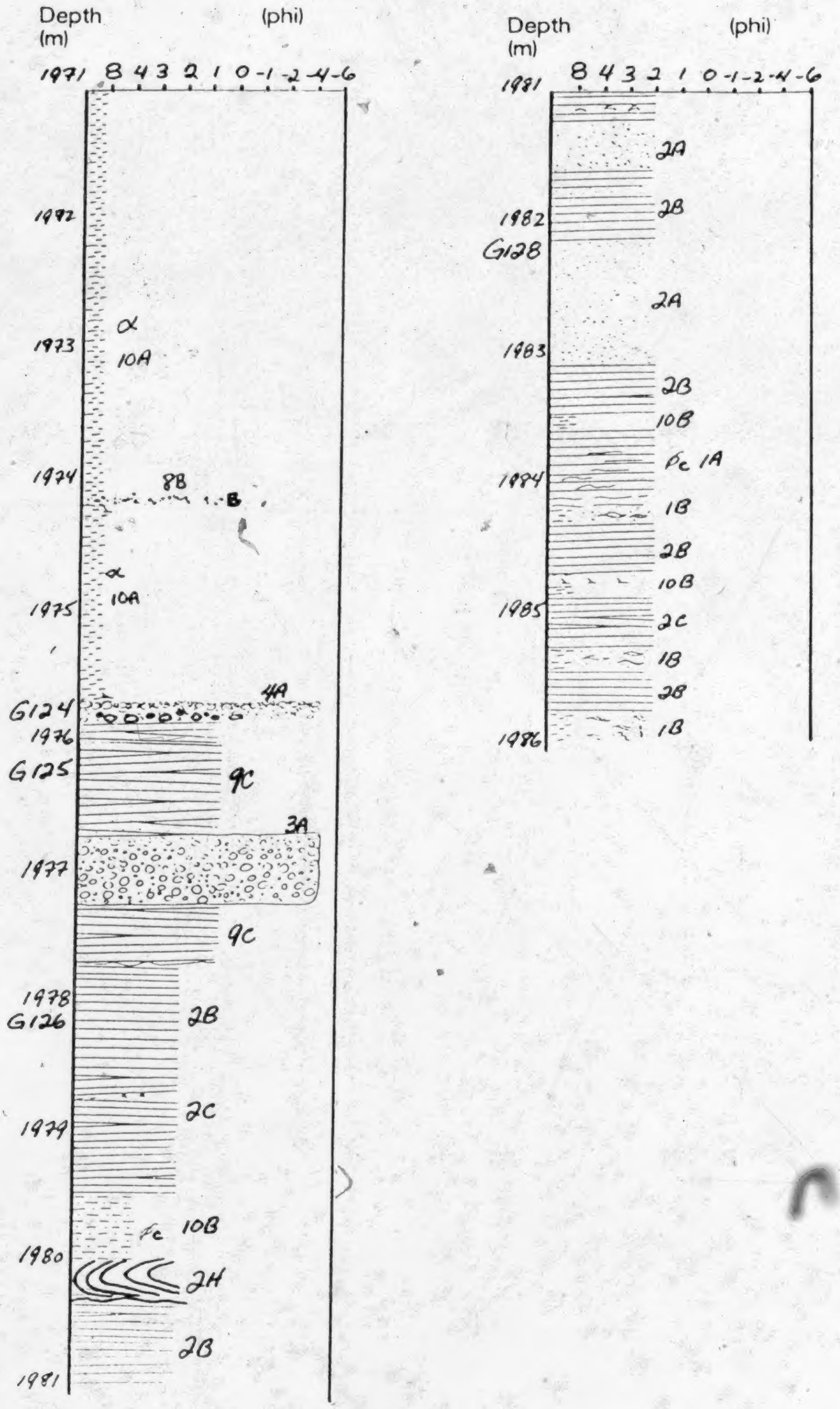
Depth (m)
(phi)
8 4 3 2 1 0 -1 -2 -4 -6
1971
1972
α
1973
10A
1974
8B
B
α
10A
1975
4A
G124
1976
G125
9C
3A
1977
9C
1978
G126
2B
2C
1979
Pc
10B
1980
2H
2B
1981
Depth (m)
(phi)
8 4 3 2 1 0 -1 -2 -4 -6
1981
2A
2B
1982
G128
2A
1983
2B
10B
Pc 1A
1984
1B
2B
10B
1985
2C
1B
2B
1B
1986

16-11-34-3W5

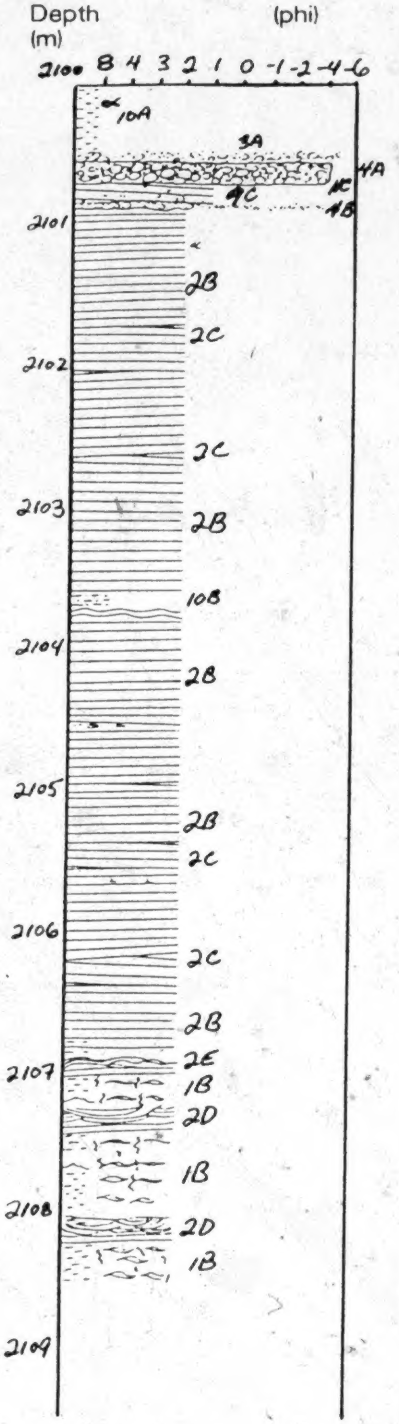
Depth
(m)
(phi)
2100
8 4 3 2 1 0 -1 -2 -4 -6
10A
3A
4A
4C
4C
4B
2101
2B
2C
2102
2C
2103
2B
10B
2104
2B
2105
2B
2C
2106
2C
2B
2E
2107
1B
2D
1B
2108
2D
1B
2109

6-13-34-3W5

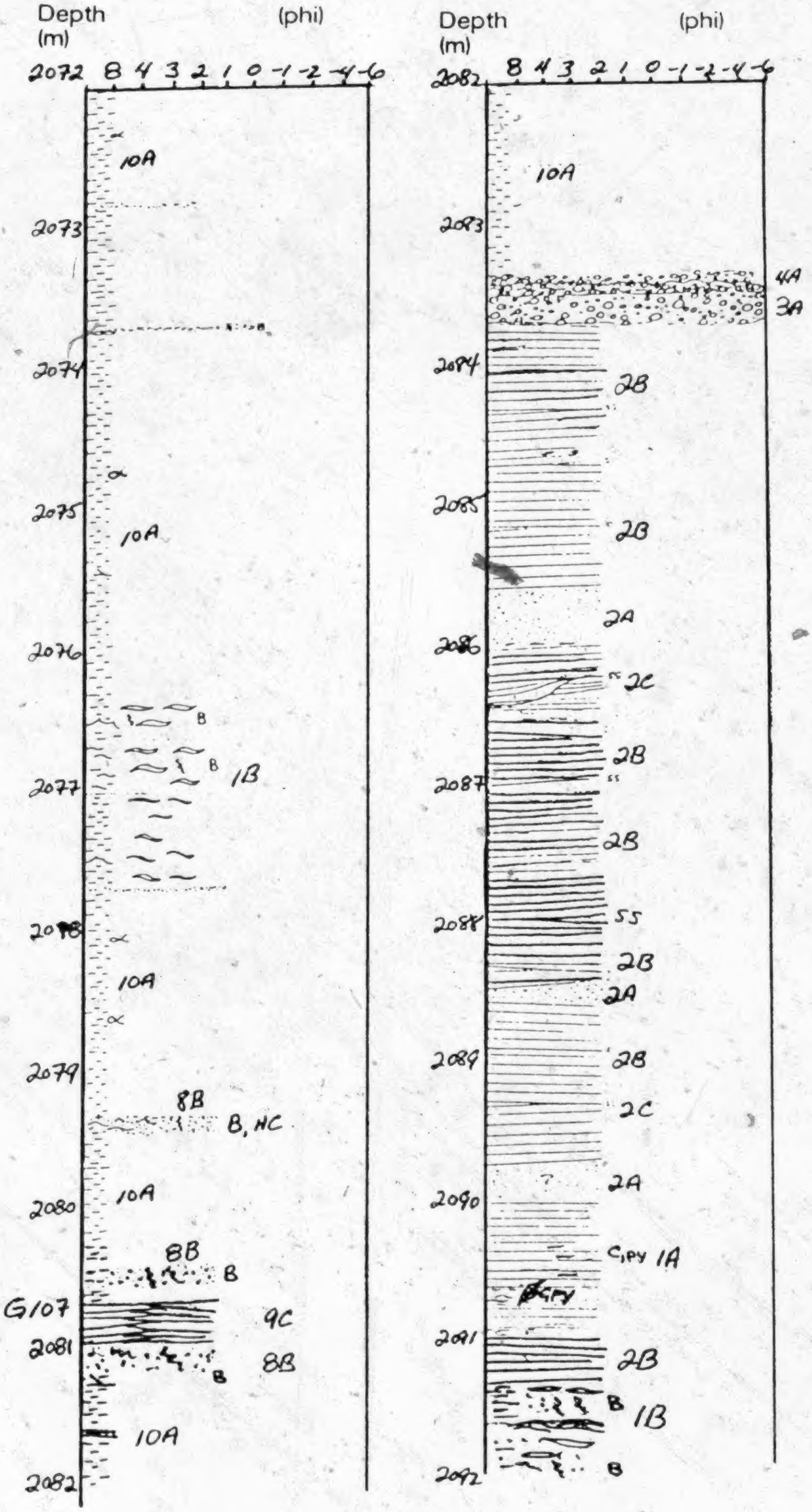
Depth (m)
(phi)
2072
8 4 3 2 1 0 -1 -2 -4 -6
10A
2073
2074
2075
10A
2076
B
B
1B
2077
2078
10A
2079
8B
B, HC
10A
2080
8B
B
G107
9C
2081
8B
B
10A
2082
Depth (m)
(phi)
2082
8 4 3 2 1 0 -1 -2 -4 -6
10A
2083
4A
3A
2084
2B
2085
2B
2A
2086
2C
2B
2087
2B
2088
SS
2B
2A
2089
2B
2C
2A
2090
C,PY 1A
C,PY
2091
2B
B
1B
2092
B

16-13-34-3W5

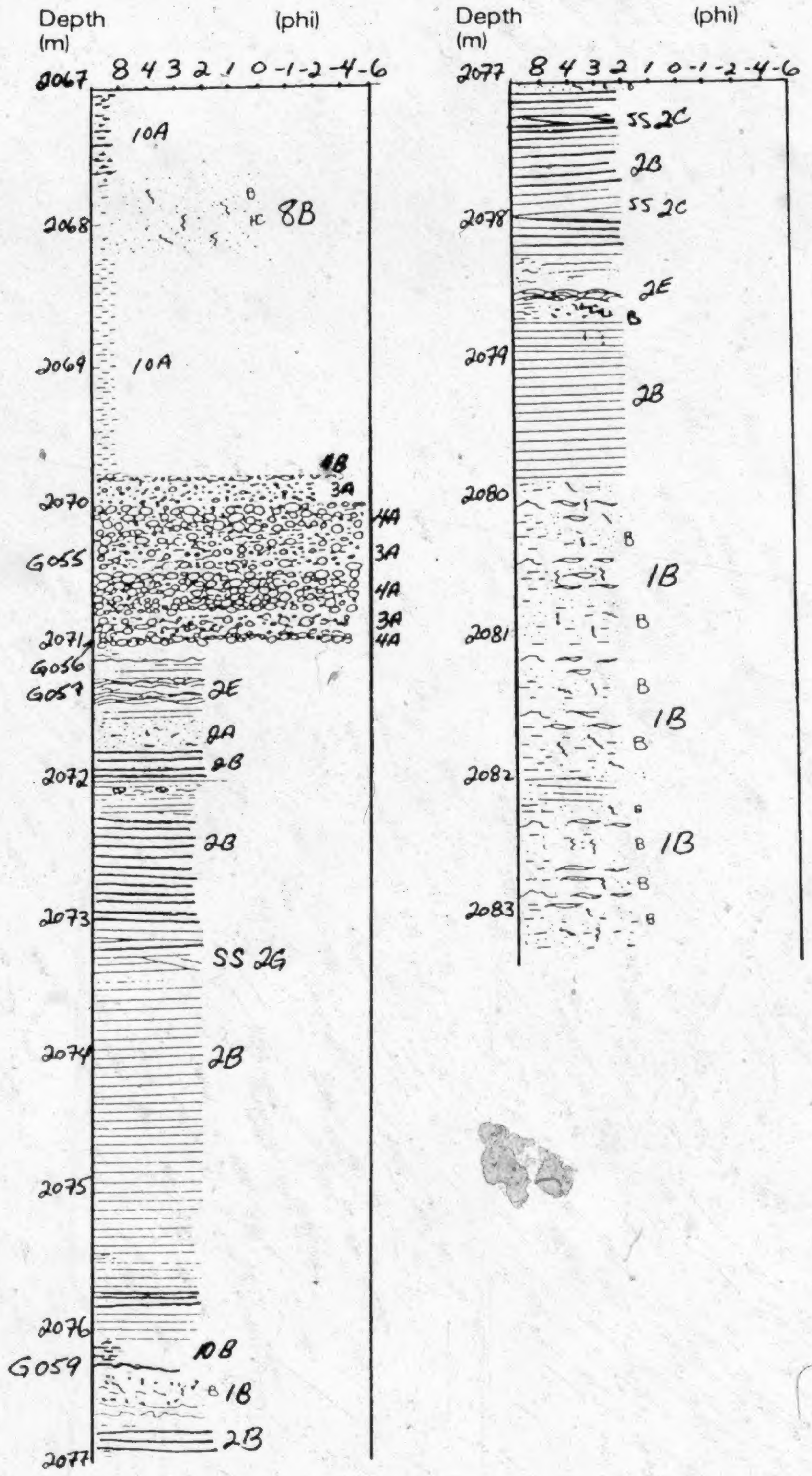
Depth (m)
(phi)
8 4 3 2 1 0 -1 -2 -4 -6
2067
10A
B
8B
2068
2069
10A
1B
3A
2070
4A
G055
3A
4A
3A
2071
4A
G056
G057
2E
2A
2B
2072
2B
2073
SS 2G
2074
2B
2075
2076
10B
G059
B
1B
2B
2077
Depth (m)
(phi)
8 4 3 2 1 0 -1 -2 -4 -6
2077
SS 2C
2B
SS 2C
2078
2E
B
2079
2B
2080
B
1B
2081
B
B
1B
B
2082
B
B
1B
B
2083
B

16-14-34-3W5

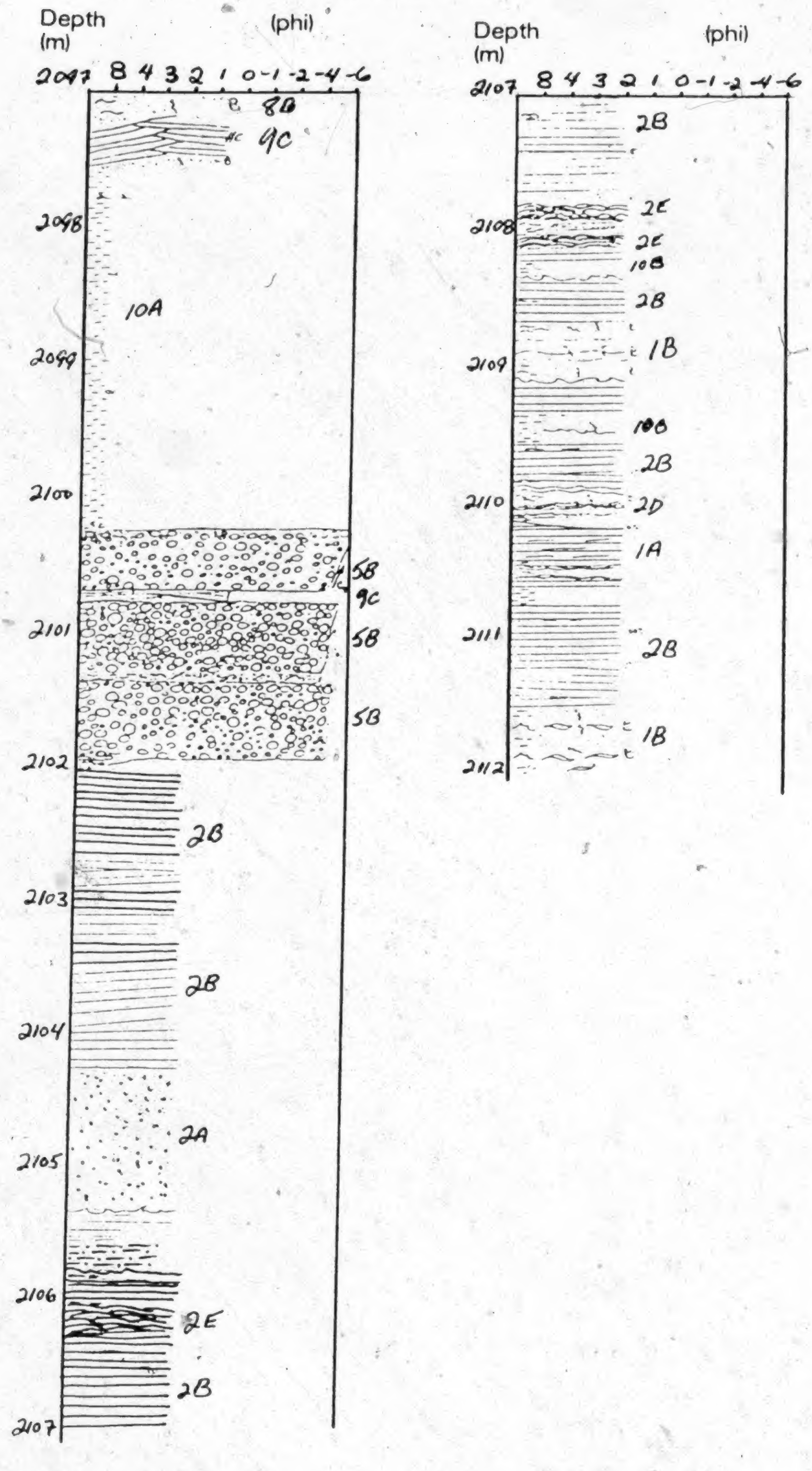
Depth (m)
(phi)
8 4 3 2 1 0 -1 -2 -4 -6
2097
2098
2099
2100
2101
2102
2103
2104
2105
2106
2107
8B
9C
10A
5B
9C
5B
5B
2B
2B
2A
2E
2B
Depth (m)
(phi)
8 4 3 2 1 0 -1 -2 -4 -6
2107
2108
2109
2110
2111
2112
2B
2E
2E
10B
2B
1B
10B
2B
2D
1A
2B
1B

16-15-34-3W5

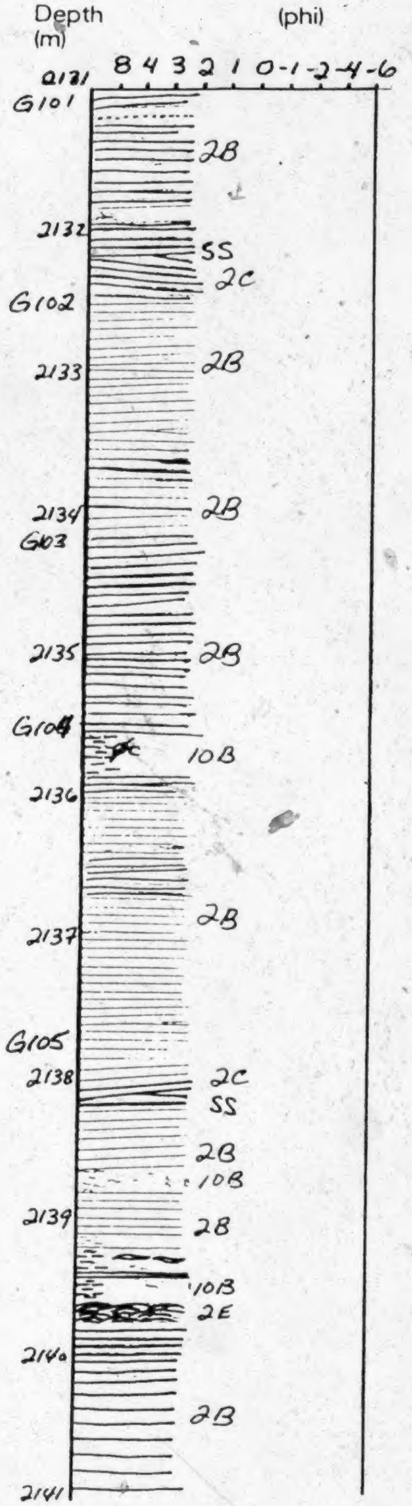
Depth (m)
(phi)
8 4 3 2 1 0 -1 -2 -4 -6
2131
G101
2B
2132
SS
2C
G102
2B
2133
2B
2134
G103
2135
2B
G104
10B
2136
2B
2137
G105
2C
2138
SS
2B
10B
2139
2B
10B
2E
2140
2B
2141

6-23-34-3W5

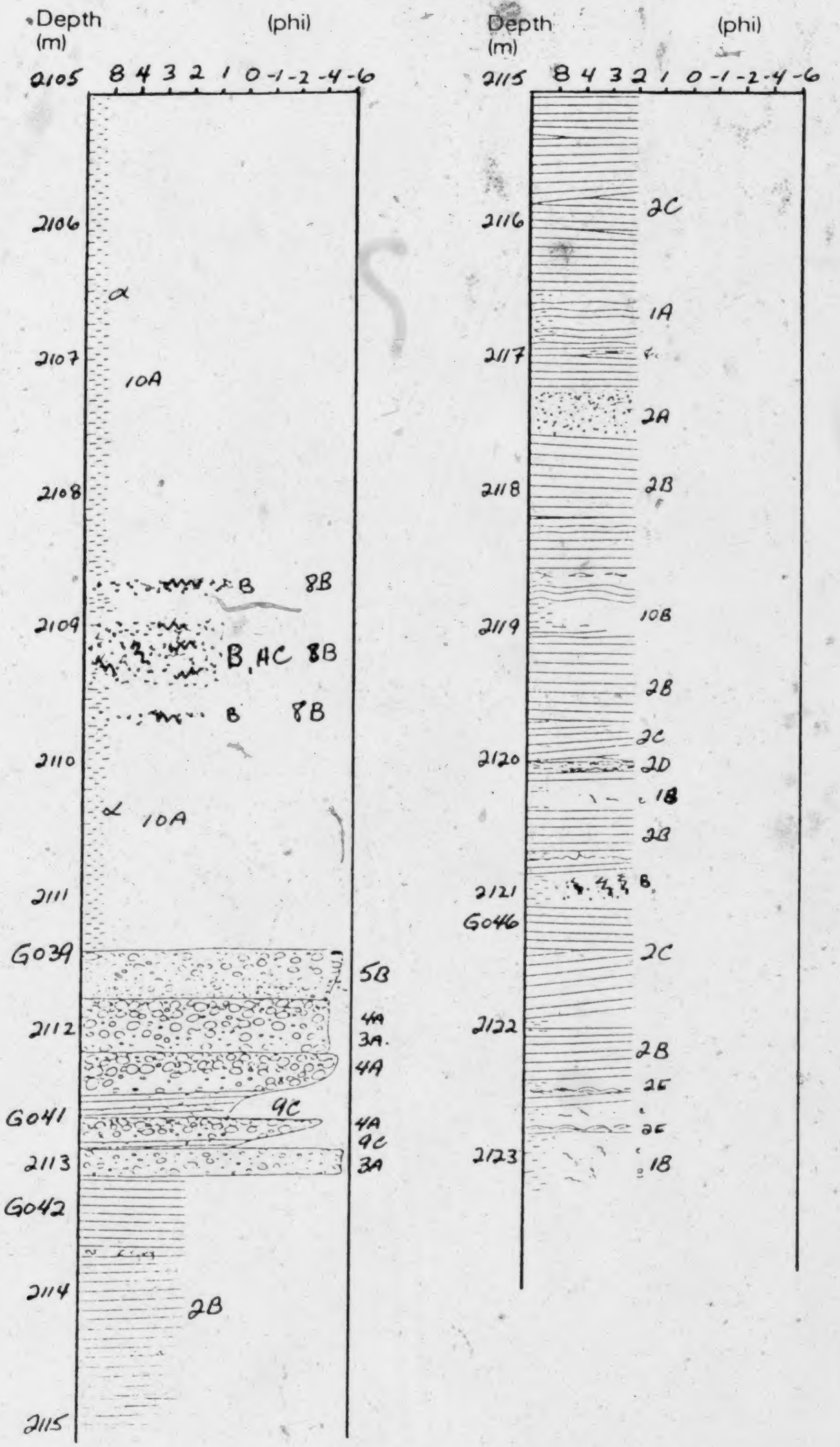
Depth (m)
(phi)
8 4 3 2 1 0 -1 -2 -4 -6
2105
2106
α
2107
10A
2108
B 8B
2109
B, AC 8B
B 8B
2110
α 10A
2111
G039
5B
2112
4A
3A.
4A
9C
G041
4A
9C
2113
3A
G042
2114
2B
2115
Depth (m)
(phi)
8 4 3 2 1 0 -1 -2 -4 -6
2115
2116
2C
1A
2117
2A
2118
2B
10B
2119
2B
2C
2120
2D
1B
2B
2121
B
G046
2C
2122
2B
2E
2E
2123
1B

16-23-34-3W5

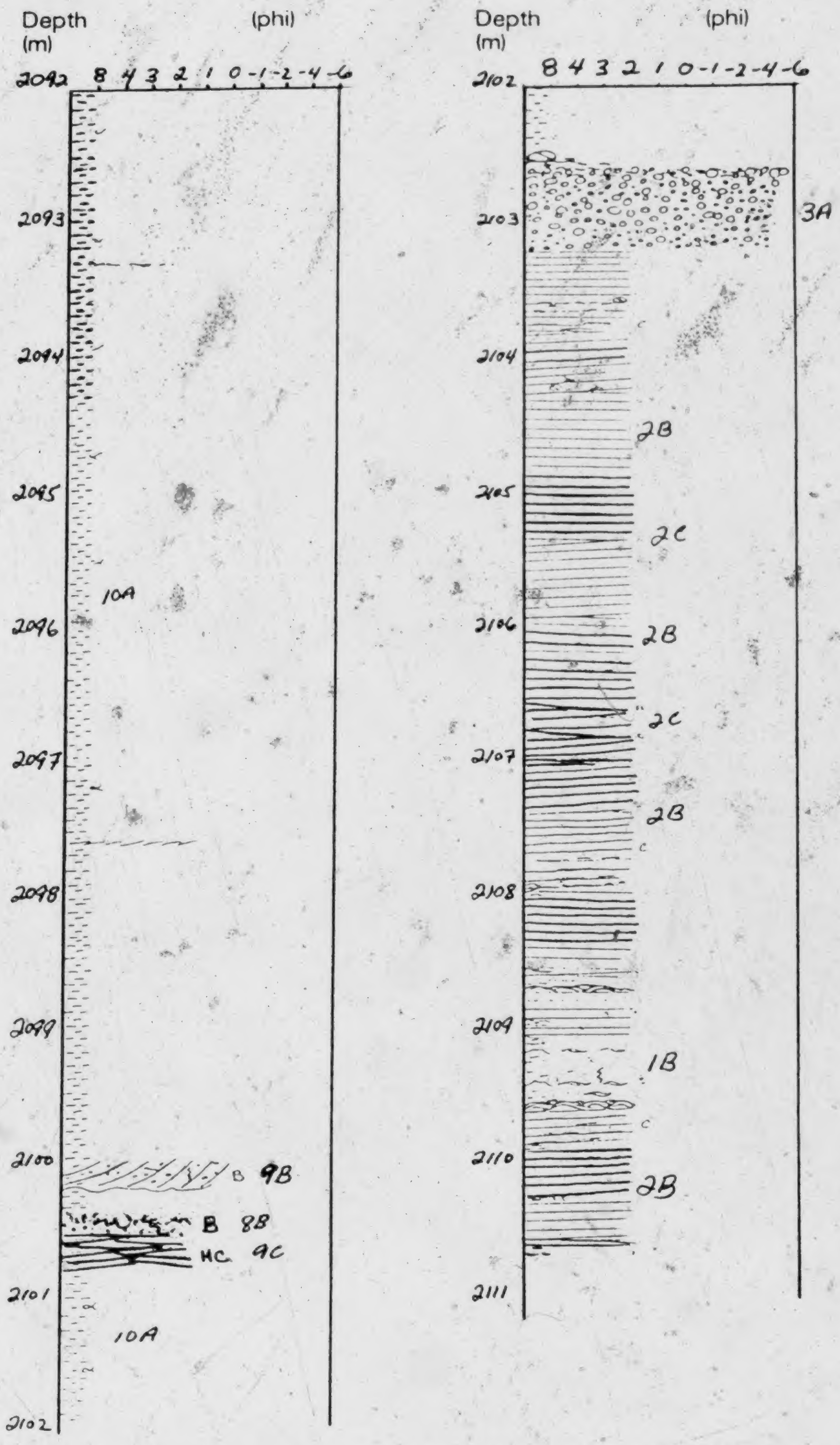
Depth (m)
(phi)
8 4 3 2 1 0 -1 -2 -4 -6
2092
2093
2094
2095
2096
2097
2098
2099
2100
2101
2102
10A
B 9B
B 8B
HC 9C
10A
Depth (m)
(phi)
8 4 3 2 1 0 -1 -2 -4 -6
2102
2103
2104
2105
2106
2107
2108
2109
2110
2111
3A
2B
2C
2B
2C
2B
1B
2B

3-24-34-3W5

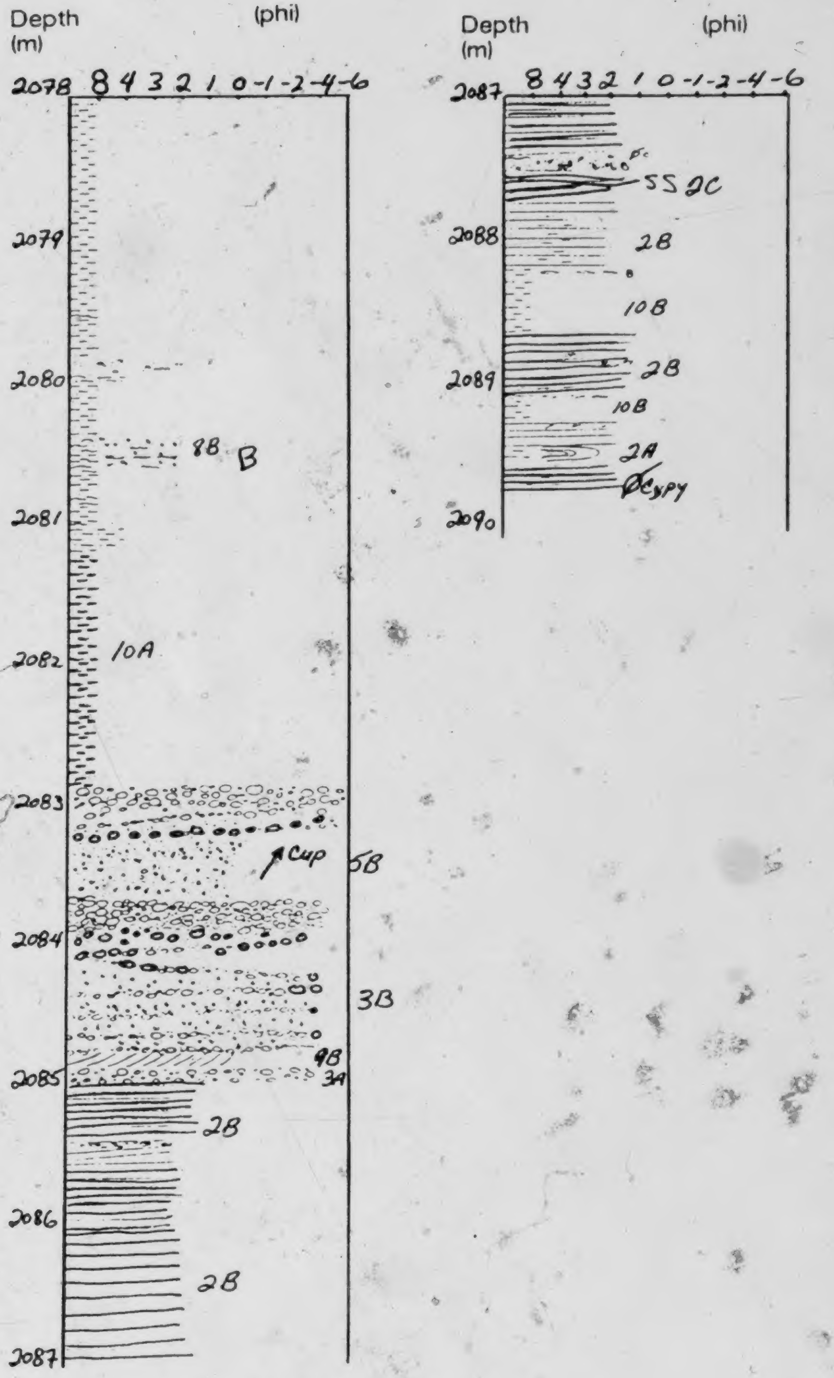
Depth (m)
(phi)
8 4 3 2 1 0 -1 -2 -4 -6
2078
2079
2080
2081
2082
2083
2084
2085
2086
2087
8B
B
10A
Cup
5B
3B
9B
3A
2B
2B
Depth (m)
(phi)
8 4 3 2 1 0 -1 -2 -4 -6
2087
2088
2089
2090
Øc
SS 2C
2B
10B
2B
10B
2A
Øcxpy

14-24-34-3W5

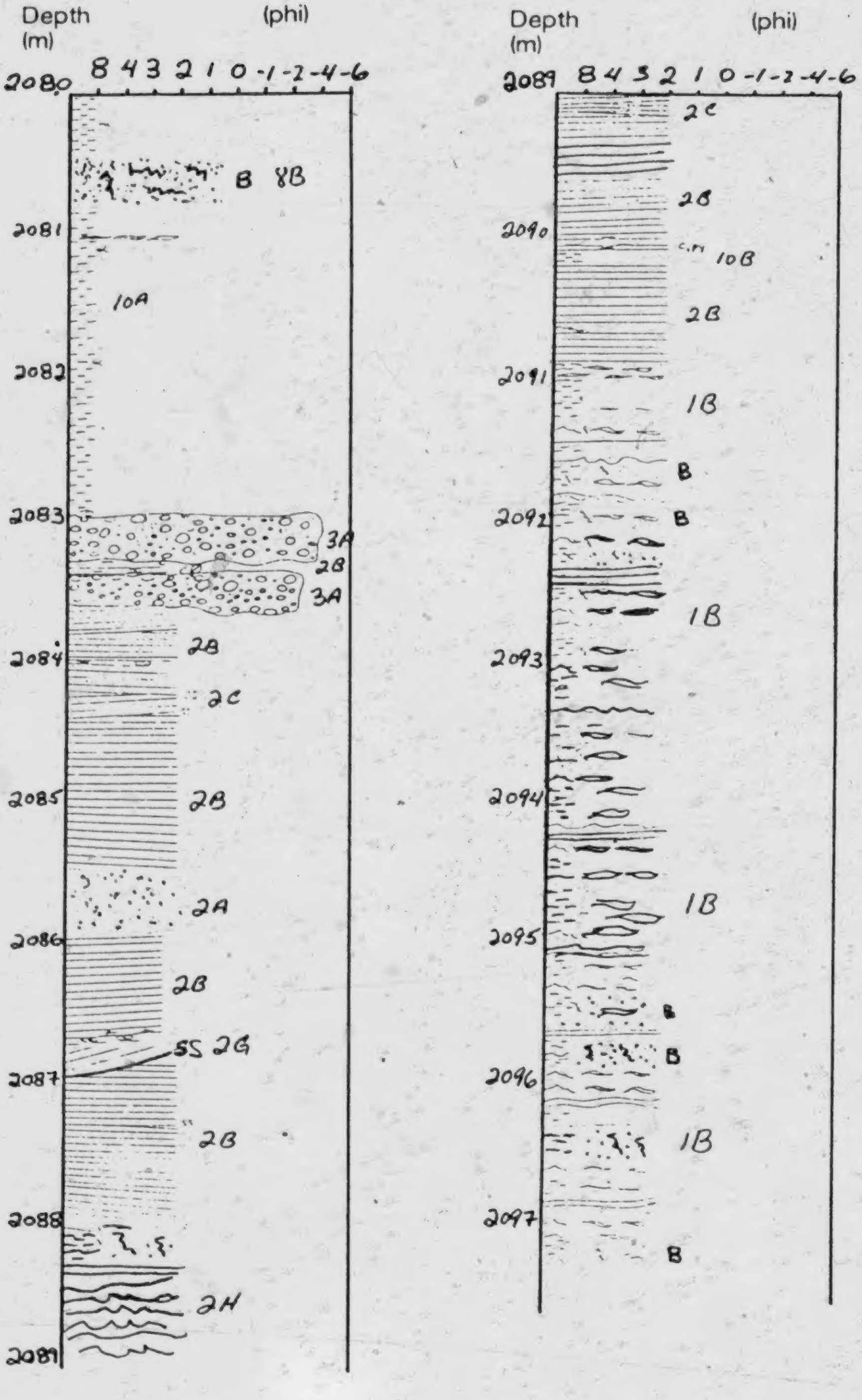
Depth (m)
(phi)
8 4 3 2 1 0 -1 -2 -4 -6
2080
B 8B
2081
10A
2082
2083
3A
2B
3A
2084
2B
2C
2085
2B
2A
2086
2B
SS 2G
2087
2B
2088
2H
2089
Depth (m)
(phi)
8 4 3 2 1 0 -1 -2 -4 -6
2089
2C
2B
2090
c.m 10B
2B
2091
1B
B
2092
B
1B
2093
2094
1B
2095
B
B
2096
1B
2097
B

16-24-34-3W5

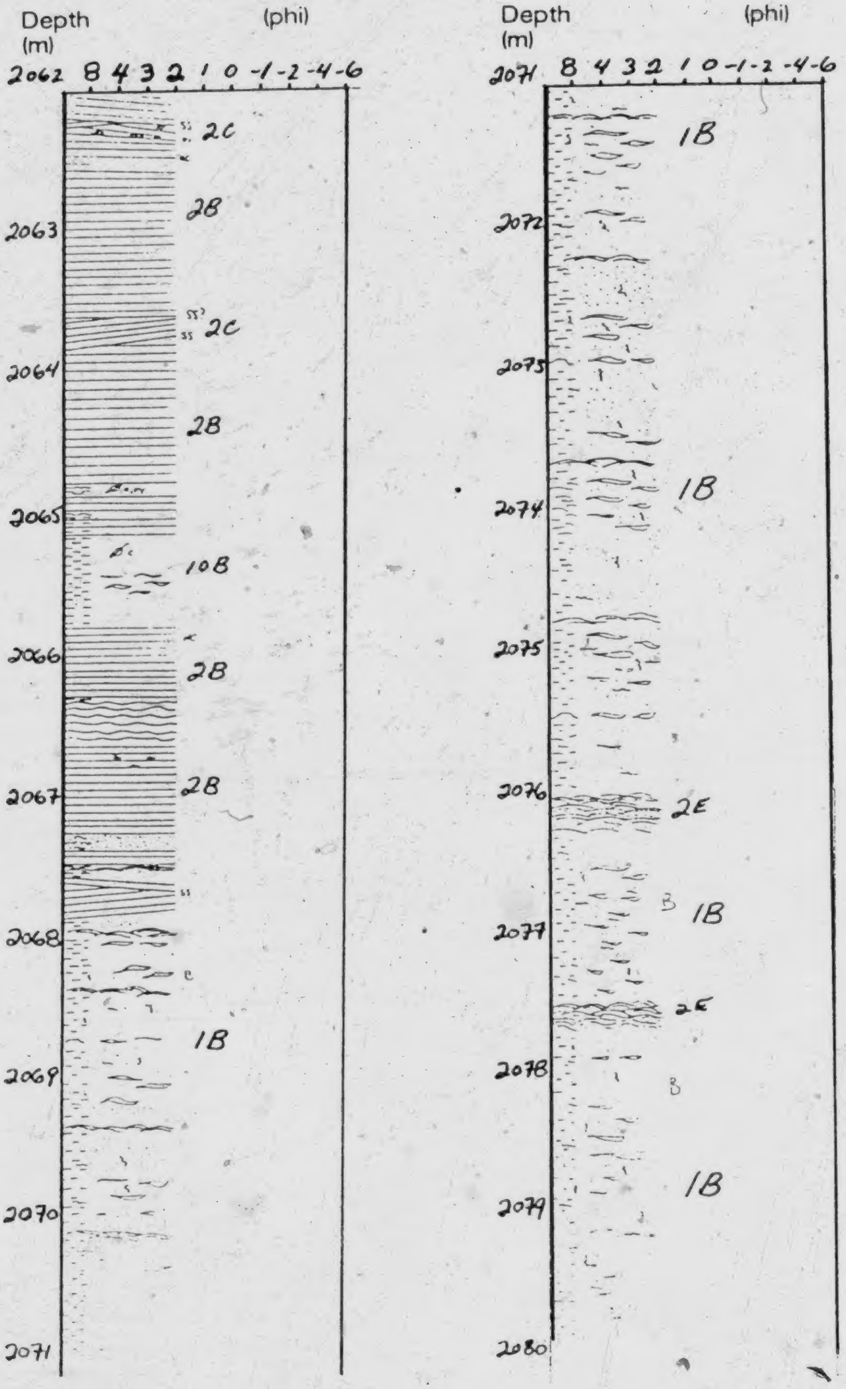
Depth (m)
(phi)
2062
8 4 3 2 1 0 -1 -2 -4 -6
2C
2B
2063
2C
2064
2B
2065
10B
2066
2B
2B
2067
2068
1B
2069
2070
2071
Depth (m)
(phi)
2071
8 4 3 2 1 0 -1 -2 -4 -6
1B
2072
2073
1B
2074
2075
2076
2E
1B
2077
2E
2078
1B
2079
2080

6-25-34-3W5

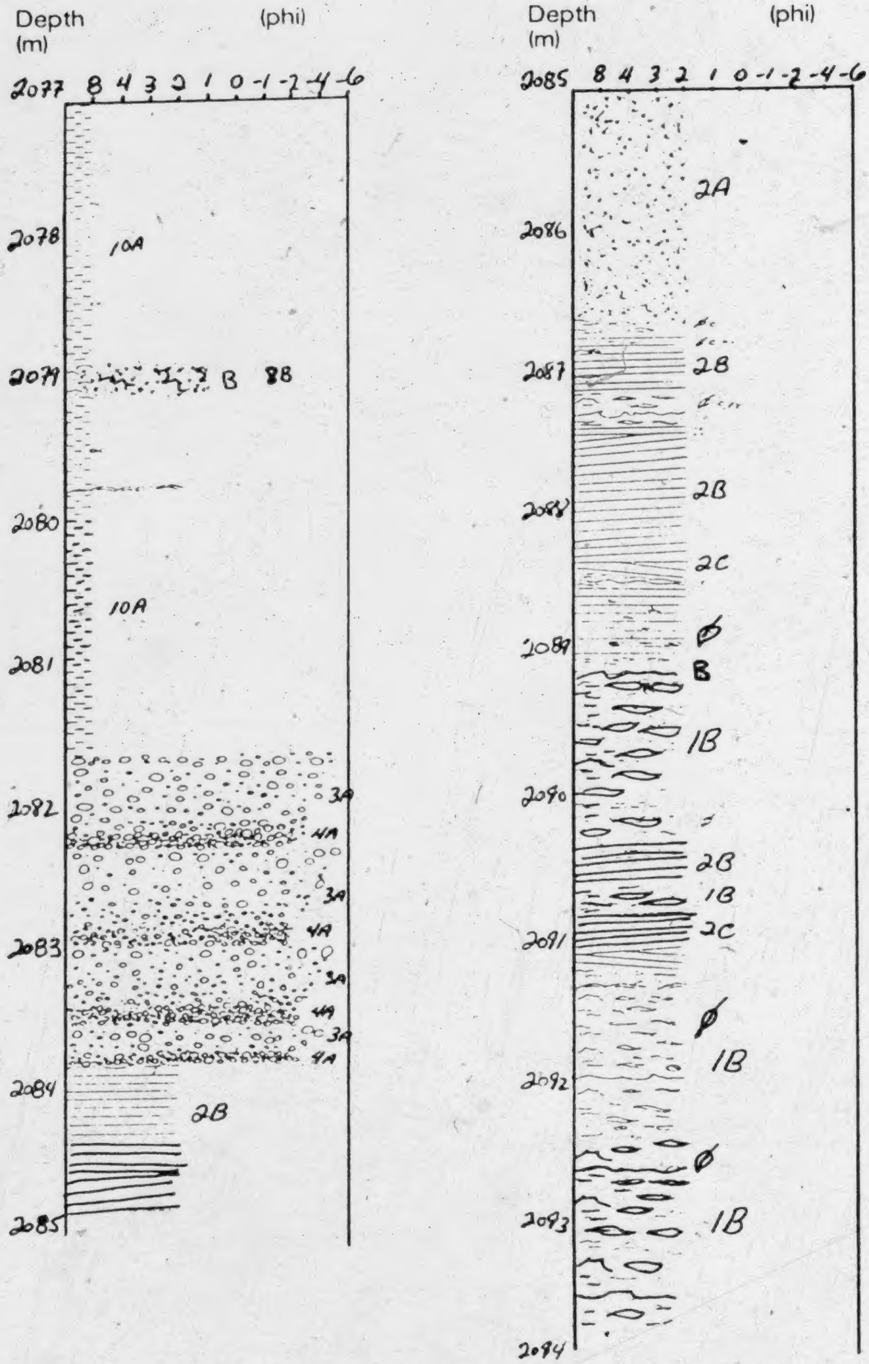
Depth (m)
(phi)
2077 8 4 3 2 1 0 -1 -2 -4 -6
2078
10A
2079
B
8B
2080
10A
2081
2082
3A
4A
3A
2083
4A
3A
4A
3A
4A
2084
2B
2085
Depth (m)
(phi)
2085 8 4 3 2 1 0 -1 -2 -4 -6
2A
2086
2B
2087
2B
2088
2C
Ø
2089
B
1B
2090
2B
1B
2C
2091
Ø
1B
2092
Ø
1B
2093
2094

8-25-34-3W5

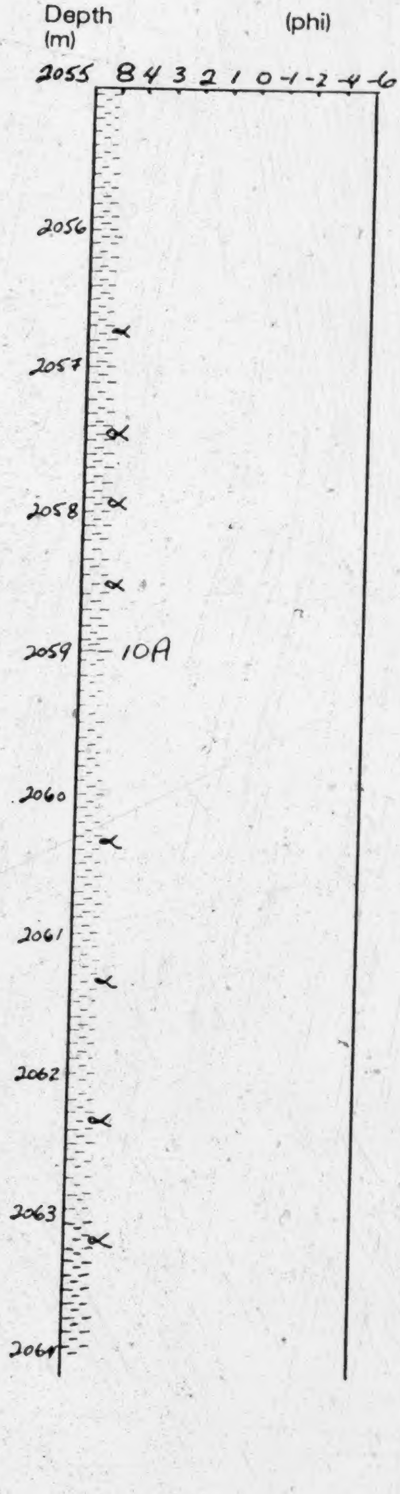
Depth (m)
(phi)
8 4 3 2 1 0 -1 -2 -4 -6
2055
2056
2057
2058
2059
10A
2060
2061
2062
2063
2064

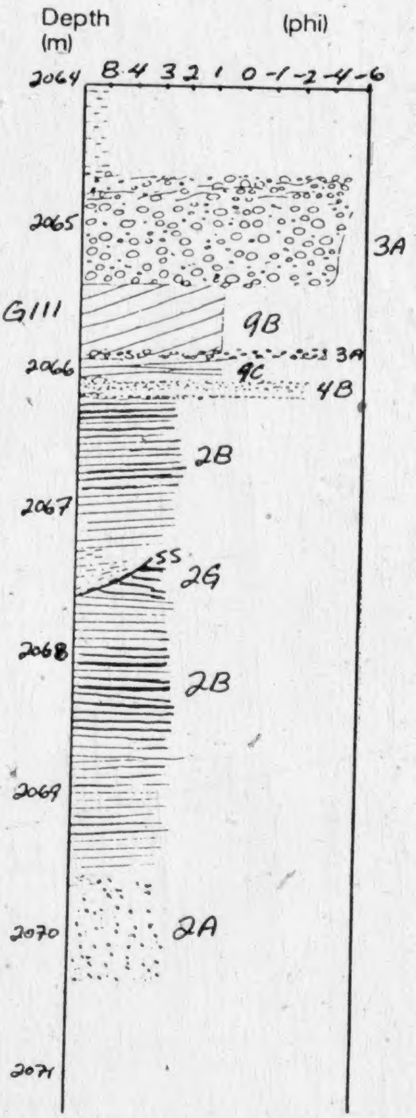
Depth (m)
(phi)
8 4 3 2 1 0 -1 -2 -4 -6
2064
2065
3A
G111
9B
3A
2066
9C
4B
2B
2067
SS
2G
2068
2B
2069
2070
2A
2071

14-25-34-3W5

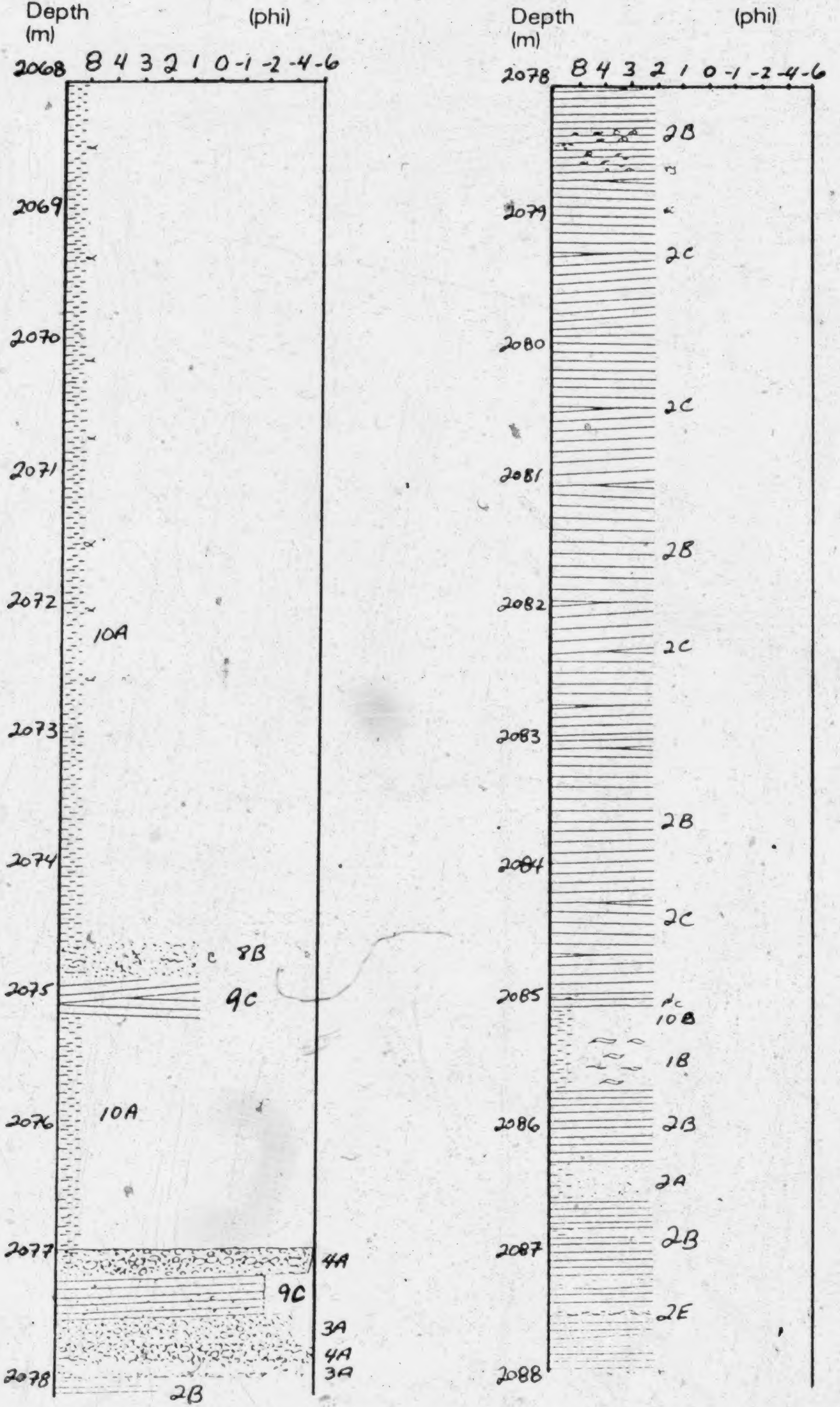
Depth (m)
(phi)
8 4 3 2 1 0 -1 -2 -4 -6
2068
2069
2070
2071
2072
10A
2073
2074
8B
2075
9C
10A
2076
2077
4A
9C
3A
4A
3A
2078
2B
Depth (m)
(phi)
8 4 3 2 1 0 -1 -2 -4 -6
2078
2B
2079
2C
2080
2C
2081
2B
2082
2C
2083
2B
2084
2C
2085
10B
1B
2086
2B
2A
2087
2B
2E
2088

16-25-34-3W5

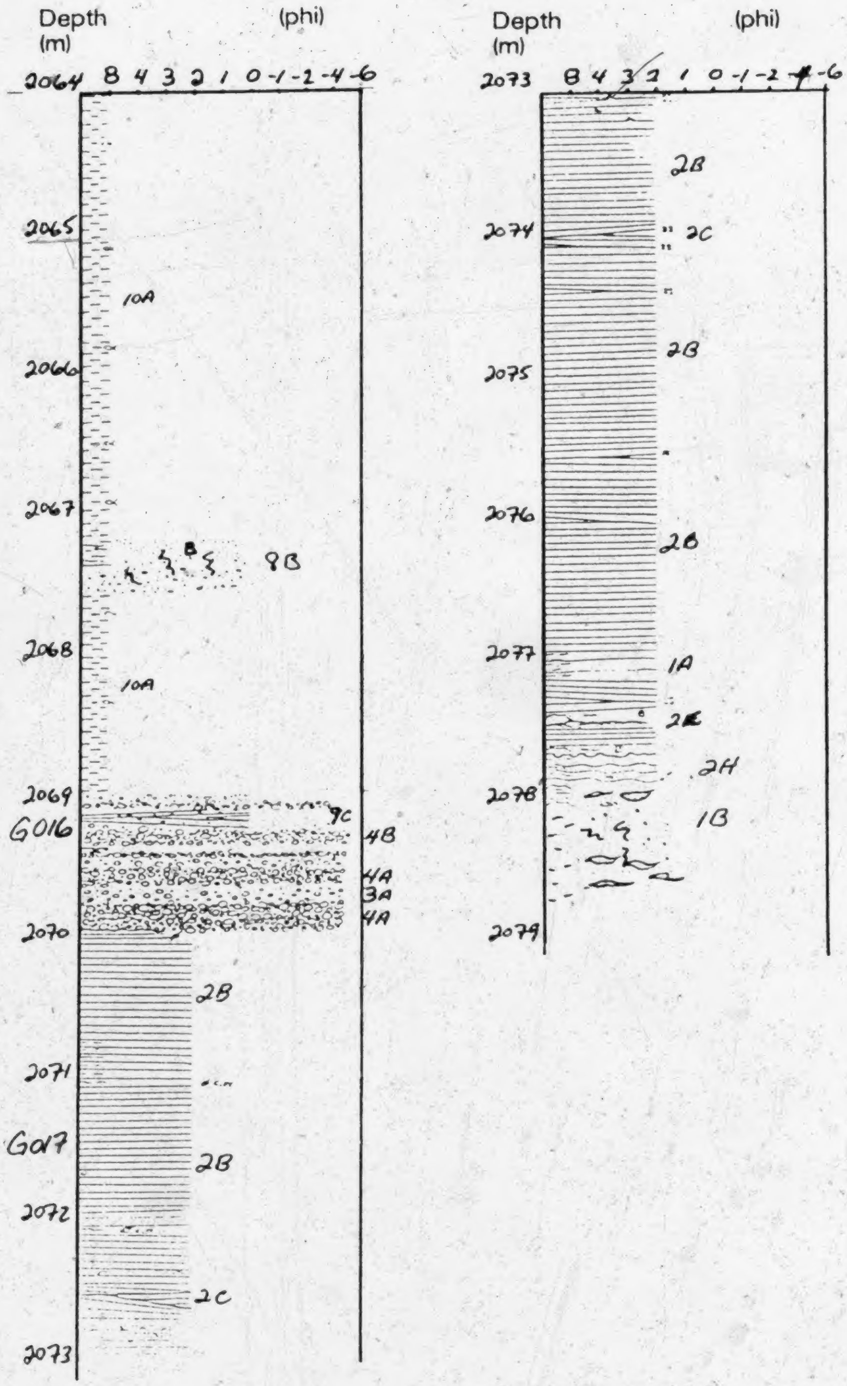
Depth (m)
(phi)
8 4 3 2 1 0 -1 -2 -4 -6
2064
2065
10A
2066
2067
8B
2068
10A
2069
G016
9C
4B
4A
3A
4A
2070
2B
2071
G017
2B
2072
2C
2073
Depth (m)
(phi)
8 4 3 2 1 0 -1 -2 -4 -6
2073
2B
2074
2C
2B
2075
2076
2B
2077
1A
2E
2H
2078
1B
2079

16-27-34-3W5

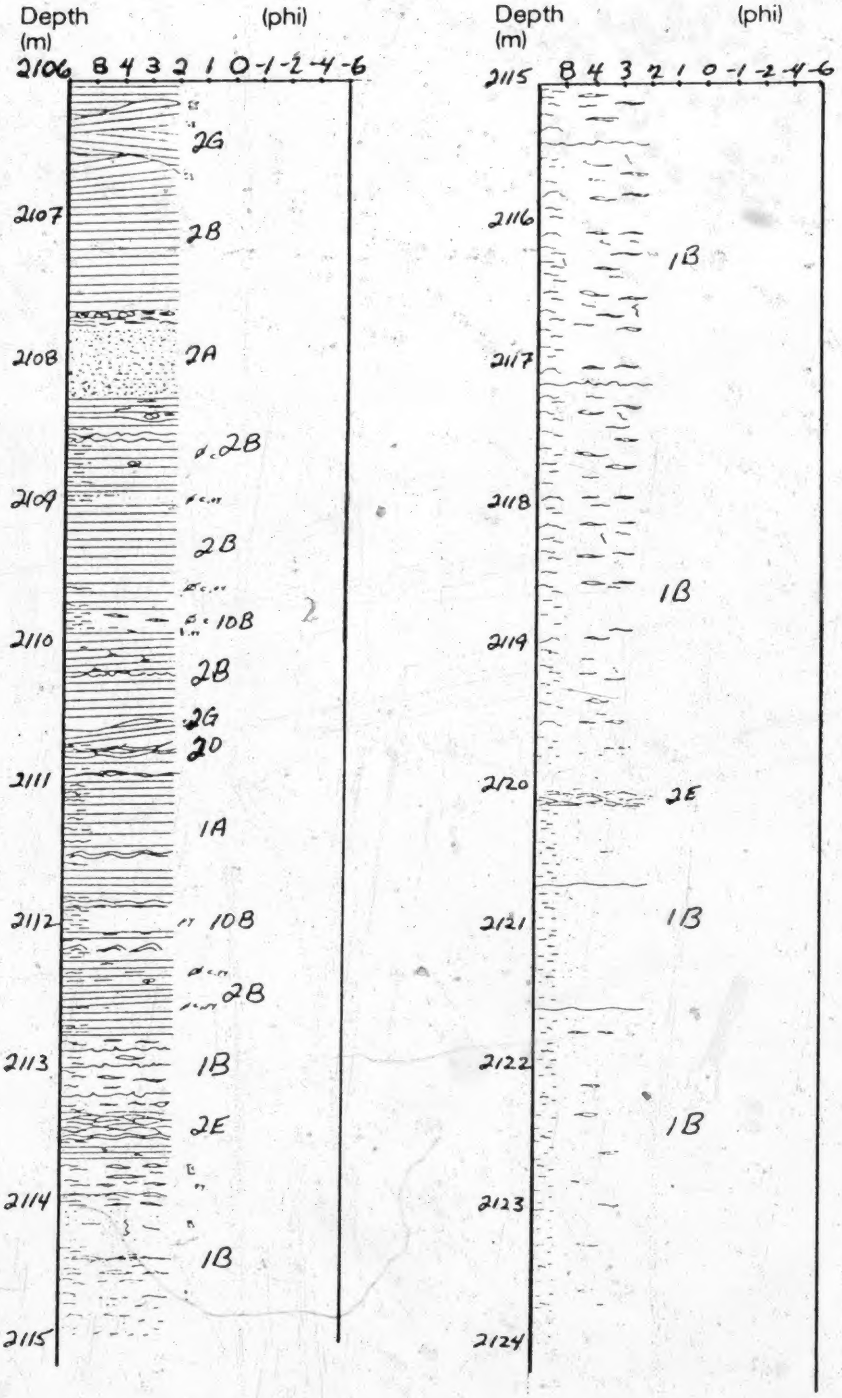
Depth
(m)
(phi)
2106
8 4 3 2 1 0 -1 -2 -4 -6
2G
2107
2B
2A
2108
2B
2109
2B
10B
2110
2B
2G
2D
2111
1A
2112
10B
2B
2113
1B
2E
2114
1B
2115
Depth
(m)
(phi)
2115
8 4 3 2 1 0 -1 -2 -4 -6
2116
1B
2117
2118
1B
2119
2120
2E
2121
1B
2122
1B
2123
2124

6-29-34-3W5

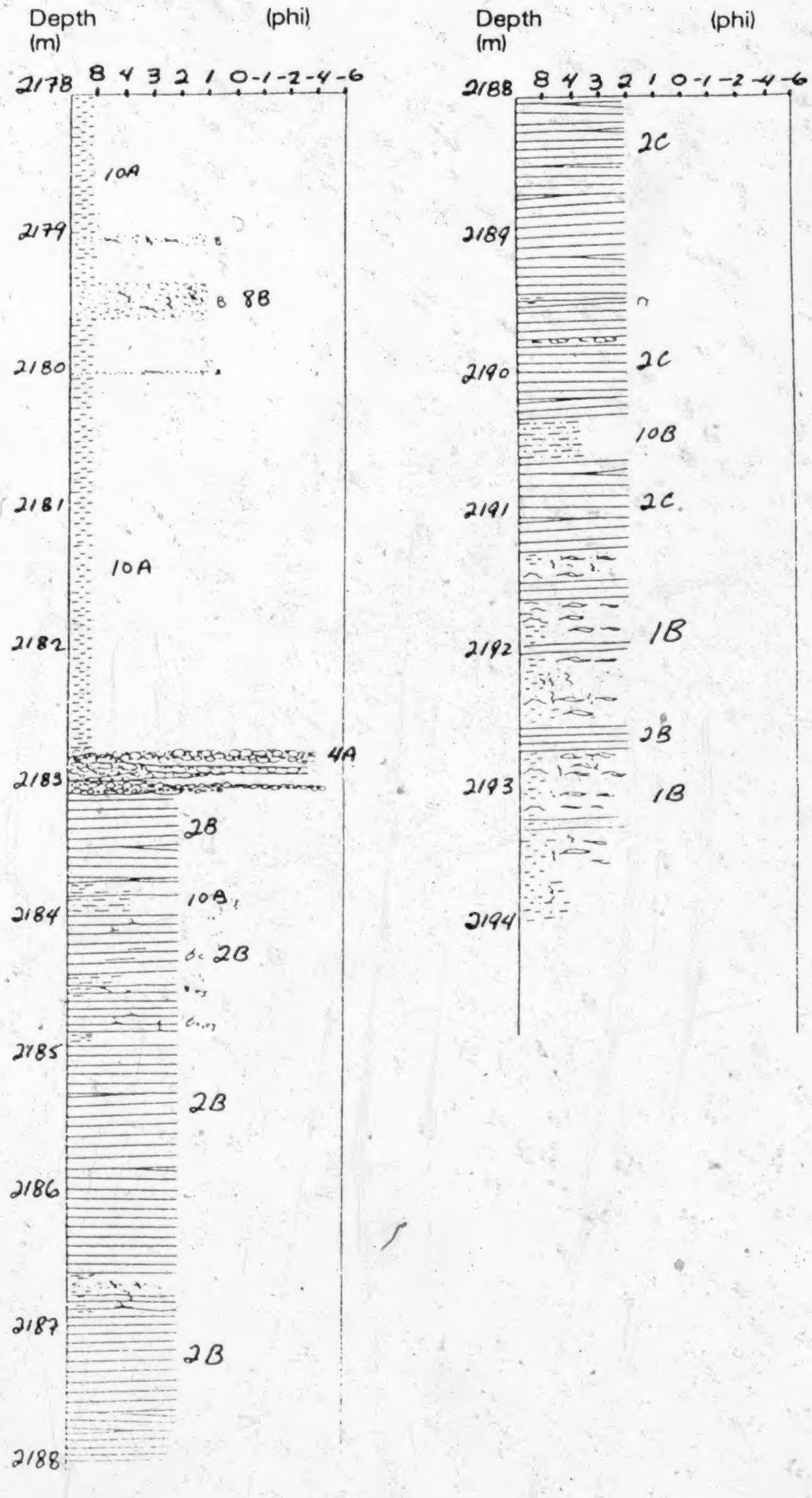
Depth (m)
(phi)
8 4 3 2 1 0 -1 -2 -4 -6
2178
2179
2180
2181
2182
2183
2184
2185
2186
2187
2188
10A
8B
10A
4A
2B
10B
2B
2B
2B
Depth (m)
(phi)
8 4 3 2 1 0 -1 -2 -4 -6
2188
2189
2190
2191
2192
2193
2194
2C
2C
10B
2C
1B
2B
1B

6-30-34-3W5

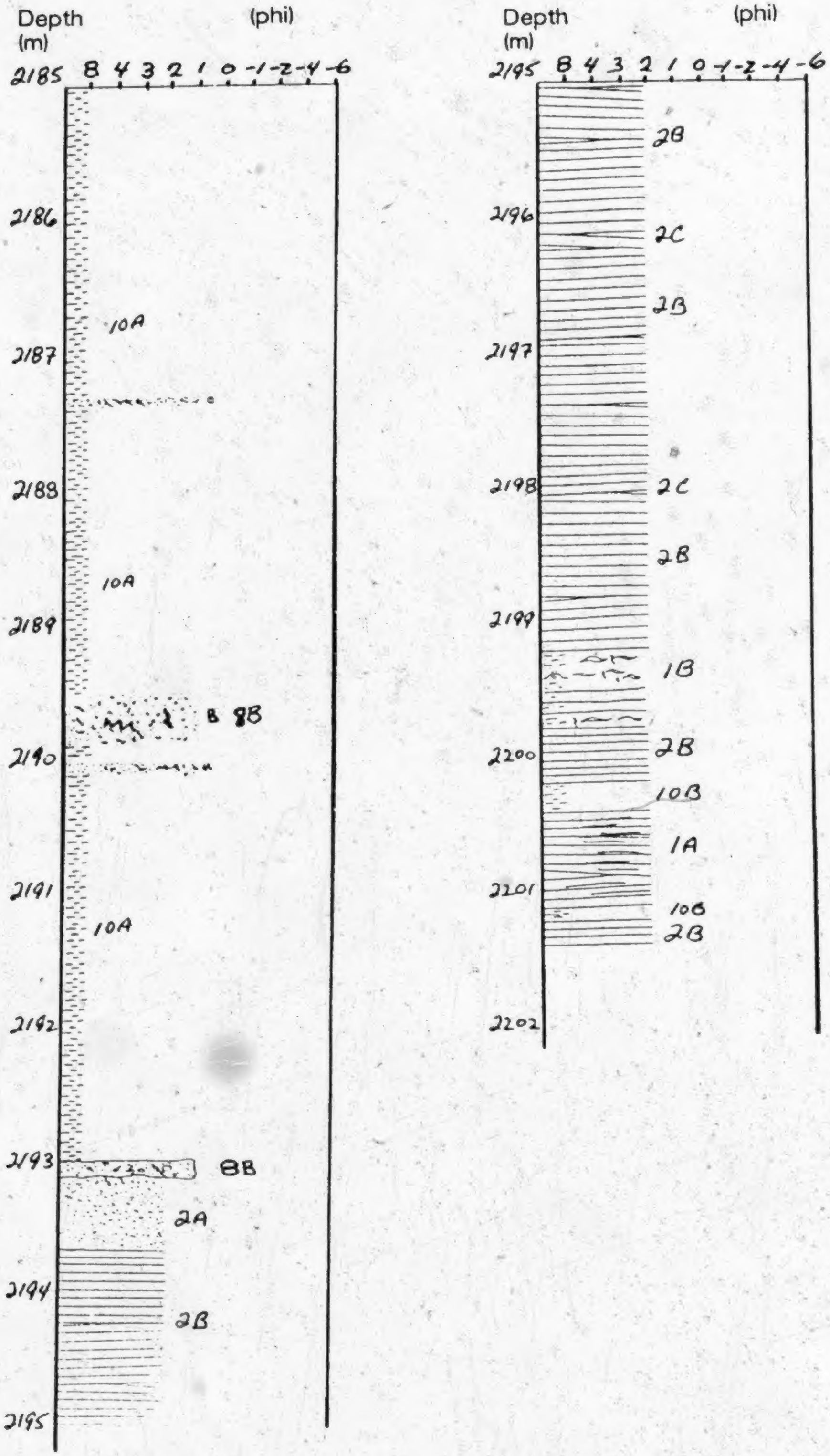
Depth (m)
(phi)
2185
8 4 3 2 1 0 -1 -2 -4 -6
2186
10A
2187
2188
10A
2189
B 8B
2190
2191
10A
2192
2193
8B
2A
2194
2B
2195
Depth (m)
(phi)
2195
8 4 3 2 1 0 -1 -2 -4 -6
2B
2196
2C
2B
2197
2198
2C
2B
2199
1B
2B
2200
10B
1A
2201
10B
2B
2202

14-32-34-3W5

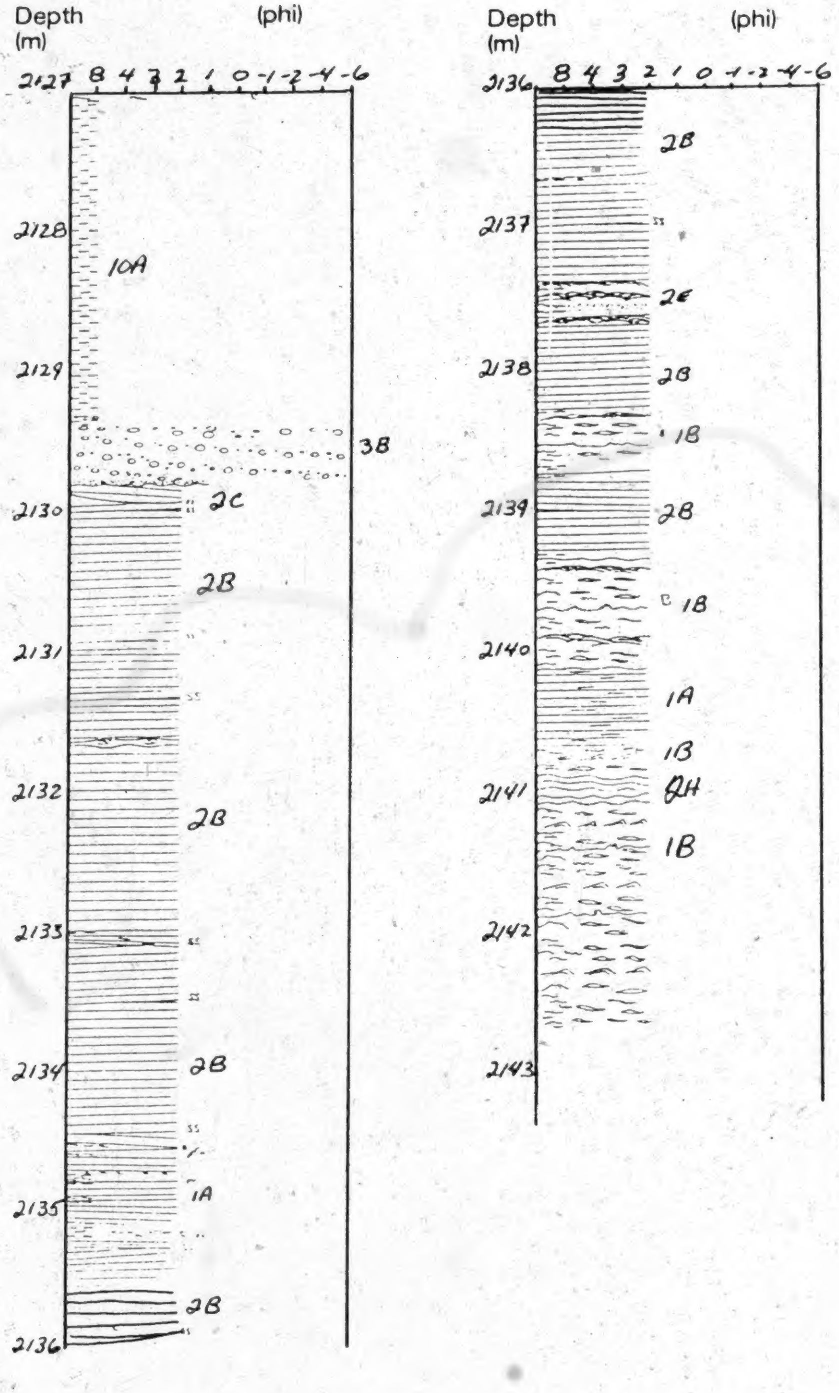
Depth (m)
(phi)
8 4 3 2 1 0 -1 -2 -4 -6
2127
2128
2129
2130
2131
2132
2133
2134
2135
2136
10A
3B
2C
2B
2B
2B
1A
2B
Depth (m)
(phi)
8 4 3 2 1 0 -1 -2 -4 -6
2136
2137
2138
2139
2140
2141
2142
2143
2B
2E
2B
1B
2B
1B
1A
1B
2H
1B

6-34-34-3W5

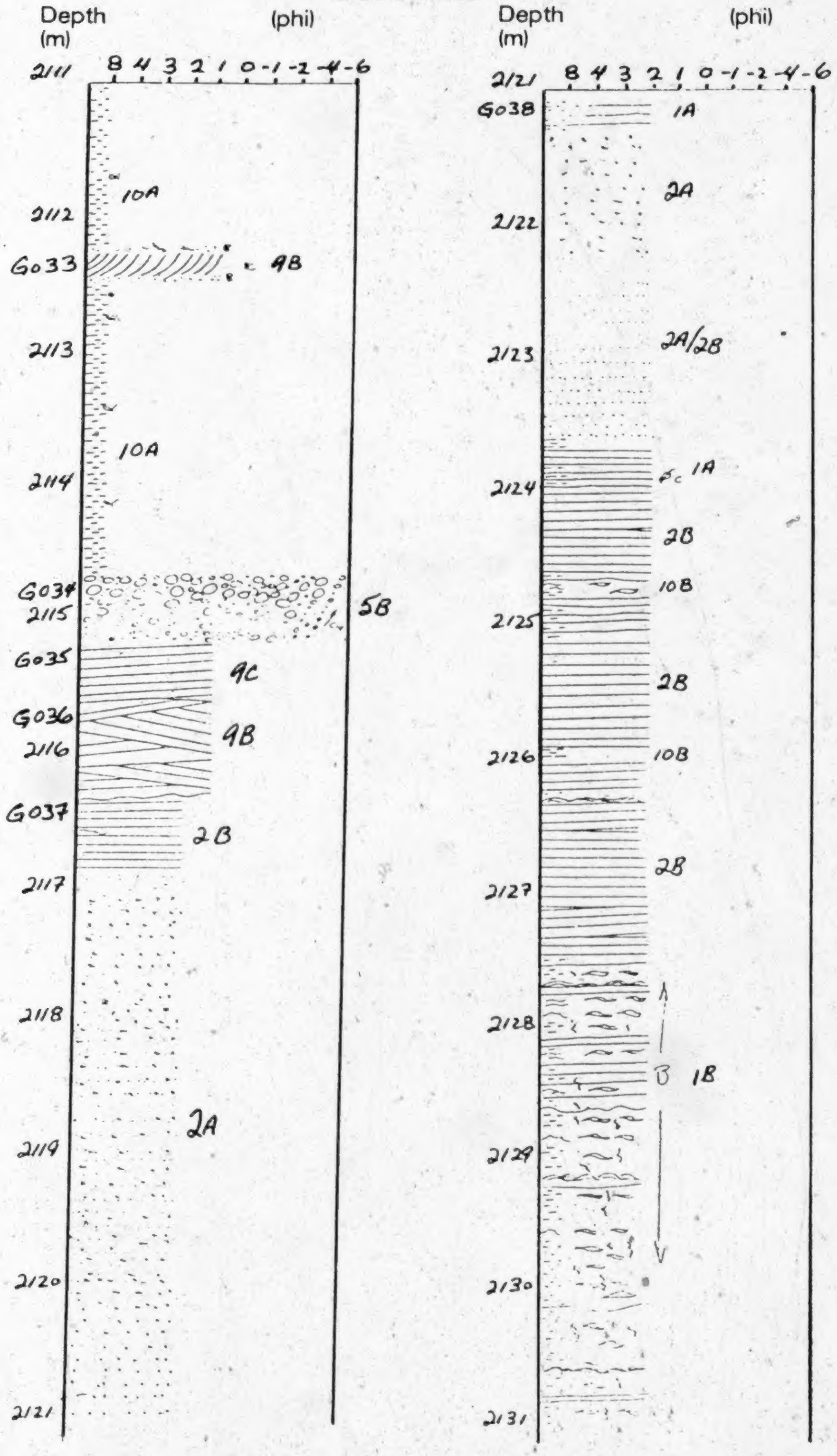
Depth
(m)
(phi)
8 4 3 2 1 0 -1 -2 -4 -6
2111
2112
2113
2114
2115
2116
2117
2118
2119
2120
2121
G033
G034
G035
G036
G037
10A
9B
10A
5B
9C
9B
2B
2A
Depth
(m)
(phi)
8 4 3 2 1 0 -1 -2 -4 -6
2121
2122
2123
2124
2125
2126
2127
2128
2129
2130
2131
G038
1A
2A
2A/2B
Fc 1A
2B
10B
2B
10B
2B
B
1B

6-35-34-3W5

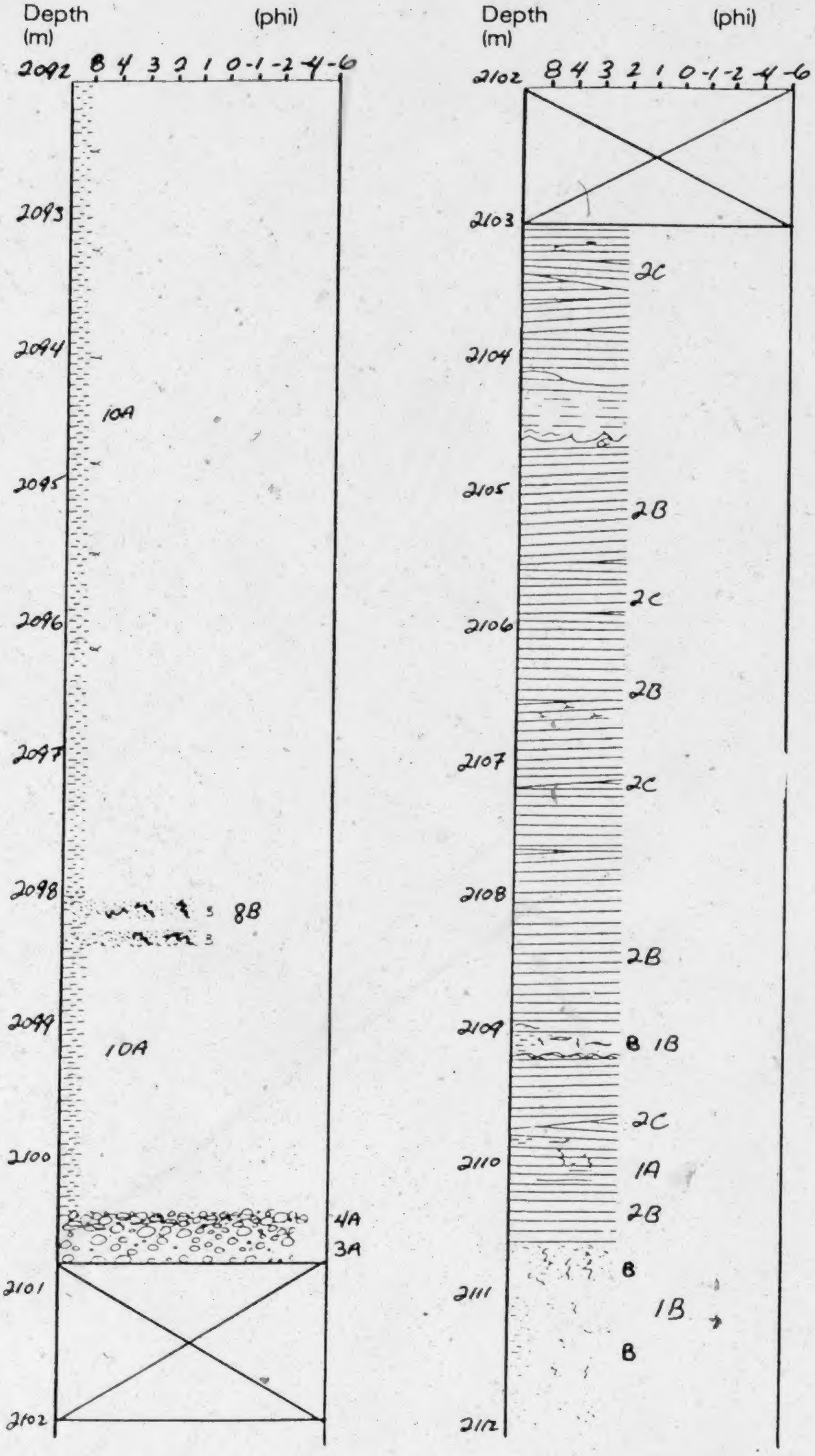
Depth
(m)
(phi)
8 4 3 2 1 0 -1 -2 -4 -6
2092
2093
2094
10A
2095
2096
2097
2098
8B
2099
10A
2100
4A
3A
2101
2102
Depth
(m)
(phi)
8 4 3 2 1 0 -1 -2 -4 -6
2102
2103
2C
2104
2105
2B
2C
2106
2B
2107
2C
2108
2B
2109
B 1B
2C
2110
1A
2B
B
2111
1B
B
2112

16-35-34-3W5

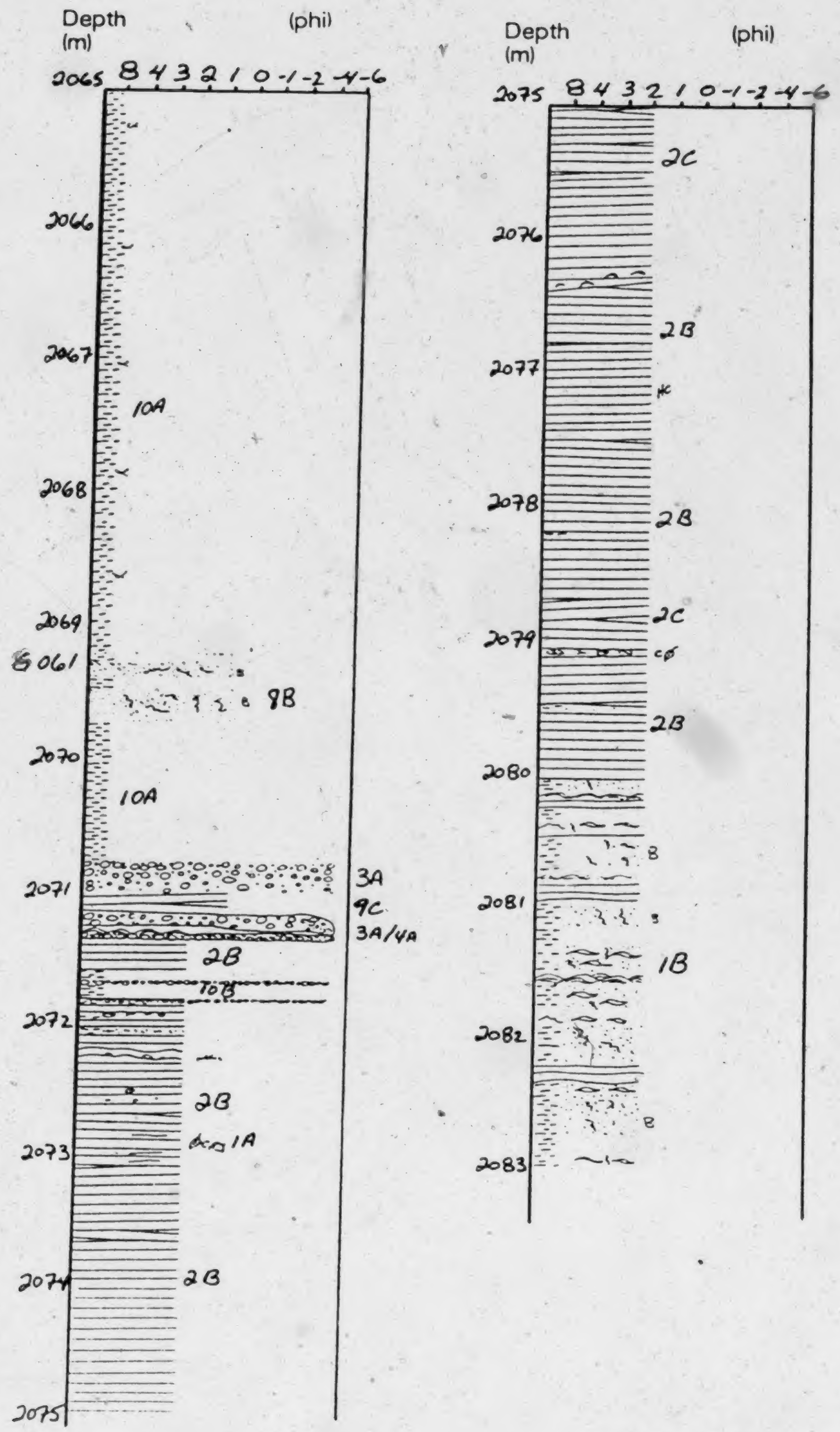
Depth (m)
(phi)
2065
8 4 3 2 1 0 -1 -2 -4 -6
2066
2067
10A
2068
2069
8061
9B
2070
10A
2071
3A
9C
3A/4A
2B
10B
2072
2B
1A
2073
2074
2B
2075
Depth (m)
(phi)
2075
8 4 3 2 1 0 -1 -2 -4 -6
2C
2076
2B
2077
2078
2B
2C
2079
cφ
2B
2080
8
2081
1B
2082
8
2083

14-36-34-3W5

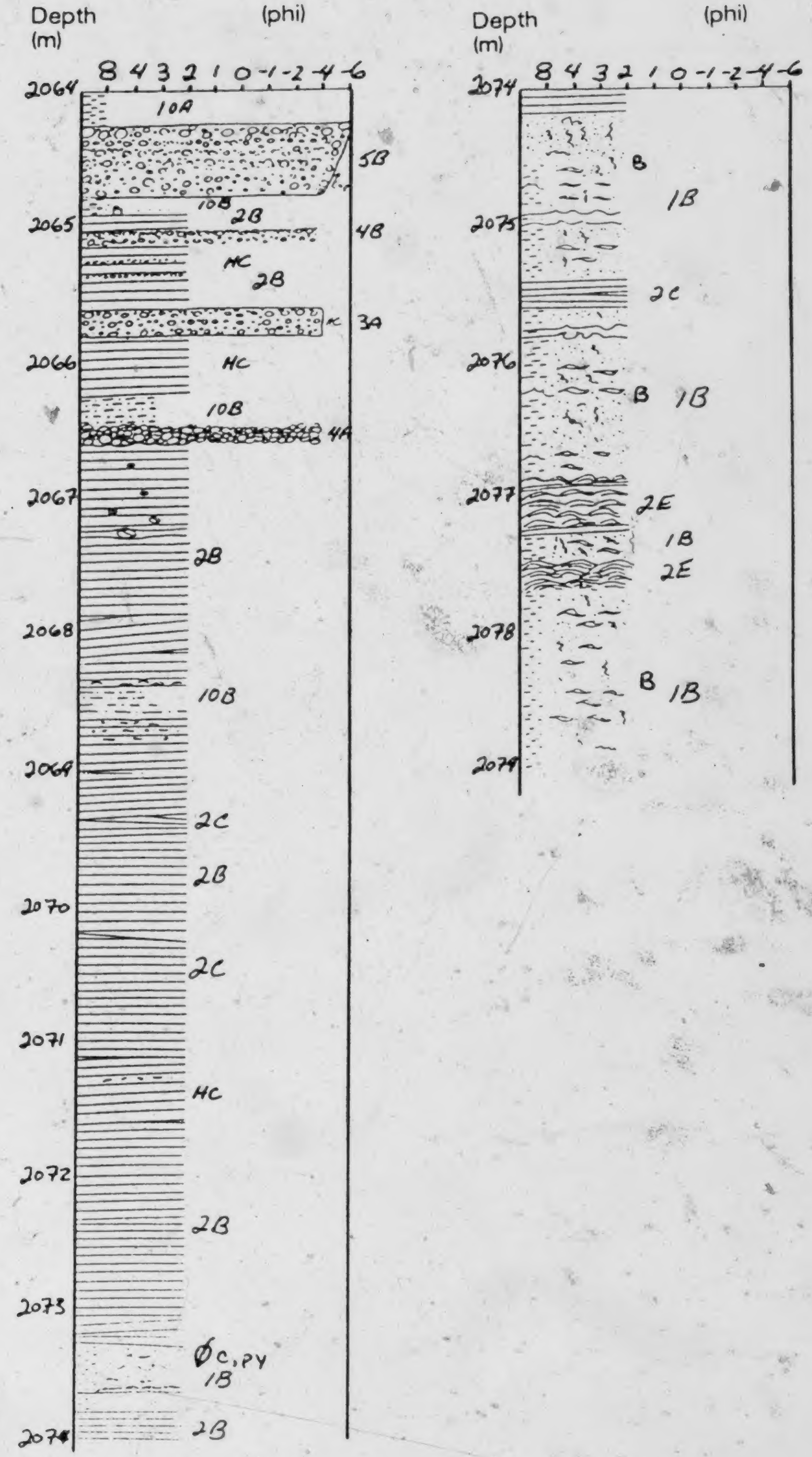
Depth (m)
(phi)
8 4 3 2 1 0 -1 -2 -4 -6
2064
10A
5B
10B
2B
2065
4B
HC
2B
3A
2066
HC
10B
4A
2067
2B
2068
10B
2069
2C
2B
2070
2C
2071
HC
2072
2B
2073
Ø C, PY
1B
2B
2074
Depth (m)
(phi)
8 4 3 2 1 0 -1 -2 -4 -6
2074
B
1B
2075
2C
2076
B
1B
2077
2E
1B
2E
2078
B
1B
2079

10-3-34-4W5

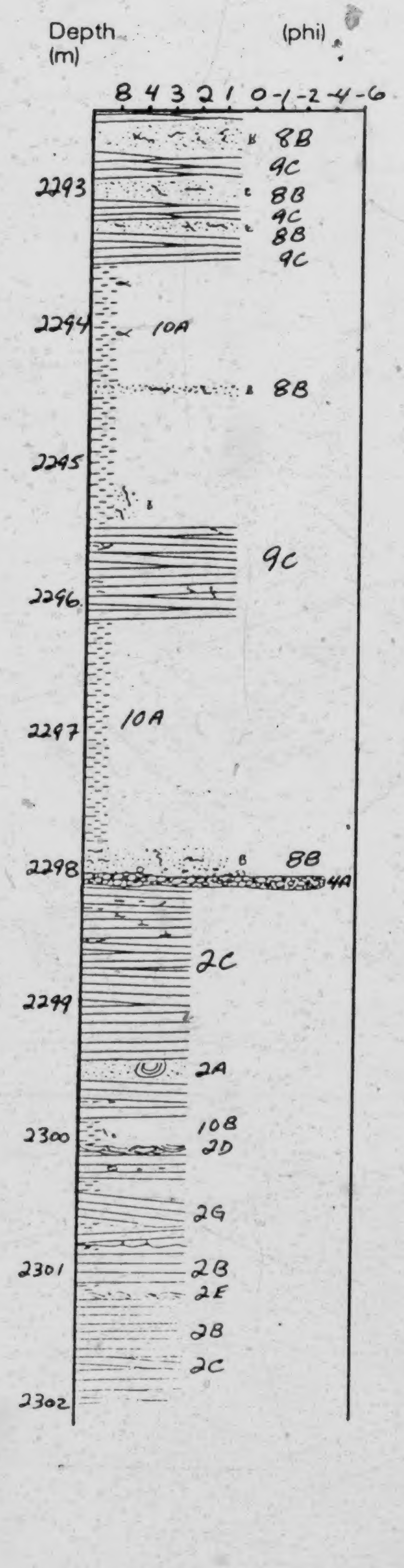
Depth (m)
(phi)
8 4 3 2 1 0 -1 -2 -4 -6
8B
9C
2293
8B
9C
8B
9C
2294
10A
8B
2295
9C
2296
10A
2297
2298
8B
4A
2C
2299
2A
10B
2300
2D
2G
2301
2B
2E
2B
2C
2302

10-7-34-4W5

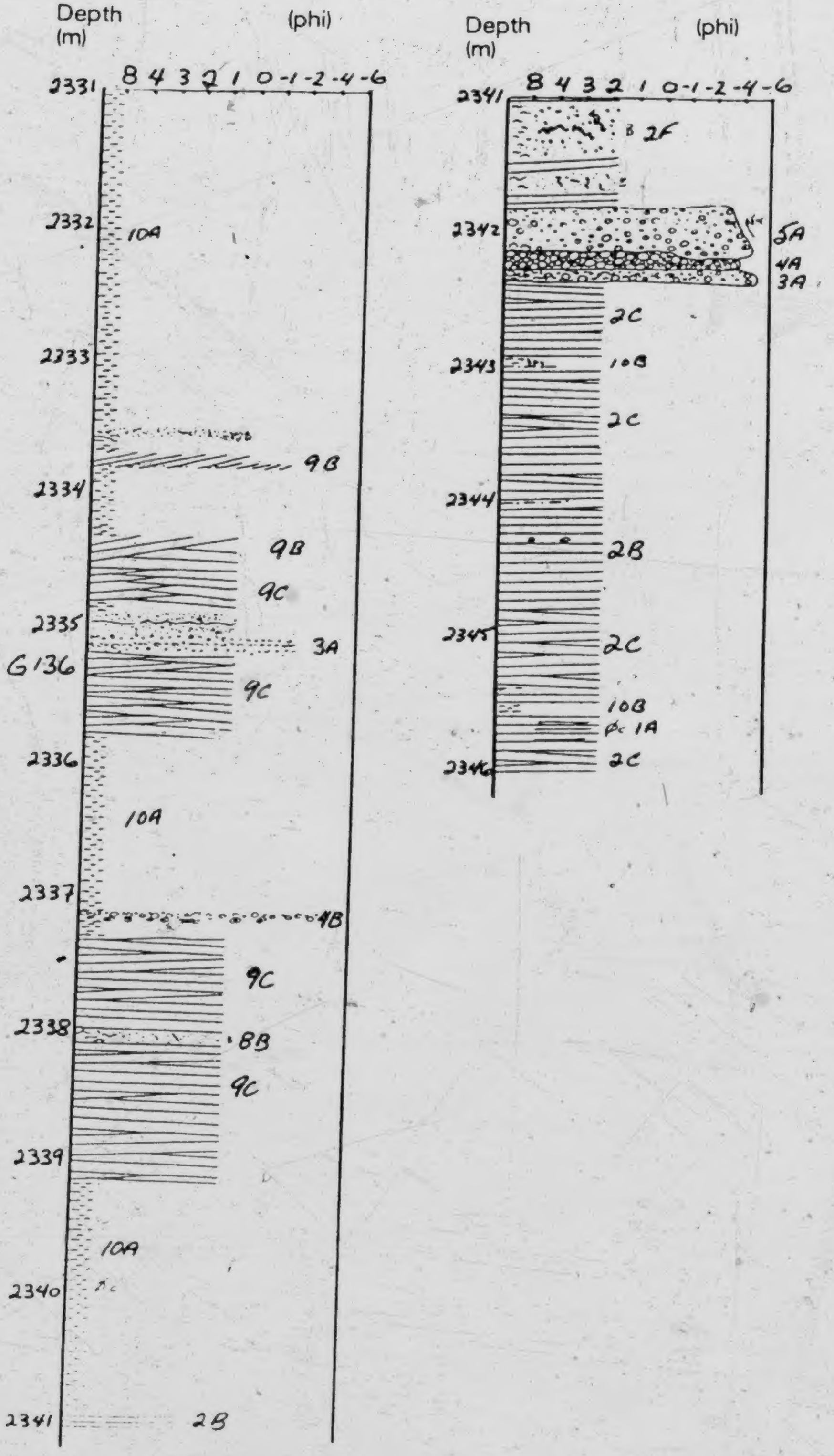
Depth (m)
(phi)
8 4 3 2 1 0 -1 -2 -4 -6
2331
2332
10A
2333
9B
2334
9B
9C
2335
3A
G136
9C
2336
10A
2337
4B
9C
2338
8B
9C
2339
10A
2340
2341
2B
Depth (m)
(phi)
8 4 3 2 1 0 -1 -2 -4 -6
2341
2F
2342
5A
4A
3A
2C
2343
10B
2C
2344
2B
2345
2C
10B
1A
2346
2C

4-20-34-4W5

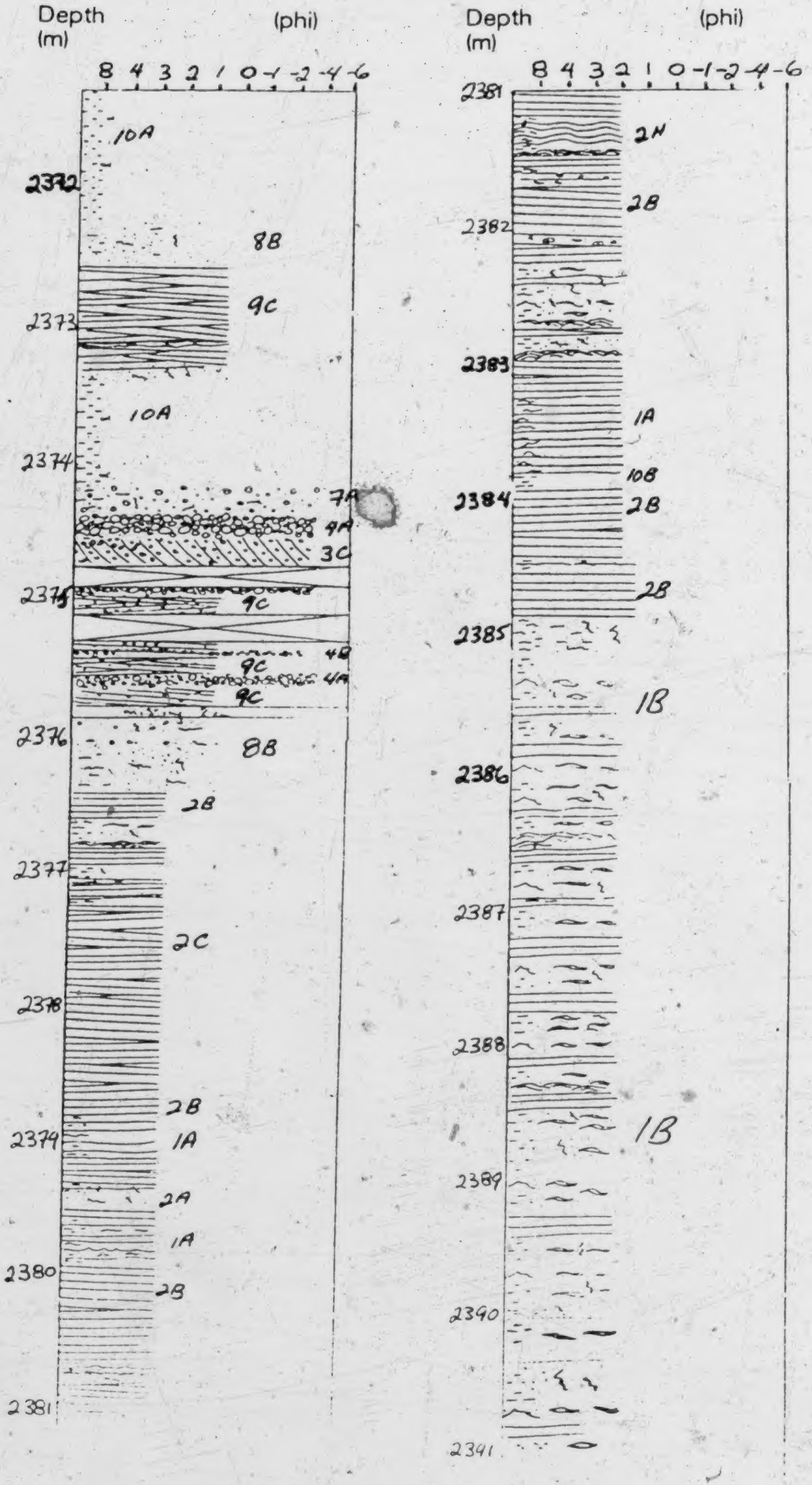
Depth (m)
(phi)
8 4 3 2 1 0 -1 -2 -4 -6
10A
2372
8B
9C
2373
10A
2374
7A
4A
3C
2375
9C
4B
9C
4A
9C
2376
8B
2B
2377
2C
2378
2B
2379
1A
2A
1A
2380
2B
2381
Depth (m)
(phi)
8 4 3 2 1 0 -1 -2 -4 -6
2381
2A
2B
2382
2383
1A
10B
2384
2B
2B
2385
1B
2386
2387
2388
1B
2389
2390
2341

11-28-34-4W5

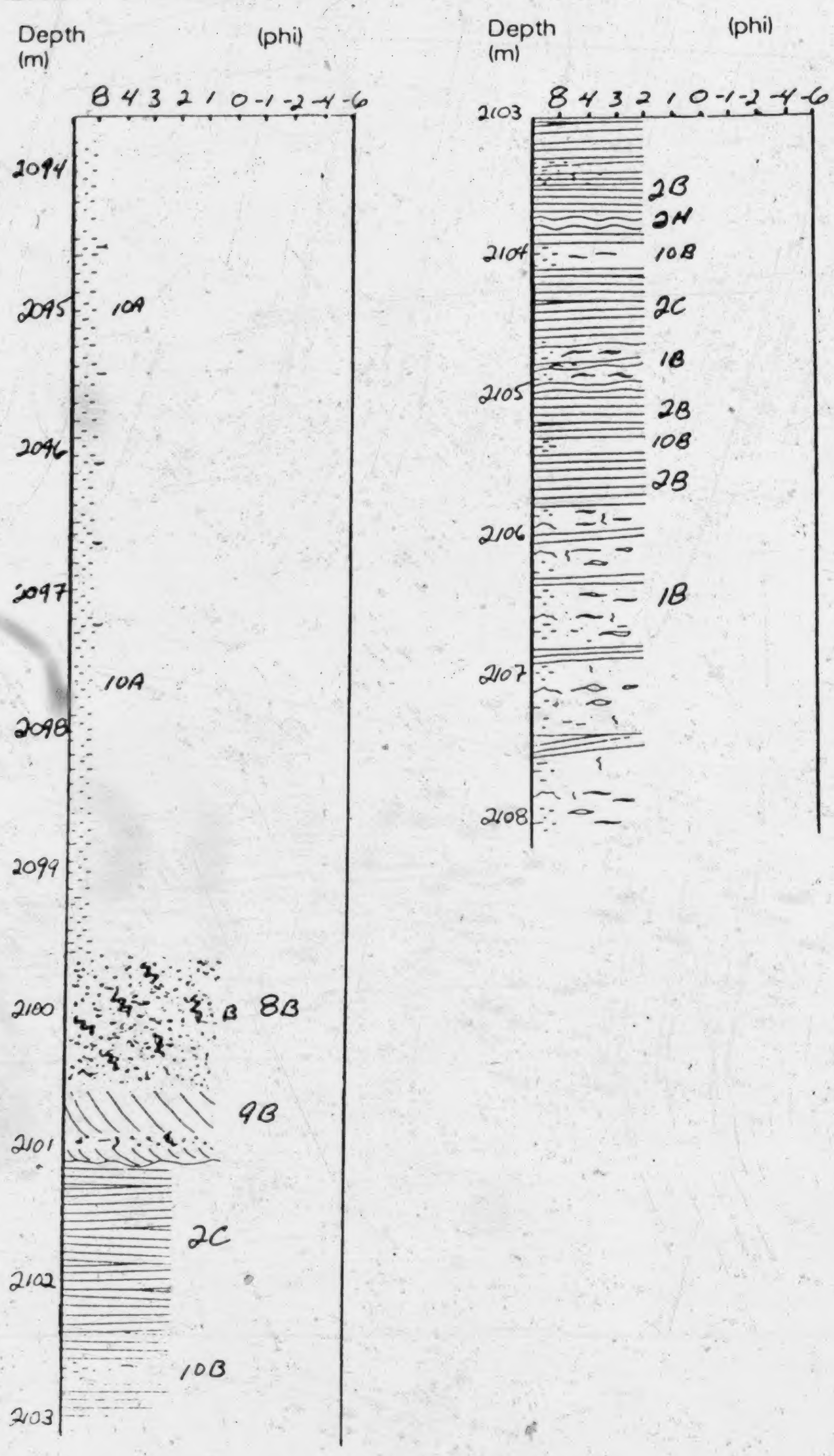
Depth (m)
(phi)
8 4 3 2 1 0 -1 -2 -4 -6
2094
2095
10A
2096
2097
10A
2098
2099
2100
B
8B
9B
2101
2C
2102
10B
2103
Depth (m)
(phi)
8 4 3 2 1 0 -1 -2 -4 -6
2103
2B
2H
2104
10B
2C
1B
2105
2B
10B
2B
2106
1B
2107
2108

6-6-35-2W5

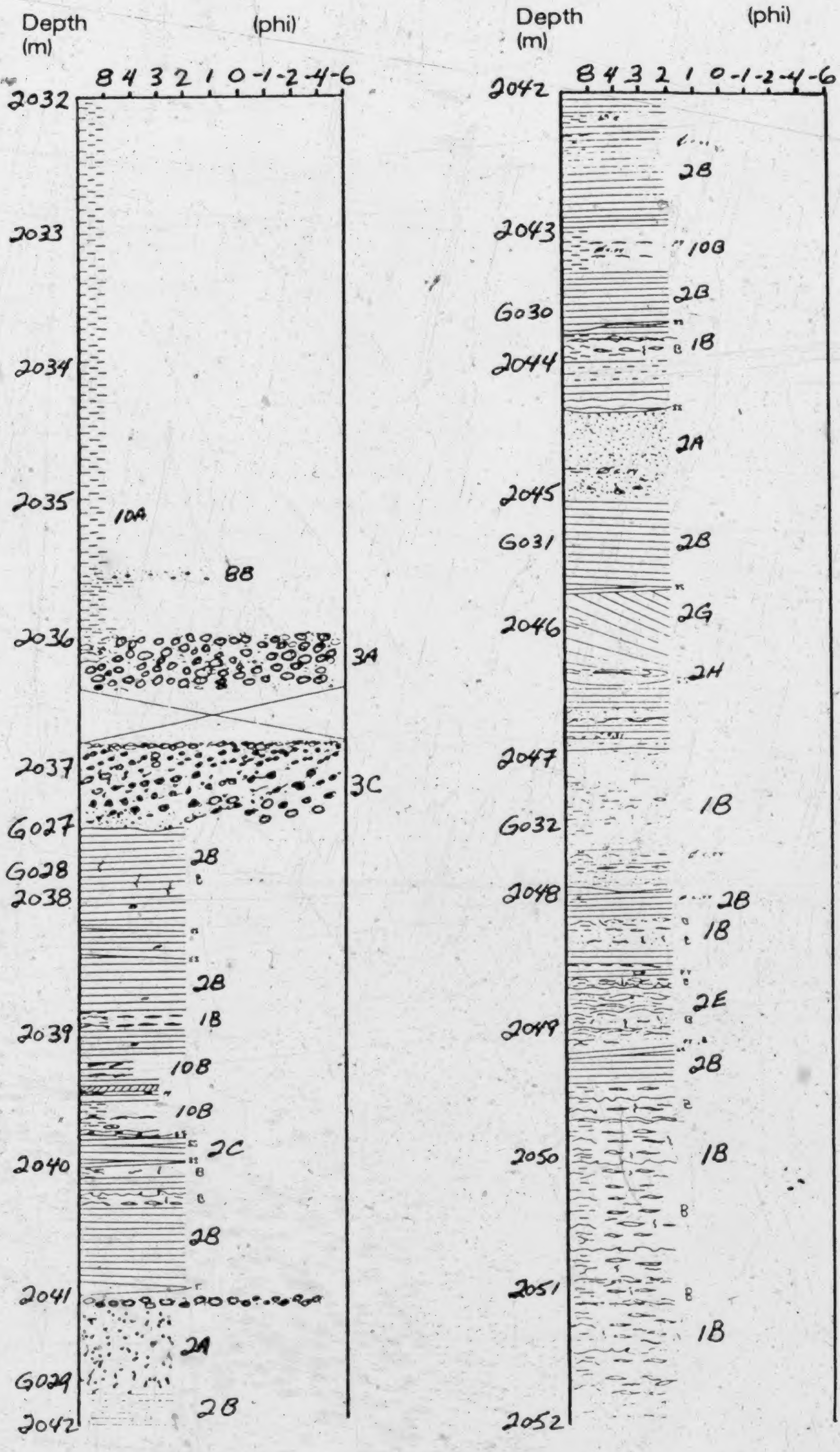
Depth (m)
(phi)
8 4 3 2 1 0 -1 -2 -4 -6
2032
2033
2034
2035
10A
8B
2036
3A
2037
3C
G027
G028
2B
2038
2B
1B
2039
10B
10B
2C
2040
2B
2041
2A
G029
2B
2042
Depth (m)
(phi)
8 4 3 2 1 0 -1 -2 -4 -6
2042
2B
2043
10B
2B
G030
1B
2044
2A
2045
G031
2B
2046
2G
2H
2047
G032
1B
2048
2B
1B
2E
2049
2B
2050
1B
2051
1B
2052

14-1-35-3W5

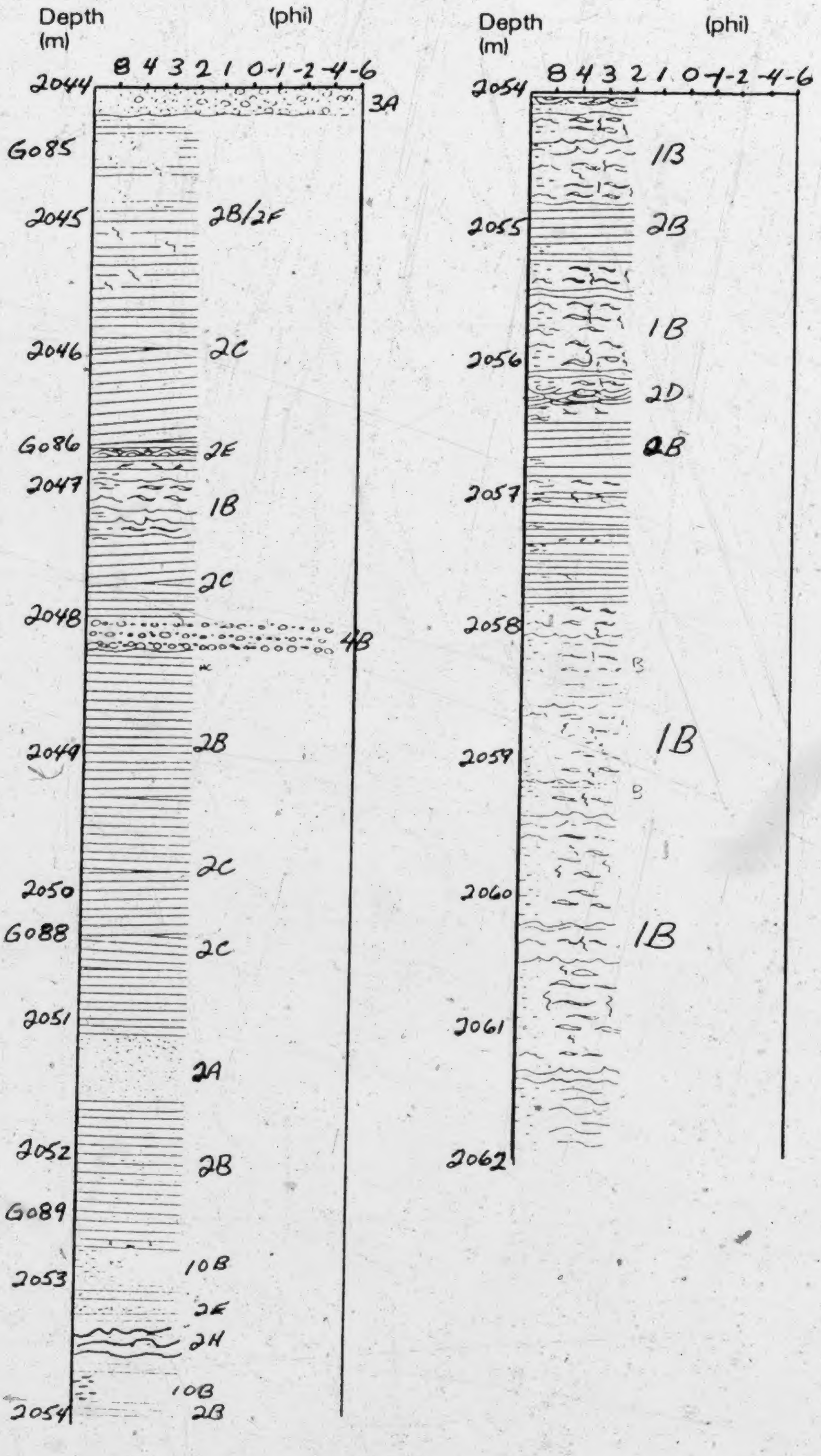
Depth (m)
(phi)
8 4 3 2 1 0 -1 -2 -4 -6
2044
3A
G085
2045
2B/2F
2046
2C
G086
2E
2047
1B
2C
2048
4B
2049
2B
2C
2050
G088
2C
2051
2A
2052
2B
G089
10B
2053
2E
2H
10B
2054
2B
Depth (m)
(phi)
8 4 3 2 1 0 -1 -2 -4 -6
2054
1B
2055
2B
1B
2056
2D
2B
2057
2058
1B
2059
2060
1B
2061
2062

14-2-35-3W5

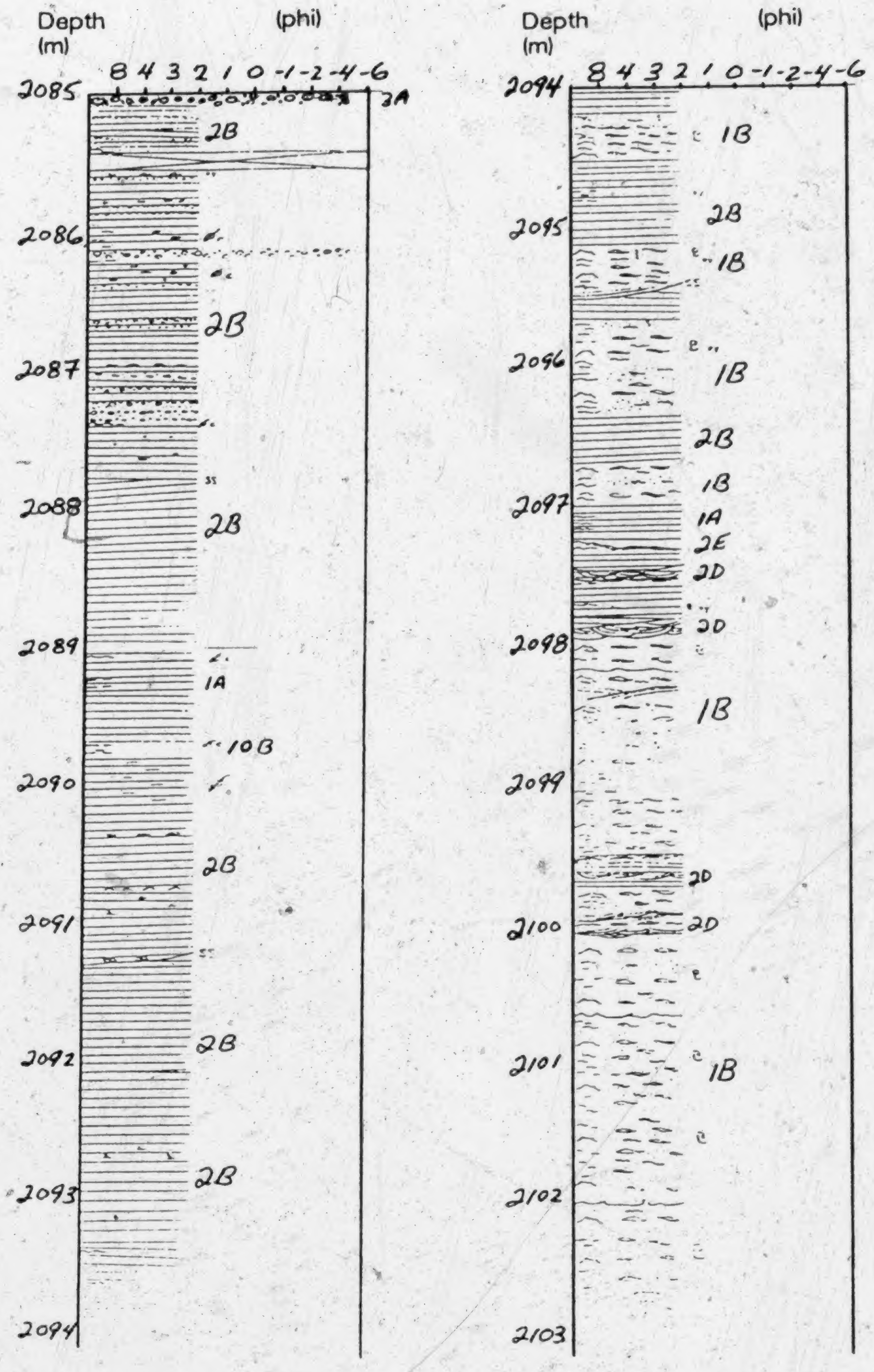
Depth (m)
(phi)
8 4 3 2 1 0 -1 -2 -4 -6
2085
2086
2087
2088
2089
2090
2091
2092
2093
2094
3A
2B
2B
2B
1A
10B
2B
2B
2B
Depth (m)
(phi)
8 4 3 2 1 0 -1 -2 -4 -6
2094
2095
2096
2097
2098
2099
2100
2101
2102
2103
1B
2B
1B
1B
2B
1B
1A
2E
2D
2D
1B
2D
2D
1B

1-3-35-3W5

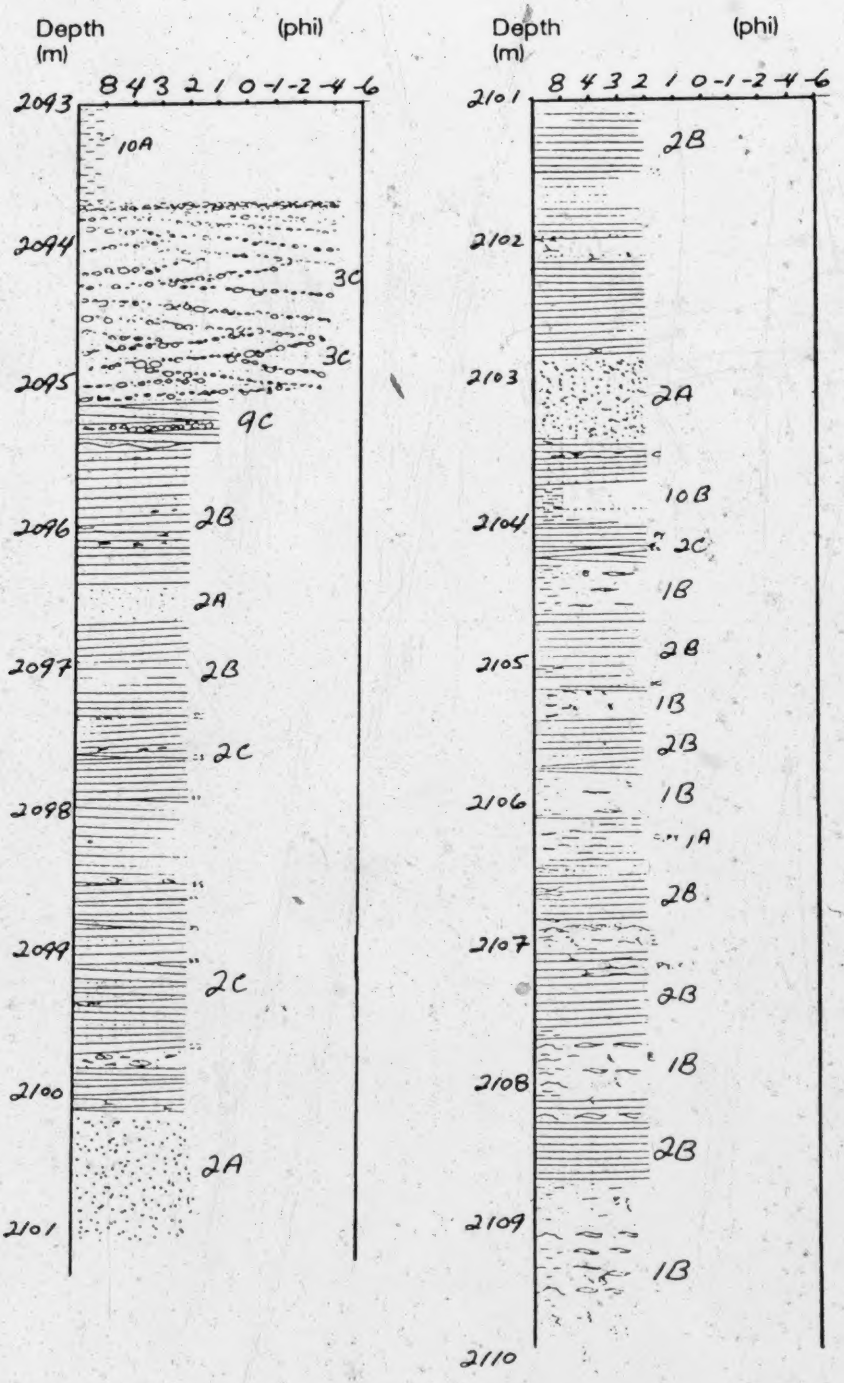
Depth (m)
(phi)
8 4 3 2 1 0 -1 -2 -4 -6
2093
10A
2094
3C
3C
2095
9C
2096
2B
2A
2097
2B
2C
2098
2099
2C
2100
2A
2101
Depth (m)
(phi)
8 4 3 2 1 0 -1 -2 -4 -6
2101
2B
2102
2103
2A
10B
2104
2C
1B
2105
2B
1B
2B
2106
1B
1A
2B
2107
2B
1B
2108
2B
2109
1B
2110

6-3-35-3W5

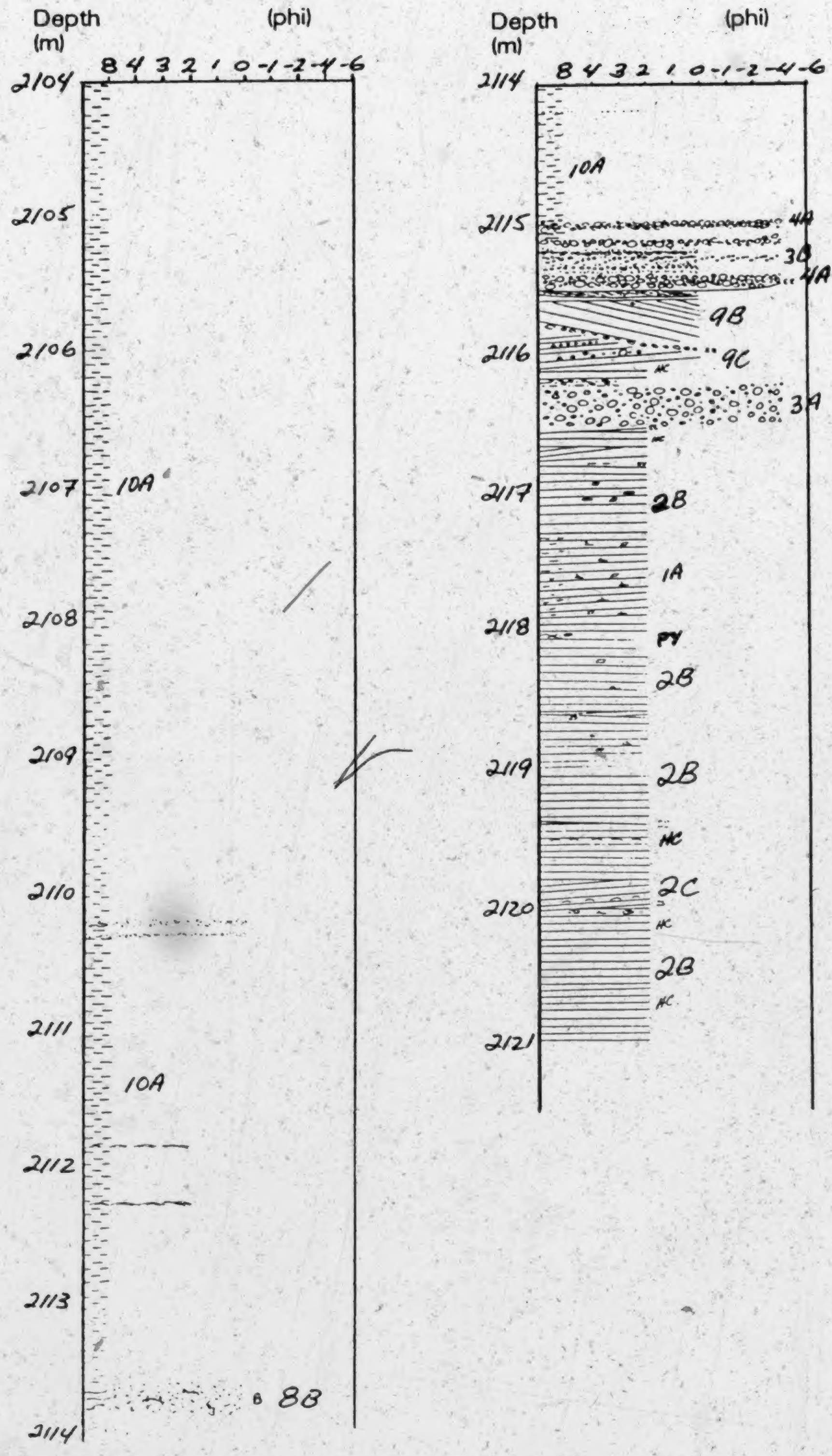
Depth (m)
(phi)
8 4 3 2 1 0 -1 -2 -4 -6
2104
2105
2106
2107
10A
2108
2109
2110
2111
10A
2112
2113
B
8B
2114
Depth (m)
(phi)
8 4 3 2 1 0 -1 -2 -4 -6
2114
10A
2115
4A
3B
4A
9B
2116
9C
HC
3A
HC
2117
2B
1A
2118
PY
2B
2119
2B
HC
2C
2120
HC
2B
HC
2121

9-3-35-3W5

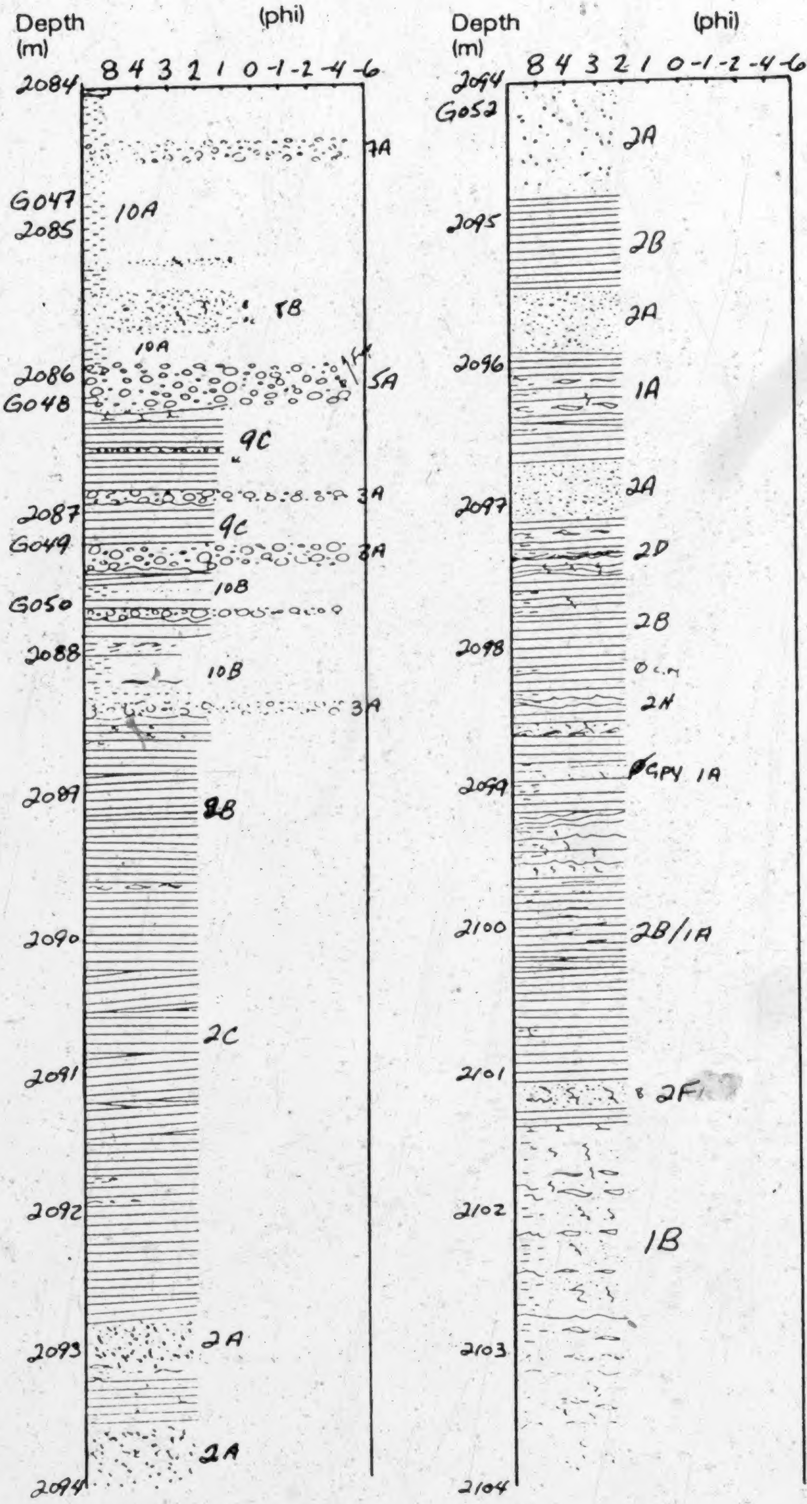
Depth (m)
(phi)
8 4 3 2 1 0 -1 -2 -4 -6
2084
7A
G047
10A
2085
8B
10A
2086
G048
5A
9C
3A
2087
9C
G049
3A
10B
G050
2088
10B
3A
2089
2B
2090
2C
2091
2092
2093
2A
2A
2094
Depth (m)
(phi)
8 4 3 2 1 0 -1 -2 -4 -6
2094
G052
2A
2095
2B
2A
2096
1A
2A
2097
2D
2B
2098
0 c.m
2H
GPY 1A
2099
2100
2B/1A
2101
2F
2102
1B
2103
2104

7-4-35-3W5

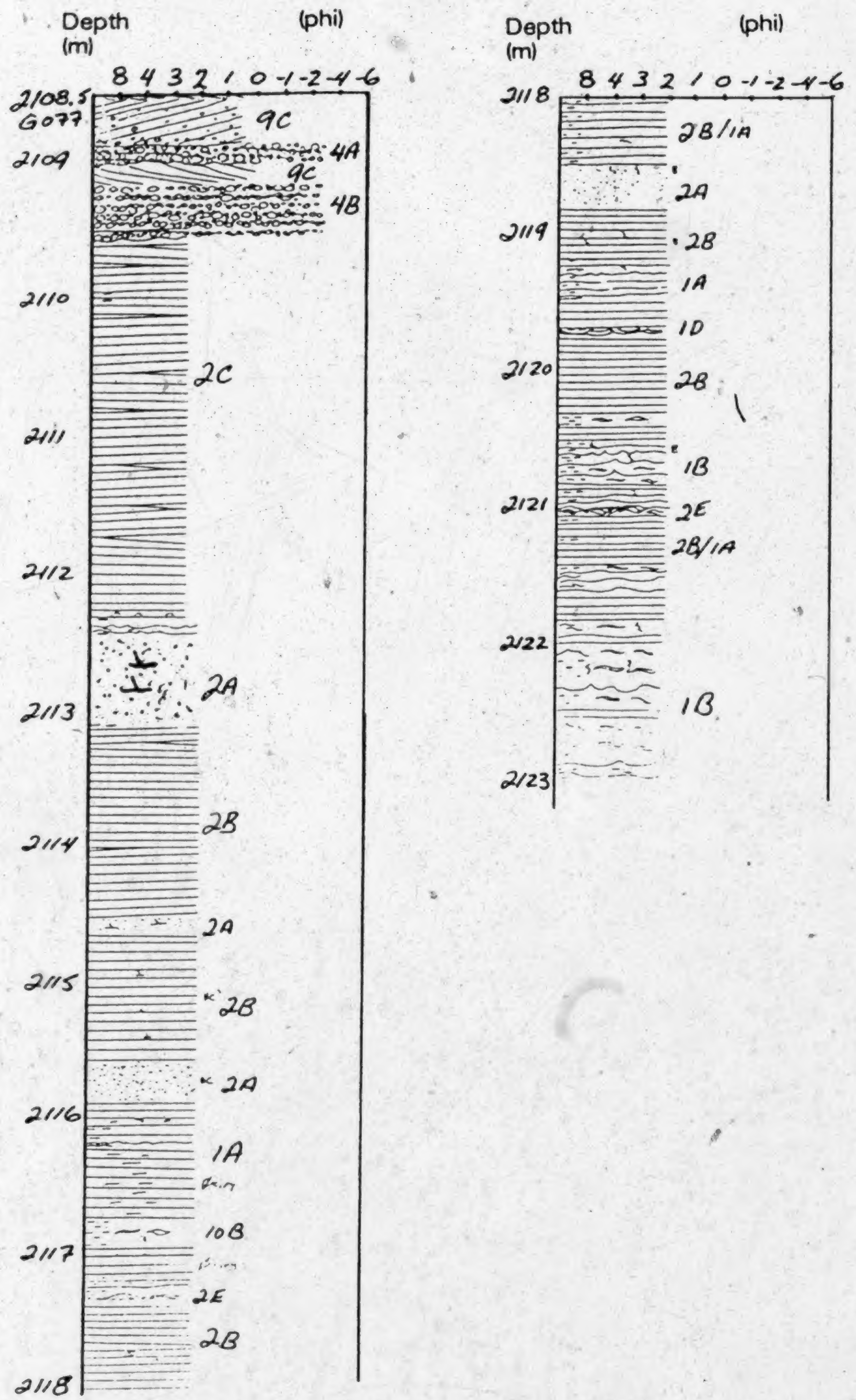
Depth (m)
(phi)
8 4 3 2 1 0 -1 -2 -4 -6
2108.5
G077
2109
2110
2111
2112
2113
2114
2115
2116
2117
2118
9C
4A
9C
4B
2C
2A
2B
2A
2B
2A
1A
10B
2E
2B
Depth (m)
(phi)
8 4 3 2 1 0 -1 -2 -4 -6
2118
2119
2120
2121
2122
2123
2B/1A
2A
2B
1A
1D
2B
1B
2E
2B/1A
1B

6-5-35-3W5

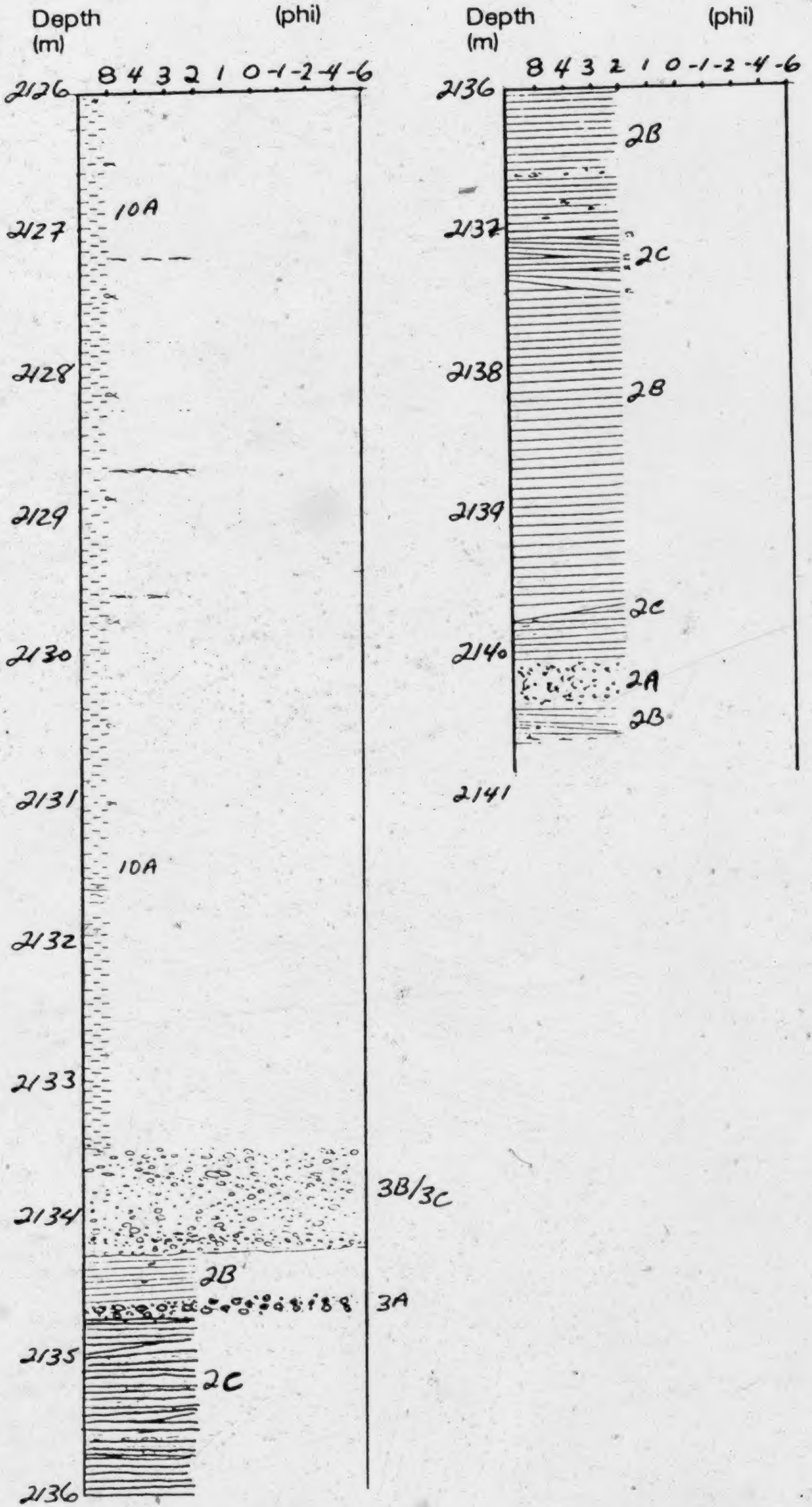
Depth
(m)
(phi)
8 4 3 2 1 0 -1 -2 -4 -6
2126
2127
2128
2129
2130
2131
2132
2133
2134
2135
2136
10A
10A
3B/3C
2B
3A
2C
Depth
(m)
(phi)
8 4 3 2 1 0 -1 -2 -4 -6
2136
2137
2138
2139
2140
2141
2B
2C
2B
2C
2A
2B

16-5-35-3W5

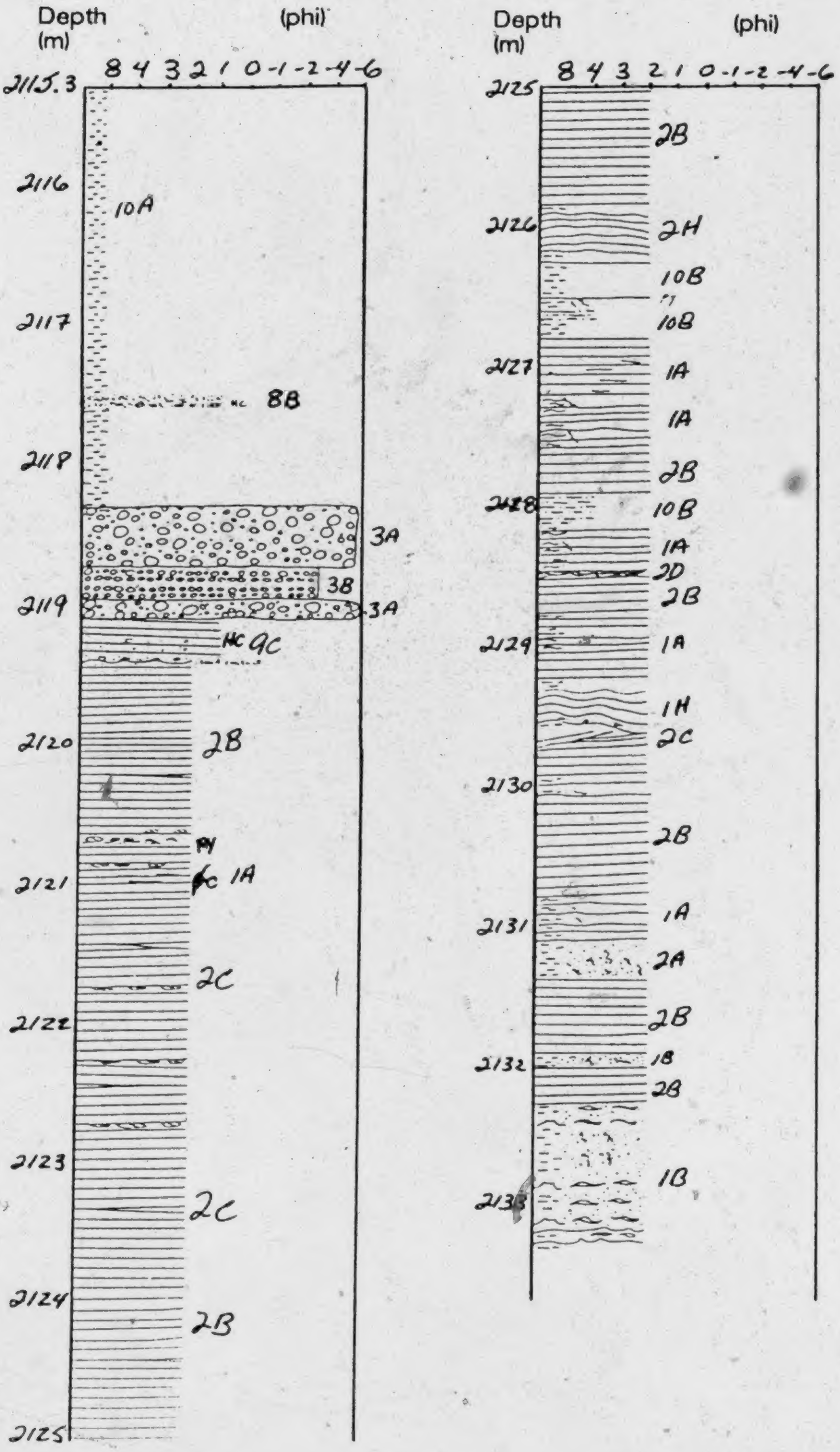
Depth (m)
(phi)
8 4 3 2 1 0 -1 -2 -4 -6
2115.3
2116
10A
2117
8B
2118
3A
3B
2119
3A
HC 9C
2120
2B
PY
2121
FC 1A
2C
2122
2123
2C
2124
2B
2125
Depth (m)
(phi)
8 4 3 2 1 0 -1 -2 -4 -6
2125
2B
2126
2H
10B
PY
10B
2127
1A
1A
2B
2128
10B
1A
2D
2B
2129
1A
1H
2C
2130
2B
2131
1A
2A
2B
2132
1B
2B
2133
1B

8-7-35-3W5

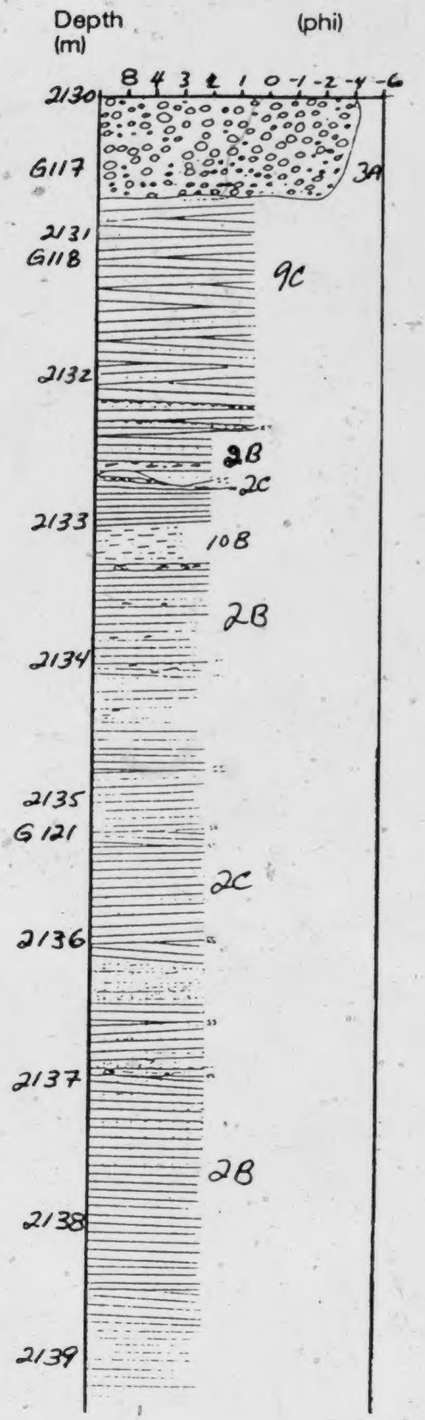
Depth
(m)
(phi)
8 4 3 2 1 0 -1 -2 -4 -6
2130
G117
3A
2131
G118
9C
2132
2B
2C
2133
10B
2B
2134
2135
G121
2C
2136
2137
2B
2138
2139

8-9-35-3W5

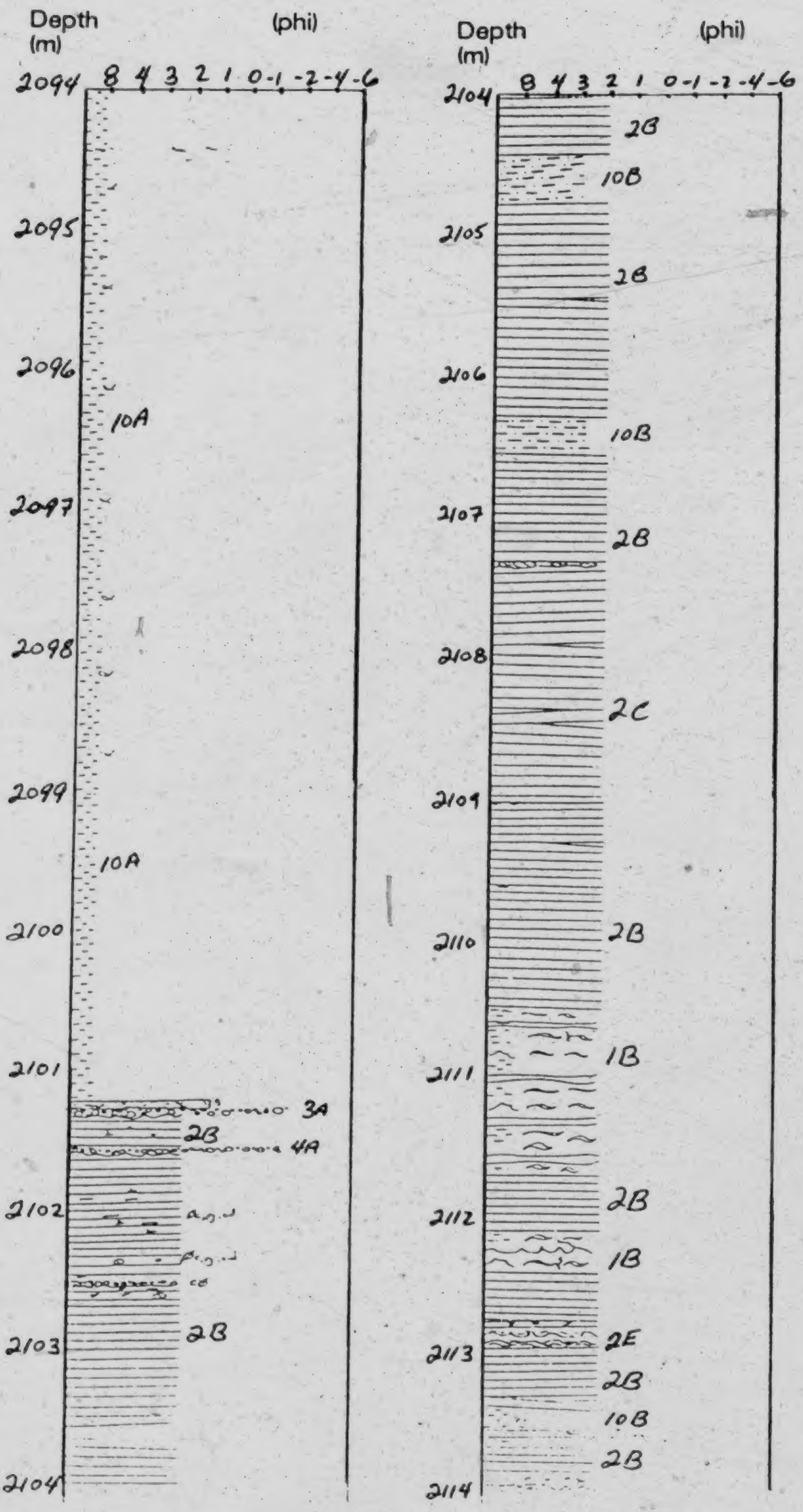
Depth (m)
(phi)
8 4 3 2 1 0 -1 -2 -4 -6
2094
2095
2096
2097
2098
2099
2100
2101
2102
2103
2104
10A
10A
3A
2B
4A
2B
Depth (m)
(phi)
8 4 3 2 1 0 -1 -2 -4 -6
2104
2105
2106
2107
2108
2109
2110
2111
2112
2113
2114
2B
10B
2B
10B
2B
2C
2B
1B
2B
1B
2E
2B
10B
2B

6-10-35-3W5

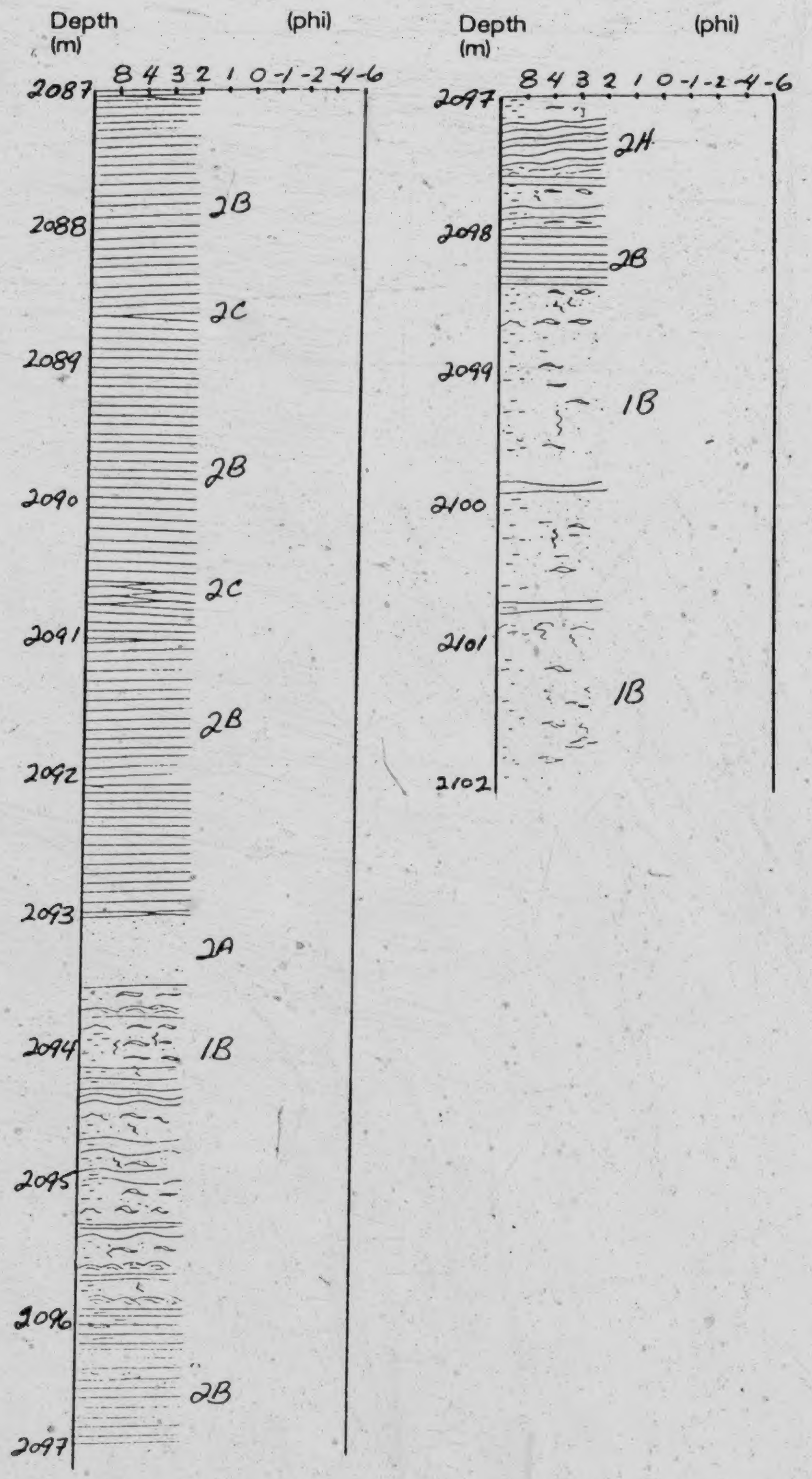
Depth (m)
(phi)
8 4 3 2 1 0 -1 -2 -4 -6
2087
2088
2089
2090
2091
2092
2093
2094
2095
2096
2097
2B
2C
2B
2C
2B
2A
1B
2B
Depth (m)
(phi)
8 4 3 2 1 0 -1 -2 -4 -6
2097
2098
2099
2100
2101
2102
2H
2B
1B
1B

10-10-35-3W5

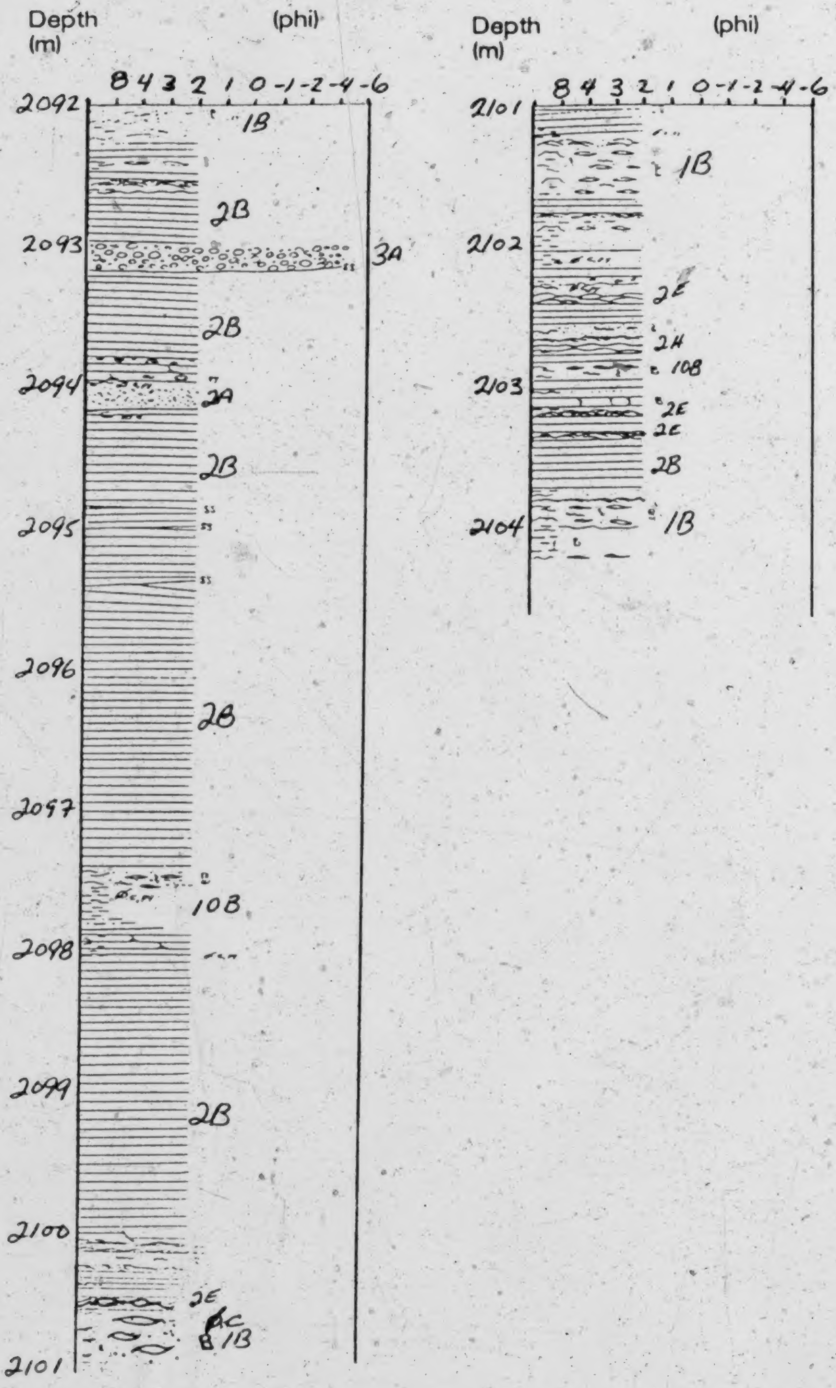
Depth (m)
(phi)
8 4 3 2 1 0 -1 -2 -4 -6
2092
1B
2B
2093
3A
2B
2094
3A
2B
2095
2096
2B
2097
10B
2098
2099
2B
2100
2E
1C
1B
2101
Depth (m)
(phi)
8 4 3 2 1 0 -1 -2 -4 -6
2101
1B
2102
2E
2H
10B
2103
2E
2E
2B
2104
1B

11-11-35-3W5

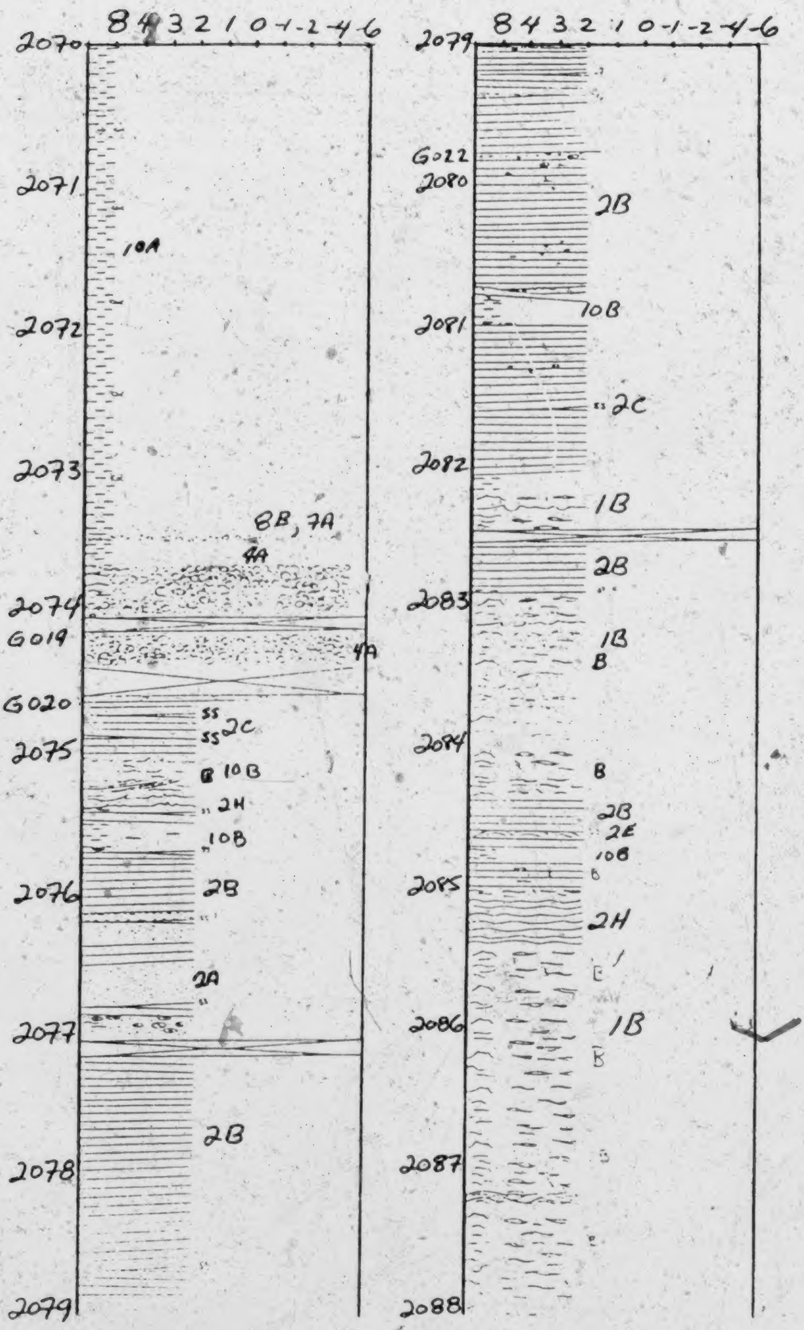
8 4 3 2 1 0 -1 -2 -4 -6
2070
2071
10A
2072
2073
8B, 7A
4A
2074
G019
4A
G020
ss
ss 2C
2075
B 10B
" 2H
" 10B
"
2076
2B
"
2A
"
2077
2B
2078
2079
8 4 3 2 1 0 -1 -2 -4 -6
2079
G022
2080
2B
10B
2081
" 2C
2082
1B
2B
" "
2083
1B
B
2084
B
2B
2E
10B
B
2085
2H
B
2086
1B
B
2087
2088

14-1-35-4W5

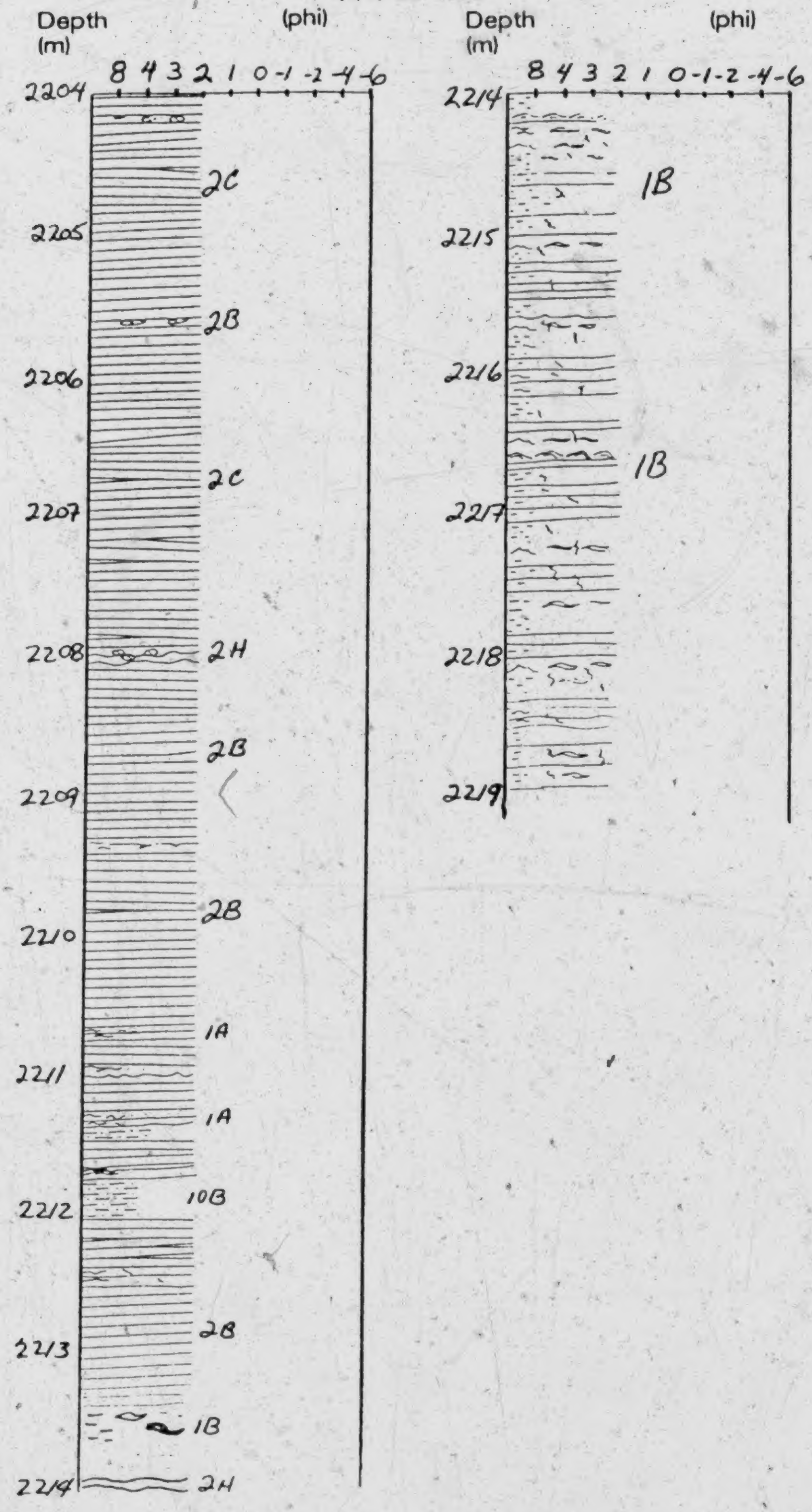
Depth (m)
(phi)
8 4 3 2 1 0 -1 -2 -4 -6
2204
2C
2205
2B
2206
2C
2207
2H
2208
2B
2209
2B
2210
1A
2211
1A
10B
2212
2B
2213
1B
2214
2H
Depth (m)
(phi)
8 4 3 2 1 0 -1 -2 -4 -6
2214
1B
2215
2216
1B
2217
2218
2219

16-1-35-4W5

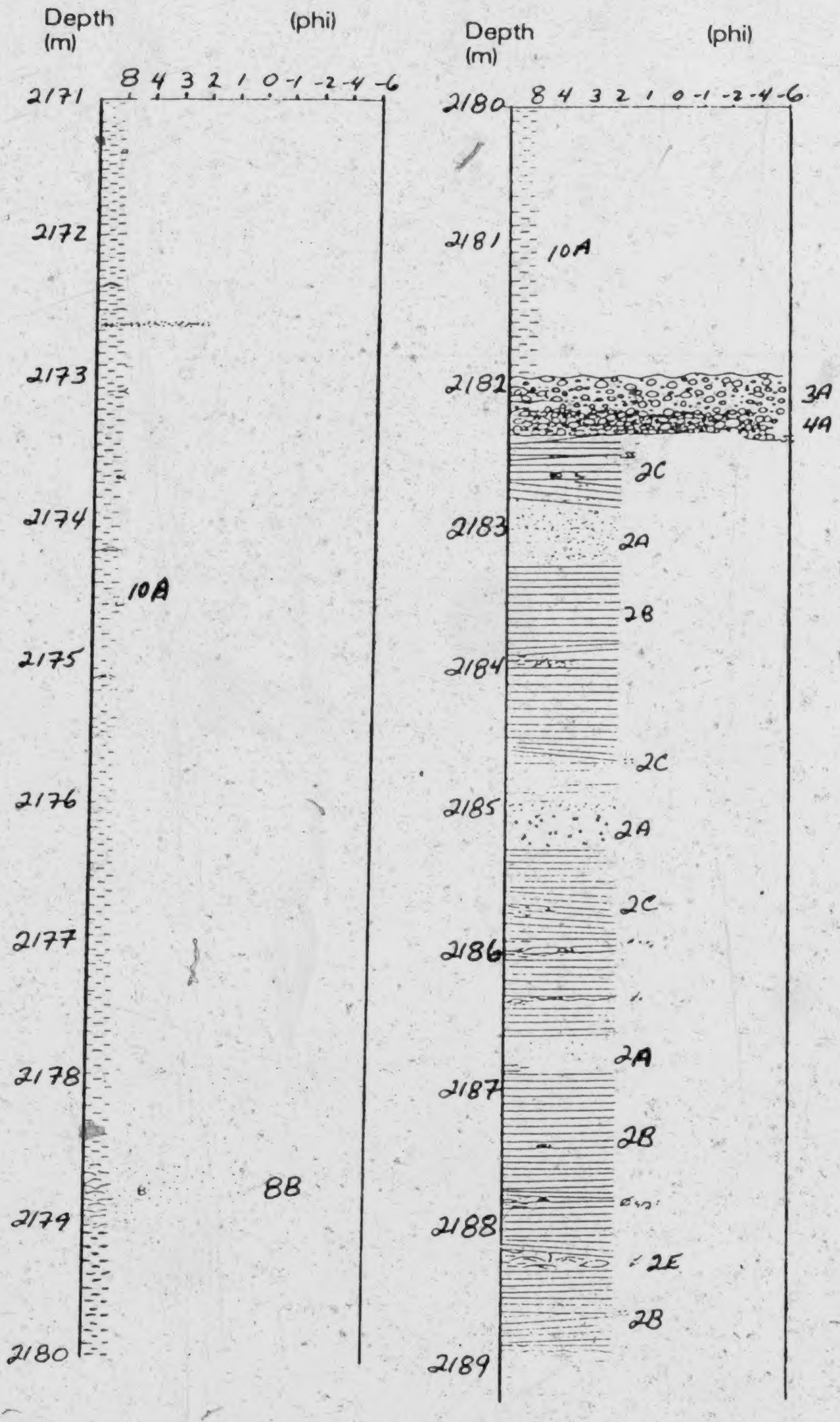
Depth (m)
(phi)
8 4 3 2 1 0 -1 -2 -4 -6
2171
2172
2173
2174
10A
2175
2176
2177
2178
8B
2179
2180
Depth (m)
(phi)
8 4 3 2 1 0 -1 -2 -4 -6
2180
2181
10A
2182
3A
4A
2C
2183
2A
2B
2184
2C
2185
2A
2C
2186
2A
2187
2B
2188
2E
2B
2189

16-2-35-4W5

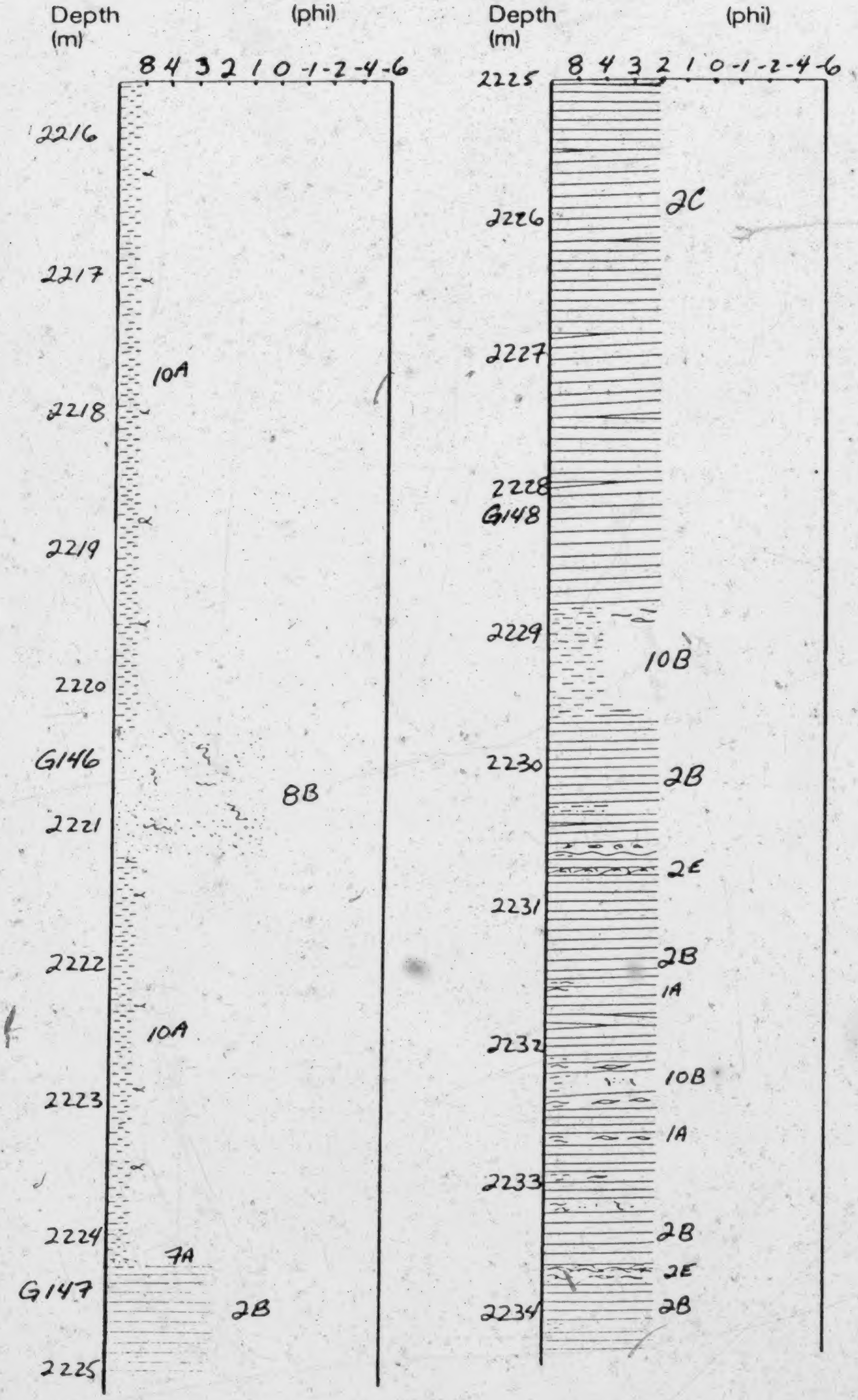
Depth
(m)
(phi)
8 4 3 2 1 0 -1 -2 -4 -6
2216
2217
10A
2218
2219
2220
G146
8B
2221
2222
10A
2223
2224
7A
G147
2B
2225
Depth
(m)
(phi)
8 4 3 2 1 0 -1 -2 -4 -6
2225
2C
2226
2227
2228
G148
2229
10B
2230
2B
2E
2231
2B
1A
2232
10B
1A
2233
2B
2E
2234
2B

6-11-35-4W5

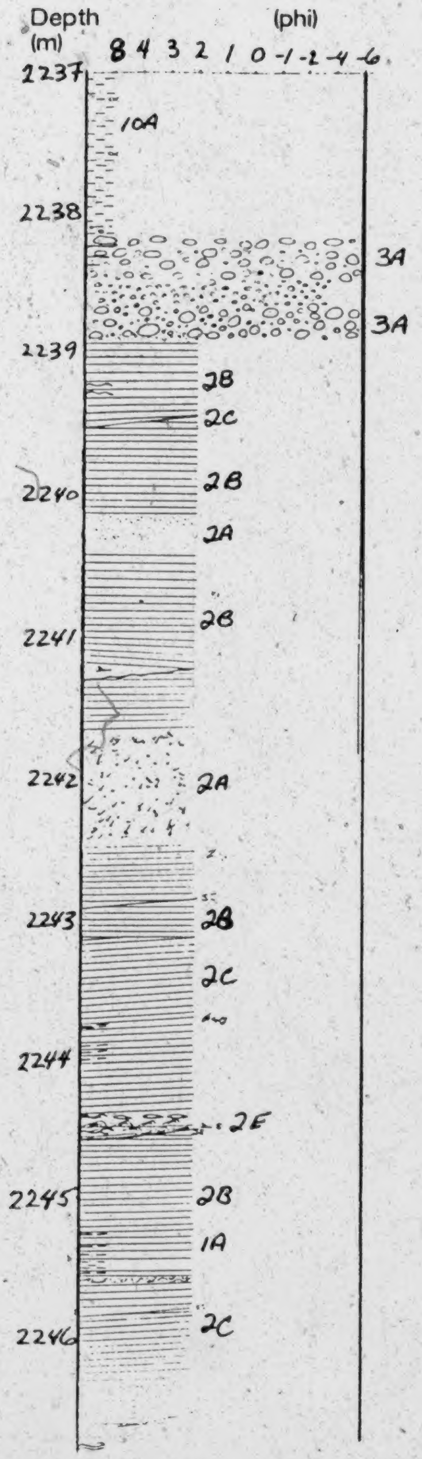
Depth
(m)
(phi)
8 4 3 2 1 0 -1 -2 -4 -6
2237
10A
2238
3A
3A
2239
2B
2C
2240
2B
2A
2241
2B
2242
2A
2243
2B
2C
2244
2E
2245
2B
1A
2246
2C

8-11-35-4W5

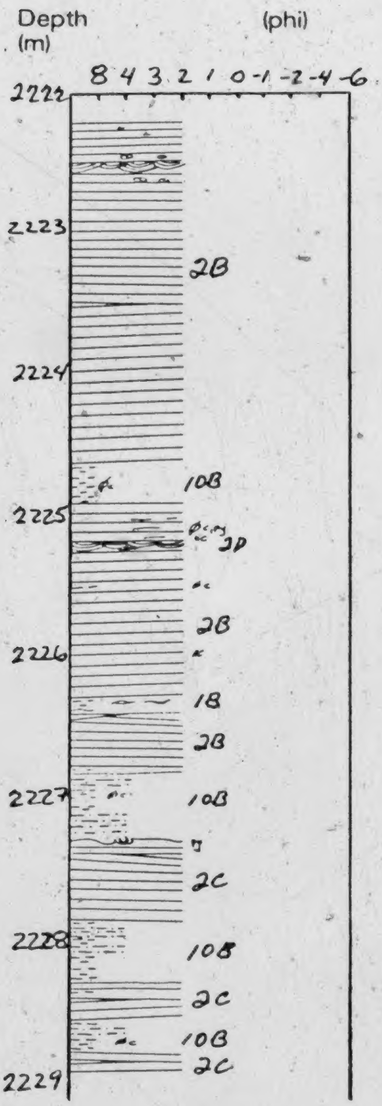
Depth (m)
(phi)
8 4 3 2 1 0 -1 -2 -4 -6
2222
2223
2B
2224
10B
2225
2D
2B
2226
1B
2B
2227
10B
2C
2228
10B
2C
10B
2C
2229

14-11-35-4W5

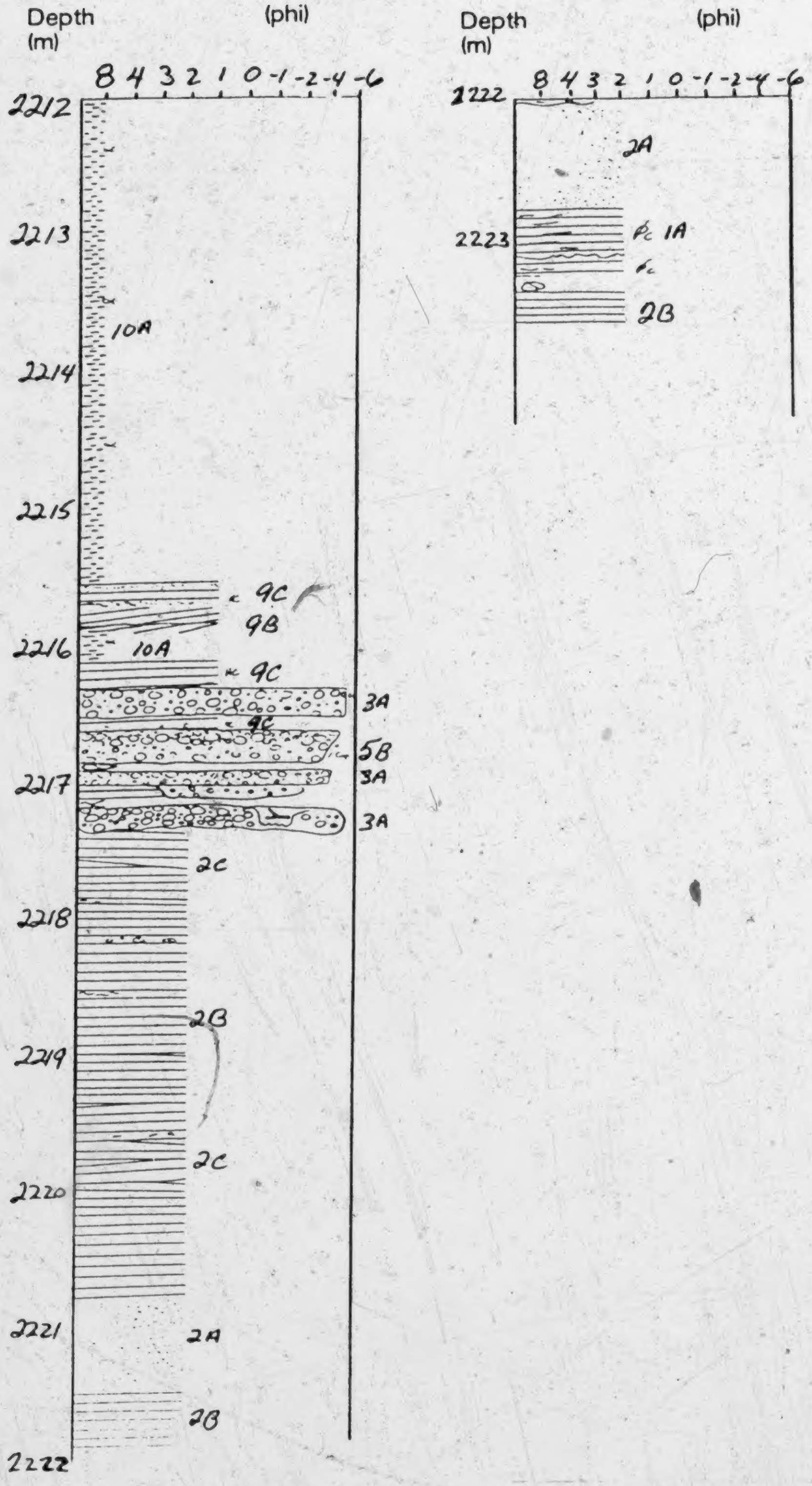
Depth (m)
(phi)
8 4 3 2 1 0 -1 -2 -4 -6
2212
2213
10A
2214
2215
9C
9B
2216
10A
9C
3A
9C
5B
3A
2217
3A
2C
2218
2B
2219
2C
2220
2221
2A
2B
2222
Depth (m)
(phi)
8 4 3 2 1 0 -1 -2 -4 -6
2222
2A
2223
Pc 1A
Pc
2B

1-12-35-4W5

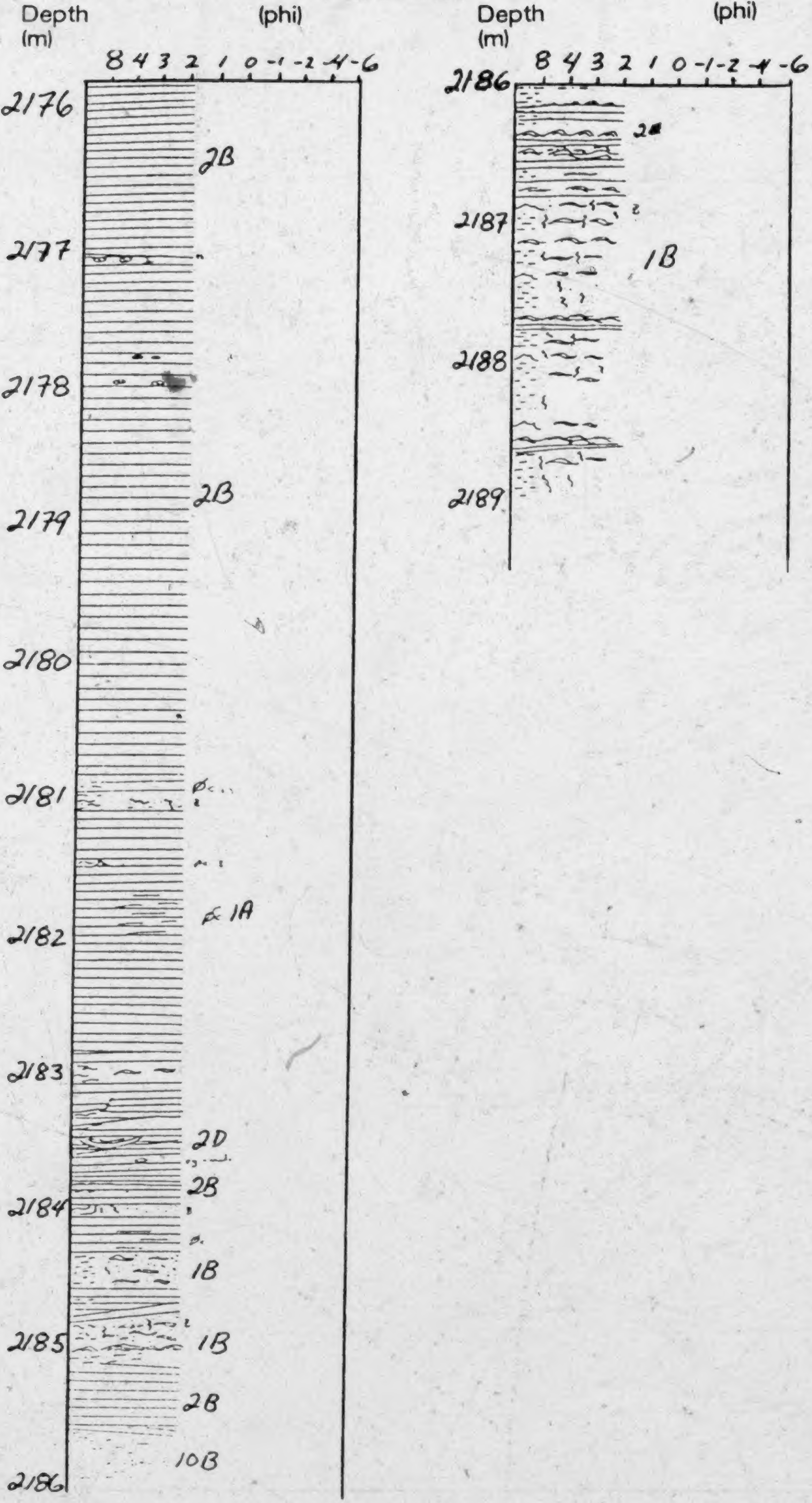
Depth (m)
(phi)
8 4 3 2 1 0 -1 -2 -4 -6
2176
2B
2177
2178
2B
2179
2180
2181
1A
2182
2183
2D
2B
2184
1B
2185
1B
2B
10B
2186
Depth (m)
(phi)
8 4 3 2 1 0 -1 -2 -4 -6
2186
2
2187
1B
2188
2189

6-12-35-4W5

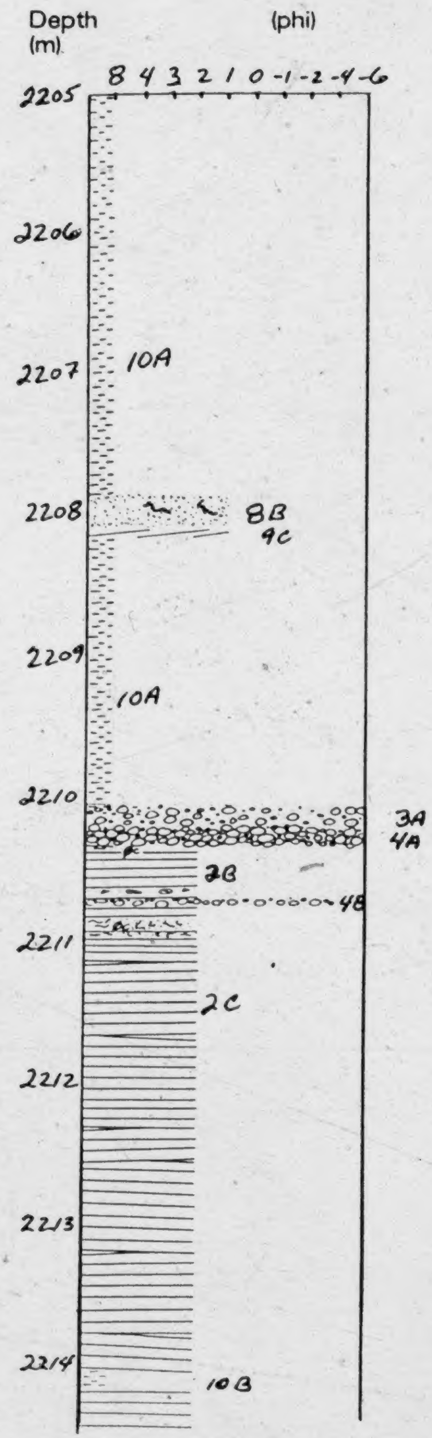
Depth
(m)
(phi)
8 4 3 2 1 0 -1 -2 -4 -6
2205
2206
2207
10A
2208
8B
9C
2209
10A
2210
3A
4A
2B
4B
2211
2C
2212
2213
2214
10B

10-13-35-4W5

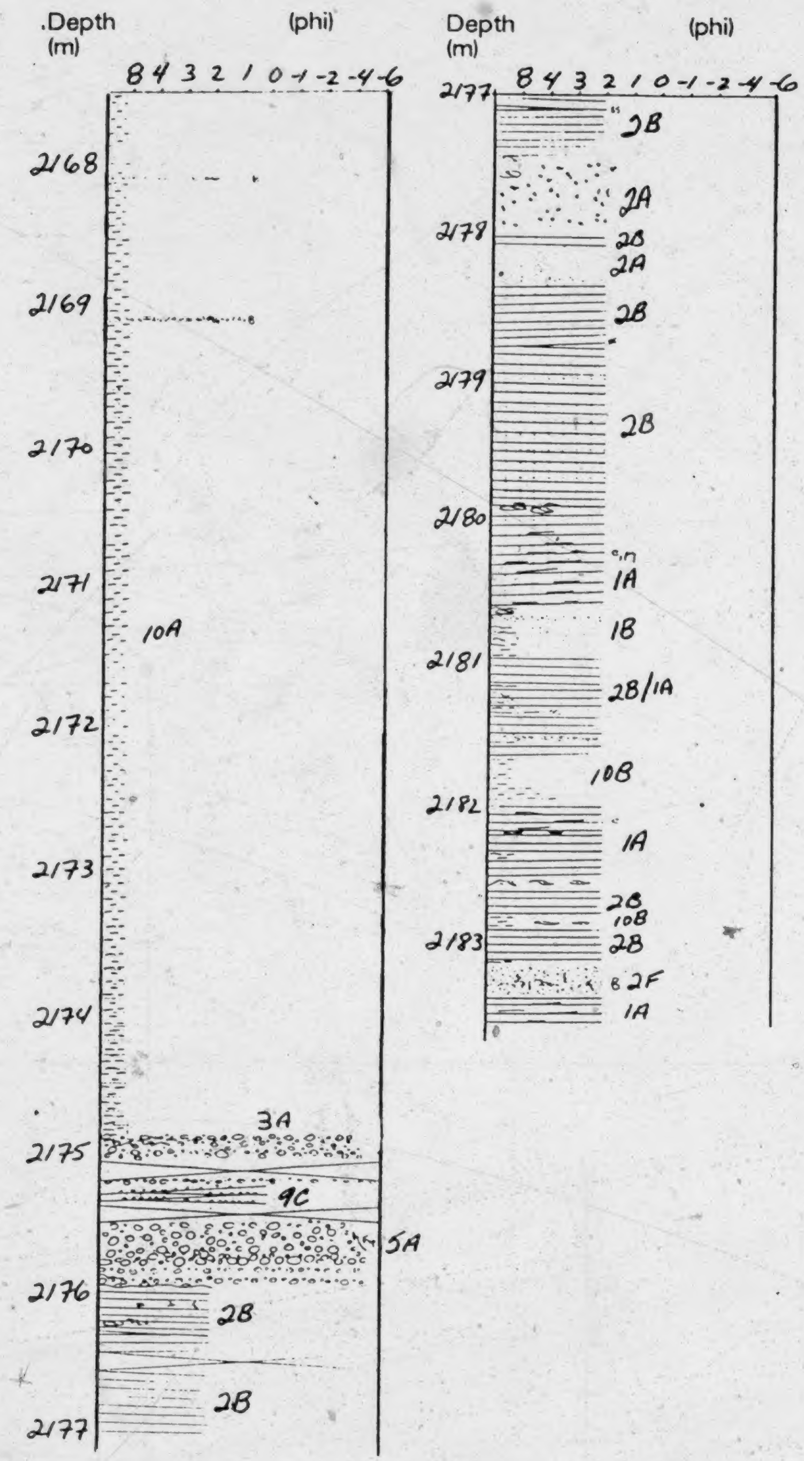

Depth (m)
(phi)
8 4 3 2 1 0 -1 -2 -4 -6
2168
2169
2170
2171
10A
2172
2173
2174
3A
2175
9C
5A
2176
2B
2B
2177
Depth (m)
(phi)
8 4 3 2 1 0 -1 -2 -4 -6
2177
2B
2A
2178
2B
2A
2B
2179
2B
2180
1A
1B
2181
2B/1A
10B
2182
1A
2B
10B
2183
2B
2F
1A

6-14-35-4W5

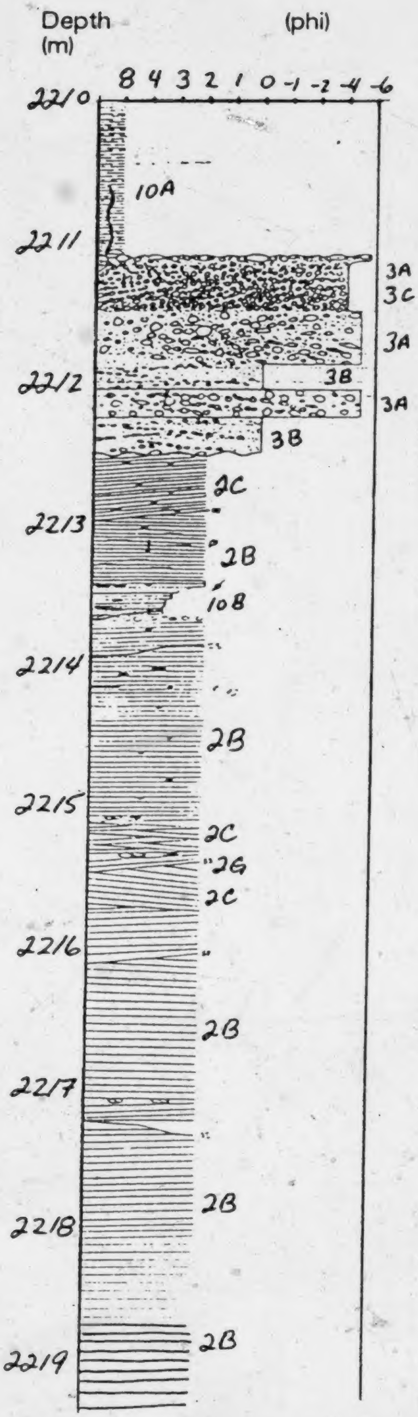
Depth
(m)
(phi)
8 4 3 2 1 0 -1 -2 -4 -6
2210
10A
2211
3A
3C
3A
2212
3B
3A
3B
2C
2213
2B
10B
2214
2B
2215
2C
2G
2C
2216
2B
2217
2B
2218
2B
2219

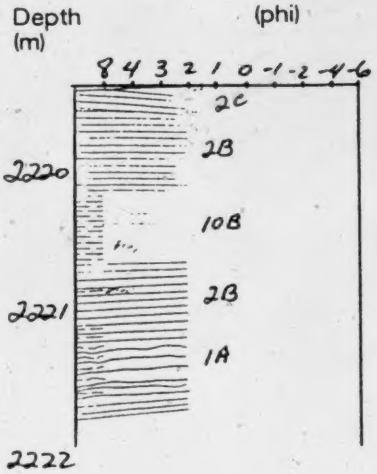
Depth
(m)
(phi)
8 4 3 2 1 0 -1 -2 -4 -6
2C
2B
2220
10B
2B
2221
1A
2222

8-14-35-4W5

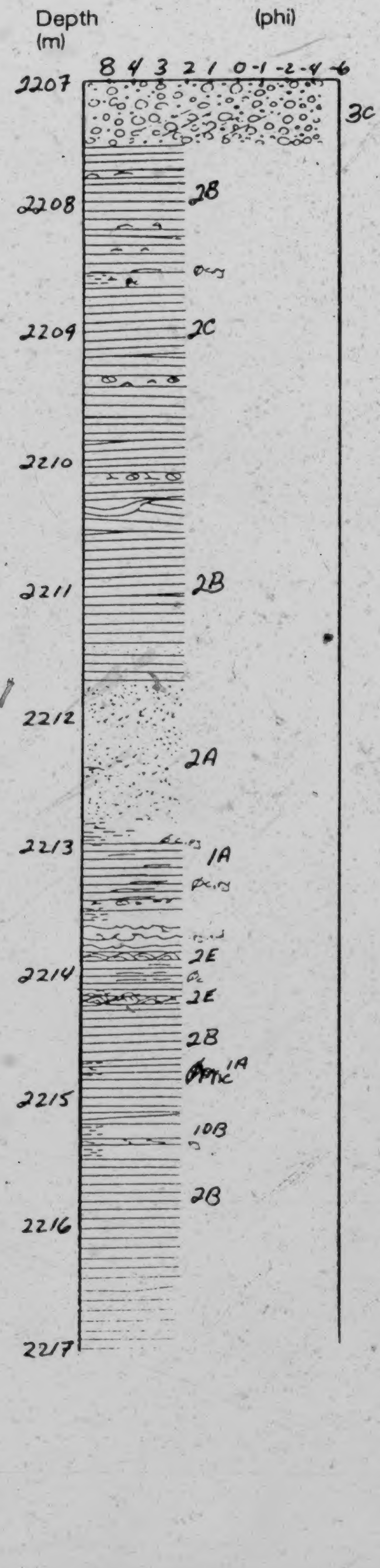
Depth (m)
(phi)
8 4 3 2 1 0 -1 -2 -4 -6
2207
3C
2B
2208
2C
2209
2210
2B
2211
2212
2A
2213
1A
2E
2214
2E
2B
1A
2215
10B
2B
2216
2217

8-15-35-4W5

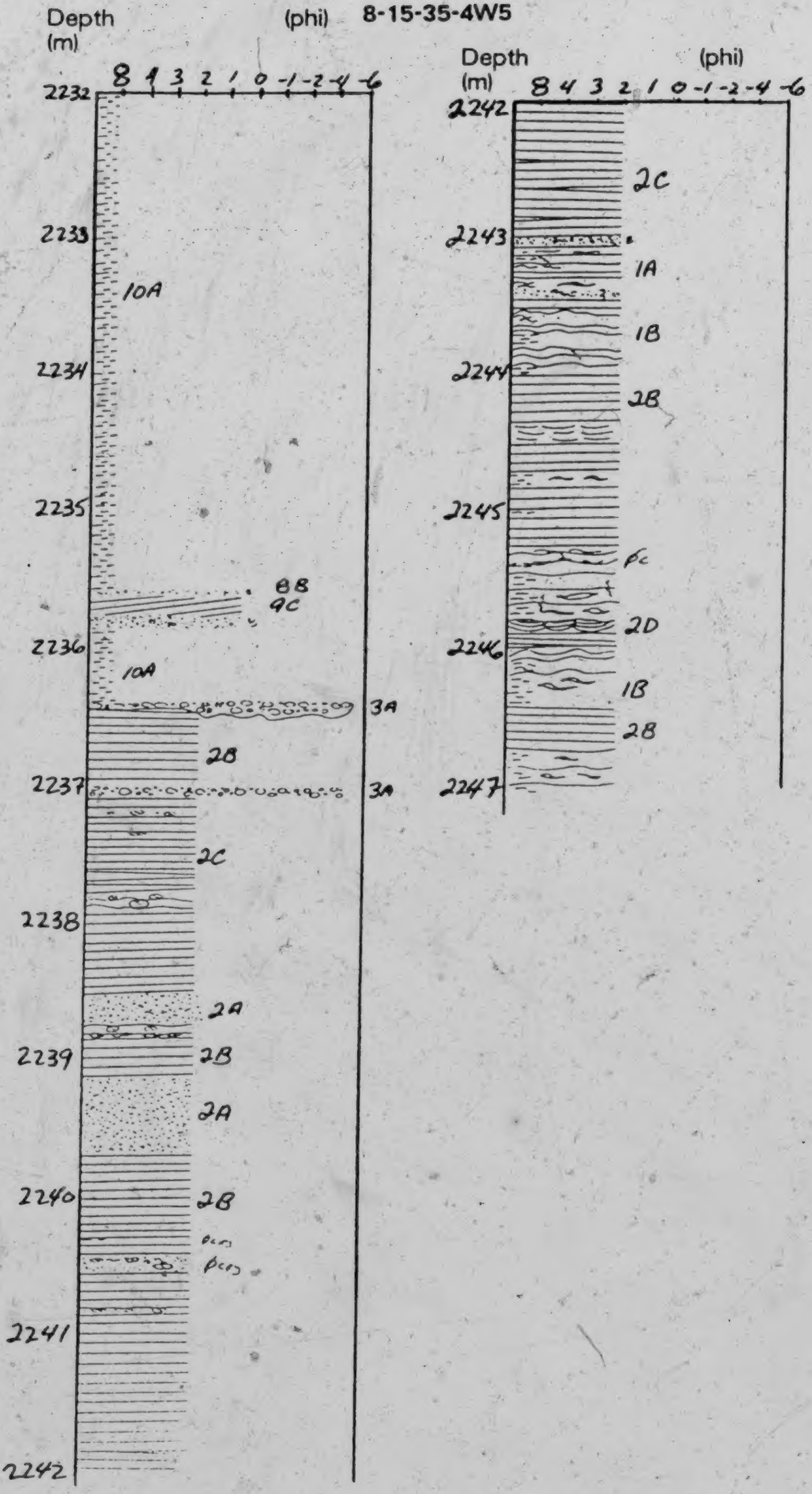
Depth (m)
(phi)
8 4 3 2 1 0 -1 -2 -4 -6
2232
2233
10A
2234
2235
8B
9C
2236
10A
3A
2B
2237
3A
2C
2238
2A
2B
2239
2A
2240
2B
Pc?
Pc?
2241
2242
Depth (m)
(phi)
8 4 3 2 1 0 -1 -2 -4 -6
2242
2C
2243
1A
1B
2244
2B
2245
Pc
2D
2246
1B
2B
2247

7-21-35-4W5

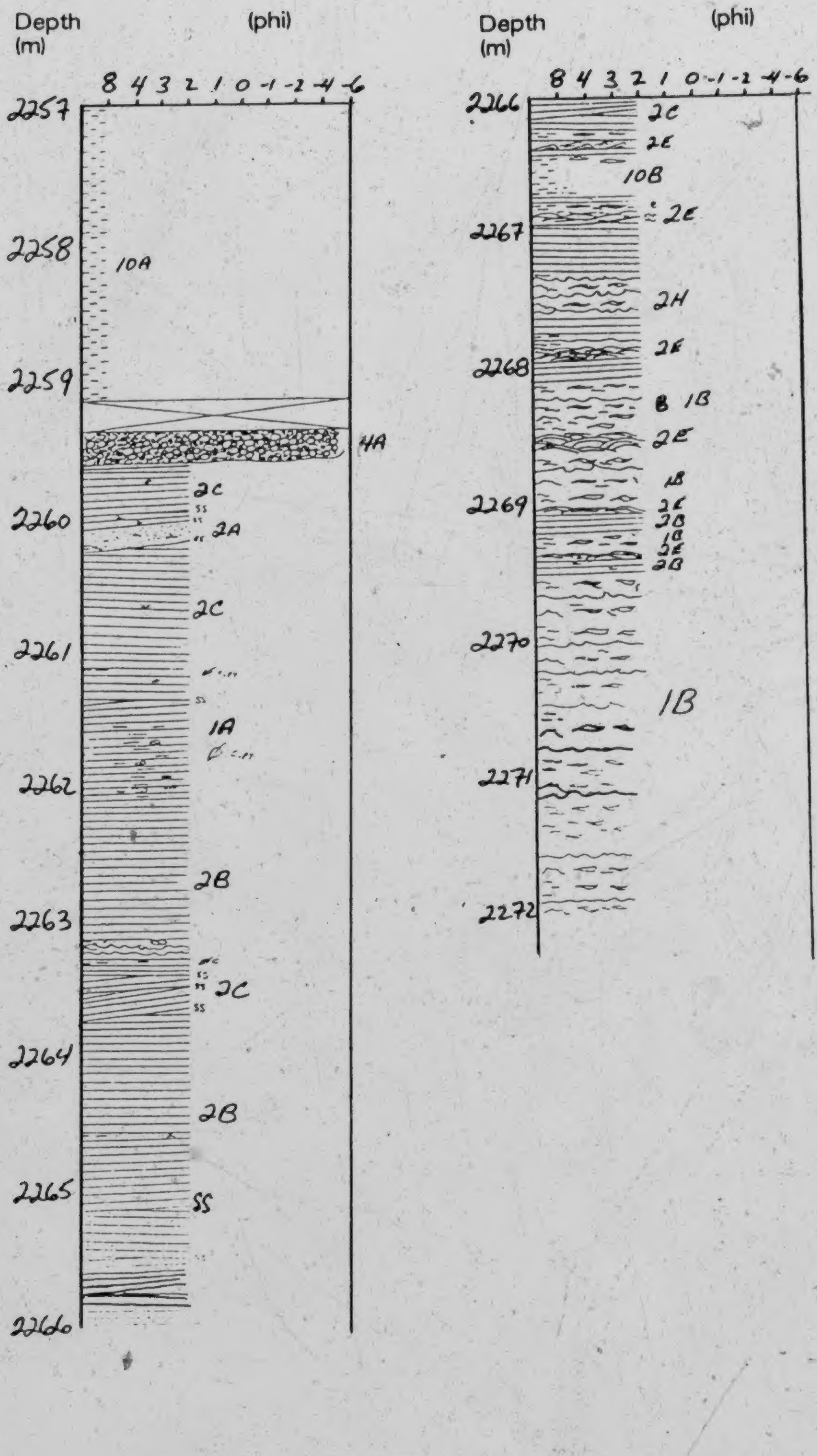
Depth (m)
(phi)
8 4 3 2 1 0 -1 -2 -4 -6
2257
2258
2259
2260
2261
2262
2263
2264
2265
2266
10A
4A
2C
SS
2A
2C
1A
2B
2C
SS
2B
SS
Depth (m)
(phi)
8 4 3 2 1 0 -1 -2 -4 -6
2266
2267
2268
2269
2270
2271
2272
2C
2E
10B
2E
2H
2E
B 1B
2E
1B
2E
2B
1B
2E
2B
1B

11-21-35-4W5

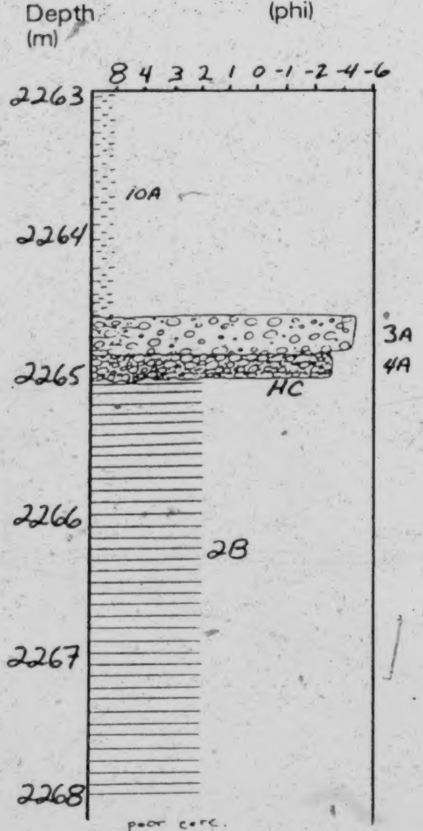
Depth (m)
(phi)
8 4 3 2 1 0 -1 -2 -4 -6
2263
2264
2265
2266
2267
2268
10A
3A
4A
HC
2B

poor core.
Questionable
Interpretation

7

11-24-35-4W5

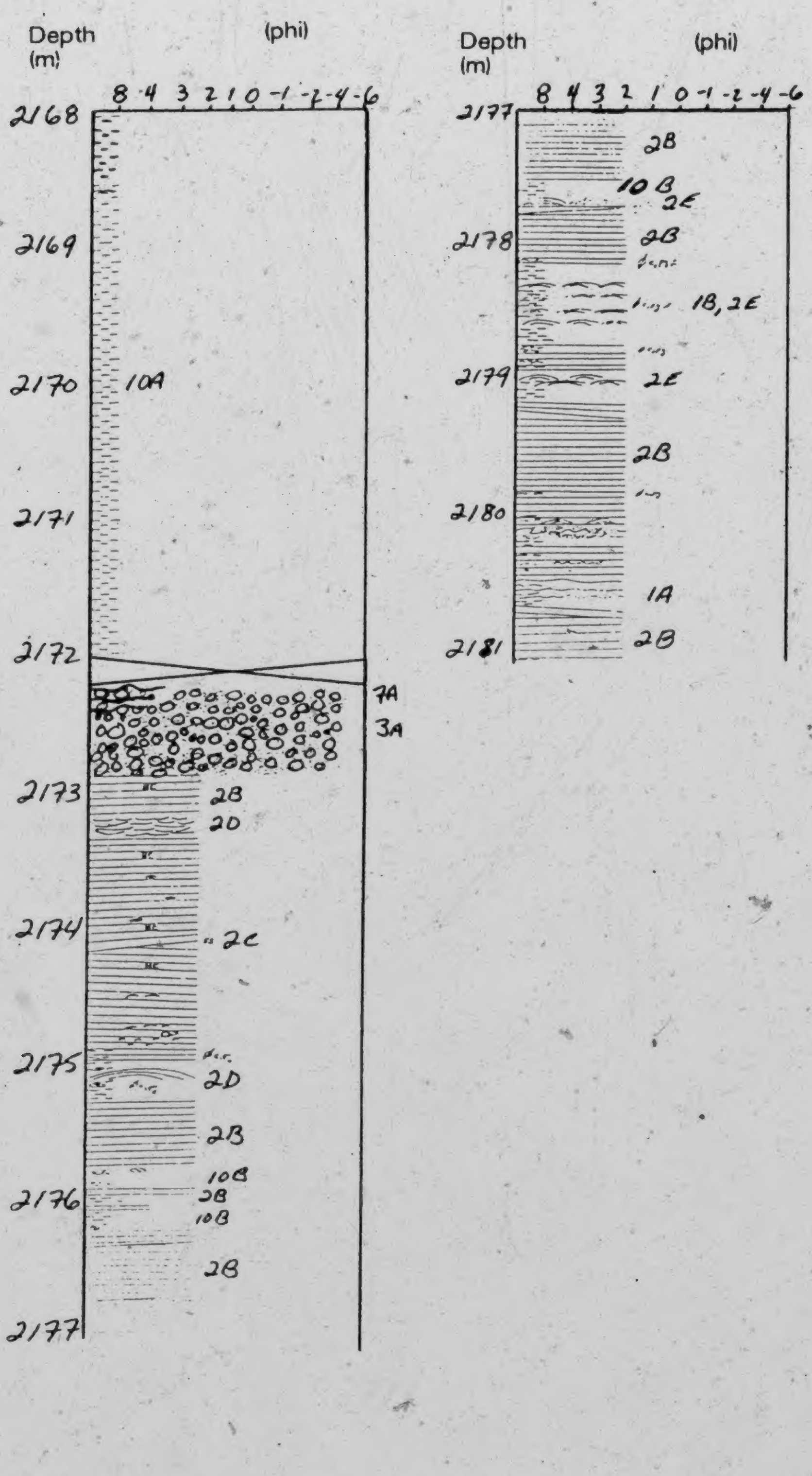
Depth (m)
(phi)
8 4 3 2 1 0 -1 -2 -4 -6
2168
2169
2170
10A
2171
2172
7A
3A
2173
2B
2D
2174
2C
2175
2D
2B
10B
2176
2B
10B
2B
2177
Depth (m)
(phi)
8 4 3 2 1 0 -1 -2 -4 -6
2177
2B
10B
2E
2178
2B
1B, 2E
2179
2E
2B
2180
1A
2181
2B

1-25-35-4W5

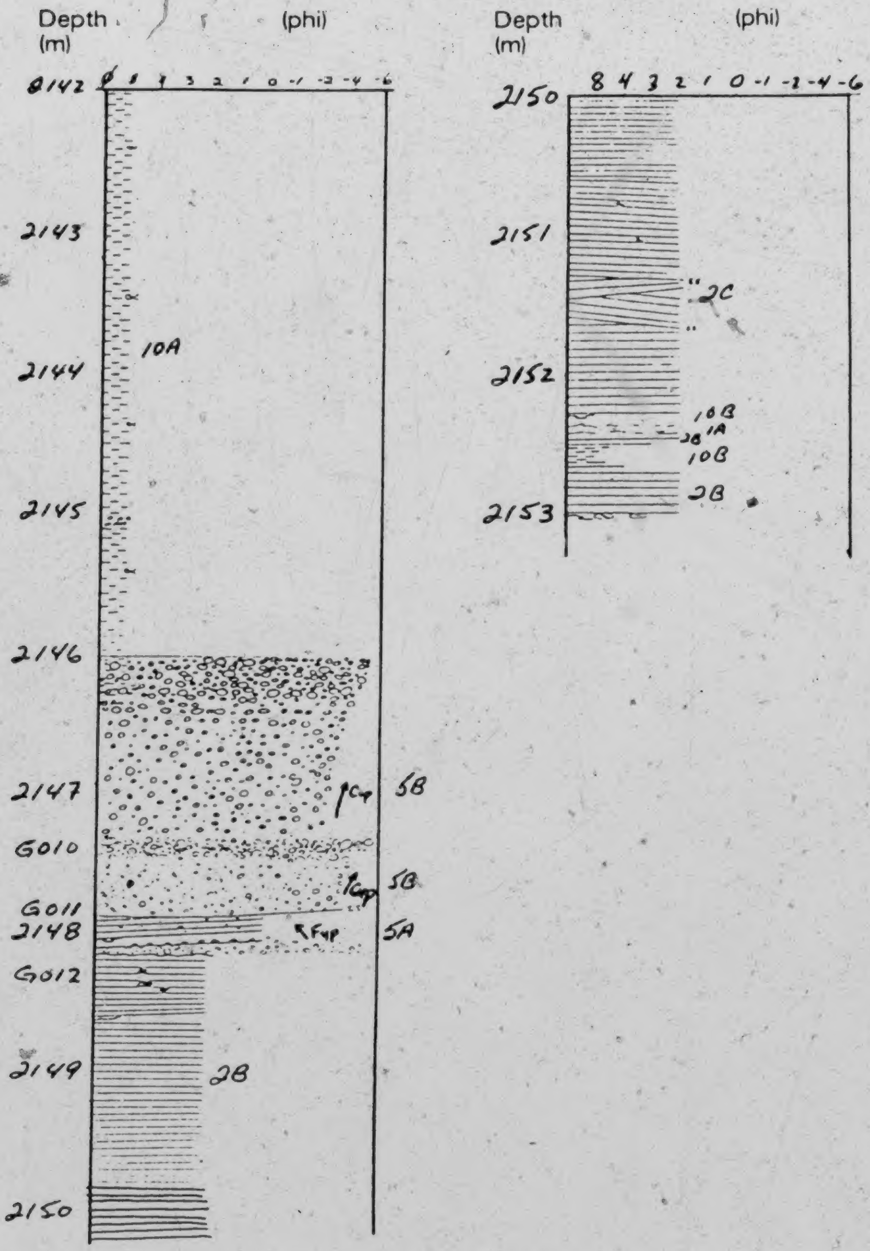
Depth (m)
(phi)
0 8 4 3 2 1 0 -1 -2 -4 -6
2142
2143
2144
2145
2146
2147
G010
G011
2148
G012
2149
2150
10A
Cp
5B
Cmp
5B
Fmp
5A
2B
Depth (m)
(phi)
8 4 3 2 1 0 -1 -2 -4 -6
2150
2151
2152
2153
2C
10B
1A
2B
10B
2B

APPENDIX B

Appendix B contains plots of gas-oil ratio (GOR) versus time for 34 wells in the Garrington Oil Field

3-24-34-3W5

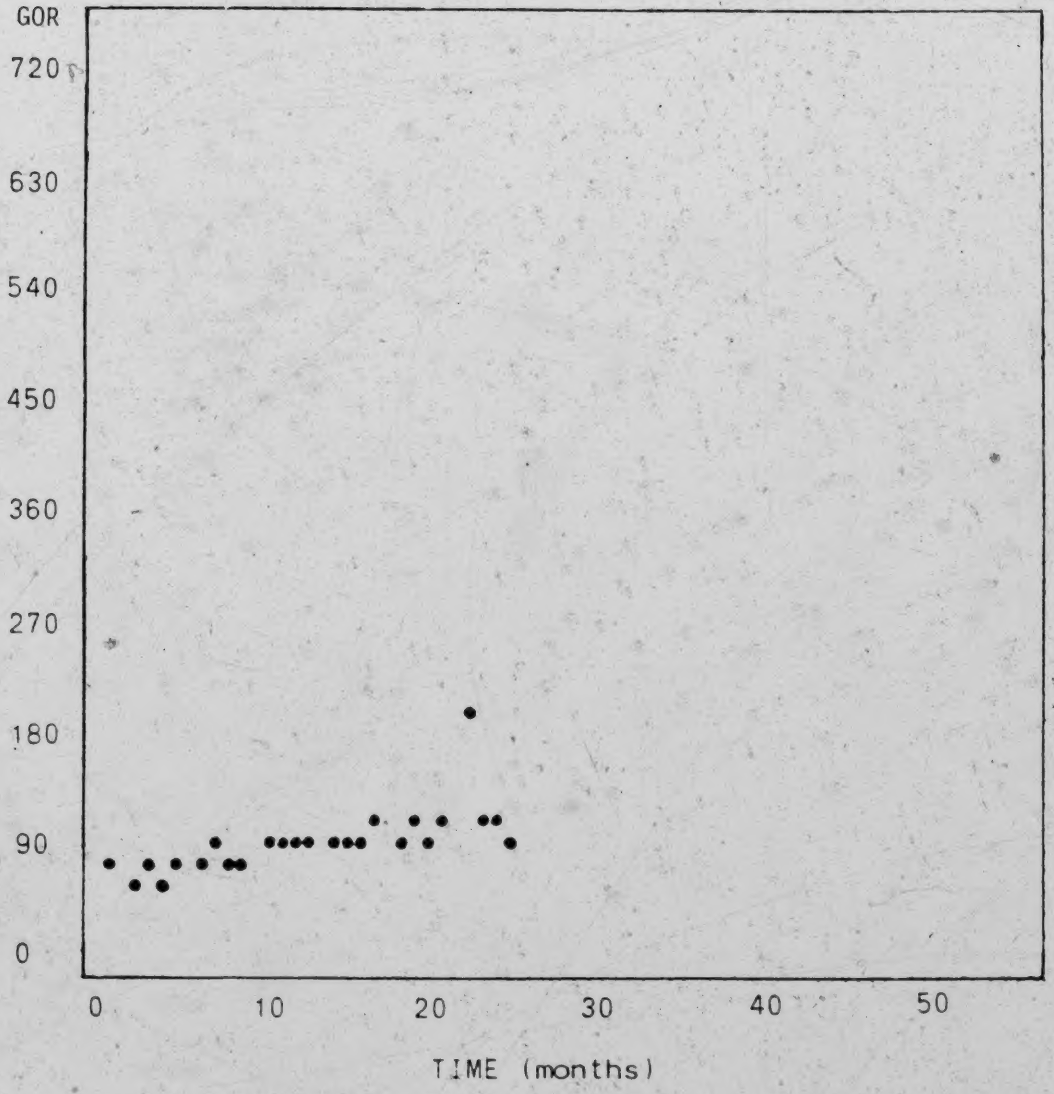

```
CORRELATION COEFFICIENT=.6555  N=25

     MEAN     ST. DEV.       REGRESSION LINE       RESIDUAL
X   13.00     7.3593      X= .19349*Y-4.5844        32.234
Y   90.88     24.934     Y= 2.2208*X+62.010       369.97
```

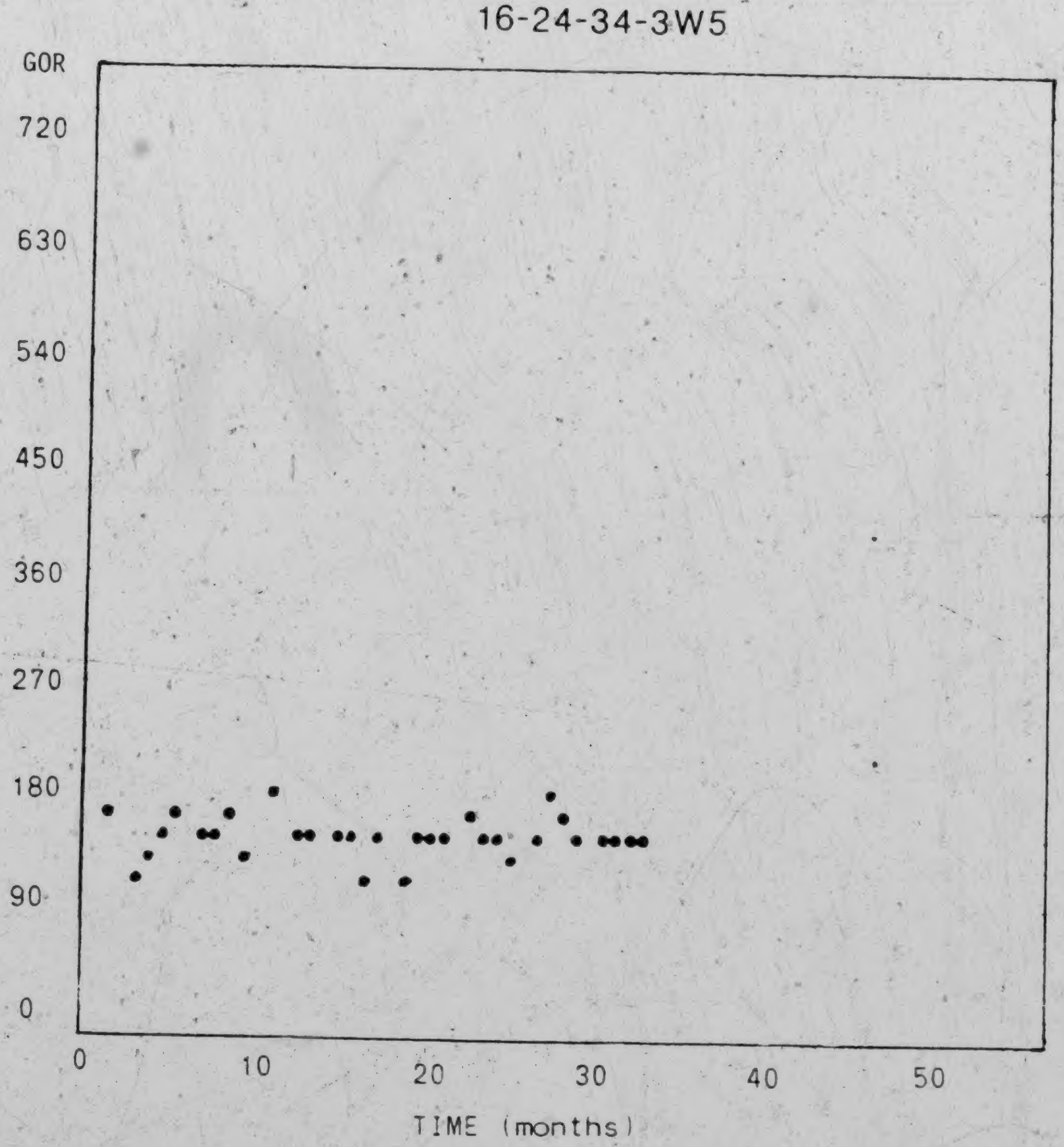

CORRELATION COEFFICIENT=.0241 N=32

```
   MEAN     ST. DEV.      REGRESSION LINE        RESIDUAL
X  17.18    9.7631      X= .01521*Y+14.990        98.439
Y  144.4    15.450      Y= .03810*X+143.75        246.51
```

16-25-34-3W5

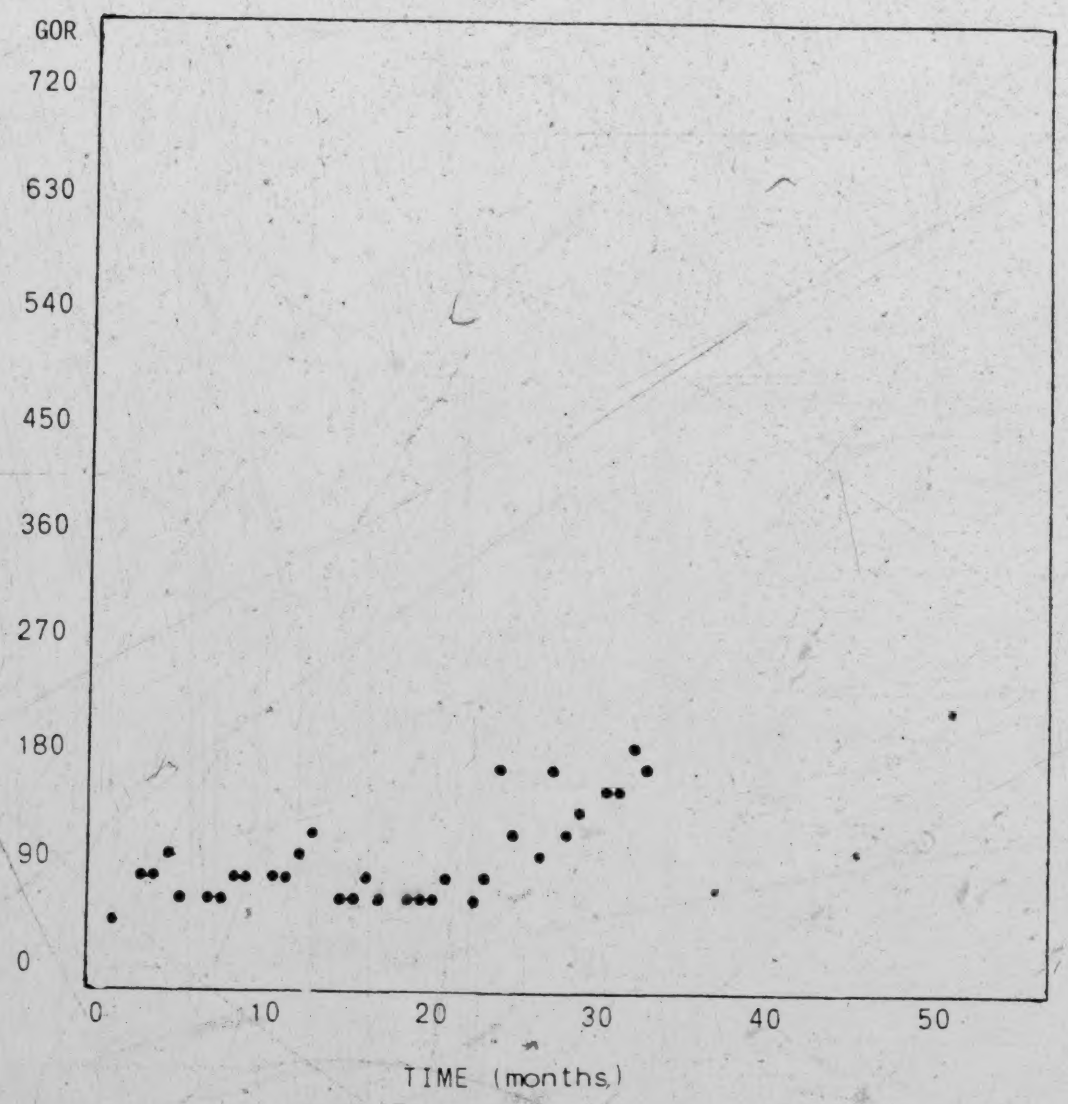

```
CORRELATION COEFFICIENT=.7114   N=33

     MEAN      ST. DEV.      REGRESSION LINE        RESIDUAL
X   17.00      9.6695      X= .18183*Y+1.1861        47.674
Y   86.97      37.830      Y= 2.7831*X+39.657        729.68
```

16-34-34-3W5

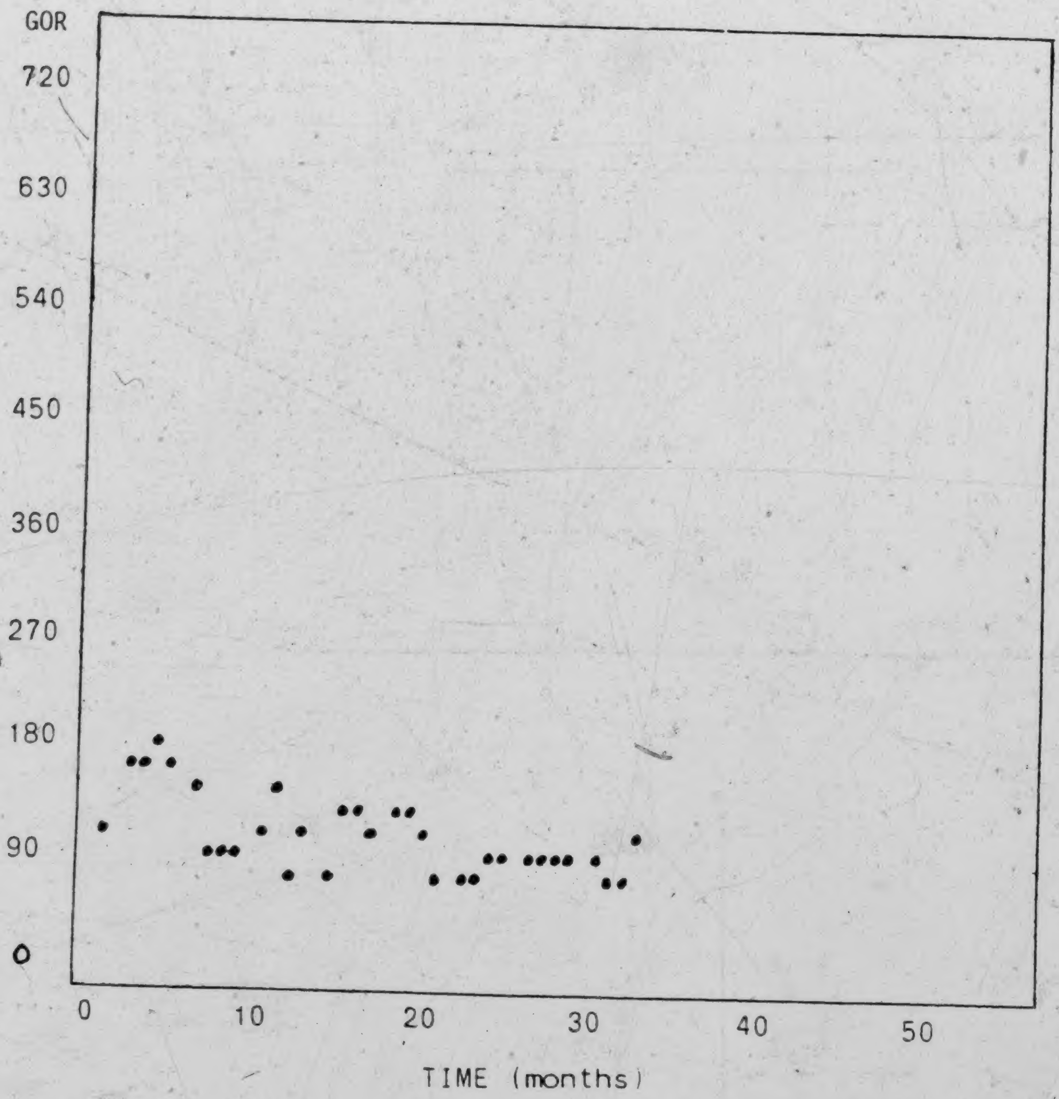

```
CORRELATION COEFFICIENT=-.5906   N=33

     MEAN      ST. DEV.      REGRESSION LINE        RESIDUAL
X   17.00      9.6695      X=-.18704*Y+36.968       62.855
Y   106.7      30.531      Y=-1.8646*X+138.46       626.62
```

6-35-34-3W5

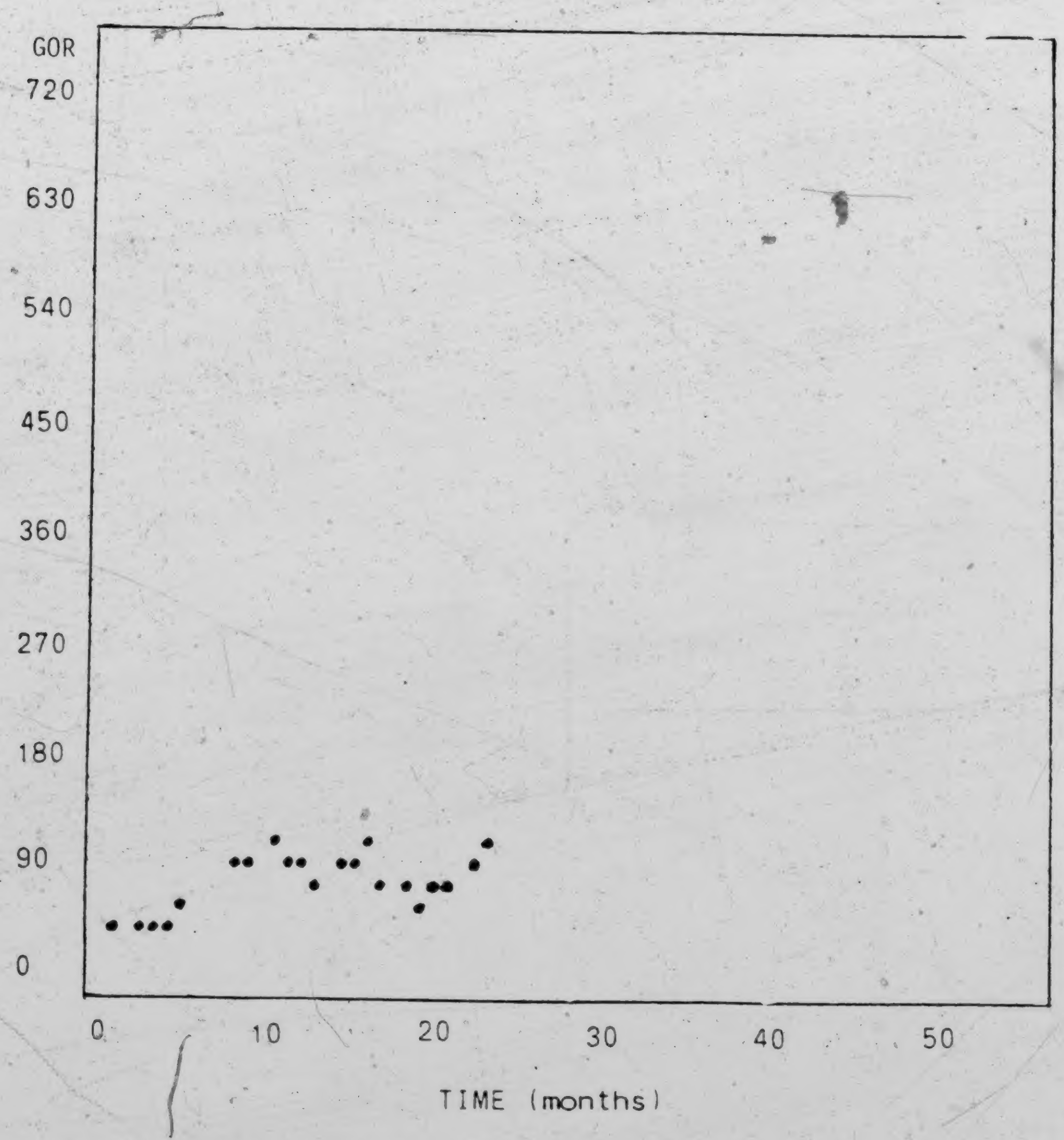

CORRELATION COEFFICIENT=.5573 N=21

```
    MEAN     ST. DEV.      REGRESSION LINE       RESIDUAL
X  12.52     6.8747      X= .15563*Y+.98267      34.296
Y  72.28     24.662      Y= 1.9994*X+49.246      441.36
```

16-35-34-3W5

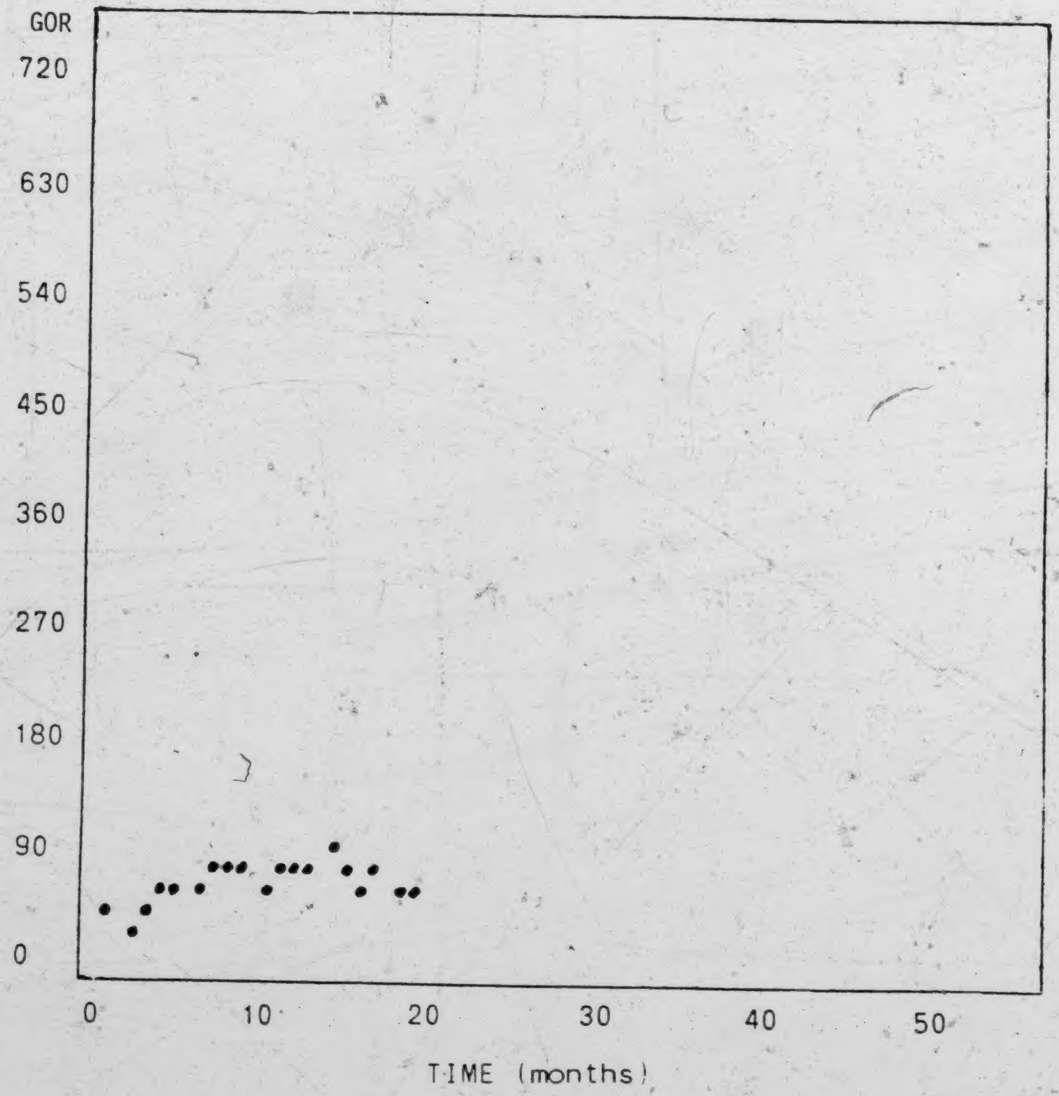

```
CORRELATION COEFFICIENT=.7022  N=19

     MEAN      ST. DEV.      REGRESSION LINE       RESIDUAL
X   10.00      5.6273      X= .24374*Y-4.0982       16.998
Y   57.84      16.211      Y= 2.0228*X+37.614       141.07
```

7-36-34-3W5

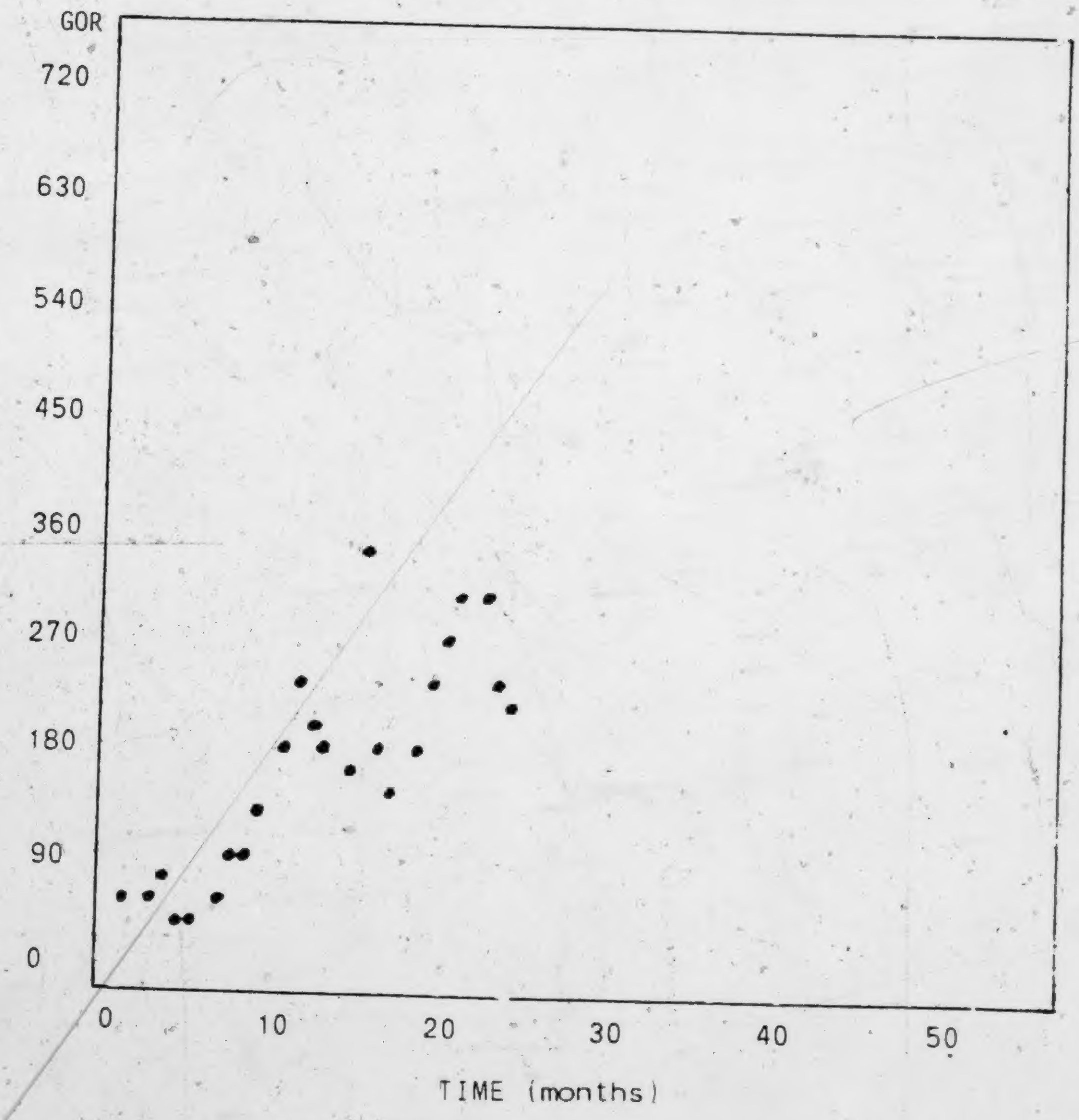

```
CORRELATION COEFFICIENT=.8389  N=24

     MEAN     ST. DEV.       REGRESSION LINE        RESIDUAL
X   12.50     7.0711     X= .04655*Y+1.9197          15.484
Y   163.9     91.903     Y= 10.903*X+27.623          2615.6
```

14-36-34-3W5

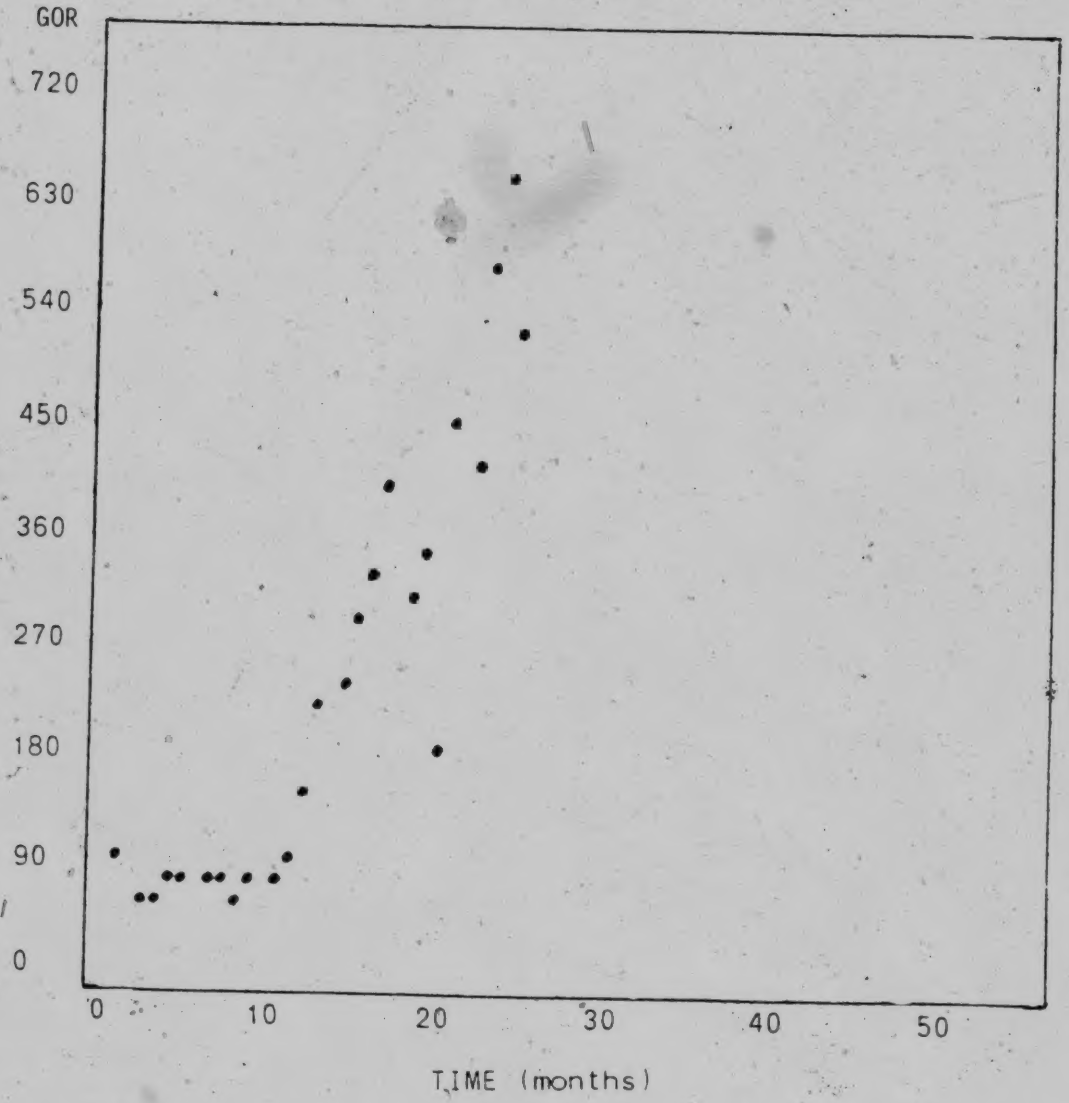

```
CORRELATION COEFFICIENT=.8984  N=25

     MEAN     ST. DEV.      REGRESSION LINE        RESIDUAL
X   13.00     7.3598     X= .03572*Y+4.7218         10.899
Y   231.7     185.09     Y= 22.594*X-62.000         6893.3
```

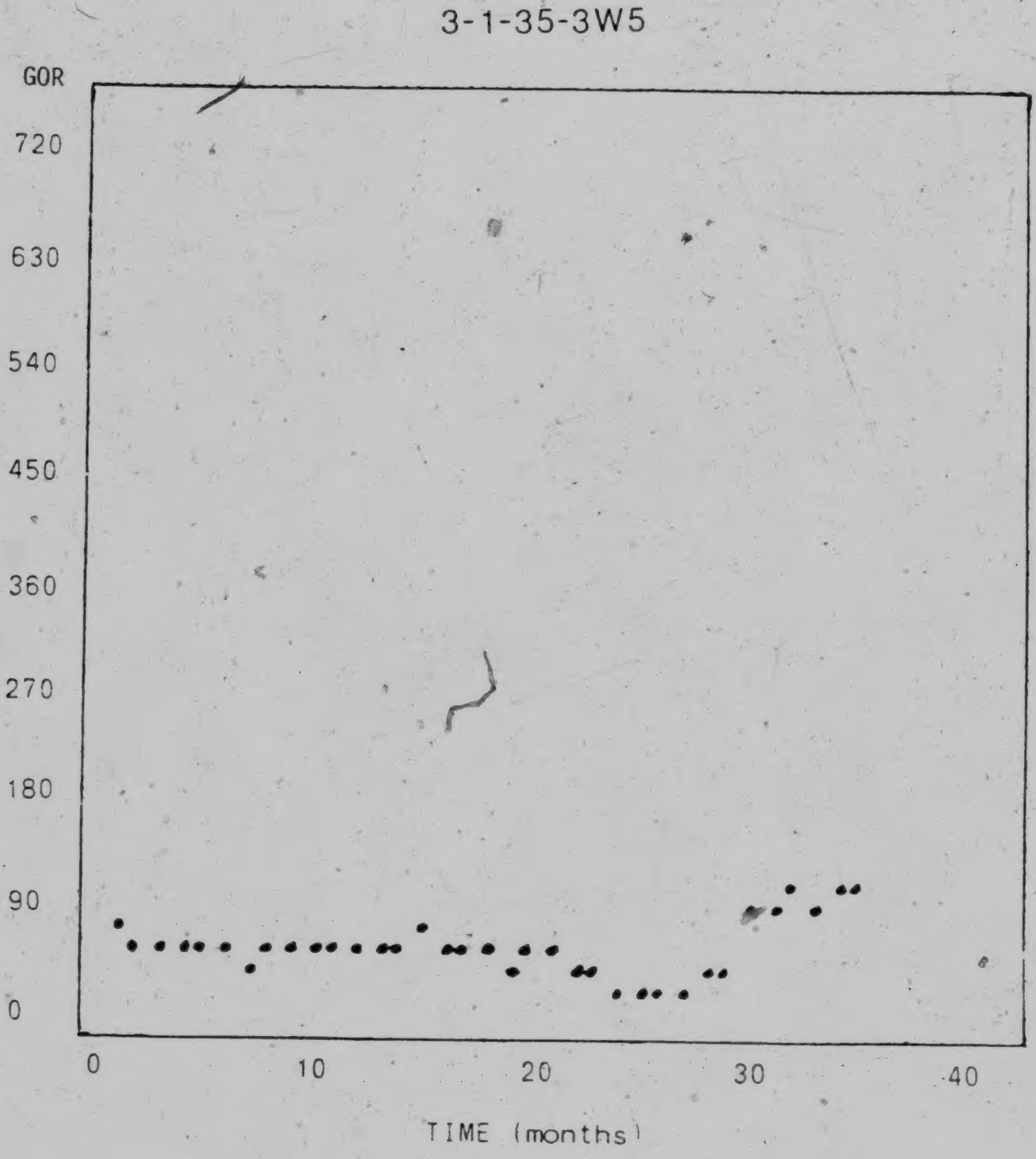

CORRELATION COEFFICIENT=.3342 N=35

```
     MEAN     ST. DEV.      REGRESSION LINE       RESIDUAL
X   18.00    10.247      X= .14764*Y+10.028       96.102
Y   54.00    23.192      Y= .75631*X+40.386       492.30
```

10-1-35-3W5

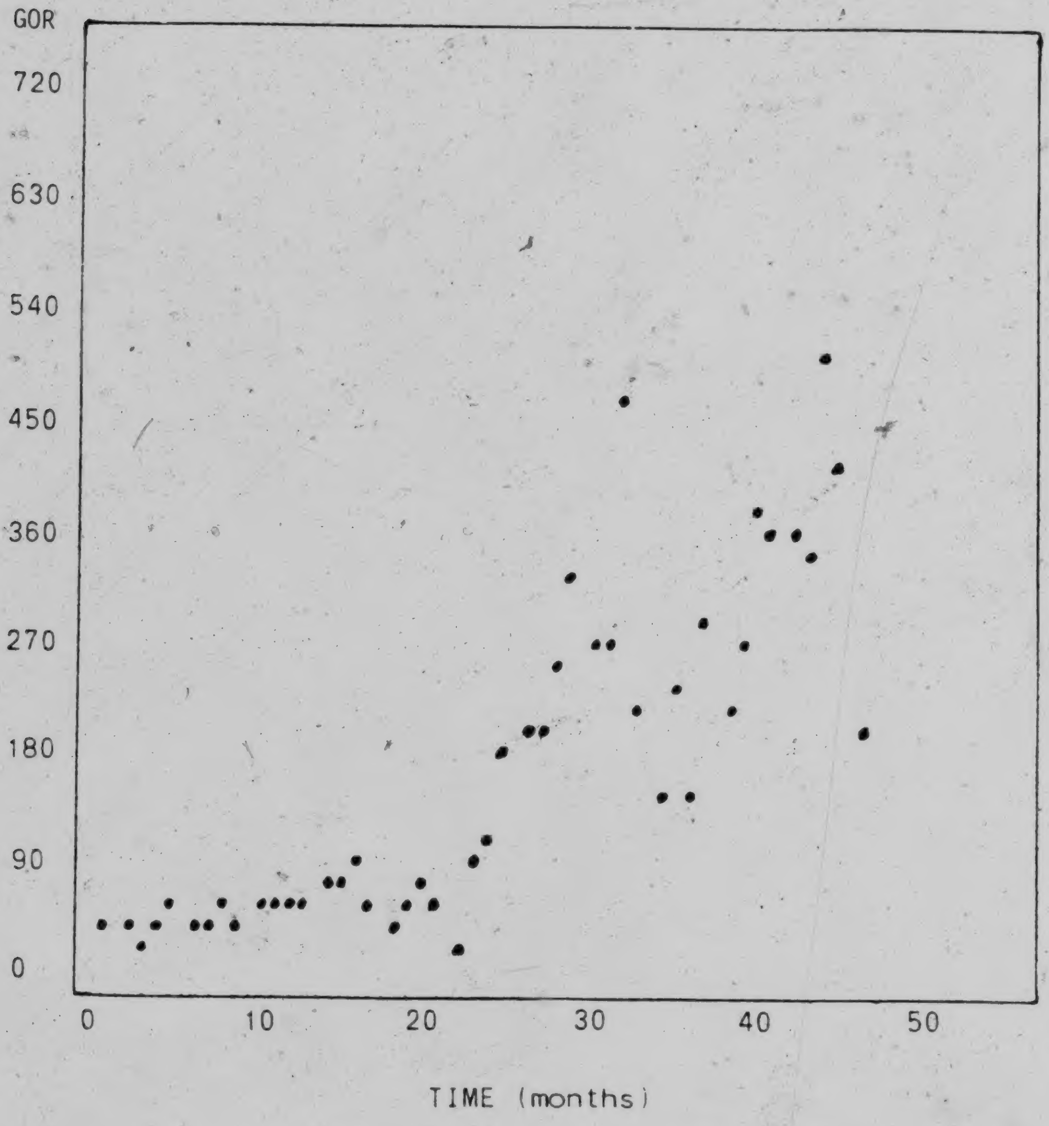

```
CORRELATION COEFFICIENT=.8395  N=46

    MEAN     ST. DEV.     REGRESSION LINE       RESIDUAL
X  23.50     13.423     X= .08328*Y+9.9539      54.386
Y  162.6     135.31     Y= 8.4633*X-36.235      5526.8
```

6-2-35-3W5

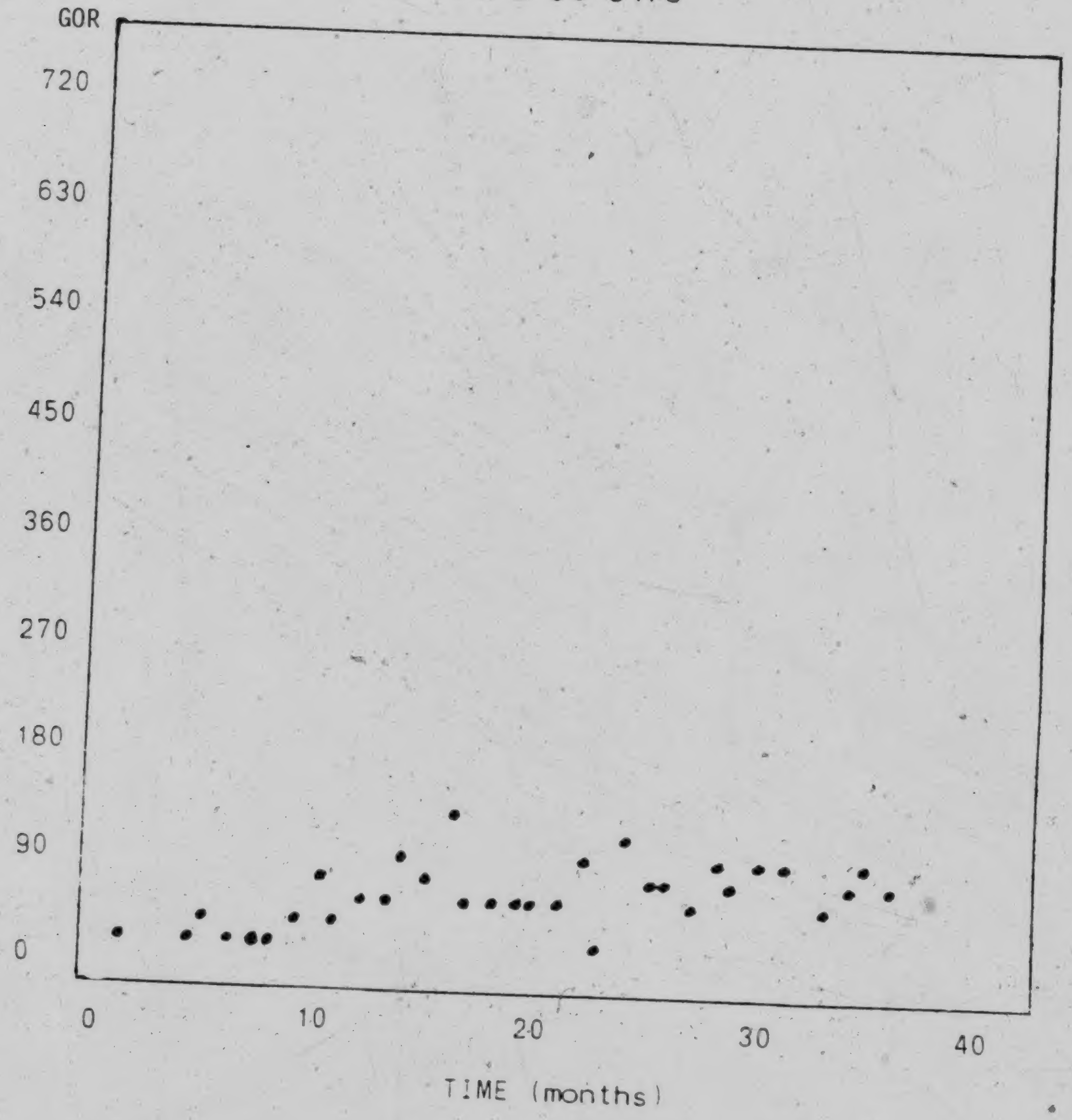

```
CORRELATION COEFFICIENT=.5694   N=33

     MEAN      ST. DEV.        REGRESSION LINE        RESIDUAL
X   19.08      9.9685       X= .20346*Y+6.9517         69.321
Y   59.51      27.897       Y= 1.5934*X+29.143         542.91
```

10-2-35-3W5

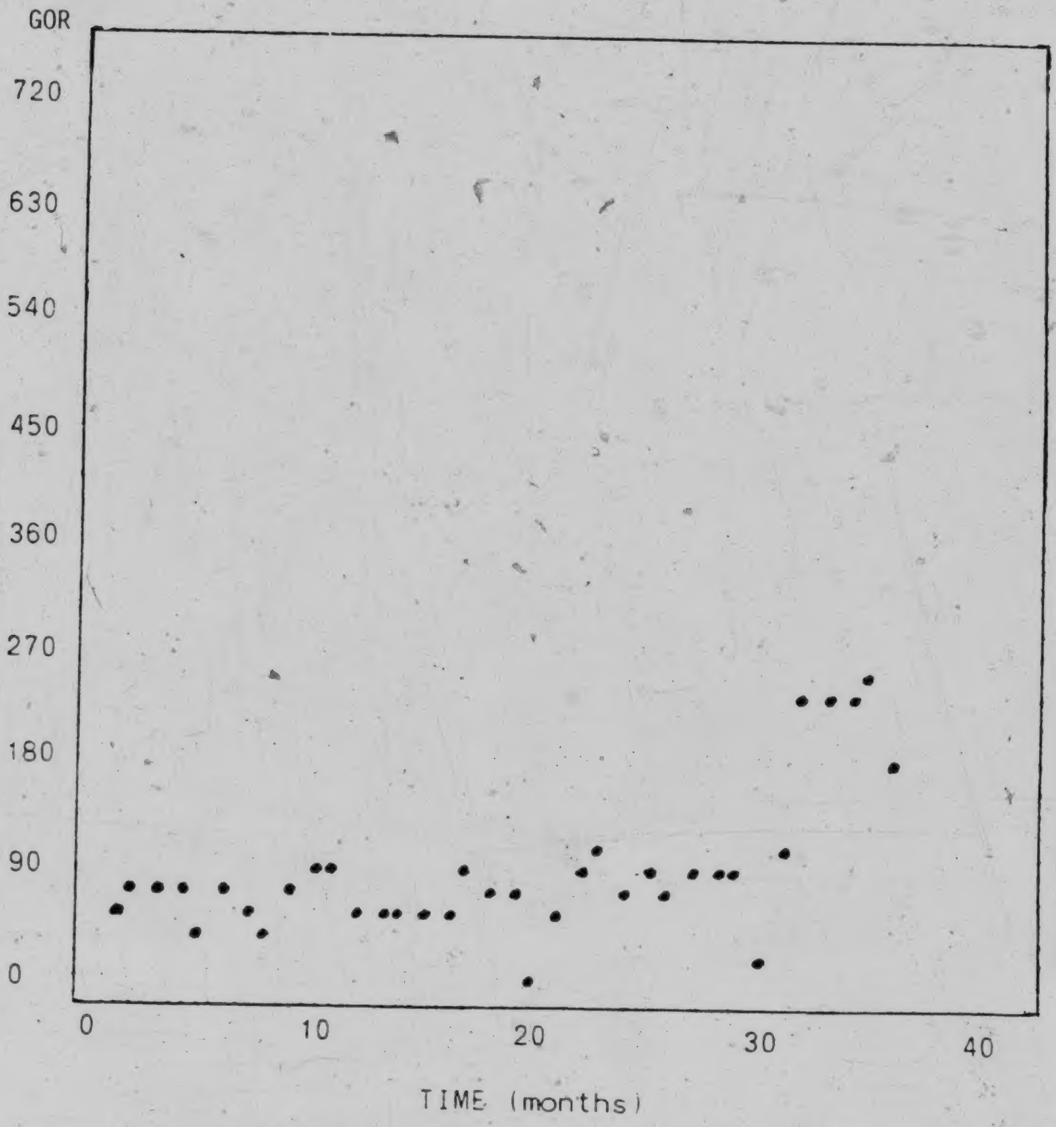

```
CORRELATION COEFFICIENT=.6169  N=36

     MEAN      ST. DEV.      REGRESSION LINE        RESIDUAL
X   18.50     10.536      X=  .10323*Y+9.1521       70.778
Y   90.55     62.963      Y= 3.6867*X+22.351        2527.8
```

14-2-35-3W5

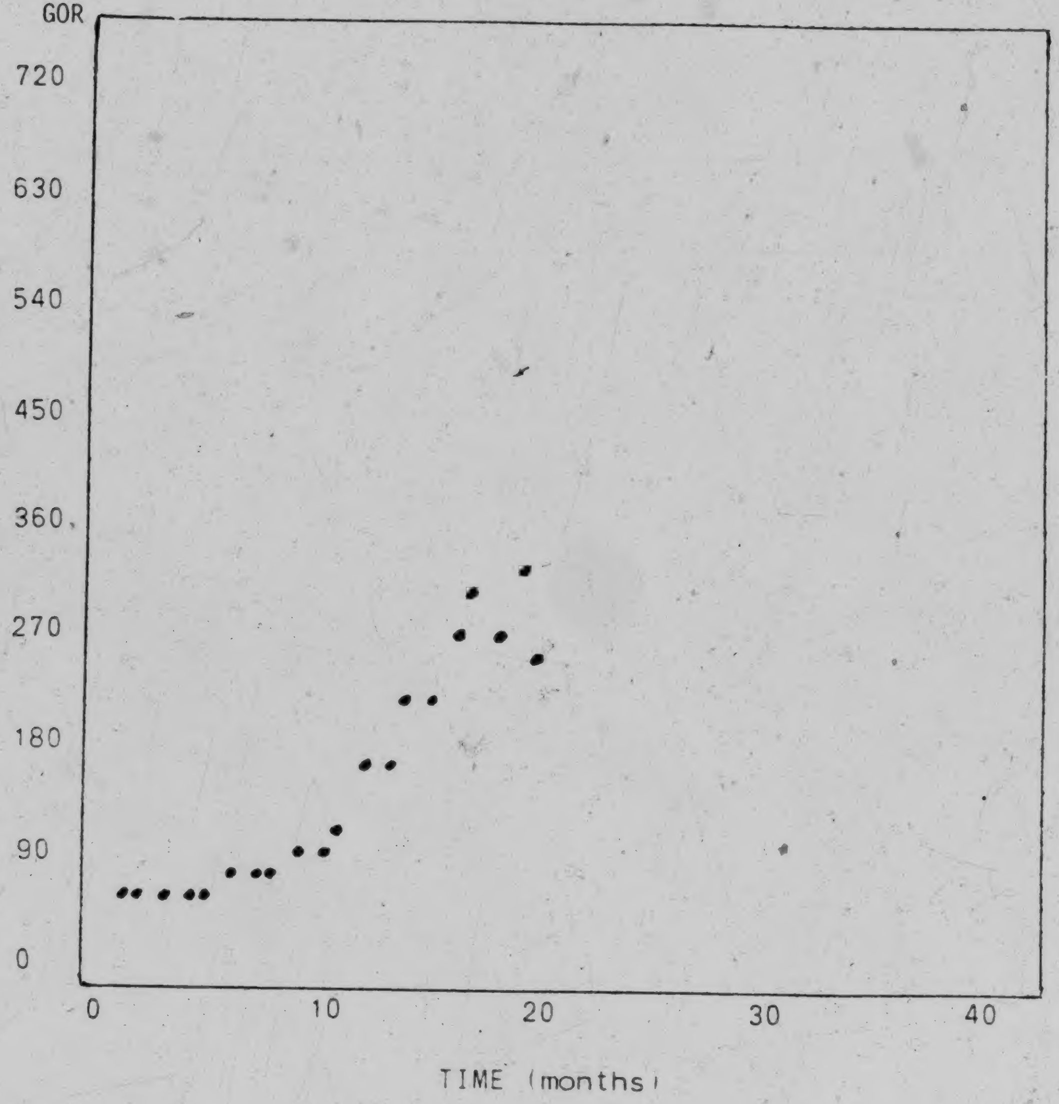

CORRELATION COEFFICIENT=.3969 N=20

	MEAN	ST. DEV.	REGRESSION LINE	RESIDUAL
X	10.50	5.9161	X= .05799*Y+1.9403	4.5193
Y	147.6	95.580	Y= 15.137*X-11.337	1178.2

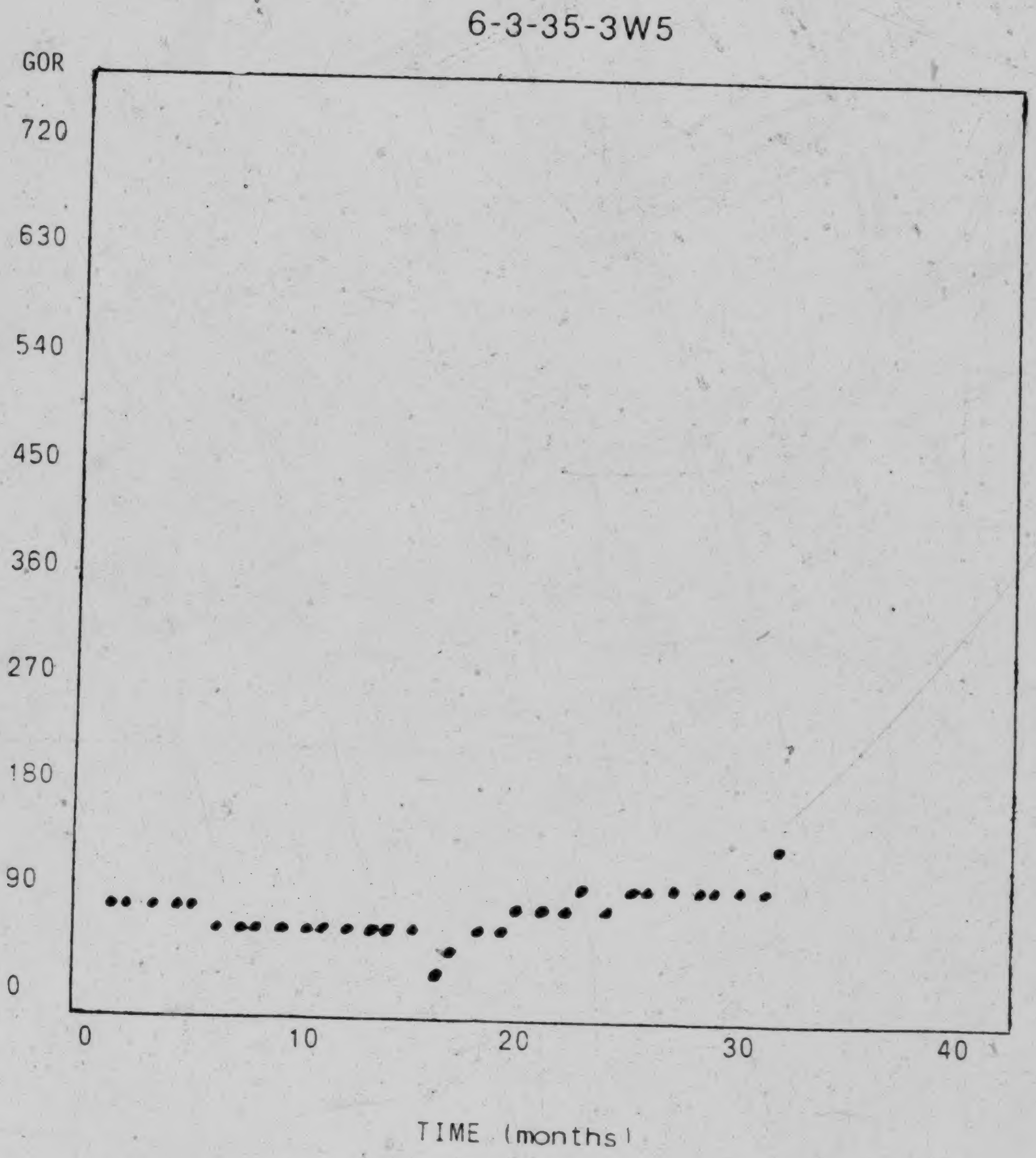

CORRELATION COEFFICIENT=.6135 N=32

```
     MEAN      ST. DEV.       REGRESSION LINE        RESIDUAL
X   16.50      9.3808       X= .26721*Y-1.7119       56.706
Y   68.15      21.538       Y= 1.4085*X+44.915       298.93
```

9-3-35-3W5

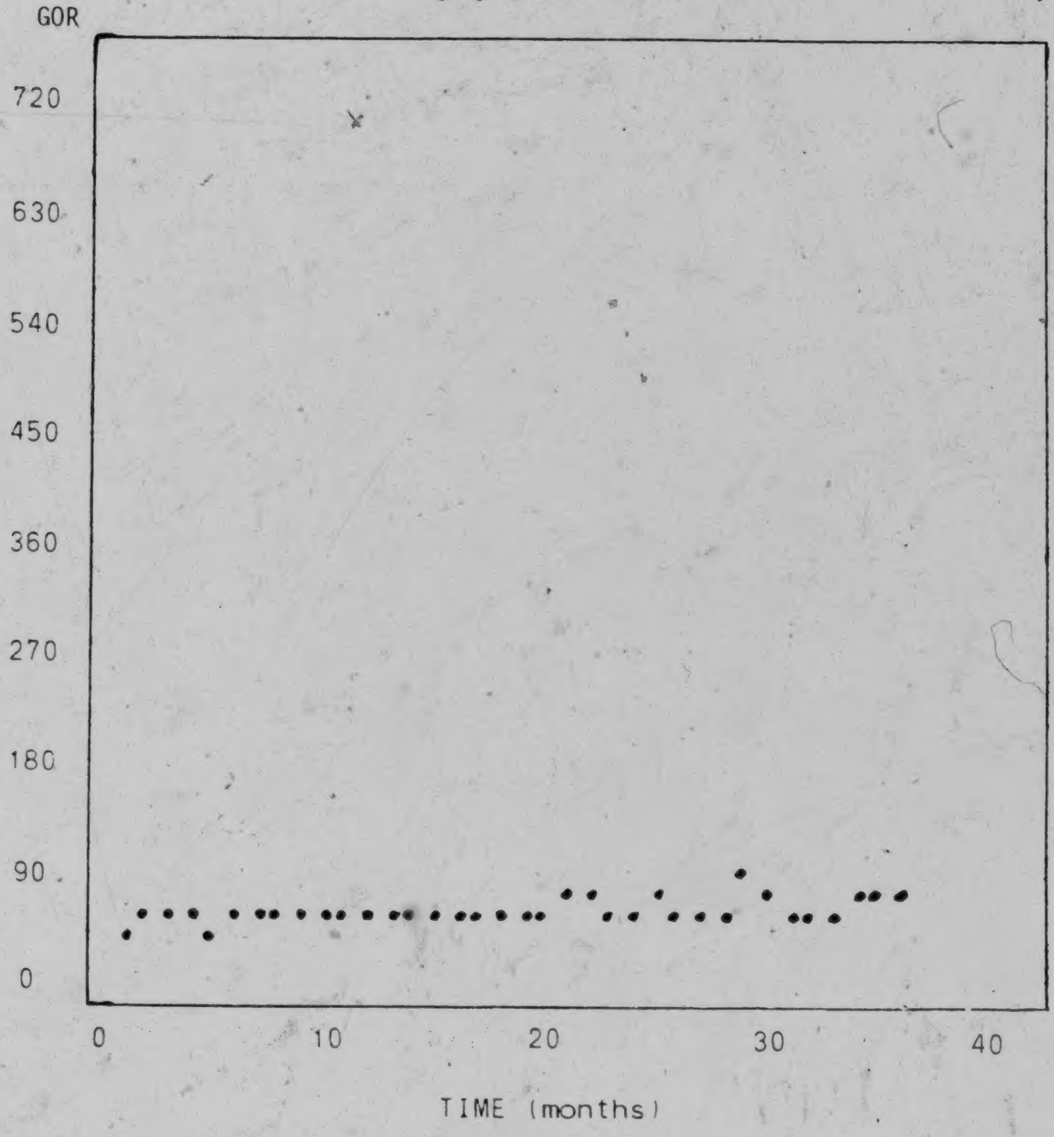

```
CORRELATION COEFFICIENT=.7051  N=36

     MEAN     ST. DEV.      REGRESSION LINE       RESIDUAL
X   18.50     10.536     X= .69186*Y-19.725       57.460
Y   55.25     10.737     Y= .71854*X+41.957       59.675
```

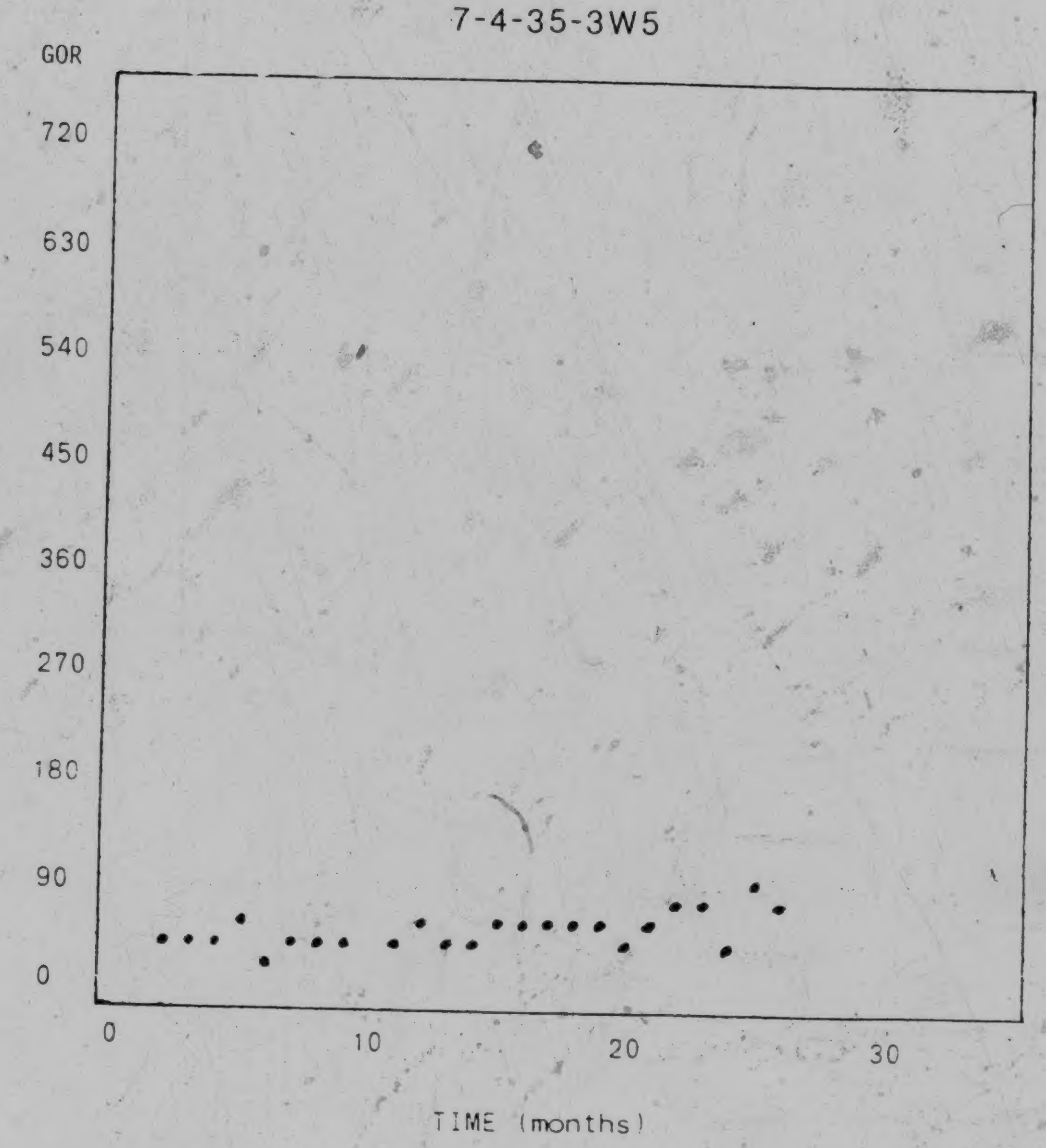

```
CORRELATION COEFFICIENT=.6861  N=26

    MEAN     ST. DEV.     REGRESSION LINE       RESIDUAL
X  14.16     7.4697      X= .36898*Y-3.6369      30.877
Y  48.25     13.889      Y= 1.2756*X+30.179      106.74
```

12-4-35-3W5

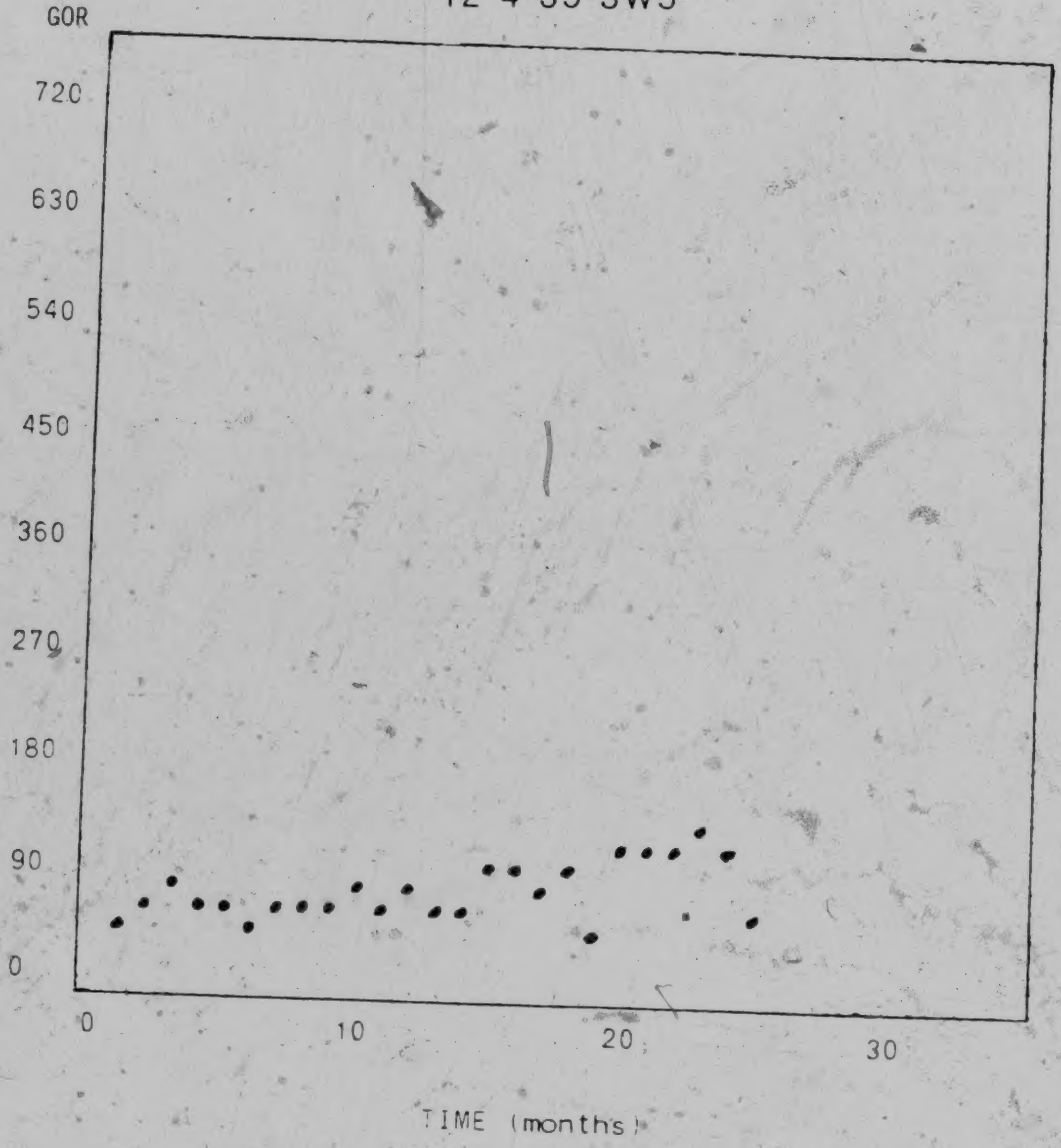

```
CORRELATION COEFFICIENT=.7007  N=25

   MEAN      ST. DEV.      REGRESSION LINE        RESIDUAL
X  13.00     7.3598      X= .21832*Y-1.9939        28.767
Y  68.68     23.623      Y= 2.2492*X+39.440        296.38
```

6-5-35-3W5

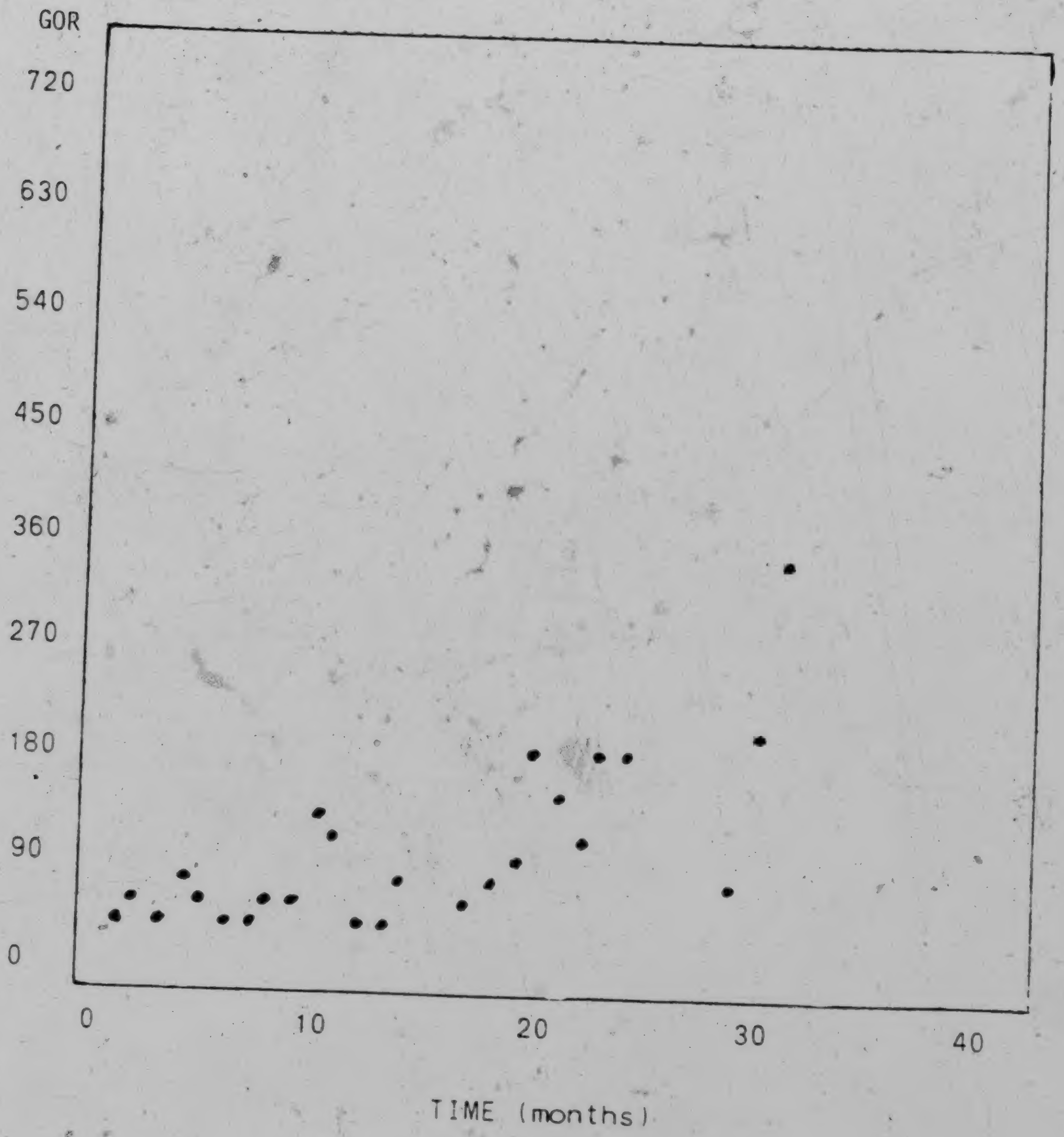

```
CORRELATION COEFFICIENT=.7286  N=25

    MEAN     ST. DEV.     REGRESSION LINE         RESIDUAL
X   14.36    9.0502     X= .09062*Y+5.5483        40.100
Y   97.24    72.764     Y= 5.8577*X+13.123        2592.2
```

6-8-35-3W5

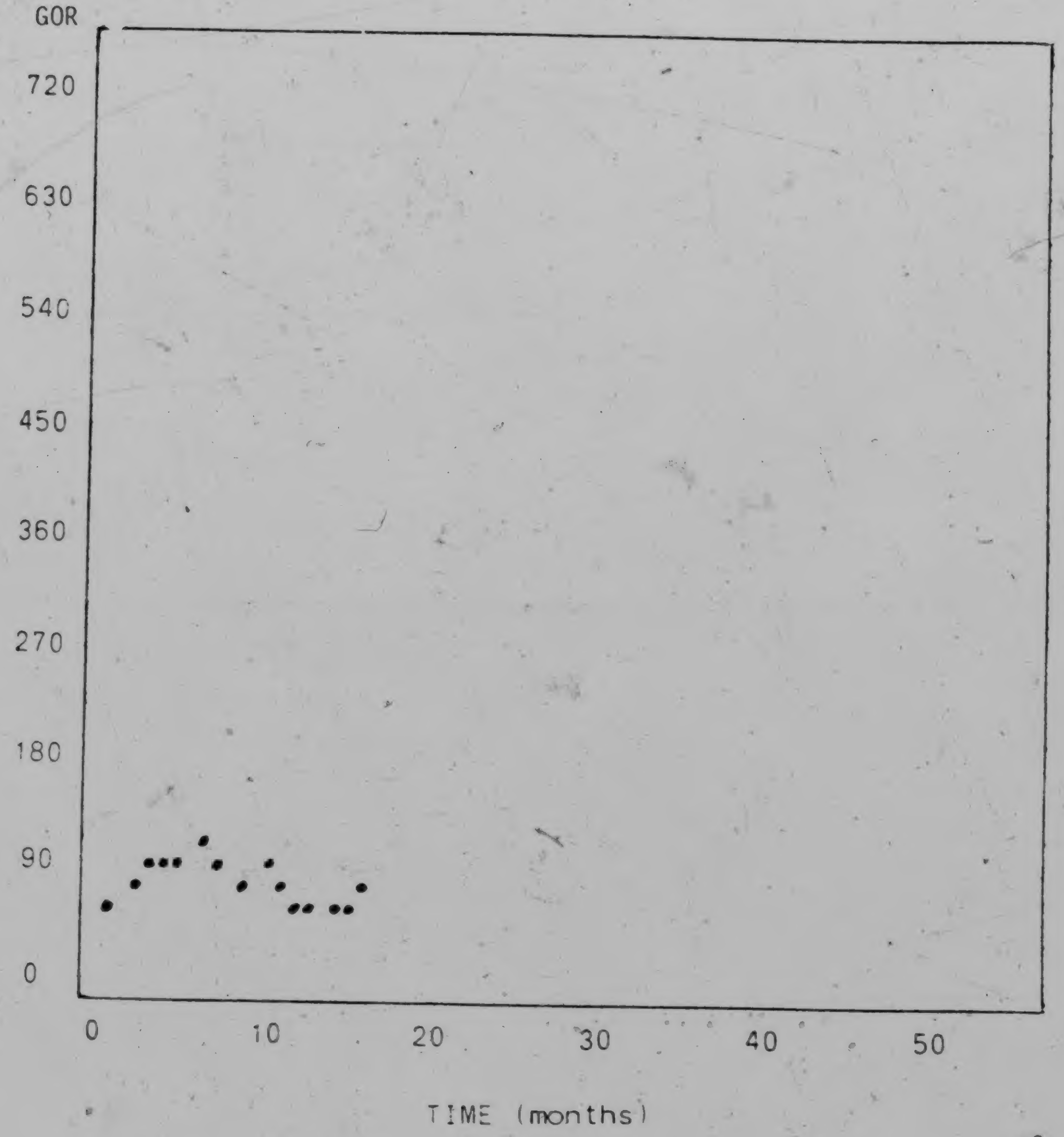

CORRELATION COEFFICIENT=-.3256 N=15

	MEAN	ST. DEV.	REGRESSION LINE	RESIDUAL
X	8.700	4.7610	X=-.06879*Y+12.872	21.711
Y	63.62	24.687	Y=-1.6882*X+83.975	583.76

8-9-35-3W5

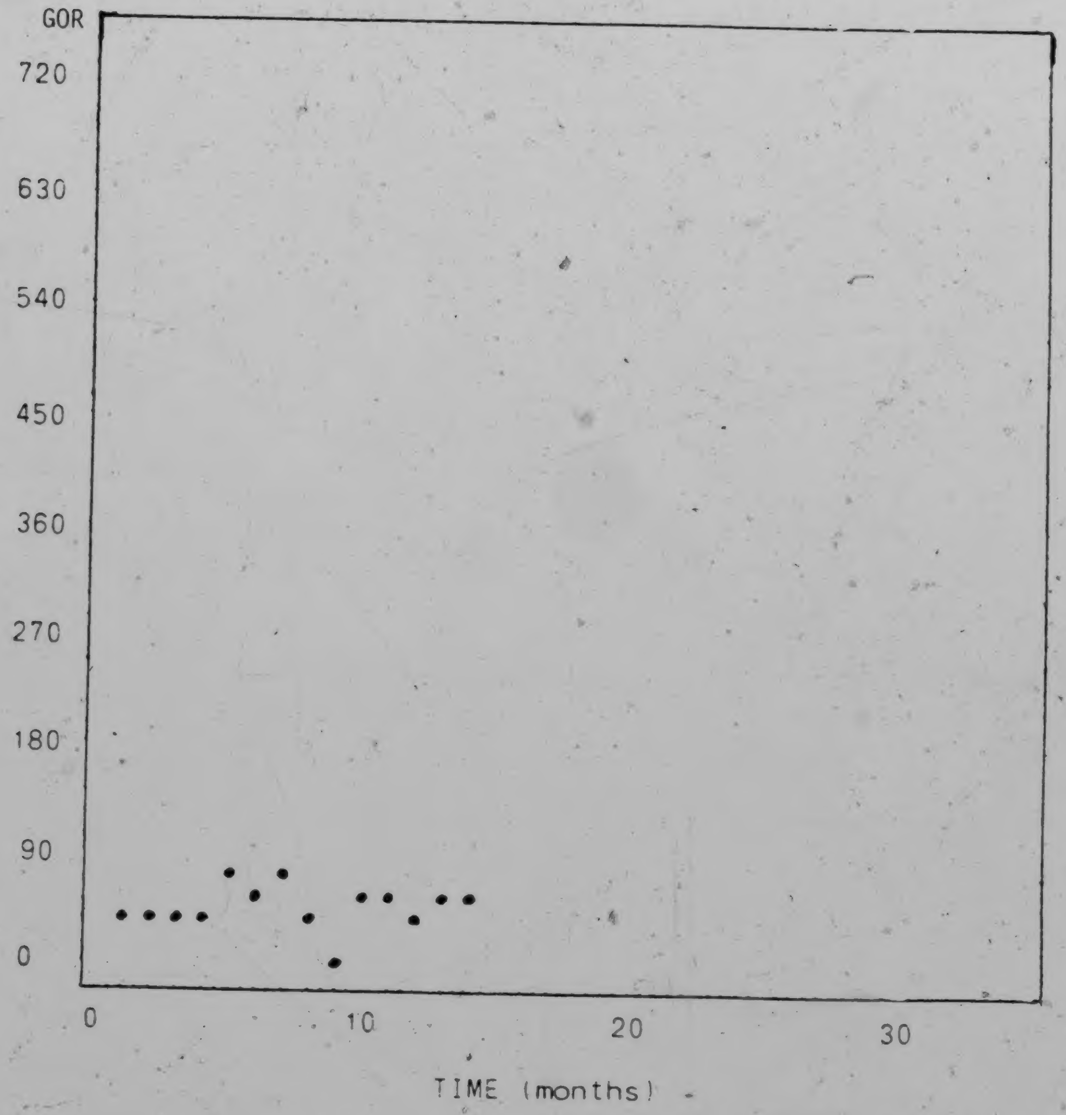

```
CORRELATION COEFFICIENT=.2616   N=14

     MEAN      ST. DEV.      REGRESSION LINE        RESIDUAL
X  7.500      4.1833      X= .06289*Y+4.7731        17.661
Y  43.35      17.399      Y= 1.0879*X+35.198        305.50
```

6-10-35-3W5

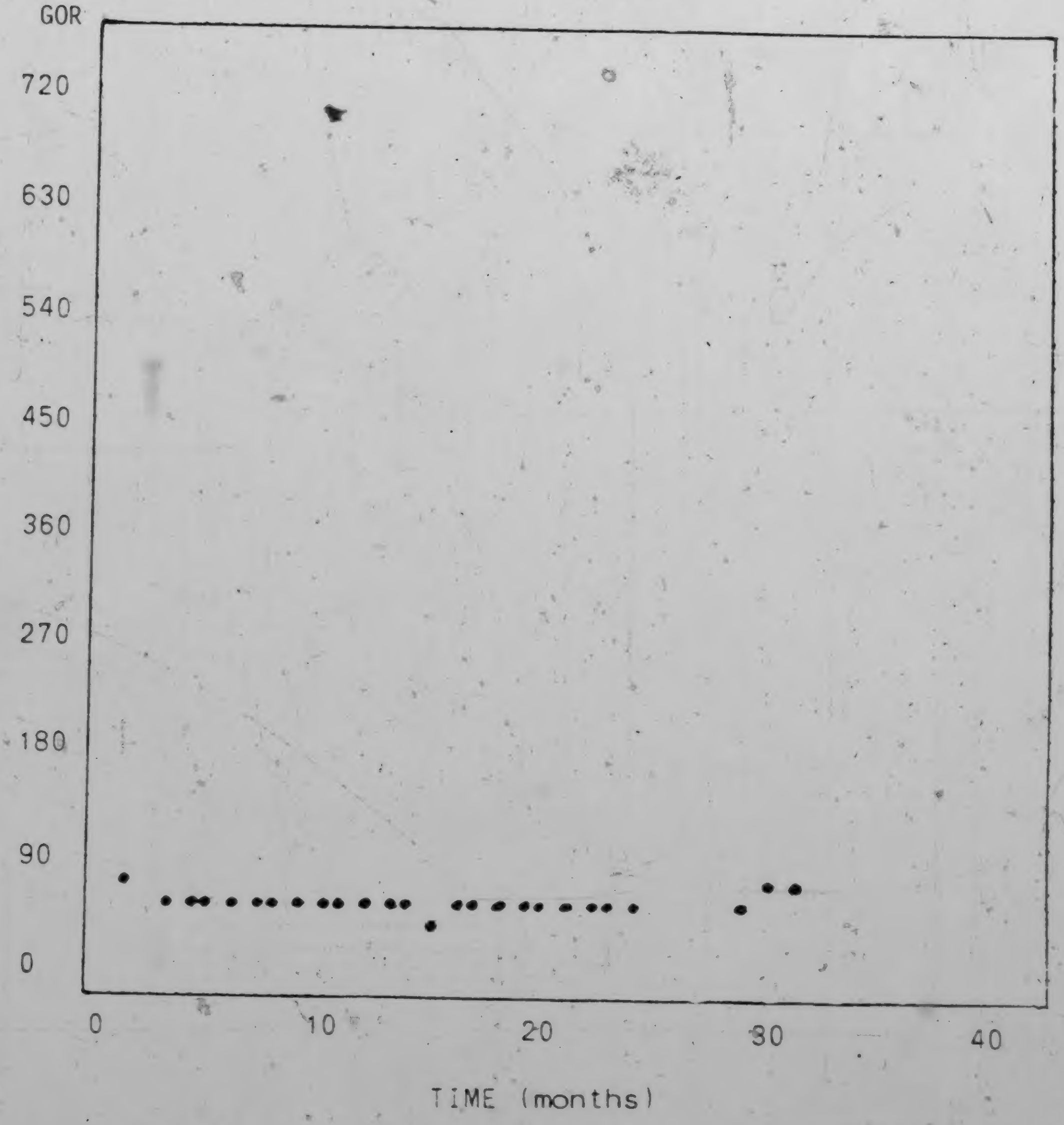

```
CORRELATION COEFFICIENT=.2654  N=26

    MEAN      ST. DEV.      REGRESSION LINE       RESIDUAL
X  14.92      8.5038     X= .32327*Y-2.3471       70.022
Y  53.42      6.9810     Y= .21786*X+50.172       47.189
```

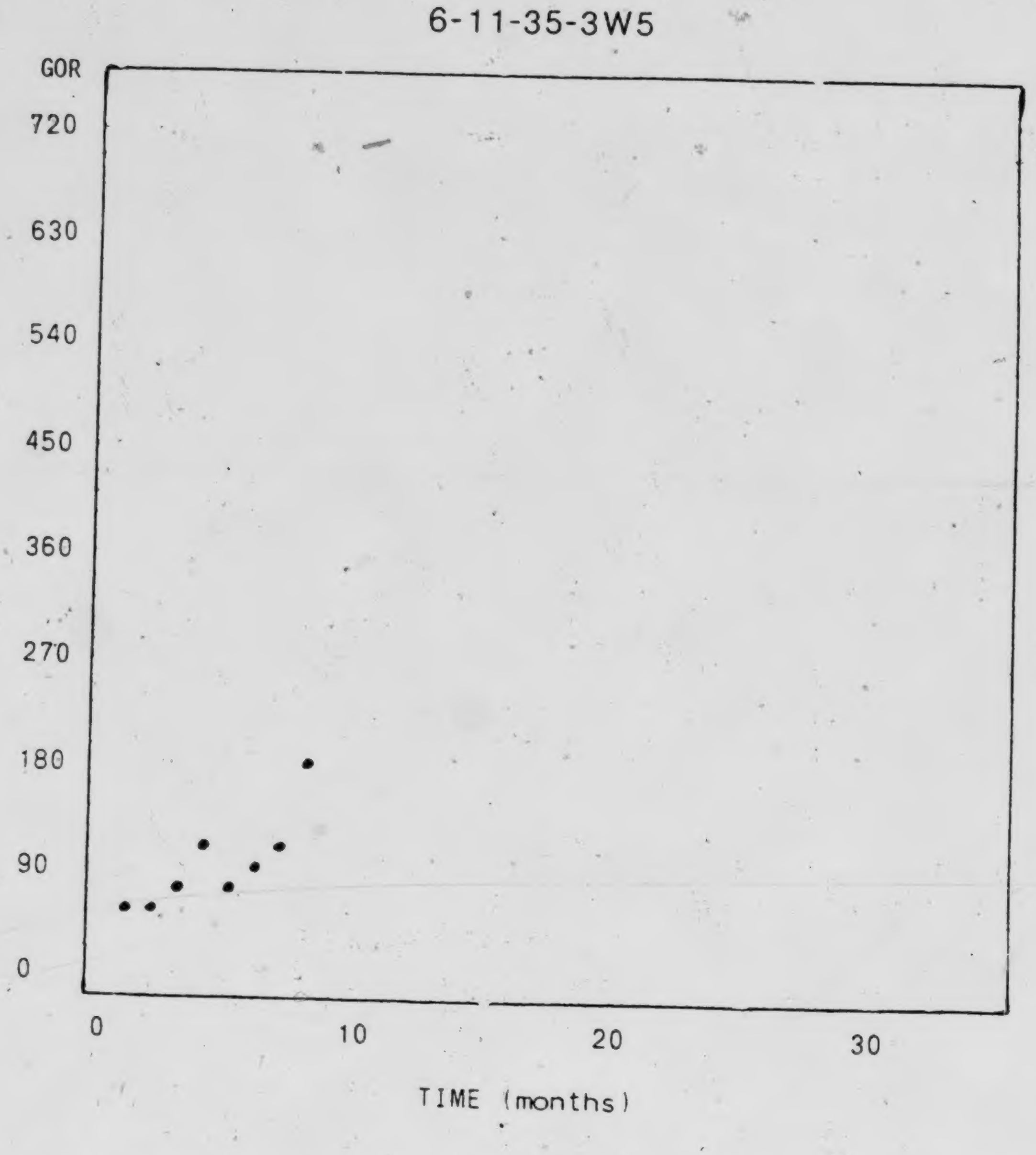

CORRELATION COEFFICIENT=.8347 N=8

```
     MEAN      ST. DEV.       REGRESSION LINE        RESIDUAL
X   4.500      2.4495      X= .05016*Y-.03278        2.1224
Y   90.37      40.767      Y= 13.893*X+27.857        587.90
```

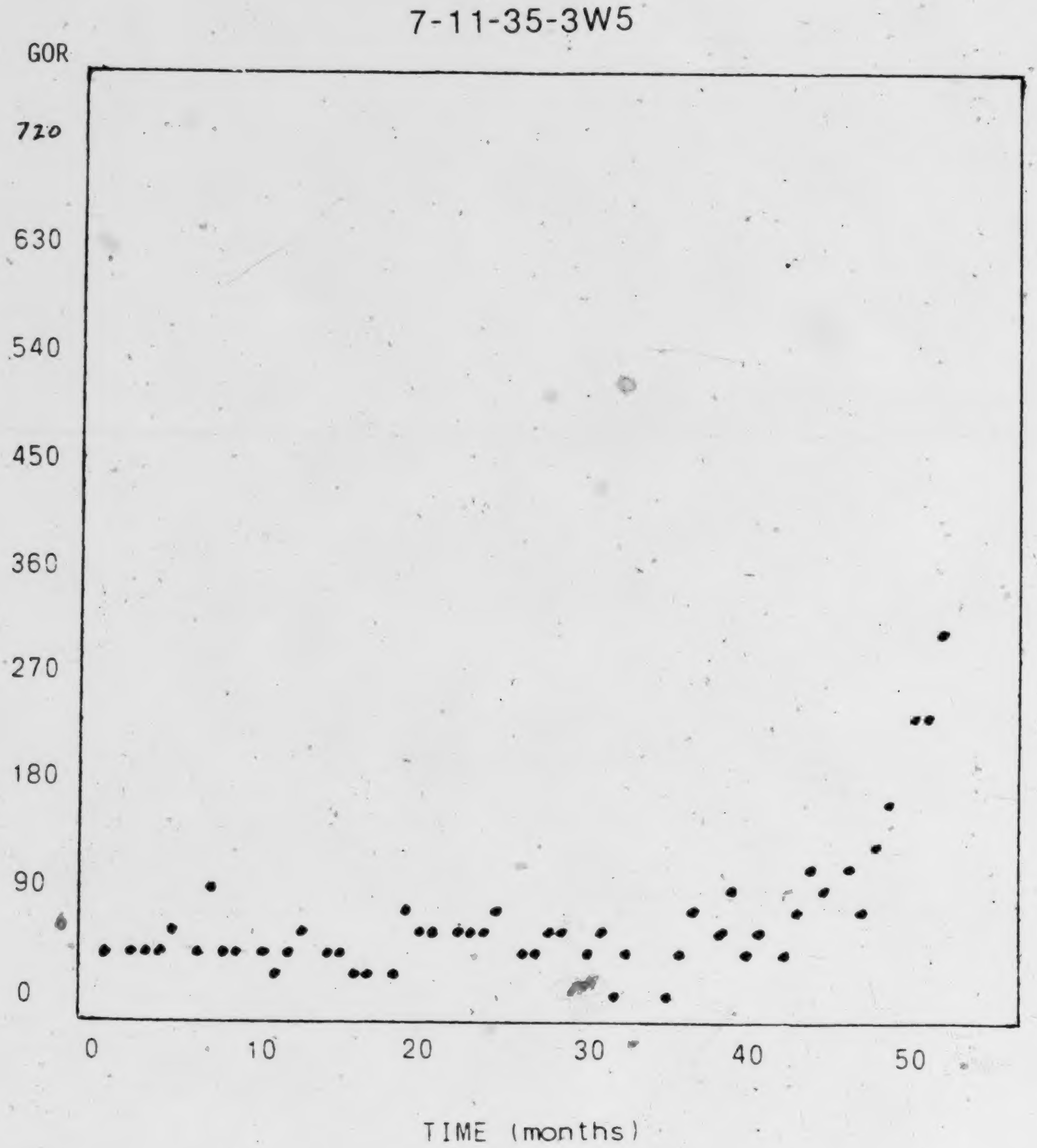

```
CORRELATION COEFFICIENT=.5893  N=51

     MEAN      ST. DEV.      REGRESSION LINE        RESIDUAL
X   26.35      15.268     X= .15807*Y+16.348        155.25
Y   63.29      56.923     Y= 2.1972*X+5.3914        2158.0
```

3-12-35-3W5

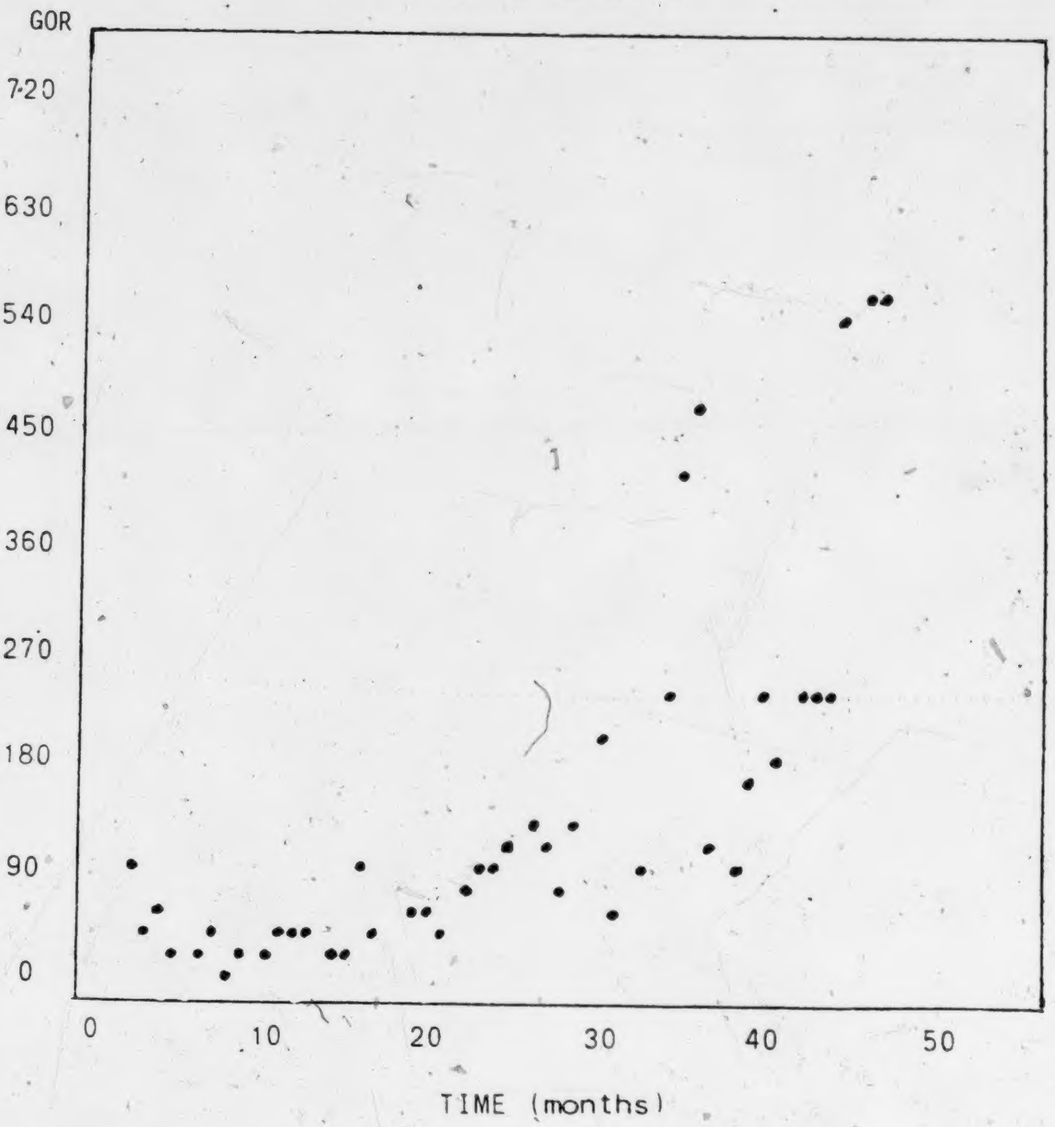

```
CORRELATION COEFFICIENT=.7494  N=44

     MEAN      ST. DEV.      REGRESSION LINE        RESIDUAL
X   24.47      13.648     X= .06765*Y+15.154         83.605
Y   137.8      151.19     Y= 8.3017*X-65.383         10260.
```

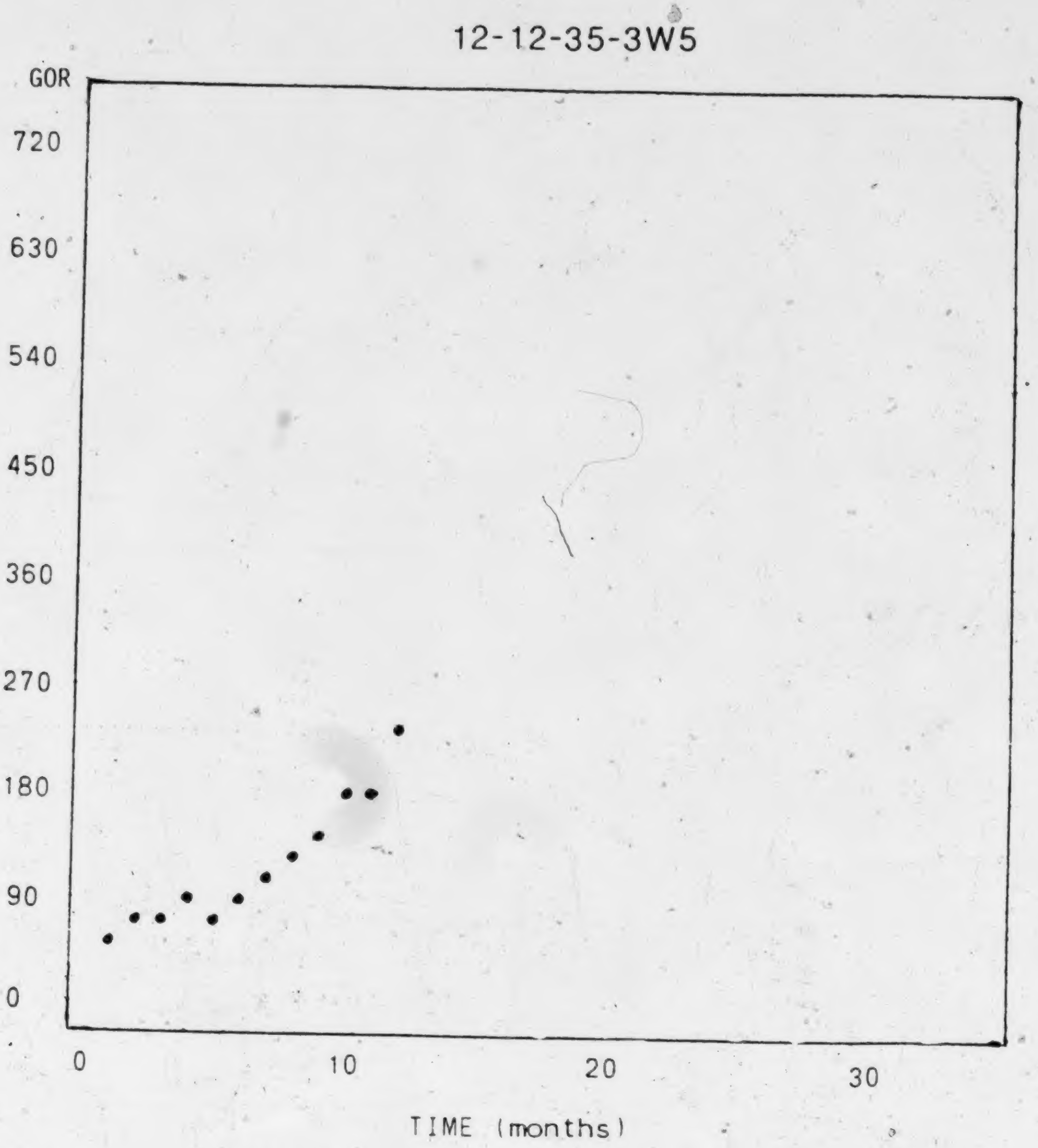

CORRELATION COEFFICIENT=.9342 N=12

```
     MEAN     ST. DEV.     REGRESSION LINE          RESIDUAL
X   6.500    3.6056      X= .06161*Y-.68730         1.8187
Y   116.7    54.687      Y= 14.168*X+24.576         418.26
```

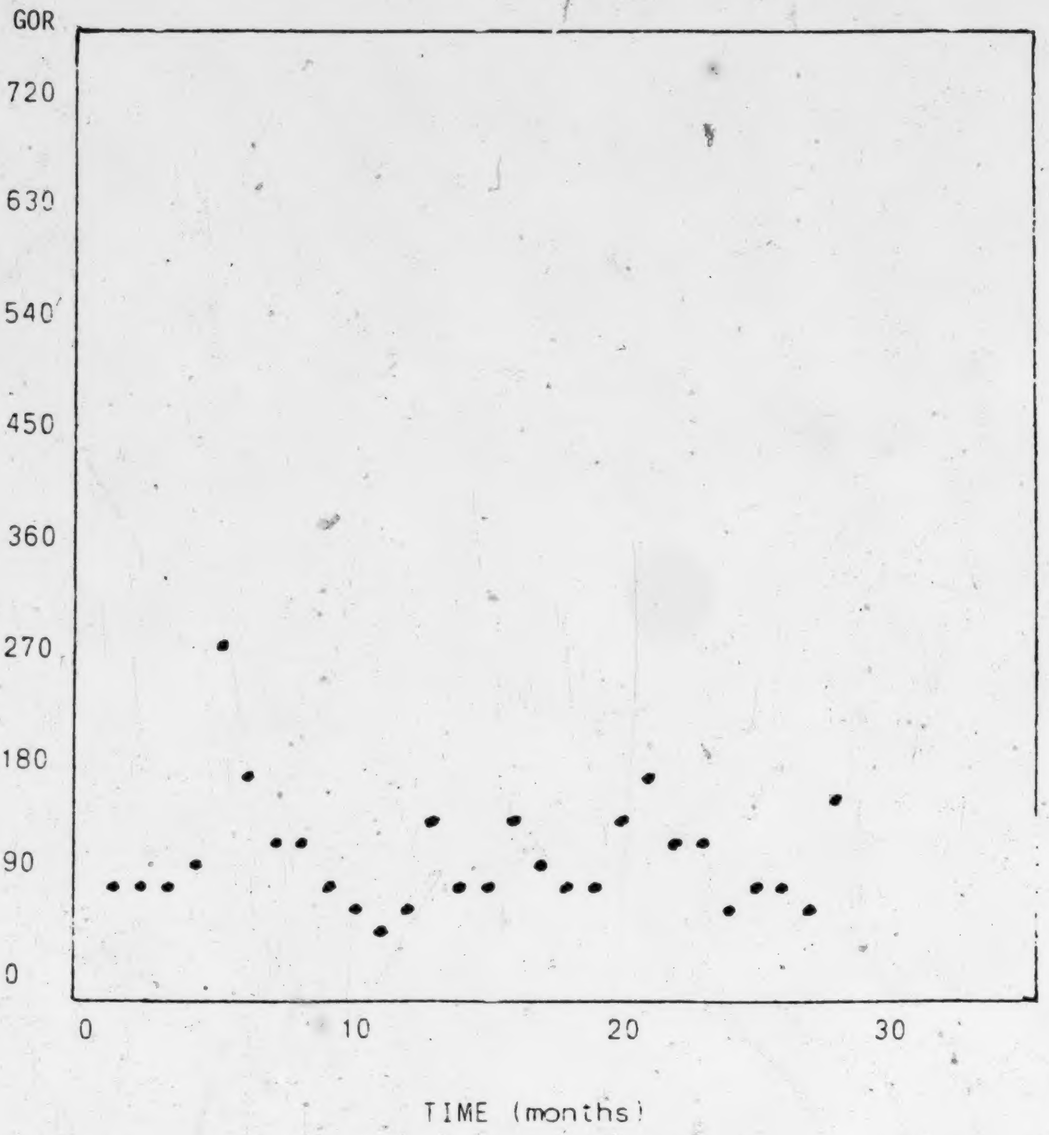

8-11-35-4W5

```
CORRELATION COEFFICIENT=-.0706  N=28

    MEAN     ST. DEV.      REGRESSION LINE      RESIDUAL
X  14.50     8.2250      X=-.01277*Y+15.723      69.916
Y  95.78     45.502      Y=-.39080*X+101.45      2139.3
```

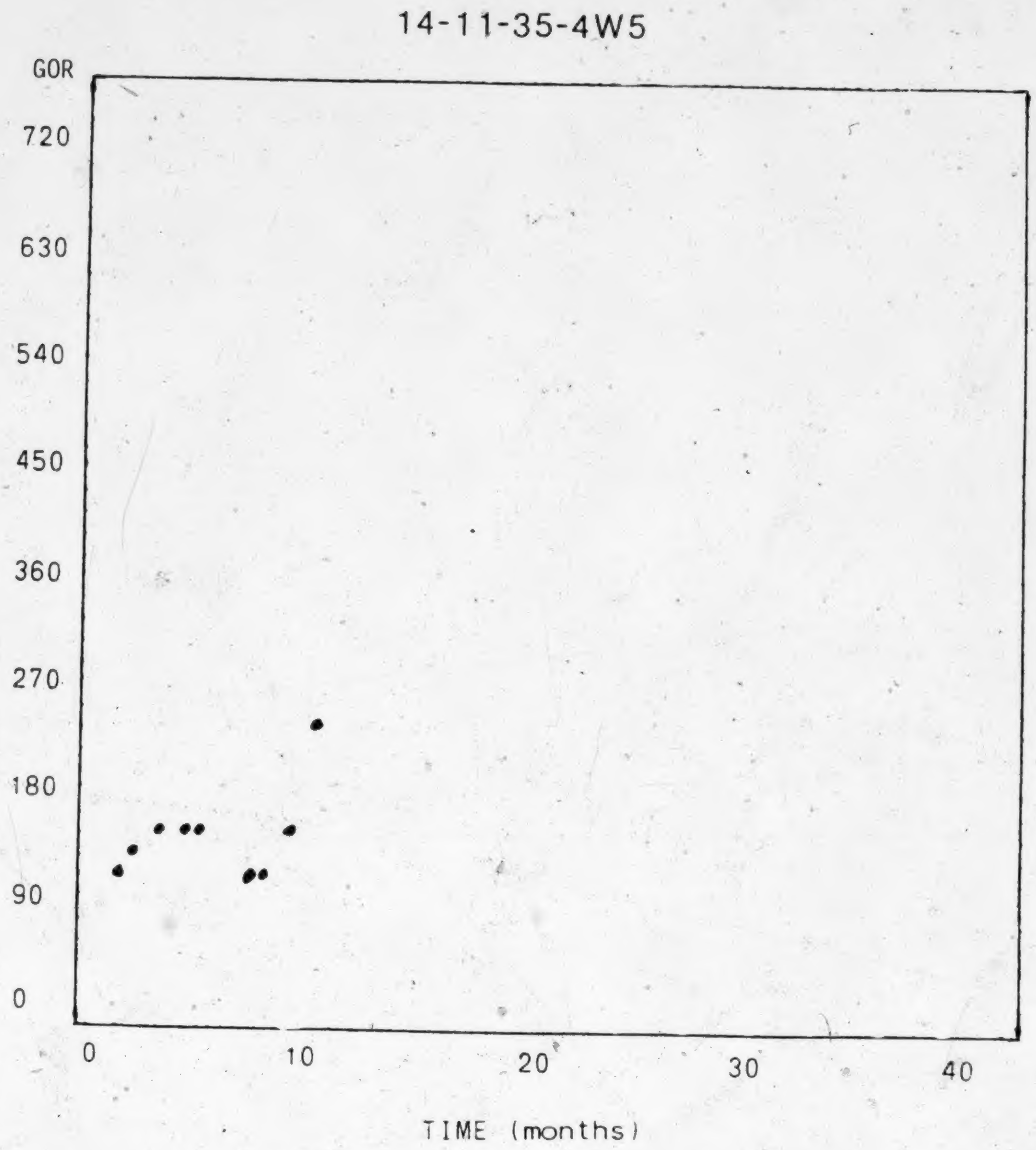

```
CORRELATION COEFFICIENT=.3894   N=9

     MEAN      ST. DEV.      REGRESSION LINE        RESIDUAL
X  5.444      3.2059      X= .03181*Y+1.0231        9.9648
Y  139.0      39.249      Y= 4.7676*X+113.04        1493.6
```

1-12-35-4W5

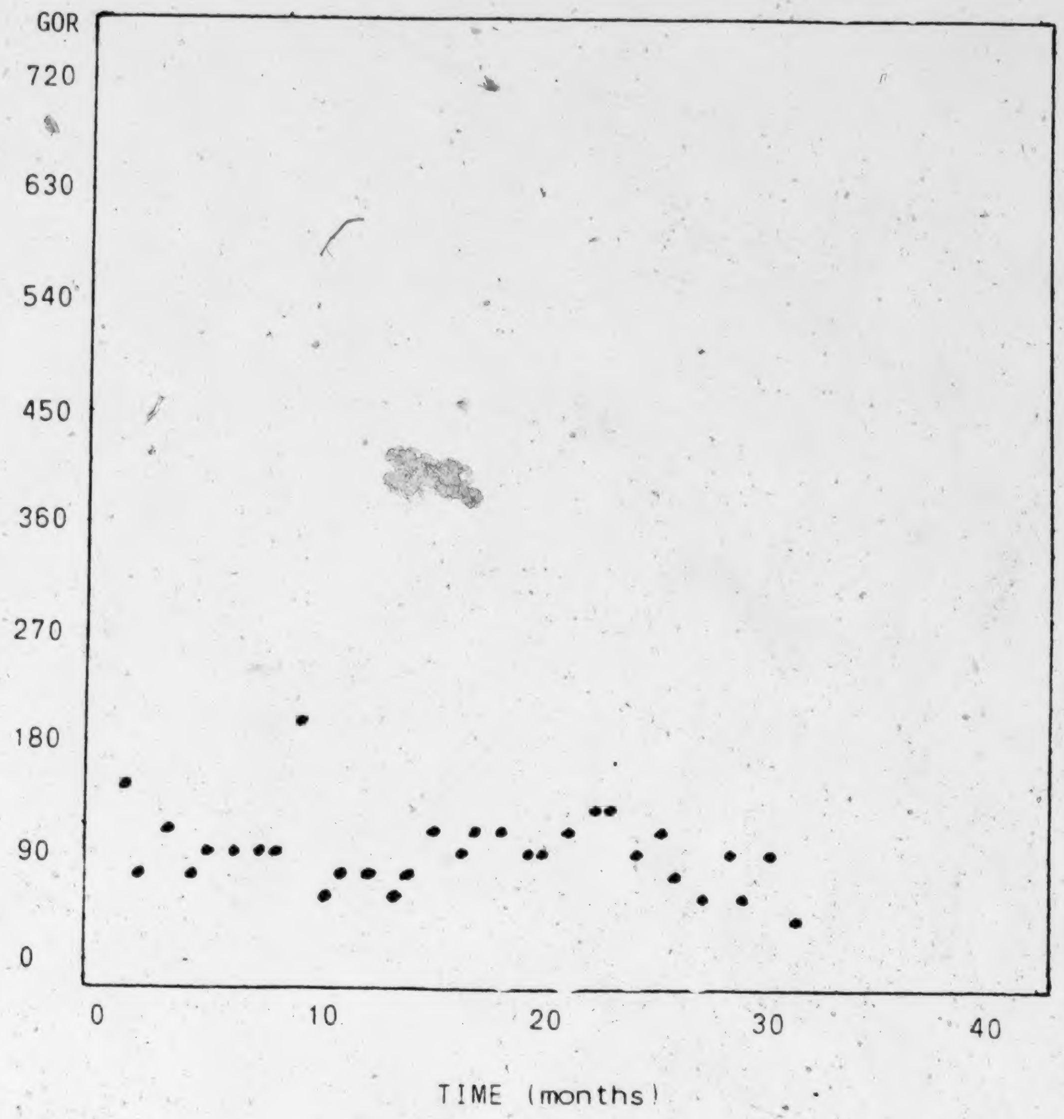

```
CORRELATION COEFFICIENT=-.2195  N=31

     MEAN     ST. DEV.      REGRESSION LINE        RESIDUAL
X   16.00     9.0291     X=-.06702*Y+22.032        81.396
Y   90.00     29.778     Y=-.71894*X+101.50        873.11
```

6-12-35-4W5

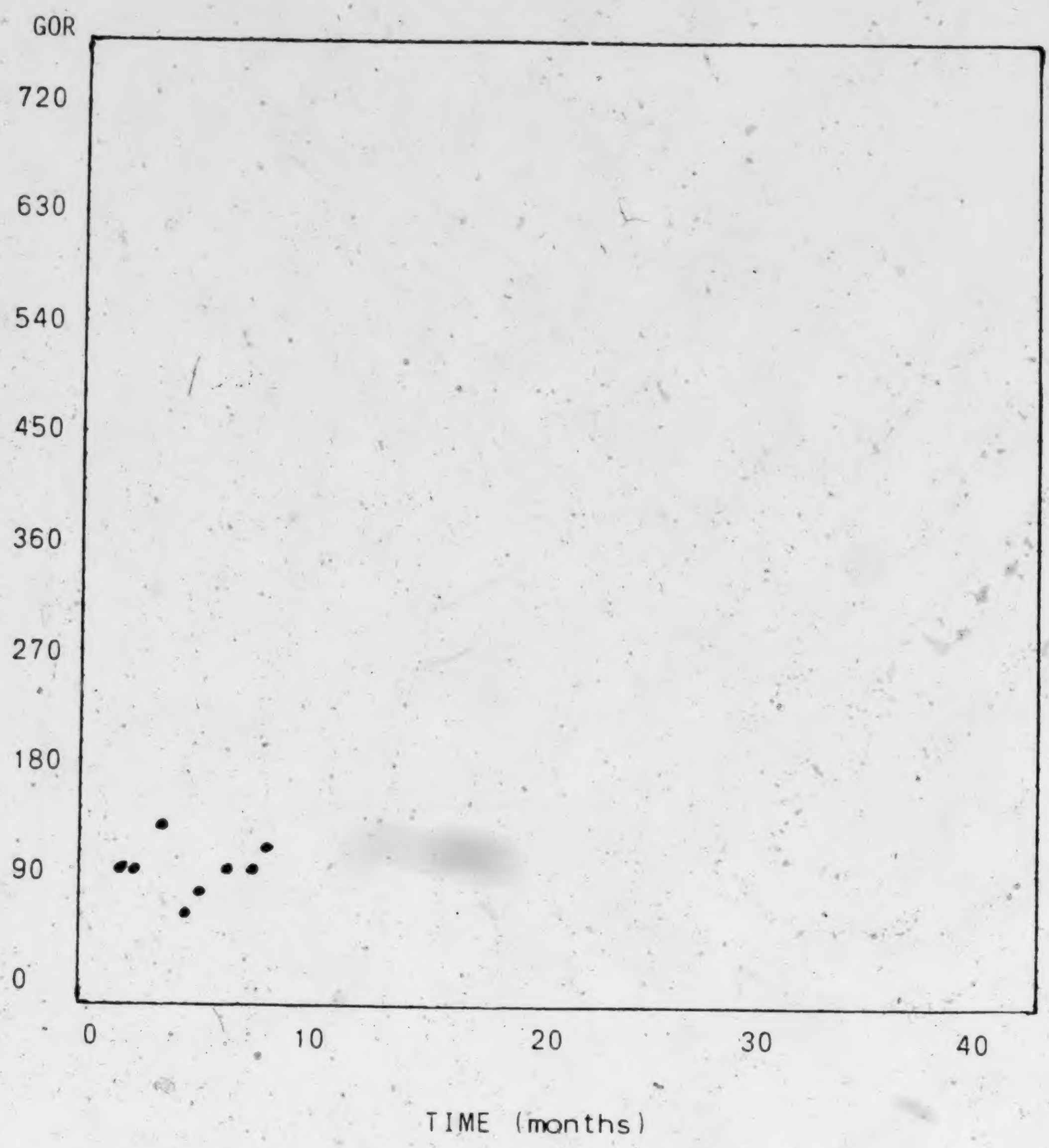

```
CORRELATION COEFFICIENT=.2185  N=8

     MEAN      ST. DEV.       REGRESSION LINE        RESIDUAL
X   4.500      2.4495     X= .02429*Y+2.2801         6.6660
Y   91.37      22.026     Y= 1.9643*X+82.536         538.97
```

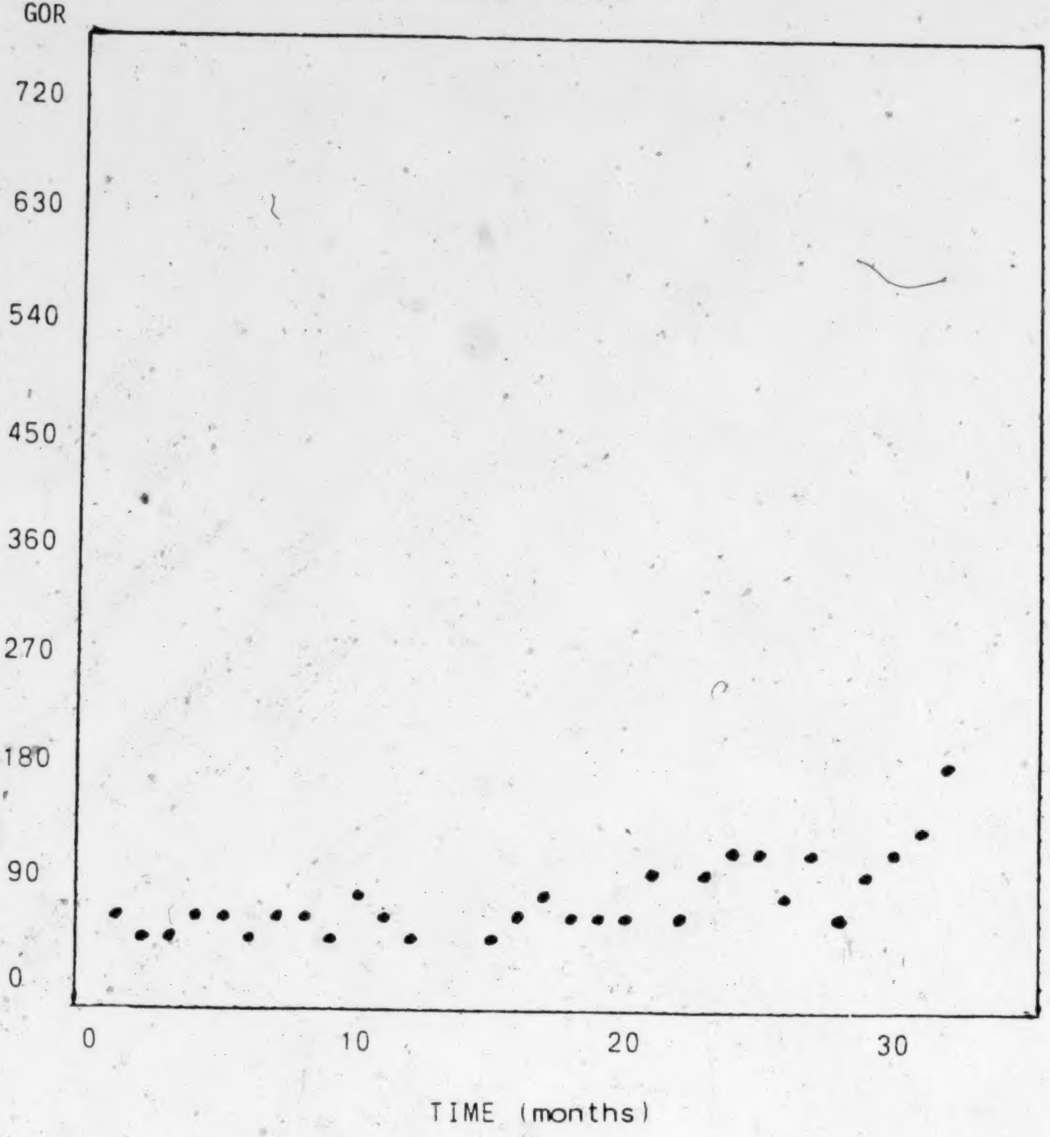
11-12-35-4W5

CORRELATION COEFFICIENT=.7686 N=30

	MEAN	ST. DEV.	REGRESSION LINE	RESIDUAL
X	16.70	9.6638	X= .23364*Y+.60249	39.592
Y	68.90	31.790	Y= 2.5282*X+26.697	428.43

6-13-35-4W5

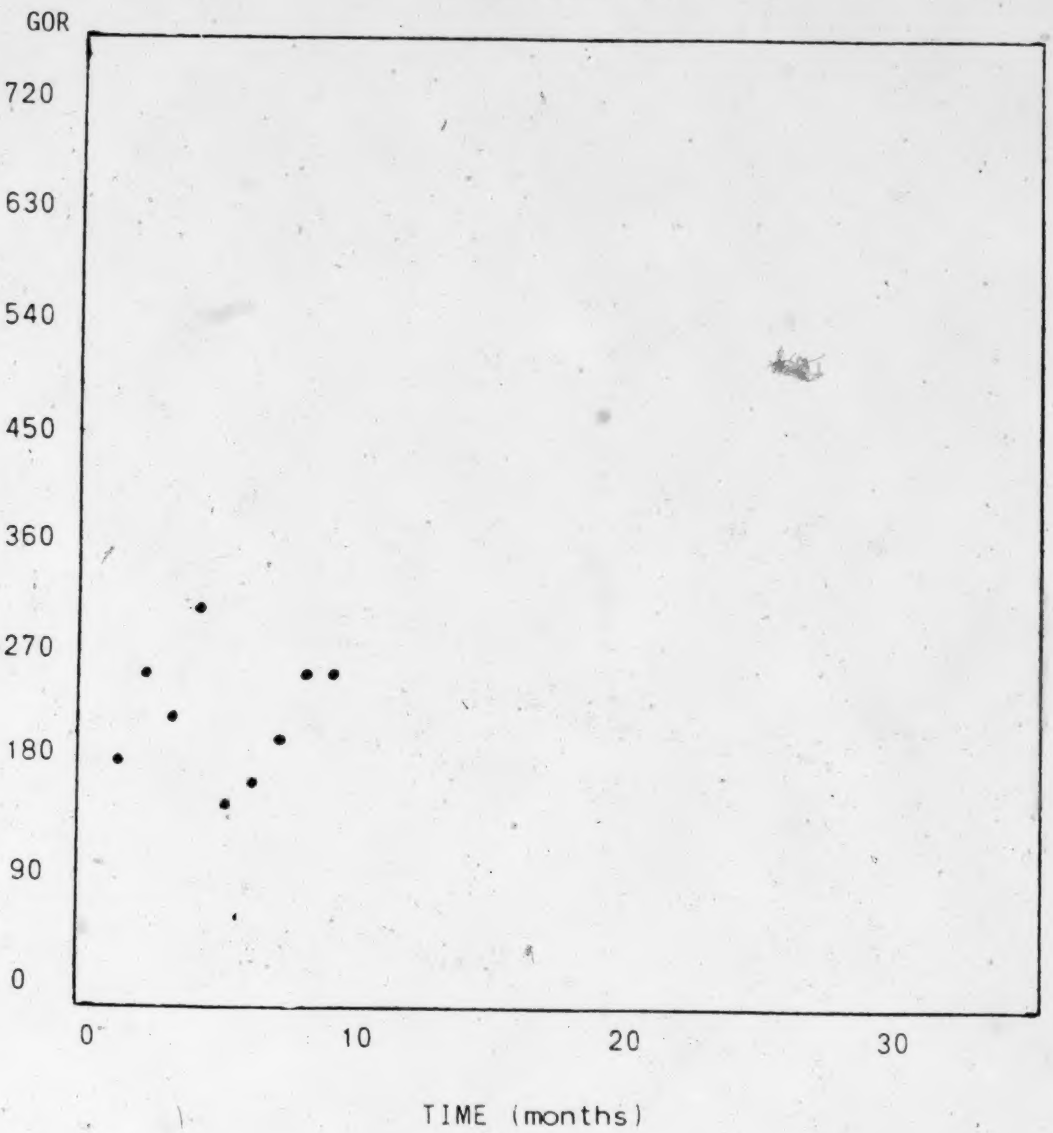

```
CORRELATION COEFFICIENT=.1387   N=9

    MEAN      ST. DEV.       REGRESSION LINE        RESIDUAL
X  5.000     2.7386      X= .00735*Y+3.4098        8.4066
Y  216.3     51.670      Y= 2.6167*X+203.25        2992.5
```

6-14-35-4W5

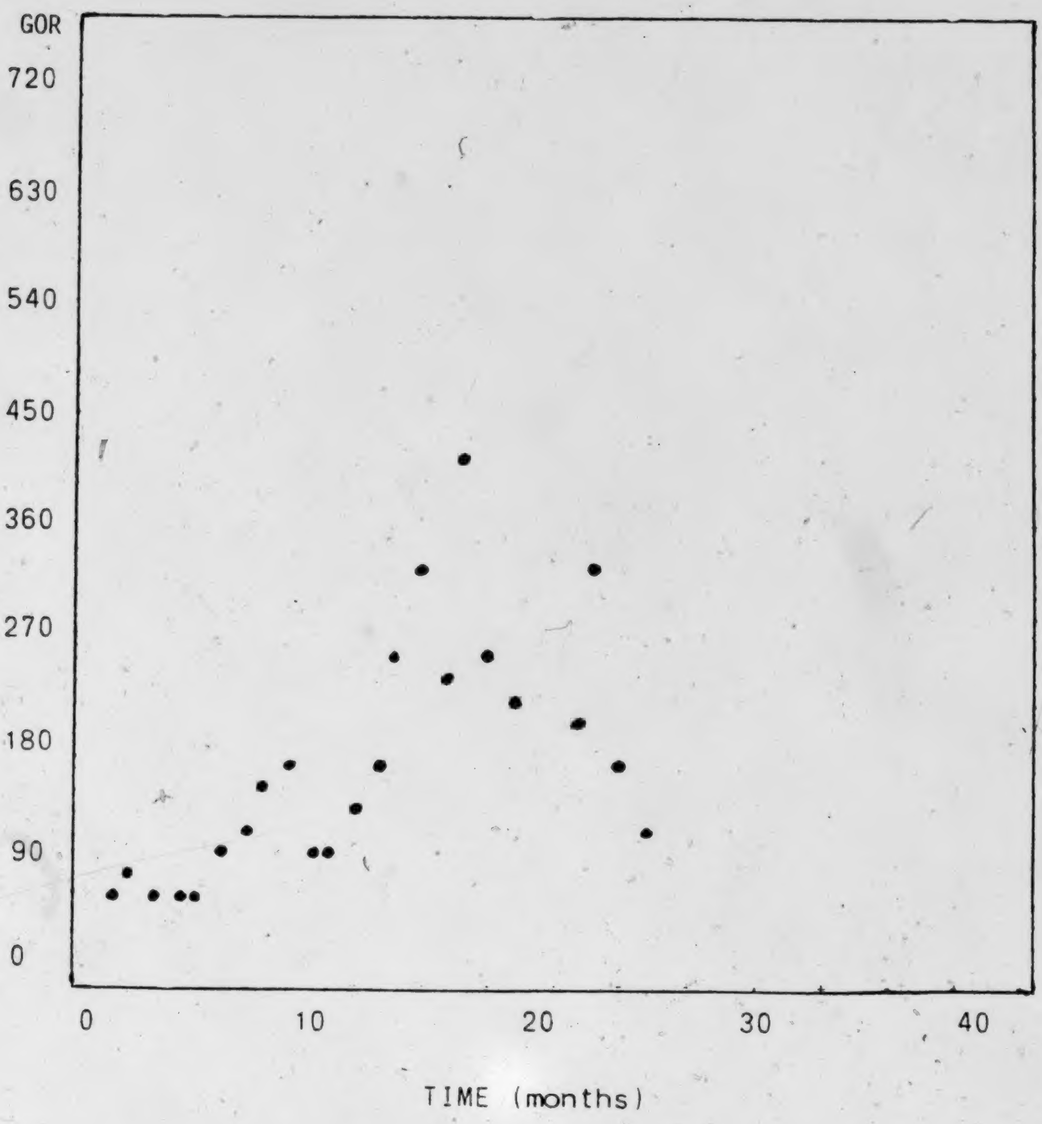

```
CORRELATION COEFFICIENT=.6419  N=23

     MEAN      ST. DEV.      REGRESSION LINE        RESIDUAL
X   12.34      7.3150      X= .04694*Y+4.7092        32.962
Y   162.7      100.03      Y= 8.7776*X+54.355        6164.0
```

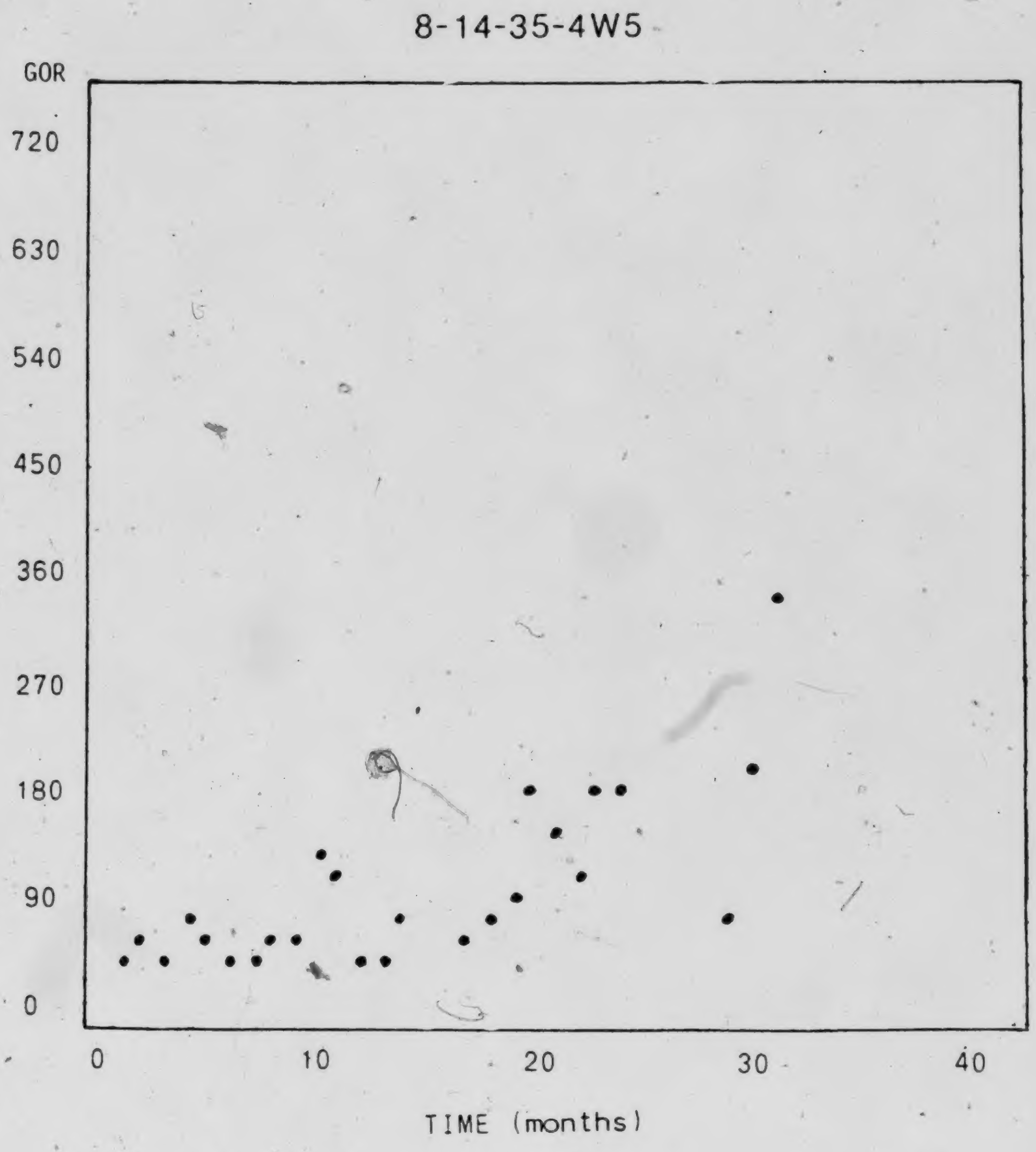

CORRELATION COEFFICIENT=.7286 N=25

	MEAN	ST. DEV.	REGRESSION LINE	RESIDUAL
X	14.36	9.0502	X= .09062*Y+5.5483	40:100
Y	97.24	72.764	Y= 5.8577*X+13.123	2592.2

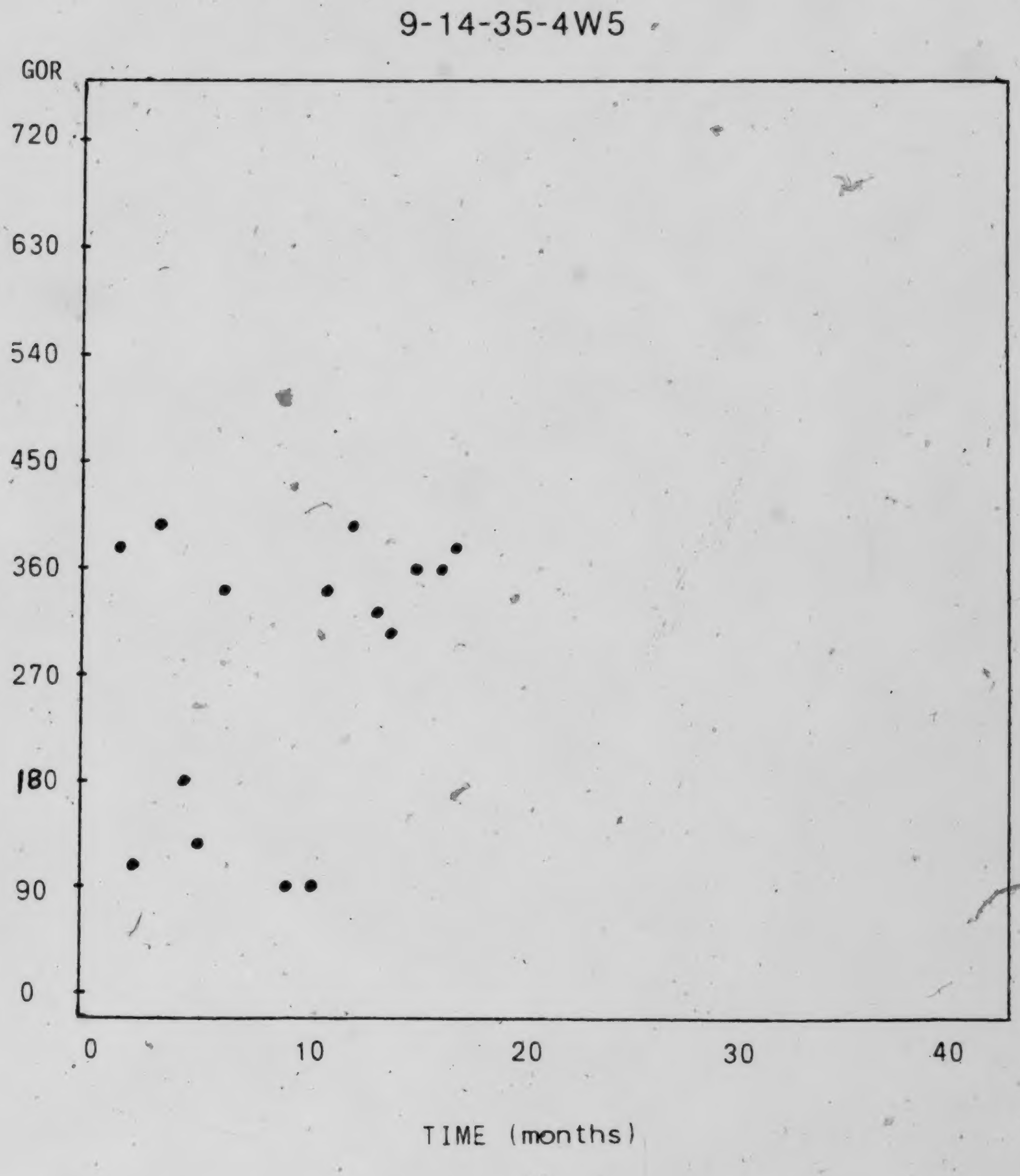

```
CORRELATION COEFFICIENT=.3407  N=15

     MEAN     ST. DEV.     REGRESSION LINE        RESIDUAL
X  9.200     5.3612     X= .01525*Y+4.9392      27.359
Y  279.4     119.84     Y= 7.6183*X+209.38      13671.
```

17

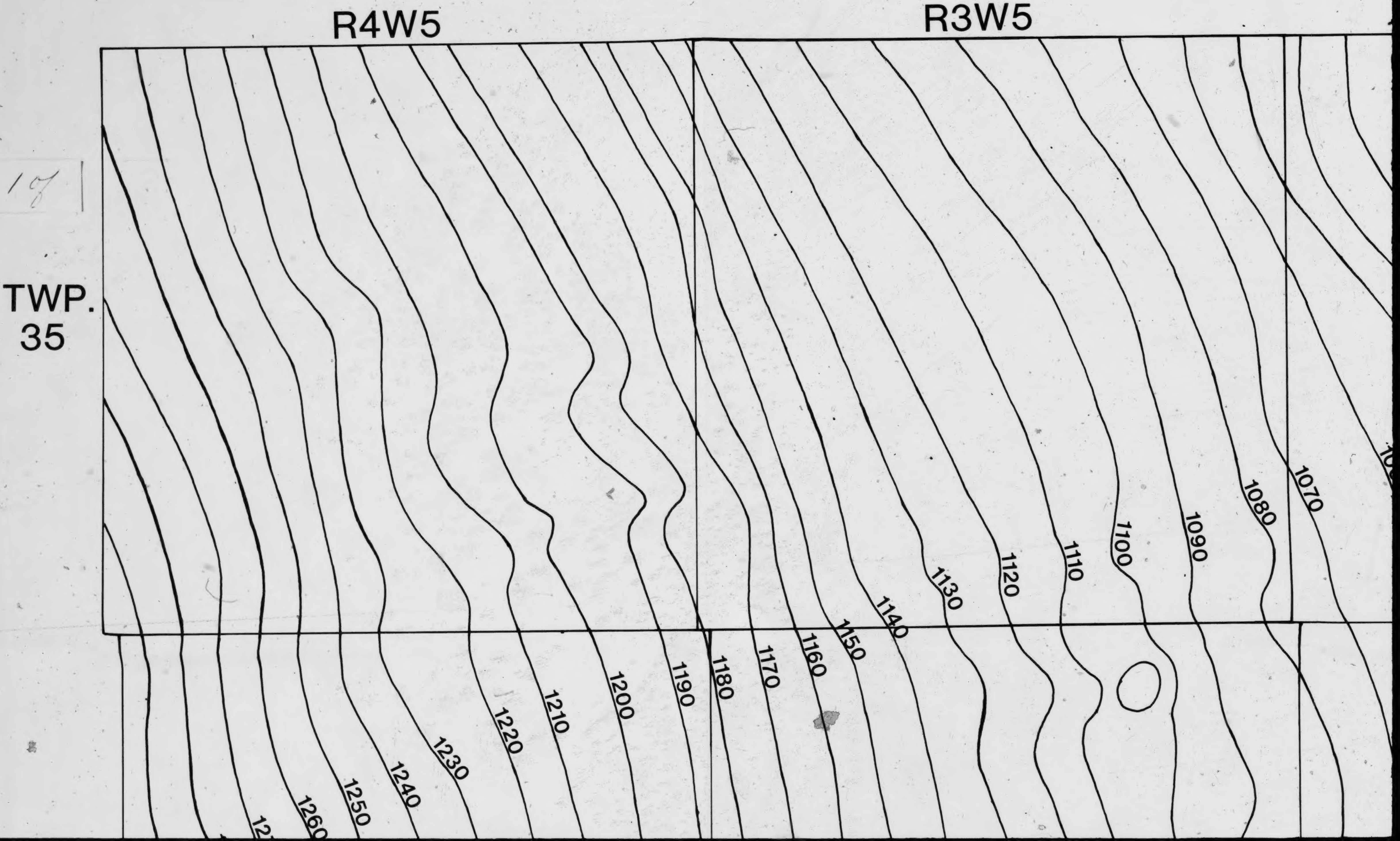
R4W5
R3W5
TWP.
35
1260
1250
1240
1230
1220
1210
1200
1190
1180
1170
1160
1150
1140
1130
1120
1110
1100
1090
1080
1070

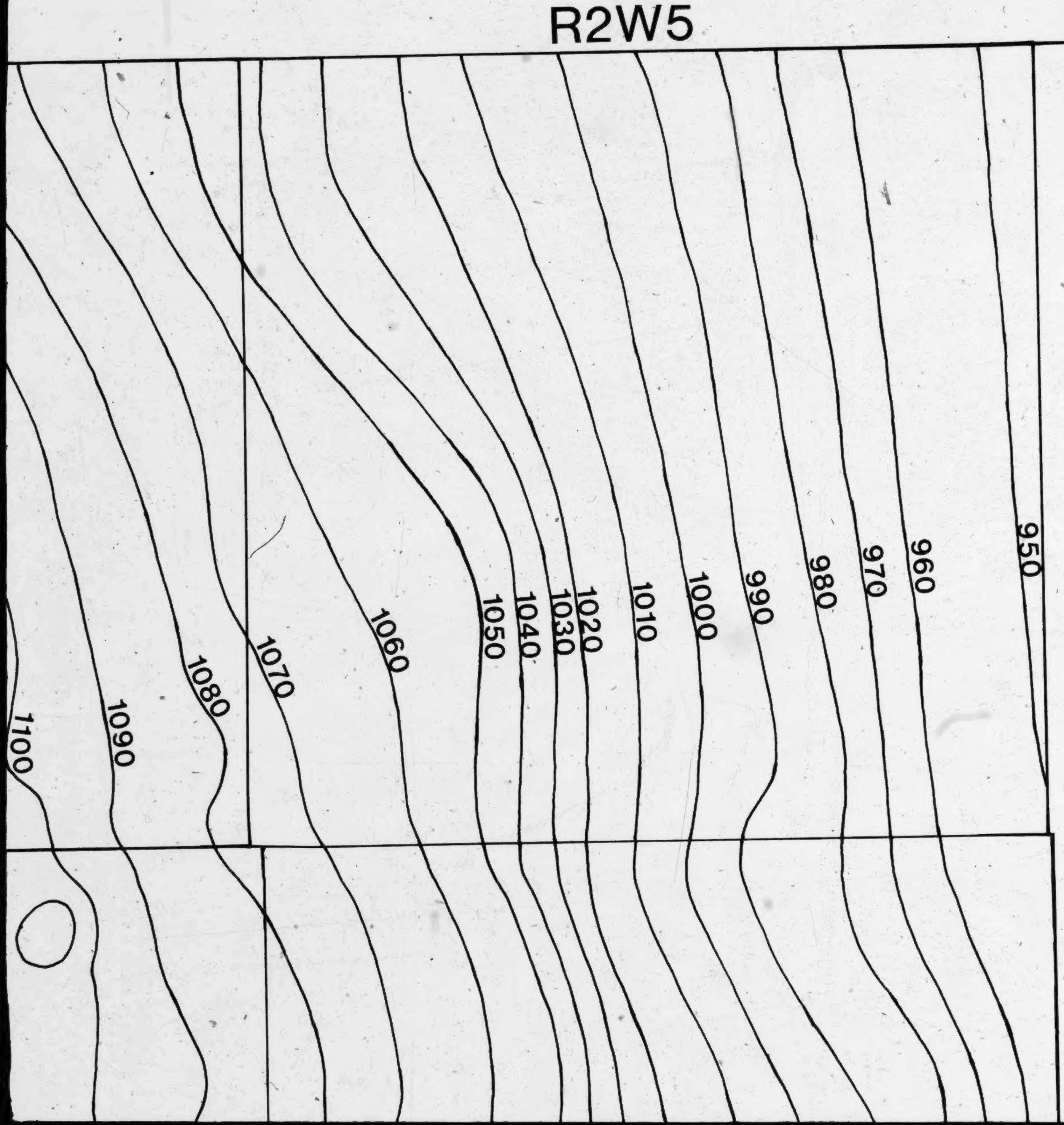
R2W5
1100
1090
1080
1070
1060
1050
1040
1030
1020
1010
1000
990
980
970
960
950

2 of

GARRINGTON OIL FIELD

VIKING "B" STRUCTURE MAP

DATUM SEA LEVEL
CONTOUR INTERVAL 10m

TWP.
34

3 of

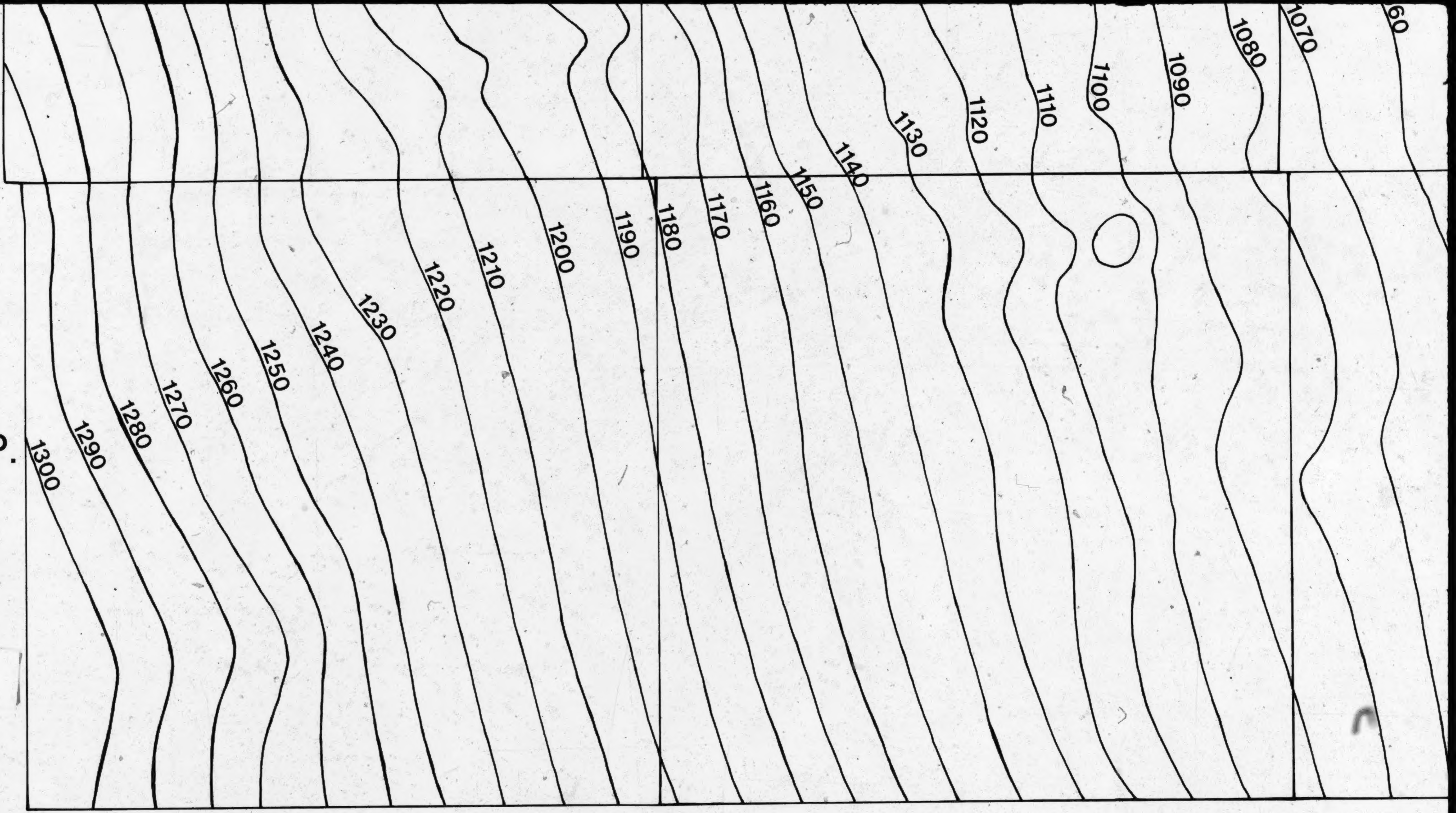
1300
1290
1280
1270
1260
1250
1240
1230
1220
1210
1200
1190
1180
1170
1160
1150
1140
1130
1120
1110
1100
1090
1080
1070
60

DATUM SEA LEVEL

CONTOUR INTERVAL 10m

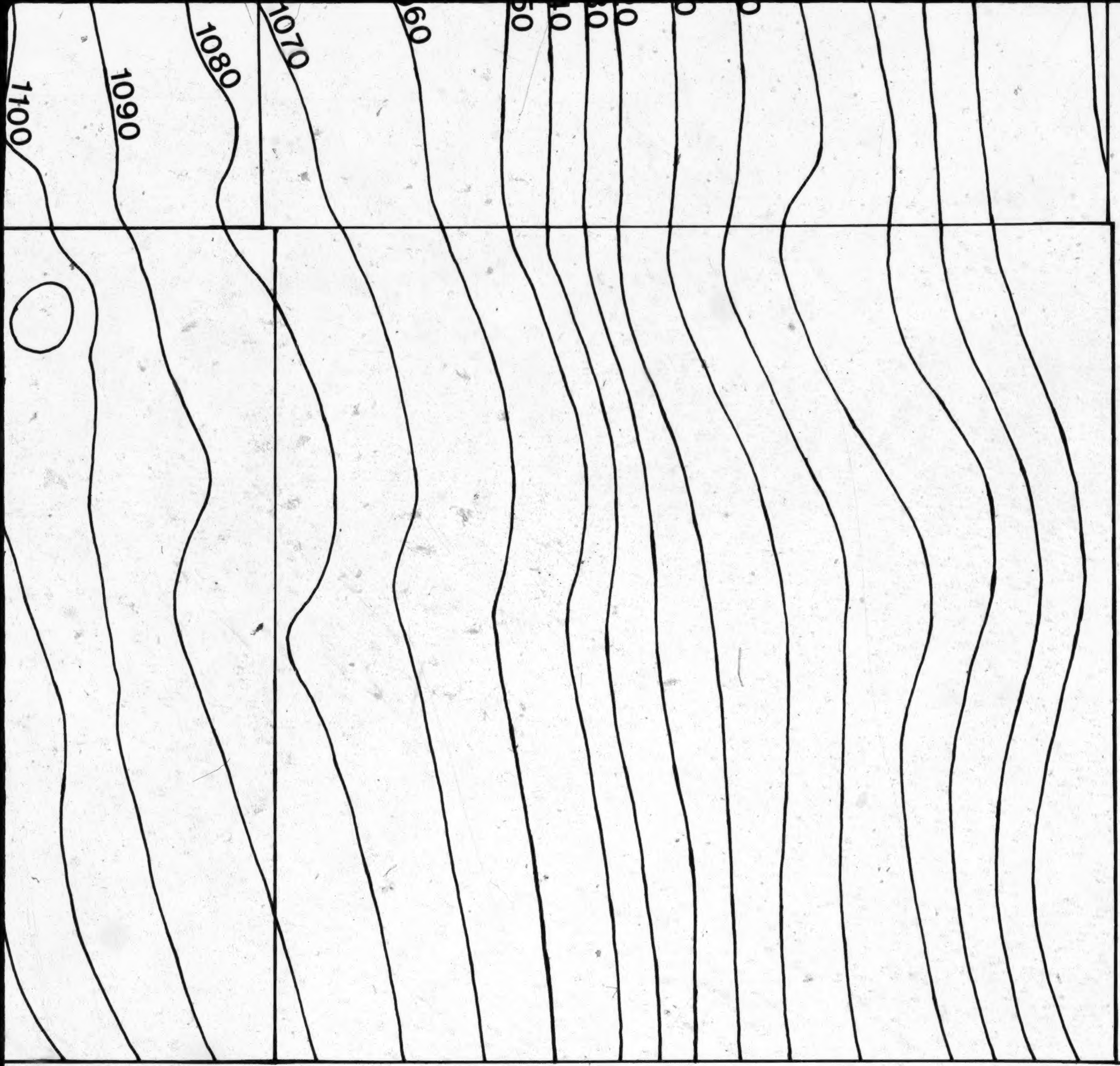
1100
1090
1080
1070
60

4 of 4

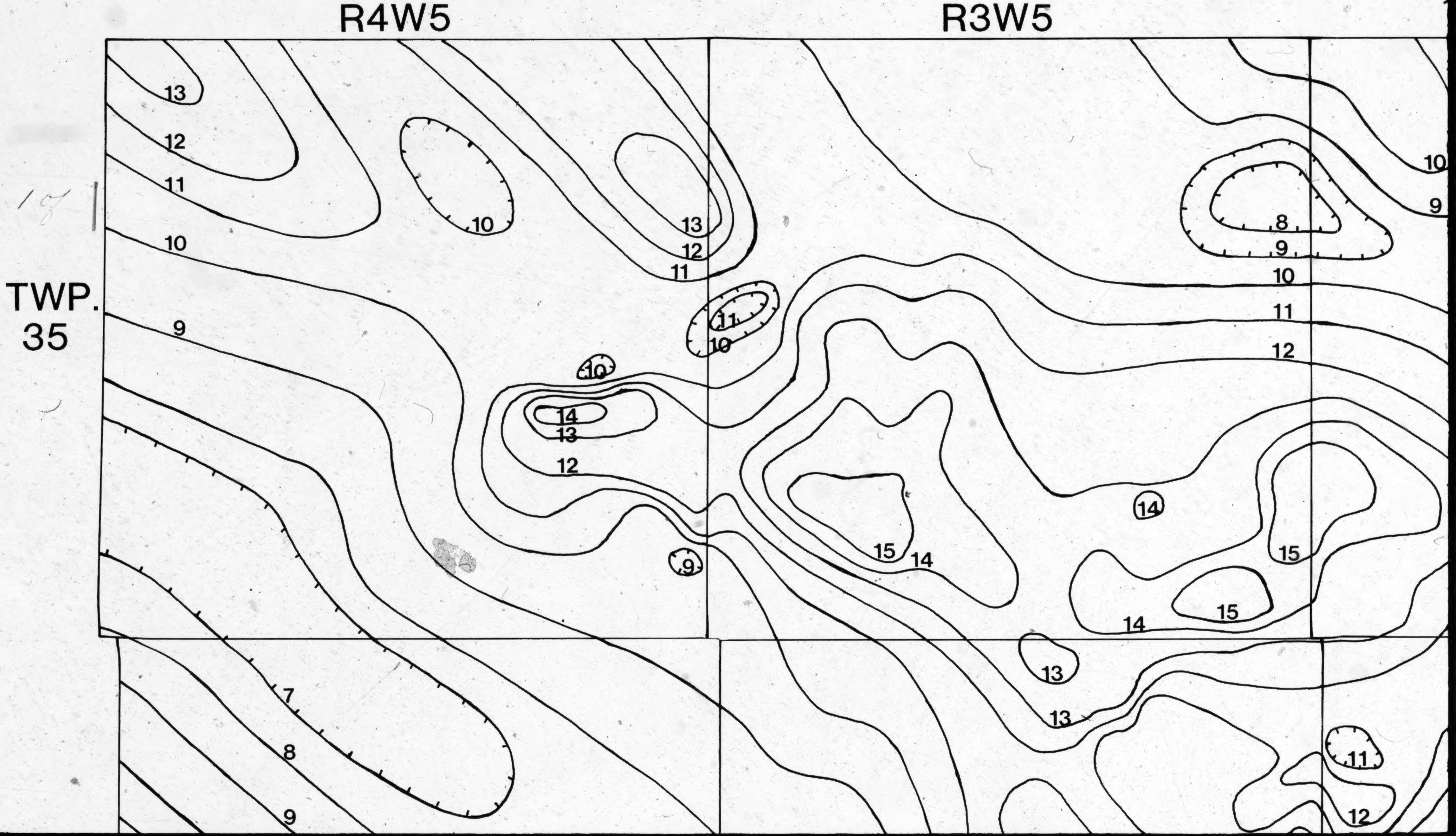
R4W5
R3W5
TWP.
35
13
12
11
10
9
10
13
12
11
11
10
10
14
13
12
9
7
8
9
8
9
10
11
12
10
9
15
14
14
15
15
14
13
13
11
12

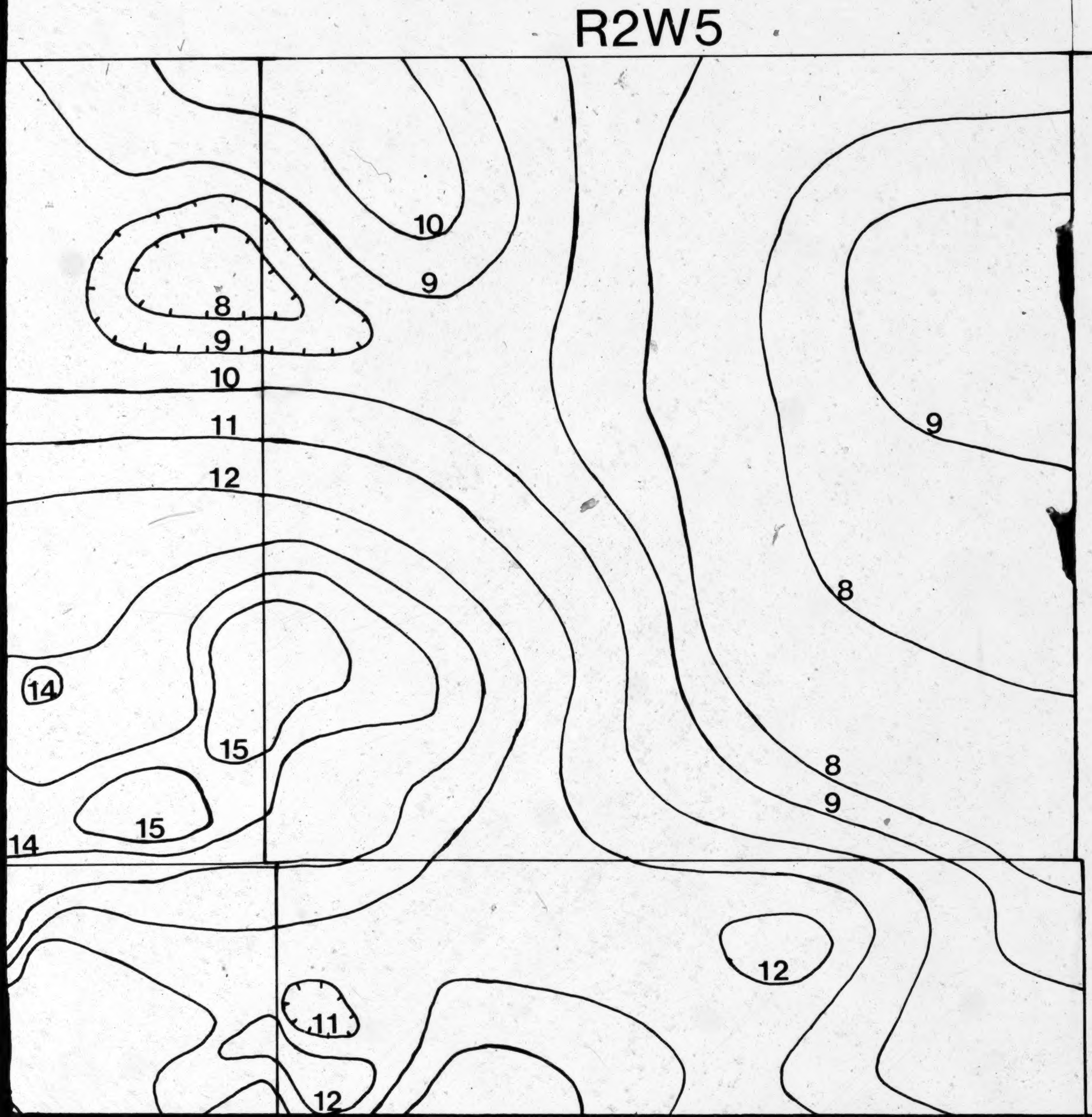
R2W5
10
9
8
9
10
11
12
14
15
15
14
9
8
8
9
12
11
12

2 of

GARRINGTON OIL FIELD

VIKING "B" CONGLOMERATE AND FINE-GRAINED SANDSTONE ISOPACH

CONTOUR INTERVAL 1m

TOPOGRAPHIC LOW

TWP.
34

3 of

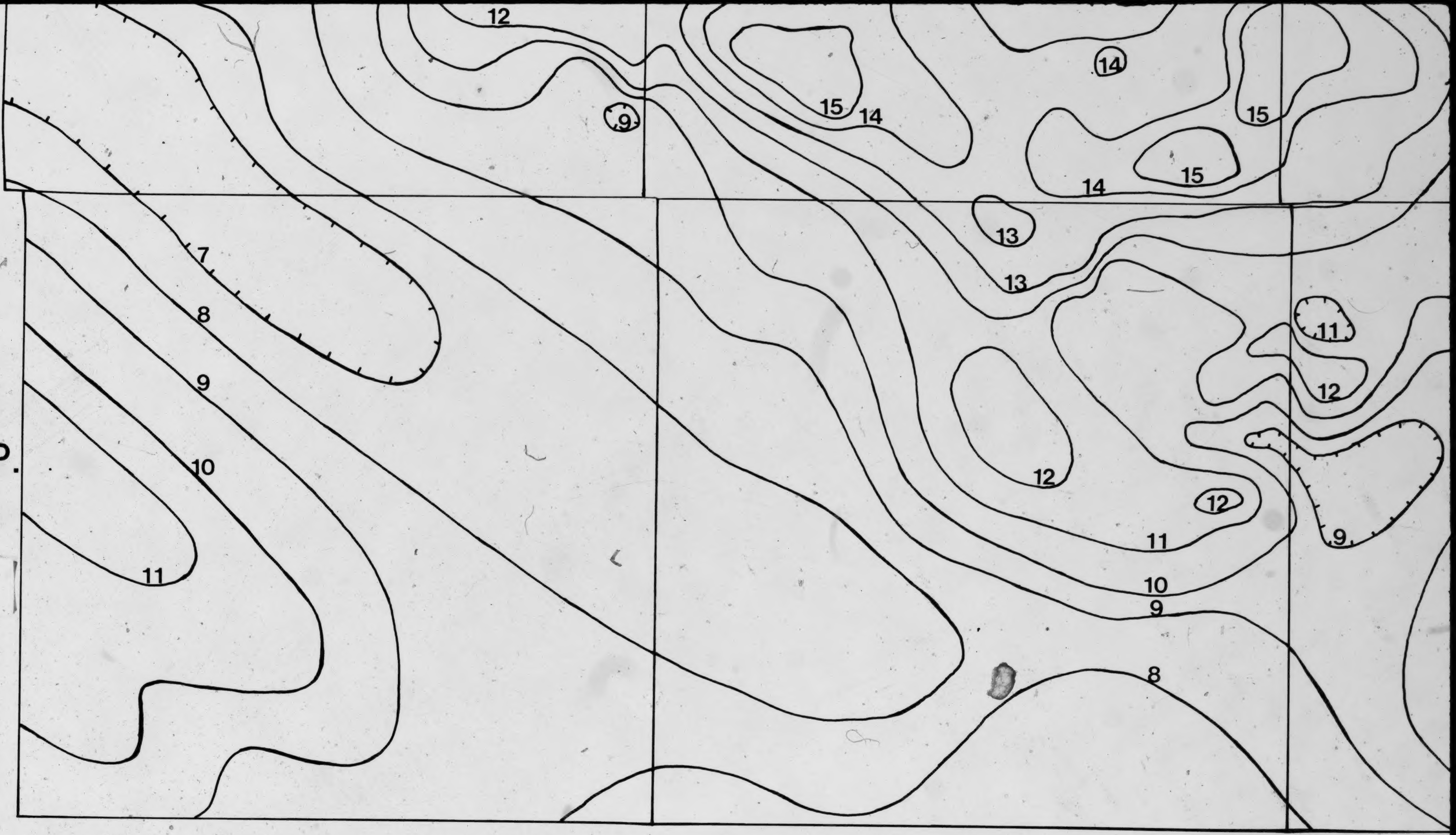
12
9
15
14
14
15
15
14
13
13
7
8
9
10
11
11
12
12
12
11
10
9
9
8

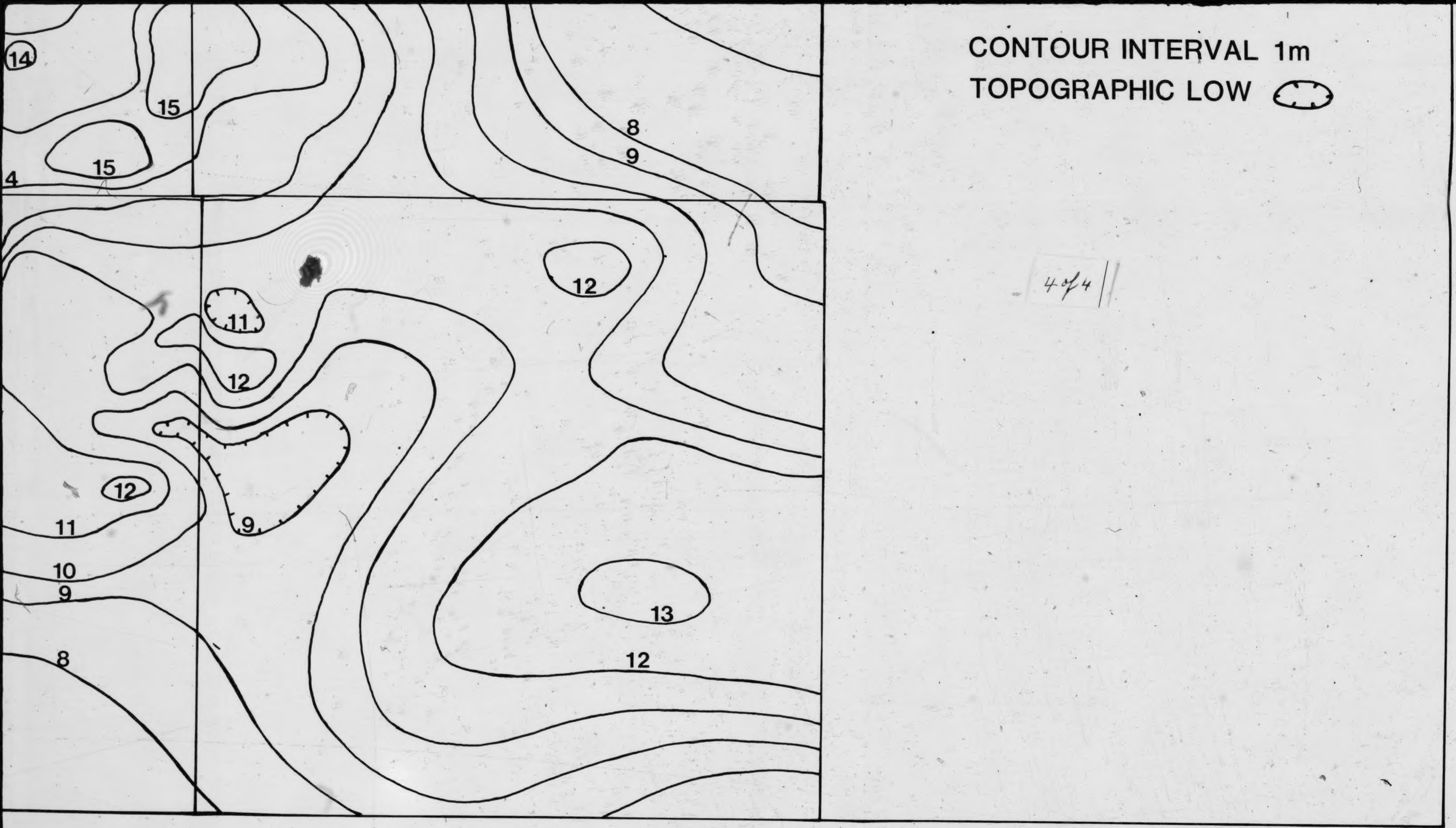
CONTOUR INTERVAL 1m
TOPOGRAPHIC LOW
14
15
15
4
8
9
12
11
12
12
11
9
10
9
8
13
12

4 of 4

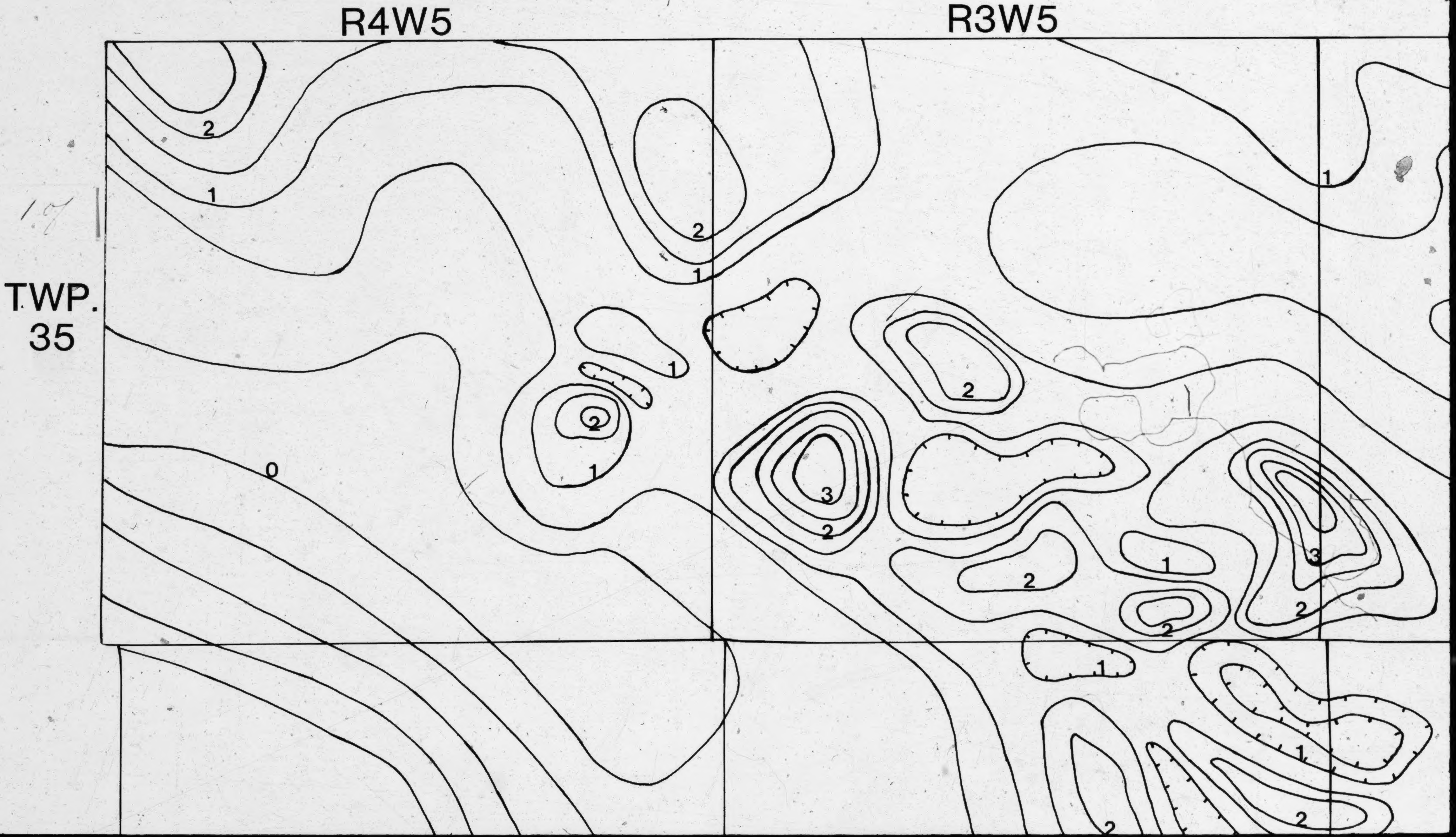
R4W5
R3W5
TWP.
35
2
1
2
1
1
2
1
0
2
3
2
1
2
1
2
3
2
1
1
2
2

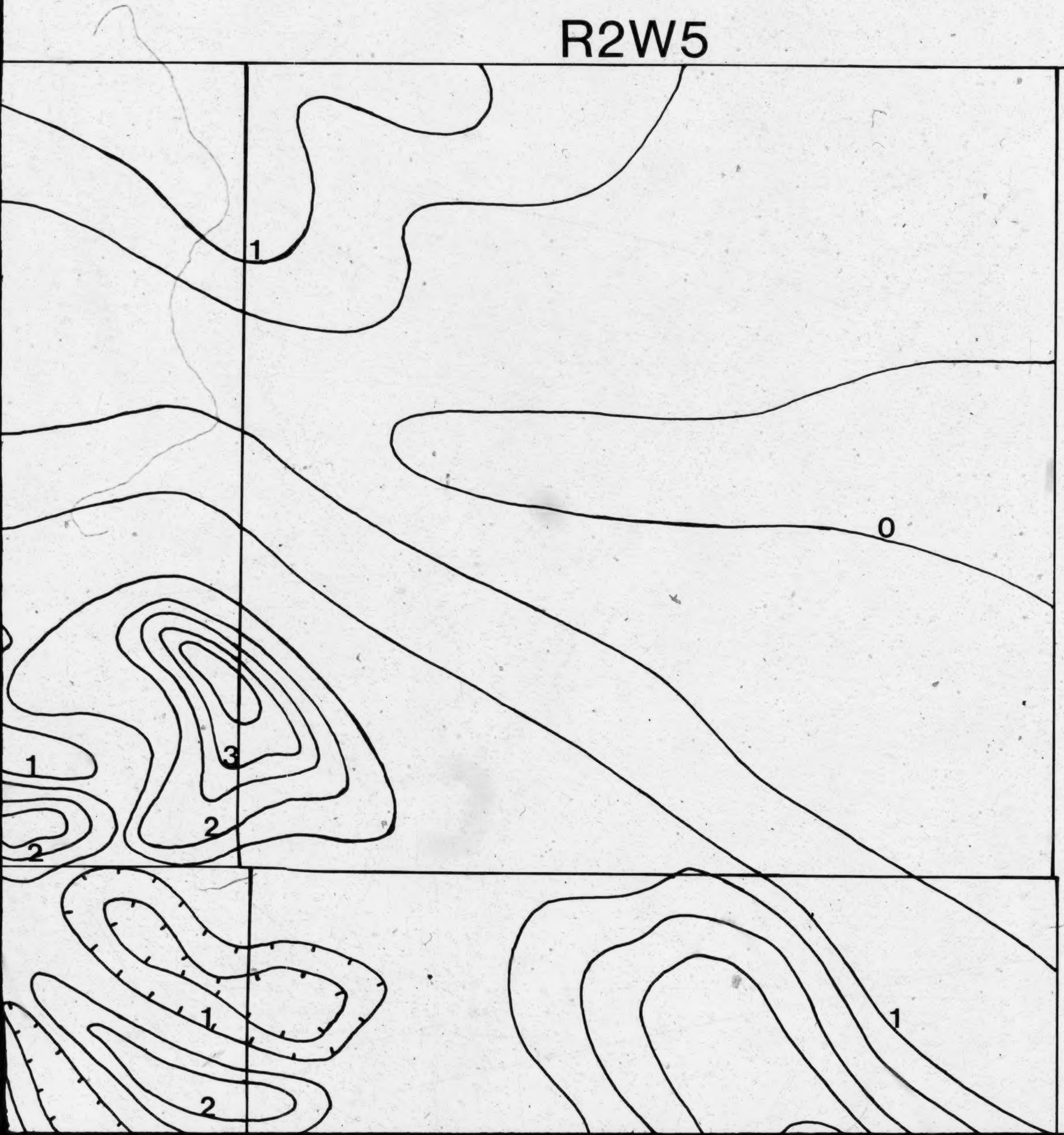
R2W5
1
0
1
3
2
2
1
1
2

2 of

GARRINGTON OIL FIELD

VIKING "B" CONGLOMERATE ISOPACH

CONTOUR INTERVAL .5m

TOPOGRAPHIC LOW

3 f

TWP.
34

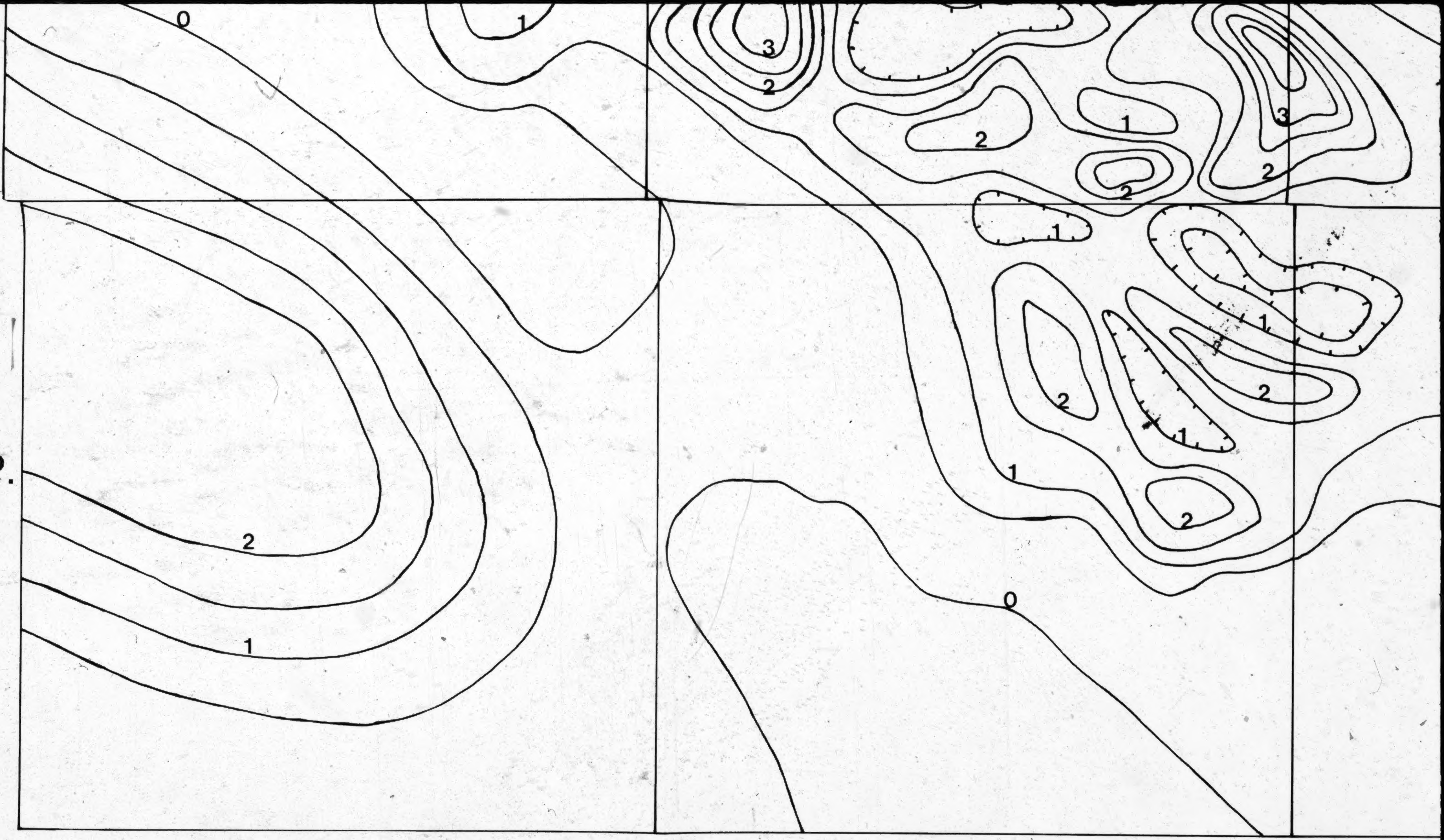
0
1
3
2
2
1
2
3
2
2
1
1
1
2
2
2
1
1
2
0
2
1

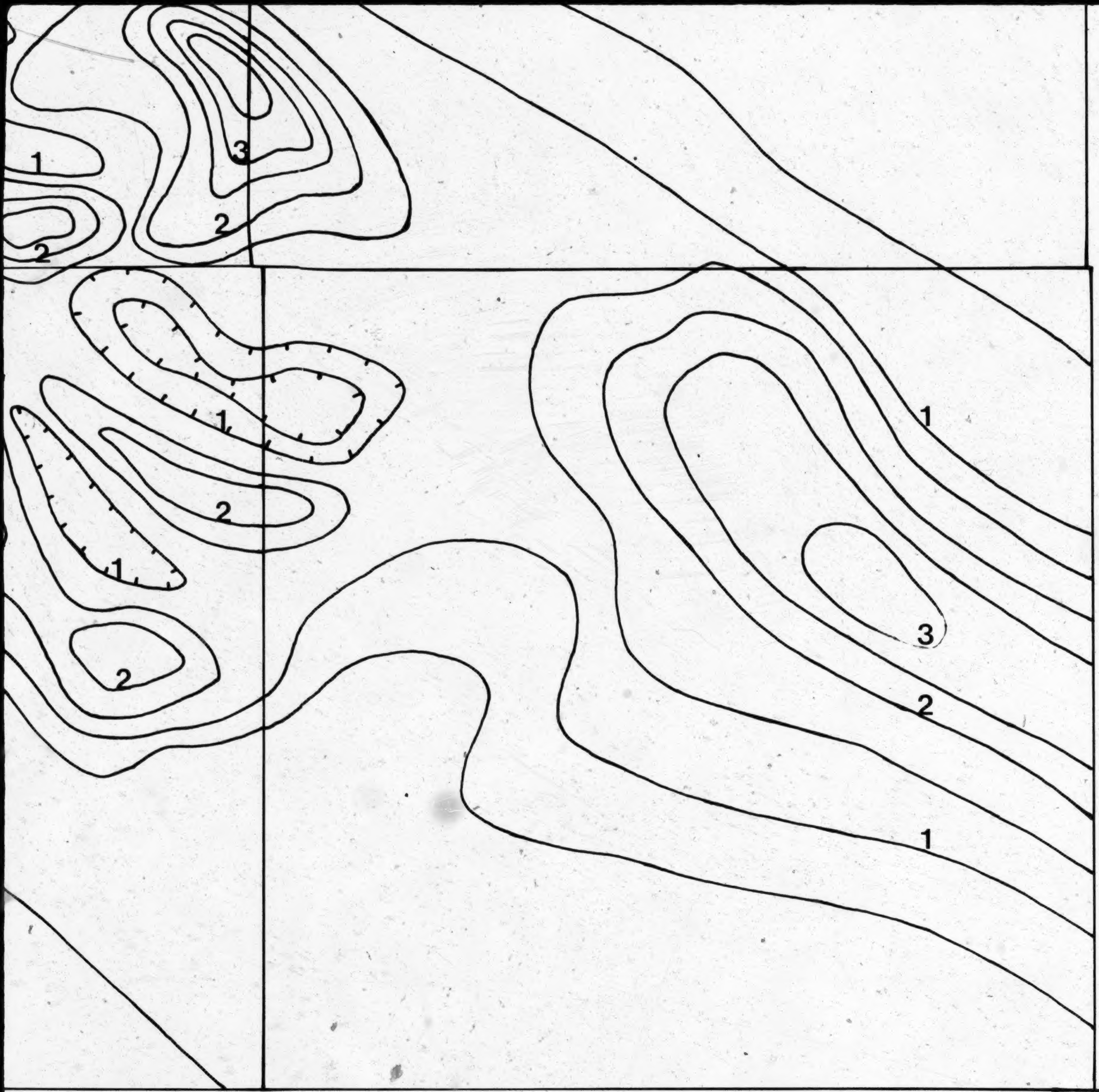
1
3
2
2
1
2
1
2
1
3
2
1

CONTOUR INTERVAL .5m

TOPOGRAPHIC LOW

4 of 4

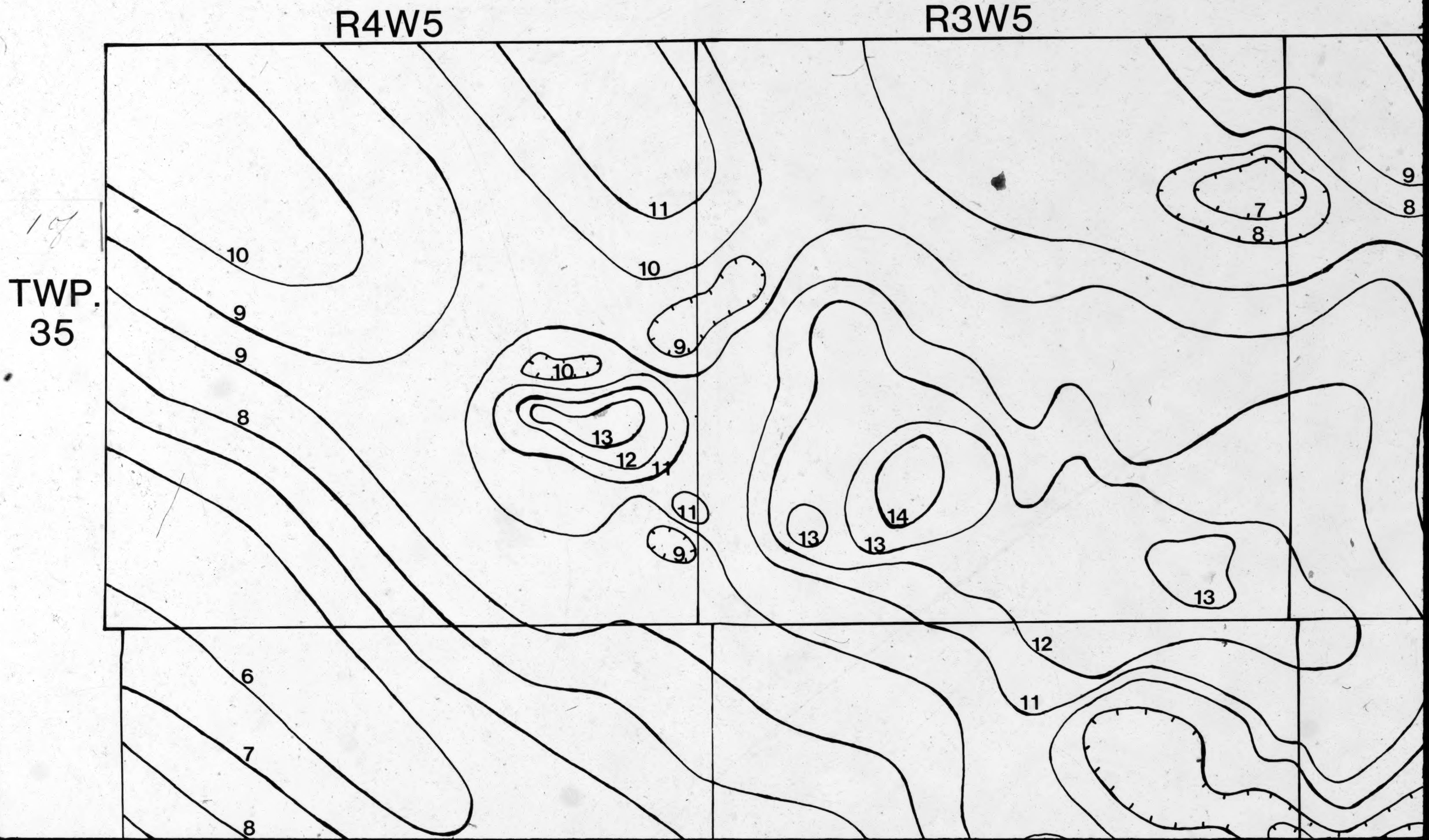
R4W5
R3W5
TWP.
35
17
10
9
9
8
11
10
9
10
13
12
11
11
9
9
8
7
8
13
13
14
13
12
11
6
7
8

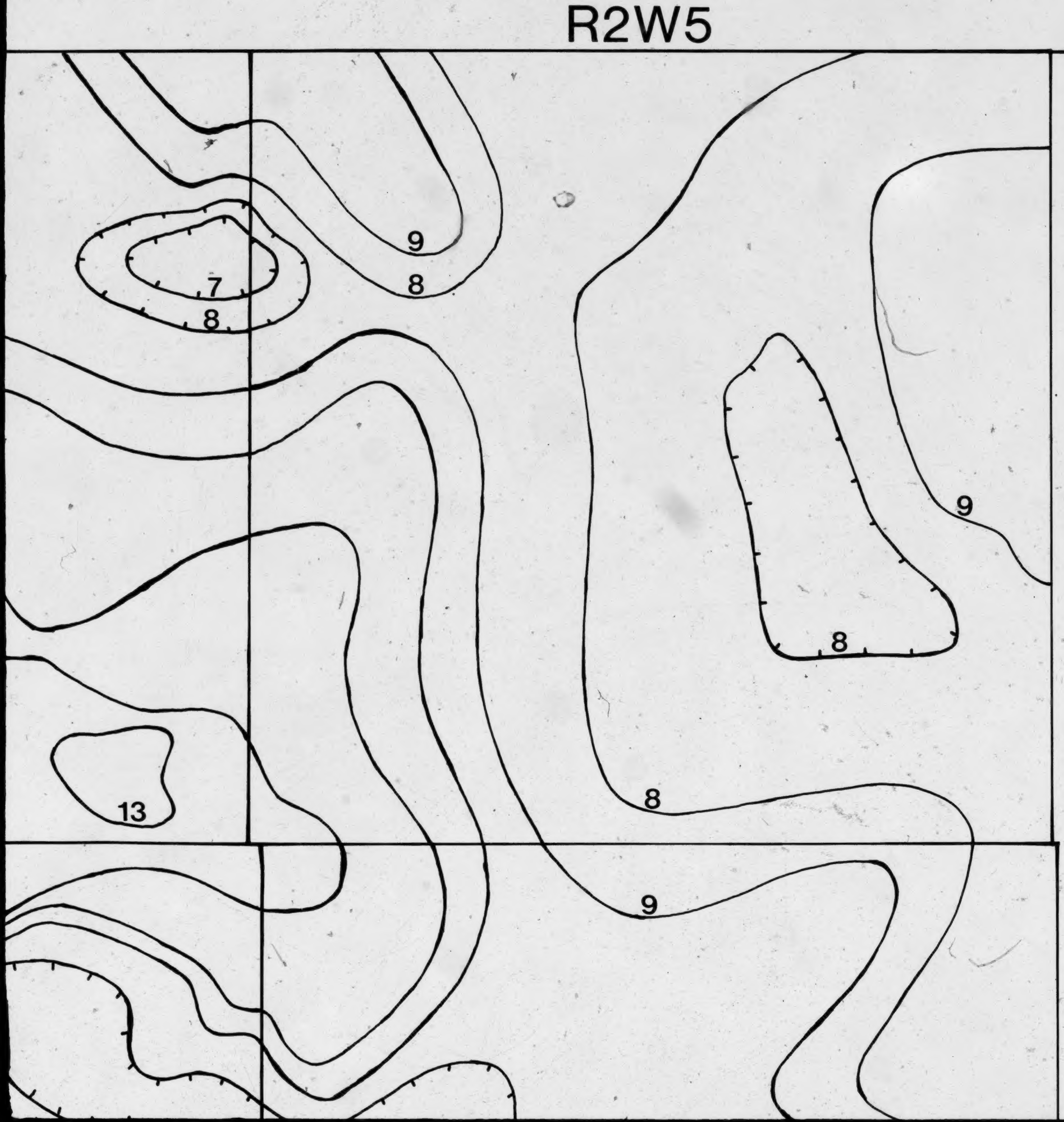
R2W5
9
8
7
8
9
8
13
8
9
9
8

2 of

GARRINGTON OIL FIELD

VIKING "B" FINE-GRAINED SANDSTONE ISOPACH

CONTOUR INTERVAL 1m

TOPOGRAPHIC LOW

TWP.
34

3 f

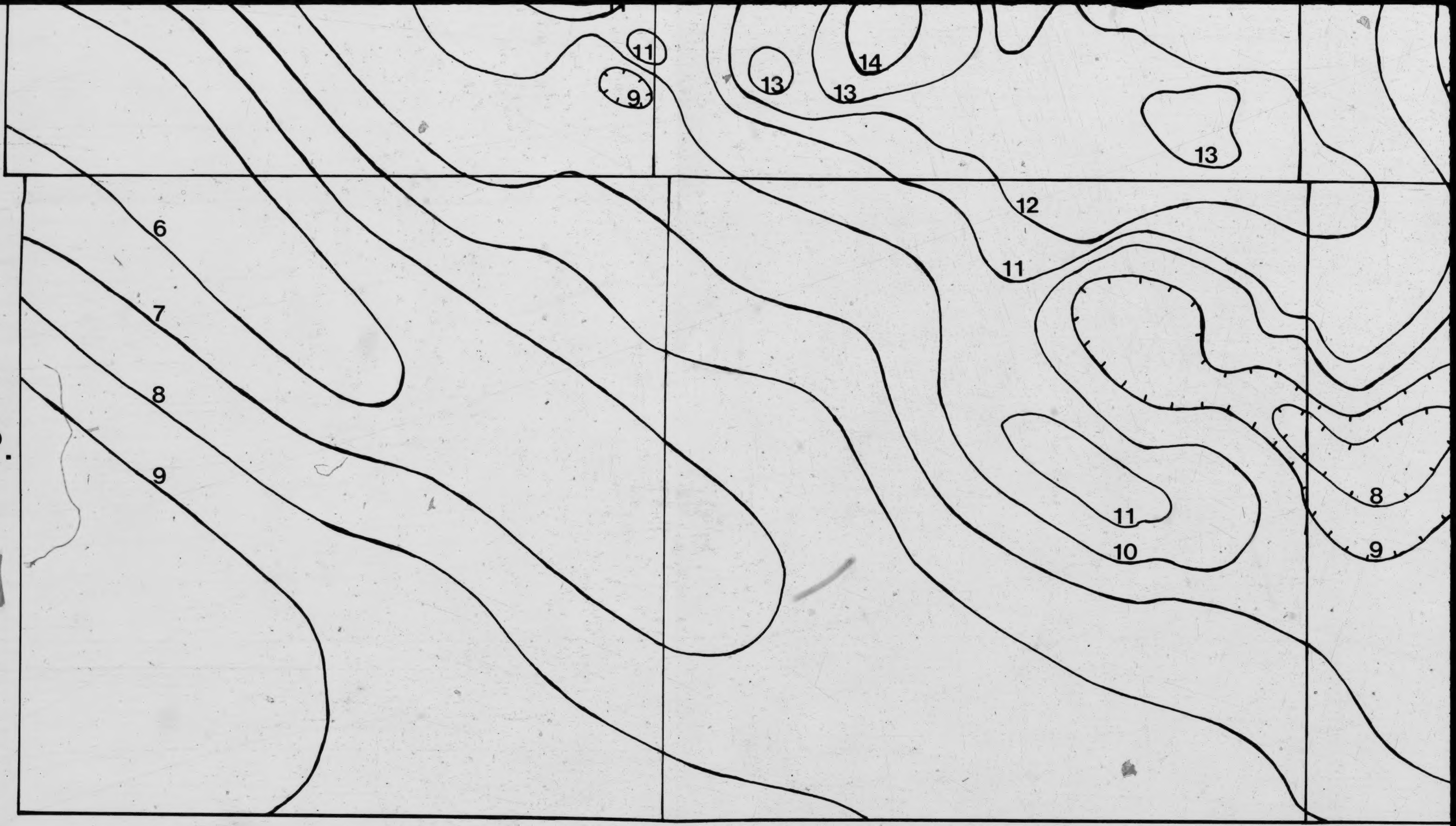
11
9
13
14
13
13
12
11
6
7
8
9
11
10
8
9

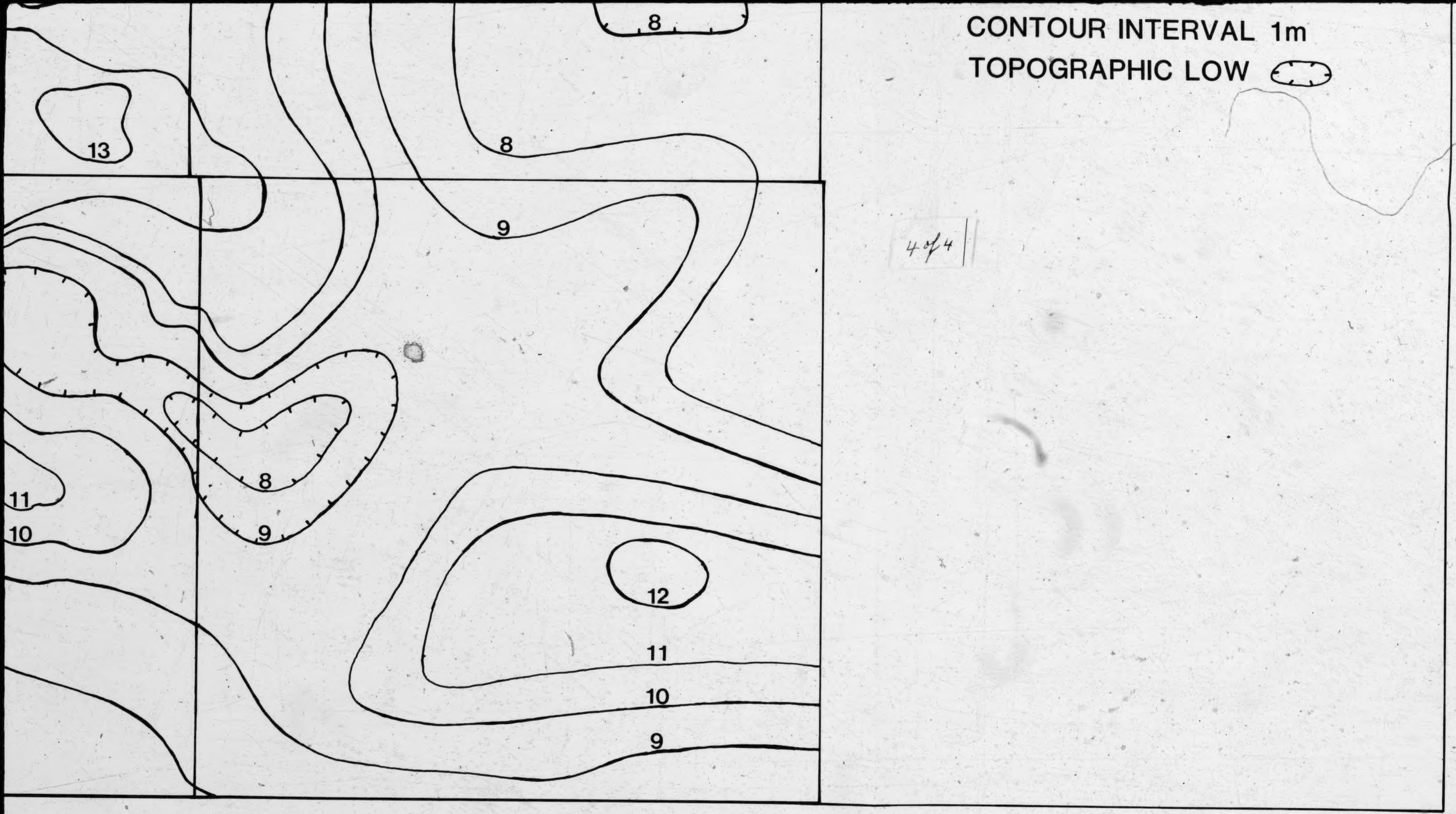
CONTOUR INTERVAL 1m
TOPOGRAPHIC LOW
8
13
8
9
11
10
8
9
12
11
10
9

4 of 4

17

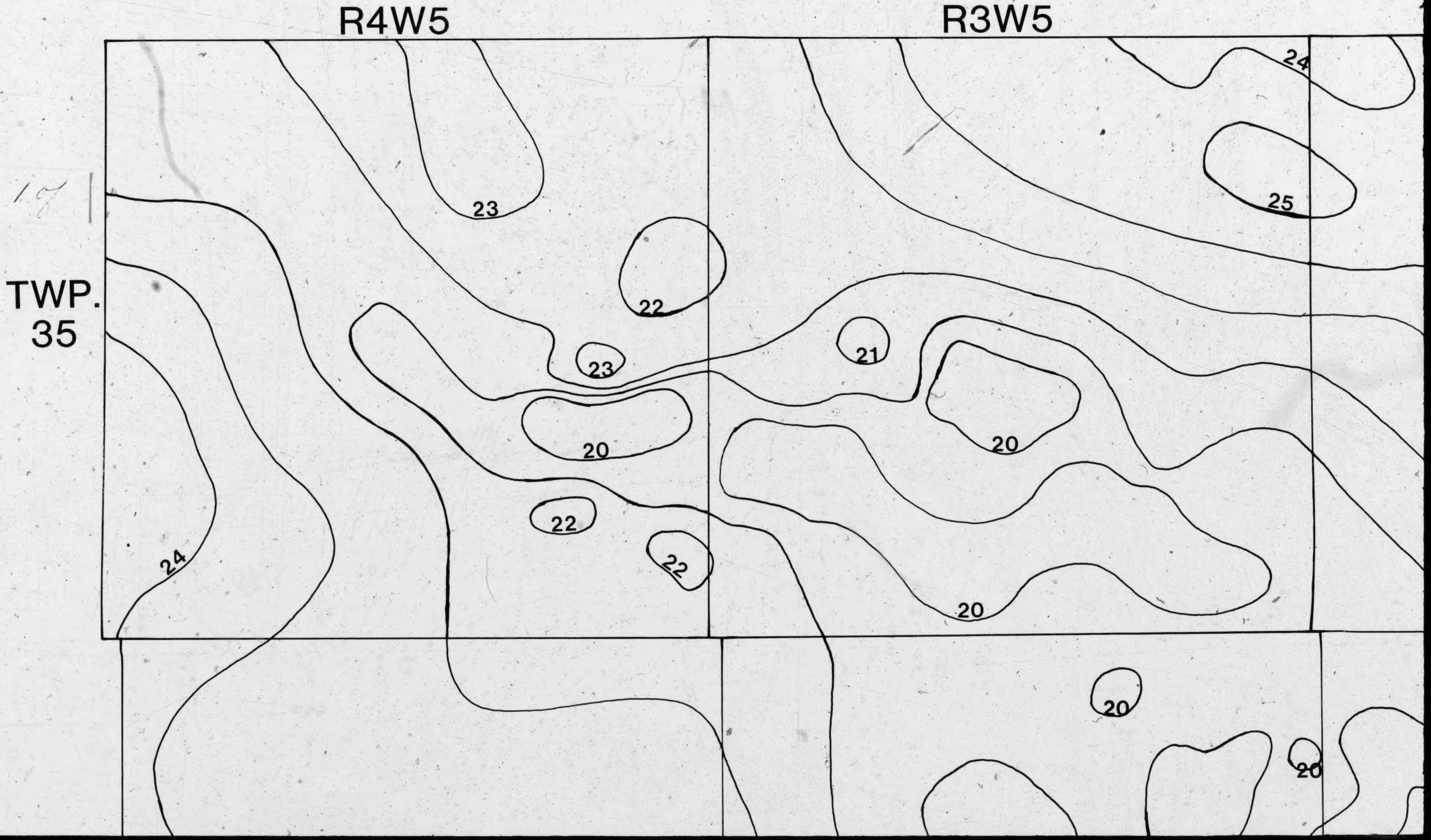
R4W5
R3W5
TWP.
35
23
24
25
22
23
21
20
20
22
22
24
20
20
20

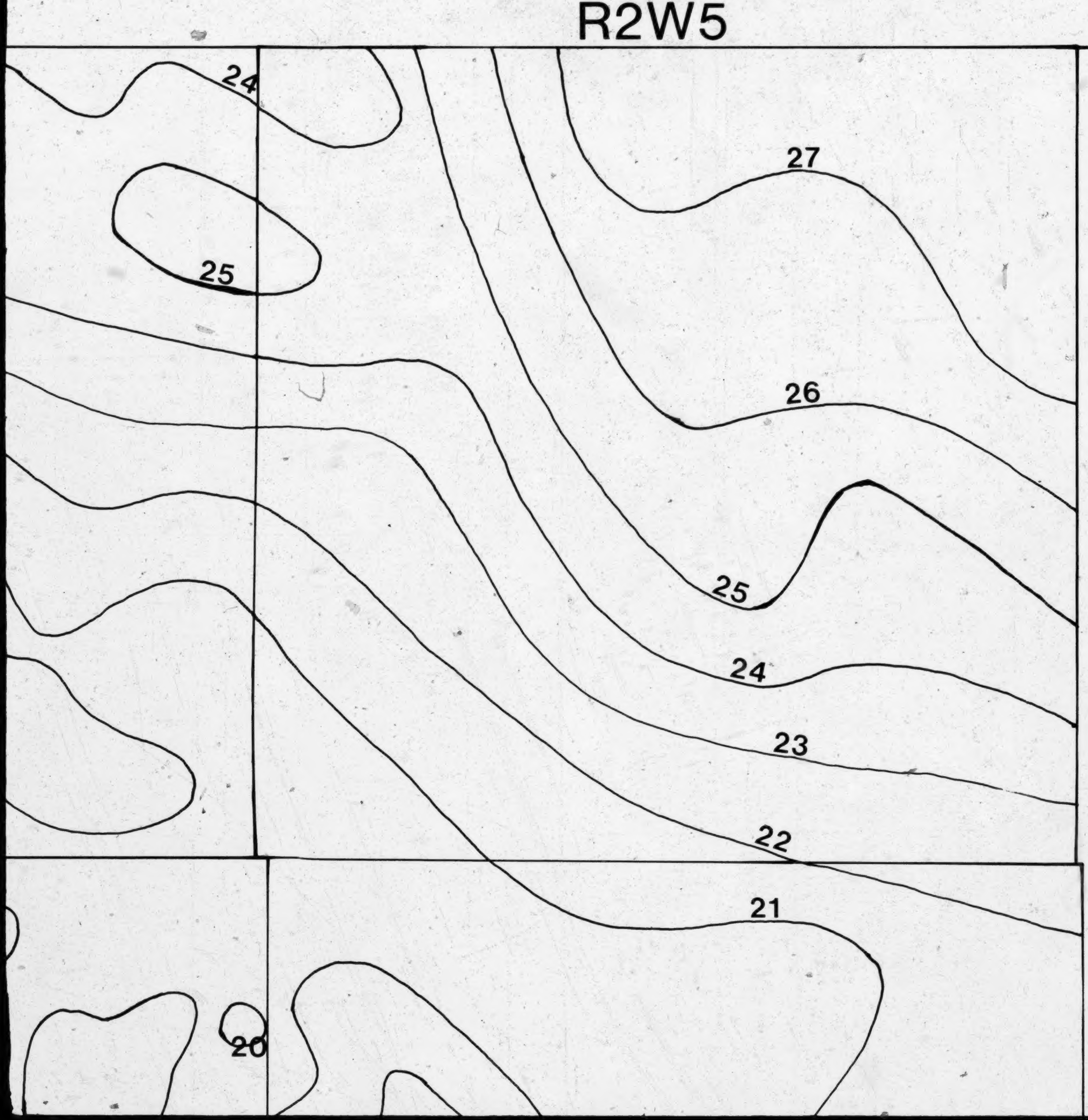
R2W5
24
27
25
26
25
24
23
22
21
20

2 of

GARRINGTON OIL FIELD

LLOYDMINSTER SHALE ISOPACH

CONTOUR INTERVAL 1m

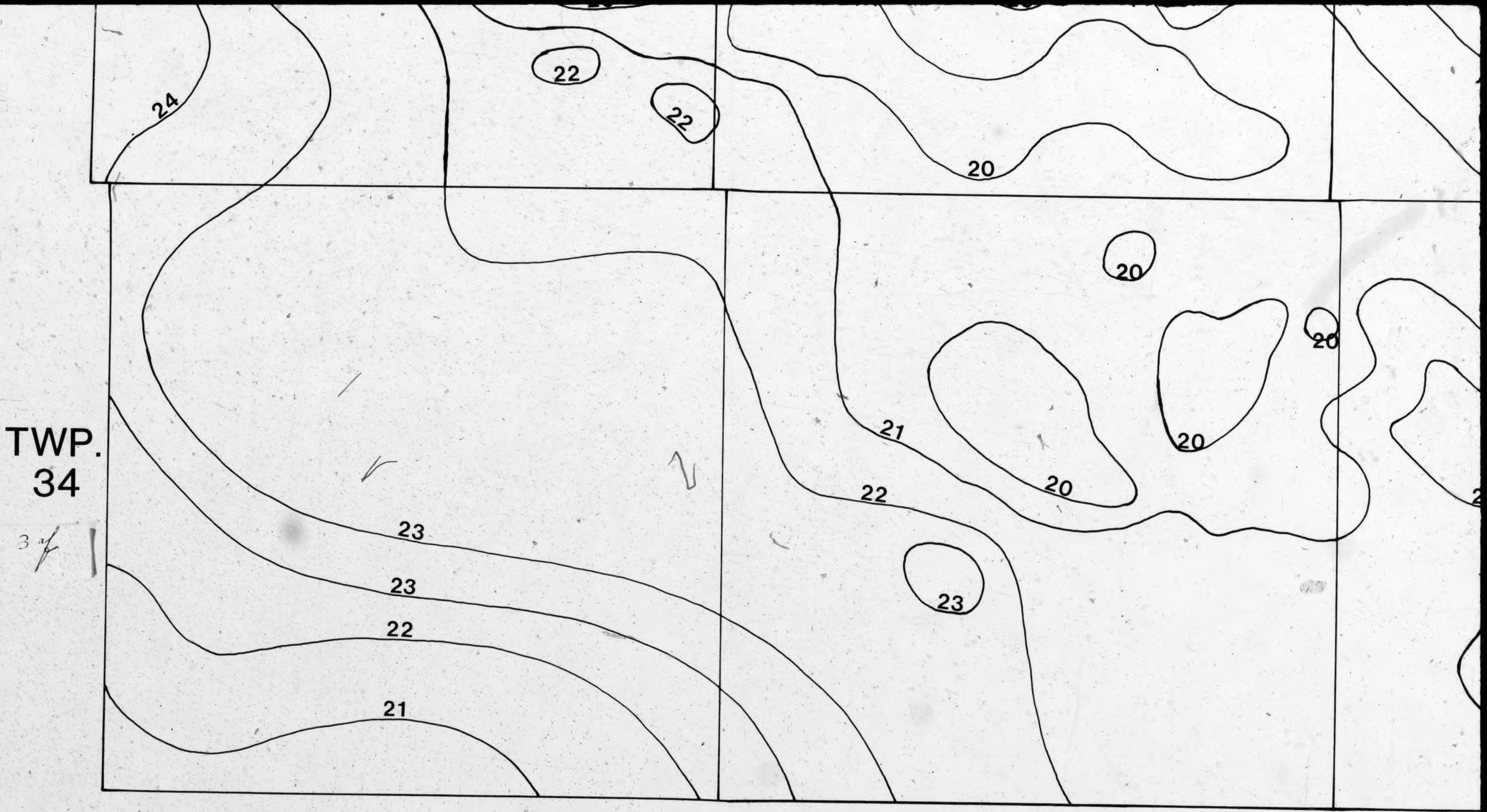
24
22
22
20
20
20
20
21
20
22
23
TWP.
34
23
23
22
21

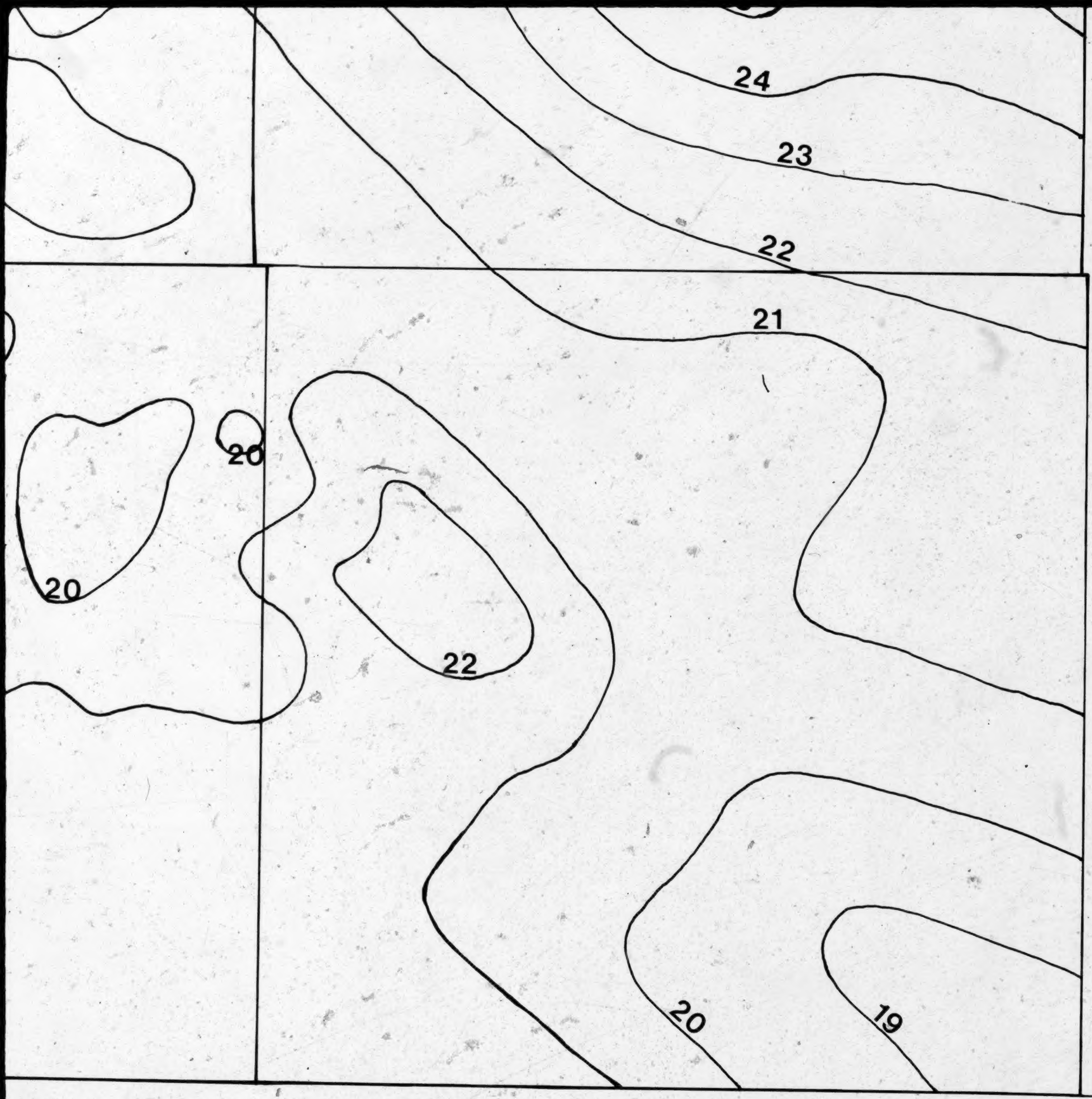
24
23
22
21
20
20
22
20
19

CONTOUR INTERVAL 1m

4 of 4

17

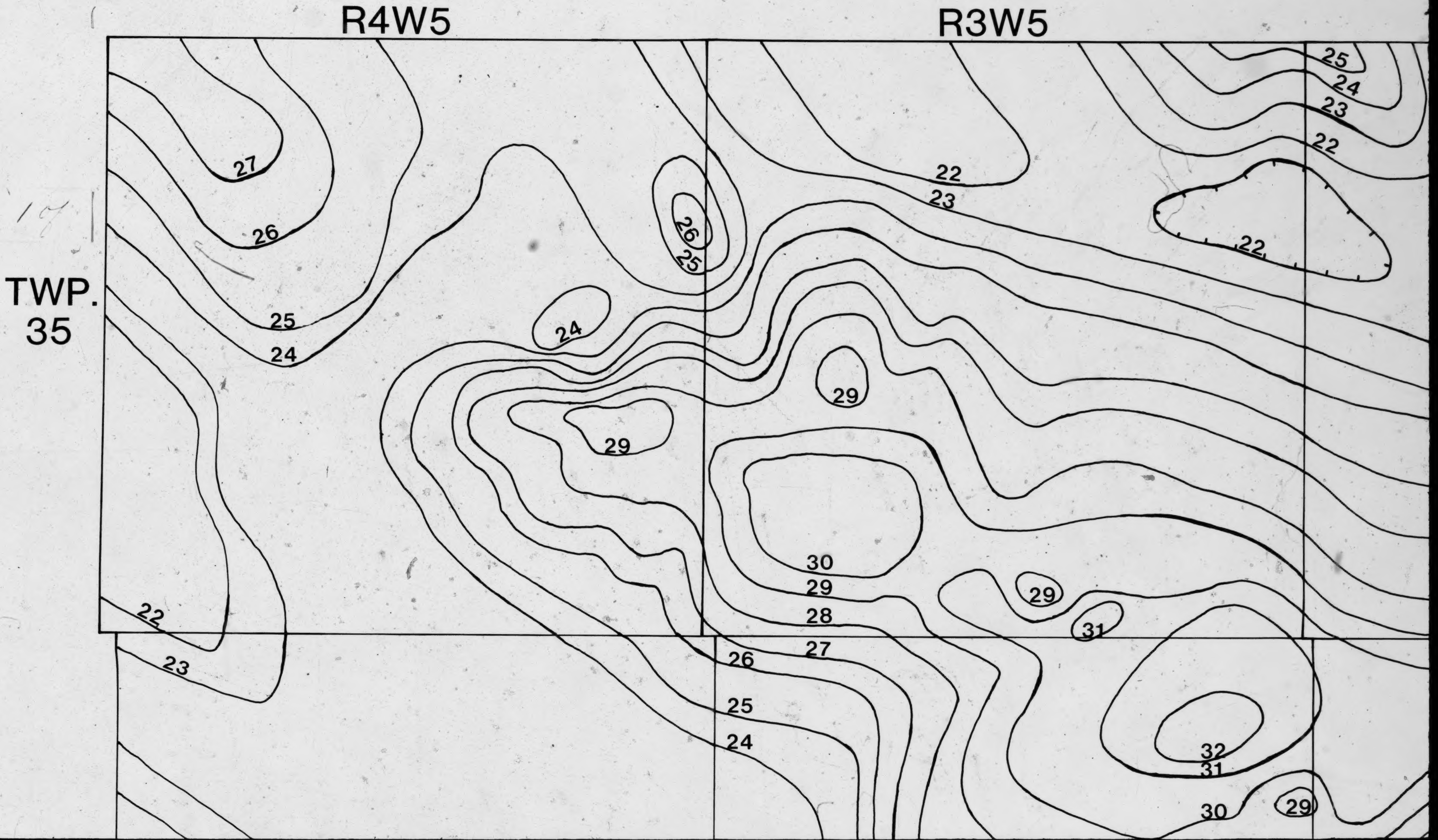
R4W5
R3W5
TWP.
35
27
26
25
24
22
23
26
25
24
29
22
23
25
24
23
22
22
29
30
29
28
27
26
25
24
29
31
32
31
30
29

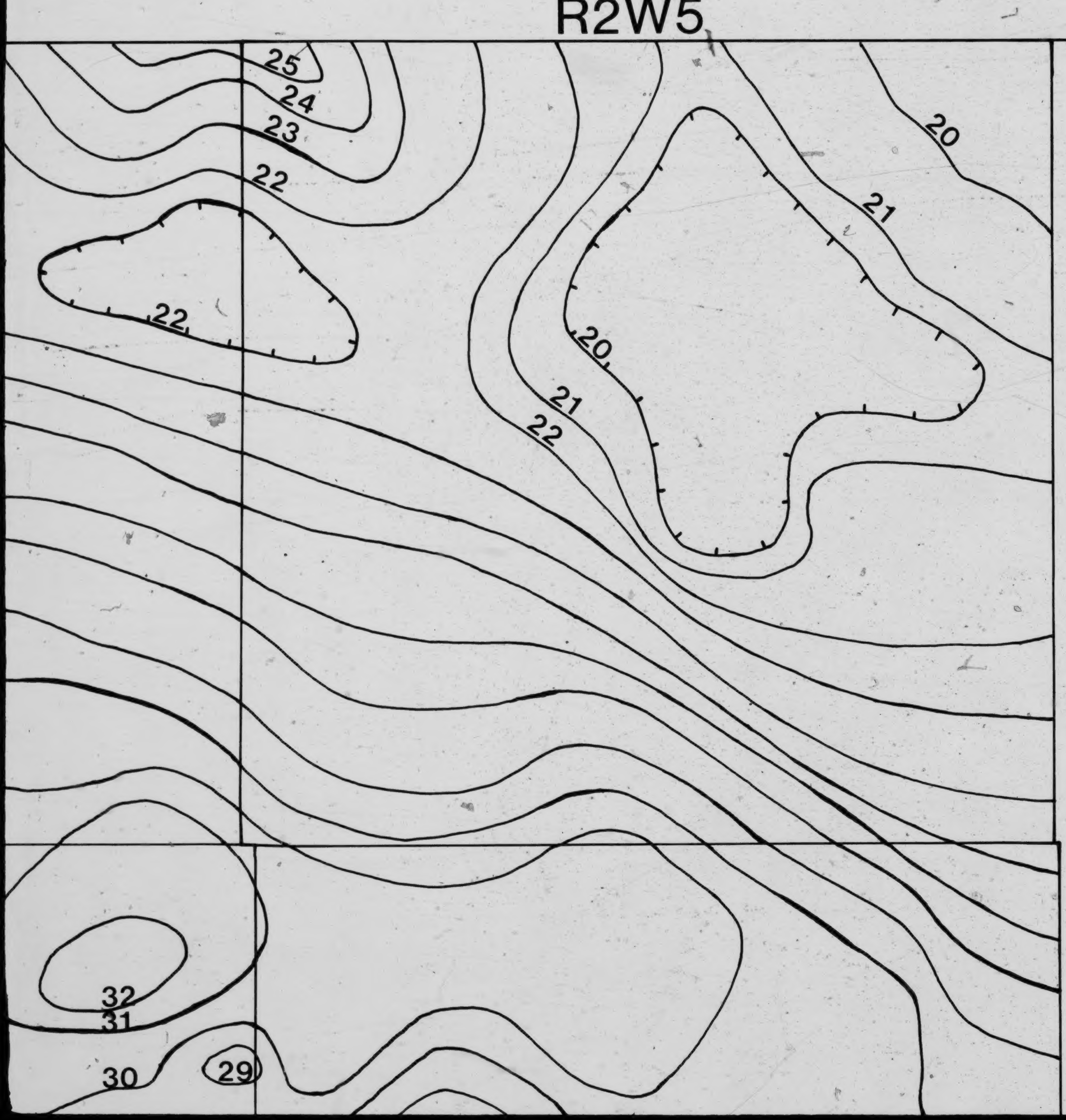
R2W5
25
24
23
22
22
20
21
20
21
22
32
31
30
29

2 of

GARRINGTON OIL FIELD

BENTONITE MARKER TO TOP OF VIKING "B" ISOPACH

CONTOUR INTERVAL 1m

TOPOGRAPHIC LOW ⬭

TWP.
34

3 of

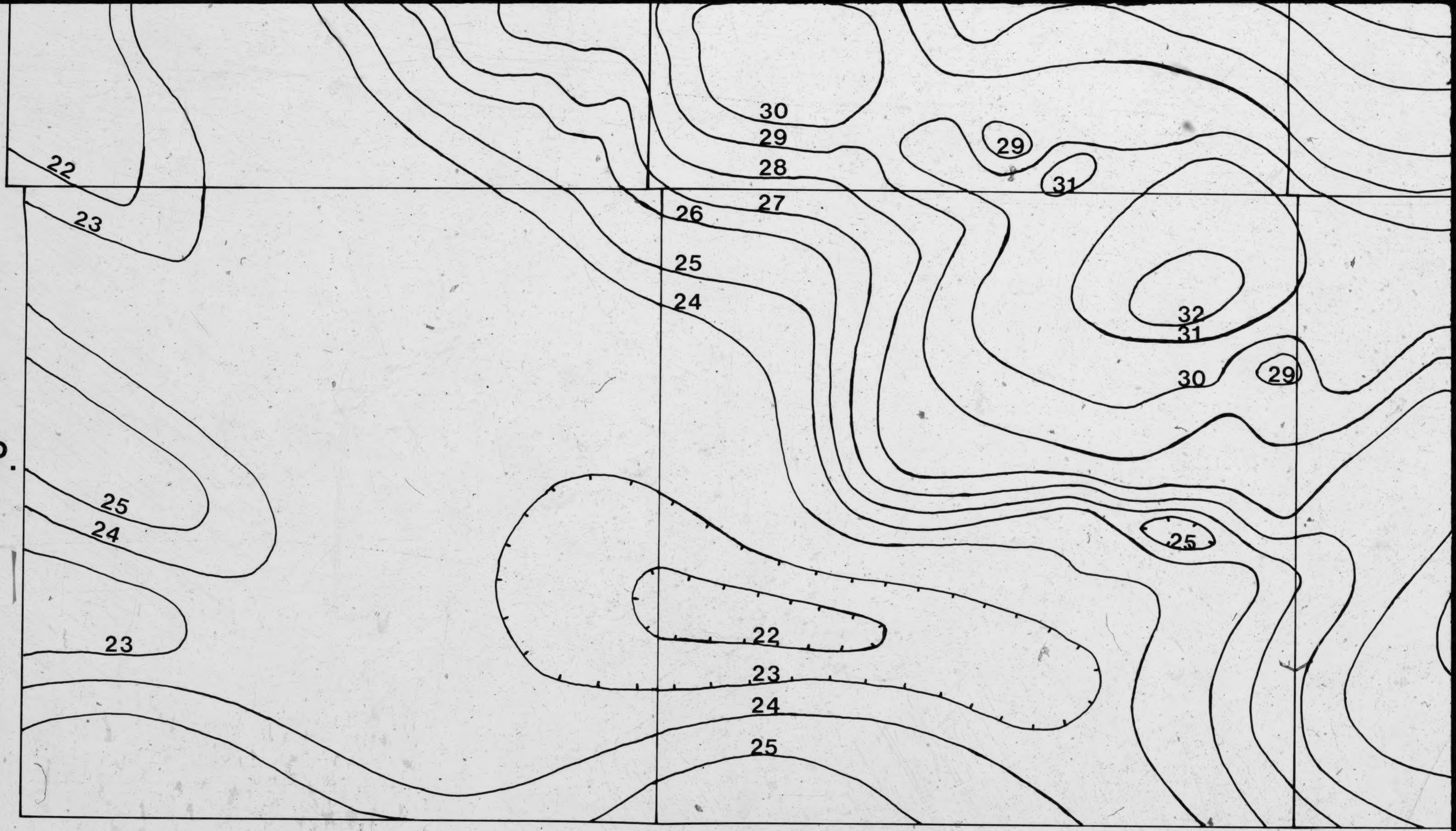
30
29
28
27
26
25
24
22
23
29
31
32
31
30
29
25
24
23
25
22
23
24
25

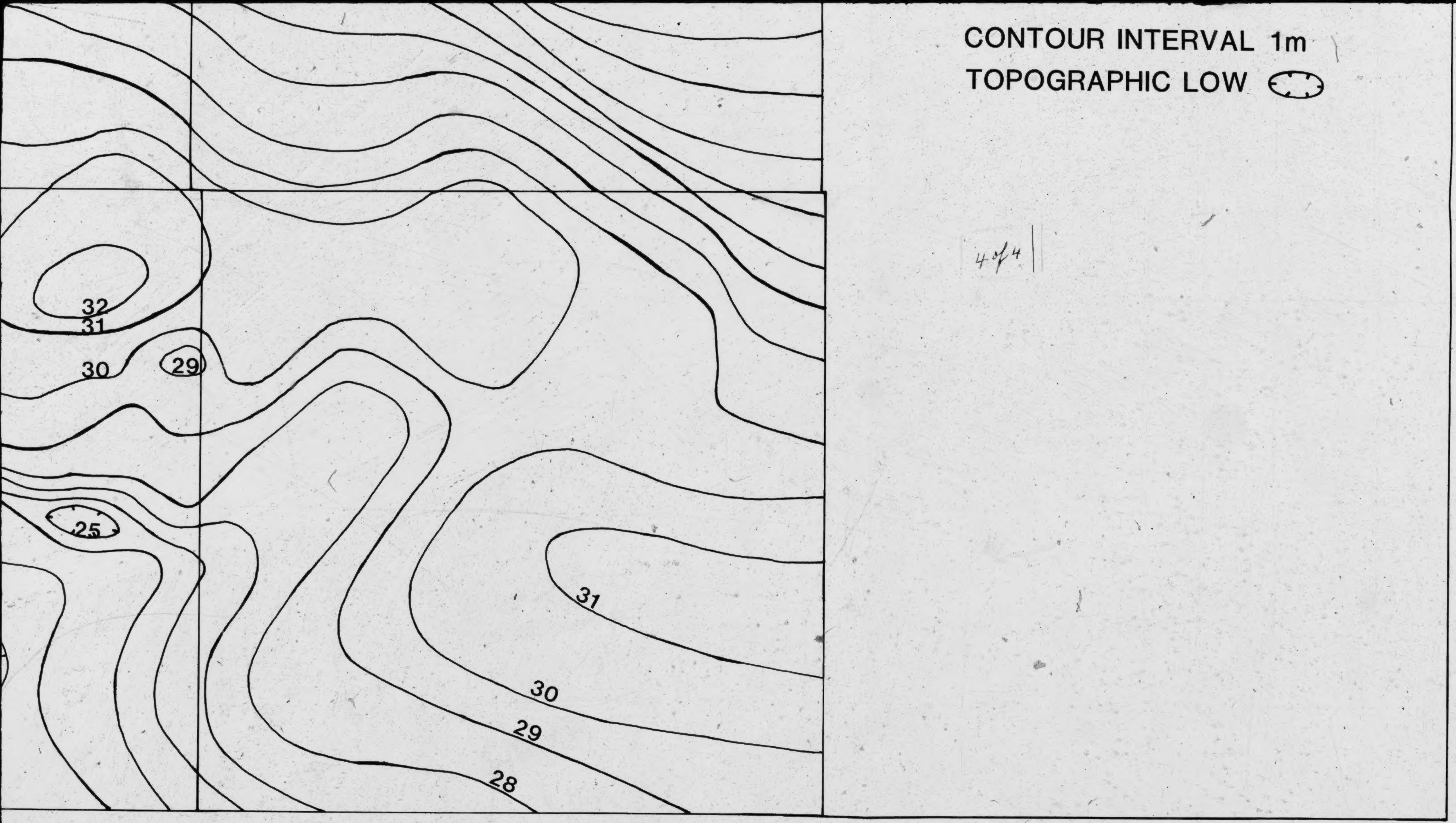
CONTOUR INTERVAL 1m
TOPOGRAPHIC LOW
32
31
30
29
25
31
30
29
28

4 of 4

17

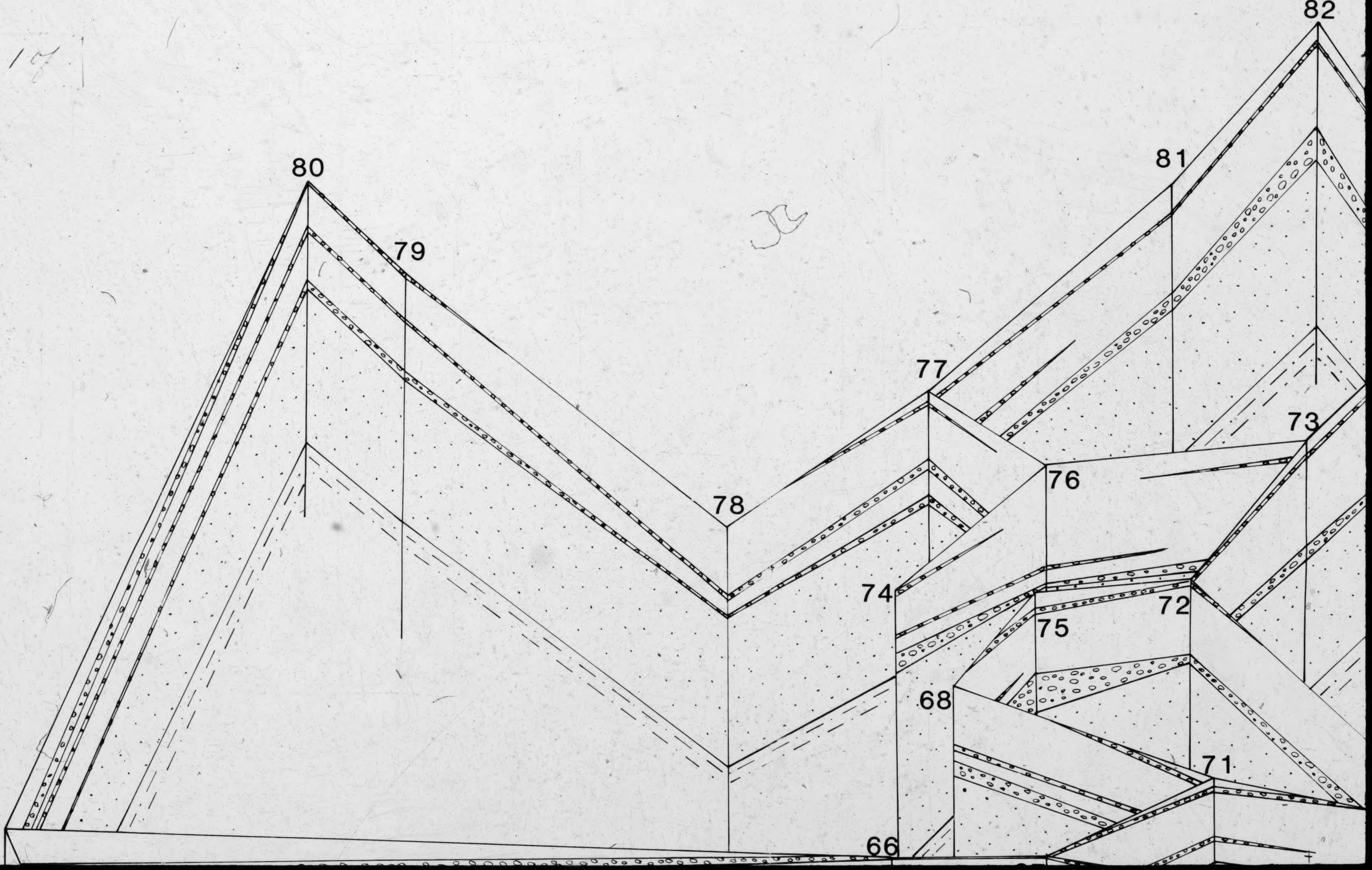

82
80
81
79
77
73
76
78
74
72
75
68
71
65
66

2 of

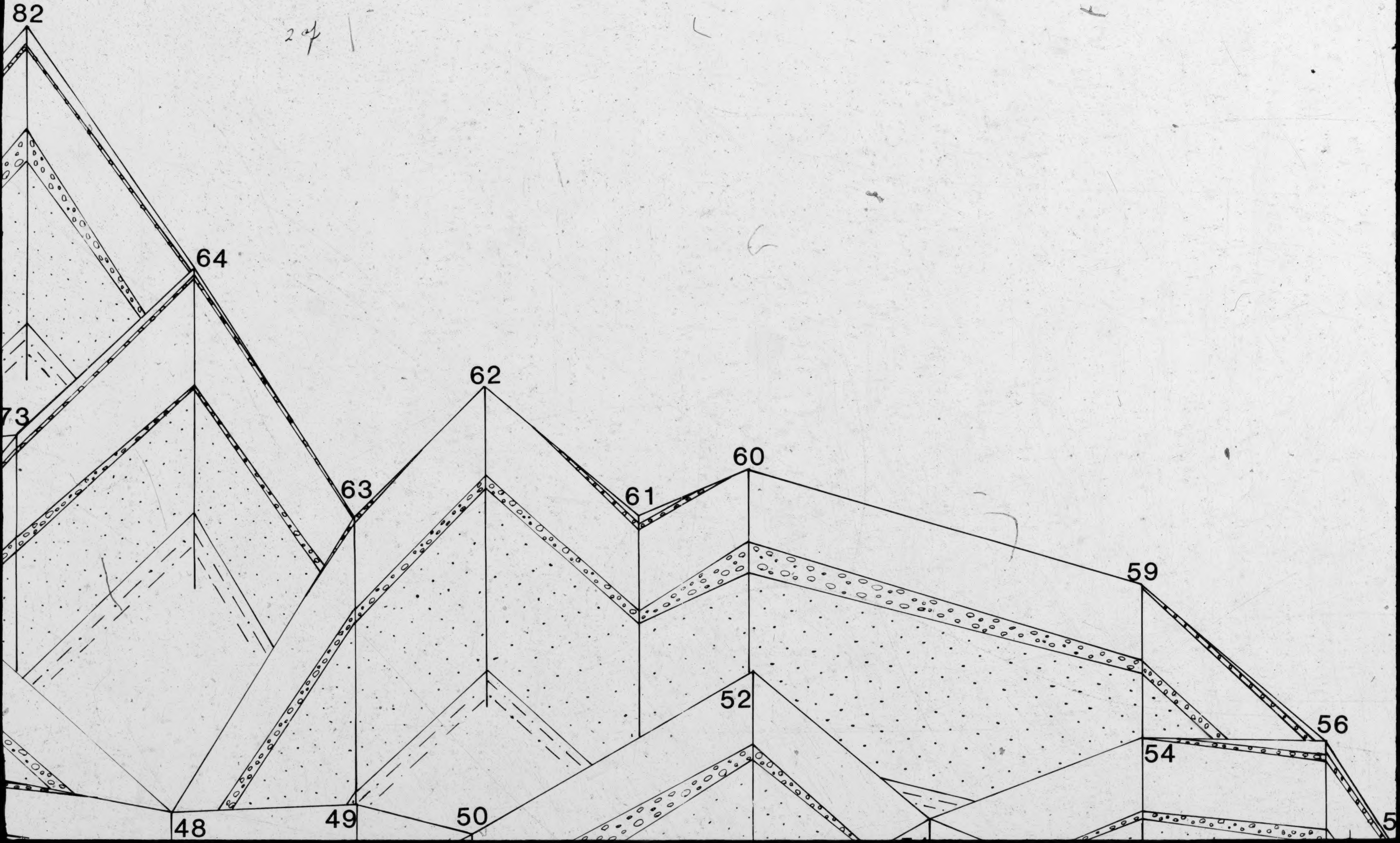
82
64
73
62
63
61
60
59
52
56
54
48
49
50
5

3 of

GARRINGTON FENC

LEGEN

☐ **LLOYDMINSTER SHALE**

⁘ CONGLOMERATE AND COARSE-GRAINED SANDSTONE

⋰ FINE-GRAINED SANDSTONE

▤ FINE-GRAINED SANDSTONE AND SHALE

WELL LO

1. 10-9-34-2W5
2. 5-14-34-2W5
3. 16-19-34-2W5
4. 11-23-34-2W5
5. 7-26-34-2W5
6. 13-30-34-2W5
7. 7-33-34-2W5
8. 7-34-34-2W5
9. 16-11-34-3W5

17. 14-24-34-3W5
18. 16-24-34-3W5
19. 6-25-34-3W5
20. 8-25-34-3W5
21. 14-25-34-3W5
22. 16-26-34-3W5
23. 16-27-34-3W5
24. 6-29-34-3W5
25. 6-30-34-3W5

33. 4-20-
34. 11-2
35. 6-6-
36. 3-1-
37. 10-1-
38. 10-2-
39. 14-2-
40. 1-3-
41. 6-2-

GARRINGTON FENCE DIAGRAM

LEGEND

ER SHALE

AND COARSE-GRAINED SANDSTONE

NDSTONE

NDSTONE AND SHALE

4 of

DATUM 15m BELOW BASE OF FISH SCALES

HORIZONTAL SCALE 6cm : 1000m

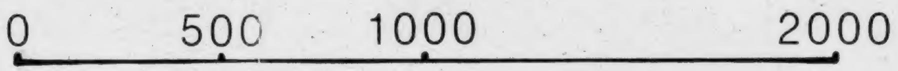

VERTICAL SCALE 1cm : 2m

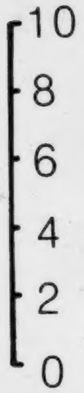

VERTICAL EXAGGERATION 83.3X

WELL LOCATIONS

17. 14-24-34-3W5
18. 16-24-34-3W5
19. 6-25-34-3W5
20. 8-25-34-3W5
21. 14-25-34-3W5
22. 16-26-34-3W5
23. 16-27-34-3W5
24. 6-29-34-3W5
25. 6-30-34-3W5
33. 4-20-34-4W5
34. 11-28-34-4W5
35. 6-6-35-2W5
36. 3-1-35-3W5
37. 10-1-35-3W5
38. 10-2-35-3W5
39. 14-2-35-3W5
40. 1-3-35-3W5
41. 6-3-35-3W5
49. 8-7-35-3W5
50. 6-8-35-3W5
51. 8-9-35-3W5
52. 14-9-35-3W5
53. 6-10-35-3W5
54. 10-10-35-3W5
55. 7-11-35-3W5
56. 11-11-35-3W5
57. 3-12-35-3W5
66. 6-11-35-4W5
67. 8-11-35-4W5
68. 14-11-35-4W5
69. 1-12-35-4W5
70. 6-12-35-4W5
71. 11-12-35-4W5
72. 6-13-35-4W5
73. 10-13-35-4W5
74. 6-14-35-4W5

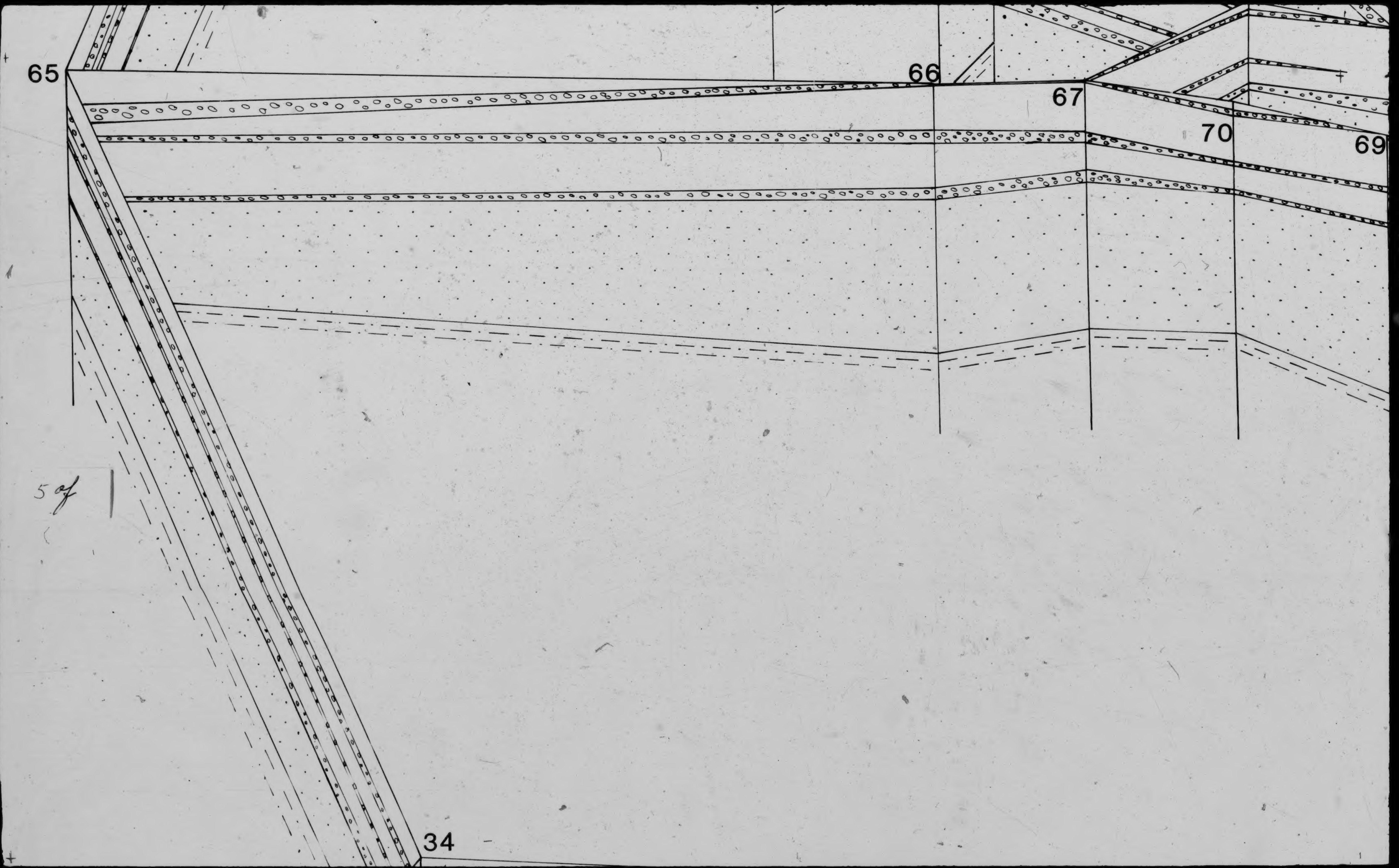
5 of

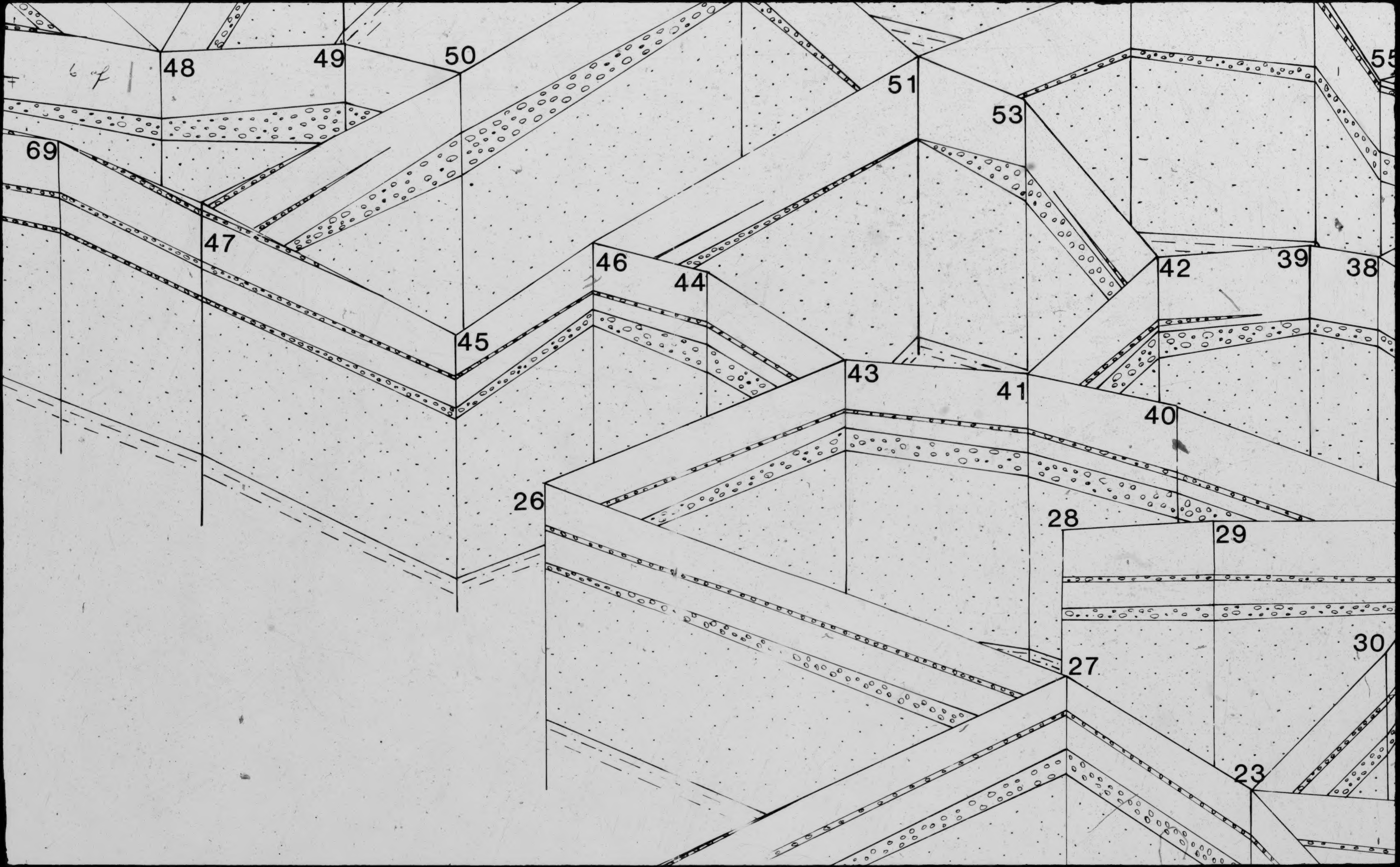
6 of

7 of

9. 16-11-34-3W5
10. 6-13-34-3W5
11. 16-13-34-3W5
12. 16-14-34-3W5
13. 16-15-34-3W5
14. 6-23-34-3W5
15. 16-23-34-3W5
16. 3-24-34-3W5

25. 6-30-34-3W5
26. 14-32-34-3W5
27. 6-34-34-3W5
28. 14-34-34-3W5
29. 16-34-34-3W5
30. 6-35-34-3W5
31. 16-35-34-3W5
32. 14-36-34-3W5

41. 6-3-3
42. 9-3-3
43. 7-4-3
44. 12-4-
45. 6-5-3
46. 16-5-
47. 14-6-
48. 6-7-3

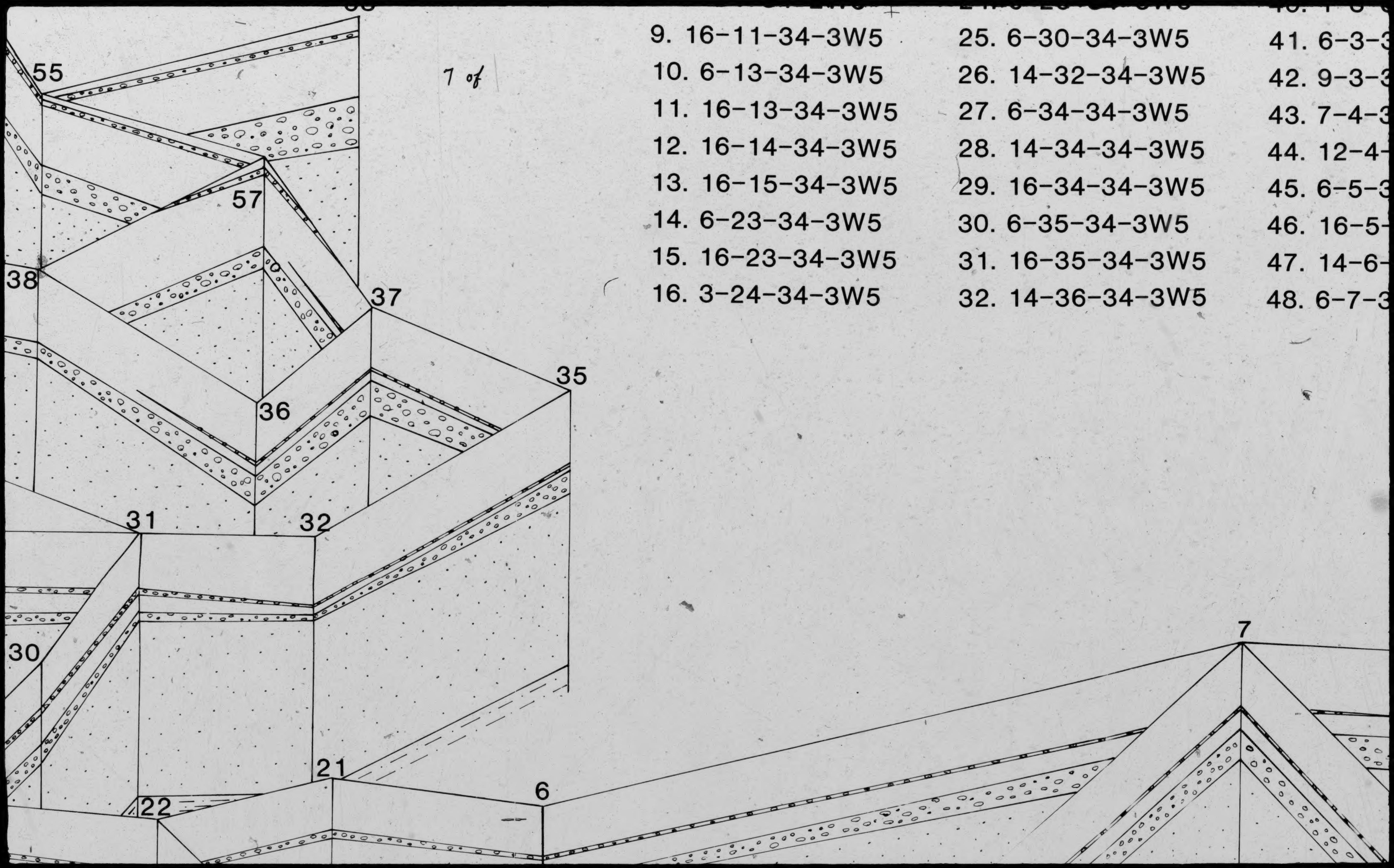
55
57
38
37
35
36
31
32
30
7
21
22
6

24. 6-29-34-3W5
25. 6-30-34-3W5
26. 14-32-34-3W5
27. 6-34-34-3W5
28. 14-34-34-3W5
29. 16-34-34-3W5
30. 6-35-34-3W5
31. 16-35-34-3W5
32. 14-36-34-3W5
40. 1-3-35-3W5
41. 6-3-35-3W5
42. 9-3-35-3W5
43. 7-4-35-3W5
44. 12-4-35-3W5
45. 6-5-35-3W5
46. 16-5-35-3W5
47. 14-6-35-3W5
48. 6-7-35-3W5
56. 11-11-35-3W5
57. 3-12-35-3W5
58. 10-12-35-3W5
59. 2-15-35-3W5
60. 11-16-35-3W5
61. 8-17-35-3W5
62. 14-17-35-3W5
63. 8-18-35-3W5
64. 6-19-35-3W5
65. 6-8-35-4W5
73. 10-13-35-4W5
74. 6-14-35-4W5
75. 8-14-35-4W5
76. 9-14-35-4W5
77. 14-14-35-4W5
78. 8-15-35-4W5
79. 7-21-35-4W5
80. 11-21-35-4W5
81. 11-24-35-4W5
82. 1-25-35-4W5

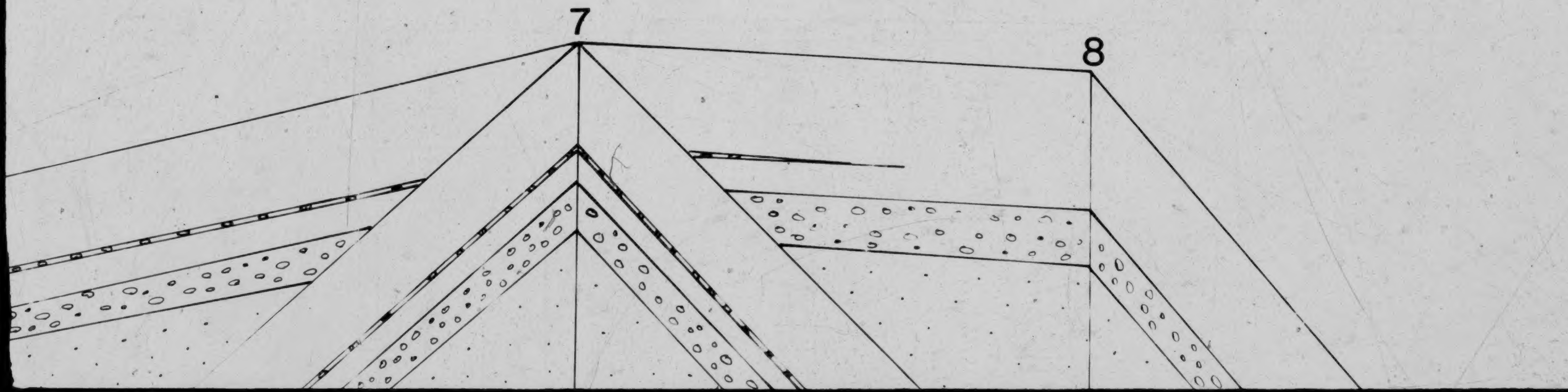

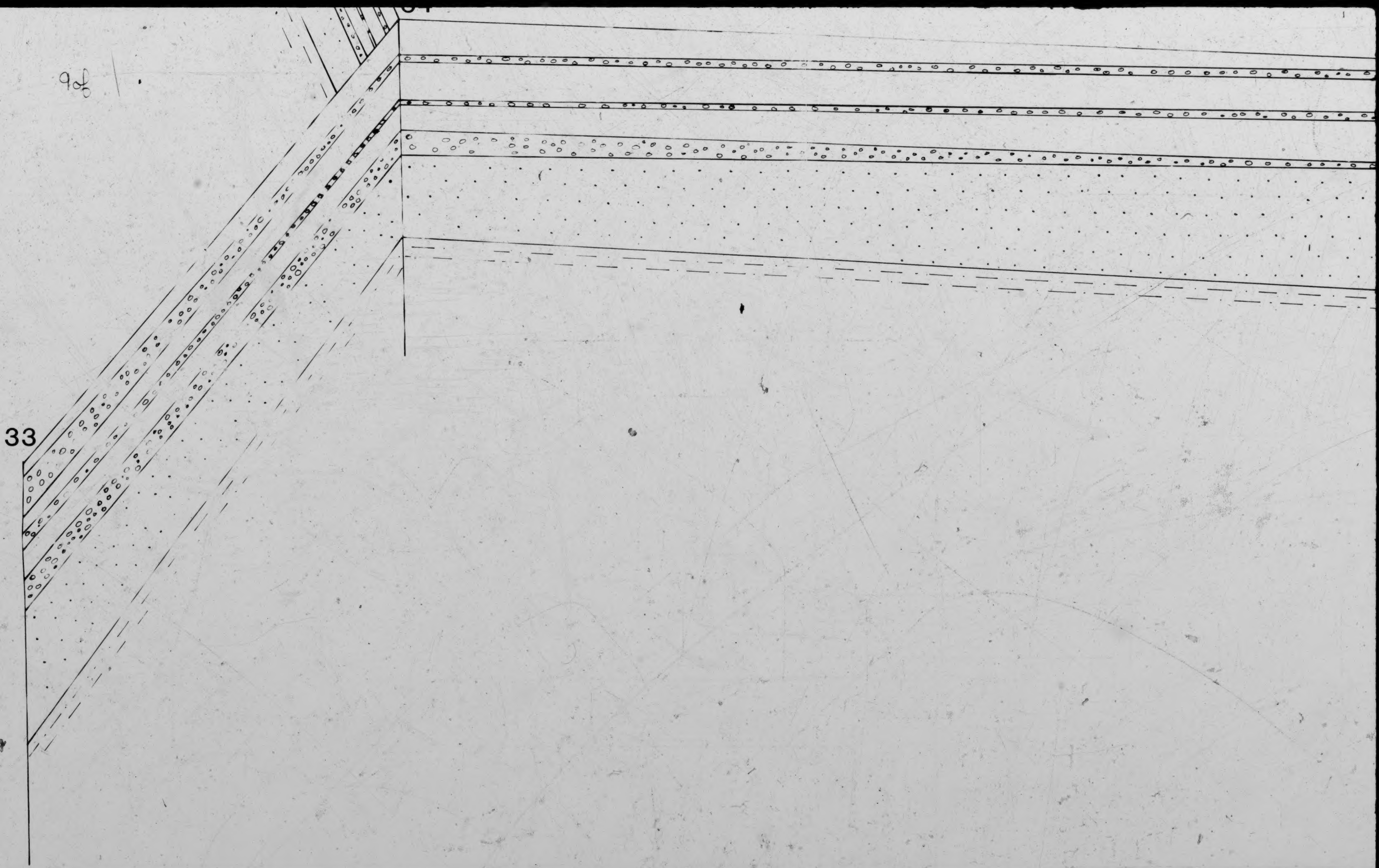
9f
33

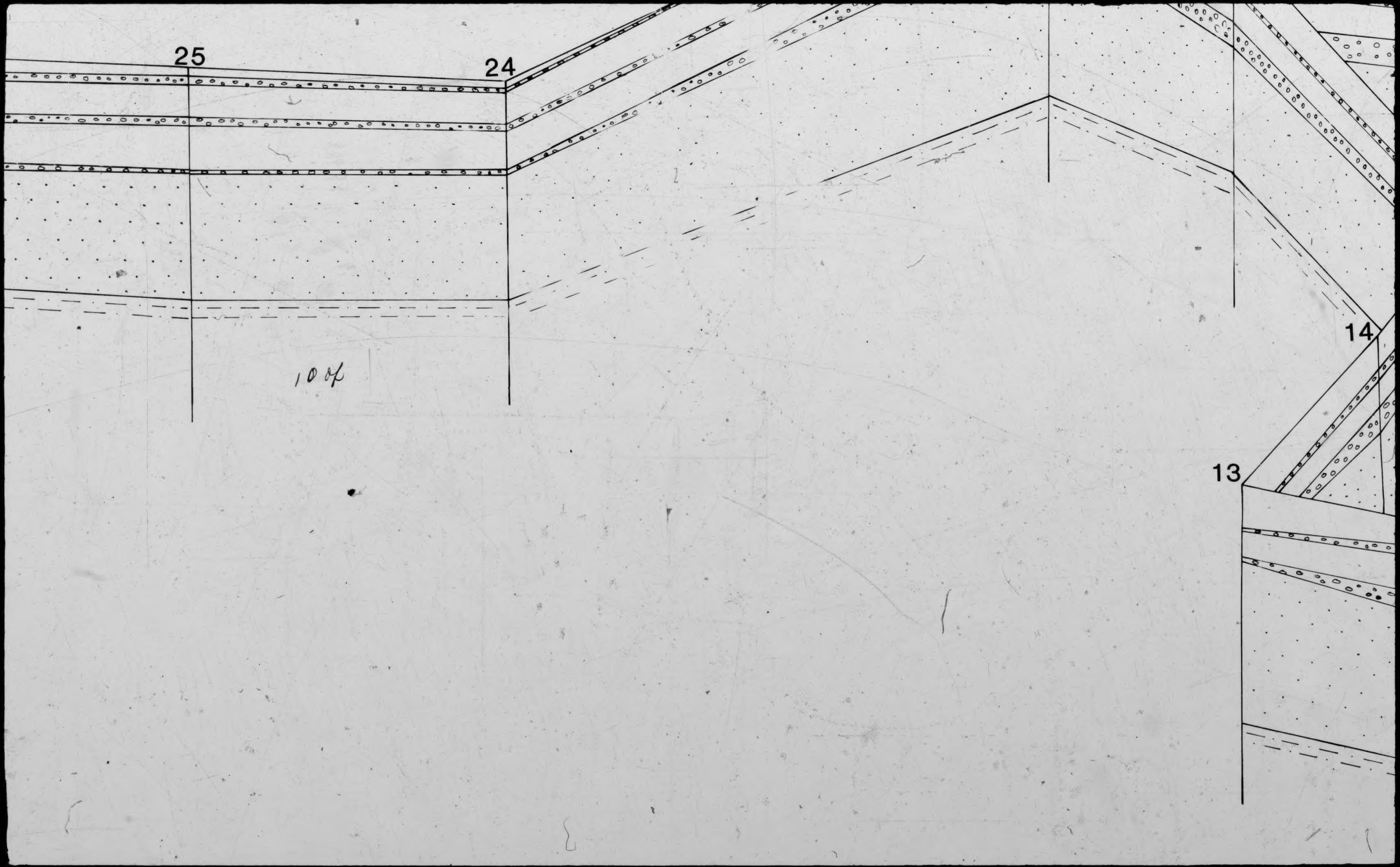

10 of

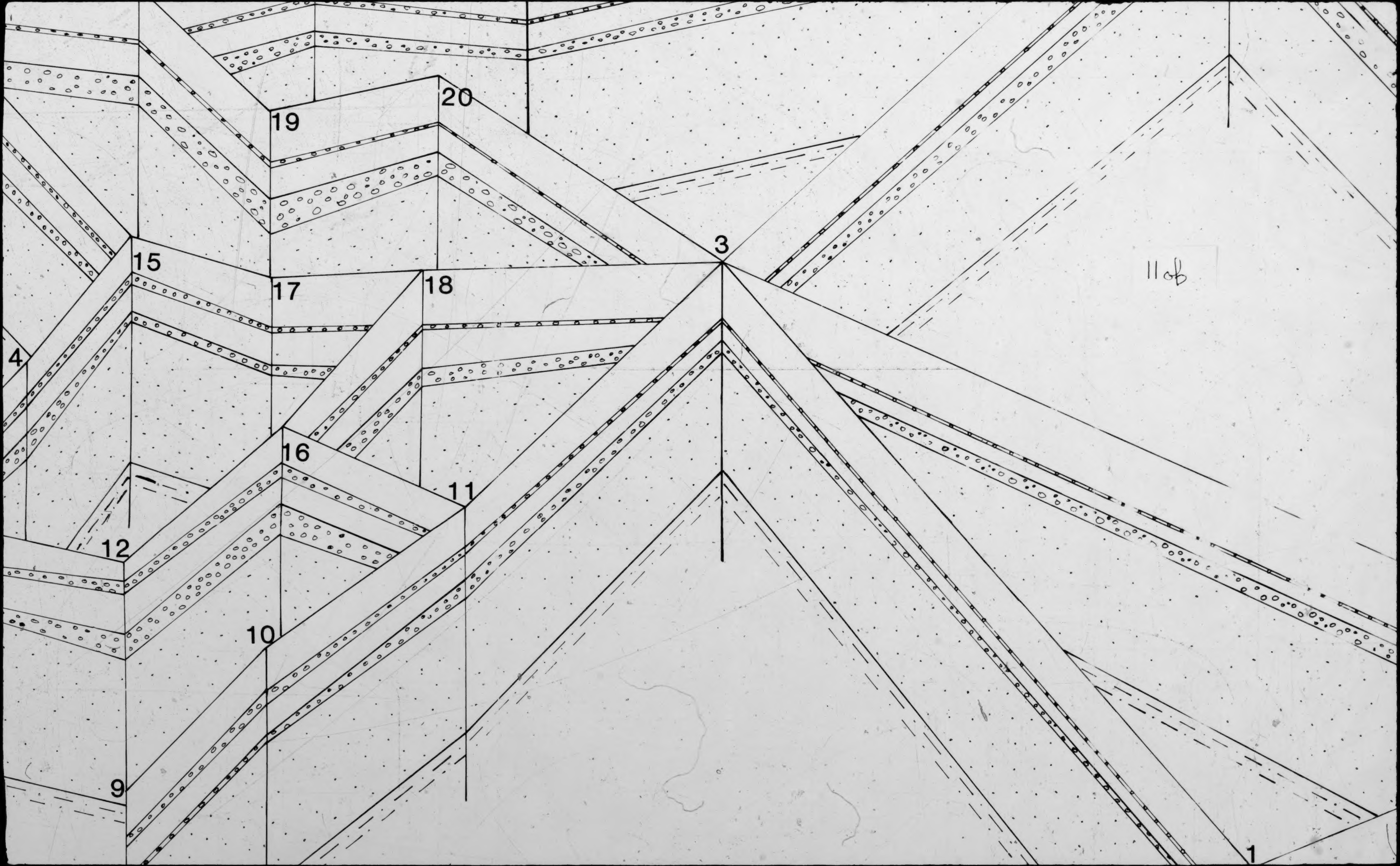
11ob

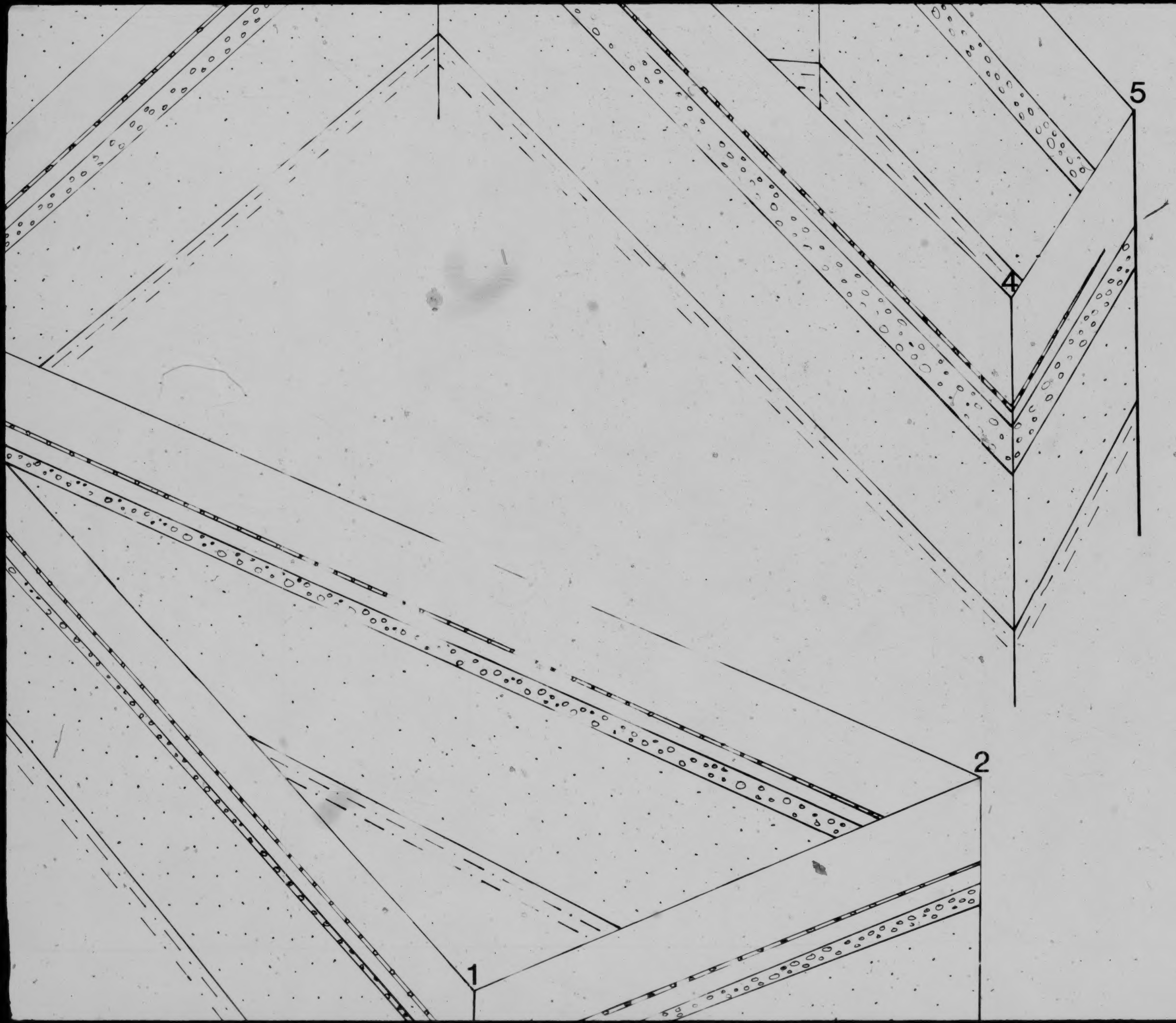

12 of
504 (r. 3/82)

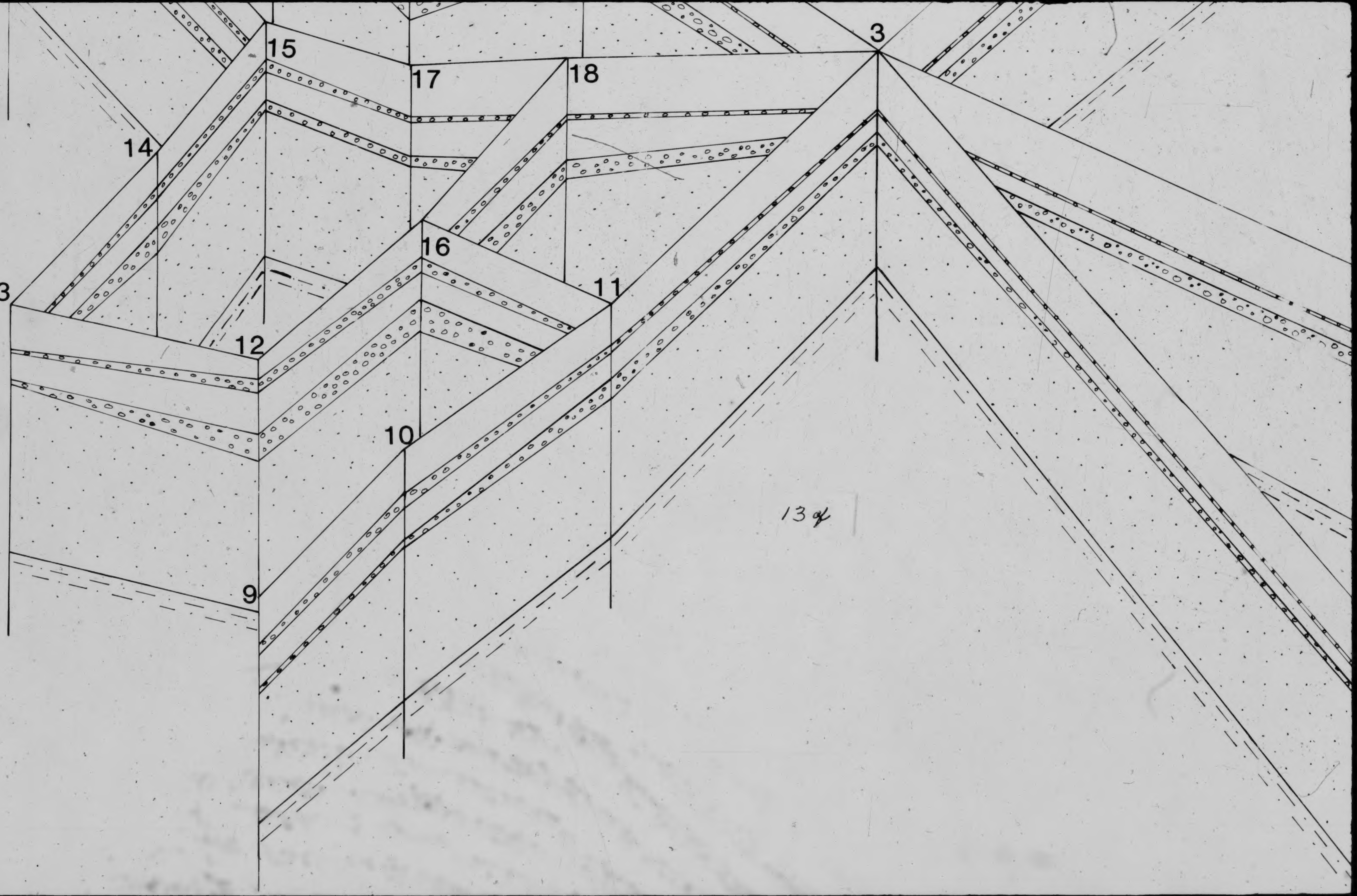
3
15
17
18
14
13
16
11
12
10
9

13 of

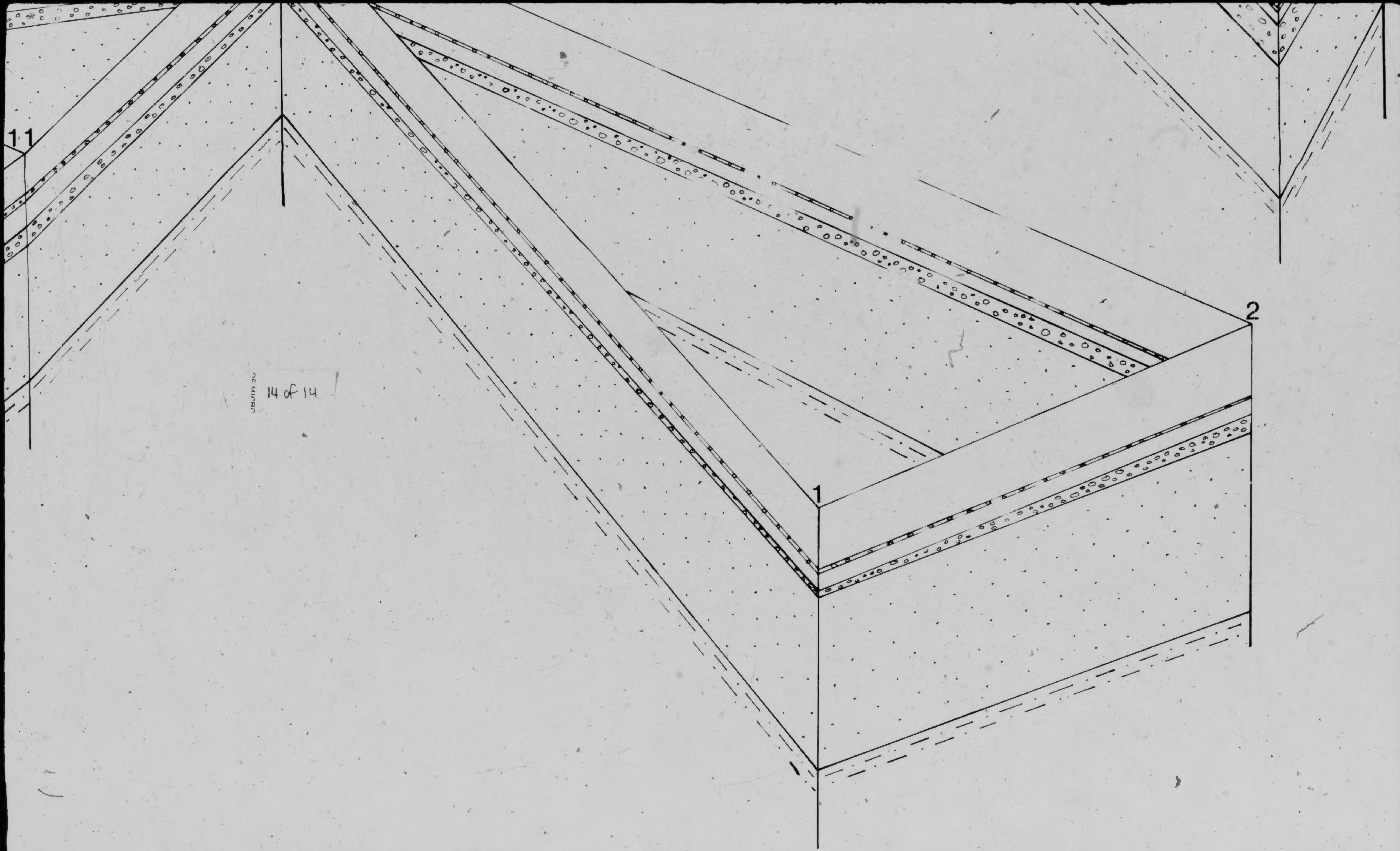

14 of 14